

DEVELOPMENT OF NEW TRANSITION METAL
COMPLEXES FOR THEIR USE IN
SUSTAINABLE CATALYTIC PROCESSES AND
AS ANTITUMORAL AGENTS

Ester Manrique Salas

Per citar o enllaçar aquest document:
Para citar o enlazar este documento:
Use this url to cite or link to this publication:
<http://hdl.handle.net/10803/668830>



<http://creativecommons.org/licenses/by/4.0/deed.ca>

Aquesta obra està subjecta a una llicència Creative Commons Reconeixement

Esta obra está bajo una licencia Creative Commons Reconocimiento

This work is licensed under a Creative Commons Attribution licence



Doctoral Thesis

Development of new transition metal complexes for
their use in sustainable catalytic processes and as
antitumoral agents

Ester Manrique Salas

2018

Doctoral programme in Chemistry

Supervised by: Dra. M. Isabel Romero García

Dra. Montserrat Rodríguez Pizarro

Tutor: Dra. M. Isabel Romero García

Presented in partial fulfilment of the requirements for a doctoral degree from the
University of Girona



Dra. M. Isabel Romero García and Dra. Montserrat Rodríguez Pizarro, from the Universitat de Girona,

WE DECLARE:

That the thesis *Development of new transition metal complexes for their use in sustainable catalytic processes and as antitumoral agents*, presented by Ester Manrique Salas to obtain a doctoral degree, has been completed under our supervision.

For all intents and purposes, we hereby sign this document.

Dra. M. Isabel Romero García

Dra. Montserrat Rodríguez Pizarro

Girona, 11th of June, 2018

The work performed in the present thesis has been possible thanks to the funding of:

- Universitat de Girona through a BR predoctoral grant.
- Universitat de Girona through project: MPCUdG2016/048
- Ministerio de Economía y Competitividad (MINECO) through project: CTQ2015-66143-P
- Generalitat de Catalunya (AGAUR) through project: 2014-SGR-149

Agraïments

Per començar voldria agrair a les meves directores de tesi Dra. Marisa Romero i Dra. Montse Rodríguez. Gràcies per donar-me l'oportunitat d'entrar en el món de la recerca inorgànica per fer el doctorat, un camí que mai havia contemplat fer. Moltes gràcies per tot allò que m'heu ensenyat durant tots aquests anys, gairebé 6 anys contant Treball Experimental i TFM, i per tot el suport que m'heu donat tant a nivell científic com personal.

També vull agrair a tots els col·laboradors que han fet possible aquesta tesi. Al Dr. Josep Ros de l'ICMAB per les nanopartícules magnètiques. Als Serveis Tècnics de Recerca de la UdG: la Dra. Lluïsa Matas pels espectres de RMN, l'Anna Costa pels anàlisis elementals i masses, en Xavier Fontrodona per les estructures de Raigs X, en Joan Pere López pels anàlisis termogravimètrics i la Carme Carulla i en Daniel Reyes pels serveis de microscopia electrònica. A la Dra. Mònica Iglesias pel seu temps a l'ICP. I a la Dra. Jessica Castro pel seu temps i la feina feta.

Un agraïment especial a les companyes de laboratori de quan vaig arribar al grup: Mònica F. i Íngrid. Mònica F., vam coincidir poc temps però de tu vaig heretar el teu lloc de treball al lab, l'*entusiasme* pels horòscops, el noi guapo de la paret i la tradició dels calendaris. Íngrid, agrair-te tota la paciència que vas tenir amb mi quan et venia a buscar cada dos segons al despatx per problemes diversos amb el nostre estimat GC i, en general, per tota la resta del teu temps que vas dedicar a ensenyar-me al laboratori.

També a tots els estudiants que heu anat passant pel grup (espero que la memòria no em falli): Juan, Ming-Zheng, Judit, Josep Maria, Anna B., Adrià S., Yoel, Patrícia, Lorena, Alba, David H., Yasmina, Andrés, Isabel, Anna C., Lorenzo, Tess i David M.; per fer més amenes totes les hores al laboratori. Sento que de tots he après alguna cosa i amb alguns m'emporto una amistat molt especial.

Agrair també a la resta de becaris i companys de passadís amb qui hem compartit esmorzars, dinars i/o sopars: Magda, Ewelina, Dani, Agustí, Albert, Iteng, Àngel, Ruben, Laura i Gemma.

A en Martí i a la Cristina... què us haig de dir!!

Martí, ja saps que *a mi aquestes coses em costen*. Gràcies per tots els moments de convivència (tant a dins del context educatiu com a fora), pels riures, per la teva amistat, per ser com ets (*Dios*). Són deu anys d'amistat que porto compartint amb tu i espero que en siguin molts més

(o potser no... *què??!*). Malauradament no hi seràs el dia que presento la tesi, però no pateixis, ja et faré arribar uns croissanets del *pica-pica* que sé que són el més important per tu, *foqueta!*

Cristina, gràcies per tots els somriures, per tots els moments *punkys*, per tots els moments de plorera i per tots els moments que *he vingut a pesar a la balança*. Els enanitos et trobaran a faltar, però jo no, perquè estic segura que la nostra amistat perdurarà al llarg del temps! (igual que el teu quadern *para colorear* ☺).

Agrair als participants incondicionals de l'hora del cafè, pels riures i les anècdotes explicades: Martí, Cristina, Pep Duran, Montse, Àngel, Aythami... i tots aquells que heu participat en alguna de les sessions. L'hora del cafè és, sens dubte, on guardo més bons records de la tesi. Gràcies!

Gràcies també als amics, Júlia, Carlota, Isma, Ming-Zheng, Juan, Jona i Toni, per tots els moments compartits (dinars, brenars, sopars, *Grannys* i *Aquagrannys*, Karokes, màsters i d'altres). I en especial, a l'Adrià, per haver compartit part d'aquest trajecte amb mi, pel seu suport i la seva amistat.

I, finalment, gràcies a la meva família pel seu suport i paciència. No cal afegir res més perquè sabeu de sobres que sense vosaltres jo no seria qui sóc i no hauria arribat fins aquí.

A tots vosaltres... moltes gràcies!!

List of publications

Publications related to the thesis content:

- *Reusable manganese compounds containing pyrazole-based ligands for olefin epoxidation reactions.*

Manrique, E., Poater, A., Fontrodona, X., Solà, M., Rodríguez, M. and Romero, I. *Dalton Trans.* **2015**, 44, 17529-17543.

- *A family of manganese complexes containing heterocyclic-based ligands with cytotoxic properties.*

Castro, J., Manrique, E., Bravo, M., Vilanova, M., Benito, A., Fontrodona, X., Rodríguez, M. and Romero, I. *J. Inorg. Biochem.* **2018**, 182, 124-132.

Abbreviations

| | |
|---------------------|--------------------------------------|
| AA | ascorbic acid |
| acac | acetylacetonate |
| Anal. Found (Calc.) | analysis found (analysis calculated) |
| bmim | 1-butyl-3-methyl-imidazolium |
| bpy | 2,2'-bipyridine |
| DFT | density functional theory |
| dmso | dimethyl sulfoxide |
| DPV | differential pulse voltammetry |
| conv. | conversion |
| COSY | correlation spectroscopy |
| CV | cyclic voltammetry |
| δ | chemical shift |
| d | doublet |
| dd | doublet of doublets |
| ddd | doublet of doublet of doublets |
| dt | doublet of triplets |
| ε | extinction coefficient |
| E | potential |
| ee | enantiomeric excess |
| $E_{1/2}$ | half wave potential |

| | |
|----------------------|---|
| E_{init} | starting potential |
| E_{pa} | anodic peak potential |
| E_{pc} | cathodic peak potential |
| eq. | equivalents |
| ESI-MS | electrospray ionization mass spectroscopy |
| FTIR | Fourier transform infrared |
| GC | gas chromatography |
| H ₂ DCFDA | 2',7'-dichlorofluorescin diacetate |
| HMBC | heteronuclear multiple bond correlation |
| HSQC | heteronuclear single-quantum correlation |
| IC ₅₀ | half maximal inhibitory concentration |
| ICP-AES | inductively coupled plasma atomic emission spectroscopy |
| ILs | ionic liquids |
| J | coupling constant |
| λ | wavelength |
| LMCT | ligand to metal charge transfer |
| m | multiplet |
| MLCT | metal to ligand charge transfer |
| MNP | magnetic nanoparticles |
| MSNP | magnetic silica nanoparticles |
| m/z | mass-to-charge ratio |

| | |
|-------|--|
| MSNP | magnetic silica nanoparticles |
| m/z | mass-to-charge ratio |
| NAC | N-acetyl cysteine |
| NMR | nuclear magnetic resonance |
| NOESY | nuclear Overhauser effect spectroscopy |
| NP | nanoparticles |
| PAA | peracetic acid |
| PBS | phosphate buffered saline |
| PCD | programmed cell death |
| PCET | proton-coupled-electron transfer |
| PI | propidium iodide |
| ppm | parts per million |
| py | pyridine |
| pz | pyrazole |
| ROS | reactive oxygen species |
| RT | room temperature |
| RTILs | room temperature ionic liquids |
| s | singlet |
| SCE | saturated calomel electrode |
| SE | standard error |
| sel. | selectivity |

| | |
|--------|--|
| SEM | scanning electron microscopy |
| SP | silica particles |
| T | temperature |
| t | triplet |
| TBAH | tetra(n-butyl)ammonium hexafluorophosphate |
| TBE | 89 mM Tris-borate (pH 8.3) + 2 mM EDTA |
| TE | 10 mM Tris-HCl (pH= 7.6) + 1 mM EDTA |
| TGA | thermogravimetric analysis |
| THF | tetrahydrofuran |
| TON | turnover number |
| Tris | 2-amino-2-hydroxymethyl-propane-1,3-diol |
| trpy | 2,2':6,2''-terpyridine |
| UV-Vis | ultraviolet-visible spectroscopy |
| v | frequency |
| vs. | versus |
| XPS | X-ray photoelectron spectroscopy |

Electronic supporting information

The material listed below can be found in the attached CD:

- pdf file of the PhD dissertation
- pdf file of the publications
- cif files for each crystal structure presented within this thesis:

| Chapter | Crystal Structure | Code |
|-----------|--|------|
| Chapter 4 | $[\text{Mn}^{\text{II}}\text{Cl}_2(\text{pypz-H})_2]$ | Mn1 |
| | $[\text{Mn}^{\text{II}}(\text{CF}_3\text{SO}_3)_2(\text{pypz-H})_2]$ | Mn2 |
| | $[\text{Mn}^{\text{II}}(\text{OAc})_2(\text{pypz-H})_2]$ | Mn3 |
| | $[\text{Mn}^{\text{II}}(\text{NO}_3)_2(\text{pypz-H})_2]$ | Mn4 |
| | $[\text{Mn}^{\text{II}}\text{Cl}_2(\text{pypz-H})(\text{H}_2\text{O})_2]$ | Mn5 |
| | $[\text{Mn}^{\text{II}}\text{Cl}_2(\text{pypz-Me})_2]$ | Mn6 |
| | $[\text{Mn}^{\text{II}}(\text{CF}_3\text{SO}_3)_2(\text{pypz-Me})_2]$ | Mn7 |
| | $[\text{Mn}^{\text{II}}(\text{CF}_3\text{SO}_3)_2(\text{pypz-CH}_2\text{COOEt})_2]$ | Mn8 |
| | $[\text{Mn}^{\text{III}}\text{Cl}(\text{Ophpz-H})_2]$ | Mn9 |
| Chapter 5 | <i>cis,cis</i> - $[\text{Ru}^{\text{II}}\text{Cl}_2(\text{pypz-CH}_2\text{COOEt})(\text{dmsO})_2]$ | Ru1a |
| | <i>cis,trans</i> - $[\text{Ru}^{\text{II}}\text{Cl}_2(\text{pypz-CH}_2\text{COOEt})(\text{dmsO})_2]$ | Ru1b |
| | $[\text{Ru}^{\text{II}}\text{Cl}_2(\text{HOphpz-H})_2(\text{dmsO})_2]$ | Ru2' |
| | $[\text{Ru}^{\text{II}}\text{Cl}_2(\text{MeOphpz-H})(\text{dmsO})_3]$ | Ru3 |
| | $[\text{Ru}^{\text{II}}\text{Cl}_2(3,4\text{-dmpzH})_2(\text{dmsO})_2]$ | Ru5 |
| Chapter 6 | <i>trans</i> - $[\text{Ru}^{\text{II}}\text{Cl}(\text{pypz-H})(\text{trpy})](\text{PF}_6)$ | Ru7b |
| | $[\text{Ru}^{\text{II}}(\text{pypz-H})(\text{trpy})(\text{dmsO})](\text{PF}_6)_2$ | Ru8 |
| | $[\text{Ru}_2^{\text{II}}\text{Cl}(\text{trpy})_2(\mu\text{-Cl})(\mu\text{-pypz})](\text{PF}_6)$ | Ru9 |
| | $[\text{Ru}_2^{\text{II}}(\text{trpy})_2(\mu\text{-pypz})_2](\text{PF}_6)_2$ | Ru11 |

List of figures

| | |
|---|----|
| Figure I.1. Schematic representation of different strategies for catalyst immobilization: adsorption (a), electrostatic immobilization (b), encapsulation (c), ionic liquid (d) and covalent binding (e). | 37 |
| Figure I.2. Structures of common cations and anions in ionic liquids. | 40 |
| Figure I.3. General process for anchoring a homogeneous catalyst onto a solid support. | 41 |
| Figure I.4. Possible binding modes of a phosphonate unit (monodentate (a), bidentate (b), tridentate (c)), alkoxy silane unit (d) (only the tridentate mode is represented but the other two are possible) and carboxylate unit (e) to an oxide-type surface..... | 41 |
| Figure I.5. Magnetic nanoparticle (a) and a silica-coated magnetic nanoparticle (b). | 43 |
| Figure I.6. From left to right: pyrolusite (MnO_2), hausmannite (Mn_3O_4) and rhodochrosite ($MnCO_3$) (Images from http://www.mindat.org)..... | 47 |
| Figure I.7. Examples of Mn (II) coordinated by N-donor ligands. | 48 |
| Figure I.8. A pure ruthenium(0) bar (image from http://www.mindat.org). | 49 |
| Figure I.9. Common polypyridyl ligands used in ruthenium coordination chemistry. | 51 |
| Figure I.10. Bioinorganic chemistry gain inspiration from metal active site of enzymes to design structural and functional model compounds..... | 56 |
| Figure I.11. Schematic representation of the atomic structure of the oxygen evolving complex OEC. Color codes for atoms: grey, manganese; blue, calcium; red, oxo- oxygen; yellow, oxygen; orange, water. Roman numerals in the grey spheres indicate the valences of the manganese atoms assigned by Suga et. al. ^{122c} | 57 |
| Figure I.12. Schematic representation of the proposed catalytic cycle for <i>Lactobacillus plantarum</i> manganese catalase. ^{126b} Oxidative half-reaction: (1) resting oxidized $Mn_2(III, III)$ state. (2) Terminal peroxide adduct. (3) Terminal dioxygen adduct. Reductive half-reaction: (4) resting or reduced $Mn_2(II, II)$ state. (5) Activated hydrogen peroxide complexes: (a) terminally bound substrate; (b) $\mu 1,1$ bridging substrate. | 57 |
| Figure I.13. Structure of the best Jacobsen's catalyst prepared on a large scale ^{151c} and currently commercially available..... | 60 |
| Figure I.14. Some ligands used by Stack and co-workers, to synthesize new manganese N-based complexes able to oxidize terminal olefins with PAA as oxidant. ^{55b,142e} | 61 |
| Figure I.15. Structure of the ligands reported by Pfaltz. | 61 |
| Figure I.16. Structure of some ligands reported by Palaniandavar and co-workers. | 62 |
| Figure I.17. Structure of a bipyridine-based manganese complex described by Watkinson et al. | 62 |
| Figure I.18. 1,10-phenantroline ligand and its derivatives used by Jiang et al..... | 63 |
| Figure I.19. Structure of the complexes containing the (-)-L chiral ligands..... | 63 |

| | |
|---|----|
| Figure I.20. Structure of ruthenium hydride complexes: tetranuclear cluster (a) and mononuclear complex (b). | 70 |
| Figure I.21. Structure of the bis(acac)-ruthenium(II) complexes..... | 70 |
| Figure I.22. Examples of arene-ruthenium(II) complexes..... | 71 |
| Figure I.23. Structure of water-soluble arene-ruthenium(II) complexes reported by Cadierno et al. ¹⁸³ | 72 |
| Figure I.24. Pyrazole-based ligands used in the synthesis of Ru-dmsO complexes described by Ferrer et al. ¹⁸⁴ | 72 |
| Figure I.25. Schematic representation of the bis-functionalized silica with sulfonatophenyl and propylimidazole groups..... | 76 |
| Figure I.26. Host-guest nanocatalysts with octahydro-Schiff base ligands described by Salvati-Niasari, Salimi and co-workers. | 77 |
| Figure I.27. Schematic representation of the ways of immobilization employed by Luts et al. to anchor a Mn(III)-Salen compound, through peptide bonding (a) and ester bonding (b), onto a mesoporous silica support. | 78 |
| Figure I.28. Schematic representation of the immobilized modified Mn(III)-Salen complex onto the modified silica surface as described by Khalil et al..... | 79 |
| Figure I.29. Schematic representation of the synthesis of the immobilized manganese(III) porphyrin onto silica-coated Fe ₃ O ₄ magnetic nanoparticles, as described by Bagherzadeh et al. | 80 |
| Figure I.30. Structure of SiO ₂ -supported Ru catalyst. | 80 |
| Figure I.31. Structure of biomimetic ruthenium complex. | 81 |
| Figure I.32. Structure of the heterogeneous [Ru(trpy)(pypz-Me)(OH ₂)] ²⁺ complex. | 81 |
| Figure I.33. Poly(N-vinyl-2-pyrrolidone) (PVP), a water-soluble polymer commonly used as a nanoparticle stabilizer..... | 82 |
| Figure I.34. Structure of a ruthenium(II) complex supported on silica-coated magnetic nanoparticles..... | 83 |
| Figure I.35. Representation of the morphological features of apoptosis (blue), autophagy (red) and necrosis (green). Apoptotic cells are characterized by cell shrinkage, membrane blebbing (I) and nuclear fragmentation (II). Autophagy is characterized by the accumulation of autophagosomes and autophagolysosomes (I) and protein degradation (II). Necrosis is characterized by the swelling of the cell and its organelles (II) as well as early membrane damage (I). | 84 |
| Figure I.36. Structures of some platinum complexes being investigated as anticancer agents. | 85 |
| Figure I.37. Structures of some ruthenium complexes being investigated as anticancer agents. | 86 |
| Figure I.38. Structure of Adpa-Mn described by Gao et al. | 88 |

| | |
|--|-----|
| Figure I.39. Structure of a Mn(III)-salphen compound described by Ansari et al. active towards malignant breast cells (MCF7)..... | 89 |
| Figure I.40. Structure of a manganese(II) complex bearing the 2-acetylpyridine thiosemicarbazone ligand, synthesized and characterized by Li, Chen, Zang et al. | 89 |
| Figure I.41. The [Mn(Phpyk) ₂ (SCN) ₂] complex described by Dash et al..... | 90 |
| Figure II.1. N-donor ligands used to synthesize the new manganese(II), manganese(III) and ruthenium(II) complexes of this work..... | 97 |
| Figure IV.1.1. Ortep plots with the corresponding atom labels for the X-ray structures of compounds Mn1-Mn5 , which contain the <i>pypz-H</i> ligand..... | 129 |
| Figure IV.1.2. Ortep plots with the corresponding atom labels for the X-ray structures of compounds Mn6 and Mn7 , which contain the <i>pypz-Me</i> ligand, and Mn8 , with the <i>pypz-CH₂COOEt</i> ligand..... | 130 |
| Figure IV.1.3. Ortep plot with the corresponding atom labels for the X-ray structure of compound Mn9 , which presents the <i>Ophpz-H</i> ligand. | 131 |
| Figure IV.1.4. Intramolecular hydrogen bonding interactions and packing diagram for complex Mn5 | 136 |
| Figure IV.1.5. Cyclic voltammetry for complexes Mn1 (a) and Mn5 (b) in CH ₃ CN vs. Ag/AgNO ₃ | 138 |
| Figure IV.1.6. Cyclic voltammetry for complex Mn6 in CH ₃ CN vs. Ag/AgNO ₃ | 139 |
| Figure IV.1.7. CV of a 1 mM acetonitrile solution containing 0.1 M TBAH of Mn1 a) before electrolysis, b) and c) after electrolysis at 0.63 V, d) after back-electrolysis at 0.3 V. The initial scan direction is indicated by arrows in all cases..... | 140 |
| Figure IV.1.8. A) Evolution of UV-Vis spectrum of complex Mn1 in CH ₃ CN (1.4 mM), upon addition of 2 eq. of peracetic acid at -10 °C and 10 eq. of styrene substrate at 15 °C: (a) initial, (b) 1 minute after addition of PAA, (c) 15 minutes after addition of PAA (addition of styrene at this point), (d) 1 hour after addition of styrene (e) 20 hours after addition of styrene; B) Evolution of UV-Vis spectrum of complex Mn9 in CH ₃ CN (1.4 mM), upon addition of 2 eq. of PAA at 25 °C and 10 eq. of styrene substrate at 25 °C: (a) initial, (b) 1 minute after addition of PAA, (c) 15 minutes after addition of PAA (addition of styrene at this point), (d) 1 hour after addition of styrene (e) 20 hours after addition of styrene. | 147 |
| Figure IV.1.9. Reaction pathway for the epoxidation of the <i>cis</i> -β-methylstyrene substrate by the catalyst Mn1 (Gibbs energies in Kcal mol ⁻¹)..... | 149 |
| Figure IV.1.10. Conversion (orange bars) and selectivity (pink bars) values obtained throughout consecutive reuses of complex Mn1 (a) and complex Mn9 (b) in the epoxidation of <i>trans</i> -β-methylstyrene in [bmim]PF ₆ :CH ₃ CN (see text for experimental conditions)..... | 154 |
| Figure IV.1.11. Synthetic strategy for the immobilization of Mn8 onto silica particles (SP)..... | 155 |
| Figure IV.1.12. UV-vis spectrum for homogeneous complex Mn8 (blue) and heterogeneous SP@Mn8 catalyst (red) in MeOH. | 156 |

| | |
|--|-----|
| Figure IV.1.13. Conversion (orange bars) and selectivity (pink bars) values obtained throughout consecutive reuses of heterogeneous SP@Mn8 in the epoxidation of cyclooctene in CH ₃ CN (see text for experimental conditions)..... | 157 |
| Figure IV.2.1. ORTEP plots and labeling schemes for complex Ru1a and Ru1b | 160 |
| Figure IV.2.2. ORTEP plot and labeling scheme for compound Ru3 | 162 |
| Figure IV.2.3. ORTEP plot and labeling scheme for compound Ru5 | 164 |
| Figure IV.2.4. Black, ¹ H-NMR spectrum (400 MHz, CDCl ₃) of an isomeric mixture of Ru1a and Ru1b in a 1:0.5 ratio. Blue, ¹ H-NMR spectrum of the pure complex Ru1b at the same scale to facilitate the identification of the Ru1a signals. | 165 |
| Figure IV.2.5. Different regions of the ¹ H-NMR spectrum of an isomeric mixture of Ru1a and Ru1b in a 1:0.5 ratio, 400 MHz, CDCl ₃ . The figure shows some examples of the high asymmetry of the Ru1a molecule: A) four methyl dmsu signals (black dots), whereas only two dmsu signals for Ru1b isomer (grey crosses); B) signals of the methylene protons (green dots), and C) signals which correspond to the aliphatic chain of the terminal ester group (red dots). | 166 |
| Figure IV.2.6. CV of complex Ru1 (as a mixture of isomers Ru1a and Ru1b) performed in CH ₃ CN (TBAH 0.1 M) vs. SCE starting the scanning potential at $E_{init}= 0$ V. Red dots indicate the anodic and cathodic peaks of isomer Ru1b which does not present dmsu linkage isomerization process. | 169 |
| Figure IV.2.7. CV of complex Ru1 (as a mixture of isomers Ru1a and Ru1b) performed in CH ₃ CN (TBAH 0.1 M) vs. SCE starting the scanning potential at $E_{init}= 1.6$ V. Red dots indicate the anodic and cathodic peaks of isomer Ru1b which does not present dmsu linkage isomerization process. | 170 |
| Figure IV.2.8. CV of complex Ru1 (as a mixture of isomers Ru1a and Ru1b) performed in CH ₃ CN (TBAH 0.1 M) vs. SCE starting the scanning potential at $E_{init}= 1.2$ V, at scan rates between 0.05 and 0.4 V·s ⁻¹ , applying an equilibration time of 1 min. | 171 |
| Figure IV.2.9. Intensity of the cathodic Ru ^{III} -O → Ru ^{II} -O peak at different scan rates..... | 173 |
| Figure IV.3.1. Hydrogen bond formation (red dashed line) between the Cl ligand and the pyrazolic N-H proton (<i>cis</i> - Ru7a) or the pyridylic H(1) proton (<i>trans</i> - Ru7b)..... | 180 |
| Figure IV.3.2. ORTEP plot and labeling scheme for the cationic moiety in the X-ray structure of complex Ru7b | 181 |
| Figure IV.3.3. ORTEP plots and labeling schemes for the cationic moieties in the X-ray structures of complexes Ru8 (a), Ru9 (b) and Ru11 (c) isolated as minor products during the synthesis of the chloro compounds Ru7a and Ru7b | 182 |
| Figure IV.3.4. ¹ H-NMR spectra of complexes a) Ru7a and b) Ru7b in methanol-d ₄ | 184 |
| Figure IV.3.5. ¹ H-NMR spectrum of complex Ru10 in methanol-d ₄ | 184 |
| Figure IV.3.6. UV-Vis spectra of Ru7a (solid line), Ru7b (dotted line) in CH ₂ Cl ₂ and Ru10 (dashed line) in phosphate buffer (pH= 7)..... | 185 |
| Figure IV.3.7. CV for complex Ru7a (blue) and Ru7b (red) registered in CH ₂ Cl ₂ vs. SCE. | 185 |
| Figure IV.3.8. DPV of complex Ru10 in phosphate buffer (pH adjusted to 11.8) vs. SCE. | 186 |

| | |
|---|-----|
| Figure IV.3.9. Pourbaix diagram for complex Ru10 . The pH-potential regions of stability and the proton composition for the different redox species are indicated. The pKa of each species is represented with a dashed vertical line..... | 187 |
| Figure IV.4.1. SEM images of a) SP and b) MSNP after the anchoring of the Ru complex. | 194 |
| Figure IV.4.2. TEM images of a) SP and b) MSNP after the anchoring of the Ru complex. | 195 |
| Figure IV.4.3. Thermogravimetric profiles of naked SP support (green), SP@Ru1 (blue) and MSNP@Ru1 (red). | 196 |
| Figure IV.4.4. XPS survey scans of SP@Ru1 : a) overall XPS spectra and b) C 1s signal together with Ru(3d _{5/2}) band. | 197 |
| Figure IV.4.5. IR spectra of a) SP@Ru1 and b) MSNP@Ru1 . Blanks of SP and MSNP respectively are represented in blue, and the heterogeneous complex in red lines..... | 198 |
| Figure IV.4.6. UV-Vis spectra (red lines) for a) SP@Ru1 and b) MSNP@Ru1 . In each figure, spectra of the corresponding naked SP and MSNP supports are depicted in green and that of complex Ru1 in blue..... | 199 |
| Figure IV.4.7. Conversion (orange bars) and selectivity (pink bars) values obtained throughout consecutive reuses of SP@Ru1 (a) and MSNP@Ru1 (b) in the hydration of benzonitrile to benzamide in water (see text for experimental conditions)..... | 201 |
| Figure IV.4.8. Conversion (orange bars) and selectivity (pink bars) values obtained throughout consecutive reuses of SP@Ru1 (a) and MSNP@Ru1 (b) in the hydration of acrylonitrile to acrylamide in water (see text for experimental conditions)..... | 202 |
| Figure IV.5.1. Structure of complex [Mn(CF ₃ SO ₃) ₂ ((-)-L) ₂] (Mn10) and the ligand (-)-pinene[5,6]bipyridine ((-)-L)..... | 204 |
| Figure IV.5.2. VC of compound Mn7 in H ₂ O + 0.103 M NaCl/0.0049 M KCl vs. SCE. The solid lines correspond to the voltammograms registered after complex solubilization at different times (blue, 25 s; red, 7 min; green, 30 min). The purple dashed line corresponds to the CV obtained after addition of p-toluene sulfonic acid, whereas that recorded after addition of NaOH is displayed as a blue dotted line..... | 205 |
| Figure IV.5.3. ROS production triggered by compound Mn10 and its ligand in OVCAR-8 (A) and NCI-H460 (B) cell lines. Cells were treated for 48 and 72 h with the compound or (-)-L and generation of ROS was measured by flow cytometry after labelling with carboxy-H2DCFDA (see the text for more details). ROS levels are indicated as fold-increase vs. control (non-treated cells). Values were analyzed from 10,000 total events. Data are presented as mean ± SE of at least three independent experiments. Differences versus untreated cells were considered significant at *p < 0.05. | 211 |
| Figure IV.5.4. Cellular viability of NCI-H460 cells after treatment with compound Mn10 and its ligand in the presence and absence of N-acetyl cysteine (NAC). Cellular viability was measured by the MTT assay. Data are presented as mean ± SE of at least three independent experiments. Differences in the cell viability values of cells with and without NAC treatment were considered significant at *p < 0.05. | 212 |
| Figure IV.5.5. Agarose gel electrophoresis of pUC18 plasmid DNA treated with different concentrations (indicated in μM) of compound Mn10 and its ligand in the absence (A) and presence (B) of H ₂ O ₂ . (A) From left to right, lane 1, cisplatin (positive control), lane 2 plasmid | |

pUC18 alone (negative control), lanes 3–6 increasing amounts of compound **Mn10** and lanes 7–10 increasing amounts of ligand (-)-L; (B) From left to right in both gels (Mn10 and (-)-L), lane 1 cisplatin (positive control), lane 2 plasmid pUC18 alone (negative control), lanes 3–6 increasing amounts of compound Mn10 or its ligand ((-)-L). OC = open circular form; CCC = covalently closed circular form; L = linear form. 216

Figure IV.5.6. Structures of complexes [RuCl₂(pypz-H)(dmsO)₂] (**P2**), [RuCl₂(bpea)(dmsO)] (**Ru12**), [RuCl₂(NO₂-pzH)(dmsO)₃] (**Ru13**), [RuCl(pypz-H)(9S3)]Cl (**Ru14**) and the free ligands *N,N*-bis(pyridin-3-ylmethyl)ethanamine (bpea), 4-nitro-1*H*-pyrazole (NO₂-pz-H) and 1,4,7-trithionane (9S3). 217

Figure IV.5.7. Agarose gel electrophoresis of pUC18 plasmid DNA treated with different concentrations (indicated in μM) of compounds Ru5-6 and ligand *bpea*. From left to right, lane 1, cisplatin (positive control), lane 2 plasmid pUC18 alone (negative control), lanes 3–8 indicated concentrations of *bpea* and complexes Ru5 and Ru6. OC = open circular form; CCC = covalently closed circular form. 219

Figure SIII.1. ¹H-NMR in CDCl₃ of *L* (a), *L4* (b), *L5* (c), *L5'* (d) and *L5''* (e). 263

Figure SIV.1.2. FTIR spectra of **Mn1**. 266

Figure SIV.1.3. FTIR spectra of **Mn2**. 267

Figure SIV.1.4. FTIR spectra of **Mn3**. 267

Figure SIV.1.5. FTIR spectra of **Mn4**. 268

Figure SIV.1.6. FTIR spectra of **Mn5**. 268

Figure SIV.1.7. FTIR spectra of **Mn6**. 269

Figure SIV.1.8. FTIR spectra of **Mn7**. 269

Figure SIV.1.9. FTIR spectra of **Mn8**. 270

Figure SIV.1.10. FTIR spectra of **Mn9**. 270

Figure SIV.1.10. Packing diagram for the structures of **Mn1** (a), **Mn2** (b), **Mn3** (c) and **Mn4** (d). The intermolecular H-bonding interactions are depicted in pale blue color. 271

Figure SIV.1.11. Packing diagram for complexes **Mn6** (a), **Mn7** (b) and **Mn8** (c). 271

Figure SIV.1.12. Intramolecular hydrogen bonding interactions and packing diagram for complex **Mn9**. 272

Figure SIV.1.13. Cyclic voltammetry of **Mn2-4** and **Mn7-8** compounds (**Mn2** (a), 2 mM; **Mn3** (b), 1 mM; **Mn4** (c), 1 mM; **Mn7** (d), 1 mM; **Mn8** (e), 1 mM and **Mn9** (f) 1 mM). Experiments have been performed in CH₃CN containing, 0.1 M of *n*-Bu₄NPF₆ (TBAH) using a graphite working electrode (3 mm diameter) and Ag/AgNO₃ as reference electrode; scan rate: 200mV/s. 273

Figure SIV.1.14. DPV of **Mn2-4** and **Mn7-8** compounds (**Mn2** (a), 2 mM; **Mn3** (b), 1 mM; **Mn4** (c), 1 mM; **Mn7** (d), 1 mM; **Mn8** (e), 1 mM). Experiments have been performed in CH₃CN containing, 0.1 M of *n*-Bu₄NPF₆ (TBAH) using a graphite working electrode (3 mm diameter); scan rate: 100mV/s. 274

| | |
|---|-----|
| Figure SIV.1.15. UV-vis spectra for complex Mn1 and for the species formed after exhaustive oxidation. | 275 |
| Figure SIV.1.16. ESI-MS spectrum formed after addition of 2 eq of peracetic acid to a solution of complexes A) Mn1 and B) Mn9 in CH ₃ CN at 0 °C (2.5mM) together with the corresponding simulations of some selected peaks (experimental values, black bars; simulated, grey bars). 277 | 277 |
| Figure SIV.1.17. Lewis structures of catalysts 1-3 | 278 |
| Figure SIV.1.18. Molecular structures of intermediates lics of catalysts a) Mn1 , b) 2 and c) 3 (distances in Å). | 279 |
| Figure SIV.1.19. Conversion (orange bars) and selectivity (pink bars) values obtained throughout consecutive reuses of complex Mn1 (A) and complex Mn9 (B) in the epoxidation of <i>cis</i> -β-methylstyrene in [bmim]PF ₆ :CH ₃ CN (see text for experimental conditions). | 280 |
| Figure SIV.1.20. Conversion (orange bars) and selectivity (pink bars) values obtained throughout consecutive reuses of complex Mn1 in the epoxidation of cyclooctene in [bmim]PF ₆ :CH ₃ CN (see text for experimental conditions). | 281 |
| Figure SIV.2.1. Left, ortep plot and labeling scheme for the X-ray diffraction of compound Ru2' . Right, detail of the intramolecular H-bonding interactions taking place..... | 282 |
| Figure SIV.2.2. CV of complex Ru2' in CH ₃ CN + 0.1 M TBAH. | 283 |
| Figure SIV.2.3. UV-Vis spectra of a 0.1 mM solution of complex Ru2' in MeOH. | 283 |
| Figure SIV.2.4. NMR of Ru2' , 400 MHz, acetone-d ₆ : a) ¹ H-NMR; b) COSY; c) NOESY..... | 285 |
| Figure SIV.2.5. FTIR spectra of Ru1b | 289 |
| Figure SIV.2.6. FTIR spectra of a mixture of Ru1a and Ru1b isomers. | 289 |
| Figure SIV.2.7. FTIR spectra of Ru2 | 289 |
| Figure SIV.2.8. FTIR spectra of Ru3 | 290 |
| Figure SIV.2.9. FTIR spectra of Ru5 | 290 |
| Figure SIV.2.10. Intermolecular and intramolecular hydrogen-bonding interactions and packing diagram for complex Ru1 , A) Λ/Δ <i>cis</i> -Cl <i>cis</i> -dmsO isomer (a) (Ru1a) and B) <i>cis</i> -Cl <i>trans</i> -dmsO isomer (d) (Ru1b). | 291 |
| Figure SIV.2.11. Intermolecular and intramolecular hydrogen-bonding interactions and packing diagram for complex Ru3 | 291 |
| Figure SIV.2.12. Intermolecular and intramolecular hydrogen-bonding interactions and packing diagram for complex Ru5 | 292 |
| Figure SIV.2.13. UV-Vis spectra of complexes a) Ru1 (0.2 mM in CH ₂ Cl ₂), b) Ru2 (0.1 mM in MeOH), c) Ru3 (0.1 mM in CH ₂ Cl ₂), d) Ru4 (0.1 mM in H ₂ O), e) Ru5 (0.1 mM in H ₂ O) and f) Ru6 (0.2 mM in MeOH). | 294 |
| Figure SIV.2.14. Cyclic voltammograms in CH ₂ Cl ₂ vs. SCE of a) Ru1 (pure isomer Ru1b (blue) and the mixture of isomers Ru1a and Ru1b (red), b) Ru2 , c) Ru3 d) Ru4 , e) Ru5 and f) Ru6 . . | 296 |

| | |
|---|-----|
| Figure SIV.2.15. NMR of Ru1a , as mixture of isomers Ru1a and Ru1b (1: 0.5), 400 MHz, CDCl ₃ : a) ¹ H-NMR; b) ¹³ C-NMR; c) COESY; d) NOESY; e) ¹ H- ¹³ C HSQC; f) ¹ H- ¹³ C HMBC. | 299 |
| Figure SIV.2.16. NMR of Ru1b , 400 MHz, CDCl ₃ : a) ¹ H-NMR; b) ¹³ C-NMR; c) COESY; d) NOESY; e) ¹ H- ¹³ C HSQC; f) ¹ H- ¹³ C HMBC. | 302 |
| Figure SIV.2.17. NMR of Ru2 , 400 MHz, acetone-d ₆ : a) ¹ H-NMR; b) ¹³ C-NMR; c) COESY; d) NOESY; e) ¹ H- ¹³ C HSQC; f) ¹ H- ¹³ C HMBC. | 305 |
| Figure SIV.2.18. NMR of Ru3 , 400 MHz, acetone-d ₆ : a) ¹ H-NMR; b) ¹³ C-NMR; c) COESY; d) NOESY; e) ¹ H- ¹³ C HSQC; f) ¹ H- ¹³ C HMBC. | 308 |
| Figure SIV.2.19. ¹ H-NMR of Ru4 , 400 MHz, CD ₂ Cl ₂ | 309 |
| Figure SIV.2.20. NMR of Ru5 , 400 MHz, CDCl ₃ : a) ¹ H-NMR; b) ¹³ C-NMR; c) COESY; d) NOESY; e) ¹ H- ¹³ C HSQC; f) ¹ H- ¹³ C HMBC. | 312 |
| Figure SIV.2.21. ¹ H-NMR of Ru6 , 400 MHz, CDCl ₃ | 312 |
| Figure SIV.2.22. CV of complex Ru1a registered in CH ₃ CN (TBAH, 0.1 M) vs SCE starting at $E_{init}=0.3$ V and scanning towards increasing potential values at scan rates between 0.05 and 0.6 V/s (equilibration time = 2 s). | 313 |
| Figure SIV.2.23. Plot of i_{c1}/i_{c2} vs. v^{-1} to obtain k'''_{o-s} for complex Ru1a | 313 |
| Figure SIV.2.24. Plot of $v^{1/2}$ vs. i_d/i_k to obtain k'''_{o-s} and k'''_{s-o} for complex Ru1a | 314 |
| Figure SIV.2.25. Plot of $\ln(i_{a1}/v^{1/2})$ vs. v^{-1} to obtain k''_{o-s} for complex Ru1a | 314 |
| Figure SIV.3.1. FTIR spectra of a mixture of the chlorido complexes Ru7a and Ru7b (a), and the <i>trans</i> aqua complex Ru10 (b). | 318 |
| Figure SIV.3.2. DPV experiment for dmsO complex Ru8 (CH ₂ Cl ₂ + 0.1 M TBAH vs. SCE). | 319 |
| Figure SIV.3.3. VC (a) and DPV experiment (b) for the dimeric complex Ru9 (CH ₂ Cl ₂ + 0.1 M TBAH vs. SCE). | 319 |
| Figure SIV.3.4. NMR of Ru7a , 400 MHz, methanol-d ₅ : a) ¹ H-NMR; b) ¹³ C-NMR; c) COESY; d) NOESY; e) ¹ H- ¹³ C HSQC; f) ¹ H- ¹³ C HMBC. | 322 |
| Figure SIV.3.5. NMR of Ru7b , 400 MHz, methanol-d ₅ : a) ¹ H-NMR; b) ¹³ C-NMR; c) COESY; d) NOESY; e) ¹ H- ¹³ C HSQC; f) ¹ H- ¹³ C HMBC. | 325 |
| Figure SIV.3.6. NMR of Ru9 , 400 MHz, acetone-d ₆ : a) ¹ H-NMR; b) ¹³ C-NMR; c) COESY; d) NOESY; e) ¹ H- ¹³ C HSQC; f) ¹ H- ¹³ C HMBC. | 328 |
| Figure SIV.3.7. ¹ H-NMR of Ru10 , 400 MHz, methanol-d ₅ | 329 |
| Figure SIV.3.8. Schematic structures for the <i>cis</i> and <i>trans</i> isomers of complexes (a) [RuCl(pypz-Me)(trpy)] ⁺ and (b) [RuCl(CN-Me)(trpy)] ⁺ | 330 |
| Figure SIV.4.1. SEM images of a) SP and b) MSNP before the anchoring of the Ru complex. Notice that for magnetic nanoparticles (b) the resolution is not as good as for the SP caused for aggregation. | 331 |
| Figure SIV.4.2. TEM images of a) SP and b) MSNP before the anchoring of the Ru complex (Image (b) was obtained by the group of Dr. Josep Ros from ICMAB). | 332 |

| | |
|--|-----|
| Figure SIV.4.3. XPS survey scans of SP@Ru1: a) deconvoluted XPS spectra for C 1s and Ru (3d _{5/2}) signals, b) Si 2p signal and c) O 1s signal. | 333 |
| Figure SIV.4.4. XPS survey scans of MSNP@Ru1: a) overall XPS spectra, b) C 1s and Ru (3d _{5/2}) signals, c) deconvoluted XPS spectra for C 1s and Ru (3d _{5/2}) signals, d) Si 2p signal and e) O 1s signal. | 334 |
| Figure SIV.5.1. UV-Vis spectra registered in PBS of complexes a) Mn6 , b) Mn7 and c) Mn8 . Blue lines correspond to the initial spectrum registered and red lines after 72 h. | 336 |
| Figure SIV.5.2. a) Mn6 and b) Mn8 in H ₂ O + 0.103 M NaCl/0.0049 M KCl; c) Mn6 , d) Mn7 and e) Mn8 in H ₂ O + 0.1M NH ₄ PF ₆ ; f) Mn7 and g) Mn8 in H ₂ O + 0.1 M Na(OSO ₂ CF ₃) vs. SCE. The solid lines correspond to the voltammograms registered after complex solubilization at different times. The purple dashed line corresponds to the CV obtained after addition of p-toluene sulfonic acid, whereas that recorded after addition of NaOH is displayed as a blue dotted line. | 339 |
| Figure SIV.5.3. Time-course of UV-Vis spectra of compound Mn10 (B, D and F)) and its ligand (-)-L (A, C and E) dissolved in 10 mM phosphate buffer, pH 7.4, in the presence of chicken egg lysozyme (A and B), human pancreatic ribonuclease (C and D) and cytochrome C (E and F) at a stoichiometric ratio of 4:1 (compound or ligand/protein). Pink: spectra of compound or ligand before the addition of the protein; purple: protein spectra before the incubation with the compound or ligand; green: mix of compound 8 or ligand (-)-L with protein at t= 0 h of incubation; red: at t= 4 h of incubation; blue: at t= 20 h of incubation; and black: at t= 48 h of incubation. | 340 |
| Figure SIV.5.4. UV-Vis spectra registered in H ₂ O of complexes a) Ru4 , b) Ru5 , c) Ru6 , d) P2 , e) Ru12 , f) Ru13 (+ 1 % dmsol) and g) Ru14 . Blue lines correspond to the initial spectrum registered and red lines after 72 h. | 343 |
| Figure SIV.5.5. The cell cycle phases a) G ₀ : growth and normal metabolic roles; b) G ₁ , first growth phase (growth and normal metabolic roles) plus preparation for DNA synthesis: cellular contents excluding the chromosomes, are duplicated; c) S, synthesis phase: duplication of chromosomes; d) G ₂ , second growth phase and preparation for division: the cell “double checks” the duplicated chromosomes for error, making any needed repairs; and e) M, mitosis: cell division. | 343 |

List of tables

| | |
|---|-----|
| Table I.1. Schematic comparison between a homogeneous, heterogeneous and a supported catalyst..... | 36 |
| Table I.2. Electrochemical parameters for aqua complexes for Ru (table extracted from ref.102) ^a | 53 |
| Table I.3. Ligand effects on the epoxidation of <i>trans</i> -stilbene with Ru-aqua complexes. ¹⁵ | 67 |
| Table III.1. Parameters for all crystal structures..... | 119 |
| Table IV.1.1. Catalytic epoxidation of styrene by Mn1-9 compounds using PAA as oxidant. ^a Conversion (conv.) and selectivity (sel.) values are given in %..... | 142 |
| Table IV.1.2. Catalytic epoxidation of different alkenes with compounds Mn1 , Mn5 and Mn6-9 , using peracetic acid as oxidant. ^a Conversion (conv.) and selectivity (sel.) values are given in %..... | 144 |
| Table IV.1.3. Reaction coordinate energies (in Kcal mol ⁻¹) for epoxidation of <i>cis</i> - β -methylstyrene with catalysts Mn1 , 1 , 2 and 3 | 150 |
| Table IV.1.4. Optimization of the procedure for the epoxidation of <i>trans</i> - β -methylstyrene substrate in ionic liquid:solvent media with Mn1 as catalyst. Conditions: <i>trans</i> - β -methylstyrene (250 μ mol), catalyst (2.5 μ mol), peracetic acid (500 μ mol), RT, 3h. Conversion (conv.) and selectivity (sel.) values are given in % and were evaluated by GC analysis with biphenyl as internal standard..... | 151 |
| Table IV.1.5. Epoxidation tests performed with complexes Mn1 , Mn5 and Mn9 in different media. ^a Conversion (conv.) and selectivity (sel.) values are given in %..... | 152 |
| Table IV.1.6. Epoxidation tests performed with heterogeneous complex SP@Mn8 in CH ₃ CN. ^a Conversion (conv.) and selectivity (sel.) values are given in %..... | 156 |
| Table IV.2.1. UV-Vis spectroscopic features in CH ₂ Cl ₂ (Ru1 , as a mixture of isomers Ru1a and Ru1b), MeOH (Ru2 , Ru3 and Ru6) and in H ₂ O (Ru4-5)..... | 169 |
| Table IV.2.2. Electrochemical data (CH ₂ Cl ₂ + 0.1M TBAH vs. SCE) for complexes Ru1-Ru6 | 170 |
| Table IV.2.3. Thermodynamic and kinetic parameters for the linkage isomerization in complex Ru1a , together with related Ru-dmso complexes. ^a | 174 |
| Table IV.2.4. Optimization of the catalytic hydration conditions for complex Ru1 using benzonitrile as substrate..... | 176 |
| Table IV.2.5. Catalytic hydration of nitriles to amides in water mediated by compounds Ru1-6 . ^a Conversion (conv.) and selectivity (sel.) values are given in %..... | 177 |
| Table IV.3.1. pKa and electrochemical data (pH= 7, $E_{1/2}$ in V vs. SCE) for aqua complexes described in this work and others for purposes of comparison..... | 191 |
| Table IV.3.2. Ru-catalyzed alkene epoxidation mediated by complex Ru10 . ^a Conversion (conv.) and selectivity (sel.) values are given in %..... | 192 |
| Table IV.4.1. Physical parameters of the different supports used..... | 195 |

| | |
|--|-----|
| Table IV.4.2. Amount of Ru anchored in the different supports..... | 196 |
| Table IV.4.3. Ru-catalyzed hydration of nitriles to amides in water using homogeneous complex Ru1 and the heterogenized systems SP@Ru1 and MSNP@Ru1 . ^a Conversion (conv.) and selectivity (sel.) values are given in %..... | 202 |
| Table IV.5.1. IC ₅₀ * values (μM) of tested ligands and compounds Mn1-2 , Mn4-8 and Mn10 on the indicated cell lines..... | 208 |
| Table IV.5.2. IC ₅₀ ^a values (μM) of compound Mn10 and its ligand on the indicated cell lines..... | 211 |
| Table IV.5.3. Effects of compound Mn10 and its ligand at the indicated concentrations on the OVCAR-8 and NCI-H460 cell cycle phase distribution after treatment for 72 h. Untreated OVCAR-8 and NCI-H460 cells were used as control..... | 212 |
| Table IV.5.4. IC ₅₀ * values (μM) of tested ligands and compounds Ru4-6 , P2 and Ru12-14 on the indicated cell lines..... | 218 |
| Table SIV.1.1. Crystallographic data for complexes Mn1-Mn9..... | 264 |
| Table SIV.1.2. Selected bond lengths (Å) and angles (°) for Mn1-Mn9..... | 265 |
| Table SIV.2.1. Crystallographic data for complexes Ru1-3 and Ru5 | 286 |
| Table SIV.2.2. Selected bond lengths (Å) and angles (°) for Ru1-3 and Ru5 | 287 |
| Table SIV.2.3. Formulas used for the calculation of rate (k) and equilibrium (K) constants.... | 315 |
| Table SIV.3.1. Crystallographic data for complexes Ru7b-9 and Ru11 | 316 |
| Table SIV.3.2. Selected bond lengths (Å) and angles (°) for Ru7b-9 and Ru11 | 317 |

List of schemes

| | |
|--|-----|
| Scheme I.1. General reaction for olefin epoxidation (a) and hydration of nitriles (b). | 43 |
| Scheme I.2. Epoxide formation and possible further transformations. | 44 |
| Scheme I.3. The nitrile hydration and amide hydrolysis reactions..... | 45 |
| Scheme I.4. Synthetic route of levetiracetam employing a nitrile hydratase. | 46 |
| Scheme I.5. Possible chemical transformations of styrene as function of the catalyst used..... | 50 |
| Scheme I.6. PCET oxidation process characteristic of Ru-aqua complexes..... | 51 |
| Scheme I.7. The stabilization of the Ru metal center promoted by the successive deprotonation of the aqua ligand. | 52 |
| Scheme I.8. Latimer diagrams of Ru polypyridyl complexes (a) non-containing and (b) containing a coordinated water molecule (V vs. SCE, pH= 7). | 52 |
| Scheme I.9. Dismutation of the superoxide ion (O_2^-) to oxygen (O_2) and hydrogen peroxide (H_2O_2) catalyzed by MnSOD. | 56 |
| Scheme I.10. Catalytic cycle for oxygen activation and transfer by cytochrome P450. | 59 |
| Scheme I.11. Scheme of a catalytic cycle of oxidation of a substrate (S) with $Ru^{IV}=O$ species. . | 64 |
| Scheme I.12. Proposed mechanistic pathways for oxygen atom transfer process. | 65 |
| Scheme I.13. Proposed mechanism for the oxidation of aromatic olefins by ruthenium(IV) oxocomplexes..... | 66 |
| Scheme I.14. The reaction pathway proposed by Murahashi and co-workers for the catalytic hydration of nitriles by $[RuH_2(PPh_3)_4]$ complex..... | 68 |
| Scheme I.15. Promoting effect of the hydride ligand of $[RuH(\eta^5-C_9H_7)(dppm)]$ complex during the catalytic hydration of nitriles. | 69 |
| Scheme I.16. Epoxidation with Jacobsen-type catalyst in IL. | 73 |
| Scheme I.17. Epoxidation with Katsuki-type catalyst in IL. | 74 |
| Scheme I.18. Epoxidation with manganese porphyrins in IL..... | 74 |
| Scheme I.19. Epoxidation with manganese(II) compounds bearing bipyridine* ligands. | 75 |
| Scheme I.20. Oxidation of cyclohexene catalyzed by a host-guest nanocatalyst using a manganese(II) compound. | 77 |
| Scheme IV.1.1. Synthetic routes for the preparation of complexes Mn1-9 and ligands used. The metal:ligand ratio was 1:2 unless specified otherwise. | 125 |
| Scheme IV.1.2. Possible diastereoisomers for $[MnX_2(pypz-R)_2]$ complexes (R= -H, $-CH_3$ or $-CH_2COOEt$), Mn1-4 and Mn6-8 | 131 |
| Scheme IV.1.3. Possible diastereoisomers for complex Mn5 | 133 |
| Scheme IV.1.4. Possible diastereoisomers for complex Mn9 | 134 |

| | |
|--|-----|
| Scheme IV.2.1. Synthetic strategy for Ru1-Ru6 compounds and ligands used. | 157 |
| Scheme IV.2.2. A, Tautomerization of the ligands 3(5)-(2'-hydroxyphenyl)pyrazole, <i>L4</i> (R= H), and 3-(2-methoxyphenyl)-1H-pyrazole, <i>L5'</i> (R= CH ₃). B, ligand 2-(1-methyl-1H-pyrazol-3-yl)phenol, <i>L5</i> | 158 |
| Scheme IV.2.3. Possible stereoisomers for complex Ru1 | 159 |
| Scheme IV.2.4. Possible stereoisomers for complexes Ru2 (R= H) and Ru3 (R= -CH ₃). | 161 |
| Scheme IV.2.5. Possible stereoisomers for compounds Ru2' (R ¹ = R ² = H; R ³ = -phOH), Ru4 (R ¹ = R ² = R ³ = H), Ru5 (R ¹ =H; R ² = R ³ = -CH ₃) and Ru6 (R ¹ = -CH ₃ ; R ² = H, R ³ = -CH ₃). | 163 |
| Scheme IV.2.6. Electron transfer and linkage isomerization processes observed for Ru-dmso complexes. | 170 |
| Scheme IV.3.1. Schematic pathways for the synthesis of the Ru(II)-chlorido complexes Ru7a and Ru7b and the aqua-complex Ru10 (other minor products were obtained in the different synthesis but are not displayed, see text for details). | 178 |
| Scheme IV.4.1. Modification of the <i>pypz-H</i> ligand by the introduction of a terminal ester group, <i>pypz-CH₂COOEt</i> | 192 |
| Scheme IV.4.2. Synthetic strategies for the immobilization of complex Ru1 (as mixture of isomers Ru1a and Ru1b) onto SP (grey spheres) and MSNP (orange-core and grey-shell spheres). | 193 |
| Scheme IV.5.1. Diastereoisomers obtained for [MnX ₂ (pypz-R) ₂] complexes (R= -H, -CH ₃ or -CH ₂ COOEt), Mn1-4 and Mn6-8 | 208 |

Table of contents

| | |
|---|------------|
| Chapter I. Introduction | 35 |
| I.1. Towards a new "Green Chemistry" | 35 |
| I.1.1. Supported Catalysts. Homogeneous vs. heterogeneous systems. | 35 |
| I.1.2. Immobilization methods | 37 |
| I.1.3. Supports | 41 |
| I.2. Metal-catalyzed chemical transformations..... | 43 |
| I.2.1. Epoxidation of alkenes | 43 |
| I.2.2. Nitrile hydration | 45 |
| I.3. Manganese and ruthenium compounds as catalysts..... | 46 |
| I.3.1. Generalities of manganese..... | 46 |
| I.3.2. Generalities of ruthenium | 49 |
| I.3.3. Catalytic properties in homogeneous phase..... | 55 |
| I.3.4. Heterogeneous catalytic systems for oxidation reactions | 72 |
| I.3.5. Heterogeneous catalysts for hydration of nitriles | 81 |
| I.4. Biological roles of transition metals | 83 |
| I.4.1. Cell death mechanisms | 84 |
| I.4.2. Anticancer metallotherapeutics in clinical development | 85 |
| I.4.3. Biological application of manganese compounds..... | 87 |
| I.4.4. Biological application of ruthenium compounds | 90 |
| | |
| Chapter II. Objectives | 95 |
| II.1. General Objectives | 95 |
| II.2. Specific Objectives..... | 96 |
| | |
| Chapter III. Experimental section | 101 |
| III.1. Materials | 101 |
| III.2. Preparations | 101 |
| III.2.1. Synthesis of ligands | 101 |
| III.2.2. Synthesis of manganese compounds | 102 |
| III.2.3. Synthesis of ruthenium compounds | 105 |
| III.2.4. Preparation of the heterogeneous systems..... | 112 |
| III.3. Cytotoxicity assays | 113 |

| | | |
|---|--|------------|
| III.3.1. | Tested compounds | 113 |
| III.3.2. | Cell lines and culture conditions | 114 |
| III.3.3. | Cell proliferation assays | 114 |
| III.3.4. | Cell cycle phase analysis..... | 115 |
| III.3.5. | Flow cytometric analysis of ROS generation..... | 115 |
| III.3.6. | Spectrophotometric and spectrofluorometric studies | 115 |
| III.3.7. | DNA interaction analysis | 117 |
| III.3.8. | Statistical analysis..... | 118 |
| III.4. | X-ray structure determination | 118 |
| III.5. | Catalytic studies | 120 |
| III.5.1. | Epoxidation of alkenes | 120 |
| III.5.2. | Hydration of nitriles | 121 |
| III.6. | Additional instrumentation and measurements..... | 122 |
| Chapter IV. Results and discussion | | 127 |
| IV.1. | Reusable manganese complexes containing pyrazole-based ligands as catalysts for epoxidation reactions..... | 127 |
| IV.1.1. | Synthesis and Structure..... | 127 |
| IV.1.2. | Electrochemical properties | 137 |
| IV.1.3. | Catalytic olefin epoxidation in acetonitrile medium..... | 140 |
| IV.1.4. | Computational studies on the epoxidation of <i>cis</i> olefins..... | 148 |
| IV.1.5. | Catalytic olefin epoxidation in different media. Reusability of catalysts in ionic liquid:CH ₃ CN. | 151 |
| IV.1.6. | Heterogeneization of complex [Mn(CF ₃ SO ₃) ₂ (pypz-CH ₂ COOEt) ₂] onto a SiO ₂ support..... | 154 |
| IV.2. | Ru(II) complexes containing dmsO and pyrazolyl ligands as catalysts for nitrile hydration..... | 159 |
| IV.2.1. | Synthesis and structure..... | 159 |
| IV.2.2. | Spectroscopic properties..... | 166 |
| IV.2.3. | Electrochemical properties and linkage isomerization | 170 |
| IV.2.4. | Catalytic hydration of nitriles | 176 |
| IV.3. | Ru(II) complexes containing trpy and pyridylpyrazole ligands as catalysts for epoxidation of alkenes. | 180 |
| IV.3.1. | Synthesis and structure..... | 180 |
| IV.3.2. | Spectroscopic properties..... | 185 |

| | | |
|--|---|------------|
| IV.3.3. | Electrochemical properties | 185 |
| IV.3.4. | Catalytic epoxidation of alkenes | 189 |
| IV.4. | Heterogenization of complex [RuCl ₂ (pypz-CH ₂ COOEt) (dmsO) ₂]. Evaluation of the catalytic activity in the hydration of nitriles..... | 192 |
| IV.4.1. | Strategies for the immobilization of Ru complexes | 192 |
| IV.4.2. | Characterization of supports..... | 193 |
| IV.4.3. | Catalytic hydration of nitriles | 199 |
| IV.5. | Biological application of some manganese and ruthenium complexes. Evaluation of the activity against tumoral cells. | 203 |
| IV.5.1. | Manganese complexes..... | 203 |
| IV.5.2. | Ruthenium complexes..... | 214 |
| IV.5.3. | Summary | 217 |
| Chapter V. Conclusions | | 221 |
| Chapter VI. References | | 231 |
| ANNEX. Supporting Information | | 261 |

Resum

En aquesta tesi es presenta la síntesi i caracterització de diferents tipus de complexos de manganès i de ruteni amb la idea d'estudiar la seva química de coordinació, així com l'activitat catalítica dels complexos sintetitzats en les reaccions d'epoxidació d'olefines i d'hidròlisi de nitrils. Per altra banda, tenint en compte la importància i els avantatges de la reutilització i l'heterogeneïtzació dels catalitzadors per al seu ús a gran escala, s'han utilitzat líquids iònics com a co-dissolvents, permetent el disseny d'un sistema catalític reutilitzable, així com també s'ha dut a terme la immobilització d'alguns d'aquests complexos sobre suports tipus sílice i nanopartícules magnètiques amb la finalitat d'aplicar-los en els mateixos processos catalítics en fase heterogènia i avaluar-ne l'activitat al llarg de successives reutilitzacions.

A més a més, tenint en compte la importància actual dels complexos metàl·lics en tractaments quimioterapèutics i la necessitat de minimitzar efectes secundaris derivats del seu ús (en paral·lel a intentar reduir costos de producció), alguns dels complexos de manganès i ruteni sintetitzats en aquesta tesi han estat avaluats com a agents anticancerígens en les línies cel·lulars OVCAR-8 i NCI-H460.

En concret, al capítol 4 es descriu la coordinació dels lligands tipus piridina-pirazole i fenol-pirazole a sals de manganès (II), generant una sèrie de complexos mononuclears que s'han caracteritzat completament a partir de les tècniques estructurals i espectroscòpiques habituals. També es descriu l'activitat catalítica dels complexos sintetitzats en l'epoxidació d'alquens utilitzant àcid peracètic com a oxidant, obtenint en general bons valors de conversió i de selectivitat. S'ha avaluat l'ús del líquid iònic [bmim]:PF₆ com a co-dissolvent, permetent el disseny d'un sistema catalític reutilitzable, i s'han dut a terme estudis preliminars d'heterogenització del complex [Mn^{II}(CF₃SO₃)₂(pypz-CH₂COOEt)₂] en partícules de sílica així com del seu comportament en la catàlisi heterogènia d'epoxidació d'alquens.

Al capítol 5 es descriu la síntesi i caracterització de nous complexos Ru(II)-dmsO que contenen lligands tipus piridina-pirazole i pirazole-fenol. S'estudia la isomerització d'enllaç de Ru^{II}(dmsO-S) a Ru^{III}(dmsO-O) induïda per la transferència electrònica en els complexos *cis,cis*-[Ru^{II}Cl₂(pypz-CH₂COOEt)(dmsO)₂] i [Ru^{II}Cl₂(HOphpz-H)(dmsO)₂]. També es descriu l'activitat catalítica dels complexos sintetitzats en l'hidròlisi de nitrils en aigua, on s'observa en general una efectivitat més elevada en el cas de substrats activats, però amb certa influència estructural en el cas dels complexos amb substituents voluminosos als lligands.

Al capítol 6 es descriu la síntesi, estructura i propietats espectroscòpiques i redox de nous complexos Ru-Cl i Ru-OH₂ que contenen el lligand neutre meridional *trpy* i el lligand no-simètric bidentat *pypz-H*. Es descriu la influència de les propietats electròniques i geomètriques dels lligands sobre el pKa i el comportament electroquímic d'aquests compostos i es porta a terme una comparació amb complexos prèviament sintetitzats al nostre grup. També es descriu l'activitat catalítica de l'aquo-complex en l'epoxidació d'olefines utilitzant diacetat de iodobenzè com agent oxidant, i observant-se millors valors de conversió per als substrats alifàtics, fet que indicaria la participació d'una espècie activa de tipus electrofílic.

Al capítol 7 es descriu l'heterogeneïtzació de la mescla d'isòmers *cis,cis-* i *cis,trans-* [Ru^{II}Cl₂(*pypz-CH₂COOEt*)(dmsO)₂] en suports de sílica i de nanopartícules magnètiques recobertes de sílica. S'ha realitzat una caracterització exhaustiva del sistema catalític heterogeni amb les tècniques ICP-AES, IR, UV-Vis, SEM, TEM, TGA i XPS, confirmant la presència del lligand *pypz-CH₂COOEt* i de Ru(II) en tots els casos. S'ha avaluat la seva activitat catalítica en la hidròlisi del benzonitril i de l'acrilonitril en condicions suaus i utilitzant aigua com a dissolvent, obtenint millors valors de conversió i selectivitat que en el cas dels sistemes homogenis anàlegs.

Finalment, al capítol 8 s'investiga l'aplicació d'alguns dels complexos de manganès i ruteni sintetitzats en la tesi, junt amb d'altres prèviament sintetitzats al grup de recerca, com a agents anticancerígens per les línies cel·lulars OVCAR-8 i NCI-H460. Tots els complexos de manganès estudiats presenten una citotoxicitat més elevada que els seus lligands lliures, confirmant que l'activitat antitumoral s'afavoreix quan aquests lligands es coordinen al metall. El complex [Mn^{II}(CF₃SO₃)₂((-)-pinene[5,6]bipyridine)₂] presenta activitats similars al cisplatí en les dues línies cel·lulars estudiades. Per contra, els complexos de ruteni estudiats han mostrat valors d'IC₅₀ relativament elevats.

Resumen

En esta tesis se presenta la síntesis y caracterización de diferentes tipos de complejos de manganeso y de rutenio con la idea de estudiar su química de coordinación, así como la actividad catalítica de los complejos sintetizados en reacciones de epoxidación de olefinas y de hidrólisis de nitrilos. Por otro lado, teniendo en cuenta la importancia y las ventajas de la reutilización y la heterogeneización de los catalizadores para su uso a gran escala, se han usado líquidos iónicos como co-disolventes, permitiendo el diseño de un sistema catalítico reutilizable, y también se ha llevado a cabo la inmovilización de algunos de estos complejos sobre soportes tipo sílice y nanopartículas magnéticas con la finalidad de aplicarlos en los mismos procesos catalíticos en fase heterogénea y evaluar su actividad a lo largo de sucesivas reutilizaciones.

Además, teniendo en cuenta la importancia actual de los complejos metálicos en tratamientos quimioterapéuticos y la necesidad de minimizar efectos secundarios derivados de su uso (en paralelo a intentar reducir costes de producción), algunos de los complejos de manganeso y rutenio sintetizados en esta tesis han sido evaluados como agentes anticancerígenos en las líneas celulares OVCAR-8 y NCI-H460.

En concreto, en el capítulo 4 se describe la coordinación de los ligandos tipo piridina-pirazola y fenol-pirazola a sales de manganeso (II), generando una serie de complejos mononucleares que se han caracterizado completamente a partir de las técnicas estructurales y espectroscópicas habituales. También se describe la actividad catalítica de los complejos sintetizados en la epoxidación de alquenos utilizando ácido peracético como oxidante, y obteniendo en general buenos valores de conversión y de selectividad. Se ha evaluado el uso del líquido iónico [bmim]:PF₆ como co-disolvente, permitiendo el diseño de un sistema catalítico reutilizable, y se han llevado a cabo estudios preliminares de heterogeneización del complejo [Mn^{II}(CF₃SO₃)₂(pypz-CH₂COOEt)₂] en partículas de sílice así como su comportamiento en la catálisis heterogénea de epoxidación de alquenos.

En el capítulo 5 se describe la síntesis y caracterización de nuevos complejos Ru(II)-dmsO que contienen ligandos tipo piridina-pirazola y pirazola-fenol. Se estudia la isomerización de enlace de Ru^{II}(dmsO-S) a Ru^{III}(dmsO-O) inducida por la transferencia electrónica en los complejos *cis,cis*-[Ru^{II}Cl₂(pypz-CH₂COOEt)(dmsO)₂] y [Ru^{II}Cl₂(HOphz-H)(dmsO)₂]. También se describe la actividad catalítica de los complejos sintetizados en hidrólisis de nitrilos en agua, donde se observa en general una efectividad más elevada en el caso de sustratos activados, pero con

cierta influencia estructural en el caso de los complejos con sustituyentes voluminosos en los ligandos.

En el capítulo 6 se describe la síntesis, estructura y propiedades espectroscópicas y redox de nuevos complejos Ru-Cl i Ru-OH₂ que contienen el ligando neutro meridional *trpy* y el ligando no-simétrico bidentado *pypz-H*. Se describe la influencia de las propiedades electrónicas y geométricas de los ligandos sobre el pKa y el comportamiento electroquímico de estos compuestos y se lleva a cabo una comparación con otros complejos previamente sintetizados en nuestro grupo. También se describe la actividad catalítica del aquo-complejo en epoxidación de olefinas utilizando diacetato de yodobenceno como agente oxidante, y se observan mejores valores de conversión por los sustratos alifáticos, hecho que indica la participación de una especie activa de tipo electrofílico.

En el capítulo 7 se describe la heterogeneización de la mezcla de isómeros *cis,cis-* y *cis,trans-* [Ru^{II}Cl₂(*pypz-CH₂COOEt*)(*dmsO*)₂] en soportes de sílice y de nanopartículas magnéticas recubiertas de sílice. Se ha realizado una caracterización exhaustiva del sistema catalítico heterogéneo con las técnicas ICP-AES, IR, UV-Vis, SEM, TEM, TGA y XPS, confirmando la presencia del ligando *pypz-CH₂COOEt* y de Ru(II) en todos los casos. Se ha evaluado su actividad catalítica en la hidrólisis del benzonitrilo y del acrilonitrilo en condiciones suaves y utilizando agua como disolvente, obteniéndose mejores valores de conversión y selectividad que en el caso de los sistemas homogéneos análogos.

Finalmente, en el capítulo 8 se investiga la aplicación de algunos de los complejos de manganeso y rutenio sintetizados en la tesis, junto con otros previamente sintetizados en el grupo de investigación, como agentes anticancerígenos para las líneas celulares OVCAR-8 i NCI-H460. Todos los complejos de manganeso estudiados presentan una citotoxicidad más elevada que sus ligandos libres, confirmando que la actividad antitumoral está favorecida cuando estos ligandos se coordinan al metal. El complejo [Mn^{II}(CF₃SO₃)₂((-)-pinene[5,6]bipyridine)₂] presenta actividades similares al cisplatino en las dos líneas celulares estudiadas. Por el contrario, los complejos de rutenio estudiados han mostrado valores de IC₅₀ relativamente elevados.

Summary

In this thesis we present the synthesis and characterization of different types of manganese and ruthenium complexes with the idea of studying their coordination chemistry, as well as the performance of the complexes synthesized in alkene epoxidation and nitrile hydration reactions. On the other hand, taking into account the importance and the advantages of the reutilization and heterogeneization of the catalysts for their use in a large-scale processes, ionic liquids have been used as a co-solvent allowing the design of a reusable catalytic system, and the immobilization of some of these complexes on silica-type and magnetic nanoparticles supports has also been carried out with the aim to apply them in the corresponding heterogeneous processes and evaluate their activity throughout successive reuses.

In addition, taking into account the current importance of the metal complexes in chemotherapeutic treatments and the need to minimize its toxic side-effects derived from their use (in parallel to a decrease the production costs), some of the manganese and ruthenium complexes synthesized in this thesis have been evaluated as antitumor agents in the OVCAR-8 and NCI-H460 cell lines.

In particular, in chapter 4 we describe the coordination of the pyridine-pyrazole and phenol-pyrazole types of ligands to manganese (II) salts, obtaining different mononuclear complexes that have been fully characterized throughout structural and spectroscopic techniques. We also describe the performance of these complexes towards alkene epoxidation using peracetic acid as oxidant, leading in general to good conversion and selectivity values. Moreover, the use of the ionic liquid [bmim]:PF₆ as a co-solvent has been studied for this purpose, allowing the design of a reusable catalytic system, and preliminary studies on the heterogenization of complex [Mn^{II}(CF₃SO₃)₂(pypz-CH₂COOEt)₂] onto silica particles along with its performance towards alkene epoxidation have been carried out.

In chapter 5 we describe the synthesis and characterization of new Ru(II)-dmsO complexes which contain pyridine-pyrazole and pyrazole-phenol types of ligands. We study the electron-transfer-induced linkage isomerization of the dmsO ligands, from Ru^{II}(dmsO-S) to Ru^{III}(dmsO-O), in compounds *cis,cis*-[Ru^{II}Cl₂(pypz-CH₂COOEt)(dmsO)₂] and [Ru^{II}Cl₂(HOphpz-H)(dmsO)₂]. We also describe the catalytic performance of all complexes towards nitrile hydration in water, and better results are obtained for the activated substrates, but with a certain structural influence in the case of the complexes bearing ligands with bulky substituents.

In chapter 6 we describe the synthesis, structure, spectroscopy and redox properties of new Ru-Cl i Ru-OH₂ complexes which contain the neutral meridional *trpy* and the non-symmetric bidentate *pypz-H* ligands. The influence of electronic and geometrical effects of the ligands over the pKa and the electrochemical behaviour of these compounds is discussed, and a comparison with the analogous complexes previously synthesized in our group is also carried out. We describe the catalytic performance of the aqua-complex with regard to the alkene epoxidation reaction using iodobenzene diacetate as oxidant, obtaining better conversion values for the aliphatic substrates, which would indicate the involvement of an active electrophilic species.

In chapter 7 we describe the heterogenization of the isomeric mixture *cis,cis*- and *cis,trans*-[Ru^{II}Cl₂(pypz-CH₂COOEt)(dmsO)₂] onto silica and silica core-shell magnetic nanoparticles. A fully characterization of the new heterogeneous systems has been done using ICP-AES, IR, UV-Vis, SEM, TEM, TGA and XPS techniques, confirming the presence of the ligand *pypz-CH₂COOEt* and the Ru(II) in all cases. The catalytic activity of these heterogeneous systems has been evaluated towards benzonitrile and acrylonitrile hydration in mild conditions and using water as solvent, obtaining better conversion and selectivity values than those observed for the analogous homogeneous system.

Finally, in chapter 8 we have investigated the application of some of the manganese and ruthenium complexes synthesized in this thesis, together with some others previously synthesized in our research group, as antitumor agents in two cancerous cell lines, OVCAR-8 and NCI-H460. All the manganese complexes studied showed a higher cytotoxicity than their free ligands, confirming that the antitumor activity is favored when these ligands are coordinated to the metal. Complex [Mn^{II}(CF₃SO₃)₂((-)-pinene[5,6]bipyridine)₂] showed similar activities as cisplatin for both studied cell lines. On the other hand, the ruthenium complexes studied in this thesis presented relatively high IC₅₀ values.

Chapter I. Introduction

I.1. Towards a new “Green Chemistry”

Chemical transformations, as well as other industrial productive processes, are experiencing a profound renovation to meet sustainability criteria, moving from old methods to new ones developed in agreement with *green chemistry* principles.¹ Substitution of harmful and hazardous chemicals with others more compatible with human health and the environment is mandatory, and among these the solvent replacement is especially important since amounts of solvents are usually much larger than those of reagents products.

In this context, new solvents should exhibit small environmental impact, no toxicity and no volatility to meet the demands of sustainability.² Glycerol derivatives are promising solvents in this respect, and glycerol itself appears as a valuable green solvent that is produced as a concomitant product in biodiesel preparation.³ Glycerol derivatives have been studied in some epoxidation reactions using hydrogen peroxide as oxidant,^{2b,4} but their application is limited so far. Water has been much under-investigated as solvent for chemical transformations basically because of poor solubility of organic molecules; however, water is the “ideal solvent”⁵ being economic, non-toxic, non-inflammable and compatible with the environment. Substitution of organic solvents by water is desirable, but it becomes especially suited for those chemical transformations in which water is one of the reagents such as hydration of nitriles.

On the other hand, new methods based on heterogeneous catalysts not only show the attractive and the powerful alternatives of avoiding the extreme acidity and basicity conditions of those nonmetal-catalyzed systems, but also exhibit the capability to recover and reuse the catalysts towards their application in large-scale processes.⁶

I.1.1. Supported Catalysts. Homogeneous vs. heterogeneous systems.

In general, catalysis is divided into homogeneous⁷ and heterogeneous⁸ catalytic systems. In the first type both catalyst and substrate are in the same phase, whereas in the second one are in a different phase (solid and liquid respectively). Among these, a supported catalyst is the result of the immobilization of a homogeneous catalyst on the surface of an insoluble solid, and can be also regarded as a heterogeneous catalyst. These types of systems are developed nowadays in order to satisfy the stringent ecological and economical demands for sustainability lead by a *green chemistry* approach for catalytic reactions.⁹ Table I.1 summarizes the principal differences between homogeneous and heterogeneous/supported catalysis.¹⁰

Homogeneous catalysts have the advantage that they are well characterized at a molecular level with well-defined active sites and they are readily soluble in the reaction medium. Such

Chapter I

single-site catalysts are highly accessible to the substrates and often show high catalytic activity and selectivity even under mild conditions, thus involving a constant energetic interaction between each active site and the substrate. However, removing them from the reaction mixture to avoid contamination of the product requires expensive and tedious purification steps.

Table I.1. Schematic comparison between a homogeneous, heterogeneous and a supported catalyst.

| Features | Homogeneous catalyst | Heterogeneous catalyst | Supported catalyst |
|---|-------------------------|-----------------------------------|--------------------------------------|
| Form | Metal complex | Solid, often metal or metal oxide | Solid with a soluble active molecule |
| Active centers | Well defined | Not defined | Defined |
| Activity | High | Variable | High |
| Selectivity | High | Variable | High |
| Reaction conditions | Mild | Drastic | Mild |
| Average time of life | Variable | Long | Long |
| Sensitivity to poisons | Low | High | Low |
| Problems of diffusion | None | Possible | Possible |
| Recycling | Difficult and expensive | Easy | Easy |
| Separation from products | Difficult | Easy | Easy |
| Variation of steric and electronic features | Possible | Difficult | Possible |
| Mechanism studies | Possible | Difficult | Possible |

On the other hand, the catalyst often consists of a high-priced noble metal and/or ligand. Recycling of the homogeneous catalysts is thus an important issue in the sustainable and large-scale production of fine chemicals. It is of special importance for enantioselective transformations, in which the cost of sophisticated ligands often exceeds that of the noble metal employed.¹¹ For these reasons, despite their intrinsic advantages, homogeneous catalysts are used in less than 20 % of the industrially relevant processes.¹²

In contrast, heterogeneous catalysts allow easy product/catalyst separation and recovery from the solution, easy handling and potential catalyst recycling. However, there are often different catalytically active sites with differing activities and selectivities in the bulk material of a heterogeneous catalyst, which are challenging to understand at a molecular level. Also, the preparation procedures are concerted and consequently not always easy to reproduce.¹³ In addition, the fact that active sites are located in a microporous environment often causes diffusion control of the catalyzed reaction and reduces the activity and the selectivity.

Therefore, the development of new catalysts that combine the best homogeneous and heterogeneous features is an interesting and growing area in catalysis. These hybrid catalysts are named immobilized heterogeneous catalyst or supported catalysts.¹⁴

I.1.2. Immobilization methods

The aim of supported catalysts is to combine the mentioned advantages of both homogeneous and heterogeneous catalysis such as: (1) high activity, selectivity and reaction rates (homogeneous catalysis), (2) easy catalyst recovery and long-term recyclability, and preparation of multifunctional catalysts (heterogeneous catalysis). Among the different techniques described to immobilize catalysts into solid supports, the most common methods used¹⁵ (see Figure I.1) are adsorption,¹⁶ electrostatic immobilization,¹⁷ encapsulation,¹⁸ ionic liquid¹⁹ and covalent binding (anchoring).²⁰

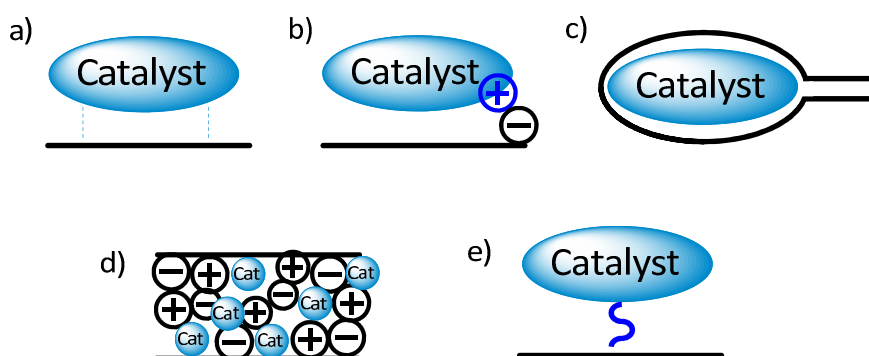


Figure I.1. Schematic representation of different strategies for catalyst immobilization: adsorption (a), electrostatic immobilization (b), encapsulation (c), ionic liquid (d) and covalent binding (e).

a) Adsorption

The adsorption is usually established by Van der Waals interactions between groups such as aromatic systems or by hydrogen bonds (Figure I.1a). These interactions are rather weak and can be disrupted easily by solvent effects or competition from oxidation products or polar oxidants. Also, the scope of this technique is quite limited taking into account that the surface

Chapter I

of most supports is polar (limiting the application to the immobilization of polar catalysts). However, the range of supports that are used with this methodology is broad, including amorphous and crystalline materials such as silica and zeolites, but in overall this method is one of the most time- and cost-effective procedures.

b) Electrostatic immobilization

An obvious limitation comes up when using this method since only a charged catalyst can be immobilized in this manner (Figure I.1b). Also, possible interactions between the support and ionic substrates or reagents that could compete with the catalyst must be considered. However, this method is a simple and fast approach to the fabrication of heterogenized catalytic systems. The most common supports used are ion-exchange resins, zeolites, clays, layered double-hydroxides, etc.

c) Encapsulation

This technique is based on the encapsulation of the catalyst inside the pores of the support (Figure I.1c). Encapsulation presents the advantage that the homogeneous catalyst does not suffer any change in its structure or chemical properties when being immobilized. Another advantage is the impossibility of deactivation by oligomerization, since each molecule, and just one, is encased in a well-defined cage, precluding the interaction with neighbouring molecules. However, this limits the application of the technique to complexes with well-defined size, and possible diffusion problems of the substrate through the pores should be considered. Nevertheless, this technique is very useful for the immobilization of complexes with bulky ligands such as porphyrins, phthalocyanines, bipyridines, tetradentate Schiff bases, etc. The supports used are often crystalline and contain cages such as zeolites, mesoporous silica and MOFs.

d) Ionic liquid matrices

Over the last decade, growing attention has been devoted to the use of ionic liquids (ILs) as solvents for organic synthesis. The strong interest in ILs for catalyzed reactions is due to the expected immobilization of the catalyst in the IL that would allow the recycling of the tandem catalyst/solvent (Figure I.1d). Furthermore, ILs have a rate acceleration effect on some catalytic reactions, and they are often considered as green alternatives to volatile organic solvents although their toxicity and biodegradability are yet to be fully determined.²¹

Ionic liquids are in general defined as liquid electrolytes composed entirely of ions. Generally, ionic liquids include liquid compounds which involve organic compounds and organominerals.

Those ionic liquids, based on quaternary ammonium or phosphonium salts and usually named room temperature ionic liquids (RTILs), have received in recent years a good deal of attention as potential alternative solvents or co-solvents in catalysis²² given their physicochemical properties and so their potential benefits:^{23,24}

- Good electrical conductivity and a relatively wide electrochemically stable window.
- Non-volatility.
- Reasonable thermal and chemical stabilities.
- Non-flammability.
- Wide range of solubility for organic, inorganic and organometallic compounds.
- They are suitable solvents for catalytic hydrogenations, carbonylations, hydroformylations and aerobic oxidations, as the solubility of gases into ILs are generally good.
- Immiscibility with a large number of organic solvents.
- Easy-tuning of their physicochemical properties.
- Non-coordinating anions.

As mentioned earlier, room temperature ionic liquids are generally salts of organic cations. The most common salts in use are those with alkylammonium, alkylphosphonium, N-alkylpyridinium and N,N'-dialkylimidazolium cations (Figure I.2). In order to be liquid at room temperature, the cation should preferably be unsymmetrical. Typically, the anions are inorganic and include $[\text{PF}_6]^-$, $[\text{BF}_4]^-$, $[\text{CF}_3\text{SO}_3]^-$ and $[(\text{CF}_3\text{SO}_2)_2\text{N}]^-$.

Chapter I

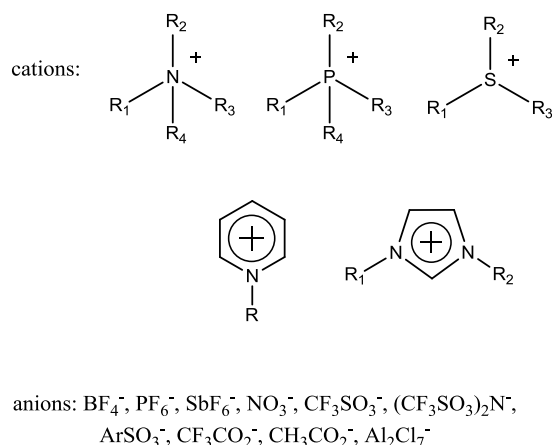


Figure I.2. Structures of common cations and anions in ionic liquids.

Numerous combinations of cations and anions offer convenient ways to fine-tune the physicochemical properties of ILs such as polarity, viscosity and miscibility with other reagents.²⁴ Most metal catalysts are soluble in ILs without modification of the ligands,²⁵ and usually the non-coordinating anions of ILs leave the active sites of catalysts available for interaction with the substrates.

Ionic liquids represent a new class of solvents with non-molecular ionic character. Even though the first representative has been known since 1914, ionic liquids have only been investigated as solvents for transition metal catalysis in the past twenty years, and this has led to a greater than exponential growth in the number of papers published. Publications to date show that replacing an organic solvent by an ionic liquid can lead to remarkable improvements in well-known processes.^{6b,26} There are also evidences that switching from a normal organic solvent to an ionic liquid can lead to novel and unusual chemical reactivity. This opens up a wide field for future investigations into this new class of solvents in catalytic applications.

e) Covalent binding (anchoring)

This type of immobilization gives a stronger interaction between catalyst and support (Figure I.1e). This immobilization method has been used to support a wide variety of active homogeneous catalysts. One of its advantages is that the chemical surrounding of the metal center is maintained as in the homogeneous parent precursor, but with all the advantages of a heterogeneous system.²⁷ The covalent immobilization process for an active homogeneous catalyst is represented in Figure I.3.

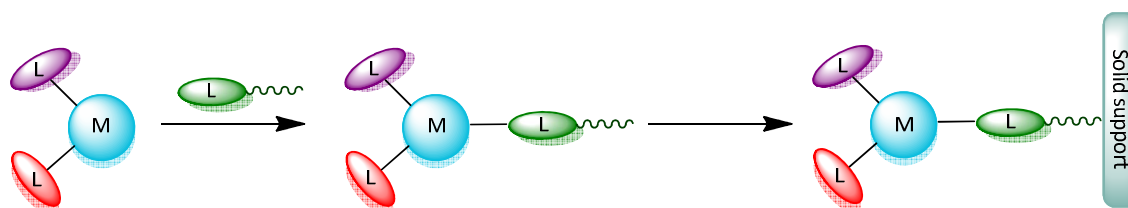


Figure I.3. General process for anchoring a homogeneous catalyst onto a solid support.

Following this methodology, the catalyst must be modified by adding a linking group that enables its attachment to the solid support. The most common linking groups used are organosilanes, of general formula R_nSiX_{3-n} (Cl, alkoxy)²⁸ and organophosphorus acids resulting in the formation of a M-O-Si, M-O-P or M-O-C bond between the inorganic support and the linker. In the case of phosphonic acid up to three M-O-P bonds can be formed with oxide-type surfaces, as represented in Figure I.4.

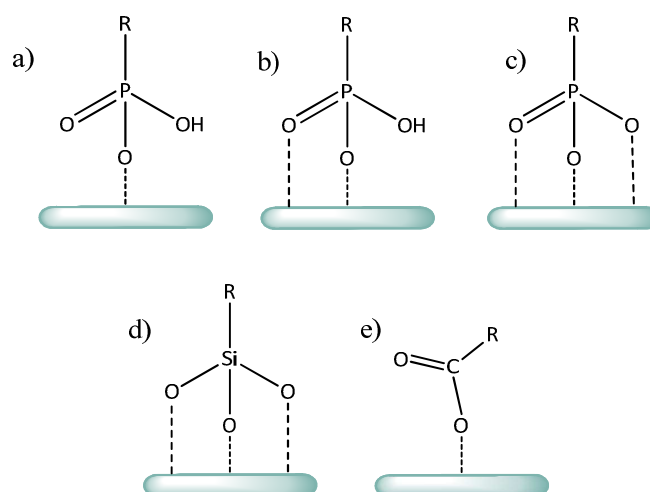


Figure I.4. Possible binding modes of a phosphonate unit (monodentate (a), bidentate (b), tridentate (c)), alkoxy silane unit (d) (only the tridentate mode is represented but the other two are possible) and carboxylate unit (e) to an oxide-type surface.

I.1.3. Supports

When choosing a support for the immobilization of a catalyst, two main aspects must be taken into account. First, the metal complex must be well dispersed through the surface of the support in order to achieve proper activities and good diffusion conditions. For this reason, parameters such as surface charge, polarity, or particle and pore size must be considered. Secondly, the system must be chemically and physically stable in the catalytic conditions.

The supports can be organic²⁹ (such as polymers with a polystyrene, polypyrrole or polyacrylate backbone), inorganic³⁰ (such as silica, alumina, titania, zeolites, metallic nanoparticles or core-shell nanoparticles) or metal-organic frameworks (MOFs).³¹ In the present work, some of the inorganic oxides will be explained.

Chapter I

a) Titanium dioxide

Structural modifications of titanium dioxide (TiO_2) can affect its band gap energy allowing it to absorb light in the visible zone, then being of interest in the solar cells research field. These modifications can be carried out by synthesizing new TiO_2 -based composite materials,³² through n-doping or by surface immobilization of sensitizing dyes.³³ The latest approach is especially interesting because by introducing adequate functional groups in the organic structure of the ligands, a complex can be easily anchored onto the TiO_2 surface.³⁴

b) Silicon dioxide

The origin of the almost exclusive use of alumina as support has been ascribed to its outstanding textural and mechanical properties and its relatively low cost.³⁵ However, the presence of undesirable strong metal-support interactions in the alumina-supported catalysis has triggered research devoted to the development of new supports.³⁶ Silica gel is a granular, vitreous, and porous form of silicon dioxide. It is a tough and hard material with good ability to adsorb compounds on its surface. It has a large surface area ($800 \text{ m}^2/\text{g}$) that can be effectively used for catalytic applications. The silanol (Si-OH) groups of silica gel provide an attractive center for the synthesis of silica-supported/functionalized novel heterogeneous catalysts. Furthermore, chelating groups can also be covalently bonded to silica gel. When silica is used as a support, its polar surface helps to change the spatial orientation of reactants toward catalysts through hydrogen bonding with functional groups of reactant molecules.³⁷

c) Nanoparticles and core-shell nanoparticles

Nanoparticles (NP) can be defined as microscopic particles with a diameter of 1-100 nm. They are considered as a bridge between molecular structures and bulk materials or, in catalytic terms, a bridge between homogeneous and heterogeneous catalysis as these systems are often referred to as "quasihomogeneous" (or soluble heterogeneous) systems.³⁸ Nowadays, magnetic nanoparticles (MNP), especially iron oxide nanoparticles, have attracted increasing interest because of their unique physical properties including high surface area, supermagnetism and low toxicity, that broadens their potential applications to many fields.³⁹ There are three common iron oxides: iron (II) oxide (FeO), iron (III) oxide (Fe_2O_3) and iron (II, III) oxide (Fe_3O_4). Among these, $\gamma\text{-Fe}_2\text{O}_3$ (maghemite) and Fe_3O_4 (magnetite) have received an especial attention in catalysis. The Fe_3O_4 nanoparticles are easily prepared and surface-functionalized and they can be recycled from the solution by an external magnetic field. Hence, the catalyst supported on Fe_3O_4 nanoparticles can be separated from the reaction system and reused.^{39a,40}

In recent years, core-shell multi-components have attracted intense attention because of their potential applications in catalysis.⁴¹ These core-shell multi-components can integrate various functions into one system for specific applications.^{38i,42} Among the core-shell structured composites, the silica-coated magnetic nanoparticles not only stand out for their potential applications in catalysis, as each nanoparticle is formed by a well-defined magnetic nucleus which is surrounded by a microporous silica shell (see Figure I.5),⁴³ but also for their large surface area-to-volume ratio and easy functionalization.

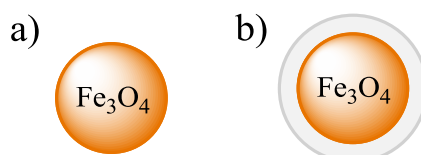
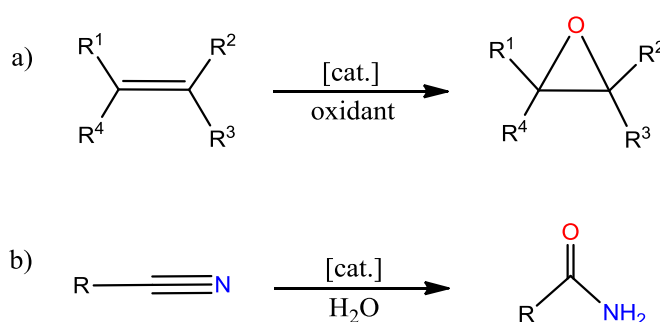


Figure I.5. Magnetic nanoparticle (a) and a silica-coated magnetic nanoparticle (b).

I.2. Metal-catalyzed chemical transformations

Transition metal-catalyzed reactions are a field of unquestionable importance in inorganic chemistry for their wide range of applications. In the present work, metal-catalyzed oxidation, one of the most important transfer reactions in chemistry and biology,⁴⁴ is one the main application of the prepared manganese and ruthenium complexes, together with catalytic hydrolysis reactions. More specifically, the studied chemical transformations are olefin epoxidation and hydration of nitriles (see Scheme I.1) which have received considerable interest from both academic and industrial points of view, since epoxides⁴⁵ and amides^{46,47} play a significant role as intermediates and building blocks in synthesis and material science.



Scheme I.1. General reaction for olefin epoxidation (a) and hydration of nitriles (b).

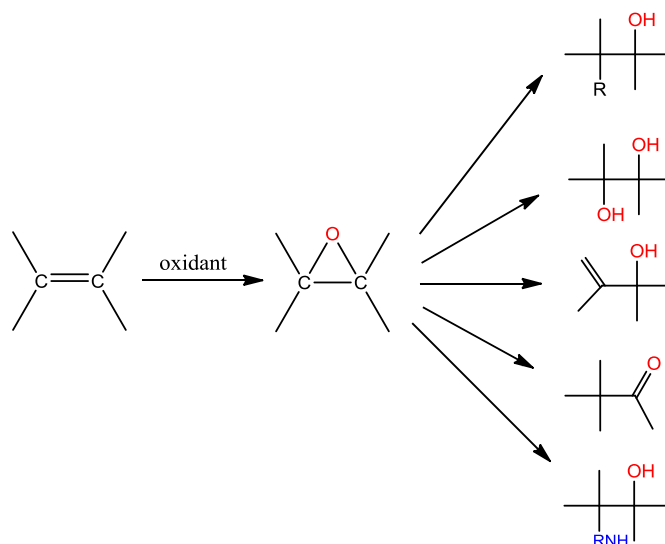
I.2.1. Epoxidation of alkenes

As mentioned earlier, olefin epoxidation has received considerable interest from both academics and industry since epoxides are key intermediates in the synthesis of more elaborated chemical products for the industrial production of bulk and fine chemicals.^{45c,45f, 48} For instance, the fine chemical Medrol, which is an anti-inflammatory and anti-allergic

Chapter I

corticosteroid, is synthesized from an epoxide.⁴⁹ Also, epoxy polymers are widely used in the marine, automotive, aerospace and building industries.

Epoxides can be transformed into a wide variety of functionalized products. For example their reductions, rearrangements or ring-opening reactions with various nucleophiles can lead to the formation of diols, aminoalcohols, allylic alcohols, ketones, etc., as depicted in Scheme I.2.⁵⁰



Scheme I.2. Epoxide formation and possible further transformations.

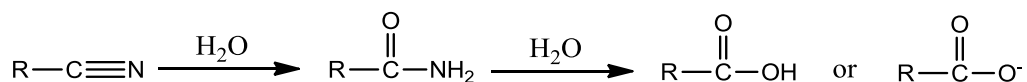
Epoxidation of alkenes can be achieved by a variety of oxidants. These include perbenzoic acids (among which metachloroperbenzoic acid, MCPBA, is the most commonly used for this purpose in the laboratory),⁵¹ dioxiranes,⁵² alkylhydroperoxides, hydrogen peroxide,⁵¹ hypochlorite,⁵³ iodosylbenzene⁵³ and molecular oxygen.⁵¹ Most of these oxidants have the disadvantage that, besides oxygenated products, stoichiometric amounts of waste products are generated and have to be separated from the desired epoxides. Thus, there is special interest on the use of environmentally friendly “green” oxidants. The most efficient are peroxides, in particular hydrogen peroxide since it is relatively cheap and the only side product after the oxidation reaction is water. However, hydrogen peroxide also presents some disadvantages such as the easy generation of highly reactive hydroxyl radicals ($\cdot\text{OH}$) giving rise to non-selective oxidation reactions, and its prevalent self-disproportionation in the presence of transition metals.⁵⁴

Uncatalyzed epoxidations of alkenes with peracetic acid are well known reactions to obtain epoxides as many terminal alkenes are susceptible to it, but these epoxidation reactions require extended reaction times at elevated temperatures that often lead to a reduced

selectivity.⁵⁵ Combining transition metal catalysts with peracetic acid can enhance the epoxidation selectivity and reduce reaction times.⁵⁶

I.2.2. Nitrile hydration

As it has been mentioned earlier, the hydration of nitriles to generate the corresponding amides is an important transformation for a wide range of fields, since the amide bond is one of the most important functional groups in contemporary chemistry. This reaction is also of biotechnological interest since nitrile hydratases, a family of non-heme iron enzymes,⁵⁷ are used in the industrial preparation of relevant amides, such as acrylamide, nicotinamide and 5-cyanovaleramide.^{46b,58} In addition, amides can be reduced to the corresponding amines under remarkably mild conditions, making the catalytic hydration of nitriles also interesting from this point of view.⁵⁹



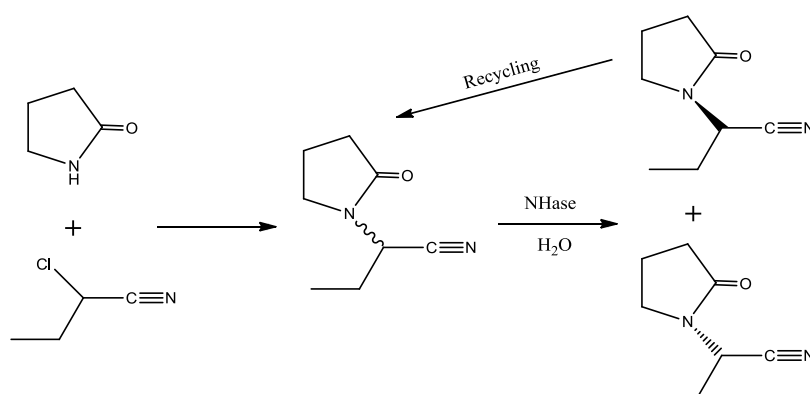
Scheme I.3. The nitrile hydration and amide hydrolysis reactions.

Amides are commonly prepared by the reaction of activated carboxylic acid derivatives (acid chlorides, anhydrides and esters) with amines including ammonia,⁶⁰ or by direct union of the acids with the amines assisted by coupling reagents, such as carbodiimides or 1H-benzotriazole derivatives.⁶¹ However, despite being of great applicability, these methods suffer from low atom economy, making their environmental profile unfavorable. For these reasons, the development of atom-efficient catalytic methods for amide formation is currently an extremely active area of research.⁶² An increasing attention is being devoted to the development of more efficient and sustainable synthetic routes that allow access to this important class of compounds.⁶³

In this context, one of the simplest methods of synthesizing primary amides is the catalytic hydration of nitriles. Conventionally, this reaction has been carried out by using strong acids⁶⁴ and bases,⁶⁵ thus suffering several drawbacks as for example the formation of undesired by-products (such as carboxylic acids by over-hydrolysis of the amides), or the formation of a large amount of salts generated after the neutralization step. Moreover, many sensitive functional groups do not endure such harsh conditions, which consequently decrease the selectivity of the reaction. Therefore, the development of new efficient procedures for the synthesis of amides that avoid the use of stoichiometric reagents and/or acidic and basic media is highly desirable.

Chapter I

To overcome these drawbacks, considerable efforts have been expended in the search of alternative methods for the nitrile hydration process. In this context, nitriles hydratases (NHases), a family of enzymes containing non-heme low spin Fe(III) or non corrinoid low-spin Co(III) active centers, have demonstrated great potential to promote the selective transformation of nitriles into amides under mild conditions.⁶⁶ In fact, these types of biocatalysts have found application in commercial production of some relevant amides, such as levetiracetam, an antiepileptic drug marketed under the trade name Keppra® (Scheme I.4).⁶⁷



Scheme I.4. Synthetic route of levetiracetam employing a nitrile hydratase.

I.3. Manganese and ruthenium compounds as catalysts

I.3.1. Generalities of manganese

Manganese is a relatively abundant metal, constituting about 0.1 % of the earth's crust (1000 ppm), making it the 12th most abundant element and the third most abundant transition element (exceeded only by iron and titanium). It is found in over 300 different and widely distributed minerals of which about twelve are commercially important. As a class-A metal it occurs in primary deposits as the silicate. Of more commercial importance are the secondary deposits of oxides and carbonates such as pyrolusite (MnO₂), hausmannite (Mn₃O₄) and rhodochrosite (MnCO₃). Millions of tons of manganese are used annually, and its most common mineral, pyrolusite, has been used in glassmaking since the time of the Pharaohs. The metal is produced by reduction of its oxides with sodium, magnesium and aluminum, or by electrolysis. Nearly all manganese produced commercially is used in the steel industry as ferromanganese.



Figure 1.6. From left to right: pyrolusite (MnO_2), hausmannite (Mn_3O_4) and rhodochrosite (MnCO_3) (Images from <http://www.mindat.org>).

The most common oxidation states of manganese are +2, +3, +4 and +7. The +2 oxidation state is the most stable, with the +3, +4, +5 and +6 states becoming increasingly less stable. Manganese (VII) compounds are powerful oxidizing agents, though the oxidation state +7 are restricted to the unstable oxide Mn_2O_7 and compounds of intensely purple permanganate anion MnO_4^- . Compounds with oxidation states +5 (blue) and +6 (green) are also strong oxidizing agents, but show vulnerability to disproportionation.

I.3.1.1. Manganese (II) compounds

This is the dominant oxidation state and the most stable. Manganese (II) is a relatively hard acid and this is manifested, for example, in the preference for O-donor rather than N-donor ligands. Few compounds are also known with P, As and S-donor ligands.⁶⁸ Manganese (II) compounds are generally quite labile. Most of the Mn(II) complexes are high-spin d^5 , due to their stable half-filled d electron shell, but few low-spin compounds have been isolated,⁶⁹ as $[\text{Mn}(\text{CN})_6]^{4-}$. The lack of the ligand-field stabilization energy for the high-spin configuration gives a large variability of coordination numbers and geometries, which seem to depend mostly on the ligand steric and electronic effects. Lower coordination numbers (three, four and five) are fairly rare, whereas higher coordination numbers (seven and eight) are more common than for other first-row (+2) transition elements, a reflection of the larger size of Mn(II).⁶⁸ Coordination geometry six is the most common for Mn(II) compounds.

In octahedral fields, in terms of electronic transitions, the high-spin configuration involves the pairing of some electrons and therefore spin-forbidden as well as parity-forbidden character, thus accounting for the extremely pale color of such compounds. In tetrahedral environments, the transitions are still spin-forbidden but no longer parity-forbidden; these transitions are therefore approximately 100 times stronger and the compounds have a noticeable green-yellow color. In low-spin configuration, compounds are strongly colored since a spin-allowed absorption band is expected in the visible region.⁷⁰

Chapter I

Many compounds, generally high-spin, with a variety of open-chain polydentate nitrogen ligands (bidentate to heptadentate), have been isolated in some cases with additional anion ligands, for example, halides or carboxylates. For instance, the tripodal tetradentate ligand ntb, (tris(2-benzimidazolymethyl)amine), with chloride, acetate, or nitrate anions, forms the five to seven-coordinate mononuclear complexes $[\text{Mn}(\text{ntb})\text{X}]\text{Cl}$ ($\text{X} = \text{Cl}, \text{O}_2\text{CMe}$) and $[\text{Mn}(\text{ntb})(\text{NO}_2)_2]$, having trigonal bipyramidal or distorted octahedral geometries.⁷¹ 8N and 7N coordination are found respectively in $[\text{Mn}(\text{L}^1)_2]^{2+}$ (Figure 1.7a),⁷² and $[\text{MnL}^2]^{2+}$ (Figure 1.7b);⁷³ the latter complex has been investigated as superoxide dismutase mimic. The structure of a rare low-spin, six-coordinate complex $[\text{Mn}(\text{L}^3)_2]$ (Figure 1.7c) has also been obtained.^{69b}

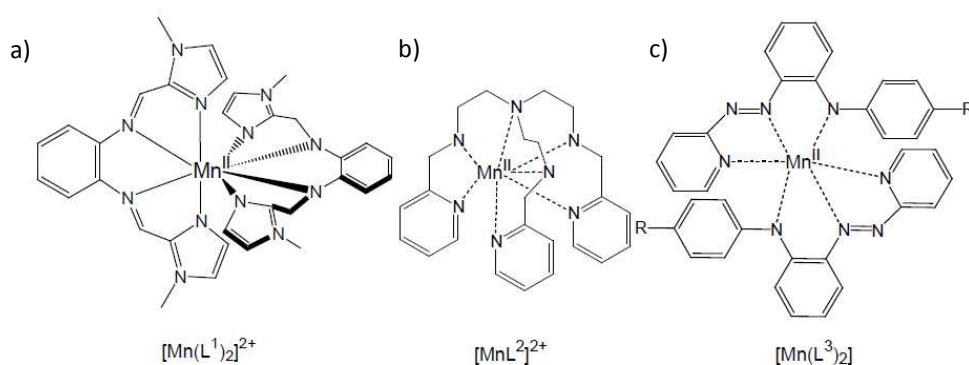


Figure 1.7. Examples of Mn (II) coordinated by N-donor ligands.

I.3.1.2. Manganese (III) compounds

The aqua ion of manganese (III) can be obtained by electrolytic or peroxy sulphate oxidation of Mn^{2+} solutions or by reduction of MnO_4^- .^{70b} The latter ion is often subject to disproportionation into manganese (IV) and manganese (II). The chemistry of manganese (III) is dominated by dinuclear, trinuclear and tetranuclear complexes with oxo, alkoxo and carboxylate bridges. The propensity of these complexes to be in mixed-valence states such as manganese (II, III) or manganese (III, IV) requires the confirmation of their structures by spectroscopic and X-ray structural methods. Mononuclear compounds can be stabilized by Schiff-based ligands, nitrogen-based ligands and macrocyclic ligands. The most commonly observed coordination numbers of manganese (III) are five⁷⁴ and six.⁷⁵ The electronic configuration of manganese (III) is d^4 , so the high-spin configuration ($S = 2$) in an octahedral field is subject to Jahn-Teller distortion.⁷⁶

I.3.2. Generalities of ruthenium

Ruthenium is a metal situated in the d group of the periodic table whose electronic configuration is $[\text{Kr}] 4d^7 5s^1$. As the 74th most abundant element in the Earth's crust, ruthenium is relatively rare (100 parts per trillion). It was discovered in 1844 by Karl Ernst Claus and was named after his homeland, Russia (in Latin, Russia is Ruthenia). It is usually found as a minor component of nickel, copper and platinum metal ores, together with other platinum group metals such as palladium, platinum, rhodium and iridium. No less important is the fact that ruthenium is the least expensive among these metals. Its annual production is about 12 tones.



Figure I.8. A pure ruthenium(0) bar (image from <http://www.mindat.org>).

Ruthenium is the unique among all the elements of the periodic table, together with osmium, that covers the whole range of 11 oxidation states theoretically possible for a transition metal (from d^0 to d^{10}), from -2 as in $[\text{Ru}(\text{CO})_4]^{2-}$ to +8 as in RuO_4 (each with different coordination geometries).⁷⁷

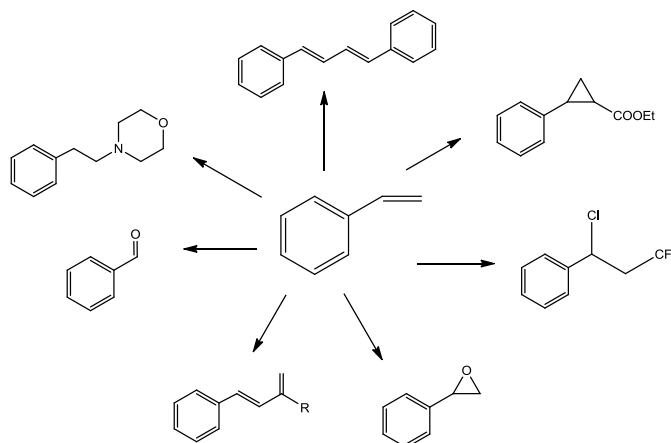
The kinetic stability of ruthenium complexes in different oxidation states, the often reversible nature of the redox pairs and their relative easy preparation make these complexes particularly interesting. Other general characteristic of ruthenium coordination compounds are their high electron transfer capacity,⁷⁸ and their ability to stabilize reactive species like oxo-metals⁷⁹ and metal-carbene complexes.⁸⁰

Ruthenium complexes are widely used and studied in different chemical fields. Their properties and so their applications are clearly correlated with the nature of the ligands coordinated to the central metal ion. Ruthenium complexes with π -conjugate ligands or systems that enable electronic delocalization have shown specific properties in nonlinear optics,⁸¹ magnetism,⁸² molecular sensors⁸³ and liquid crystals.⁸⁴ On the other hand, sulfoxide complexes have been extensively studied, as it will be seen in section I.3.2.2, due to their relevant usefulness in chemotherapy.^{85,258a} Ruthenium complexes with heterocyclic N-donor ligands are the most employed due to their interesting spectroscopic, photophysical and electrochemical properties,⁸⁶ which lead to potential applications in many different areas such

Chapter I

as photosensitizers for photoactive conversion of solar energy,^{33a,87} molecular electronic devices⁸⁸ and photoactive DNA cleavage agents for therapeutic purposes.⁸⁹

In the present work, catalysis is the most important application of the prepared ruthenium complexes. Synthetic versatility, easily available high oxidation states and a robust character of their coordination sphere make ruthenium complexes particularly useful for catalytic transformations, such as cyclopropanation,⁹⁰ isomerization,⁹¹ metal-promoted radical reactivity,⁹² oxidation,⁹³ addition,⁹⁴ hydrogen generation,⁹⁵ hydrogenation,⁹⁶ C-H and C-halogen bond activation⁹⁷ and olefin metathesis.⁹⁸ The effect of the ligands is crucial in determining the type of the catalytic reaction; in consequence the same metal complex can transform the same substrate into different products by changing the ligands. To illustrate it, in Scheme I.5 is shown how styrene can be transformed into multiple products as function of the catalyst used.⁹⁹



Scheme I.5. Possible chemical transformations of styrene as function of the catalyst used.

Due to the importance of the ligand environment, numerous studies have been focused on the understanding of their electronic and geometric properties and how these properties influence the metal reactivity.

I.3.2.1. Ruthenium polypyridyl aqua complexes

The research carried out by Frances P. Dwyer and co-workers during 1940s to 1960s can be considered the starting point of the chemistry of polypyridyl complexes of ruthenium and osmium.¹⁰⁰ Further studies have considerably improved the synthetic procedures described in these initial publications. For example, Thomas J. Meyer and collaborators began a systematic study of their relevant reactive properties or Ru and Os-aqua complexes based on their accessibility to long-lived excited states and oxidation states varying from M(II) to M(VI).^{79a,101}

It is important to notice that it is possible to create families of related complexes in which these redox properties can be varied by changing the ancillary ligands.¹⁰²

Polypyridyl ligands give a great stability to the metal ion not only thanks to their chelating effect, which enhance their coordinative capacity, but also for the resulting increased stability of the formed complex against oxidation (Figure I.9).

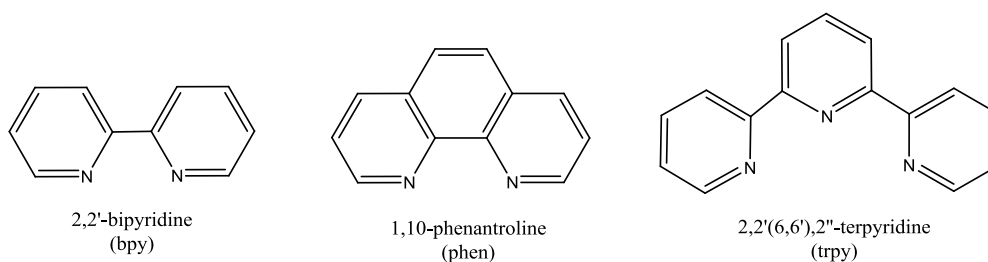
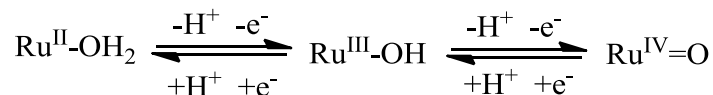


Figure I.9. Common polypyridyl ligands used in ruthenium coordination chemistry.

The redox properties of these polypyridyl-based complexes becomes especially interesting when an aqua ligand is directly bound to the metal center. In this case, proton-coupled-electron transfers (PCET) are possible, thus making high oxidation states become fairly accessible.¹⁰³



Scheme I.6. PCET oxidation process characteristic of Ru-aqua complexes.

As shown in Scheme I.6, the successive oxidation from Ru(II) to Ru(IV) are accompanied by a sequential loss of protons favored by the enhanced acidity of the bonded aqua ligand. Therefore, the initial $\text{Ru}^{\text{II}}\text{-OH}_2$ is oxidized to $\text{Ru}^{\text{IV}}\text{=O}$, passing through a $\text{Ru}^{\text{III}}\text{-OH}$ species. As a result of this behaviour, the redox potential of the aqua complexes can be directly correlated with the pH of the medium: if pH increases, the Ru(III/II) and Ru(IV/III) couples are shifted to lower potentials and viceversa. The Nernst equation (Equation I.1) correlates pH with redox potential in such a way that, for monoprotic and monoelectronic transfer, the redox potential diminishes in 59 mV by every pH unit increased.

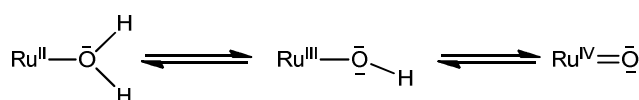
Chapter I

$$E_{1/2} = E_{1/2}^0 - 0.059 (m/n) pH$$

Equation I.1. The Nernst equation, which correlates pH with redox potential ($E_{1/2}$ = half wave redox potential at a given pH; $E_{1/2}^0$ = half wave redox potential at standard conditions; m = number of transferred protons; n = number of transferred electrons).

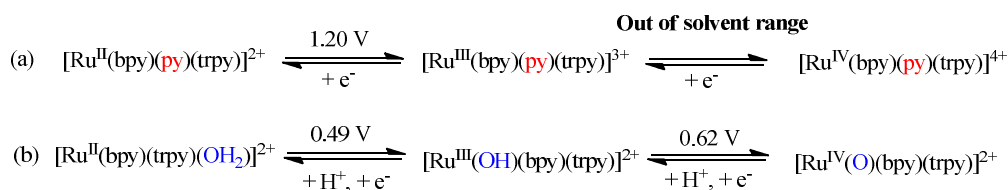
The graphical representation of this pH dependence in front the redox potential is known as Pourbaix diagram. This diagram combines the redox equilibria with the acid-base equilibria of all thermodynamically stable species involved, and represents the evolution of the half wave redox potential, $E_{1/2}$, throughout the complete pH range.

The presence of a coordinated aqua ligand to Ru lowers the redox potential values thanks to the release of protons upon oxidation. This stabilization is promoted by the successive deprotonation and subsequent electronic stabilization of the higher oxidation states by the oxocomplex formation, due to the more acidic character of the deprotonated aqua ligand (Scheme I.7).



Scheme I.7. The stabilization of the Ru metal center promoted by the successive deprotonation of the aqua ligand.

In order to illustrate this behaviour, Scheme I.8 shows the Latimer diagrams for two different polypyridylic ruthenium complexes: (a) $[\text{Ru}^{\text{II}}(\text{bpy})(\text{py})(\text{trpy})]^{2+}$ and (b) $[\text{Ru}^{\text{II}}(\text{bpy})(\text{trpy})(\text{OH}_2)]^{2+}$. As it can be seen, the substitution of a pyridyl ligand by an aqua ligand causes a dramatic decrease of the oxidation potential values.



Scheme I.8. Latimer diagrams of Ru polypyridyl complexes (a) non-containing and (b) containing a coordinated water molecule (V vs. SCE, pH= 7).

The stabilization and the $E_{1/2}$ of the ruthenium oxocomplexes, and therefore their reactivity, depend on several factors. The nature of the accompanying ligands is one of the most studied among them. The possibility of modulate the complexes reactivity by tuning their redox potentials, in addition to the need of obtain selective catalysts, has resulted in a large number of systematic studies on the redox properties of these complexes, containing a broad variety of ligands.¹⁰⁴

Table I.2. Electrochemical parameters for aqua complexes for Ru (table extracted from ref.102)^a.

| Entry | Compound | $E_{1/2}$ (V) | | $\Delta E_{1/2}$ |
|-------|---|---------------|------------|------------------|
| | | Ru(III/II) | Ru(IV/III) | |
| 1 | [Ru(NH ₃)(OH ₂) ²⁺ | -0.33 | 0.35 | 0.68 |
| 2 | [Ru(trpy)(acac)(H ₂ O)] ⁺ | 0.19 | 0.56 | 0.37 |
| 3 | [Ru(trpy)(C ₂ O ₄)(H ₂ O)] | 0.16 | 0.45 | 0.29 |
| 4 | [Ru(trpy)(H ₂ O) ₃] ²⁺ | 0.35 | 0.64 | 0.29 |
| 5 | <i>trans</i> -[Ru(trpy)(pic)(H ₂ O)] ⁺ | 0.21 | 0.45 | 0.24 |
| 6 | <i>cis</i> -[Ru(trpy)(pic)(H ₂ O)] ⁺ | 0.38 | 0.56 | 0.22 |
| 7 | <i>cis</i> -[Ru(6,6'-Me ₂ -bpy)(H ₂ O) ₂] ²⁺ | 0.57 | 0.73 | 0.16 |
| 8 | [Ru(trpy)(tmen)(H ₂ O)] ²⁺ | 0.36 | 0.59 | 0.13 |
| 9 | [Ru(trpy)(phen)(H ₂ O)] ²⁺ | 0.50 | 0.60 | 0.10 |
| 10 | <i>cis</i> -[Ru(bpy) ₂ (py)(H ₂ O)] ²⁺ | 0.42 | 0.53 | 0.11 |
| 11 | [Ru(trpy)(bpy)(H ₂ O)] ²⁺ | 0.49 | 0.62 | 0.13 |
| 12 | [Ru(trpy)(4,4'-((CO ₂ Et) ₂ bpy)(H ₂ O)] ²⁺ | 0.66 | 0.80 | 0.13 |
| 13 | [Ru(trpy)(4,4'-Me ₂ -bpy)(H ₂ O)] ²⁺ | 0.47 | 0.61 | 0.14 |
| 14 | <i>cis</i> -[Ru(bpy) ₂ (AsPh ₃)(H ₂ O)] ²⁺ | 0.50 | 0.67 | 0.17 |
| 15 | <i>cis</i> -[Ru(bpy)(biq)(PEt ₃)(H ₂ O)] ²⁺ | 0.45 | 0.63 | 0.18 |
| 16 | [Ru(tpm)(4,4'-((NO ₂) ₂ -bpy)(H ₂ O)] ²⁺ | 0.56 | 0.75 | 0.19 |
| 17 | <i>cis</i> -[Ru(bpy) ₂ (PET ₃)(H ₂ O)] ²⁺ | 0.46 | 0.67 | 0.21 |
| 18 | <i>cis</i> -[Ru(bpy)(biq)(PPh ₃)(H ₂ O)] ²⁺ | 0.48 | 0.70 | 0.22 |
| 19 | <i>cis</i> -[Ru(bpy) ₂ (P(<i>i</i> -Pr) ₃)(H ₂ O)] ²⁺ | 0.45 | 0.68 | 0.23 |
| 20 | <i>cis</i> -[Ru(bpy) ₂ (PPh ₃)(H ₂ O)] ²⁺ | 0.50 | 0.76 | 0.26 |
| 21 | <i>cis</i> -[Ru(bpy) ₂ (SbPh ₃)(H ₂ O)] ²⁺ | 0.52 | 0.80 | 0.28 |
| 22 | [Ru(trpy)(dppene)(H ₂ O)] ²⁺ | 1.17 | 1.53 | 0.36 |

^{1a}In H₂O at pH= 7.0, T= 22±2 °C, I= 0.1 M vs. SCE. ^b $E_{1/2}$ values for Ru^{III}-OH/Ru^{II}-OH₂, Ru^{IV}=O/Ru^{III}-OH and Ru^{IV}=O/Ru^{II}-OH₂ couples. ^c $\Delta E_{1/2} = E_{1/2}(\text{Ru(IV/III)}) - E_{1/2}(\text{Ru(III/II)})$. ^dpH= 4.0. ^eIn CH₂Cl₂/H₂O (3:1). Abbreviations: acac= acetyl acetate; pic= picolate anion; tmen= N,N,N,N-tetramethylethylenediamine; py= pyridine; biq= 1,1'-biquinoline; tpm= tris(pyrazolyl)methane; dppene= *cis*-1,2-bis(diphenylphosphino)ethylene.

Table I.2 shows the strong ligand effect over the Ru(IV/III) and Ru(III/II) redox couples in different families of ruthenium complexes with N-containing ligands.¹⁰² As it can be seen, the Ru(IV/III) and Ru(III/II) redox couples are clearly influenced by the ligands. Ru(II) is stabilized by ligands with low-lying π acceptor levels, such as PPh₃ or the py ligand (entries 20 and 10), then displaying relatively high Ru(III/II) $E_{1/2}$ values. On the contrary, Ru(III) oxidation state is clearly stabilized by σ -donor ligands as acetyl acetate (acac) or oxalate, C₂O₄²⁻ (entries 2 and 3) and thus oxidation from Ru(II) to Ru(III) is easily attained.

Chapter I

On the other hand, Ru(IV/III) couples are, in general, less sensitive to ligand variations than Ru(III/II). This phenomenon can be observed by comparing the complexes in entries 2 and 11 or 3 and 9, where changes in the accompanying ligands produce only a slight modification in the potential of the Ru(IV/III) couple, whereas the Ru(III/II) couple is strongly influenced. This behaviour is due to the control of the π -binding exerted by the oxo ligand through a $d_{\pi\text{Ru}}-p_0$ interaction in the Ru(IV) species.

Due to these properties, polypyridyl ruthenium complexes with aqua ligands have been extensively employed in oxidation reactions of organic and inorganic substrates, C-H insertion and proton-coupled electron transfer as it will be seen in section I.3.2.1.

I.3.2.2. Ruthenium complexes with sulfoxide ligands

In general, transition metal complexes containing sulfoxide ligands have been used since the 60s¹⁰⁵ as precursors for the synthesis of a large variety of compounds¹⁰⁶ with applications in a wide number of catalytic processes.¹⁰⁷ Nevertheless, the most remarkable applications of these complexes are their utility in medicinal chemistry as antitumor compounds^{106b,108} and antimetastatic agents.¹⁰⁹

On the other hand, the ambidentate behaviour of sulfoxide ligand, responsible for the bond isomerization observed in these type of complexes (see below), makes them interesting from an academic point of view for their basic coordination chemistry¹¹⁰ and their applications as molecular memories.¹¹¹ The characteristics of this kind of complexes are closely associated with the nature of the metal-sulfoxide bond and, for this reason, the understanding of the factors which affects the bond mode is important for the design and tuning of their properties.

Dimethyl sulfoxide (dmsO) presents a certain selectivity for different electronic population in Ru-dmsO complexes. It acts as a S-bonded molecule (S-dmsO) for Ru(II) d^6 low spin configuration and as O-bonded molecule (O-dmsO) for Ru(III) d^5 low spin configuration.¹¹² Consequently, it must be taken into account that Ru-dmsO complexes can suffer a linkage isomerization process. There are some factors that can induce such isomerization,^{112a,113} but in the present work focus is set in the S-dmsO to O-dmsO isomerization provoked by the change in metal oxidation state. According to Pearson acid-base theory,¹¹⁴ diffuse orbitals from metallic ions are well overlapped with donor orbitals from S, and this Ru-S linkage is further favored when a π -retrodonation from metal to empty $d_{(s)}$ or π^* dmsO orbitals takes place. The Ru(II)-S_{dmsO} bond has some double bond character due to the occurrence of π -retrodonation and, for this reason, it can be observed that the average Ru-S bond distance is lower than the

sum of the respective covalent radius. For harder metallic ions as Ru(III) the linkage through O is the favorite in agreement with Pearson's theory, π -retrodonation is less important due to the higher oxidation state of the metal and the absence of empty d orbitals in O, and therefore the Ru-S_{dmsO} to Ru-O_{dmsO} isomerization takes place when Ru(II) is oxidized to Ru(III).

I.3.3. Catalytic properties in homogeneous phase

I.3.3.1. Manganese in oxidation catalysis

Nowadays a lot of studies are focused to mimic natural systems that carry out chemical transformation with excellent effectiveness in terms of selectivity and energy consumption. Concretely, the oxidation of organic substrates has received a special interest.^{44a,c;48a,115}

Selective oxidation of raw materials is an important area for the chemical industry, due to the necessity to produce oxygen-containing chemicals from fossil hydrocarbons avoiding the complete conversion to carbon dioxide. This is often a difficulty during the preparation of fine chemicals, since it is still challenging to cleanly introduce an alcohol moiety at the desired position of a drug precursor in the same manner as enzymes do.

Many enzymes are present in nature acting as "biological catalysts" capable of catalyzing oxidation reactions in living organisms.¹¹⁶ Metals in enzymes participate in complex biochemical reactions and highly specialized biological functions thanks to their ability to exist in multiple oxidation states and different geometries. Manganese compounds are used as biomimetic catalysts due to Mn biological role, as is an essential trace nutrient in all form of life. The best-known manganese-containing polypeptides may be arginase, the diphtheria toxin and Mn-containing superoxide dismutase (Mn-SOD). These enzymes are frequently studied by using model complexes which provide information on the nature and reactivity of the active site (see Figure I.10) and also about possible reactions mechanisms.¹¹⁷ Several factors modulate the reactivity of the active center, such as the nature of the ligand, the type of the metal ion or the coordination geometry around the metal center. Based on the manganese or iron containing enzymes and on the related model complexes various oxidation catalysts have been studied.

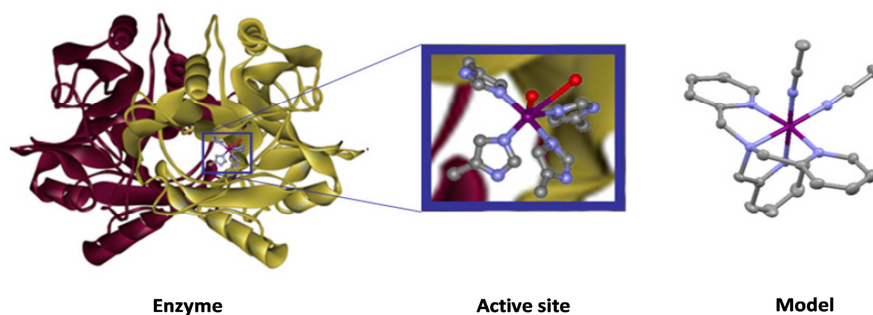
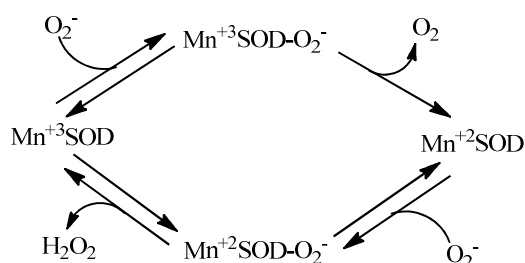


Figure I.10. Bioinorganic chemistry gain inspiration from metal active site of enzymes to design structural and functional model compounds.

Superoxide (O_2^-) is a harmful radical for living organisms and is generated by the single electron reduction of oxygen. Due to its high toxicity it needs to be transformed to less reactive species. Superoxide dismutases (SOD) are metalloenzymes which catalyze the dismutation of superoxide (O_2^-) to oxygen (O_2) and hydrogen peroxide (H_2O_2) (see Scheme I.9).¹¹⁸ This latter product can be degraded by catalase enzymes to water and oxygen. So, the SOD enzymes serve a vital role in defending oxygen-utilizing life forms from oxidative damage. There are three distinct families of SOD enzymes depending on which metal ion employs to mediate the chemistry: NiSODs, Cu,ZnSODs and Mn- or FeSODs.¹¹⁹ The active site of MnSOD contains a mononuclear five-coordinated Mn^{III} ion bound to three histidines, one aspartate residue and one water or hydroxide ligand.¹²⁰



Scheme I.9. Dismutation of the superoxide ion (O_2^-) to oxygen (O_2) and hydrogen peroxide (H_2O_2) catalyzed by MnSOD.

Manganese is also important in photosynthetic oxygen evolution in chloroplasts in plants. The oxygen-evolving complex (OEC) is a part of photosystem II contained in the thylakoid membranes of chloroplasts. It is responsible for the terminal photooxidation of two water molecules to molecular oxygen during the light reactions of photosynthesis. Based on many spectroscopic measurements it has been recognized that a tetranuclear Mn-cluster is the active catalyst for the oxygen evolution,¹²¹ which has been confirmed by the crystal structure of PSII (see Figure I.11).¹²² However, the exact mechanism of the water oxidation has not been elucidated so far.^{122c}

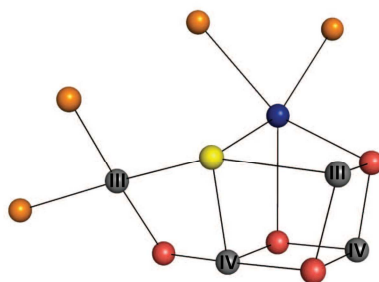


Figure I.11. Schematic representation of the atomic structure of the oxygen evolving complex OEC. Color codes for atoms: grey, manganese; blue, calcium; red, oxo- oxygen; yellow, oxygen; orange, water. Roman numerals in the grey spheres indicate the valences of the manganese atoms assigned by Suga et al.^{122c}

Catalases decompose hydrogen peroxide to water and oxygen¹²³ and some of these manganese enzymes have been isolated from different bacteria.¹²⁴ X-ray crystallographic structure analysis elucidated that these catalases contain a dinuclear manganese center.¹²⁵ During the catalytic process the dinuclear manganese active site cycle between the Mn^{II}_2 - and Mn^{III}_2 -oxidation states (see Figure I.12).¹²⁶

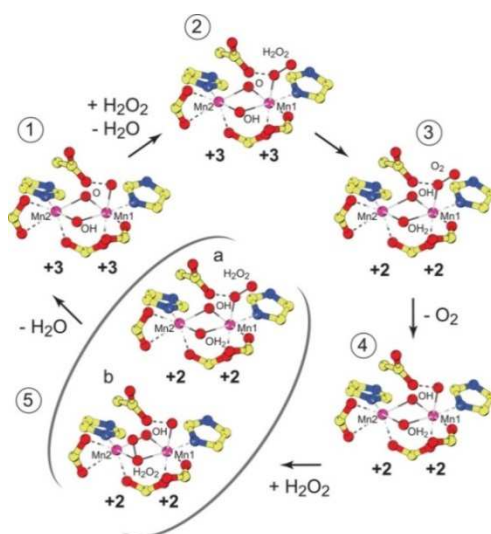


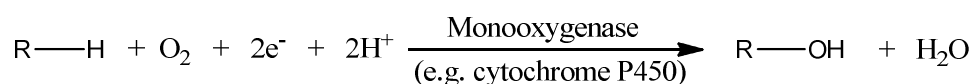
Figure I.12. Schematic representation of the proposed catalytic cycle for *Lactobacillus plantarum* manganese catalase.^{126b} Oxidative half-reaction: (1) resting oxidized $\text{Mn}_2(\text{III}, \text{III})$ state. (2) Terminal peroxide adduct. (3) Terminal dioxygen adduct. Reductive half-reaction: (4) resting or reduced $\text{Mn}_2(\text{II}, \text{II})$ state. (5) Activated hydrogen peroxide complexes: (a) terminally bound substrate; (b) $\mu 1,1$ bridging substrate.

Chapter I

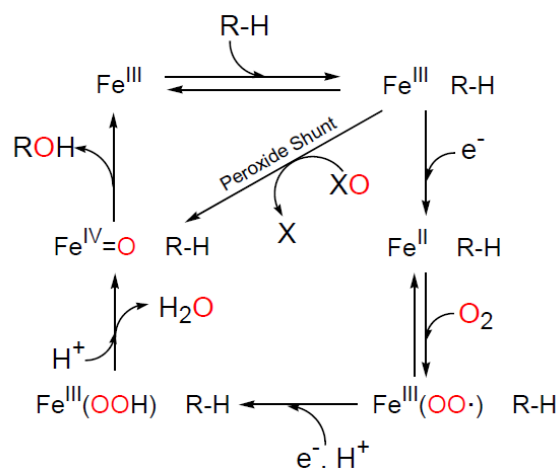
Many compounds containing a dinuclear manganese core surrounded by a variety of ligands have been employed as catalase mimic complexes.^{127a,128}

The development of artificial models of cytochrome P450 in oxidation reactions of organic substrates has also received a special attention.^{44c,129} Although iron models have received much more attention, synthetic manganese porphyrins have been extensively used as P450 models, and both Mn(IV)-oxo and Mn(V)-oxo porphyrin complexes have been characterized.¹³⁰

Nature is able to efficiently perform monooxygenation reactions by introducing one oxygen atom of molecular oxygen into a defined substrate, while the second oxygen atom of O₂ is eliminated as a water molecule with the associated consumption of two electrons provided by NAD(P)H:



Although many artificial systems based on molecular oxygen together with an electron source have been reported to catalyze hydroxylation and epoxidation reactions, it has been observed the formation of water as the main product instead of the expected alcohol or epoxide, via the 2e⁻ reduction of the intermediate metal-oxo species.¹³¹ An alternative way to avoid this difficulty is to use single oxygen atom donors such as hydrogen peroxide (H₂O₂), alkylperoxides (ROOH), iodosylbenzene (PhIO), hypochlorite (NaOCl), monopersulfate (KHSO₅) or peracids. The use of oxygen atom donors to generate the oxidized species is known as the “peroxide shunt” (Scheme I.10).¹³² In particular hydrogen peroxide is the suitable “green” oxidant since the only side product after an oxidation reaction is water. However, peroxides have weak and rather symmetrical O-O bonds. The low dissociation energy leads to spontaneous homolytic cleavage and the formation of hydroxyl radicals HO·. Alkylhydroperoxides ROOH can be easily cleaved by transition metal complexes and the resulting alkoxy radicals RO· are able to efficiently abstract hydrogen atoms from alkanes leading to a mixture of alcohols and ketones as in autoxidation reactions.¹³³



Scheme I.10. Catalytic cycle for oxygen activation and transfer by cytochrome P450.

Effective monooxygenase models are able to perform both hydroxylation of alkanes and epoxidation of olefins, since the active species is an electrophilic high-valent metal-oxo entity like in the corresponding metalloenzymes. The metal center is able to activate the oxidant and then to control the oxygen atom transfer from the metal-oxo species to the substrate (the oxygen rebound mechanism involves an organic radical intermediate controlled by the metal center, without formation of free radicals). All the different studies on the modeling of oxygenases clearly confirm that the coordination of olefins to the metal-oxo center is not necessary to produce epoxides.

All the biomimetic oxidations have largely contributed to the development of methods for the characterization of high-valent metal-oxo species¹³⁴ and to their chemical reactivity knowledge with respect to organic substrates,¹³⁵ although new studies are required to deepen in the processes and mechanisms.

Manganese complexes containing nitrogen-based ligands have emerged during the last decades as a very active and interesting compounds for oxidation catalysis, due to the well-known advantages such as chemical robustness or rich coordination chemistry of these ligands in combination with inexpensive first-row transition metal. The most developed systems are those based on sp^2 -hybridized nitrogen-donor atoms such as chiral oxazolines¹³⁶ or pyridines,^{137,138} porphyrines¹³³ and Salen ligands.¹³⁹ Specially, manganese complexes bearing non-heme ligands, such as salen-, Tacn^{140,141}-, N-based tetradentate^{55b,142} and bipyridine^{25b,142c,143}-derivated ligands (see Figures I.13-I.19), have shown a remarkable activity as catalysts in olefin epoxidation.¹⁴⁴

Chapter I

d) Salen-based ligands

In 1980, it was reported that catalytic amounts of manganese Schiff bases associated with sodium hypochlorite as oxygen source were able to epoxidize styrene (8 % yield after 3 hours).¹⁴⁵ Some years later, Kochi et al. used chromium¹⁴⁶ and manganese¹⁴⁷ Schiff base complexes as catalysts for olefin epoxidation in the presence of iodosylbenzene. Although the obtained yields were moderate, these preliminary works evidenced that Schiff base complexes were able to mimic the monooxygenase activity of heme proteins, in a similar way as synthetic metalloporphyrins. A few years after the discovery of Kochi, the groups of Katsuki¹⁴⁸ and Jacobsen¹⁴⁹ independently described a breakthrough in this olefin epoxidation by the introduction of a chiral functionality in the salen ligand. This fact was the starting point for many researchers to develop new chiral manganese systems capable to epoxidize olefines in an enantioselective way, in the presence of iodosyl-derivatives,^{148,149,150} sodium hypochlorite¹⁵¹ or MCPBA¹⁵² as the oxygen donor atom.

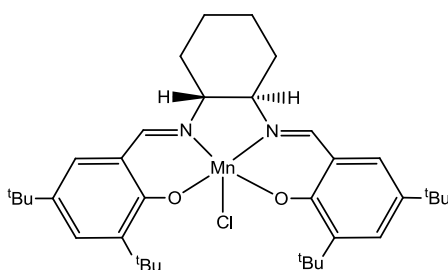


Figure I.13. Structure of the best Jacobsen's catalyst prepared on a large scale^{151c} and currently commercially available.

In order to improve the activity and selectivity, and to broaden the scope of substrates, an optically active binaphthyl moiety was introduced in the structure of the salen-based ligand,¹⁵³ but the manganese complexes obtained displayed poor catalytic activity and enantioselectivity probably due to extensive degradation of the manganese binaphthyl-based compounds under the oxidation reaction conditions (NaOCl, H₂O₂ or MCPBA as oxidant).

In overall, all these compounds showed higher ee's and yields compared to porphyrin complexes, but they also presented several limitations: a relatively limited substrate scope (especially in the epoxidation of terminal olefins), relatively high catalyst loading requirement (5-10 %) and an easy catalyst degradation.

e) N-based tetradentate ligands

In 2003 Stack et al. presented a new tetradentate N-donor system that, when coordinated to manganese, was able to catalyze epoxidation of terminal olefins with peracetic acid (PAA), with 400-1000 TON in only 5 minutes.^{55b} This new family of manganese compounds were more stable than those reported earlier under the acidic conditions created by PAA, and so allowed an efficient epoxidation reaction with a catalytic load range between 0.02-0.1 mol %.

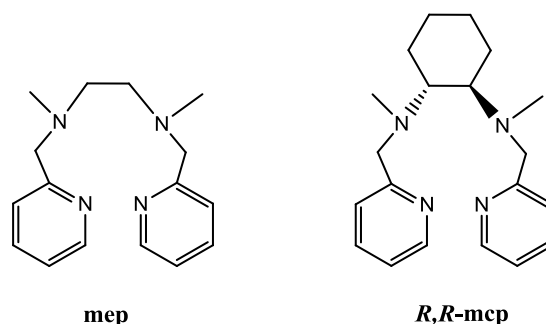


Figure I.14. Some ligands used by Stack and co-workers, to synthesize new manganese N-based complexes able to oxidize terminal olefins with PAA as oxidant.^{55b,142e}

These N-tetradentate based complexes showed a remarkable activity towards the epoxidation of some terminal olefins. For example, in the case of 1-octene, the manganese complex $[\text{Mn}^{\text{II}}(\text{R,R-mcp})(\text{CF}_3\text{SO}_3)_2]$ (0.1 mol %) achieved a conversion of 98 % and 94 % yield in the epoxide product within 5 minutes of reaction at room temperature, in acetonitrile and with PAA as oxidant.^{142e}

More recently, Pfaltz et al. reported a system based on 4N diamino-bisoxazoline manganese complexes. Modest stereoselectivity (up to 21 %) was observed using PAA as oxidant.^{142,154}

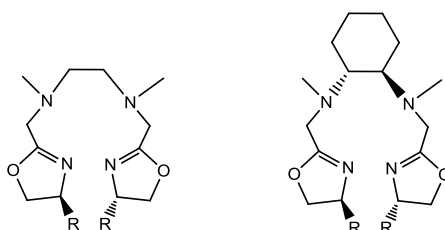


Figure I.15. Structure of the ligands reported by Pfaltz.

In 2012, Palaniandavar et al. presented a series of Mn(II) complexes containing tetradentate 4N ligands with systematically varied diazacycloalkane backbones, that were studied in the epoxidation of cyclohexene, styrene and *cis*-cyclooctene by using PhIO as the oxygen source in acetonitrile. They observed that the epoxide yield and product selectivity increase upon increasing the Lewis acidity of the Mn(II) center, modified by the variation of the

Chapter I

diazacycloalkane ligand backbone.^{142b} For the *cis*-cyclooctene substrate, they obtained moderate conversions (21-54 %) and excellent selectivities (100 %) for the *cis*-epoxide product.

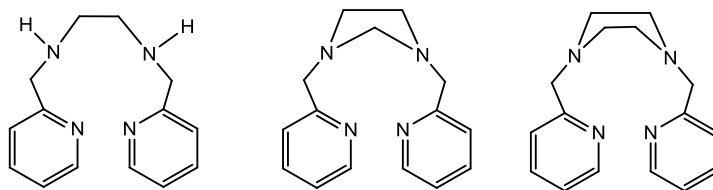


Figure I.16. Structure of some ligands reported by Palaniandavar and co-workers.

f) Bipyridine-based ligands

Among the catalysts screened by Stack and co-workers, complex $[\text{Mn}(\text{bpy})_2(\text{CF}_3\text{SO}_3)_2]$, together with $[\text{Mn}(\text{R,R-mcp})(\text{CF}_3\text{SO}_3)_2]$ and $[\text{Mn}(\text{phen})_2(\text{CF}_3\text{SO}_3)_2]$ (phen= 1,10-phenanthroline), showed the highest catalytic activity in epoxidation of alkenes, obtaining with the bipyridylic complex a conversion of 99 % and yield of 95 % (> 1000 TON/min) with 1-octene as substrate using PAA previously prepared from acidic resins.^{142c,e} Later studies demonstrated that trinuclear $[\text{Mn}_3(\text{L}_2)(\text{OAc})_6]$, complexes containing a neutral bidentate nitrogen ligand, are also highly efficient catalysts in the epoxidation of alkenes using PAA.¹⁵⁵ So, taking into account these precedents, the bipyridine (bpy) core appeared to be an ideal candidate about with develop new and better catalytic systems.

Watkinson and co-workers reported in 2008 a preliminary investigation into a rationally designed catalytic system for the epoxidation of alkenes based on a bipyridyl core.¹⁵⁶ They developed a series of new manganese compounds containing bipyridine-based ligands and tested them in the catalytic epoxidation of alkenes substrates, such as styrene, *cis*-cyclooctene and 1-octene, in acetonitrile using PAA as the oxygen source. They obtained moderate to good conversions and yields, except when 1-octene was the substrate (in this case no conversion was observed), but with a long reaction times (4 - 16 h of reaction for 1 mol % of catalyst).

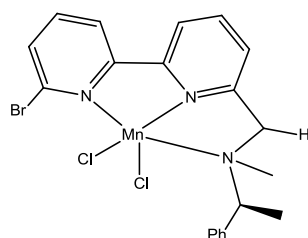


Figure I.17. Structure of a bipyridine-based manganese complex described by Watkinson et al.

Manganese complexes with electronically modified phen ligands were synthesized and described by Jiang et al. in 2012.^{142d} Electronic perturbations were introduced at the 5-position of the phen ligands in order to minimize the influence of the steric effects on the alkene epoxidation. Each of the $[\text{Mn}(\text{R-phen})_2\text{Cl}_2]$ compounds ($\text{R} = \text{NH}_2, \text{CH}_3, \text{H}, \text{NO}_2$) were able to catalyze the epoxidation of alkenes by PAA. Unexpectedly, the more electron-rich ligands lead to faster reactivity with the alkenes investigated, which suggest that $[\text{Mn}(\text{phen})_2\text{Cl}_2]$ and related complexes may oxidize alkenes to epoxides through a different pathway than Mn(III)-salen catalysts.

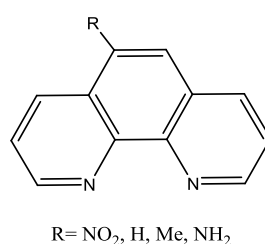


Figure I.18. 1,10-phenanthroline ligand and its derivatives used by Jiang et al.

Finally, in our group new Mn(II) complexes containing the bidentate polypyridylic chiral ligand (-)-L ((-)-L = (-)-pinene[5,6]bipyridine), were synthesized and tested towards the epoxidation of some alkenes.¹³⁷ These complexes displayed a good efficiency in the epoxidation of aromatic olefins and complete stereoselectivity in the epoxidation of *cis*- β -methylstyrene as substrate, using PAA as oxidant. This work pointed out that, although triflate Mn complexes have been extensively tested as epoxidation catalysts (sometimes invoking the lability of the monodentate triflate ligands), chlorido complexes proved to be better catalysts for styrene epoxidation than the triflate analogues.

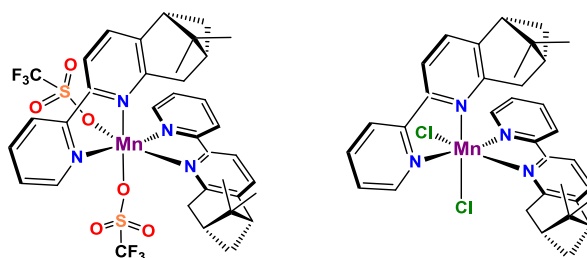


Figure I.19. Structure of the complexes containing the (-)-L chiral ligands.

The catalytic epoxidation activity of these complexes was studied in CH_3CN using commercial peracetic acid (32 %) as oxidant, both in the absence and in the presence of two different additives, imidazole and NaHCO_3 , at room temperature for 3 h. For styrene, the conversion with the chlorido complex was 70 %, whereas only a 24 % was achieved in the same conditions

Chapter I

by the triflate complex. The selectivity was also much better for the chlorido complex (74 %) than the obtained with the triflate complex (33 %).

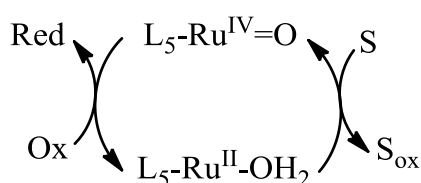
I.3.3.2. Ruthenium in oxidation catalysis

The $\text{Ru}^{\text{IV}}=\text{O}$ complexes are able to act as efficient oxidants for a wide range of substrates.¹⁵⁷ Firstly, as mentioned above, the oxo group stabilizes high oxidation states and makes them accessible at fairly low potential. In addition, from the mechanistic point of view, its ability to accept two electrons can avoid radicalary reaction pathways of high energy and reactivity.^{158(a,b),159} Finally, the robust character of the first coordination sphere of these complexes makes possible the easy exchange between $\text{Ru}(\text{II})$ and $\text{Ru}(\text{IV})$ without any dramatic changes in the catalyst structure, the oxo group being the only that modifies its environment.

Among the oxidation reactions promoted by $\text{Ru}^{\text{IV}}=\text{O}$ complexes, the oxidation of alkenes, the epoxidation of alkenes, the cleavage of double bonds, the oxidation of alcohol and ethers and the oxidation of amines and amides can be pointed out. The orbital and energetic properties of $\text{Ru}^{\text{IV}}=\text{O}$ promote different mechanistic pathways, including outer-sphere electron transfer, proton-coupled electron transfer, electrophilic ring attack, oxo transfer, hydride transfer and C-H insertion.

Among different oxidation agents used in the catalysis with oxocomplexes, PhIO and $\text{PhI}(\text{OAc})_2$, two electrons oxidation agents, remain the most effective in the oxidation of organic substrates in the presence of ruthenium complexes.¹⁶⁰

The catalytically active $\text{Ru}=\text{O}$ species act as excellent catalysts for the oxidation of different organic substrates following the catalytic cycle shown in Scheme I.11. In this cycle the catalytic oxidation of the substrate is simultaneously accompanied by the reduction of ruthenium complex from oxidation state +IV to +II.



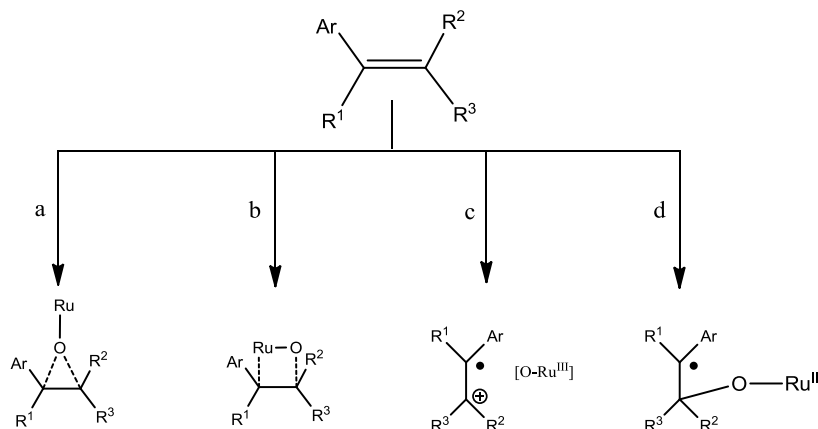
Scheme I.11. Scheme of a catalytic cycle of oxidation of a substrate (S) with $\text{Ru}^{\text{IV}}=\text{O}$ species.

Ruthenium complexes have proved efficient in the epoxidation of different olefins with relatively high selectivities,¹⁶¹ and a huge variety of ruthenium oxocomplexes with different oxidants as oxygen source have been described in the literature.¹⁶² One of the first examples of

the epoxidation by these kind of compounds was described by Griffith et al. Complex $[\text{Ru}(\text{O}_2)(\text{bpy})\{\text{IO}_3(\text{OH})_3\}]$ showed a great performance for the oxidation of different olefins in the presence of NaIO_4 and the *N*-methylnmorpholine *N*-oxide (NMO) as a co-oxidant.¹⁶³ Also, Che et al. presented in 1998 the $[\text{Ru}^{\text{IV}}(\text{ppz})(\text{bpy})\text{O}](\text{ClO}_4)_2$ complex (in where ppz= 2,6-bis[(4*S*,7*R*)-7,8,8-trimethyl-4,5,6,7-tetrahydro-4,7-methaneindazol-2-yl]pyridine) which is capable of oxidizing, stoichiometrically, different aromatic olefins.¹⁶⁴

It is believed that the oxygen atom transfer involves a side-on approach of the olefin to the Ru(IV) active site. This kind of approach explains the lower enantioselectivities generally observed for *trans*-olefins compared to *cis*-olefins, both with porphyrin-based complexes and Jacobsen type salen ligands, since the approach of *trans*-olefins is clearly more hindered.

Different mechanisms, concerted and non-concerted, have been proposed as possible pathways for oxygen atom transfer (Scheme I.12): direct transfer through a concerted oxene insertion (a); by the formation of a 4-member ring where both Ru and O atoms are respectively bonded to the C α and C β of the olefin (b); through a single electron transfer with the formation of a radical cation (c); or through the formation of a benzylic radical intermediate (d).¹⁶⁴

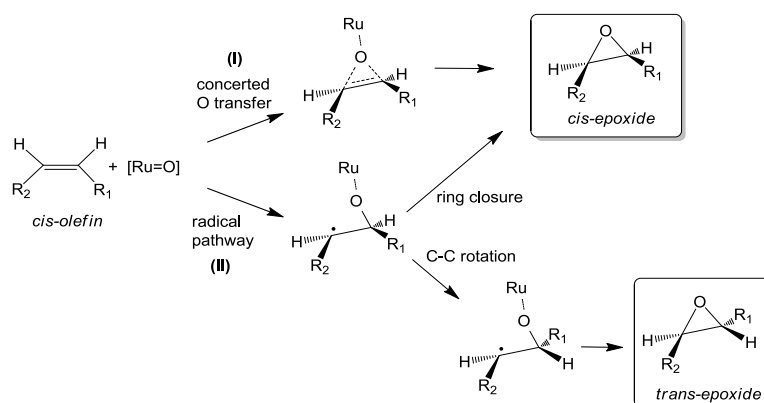


Scheme I.12. Proposed mechanistic pathways for oxygen atom transfer process.

The use of *cis*-alkenes, such as *cis*- β -methylstyrene, is known to be useful for determining whether a concerted or non-concerted pathway takes place.¹⁶⁵ If the epoxidation of the *cis*-alkene takes place in a non-concerted pathway (pathways c and d, Scheme I.12), involving a breakage of the C=C π bond, a mixture of the *cis* and *trans*-epoxide products can be obtained by the possible isomerization by the rotation of the C-C bond due to the formation of an acyclic radical intermediate. On the contrary, if the epoxidation takes place in a concerted pathway (pathways a and b, Scheme I.12), only the *cis*-epoxide product will be obtained.

Chapter I

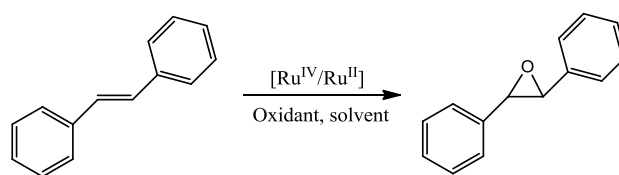
Stereoselectivities for *cis*-alkene epoxidations vary with both *cis*-alkenes and ruthenium oxidants. In the epoxidation of *cis*- β -methylstyrene mixtures of *cis* and *trans*-epoxides were observed (*cis*: *trans* ratios varying from 2:1 to 5:1). This loss of stereospecificity could not be explained with a concerted insertion of Ru^{IV}=O into the C=C bond (path a, Scheme I.12) and, hence, a non-concerted pathway was proposed. Scheme I.13 shows the radical mechanism of epoxidation reaction and the different possible products.



Scheme I.13. Proposed mechanism for the oxidation of aromatic olefins by ruthenium(IV) oxocomplexes.

Recently, Chatterjee has shown that for Ru-aqua complexes with general formula [Ru(T)(D)OH₂] (T= tridentate ligand and D= bidentate ligand), the geometry of the tridentate ligand and the electronic nature of the bidentate ligand play a key role in the catalytic performance of complexes in the epoxidation reactions. Indeed, the facial coordination of a tridentate ligand can make stereochemically easy the contact between the organic substrate and the catalytic species. The electrophilic character of ruthenium can be modulated by the auxiliary bidentate ligand. Thus, a good π -acceptor bidentate ligand would make electron deficient the ruthenium center, while a good σ -donor ligand could increase the electron density, then reducing the tendency of the metal center to have a reduction via electron transfer through the external sphere, thus allowing the ruthenium to act as epoxidation catalyst instead of hydroxylation.¹⁶⁶

In Table I.3 some examples of the effects of ligands on the reactivity of the ruthenium complexes in the case of the epoxidation of *trans*-stilbene are shown.

Table I.3. Ligand effects on the epoxidation of *trans*-stilbene with Ru-aqua complexes.¹⁵

| Entry | Complex | Oxidant | Yield (% <i>trans</i> -stilbene) | Ref. |
|-------|---|-----------------------|----------------------------------|------|
| 1 | [Ru ^{II} (trpy)(bpy)OH ₂] ²⁺ | NaOCl | 7 | 167 |
| 2 | [Ru ^{II} (trpy)(pic)OH ₂] ²⁺ | t-BuOOH | 55 | 168 |
| 3 | [Ru ^{II} (trpy)(phbox- <i>i</i> Pr)OH ₂] ²⁺ | PhI(OAc) ₂ | 37 | 169 |
| 4 | [Ru ^{II} (trpy)(box-C)OH ₂] ²⁺ | PhI(OAc) ₂ | 13 | 170 |
| 5 | [Ru ^{II} (tpm)(box-C)OH ₂] ²⁺ | PhI(OAc) ₂ | 61 | 170 |

Abbreviations: pic = picolinate; phbox-*i*Pr = 1,2-bis[4'-alkyl-4',5'-dihydro-2'-oxazolyl]benzene; box-C = 4,4'-dibenzyl-4,4',5,5'-tetrahydro-2,2'-bioxazole.

The substitution of a neutral bpy ligand (entry 1) by a stronger σ -donor pic ligand (entry 2) leads to improve the catalytic performance from 7 to 55 %. This could be explained by the fact that the ruthenium electron density increases due to the important donor effect of the anionic pic ligand, which facilitates the attack of the ruthenium to the substrate, whereas the π -acceptor nature of the phbox-*i*Pr ligand makes electron deficient the metal center and causes a yield reduction (entry 3).

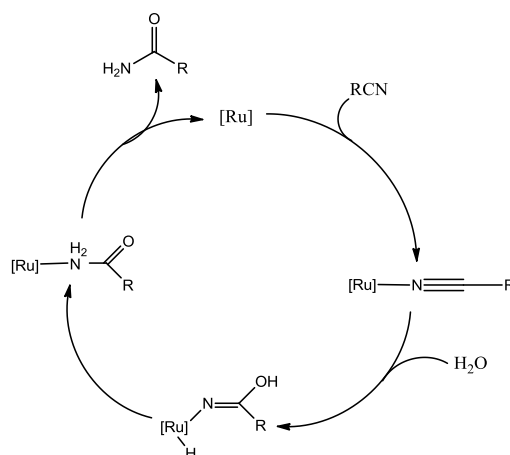
The change in the geometry of the tridentate ligand could also have an important influence on reactivity. Thus facial disposition of tpm ligand, unlike the meridional disposition of trpy ligand, promotes contact between the substrate and the active group Ru=O which leads to an increased yield (61 %) (entries 4 and 5).

I.3.3.3. Hydration of nitriles catalyzed by ruthenium complexes

The first example of a ruthenium complex which was able to catalyze the hydration of nitriles was described by Taube and co-workers in the 1970s.¹⁷¹ This system worked in a stoichiometric amount of [RuCl(NH₃)₅]Cl₂ together with Ag₂O, trifluoroacetic acid and zinc amalgam in CH₂Cl₂, obtaining in high yields the corresponding amide products from aromatic, aliphatic and α,β -unsaturated nitrile substrates. However, it was not until 1992 that the first truly catalytic system could be developed by Murahashi and co-workers employing the ruthenium dihydride complex [RuH₂(PPh₃)₄] as catalyst.¹⁷² This catalytic system worked under neutral conditions in

Chapter I

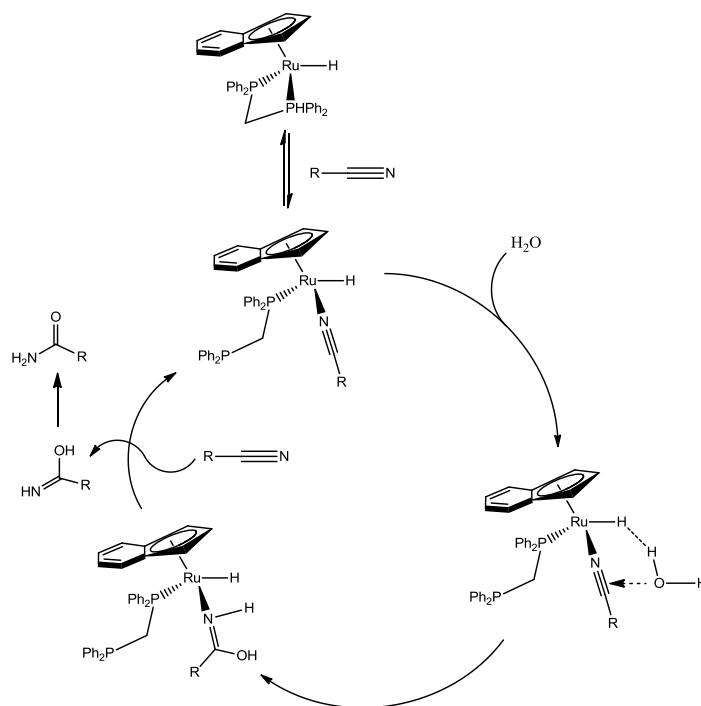
1,2-dimethoxyethane (DME), and showed an excellent functional group tolerance, therefore expanding its applicability in the syntheses of complex organic molecules and natural products. A reaction pathway involving the intermolecular nucleophilic addition of water to the coordinated nitrile, to give an iminol complex, was proposed (Scheme I.14). Reductive elimination, isomerization of the iminol to the amide and subsequent dissociation regenerates the catalytically active ruthenium species.^{172c}



Scheme I.14. The reaction pathway proposed by Murahashi and co-workers for the catalytic hydration of nitriles by $[\text{RuH}_2(\text{PPh}_3)_4]$ complex.

It is commonly accepted that the nitrile substrate has to coordinate firstly to the metal, activating the CN bond towards the nucleophilic addition of water (or the hydroxyl group if basic conditions are used), and obtaining the amide product, thus enhancing the rate of the hydration step.¹⁷³

The half-sandwich hydrido-ruthenium(II) complex $[\text{RuH}(\eta^5\text{-C}_9\text{H}_7)(\text{dppm})]$ (dppm = bis(diphenylphosphino)methane; C_9H_7 = indenyl) revealed also as a quite effective catalyst for the selective conversion of nitriles to amides in water.¹⁷⁴ Worthy of note, its chlorido counterpart $[\text{RuCl}(\eta^5\text{-C}_9\text{H}_7)(\text{dppm})]$ was found to be completely ineffective, suggesting that the hydride ligand plays a key role during the catalytic event. To clarify this point, Density Functional Theory (DFT) calculations were performed, pointing out an unusual promoting effect of the hydride (Scheme I.15). Hydride ligand activates the incoming water molecule through a $\text{Ru-H}\cdots\text{H-OH}$ dihydrogen-bonding interaction, favoring the nucleophilic attack of water on the coordinated nitrile. In this rate-determining step, an iminol intermediate is produced, which quickly tautomerizes to amide upon dissociation. Remarkably, despite the known tendency of the indenyl ligand to undergo $\eta^5\text{-}\eta^3$ slippage,¹⁷⁵ the DFT calculations indicated that coordination of the nitrile to ruthenium takes places by dissociation of one arm of the diphosphine dppm.



Scheme I.15. Promoting effect of the hydride ligand of $[\text{RuH}(\eta^5\text{-C}_9\text{H}_7)(\text{dppm})]$ complex during the catalytic hydration of nitriles.

The same promoting effect of the hydride ligand, via $\text{Ru-H}\cdots\text{H-OH}$ dihydrogen-bonding, was evidenced by means of DFT calculations in the reaction of the isoelectronic hydro(trispyrazolyl)borate complex $[\text{RuH}(\text{Tp})(\text{PPh}_3)(\text{NCMe})]$ with water.¹⁷⁶ Both complexes are able to promote the selective conversion of several organonitriles to the corresponding primary amides in 1,4-dioxane/water mixtures. However, modest results in terms of activity were in general obtained.

The tetranuclear cluster and the mononuclear derivative shown in Figure I.20 are additional examples of hydrido-ruthenium complexes which are able to promote the selective hydration of CN bonds. These systems work in *i*PrOH, THF, acetone or DME as solvent and 10 to 20 equivalents of water. In the case of the tetranuclear cluster, amides were obtained in excellent yields, whereas the mononuclear complex showed a remarkably lower activity.

Chapter I

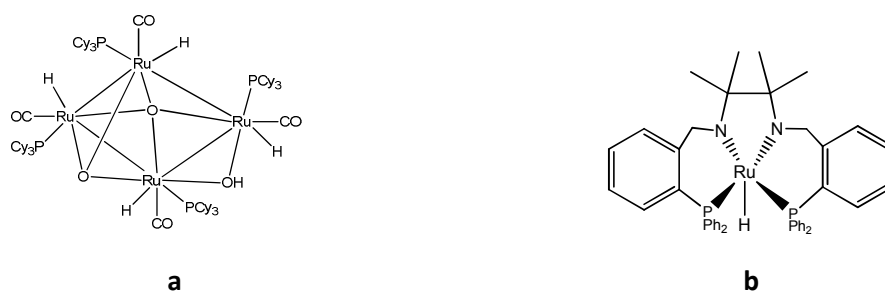


Figure I.20. Structure of ruthenium hydride complexes: tetranuclear cluster (a) and mononuclear complex (b).

Oshiki and co-workers evidenced the key role played by the auxiliary ligands in this catalytic transformation.¹⁷⁷ Complex cis -[Ru(acac)₂(PPh₂py)₂] was able to hydrolize efficiently a large number of nitriles employing DME as solvent and 4 equivalents of water. However, when complexes cis -[Ru(acac)₂(PPh₃)₂], cis -[Ru(acac)₂(PMe₃)₂] and cis -[Ru(acac)₂(PBu₃)₂] were used, which contain non-cooperative ligands,^{177b} mediocre results were obtained. This fact can be explained in terms of *bifunctional catalysis*, in which the substrates are activated by the combined action of the metal, which acts as a Lewis acid, and the ligand (in this case a pyridyl ring), that acts as a Lewis base. Such a concept has been largely exploited in homogeneous catalysis during the last years.¹⁷⁸

Inspired by the works of Oshiki and co-workers, Smejkal and Breit described the preparation and catalytic behaviour of the bis(acetylacetonate)-ruthenium(II) complexes bearing the potentially cooperative P-donor ligands 6-diphenylphosphino-*N*-pivaloyl-2-aminopyridine and 3-diphenylphosphinoisoquinoline (Figure I.21).¹⁷⁹ All of them were able to catalyze selectively the model substrate 4-methylbenzotrile. However, under the same reaction conditions, their effectiveness was comparatively lower to that shown by complex cis -[Ru(acac)₂(PPh₂py)₂].

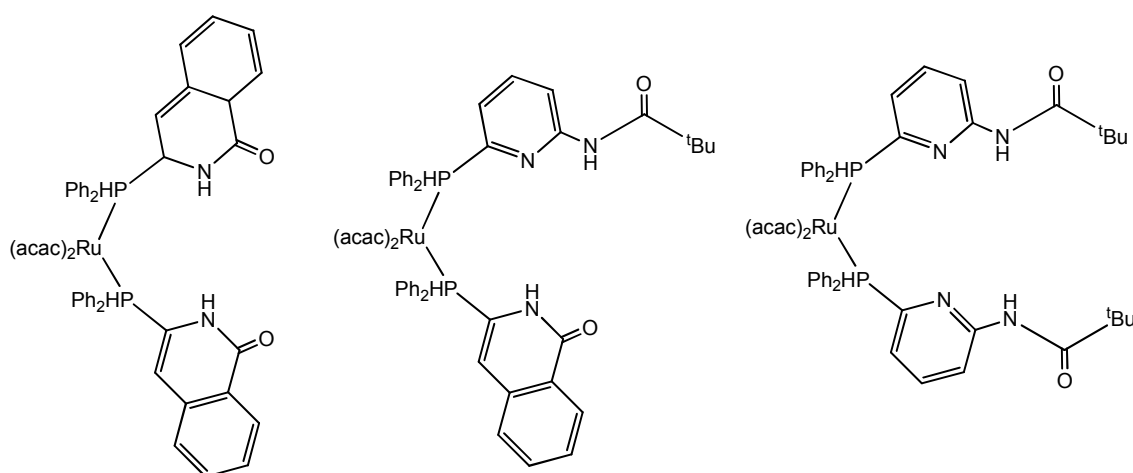


Figure I.21. Structure of the bis(acac)-ruthenium(II) complexes.

Most of the known homogeneous catalysts for nitrile hydration, including the examples commented above, operate in organic media in the presence of only small amounts of water. Therefore, in the search for cooperative effects of the ligands and being environmentally concerned, the catalytic behaviour of different arene-ruthenium(II) complexes with potentially H-bond accepting amino-aryl-phosphines was also explored by Crochet, Cadierno and co-workers.¹⁸⁰ All these complexes (5 mol %) were able to hydrolyze the model substrate benzonitrile in pure water as solvent.

In order to facilitate the solubility of the catalysts in water, remarkable efforts have been devoted in recent years to the study of ruthenium complexes bearing water-soluble phosphines. In this context, a possible cooperative effect of the “cage-like” phosphines 1,3,4-triaza-7-phosphaadamantane (PTA), 1-benzyl-1-azonia-3,5-diaza-7-phosphaadamantyl (PTA-Bn), 3,7-Diacetyl-1,3,7-triaza-5-phosphabicyclo[3.3.1]nonane (DAPTA), 2,4,10-trimethyl-1,2,4,5,7,10-hexaaza-3-phosphatricyclo[3.3.1.1(3,7)]decane (THPA) and 2,3,5,6,7,8-hexamethyl-2,3,5,6,7,8-hexaaza-1,4-diphosphabicyclo[2.2.2] octane (THDP),^{17b,181} via H-bonding of the nucleophilic water molecule with the nitrogen atoms present in their structures, has been proposed to explain the remarkably high effectiveness shown by the arene-ruthenium(II) (Figure I.22) and bis(allyl)-ruthenium(IV) complexes.¹⁸² All of these catalytic systems work in pure water solvent without the addition of any amount of acid or base, showing a wide substrate scope and high tolerance to common functional groups. In addition, after selective crystallization of the final amide, recycling of the aqueous phase containing the active species could also be demonstrated for $[\text{RuCl}_2(\eta^6\text{-C}_6\text{Me}_6)(\text{PTA-Bn})]$.^{182a}

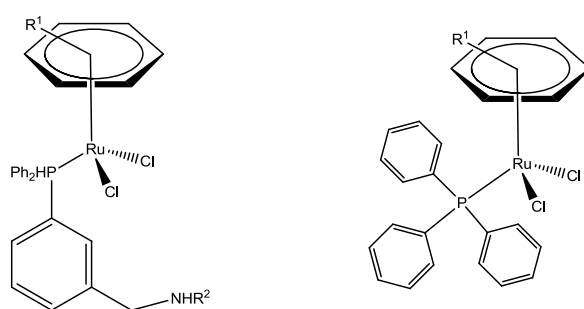


Figure I.22. Examples of arene-ruthenium(II) complexes.

Cadierno et al.¹⁸³ developed a new class of water-soluble phosphine ligands, consisting of N-protonated thiazolyl-phosphine salts (Figure I.23). One of them turned out to be an excellent auxiliary ligand in the ruthenium-catalyzed selective hydration of nitriles to primary amides in environmentally friendly aqueous medium. In addition, the high solubility of complex in water

Chapter I

allowed a facile amide product separation (by selective crystallization), and the effective reuse of the remaining aqueous solution containing the catalyst.

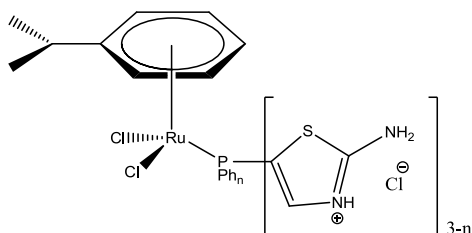


Figure I.23. Structure of water-soluble arene-ruthenium(II) complexes reported by Cadierno et al.¹⁸³

Finally, more recently our group reported a new class of phosphine-free ruthenium(II) catalysts containing N- or S- ligands.¹⁸⁴ For the first time, Ru-dmsO complexes were used as mediator complexes in nitrile hydration. The Ru-dmsO complexes described contained the non-symmetric bidentate ligand 2-(3-pyrazolyl)pyridine (*pypzH*), and a variety of monodentateazole ligands (Figure I.24). All complexes showed an excellent performance regarding to the selective hydration of nitriles in a pure water medium.

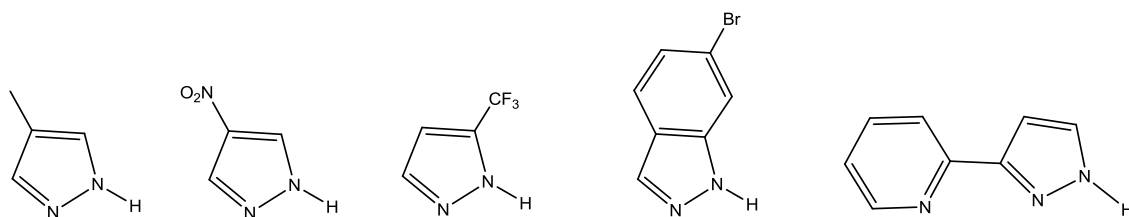


Figure I.24. Pyrazole-based ligands used in the synthesis of Ru-dmsO complexes described by Ferrer et al.¹⁸⁴

All compounds displayed good selectivity for the amide products and was demonstrated the promising potential of this kind of Ru-dmsO complexes towards the hydration of nitriles in environmentally friendly media.

I.3.4. Heterogeneous catalytic systems for oxidation reactions

Oxidation catalysis requires of the participation of an oxo-metal complex or another metal-oxygen bond, so the inhibition of undesired self-interactions between catalyst molecules will lead to the enhancement of their stability. In consequence, the heterogenization of the catalyst seems to be a suitable strategy to prevent its deactivation, either by ligand oxidative degradation or by formation of μ -oxo-bridged dimers or other oligonuclear species.

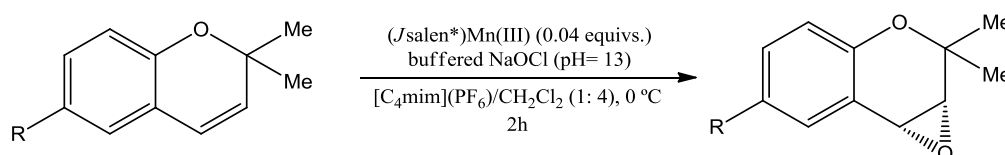
The range of immobilized catalysts used to perform the epoxidation of olefins is broad. Among the metals used we can find manganese,¹⁸⁵ iron,^{185d,186} titanium,¹⁸⁷ cobalt,¹⁸⁸ molybdenum,¹⁸⁹ vanadium,¹⁹⁰ tungsten¹⁹¹ and ruthenium.¹⁹² The immobilizing methods used involves tethering

procedures on functionalized silica surfaces and on PVA polymers, as well as using functionalized silica-coated magnetic nanoparticles.^{39b,193}

Heterogenized catalyst have been active in oxidation of alcohols,^{30a,194} olefins,¹⁹⁵ organic sulfides,¹⁹⁶ phenol¹⁹⁷ and aromatic C-H.¹⁹⁸ They also show activity in allylic oxidation¹⁹⁹ and dihydroxylation.²⁰⁰ Some examples of heterogenized Mn and Ru catalysts are described below.

I.3.4.1. Manganese compounds immobilized in ionic liquids as catalysts for oxidation reactions

In 2000, Song et al. reported the first example of a transition metal catalyzed oxidation reaction in an ionic liquid, describing a procedure to recycle an achiral Jacobsen-type (salen)Mn(III) epoxidation catalyst (Scheme I.16).²⁰¹ In that case, the asymmetric epoxidations were carried out at 0 °C in [bmim](PF₆): CH₂Cl₂ (1: 4 v/v), with NaOCl as the oxidant. Dichloromethane was added as a co-solvent in order to avoid the IL solidification at the reaction temperature. The authors described a clear enhancement of the catalyst activity by the addition of the ionic liquid to the organic solvent. In the presence of the ionic liquid a 86 % conversion of 2,2-dimethylchromene was observed after 2 h. In contrast, without the ionic liquid, the same conversion was achieved after 16 h. In both cases the enantiomeric excess was as high as 96 %. Moreover, the use of the ionic liquid solvent allowed an easy catalyst recycling without any modification or further treatment. However, after five recycles under the same conditions, the conversion dropped from 83 % to 53 %. The authors explain this loss in activity by a slow degradation of the [Mn^{III}(salen)] complex.

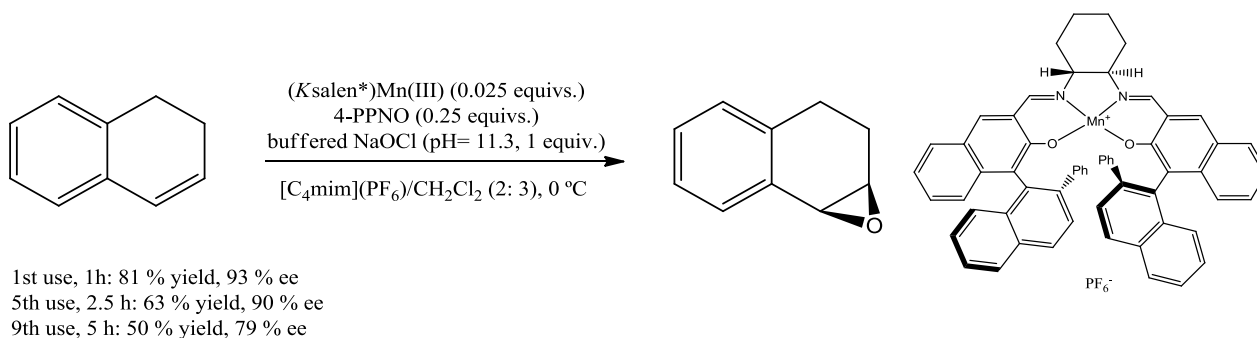


R= H: 86 % yield, 96 % ee (5th use: 53 % yield, 86 % ee)
R= CN: 72% yield, 94 % ee

Scheme I.16. Epoxidation with Jacobsen-type catalyst in IL.

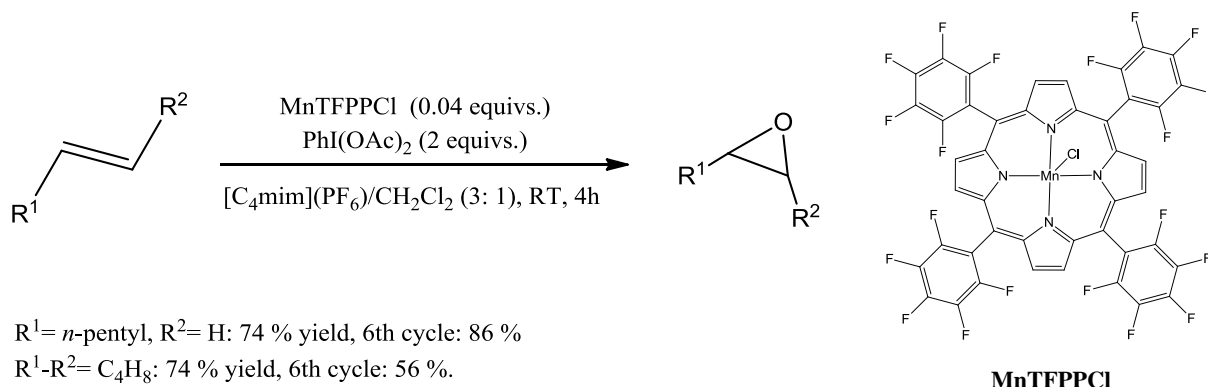
Smith et al. used a chiral Katsuki-type (salen)Mn(III) catalyst for the epoxidation at 0 °C of 1,2-dihydronaphthalene with NaOCl, in a mixture of [bmim](X) (X= PF₆ or BF₄) and an organic solvent (CH₂Cl₂ or EtOAc), in the presence of 4-phenylpyridine-N-oxide (4-PPNO) (Scheme I.17). A higher reactivity and similar ee's were achieved when compared to those obtained in chlorinated solvents. Under identical experimental conditions, (Ksalen*)Mn(III) provided a higher yield and enantioselectivity than (Jsalen*)Mn(III) but required a longer reaction time. Up to 100 % ee was obtained under some specific conditions.²⁰²

Chapter I



Scheme I.17. Epoxidation with Katsuki-type catalyst in IL.

Manganese porphyrins in a mixture of [bmim](PF₆) and CH₂Cl₂ were used, at room temperature, by Xia et al. for the efficient catalytic epoxidation of various alkenes with iodosylbenzene diacetate, this latter being more efficient than PhIO (Scheme I.18). Also, an effective recycling of the catalytic system was obtained.²⁰³



Scheme I.18. Epoxidation with manganese porphyrins in IL.

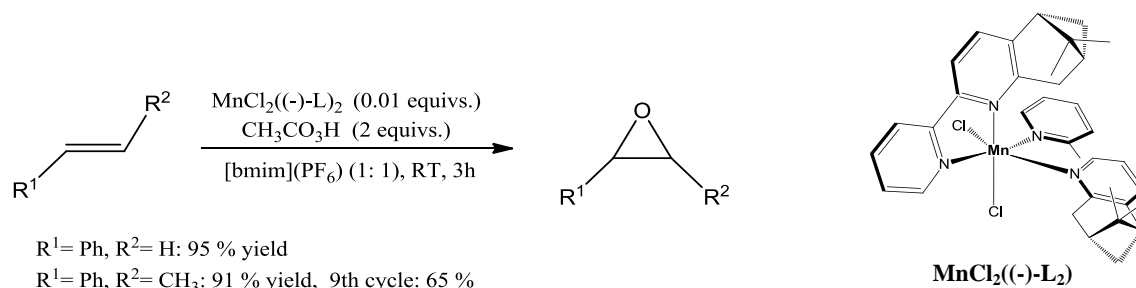
Since then, ILs have been successfully applied in olefin epoxidations, using manganese(III) catalysts with porphyrins of Schiff base ligands.^{22,204}

Moreover, effective epoxidation of various alkenes was accomplished at room temperature in [bmim](BF₄) with aqueous hydrogen peroxide, in the presence of catalytic amounts of manganese sulfate and a stoichiometric quantity of tetramethylammonium hydrogen carbonate. Good conversions and high selectivities were generally obtained, except for the case of an inactivated terminal alkene such as 1-decene, which was unmodified, and 1-phenylcyclohexene. For recycling experiments, some amounts of MnSO₄ and Me₄NHCO₃ must to be added from time to time to restore the activity of the system.²⁰⁵

The asymmetric epoxidation of limonene was investigated by the group of Bernardo Gusmano et al. They used the Jacobsen's Mn(Salen) catalyst and hydrogen peroxide as oxygen source. The catalytic procedure was performed in [bmim](BF₄) and resulted in a high diastereomeric excess of 74 % to the respective 1,2-epoxy-p-ment-8-enes, while the conversion was 70 %.²⁰⁶ Also, a Mn(salen) catalyst was used for the oxidation of styrene with molecular oxygen to benzaldehyde.²⁰⁷

Finally, in 2010 Wong et al. reported a novel and robust IL system for the rapid epoxidation of a number of aliphatic terminal alkenes under relatively mild conditions using manganese(II) acetate as an effective ligand-free catalyst precursor, with peracetic acid as oxidant.^{25a}

Recently our group has described the epoxidation activity of two manganese(II) complexes containing (-)-L ligand^{25b} in [bmim](PF₆)/CH₃CN media that constitute some of the scarce systems evaluated to date as epoxidation catalysts in such media (Scheme I.19). The Mn(II) chlorido complexes showed a remarkable effectiveness and selectivity for the epoxide product as well as a good degree of reusability.



Scheme I.19. Epoxidation with manganese(II) compounds bearing bypipinene* ligands.

I.3.4.2. Manganese compounds as supported catalysts for oxidation reactions

Previously, it has been explained that the homogeneous catalysts limitations, such as their low average life-time and the non-easy recovery and recyclability, can be avoided by attaching them onto a solid support. In this context, the first reports found in the literature for Mn complexes used metalloporphyrins bounded to silica as catalysts for oxidation reactions, with PhIO or H₂O₂ as the oxygen source²⁰⁸, since some synthetic metalloporphyrins have been found to be highly efficient homogeneous oxidation catalysts, and the solid support can act in some way analogously as the protein matrix of hemoproteins in respect of sterical hindrance and electronic effects.²⁰⁹

Chapter I

Vinhado et al. reported the preparation of three supported cationic manganese(III) porphyrins bounded to a bis-functionalized silica (see Figure I.25) as catalysts for hydrocarbons oxidation, using PhIO and H_2O_2 as oxidants.^{208c} In this case, the support provide two important benefits: (a) the sulfonatophenyl groups ensure a securely anchoring by electrostatic interactions and (b) the propylimidazole groups act as proximal ligands to the Mn(III), reflecting the role of histidine in some enzymes.

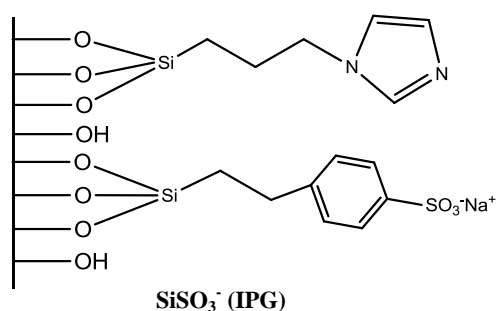
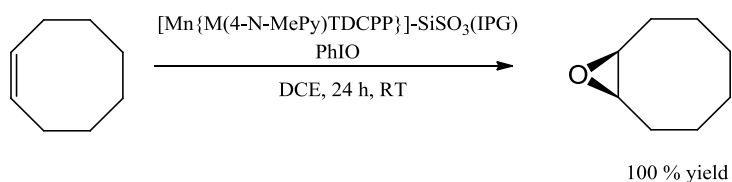
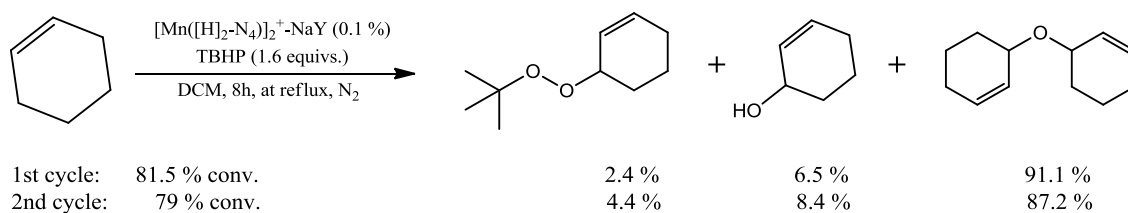


Figure I.25. Schematic representation of the bis-functionalized silica with sulfonatophenyl and propylimidazole groups.

However, none of their Mn(III) supported catalysts were efficient towards hydrocarbon oxygenation using H_2O_2 as oxidant without the addition of a co-catalyst such as $\text{CH}_3\text{COONH}_4$. In contrast, good results were achieved using PhIO as the oxygen source in the *cis*-cyclooctene epoxidation:

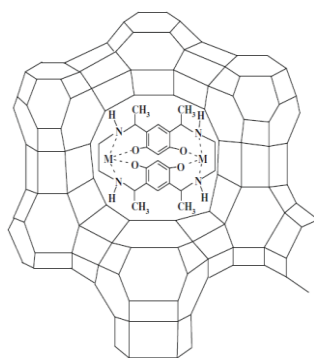


Salavati-Niasari et al. described the synthesis of manganese(II) complexes of 12-membered macrocyclic ligands, encapsulated within the nanopores of a zeolite by the Flexible-Ligand Method (FLM).^{210a} The complexes were entrapped in the nanocavities of zeolite-Y by a two-step process in the liquid phase. These host-guest nanocatalysts were used for oxidation of cyclohexene with *tert*-butylhydroperoxide (TBHP) oxidant in different solvents, obtaining better selectivities for the ether product than the same catalyst essayed in homogeneous conditions.



Scheme I.20. Oxidation of cyclohexene catalyzed by a host-guest nanocatalyst using a manganese(II) compound.

In 2009, Salvati-Niasari, Salimi et al. reported the synthesis of new host-guest nanocatalysts with octahydro-Schiff base ligands.^{210b} In this case, the catalysts were used for oxidation of cyclohexene using H₂O₂ as the oxygen source and showed a clearly preference towards the alcohol product.



[M₂([H₈-N₄O₄)]-NaY
(M= Mn(II), Co(II), Ni(II),
Cu(II))

Figure I.26. Host-guest nanocatalysts with octahydro-Schiff base ligands described by Salvati-Niasari, Salimi and co-workers.

There are several examples in the literature for the preparation of heterogenized manganese catalysts by the covalent binding method.^{143,211}

A covalent immobilization of Mn(III)-Salen complexes on an amorphous mesoporous silica support was reported by Luts et al. in 2007.^{211b} The complexes were anchored onto the silica using peptide and ester bonds, and were studied in the catalytic epoxidation of cyclooctene with TBHP as oxidant.

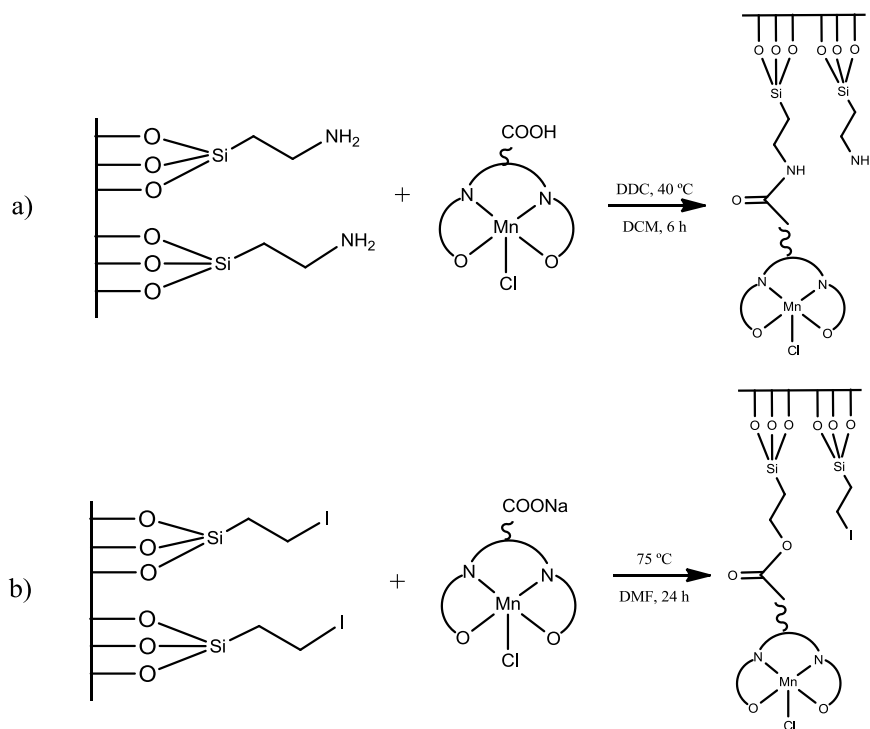


Figure I.27. Schematic representation of the ways of immobilization employed by Luts et al. to anchor a Mn(III)-Salen compound, through peptide bonding (a) and ester bonding (b), onto a mesoporous silica support.

The epoxidation of cyclooctene with the homogeneous catalysts was carried out in toluene as solvent at three different temperatures: 45, 60 and 75 °C. The cyclooctene oxide yield decreased with the increment of the temperature (yield(T °C) at 30 h: 40 %(45); 20 %(75)). The authors related this fact with the thermal decomposition of organic peroxides. The heterogenized catalysts were recycled up to three consecutive runs at the same conditions (1:2.2:0.02, substrate:oxidant:catalyst mmol) but keeping the temperature at 45 °C, and obtained similar conversions through all the runs (30 - 35 %).

Khalil et al. reported the immobilization of Mn(III)-Salen onto silica by the covalent binding method.²¹² In this case, the covalent binding was provided through a cross linker. The use of crosslinkers makes the active site far away from the surface of the support and may prevent problems such as the restricted orientation of the active site and the effect of the surface on it.²¹³ So, the crosslinker connects the solid and the complex by reaction with functional surface groups and a suitable modified ligand. Both the silica surface and the Mn(III)-Salen complex were modified. The surface was silylated using 3-aminopropyltriethoxysilane, whereas the complex was modified by adding an aryldiamine ligand containing -NH₂ groups. The crosslinker used was 1,4-phenylenediisothiocyanate which was able to react with both -NH₂ moieties

belonging to the silane groups on the silica surface and the -NH_2 groups belonging to the aryldiamine Mn(III)-Salen ligand (Figure I.28).

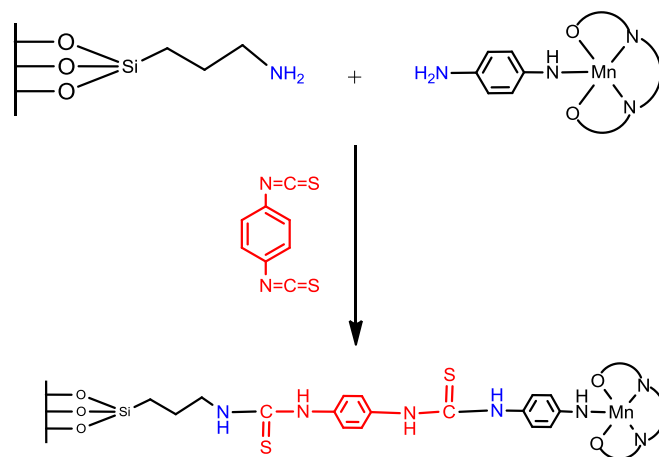


Figure I.28. Schematic representation of the immobilized modified Mn(III)-Salen complex onto the modified silica surface as described by Khalil et al.

This heterogenized complex was studied in the oxidation of cyclohexene using TBHP as the oxygen source. The results showed a highly selectivity towards both cyclohexenol (36 % yield) and cyclohexenone (44 % yield) products, although only a 25 % of conversion was achieved. Authors explained the low selectivity for the epoxide product (2 % yield) as the preference for the attack at activated C-H bond over the C=C bond, since TBHP promotes the allylic oxidation pathway.^{210a} Moreover, the epoxidation of cyclohexene is inhibited by water²¹⁴ and the heterogenized catalyst was not dehydrated before the catalytic reaction and could contain a certain amount of water. Similar results were observed at the second, and final, run of the heterogenized catalyst.

A covalent immobilization of a manganese(III) porphyrin complex onto silica-coated Fe_3O_4 magnetic nanoparticles as catalyst for oxidation reactions was reported by Bagherzadeh et al. in 2016.^{211e} The immobilization of the complex was achieved *via* an amino propyl linkage belonging to the functionalized silica-shell. First of all, the authors synthesized the Fe_3O_4 nanoparticles and coated them with a thin layer of silica.²¹⁵ Then, the functionalized silica-shell was obtained by its reaction with 3-aminopropyltriethoxysilane. Afterwards, the complex was added to a dispersion of the functionalized silica-coated Fe_3O_4 nanoparticles in toluene, and refluxed for 24 h under argon atmosphere (Figure I.29).

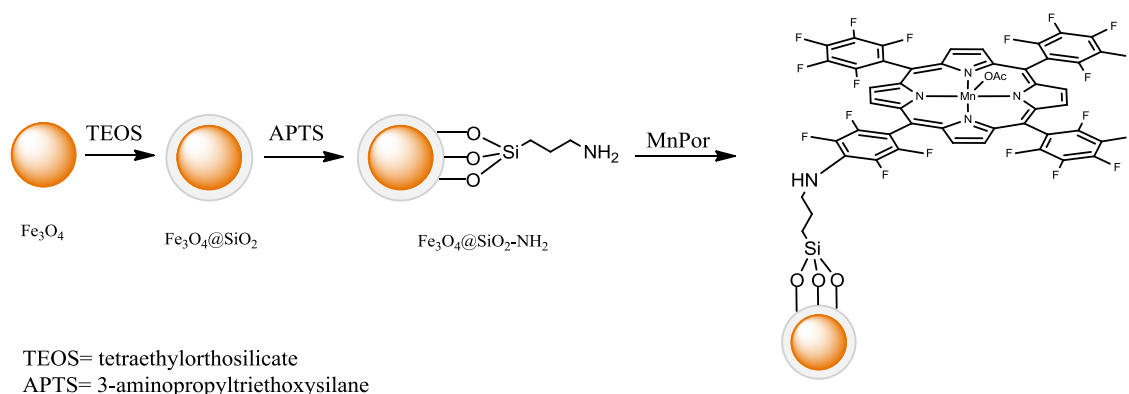


Figure I.29. Schematic representation of the synthesis of the immobilized manganese(III) porphyrin onto silica-coated Fe_3O_4 magnetic nanoparticles, as described by Bagherzadeh et al.

The heterogenized catalyst obtained, $\text{Fe}_3\text{O}_4@\text{SiO}_2\text{-NH}_2@[\text{Mn}(\text{TPFPP})\text{OAc}]$, was used in alkane oxidation in the presence of two different oxidants: tetra-*n*-butylammonium hydrogen monopersulfate ($n\text{-Bu}_4\text{NHSO}_5$) and PhIO ; and in epoxidation of alkenes using $n\text{-Bu}_4\text{NHSO}_5$ as the oxygen source. The catalysis were performed in dichloromethane at room temperature, and with a molar ratio of {catalyst:imidazole:substrate:oxidant}:{1:80:250:500} (imidazole acting as an additive). Regarding to the cyclooctene epoxidation, the heterogenized catalyst showed a remarkable activity through up six consecutive runs with a minimum leaching.

I.3.4.3. Ruthenium compounds as supported catalysts in oxidation reactions

A SiO_2 -supported unsaturated Ru-monomer complex (Figure I.30) was reported by Iwasawa and co-workers,²¹⁶ exhibiting high values of selectivity for aldehyde oxidation and alkene epoxidation at room temperature.

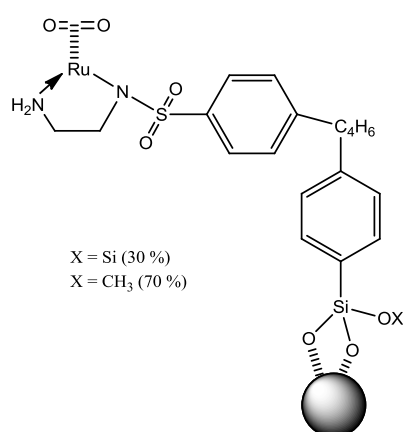


Figure I.30. Structure of SiO_2 -supported Ru catalyst.

Louloudi et al.²¹⁷ reported a biomimetic ruthenium complex covalently attached to silica surface (Figure I.31). The complex was efficient in alkene oxidation and, in some cases, it showed increased activity compared to the homogeneous ruthenium complex.

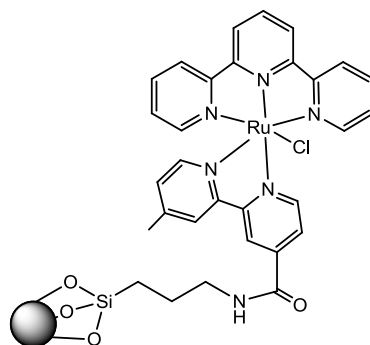


Figure I.31. Structure of biomimetic ruthenium complex.

Our group has described recently the anchoring of a Ru polypyridyl complex onto mesoporous SiO_2 and silica-coated magnetic nanoparticles (Figure I.32) via phosphonated groups attached to the trpy ligand.^{218a} The heterogeneous system was able to epoxidize aromatic and aliphatic olefins with $\text{PhI}(\text{OAc})_2$ as oxidant in dichloromethane and could be recycled for up to five runs, though with a progressive decrease in the conversion values. The selectivity values were kept around 60-80 % throughout all the catalytic cycles and were only slightly worse than that displayed by the corresponding homogenous complex in solution.^{218b}

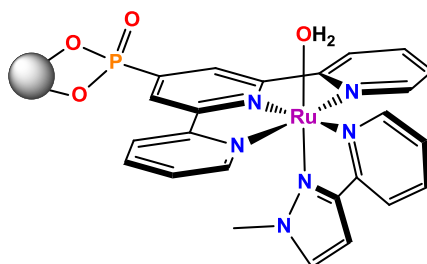


Figure I.32. Structure of the heterogeneous $[\text{Ru}(\text{trpy})(\text{pypz-Me})(\text{OH}_2)]^{2+}$ complex.

I.3.5. Heterogeneous catalysts for hydration of nitriles

The first example of nitrile hydration by a nanoparticle catalyst reported in the literature was in a short letter published by Oshiki and co-workers.²¹⁹ They prepared water soluble palladium and platinum nanoparticles stabilized by a water-soluble polymer, poly(N-vinyl-2-pyrrolidone) (PVP; Figure I.33).

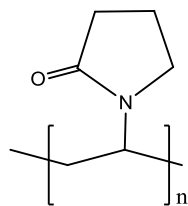


Figure I.33. Poly(N-vinyl-2-pyrrolidone) (PVP), a water-soluble polymer commonly used as a nanoparticle stabilizer.

After this first heterogeneous catalyst, other metals such as nickel,²²⁰ silver,²²¹ gold²²² and ruthenium²²³ were reported as nitrile hydration catalysts, mainly as nanoparticle catalysts or supported nanoparticles.

I.3.5.1. Ruthenium compounds as supported catalysts for hydration of nitriles

Despite the enormous interest of heterogeneous catalysts for industry due to their easier handling, higher stability, easier recovery and reusability, heterogeneous ruthenium-based systems for nitrile hydration reactions have been comparatively much less developed than the homogeneous ones.

In this context, the use of ruthenium supported on carbon (Ru/C)²²⁴ and alumina (Ru/Al₂O₃),²²⁵ as well as ruthenium nanoparticles combined with oxygen-containing copper compounds,²²⁶ have been described in a series of Japanese patents. All of them were active and selective towards amide formation. Efficient and selective hydration of a number of organonitriles in water was described by Mizuno and co-workers employing ruthenium hydroxide supported on alumina (Ru(OH)_x/Al₂O₃) as catalyst.²²⁷

Magnetic nanoparticles have also been used in hydration catalysts by means of ruthenium hydroxide supported on dopamine-functionalized Fe₃O₄ nanoparticles,²²⁸ Ru(OH)_x^{43b} or Ag²²⁹ or Mo_xO_y²³⁰ nanoparticles and a bifunctional ruthenium(II) complex^{43a} supported on silica-coated Fe₃O₄ nanoparticles (Figure I.34). All these nanocatalysts showed excellent activities and selectivities for a broad range of activated and inactivated benzonitriles, as well as heteroaromatic, aliphatic and α,β -unsaturated nitriles. Because the super-paramagnetic nature of the Fe₃O₄ support, all these nanocatalysts could be easily separated from the reaction products with the help of an external magnet.²³¹

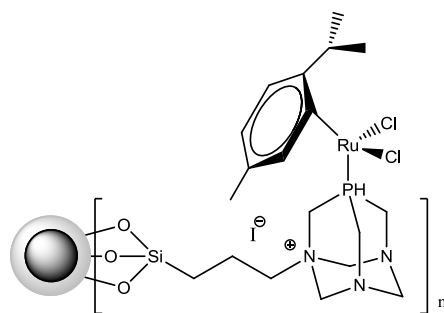


Figure I.34. Structure of a ruthenium(II) complex supported on silica-coated magnetic nanoparticles.

I.4. Biological roles of transition metals

Transition metals and metal compounds have been used in versatile platforms for biomedical applications and therapeutic intervention. Transition metal complexes have a valuable role in antitumor therapy and open a new area of research in the field of medical chemistry.²³²

The modern research regarding the development of the metal-based anticancer drugs began with the discovery of the platinum (II) complex cisplatin by Rosenberg in the 1960s.²³³ While the platinum based anti-tumor agents have an enormous impact on current cancer therapy,²³⁴ the types of cancer that can be treated with platinum agents are narrow and suffer from side effects and resistance phenomena.²³⁵ In order to overcome these problems and taking into account the good clinical success of Pt-based anticancer drugs, the exploration of other metal-based anticancer compounds has been stimulated in recent years.^{235b,236}

Inertness and stability are desirable properties for drug design, allowing the complex to reach its target site without being modified. The ligands may play important roles in target site recognition; the presence of a chelating ligand may control the reactivity toward different biomolecules (DNA, enzymes, etc.) and play a key role in the interaction with them through hydrogen bonding or intercalation. On the other hand, the coordination site occupied by good leaving groups may drive the coordination of the metal ion to target biomolecules. For example complexes as α -[Ru(azpy)₂Cl₂] containing N-chelating ligands and the chlorido ligand as leaving group showed remarkably high cytotoxicity against most of the tested cell lines.²³⁷

Cancer cells are different from healthy cells due to their unique redox balances and the generation of high level of reactive oxygen species (ROS). Consequently, metal complexes interfere with the cellular redox homeostasis, stimulate generation of ROS, and interact with DNA strands and thereby produce antiproliferative activity against cancer cells.²³⁸ Notably, most of the chemotherapeutic agents kill cancer cells by diverse mechanisms including intercalation into DNA, inhibition of DNA replication, cell membrane damage, or free radical

Chapter I

generation.²³⁹ Although the primary intracellular targets of drug action are rather distinct, the drug-induced cytotoxicity ultimately leads to a common pathway causing apoptosis. Apoptosis is a highly orchestrated cell suicidal program required to maintain a balance between cell proliferation and death, and is usually induced by a variety of physiological and external stimuli,²⁴⁰ therefore it can also be induced by a metal complex. In fact, most of the Pt-based anticancer agents in clinical use induce the apoptosis in cancer cells.^{235a,241} However, defects in the apoptotic programs may cause resistance to the therapeutic agents,²⁴² thus new chemotherapeutic agents capable to act through an alternative cell death pathway called autophagy^{232,243} (“self-cannibalistic” process) are becoming increasingly important in cancer therapy.^{243a,244}

I.4.1. Cell death mechanisms

Although there are at least 13 different types of cell death,²⁴⁵ in general the cell death mechanisms are divided into *programmed cell death* and *non-programmed cell death* (PCD and non-PCD, respectively). PCD is proposed to be the death of a cell in any pathological format associated with a series of biochemical and morphological changes, and is divided into three main categories: type I (apoptosis), type II (autophagy) and type III (necroptosis). The differences between these modes of death are established by the type of morphological, biochemical, and biomolecular alterations that induce them.²⁴⁶ For a long time, non-PCD was synonymous with necrosis, which was viewed as an accidental or uncontrolled type of cell death. However, new studies have shown recently that necrosis is in fact an active and controlled form of PCD.²⁴⁷ Apoptosis and programmed necrosis, which was named “necroptosis”, lead to cell death, whereas the role of autophagy is more complex.²⁴⁸

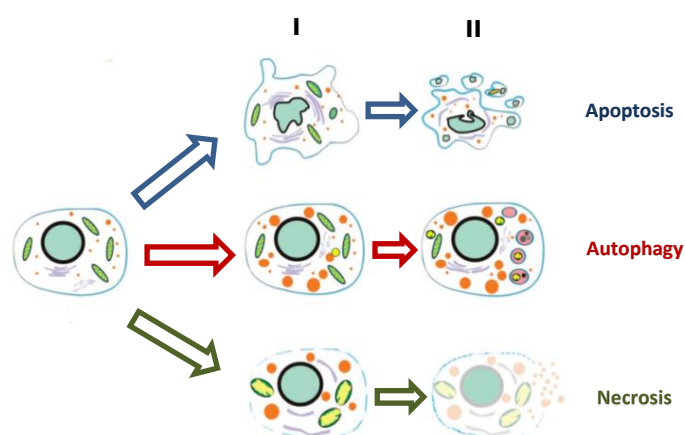


Figure I.35. Representation of the morphological features of apoptosis (blue), autophagy (red) and necrosis (green). Apoptotic cells are characterized by cell shrinkage, membrane blebbing (I) and nuclear fragmentation (II). Autophagy is characterized by the accumulation of autophagosomes and autophagolysosomes (I) and protein degradation (II). Necrosis is characterized by the swelling of the cell and its organelles (II) as well as early membrane damage (I).

I.4.2. Anticancer metallotherapeutics in clinical development

Among thousands of metal complexes that have been synthesized and evaluated as anticancer agents, only complexes of platinum,^{234e} ruthenium,²⁴⁹ titanium²⁵⁰ and gallium²⁵¹ have entered clinical trials.

a) Platinum complexes

Currently, the platinum complexes being investigated as anticancer candidates include *cis*-diamminedichloroplatinum (II), cisplatin, derivatives (e.g., carboplatin and oxaliplatin) (Figure I.36), *trans*-platinum and polynuclear platinum complexes, Pt(IV)-based prodrugs and others.²³⁴

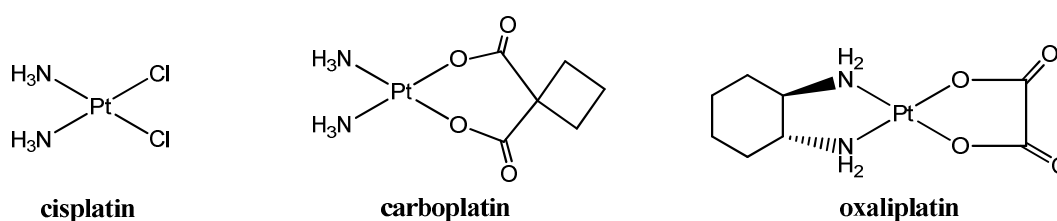


Figure I.36. Structures of some platinum complexes being investigated as anticancer agents.

The action mechanisms of the platinum-based anticancer agents are mainly the apoptotic way. However, in various cell types some Pt complexes stimulate autophagy as a cytoprotective response. For instance, both cisplatin and oxaliplatin can induce this cytoprotective process to antagonise the metal-induced apoptosis. Therefore, the inhibition of the induced autophagy could enhance their apoptotic effects.²⁵²

Although *trans*-platin was found to be inactive, platinum complexes bearing aromatic or bulky amines in the *trans* geometry showed potent antiproliferative activities.²⁵³ Among them, a series of mono- and bimetallic *trans*-N-heterocyclic carbene-amine-Pt(II) have displayed a potent cytotoxicity and the capability to overcome cisplatin resistance.²⁵⁴

Pt(IV) complexes, which are kinetically more inert than Pt(II)-compounds, have been synthesized in recent years to generate more potent and selective antitumor drugs, taking into account that they can be reduced *in vivo* to form active cisplatin species.^{241h} Two Pt(IV) complexes with ethylenediamine-N,N'-di-3-propanoate esters as ligands were found to show cytotoxicity comparable to that of cisplatin.²⁵⁵ Moreover, photoactivable Pt(IV) prodrugs offer the potential for targeted drug release and reduced side effects.²⁵⁶

Complexes as cisplatin or derivatives can interact with the DNA through a covalent intercalation. Cisplatin becomes activated once it enters into the cell. In the cytoplasm the

Chapter I

electrophile that can react with any nucleophile, such as the nitrogen donor atoms of nucleic acids. Cisplatin binds to the N reactive center on purine residues and causes DNA damage in cancer cells, blocking cell division and resulting in apoptotic cell death.²⁵⁷

b) Ruthenium complexes

Compared with platinum complexes, ruthenium complexes have similar substitution kinetics but differ in biological properties. Based on the chemical structures of NAMI-A and KP1019 (Figure I.37), the two ruthenium complexes in clinical trials,²⁴⁹ the anticancer candidates based on ruthenium currently investigated can be divided into NAMI-A type complexes, KP1019 and its derivatives, Ru(II)-arene complexes, Ru(II)-PTA complexes, Ru(II)-polypyridyl complexes and others.^{236c,258} Other families of ruthenium compounds under investigation are the so-called "RAPTA" complexes and multinuclear compounds.²⁵⁹ RAPTA complexes are characterized by the presence of a facially-coordinated aromatic ring (which is relatively hydrophobic) and a PTA (1,3,5-triaza-7-phosphaadamantane) ligand (which is highly water soluble). Regarding to the multinuclear compounds, some particularly interesting strategies include ruthenium-platinum mixed-metal compounds,²⁶⁰ ruthenium cluster complexes,²⁶¹ ruthenium DNA intercalators²⁶² and supramolecular "Trojan Horses", which contain a cytotoxic payload that is released upon entry to the cancer cell.²⁶³

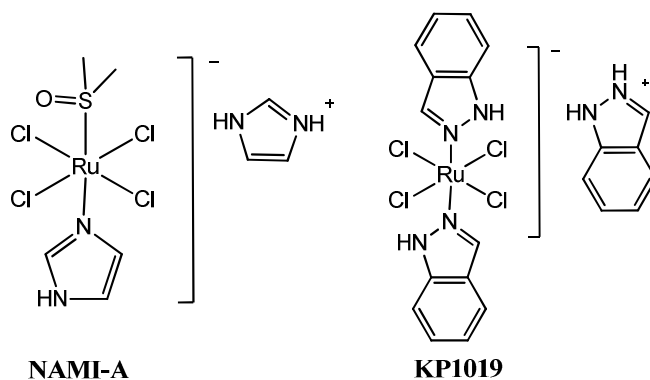


Figure I.37. Structures of some ruthenium complexes being investigated as anticancer agents.

The NAMI-A type complexes were predominantly studied for their antimetastatic activities and showed relatively low cytotoxicity.^{258a} KP1019 was reported to induce apoptosis in human colon adenocarcinoma SW480 cells.^{258c} The ruthenium-arene complexes can provide both hydrophilic and hydrophobic properties and form covalent and noncovalent interactions with DNA.²⁶⁴ A Ru(II)-arene complex developed by Bugarcic et al. was able to induce apoptosis as well as a much lower extent of necrosis.²⁶⁵ A study conducted by Chen et. al. showed that a

Ru(II) polypyridyl complex could also induce apoptosis in human malignant melanoma A375 cell line.

More recently, Pierroz et al. developed a Ru(II)-polypyridyl complex containing the 2-pyridyl-2-pyrimidine-4-carboxylic acid as the ligand, which could accumulate in mitochondria causing serious dysfunctions and therefore the caspase activation.²⁶⁶

Inhibitors of DNA topoisomerases constitute a novel family of anticancer agents. Chao et al. reported that Ru(II)-polypyridyl complexes containing an asymmetric ligand exhibited high selectivity for cancer cells over normal cells by targeting topoisomerase. The most effective complex could effectively induce apoptosis *via* mitochondrial dysfunctions, ROS generation, and the activation of caspase family proteins.²⁶⁷ A series of mononuclear and binuclear redox-active Ru(II)-polypyridyl complexes developed by Yadav et al. were found to induce apoptosis involving both the intrinsic and extrinsic pathways.²⁶⁸

Regarding the anticancer mechanism of NAMI-A, its metabolites once hydrolyzed inside the cell have been shown to bind strongly to several proteins, including integrins, transferrins, and human serum albumin.^{258b,269} In contrast to platinum drugs, NAMI-A binds to DNA weakly,²⁷⁰ indicating that its antimetastatic activity may be not related to DNA damage. Theoretical calculations carried out by Vargiu et al. confirmed that NAMI-A is easily reduced *in vivo* and that reduction strongly affects the hydrolysis. They suggest that *cis* and *trans* Ru(II)-diaqua metabolites are the most abundant, though the mono-aqua complexes cannot be discarded, and perhaps the most relevant for the biological activity of NAMI-A.²⁷¹

1.4.3. Biological application of manganese compounds

In comparison with the well-developed Mn catalysts, Mn anticancer agents are scarcely studied.^{238,272} Since the success of cisplatin, more and more attention has been paid to metal complexes, which inhibit the proliferation of cancer cells through DNA or mitochondria involved path.²⁷³ Mitochondria are the most important organelles in determining continued cell survival and cell death. Mitochondrial membranes span across a negative potential, so positive charged complexes, such as Mn(III)-salen and -salphen compounds, take advantage of electrostatic forces in locating its target and causing the cell death through the apoptotic pathway.²⁷⁴

Moreover, manganese(II) ions are the required cofactor for many ubiquitous enzymes. Mitochondria can accumulate Mn²⁺ ions through an ATP-dependent Ca transporter.²⁷⁵ Mitochondrial Ca²⁺ loading has profound consequences for mitochondrial function, such as

Chapter I

regulating cellular respiration and mediating cell death by apoptosis or necrosis.²⁷⁶ The transport mechanism of Mn(II) ions *in vivo* may make it possible for Mn(II)-based compounds to be tumor-targeted. Research has proven that Mn(II) ions were mainly taken up and transported by a divalent metal transporter (DMT-1) and a transferrin (Tf) receptor (TfR), which were highly expressed in some tumor tissues.^{276b,277} Simple Mn(II) salts have shown an antiproliferative effect on several cancer cell lines, but their application was limited because of their high dose.²⁷⁸ Mn(II) complex [(Adpa)Mn(Cl)(H₂O)] (Adpa= bis(2-pyridylmethyl)amino-2-propionic acid), Adpa-Mn, targets mitochondria and inhibits the proliferation of human glioma cell line U251, with low IC₅₀ (9.5 μM) *in vitro*.^{272f,279} So, it is possible for special Mn(II) complexes to target cancer cells through an ATP-related Ca transporter.

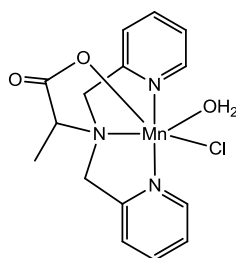


Figure I.38. Structure of Adpa-Mn described by Gao et al.

Cellular levels of H₂O₂ directly or indirectly play a key role in malignant transformation. Cancer cells use O₂ to generate excessive levels of ROS and H₂O₂. During the overexpression of H₂O₂-detoxifying enzymes, H₂O₂ concentration decreases and the cancer cells revert to normal appearance,²⁸⁰ so the alteration in the metabolism of O₂ by Mn(II) complexes plays an important role in carcinogenesis. Adpa-Mn induce mitochondrial dysfunction by the accumulation of ROS. ROS play several roles in cellular processes, including DNA damage, mitochondrial dysfunction, the activation of signaling pathways and the activation of transcription factors, leading to the upregulation of genes.²⁸¹

Ansari et al. reported several Mn(III)-salphen derivatives that induce apoptosis in human cells via mitochondrial pathway, with IC₅₀ values lying within the range 11-40 μM towards malignant breast cells (MCF7), being similar to cisplatin in terms of cytotoxicity and selectivity versus the same cell line.^{272a}

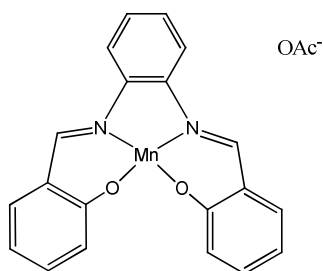


Figure I.39. Structure of a Mn(III)-salphen compound described by Ansari et al. active towards malignant breast cells (MCF7).

The synthesis of two manganese(II) complexes bearing modified acetylpyridine thiosemicarbazones were described by Li, Chen, Zang, et al. in 2010.^{272b} These compounds showed antitumor activity against K562 leukemia cancer cell line, with IC_{50} values lying within the range 2.5-0.6 μ M.

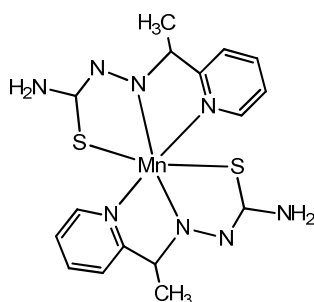


Figure I.40. Structure of a manganese(II) complex bearing the 2-acetylpyridine thiosemicarbazone ligand, synthesized and characterized by Li, Chen, Zang et al.

Dash et al. described the synthesis and characterization of a manganese(II) compound, $[Mn(Phpyk)_2(SCN)_2]$ (Phpyk= 2-benzoylpyridine), which also presents antimetastatic activity against K562 leukemia cancer cell line.²³⁸ In this case, the IC_{50} values were higher ($\sim 46 \mu$ M) but authors reported that no toxicological impact on healthy cells were detected. Despite of the observation of numerous effects in cells due to their exposition to this Mn(II) complex, such as alteration of cellular redox status, loss of mitochondrial membrane potential, and oxidative stress caused by ROS, the authors couldn't identify the exact mechanism of action for its anticancer activity.

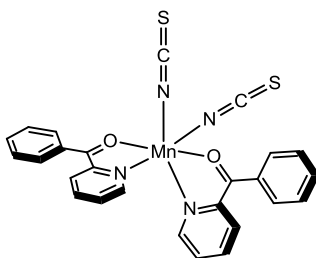


Figure I.41. The $[Mn(Phpyk)_2(SCN)_2]$ complex described by Dash et al.

Gao et al. reported the anticancer activity of manganese(II) complexes containing N-substituted di(2-pyridylmethyl)amines as ligands.^{272c} These complexes interfered with the functions of mitochondria and the metabolite of O_2 in cancer cells, exhibiting good inhibition of proliferation of U251 (glioblastoma) and HeLa (human epitheloid cervix carcinoma) cells. The inhibiting activity of these compounds is related to their disproportionating H_2O_2 activity, causing the apoptosis of cancer cells.

A manganese(II) complex capable to bind to DNA was reported by Zhang et al. in 2012.^{272d} The complex, $\{(Hapy)_2[MnII(DCA)_2] \cdot 6H_2O\}$ (Hapy= 2-aminopyridine acid; DCA= dimethylcantharate), showed antiproliferative activity against human hepatoma cells lines ($IC_{50}= 56 \mu M$) and human gastric cancer cell lines ($IC_{50}= 72 \mu M$) in vitro, through a partial intercalation mode into DNA.

To sum up, complexes containing pyridine rings have been reported for their bioactivities, such as DNA binding properties and antibacterial activity.²⁸² Meanwhile, ionic compounds possess the advantages of the better water-solubility and easy channeling through cell membranes. All Mn-anticancer agents described above possess at least one of these properties. Therefore, the combination of two of them in new manganese complexes could give a promising results in biological applications as anticancer agents.

1.4.4. Biological application of ruthenium compounds

There are four main properties that make ruthenium compounds well suited to medicinal application:

- *The low ligand exchange rate.* Their kinetics are on the timescale of cellular reproduction, meaning that if a ruthenium ion does bind to something in the cell, it is likely to remain bounded for the remainder of that cell's lifetime.
- *The range of accessible oxidation states (II, III and IV) under physiologically relevant conditions.* The energy barriers to interconversion between these oxidation states is relatively low, allowing for fast oxidation state changes when inside the cell.

- *The ability to bind to a range of biomolecules and not just DNA.* Ruthenium belongs to the same group as iron, and that has led to some chemists postulating that it is capable of taking iron's place in some proteins.
- *Preference to form compounds in octahedral geometry.* Ruthenium tends to form octahedral complexes, which gives the chemist two more ligands to exploit compared with platinum(II) complexes, which adopt a square planar geometry.

For all these reasons, there are many different applications for ruthenium compounds in medicine. For example, Ru(III) complexes with N-donor ligands such as $[\text{Ru}(\text{NH}_3)_4(\text{Im})_2]$ (Im = imidazole) are used as immunosuppressants; the complex $[\text{RuCl}_2(\text{cloroquinone})]_2$ is used against the malaria; coordinating ruthenium to organic antibiotic compounds often results in higher *in vitro* activity (e.g: the ruthenium(III) derivative of thiosemicarbazonee); and as anticancer agents (see section I.4.2).²⁸³

Interestingly, ruthenium compounds have shown to be less toxic as anticancer agents compared to platinum(II) complexes. One hypothesis is that ruthenium(III) complexes are more inert, so they can be administered causing the minimal damage to healthy cells, and can be reduced to the active II oxidation state in cancer cells. Cancerous cells tend to have a more chemically reducing environment than healthy cells, owing to their lower concentration of molecular oxygen (due to their higher metabolic rate). Moreover, the higher metabolic rate of cancer cells requires high quantities of iron, therefore they increase the number of transferrin receptors located on their cell surfaces. The ability of ruthenium to mimic iron in binding to many biomolecules enables the Ru ion to bind transferrins, so a higher amount of ruthenium will target cancer cells than healthy cells, and therefore its toxicity is reduced because less of it will reach healthy cells.^{259,283}

I.4.4.1. Anticancer activity of Ru-dmso

Ru-dmso complexes have shown an antimetastatic activity comparable to that of cisplatin in some malign tumors in animals, plus having less toxic secondary effects. The presence of dmso as ligand is a key point in the potential anticancer activity of ruthenium compounds for these reasons:

- dmso is a polar molecule which is able to cross cellular membranes. Therefore, when it is coordinated to a metal center, the solubility of this complex could be better in water and in parallel the capacity to cross the biologic membranes could increase.

Chapter I

- dmsO has a quite strong *trans* effect when dmsO is coordinated through S, which could generate free coordination positions in the metal center.

Furthermore, Ru(III) complexes with S-dmsO ligands in their coordination sphere present another characteristic: due to π -acceptor properties of S-dmsO their redox potential is especially high and their reduction *in vivo* to Ru(II) is favorable, then making them more labile and consequently more active.

Specifically, *trans*-imidazoledimethylsulfoxide-tetrachlororuthenate, known as NAMI-A (Figure I.37) is active against solid tumor metastases either in experimental mouse tumors or against human xenograft.^{109b,284} As it has been said in section 0, NAMI-A has a unique mechanism of activity which is not fully understood yet. Its high antimetastatic properties are accompanied with low antitumor effect for primary tumors *in vivo* and no cytotoxic effect *in vitro*.²⁸⁵

Due to their characteristics, different monomeric and dimeric Ru(II) complexes similar to NAMI-A have been synthesized.²⁸⁶ Preclinical studies with indazolium bis-indazole-tetrachlororuthenate, known as KP1019 (Figure I.37) showed promising activity against colorectal tumours and the phase I study seems to support this.²⁸⁷

Chapter II. Objectives

II.1. General Objectives

One of the main research lines of the group where this PhD Thesis has been developed is centered in the synthesis of new manganese and ruthenium complexes and their exhaustive characterization, as well as their evaluation as potential catalysts for different reactions such as epoxidation or nitrile hydration. As it has been seen in the introduction, these reactions are important transformations from both academic and industrial points of view.

Transition-metal complexes containing ligands with nitrogen as donor atom constitute an important class of coordination compounds that are able to perform a wide range of transformations. Nitrogen-based ligands have well-known advantages such as chemical robustness or rich coordination chemistry. In this line, it is well known that manganese and ruthenium complexes containing polypyridyl type of ligands have shown to be good catalysts for the epoxidation of alkenes, and ruthenium compounds bearingazole-based ligands have been described to be good catalysts for the nitrile hydration reaction in environmental friendly media; therefore the use of mixed ligands as pyridine/pyrazole or phenol/pyrazole is expected to generate also active compounds for these reactions, and the characteristics of the different ligands employed will help to broaden the knowledge of the factors that influence the catalysts performance.

As described also in the introduction, chemical transformations are experiencing a profound renovation to meet sustainability criteria, moving from old methods to new ones developed in agreement with *green chemistry* principles as the hazardous solvent replacement. In this context, heterogenization and reuse of catalysts are fields of unquestionable importance especially towards their application in large-scale processes.

On the other hand, transition metal compounds have been used in versatile platforms for biomedical applications and therapeutic intervention. Transition metal complexes have a valuable role in antitumor therapy and open a new area of research in the field of medical chemistry. In the specific field of chemotherapeutic agents for cancer treatment *cis-platin* is nowadays used worldwide. However, its toxic side-effects have pushed on the research on alternative drugs, in some cases based on metals such as ruthenium or manganese. Mn complexes have potentially fewer side effects and are more environment-friendly compared to platinum or ruthenium.

For this purpose, one of the general objective of this thesis was the design of new families of manganese and ruthenium complexes with different types of N-donor ligands and their

Chapter II

evaluation as potential catalysts in epoxidation or nitrile hydration reactions. From the point of view of sustainability of the processes, we were interested in studying the degree of reusability of our catalysts and their performance as heterogeneous catalytic systems. Therefore, other objectives were, on one hand, the use of new green solvents, such as RTILs or glycerol as reaction media in the catalytic reactions and, on the other hand, the immobilization of certain compounds onto silica and magnetic silica nanoparticles to use them as heterogeneous catalysts. Finally, and taking into account the versatility of our complexes, we also considered studying them as potential antitumoral agents.

II.2. Specific Objectives

In order to attain the general goals, specific objectives for manganese and ruthenium complexes have been designed.

For manganese complexes:

- The synthesis and complete characterization (elemental analysis, spectroscopic, structural and electrochemical techniques) of new manganese(II) and manganese(III) complexes containing the bidentate ligands 2-(3-pyrazolyl)pyridine, *pypz-H*, 2-(1-methyl-3-pyrazolyl)pyridine, *pypz-Me*, 2-(1H-pyrazol-3-yl)phenol, *HOphpz-H*, and 3-(2-pyridyl)-1-(pyrazolyl)acetic acid ethylester, *pypz-CH₂COOEt* (Figure II.1).
- The study of their catalytic activity in the epoxidation of some aliphatic and aromatic alkenes in different media as CH₃CN, glycerol and in ionic liquid:solvent media using peracetic acid as oxidant.
- The study of the reusability of these homogeneous systems in ionic liquid:solvent media.
- The heterogenization of the new manganese systems containing pyrazole-based ligands onto silica particles, the characterization of the new materials prepared and the study of their catalytic activity and reusability with regard to alkene epoxidation.
- To test some of synthesized manganese compounds, together with other manganese complexes previously synthesized in our group, as potential antitumor agents through the study of *in vitro* cytotoxicity tests against ovarian and lung human cancer cell lines, OVCAR-8 and NCI-H460.

For ruthenium complexes:

- The synthesis and complete characterization (structural, spectroscopic and electrochemical techniques) of two new families of ruthenium(II) complexes: i) Ru(II)-dmsO complexes containing the bidentate ligands 3-(2-pyridyl)-1-(pyrazolyl)acetic acid ethylester, *pypz-CH₂COOEt*, 2-(1H-pyrazol-3-yl)phenol, *HOphpz-H*, and 3-(2-methoxyphenyl)pyrazole, *MeOphpz-H*, and the monodentate ligand 3,4-dimethylpyrazole, *3,4-dmpzH*; and ii) Ru-Cl and Ru-OH₂ complexes, containing the tridentate ligand 2,2':6,2''-terpyridine, *trpy*, and the bidentate ligand 2-(3-pyrazolyl)pyridine, *pypz-H* (Figure II.1).
- The study of the electron-transfer-induced linkage isomerization of the dmsO ligands in representative compounds as [Ru^{II}Cl₂(*pypz-CH₂COOEt*)(dmsO)₂] or [Ru^{II}Cl₂(*MeOphpz-H*)(dmsO)₃].
- The study of the catalytic activity of the new ruthenium(II)-dmsO complexes with regard to the hydration of some aromatic and aliphatic nitriles in water, together with the heterogenization of some of the compounds onto silica particles and magnetic silica nanoparticles, including their full characterization (ICP-AES, UV-Vis, IR, SEM, TEM, TGA and XPS) and the evaluation of their heterogeneous catalytic activity.
- The study of the Ru-aqua reactivity towards the epoxidation of alkenes using iodobenzene diacetate as the oxidant, establishing a comparison with analogous complexes previously synthesized in our group.
- To test some of the ruthenium(II) complexes synthesized as antitumor agents, through the study of *in vitro* cytotoxicity tests against human ovarian and lung cancer cell lines, OVCAR-8 and NCI-H460.

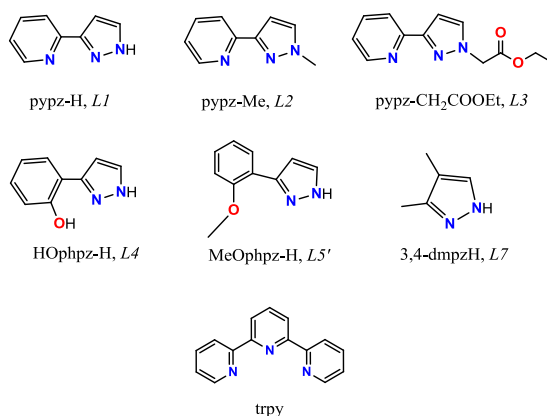


Figure II.1. N-donor ligands used to synthesize the new manganese(II), manganese(III) and ruthenium(II) complexes of this work.

Chapter III. Experimental section

III.1. Materials

All commercial reagents and mesoporous silica particles (SP) were purchased from Sigma-Aldrich and were directly used without further purification. Reagent grade organic solvents were obtained from SDS and Scharlab and high purity de-ionized water was obtained by passing distilled water through a nano-pure Mili-Q water purification system. RuCl₃·2.53H₂O was purchased from Johnson and Matthey Ltd. and was used as received. Fe₃O₄@SiO₂ core-shell nanoparticles (MSNP) were prepared in Dr. Josep Ros group in Universitat Autònoma de Barcelona (UAB) according to the literature.²⁸⁸

III.2. Preparations

III.2.1. Synthesis of ligands

2-(3-pyrazolyl)pyridine²⁸⁹ (pypz-H, L1), 2-(1-methyl-3-pyrazolyl)pyridine²⁹⁰ (pypz-Me, L2), 3-(2-pyridyl)-1-(pyrazolyl)acetic acid ethylester²⁹¹ (pypz-CH₂COOEt, L3) and N,N-bis(2-pyridylmethyl)ethylamine²⁹² (bpea, L9) ligands were prepared according to literature procedures.

For the structure and NMR numbering scheme see the Supporting Information, Figure SIII.1.

2-(1H-pyrazol-3-yl)phenol (HOphpz-H, L4). This ligand was prepared following a different method to that described in the literature.²⁹³

A 5 g (36.7 mmol) of 2'-hydroxyacetophenone and 7 mL (52.6 mmol) of N,N-dimethylformamide dimethylacetal were introduced in a round-bottomed flask. The reaction mixture was refluxed overnight at 160 °C. A solid, corresponding to 3-(dimethylamino)-1-(1-hydroxyphen-2-yl)prop-2-en-1-one, L, precipitated after cooling to room temperature. That solid was collected by filtration, washed with hexane (3 x 100 mL) and diethyl ether (3 x 100 mL), and dried at vacuum. Yield 5.05 g (72 %). ¹H-NMR (400 MHz, CDCl₃, 20 °C): δ = 2.97 (s, 3H, N-CH₃), 3.19 (s, 3H, N-CH₃), 5.78 (d, 1H, H5, ³J_{H,H} = 16 Hz), 6.81 (t, 1H, H3, ³J_{H,H} = 10.8 Hz), 6.93 (d, 1H, H1, ³J_{H,H} = 11.2 Hz), 7.34 (t, 1H, H2, ³J_{H,H} = 11.2 Hz), 7.69 (d, 1H, H4, ³J_{H,H} = 10.8 Hz), 7.88 (d, 1H, H6, ³J_{H,H} = 16 Hz), 13.92 (s, 1H, O-H) ppm. In a second step, 2.76 g (14.43 mmol) of L in ethanol (9 mL) and 6 mL (123.5 mmol) of hydrazine were introduced in a round-bottomed flask. The mixture was heated at 60 °C and stirred for 30 min at this temperature. After reducing the volume and cooling to room temperature, 30 mL of distilled water were added, giving rise to the precipitation of a brown solid corresponding to HOphpz-H ligand. This solid was filtered off, washed with hexane (2 x 200 mL) and dried at 100 °C for 1 h. After cooling, the product was recrystallized in ethanol (5 mL), obtaining a pale brown powder. Yield 1.31 g (57 %). ¹H-NMR (400 MHz, CDCl₃, 20 °C): δ = 6.73 (d, ³J_{H,H} = 3.4 Hz, 1H, H4), 6.93 (ddd, 1H, H3, ³J_{H,H}

Chapter III

= 10.3, 9.7 Hz, $^4J_{\text{H,H}} = 1.2$ Hz), 7.04 (dd, 1 H, H1, $^3J_{\text{H,H}} = 10.9$ Hz, $^4J_{\text{H,H}} = 1.6$ Hz), 7.24 (ddd, 1 H, H2, $^3J_{\text{H,H}} = 10.9$, 9.7 Hz, $^4J_{\text{H,H}} = 2.2$ Hz), 7.61 (dd, 1 H, H4, $^3J_{\text{H,H}} = 10.3$ Hz, $^4J_{\text{H,H}} = 2.2$ Hz), 7.63 (d, 1 H, H6, $^3J_{\text{H,H}} = 3.4$ Hz) ppm.

2-(1-methyl-1H-pyrazol-3-yl)phenol (HOphpz-Me, L5). This ligand was prepared following the method described in the literature.²⁹⁴ The product was purified by chromatography column of silica with CH_2Cl_2 as the eluent, and ligands 3-(2-methoxyphenyl)pyrazole (MeOphpz-H, L5') and 3-(2-methoxyphenyl)-1-methyl-1H-pyrazole (MeOphpz-Me, L5'') were also isolated in a ratio of L5: L5': L5'' = 0.5: 0.4: 0.1.

For L5: $^1\text{H-NMR}$ (400 MHz, CDCl_3 , 20 °C): $\delta = 3.95$ (s, 3H, N- CH_3), 6.61 (d, 1H, H5, $^3J_{\text{H,H}} = 3.20$ Hz), 6.90 (ddd, 1H, H2, $^3J_{\text{H,H}} = 10.91$, 10.42 Hz, $^4J_{\text{H,H}} = 2.08$ Hz), 7.02 (dd, 1H, H1, $^3J_{\text{H,H}} = 10.91$ Hz, $^4J_{\text{H,H}} = 2.12$ Hz), 7.20 (ddd, 1H, H3, $^3J_{\text{H,H}} = 10.42$, 10.28 Hz, $^4J_{\text{H,H}} = 2.12$ Hz), 7.40 (d, 1H, H6, $^3J_{\text{H,H}} = 3.20$ Hz), 7.55 (dd, 1H, H4, $^3J_{\text{H,H}} = 10.28$ Hz, $^4J_{\text{H,H}} = 2.08$ Hz), 10.80 (s, 1H, O-H) ppm.

For L5': $^1\text{H-NMR}$ (400 MHz, CDCl_3 , 20 °C): $\delta = 4.01$ (s, 3 H, O- CH_3), 6.65 (d, 1H, H5, $^3J_{\text{H,H}} = 2.24$ Hz), 7.05 (m, 2H, H1, H2), 7.32 (ddd, 1H, H3, $^3J_{\text{H,H}} = 10.5$, 9.4 Hz, $^4J_{\text{H,H}} = 2.24$ Hz), 7.62 (d, 1H, H6, $^3J_{\text{H,H}} = 2.20$ Hz), 7.70 (dd, 1H, H4, $^3J_{\text{H,H}} = 10.5$ Hz, $^4J_{\text{H,H}} = 2.24$ Hz), 11.38 (s, 1H, N-H) ppm.

For L5'': $^1\text{H-NMR}$ (400 MHz, CDCl_3 , 20 °C): $\delta = 3.89$ (s, 3H, O- CH_3), 3.96 (s, 3H, N- CH_3), 6.75 (d, 1H, H5, $^3J_{\text{H,H}} = 2.96$ Hz), 6.96-7.06 (m, 2H, H1, H2), 7.28 (ddd, 1H, H3, $^3J_{\text{H,H}} = 10.42$, 10.32 Hz, $^4J_{\text{H,H}} = 2.37$ Hz), 7.38 (d, 1H, H6, $^3J_{\text{H,H}} = 2.96$ Hz), 7.89 (dd, H4, 1H, $^3J_{\text{H,H}} = 10.32$ Hz, $^4J_{\text{H,H}} = 2.33$ Hz) ppm.

III.2.2. Synthesis of manganese compounds

$\text{Mn}(\text{CF}_3\text{SO}_3)_2$ ²⁹⁵ and $[\text{Mn}(\text{CF}_3\text{SO}_3)_2((-)\text{-L})_2]$ ¹³⁷ (**Mn10**) compounds were prepared following the method previously described in the literature.

$[\text{Mn}^{\text{II}}\text{Cl}_2(\text{pypz-H})_2]\cdot\text{H}_2\text{O}$, Mn1. A solution of *pypz-H* (L1) (0.144 g, 0.992 mmol) and 0.049 g (0.389 mmol) of MnCl_2 in ethanol (5 mL) was stirred for 30 min at room temperature. A pale yellow precipitate was obtained that was collected by filtration, washed thoroughly with diethyl ether and dried in air. The resulting pale yellow solution was left to evaporate at room temperature. After one week, air-stable, colorless crystals of **Mn1**, suitable for X-ray diffraction analysis, were obtained. Yield: 0.15 g (94 %). Anal. Found (Calc.) for $\text{C}_{16}\text{H}_{14}\text{N}_6\text{Cl}_2\text{Mn}\cdot\text{H}_2\text{O}$: C, 44.07 (44.26); H, 3.1 (3.71); N, 19.17 (19.36) %. IR (cm^{-1}): $\nu = 3106\text{-}3045$ (ν (NH)); 1600 (ν (C-N) sp^2); 1433 (ν (C-C) sp^2) cm^{-1} . $E_{1/2}$ (III/II): 0.63 V vs. Ag/AgNO_3 ($\text{CH}_3\text{CN} + 0.1$ M TBAH). ESI-MS (m/z): 457 ($[\text{MnCl}_2(\text{pypz-H})_2]\cdot\text{H}_2\text{O})\text{Na}^+$.

[Mn^{II}(CF₃SO₃)₂(pypz-H)₂], Mn2. A solution of *pypz-H* (L1) (0.115 g, 0.792 mmol) and Mn(CF₃SO₃)₂ (0.141 g, 0.399 mmol) in THF (5 mL) was stirred for one hour at room temperature. Afterwards, the volume of the solution was reduced to 1 mL and a pale yellow precipitate was obtained. This solid was filtered off, washed thoroughly with diethyl ether and dried in air. After two days, air-stable, colorless crystals, suitable for X-ray diffraction analysis, were obtained. Yield: 0.24 g (93.5 %). Anal. Found (Calc.) for C₁₈H₁₄N₆S₂O₆F₆Mn: C, 33.54 (33.60); H, 2.32 (2.19); N, 13.65 (13.06) %. IR (cm⁻¹): ν = 3238-3142 (ν (N-H)); 1607 (ν (C-N)sp²); 1434 (ν (C-C)sp²); 1223-1172 (ν (S-O)sp²). cm⁻¹. E_{1/2} (III/II): 0.72 V vs. Ag/AgNO₃ (CH₃CN + 0.1 M TBAH). ESI-MS (m/z): 494 [Mn(CF₃SO₃)(pypz-H)₂]⁺.

[Mn^{II}(OAc)₂(pypz-H)₂·H₂O, Mn3. 0.107 g (0.737 mmol) of *pypz-H* (L1) were added under stirring to a solution of Mn(OAc)₂·4H₂O (0.086 g, 0.356 mmol) in acetonitrile (5 mL). A pale yellow product was obtained after one hour. This solid was collected by filtration, washed thoroughly with diethyl ether and dried in air. By recrystallization of the product in CH₂Cl₂, colorless plates of **Mn3** suitable for X-ray diffraction were obtained. Yield: 92.4 mg (57 %). Anal. Found (Calc.) for C₂₀H₂₂N₆O₅Mn: C, 49.57 (49.90); H, 4.01 (4.60); N, 17.52 (17.45) %. IR (cm⁻¹): ν = 3145-3050 (ν (NH)); 2926 (ν (C-H)sp³); 1587 (ν (COO⁻)_{as}); 1407 (ν (COO⁻)_s); 899 (δ(COO⁻)) cm⁻¹. E_{1/2} (III/II): 0.74 V vs. Ag/AgNO₃ (CH₃CN + 0.1 M TBAH). ESI-MS (m/z): 558 [{Mn(pypz-H)₂(μ-OAc)₃}]⁺.

[Mn^{II}(NO₃)₂(pypz-H)₂], Mn4. 0.15 g (1 mmol) of *pypz-H* (L1) were added to a solution of Mn(NO₃)₂·4H₂O (0.13 g, 0.5 mmol) in ethanol (5 mL) under stirring. After one hour, diethyl ether was added, giving rise to the precipitation of a pale brown solid that was collected by filtration, washed thoroughly with diethyl ether and dried in air. Suitable crystals as colorless blocks were grown by diffusion of ethyl ether into an acetone solution of the compound. Yield: 0.18 g (74 %). Anal. Found (Calc.) for C₁₆H₁₄N₆O₆Mn: C, 39.39 (40.95); H, 2.96 (3.01); N, 22.86 (23.88) %. IR (cm⁻¹): ν = 3174 (ν (OH)); 3045-2925 (ν (NH)); 1607-1517 (ν (NO₂)); 1431 (ν (C-C)sp²); 1301 (ν (C-N)sp²). E_{pa} (III/II): 0.73 V vs. Ag/AgNO₃ (CH₃CN + 0.1M [(nBu)₄N]PF₆). ESI-MS (m/z): 489 ([Mn(NO₃)₂(pypz-H)₂·H₃O]⁺.

[Mn^{II}Cl₂(pypz-H)(H₂O)₂], Mn5. To a solution of MnCl₂ (0.087 g, 0.695 mmol) in ethanol (5 mL), 0.102 g of *pypz-H* (L1) (0.705 mmol) were added under stirring. The resulting pale yellow solution was stirred for 10 min and afterwards a white solid precipitated. This solid was filtered off, washed with diethyl ether and dried in air. Colorless plates, suitable for X-ray diffraction, were grown by recrystallization in ethanol. Yield: 0.16 g (73 %). Anal. Found (Calc.) for C₈H₁₁Cl₂Mn N₃O₂: C, 31.47 (31.29); H, 3.55 (3.61); N, 13.73 (13.69) %. IR (cm⁻¹): ν = 3328-3222

Chapter III

(ν (OH)); 3140-3119 (ν (NH)); 1606 (ν (C-N) sp^2); 1429 (ν (C-C) sp^2) cm^{-1} . $E_{1/2}$ (III/II): 0.66 V vs. Ag/AgNO₃ (CH₃CN + 0.1 M TBAH). ESI-MS (m/z): 660 [$\{MnCl(H_2O)(pypzH)\}_2(\mu-Cl)_2\} \cdot Na^+$].

[Mn^{II}Cl₂(pypz-Me)₂], Mn6. To a solution of MnCl₂ (0.030 g, 0.236 mmol) in acetonitrile (5 mL), 0.072 g of *pypz-Me* (L2) (0.472 mmol) were added under stirring. The resulting white solution was stirred for 10 min and afterwards a white solid precipitated. This solid was filtered off, washed with diethyl ether and dried in air. Colorless plates, suitable for X-ray diffraction, were obtained from the mother liquor. Yield: 73.7 mg (70 %). Anal. Found (Calc.) for C₁₈H₁₉Cl₂N₆Mn: C, 47.93 (48.27); H, 3.70 (4.08); N, 18.65 (18.92) %. IR (cm^{-1}): ν = 3238-3142, 1604 (ν (C-N) sp^2), 1431 (ν (C-C) sp^2). $E_{1/2}$ (III/II): 0.62 V vs. Ag/AgNO₃ (CH₃CN 0.1 M + TBAH). ESI-MS (m/z): 408 [MnCl(pypz-Me)₂]⁺.

[Mn^{II}(CF₃SO₃)₂(pypz-Me)₂], Mn7. 0.058 g (0.365 mmol) of *pypz-Me* were added under stirring to a solution of Mn(CF₃SO₃)₂ (0.064 g, 0.183 mmol) in anhydrous THF (5 mL). After one hour a white precipitate was obtained and collected by filtration, washed thoroughly with diethyl ether and dried in vacuum. Colorless needles, suitable for X-ray diffraction, were grown by diffusion of ethyl ether into a THF solution of the compound. Yield: 70.2 mg (57 %). Anal. Found (Calc.) for C₂₀H₁₈F₆N₆O₆S₂Mn: C, 36.11 (35.78); H, 2.63 (2.70); N, 12.28 (12.52) %. IR (cm^{-1}): ν = 3238-3142, 1608 (ν (C-N) sp^2), 1437 (ν (C-C) sp^2), 1303 (ν (C-N) sp^2), 1208-1163 (ν (S-O) sp^2). $E_{1/2}$ (III/II): 0.76 V vs. Ag/AgNO₃ (CH₃CN 0.1 M + TBAH). ESI-MS (m/z): 522 [Mn(CF₃SO₃)(pypz-Me)₂]⁺.

[Mn^{II}(CF₃SO₃)₂(pypz-CH₂COOEt)₂], Mn8. 0.115 g (0.500 mmol) of *pypz-CH₂COOEt* (L3) were added under stirring to a solution of Mn(CF₃SO₃)₂ (0.088 g, 0.250 mmol) in aqueous THF (5 mL). The resulting white solution was stirred for 30 min and afterwards a white solid precipitated. This solid was collected by filtration, washed thoroughly with diethyl ether and dried in air. Colorless needles, suitable for X-ray diffraction, were grown by diffusion of diethyl ether into a CH₂Cl₂ solution of the compound. Yield: 123.3 mg (60 %). Anal. Found (Calc.) for C₂₆H₂₆N₆F₆O₁₀S₂Mn·0.5 THF: C, 39.21 (39.49); H, 3.47 (3.55); N, 9.58 (9.87) %. IR (cm^{-1}): ν = 3122, 2977 (ν (C-C) sp^3), 1742 (ν (C-O)_{st}), 1607 (ν (C-N) sp^2), 1304 (ν (C-N) sp^2), 1210-1167 (ν (S-O) sp^2). $E_{1/2}$ (III/II): 0.80 V vs. Ag/AgNO₃(CH₃CN 0.1 M + TBAH). ESI-MS (m/z): 666 [Mn(CF₃SO₃)(pypz-CH₂COOEt)₂]⁺, 258.5 [Mn(pypz-CH₂COOEt)₂]²⁺.

[Mn^{III}Cl(Ophpz-H)₂·3H₂O], Mn9. 100 mg (0.624 mmol) of HOphpz-H (L4) were added to a solution of MnCl₂ (39.3 mg, 0.312 mmol) in ethanol (5 mL) under stirring. Afterwards, 0.3 mL of NaOH 1 M were added to the reaction mixture and this solution turned from yellow to dark

green. After one hour, 15 mL of distilled water were added, giving rise to the precipitation of a dark green solid that was collected by filtration, washed thoroughly with cool water and dried in air. After one week, air-stable, dark green crystals of **Mn9**, suitable for X-ray diffraction analysis, were obtained from the mother liquor. Yield: 27.6 mg (19 %). Anal. Found (Calc.) for $C_{18}H_{14}ClN_4O_2Mn \cdot 3H_2O$: C, 46.74 (46.71); H, 4.10(4.36); N, 12.05 (12.10) %. IR (cm^{-1}): $\nu = 3360-3258$ (ν (OH)); 1601-1560 (ν (C-N) sp^2). E_{pa} (IV/III): 0.63 V vs. Ag/AgNO₃ (CH₃CN + 0.1 M TBAH). UV-Vis (CH₃CN) [λ_{max} , nm (ϵ , M⁻¹ cm⁻¹): 636 (202.34). ESI-MS (m/z): 373 [Mn(Ophpz-H)₂]⁺.

III.2.3. Synthesis of ruthenium compounds

[RuCl₂(dmsO)₄] (**P1**),^{106a} [RuCl₂(pypz-H)(dmsO)₂] (**P2**),^{184a} [RuCl₃(trpy)] (**P3**),²⁹⁶ [RuCl₂(bpea)(dmsO)] (bpea= *N,N*-bis(pyridin-2-ylmethyl)ethanamine) (**Ru12**),^{106c} [RuCl₂(NO₂-pzH)(dmsO)₂] (**Ru13**)^{184b} were prepared according to literature procedures.

cis,cis- and **cis,trans-[Ru^{II}Cl₂(pypz-CH₂COOEt)(dmsO)₂], Ru1a and Ru1b.** A 0.046 g (0.200 mmol) sample of *pypz-CH₂COOEt* (**L3**) were added to a solution of [RuCl₂(dmsO)₄] (**P1**) (0.097 g, 0.200 mmol) in absolute ethanol (15 mL) under stirring and the resulting solution was refluxed for 2 h. Afterwards, the solvent volume was reduced to 7 mL and the solution was cooled, giving rise to the precipitation of an orange solid. The solid was filtered on a frit, washed with diethyl ether and vacuum-dried. This solid was a mixture approximately 1: 0.5 of complexes **Ru1a** and **Ru1b**. Overall yield: 54 mg (48 %). Anal. Found (Calc.) for C₁₆H₂₅Cl₂N₃O₄RuS₂: C, 34.25 (34.35); H, 4.58 (4.50); N, 7.48 (7.51) %. IR (ν_{max} , cm^{-1}): 3010 (ν (=C-H)), 2918 (ν (-C-H)), 1747 (ν (-C=O)), 1207 (ν (-C-O)), 1091-916 (ν (-C-H)). UV-Vis (CH₂Cl₂) [λ_{max} , nm (ϵ , M⁻¹ cm⁻¹): 278 (579), 376 (152). ESI-MS (m/z): 524 [RuCl(pypz-CH₂COOEt)(dmsO)₂]⁺.

Suitable crystals of **Ru1a** were obtained as orange blocks by slow evaporation of the mother liquor. $E_{1/2}$ (III/II) = 1.14 V vs. SCE (CH₂Cl₂ + 0.1 M TBAH). ¹H-NMR (400 MHz, CDCl₃, 20 °C): δ 1.33 (t, 3H, H12, ³ $J_{H,H}$ = 7.2 Hz), 2.49 (s, 3H, H14), 3.19 (s, 3H, H15), 3.51 (s, 3H, H13), 3.61 (s, 3H, H16), 4.248 (q, 1H, H11', ³ $J_{H,H}$ = 7.1 Hz), 4.252 (q, 1H, H11, ³ $J_{H,H}$ = 7.1 Hz), 4.97 (d, 1H, H9', ² $J_{H,H}$ = 18.0 Hz), 6.82 (d, 1H, H9, ² $J_{H,H}$ = 18.0 Hz), 6.98 (d, 1H, H7, ³ $J_{H,H}$ = 2.8 Hz), 7.35 (m, 1H, H2), 7.64 (d, 1H, H8, ³ $J_{H,H}$ = 2.8 Hz), 7.80-7.82 (m, 2H, H3, H4), 9.88 (ddd, 1H, H1, ³ $J_{H,H}$ = 5.6, 1.2 Hz, ⁴ $J_{H,H}$ = 0.8 Hz) ppm. ¹³C-NMR (400 MHz, CDCl₃, 20 °C): δ 14.3 (1), 44.3 (13), 45.2 (16), 45.7 (15), 45.8 (14), 54.2 (4), 62.4 (2), 105.2 (6), 121.6 (9), 124.5 (11), 137.1 (10), 137.2 (5), 152.7 (7), 153.7 (8), 157.1 (12), 168.9 (3) ppm.

Suitable crystals of **Ru1b** as pale yellow plates were grown by diffusion of diethyl ether into a chloroform solution of the orange solid. $E_{1/2}$ (III/II) = 0.96 V vs. SCE (CH₂Cl₂ + 0.1 M TBAH). ¹H-

Chapter III

NMR (400 MHz, CDCl₃, 20 °C): δ 1.34 (t, 3H, H12, ³J_{H,H}= 7.2 Hz), 3.01 (s, 6H, H13 H16), 3.16 (s, 6H, H14, H15), 4.28 (q, 2H, H11, ³J_{H,H}= 7.2 Hz), 5.95 (s, 2H, H9), 6.93 (d, 1H, H7, ³J_{H,H}=2.90 Hz), 7.35 (m, 1H, H2), 7.66 (d, 1H, H8, ³J_{H,H}= 2.90 Hz), 7.76 (ddd, 1H, H4, ³J_{H,H}= 7.90, ⁴J_{H,H}= 1.60, 0.70 Hz), 7.85 (ddd, 1H, H3, ³J_{H,H}= 7.90, 7.60 Hz, ⁴J_{H,H}= 1.50 Hz), 9.56 (ddd, 1H, H1, ³J_{H,H}= 5.90, 1.52 Hz, ⁴J_{H,H}= 0.70 Hz) ppm. ¹³C-NMR (400 MHz, CDCl₃, 20 °C): δ 14.3 (12), 41.7 (15, 14), 42.8 (13, 16), 53.4 (9), 62.3 (11), 105.8 (7), 121.1 (4), 123.9 (2), 136.4 (8), 136.7 (3), 153.2 (6), 154.4 (1), 155.9 (5), 168.0 (10) ppm.

For the NMR assignments we use the same labeling scheme as for the X-ray structures (Figure IV.2.1).

[Ru^{II}Cl₂(HOphpz-H)(dmsO)₃] and [Ru^{II}Cl₂(HOphpz-H)₂(dmsO)₂], Ru2 and Ru2'. A mixture of [RuCl₂(dmsO)₄] (**P1**) (77 mg, 0.15 mmol) and *HOphpz-H* (*L3*) (25 mg, 0.15 mmol) in CH₂Cl₂ (4 mL) was refluxed at 40 °C for 90 minutes. After this time, the reaction was cooled to room temperature and a greenish-yellow solid was formed. This greenish-yellow solid, which corresponds to the minor product **Ru2'** complex, was recovered with a glass frit and dried under vacuum. Yield: 10.2 mg (10 %). Afterwards, the volume was reduced and **Ru2** complex was obtained by adding diethyl ether to the mother liquor. The pure **Ru2** complex was obtained in this manner as a pale yellow solid. Yield: 35.3 mg (45 %).

For **Ru2'**, ¹H-NMR (400 MHz, acetone d₆, 20 °C): δ = 3.14 (s, 12H, CH₃-dmsO), 6.81 (dd, 2H, H2, ³J_{H,H}= 2.16, 2.14 Hz), 6.94 (ddd, 2H, H8, ³J_{H,H}= 7.80, 7.19 Hz, ⁴J_{H,H}= 1.09 Hz), 7.07 (dd, 2H, H6, ³J_{H,H}= 7.73 Hz, ⁴J_{H,H}= 1.09 Hz), 7.21 (ddd, 2H, H7, ³J_{H,H}= 7.73, 7.19 Hz, ⁴J_{H,H}= 1.55 Hz), 7.68 (dd, 2H, H9, ³J_{H,H}= 7.80 Hz, ⁴J_{H,H}= 1.55 Hz), 8.09 (d, 2H, H3, ³J_{H,H}= 2.14 Hz), 9.89 (s, 2H, H10), 13.41 (s, 2H, H2A) ppm. Suitable greenish crystals for X-ray diffraction were grown by slow evaporation of the mother liquor. For the NMR assignments we use the same labeling scheme as for the X-ray structure (Figure SIV.2.1). *E*_{pa} (II/III): 1.31 V vs. Ag/AgNO₃ (CH₃CN + 0.1 M TBAH). UV-Vis (MeOH) [λ_{max}, nm (ε, M⁻¹ cm⁻¹): 270 (17446), 306 (12307). ESI-MS (m/z): 646.8 [RuCl₂(Ophpz-H)(HOphpz-H)(dmsO)₂]⁻, 486.7 [RuCl₂(Ophpz-H)(dmsO)₂]⁻.

For **Ru2**, ¹H-NMR (400 MHz, acetone-d₆, 20 °C): δ = 3.19 (s, 6H, H12, H15), 3.45 (s, 6H, H11, H16), 3.48 (s, 6H, H13, H14), 6.85 (dd, 1H, H2, ³J_{H,H}= 2.1, 2.1 Hz), 6.97 (ddd, 1H, H8, ³J_{H,H}= 7.5, 7.3 Hz, ⁴J_{H,H}= 0.8 Hz), 7.10 (dd, 1H, H6, ³J_{H,H}= 7.7 Hz, ⁴J_{H,H}= 0.8), 7.25 (ddd, 1H, H7, ³J_{H,H}=7.7, 7.5 Hz, ⁴J_{H,H}= 1.5 Hz), 7.71 (dd, 1H, H9, ³J_{H,H}= 7.3 Hz, ⁴J_{H,H}= 1.5 Hz), 8.54 (dd, 1H, H3, ³J_{H,H}= 2.1, 2.1 Hz), 9.71 (s, 1H, H10), 14.36 (s, 1H, H2A) ppm. ¹³C-NMR (400 MHz, CDCl₃, 20 °C): δ 45.81 (C13, C14), 46.95 (C12, C15), 47.60 (C11, C16), 104.8 (C2), 116.2 (C4), 117.3 (C6), 121.0 (C8), 128.5 (C9), 130.9 (C7), 142.9 (C1), 143.3 (C3), 154.9 (C5) ppm. For the NMR assignment we have used

the numbering scheme shown in Figure IV.2.2. Anal Found (Calc.) for $C_{15}H_{26}Cl_2N_2O_4RuS_3 \cdot 1CH_2Cl_2 \cdot H_2O$: C, 28.76 (28.70); N, 3.79 (4.18); H, 4.41 (4.51) %. IR (cm^{-1}): $\nu = 3130$ (ν (OH)); 3010 (ν (NH)); 1594 (ν (C-N) sp^2); 1404 (ν (C-C) sp^2); 1065 (ν (S=O)). E_{pa} (II/III): 1.60 V vs. SCE ($CH_2Cl_2 + 0.1$ M TBAH). UV-Vis (MeOH) [λ_{max} , nm (ϵ , $M^{-1} cm^{-1}$)]: 302 (17593), 358 (1731). ESI-MS (m/z): 564.7 [$RuCl_2(Ophpz-H)(dmsO)_3$] $^+$, 486.7 [$RuCl_2(Ophpz-H)(dmsO)_2$] $^+$, 408.7 [$RuCl_2(Ophpz-H)(dmsO)$].

[$Ru^{II}Cl_2(MeOphpz-H)(dmsO)_3$], Ru3. A mixture of [$RuCl_2(dmsO)_4$] (**P1**) (100 mg, 0.206 mmol) and *MeOphpz-H* (**L2**) (35.9 mg, 0.206 mmol) in CH_2Cl_2 (5 mL) was refluxed at 40 °C for 3 h minutes. After this time, the reaction was cooled to room temperature and the volume was reduced to 1 mL. The addition of diethyl ether provoked the precipitation of the pale yellow **Ru3** product, which was recovered with a glass frit, washed with diethyl ether and dried at vacuum. Yield: 86 mg (77 %). Suitable pale yellow crystals for X-ray diffraction were formed by slow evaporation of the mother liquor. 1H -NMR (400 MHz, acetone- d_6 , 20 °C): $\delta = 3.21$ (s, 6H, H12, H15), 3.47 (s, 6H, H11, H16), 3.49 (s, 6H, H13, H14), 4.04 (s, 3H, H10), 6.87 (dd, 1H, H2, $^3J_{H,H} = 2.22, 2.22$ Hz), 7.07 (ddd, 1H, H8, $^3J_{H,H} = 7.58, 7.56$ Hz, $^4J_{H,H} = 1.06$ Hz), 7.19 (d, 1H, H6, $^3J_{H,H} = 7.87$ Hz, $^4J_{H,H} = 1.06$ Hz), 7.40 (ddd, 1H, H7, $^3J_{H,H} = 7.87, 7.56$ Hz, $^4J_{H,H} = 1.67$ Hz), 7.80 (dd, 1H, H9, $^3J_{H,H} = 7.58$ Hz, $^4J_{H,H} = 1.67$ Hz), 8.53 (dd, 1H, H3, $^3J_{H,H} = 2.22, 2.22$ Hz), 14.44 (s, 1H, H2A) ppm. ^{13}C -NMR (400 MHz, $CDCl_3$, 20 °C): δ 45.8 (C13, C14), 46.9 (C12, C15), 47.6 (C11, C16), 55.4 (C10), 104.9 (C2), 112.7 (C6), 121.9 (C8), 128.6 (C9), 130.6 (C4), 131.2 (C7), 142.99 (C3), 143.01 (C1), 157.1 (C5) ppm. For the NMR assignment we have used the numbering scheme shown in Figure IV.2.2. Anal Found (Calc.) for $C_{16}H_{28}Cl_2N_2O_4RuS_3$: C, 32.84 (33.10); N, 3.79 (4.83); H, 4.75 (4.86) %. IR (cm^{-1}): $\nu = 3130$ (ν (OH)); 3010 (ν (NH)); 1594 (ν (C-N) sp^2); 1404 (ν (C-C) sp^2); 1065 (ν (S=O)). E_{pa} (II/III): 1.65 V vs. SCE ($CH_2Cl_2 + 0.1$ M TBAH). UV-Vis (MeOH) [λ_{max} , nm (ϵ , $M^{-1} cm^{-1}$)]: 358 (725). ESI-MS (m/z): 545.12 [$RuCl(MeOphpz-H)(dmsO)_3$] $^+$.

[$Ru^{II}Cl_2(pz-H)_2(dmsO)_2$], Ru4. This complex was obtained from modified literature procedure.²⁹⁷

A 0.120 g (0.25 mmol) sample of [$Ru^{II}Cl_2(dmsO)_4$] (**P1**) and 0.034 g (0.50 mmol) of pyrazole were refluxed in 10 mL of methanol for 2 h. Afterwards, the volume of the solution was reduced to 5 mL and cooled at 0 °C. Orange crystals corresponding to **Ru4** were collected on a frit and washed with diethyl ether and dried in vacuum. Yield: 70 mg (60 %). 1H -NMR (400 MHz, CD_2Cl_2 , 20 °C) = δ 3.14 (s, 12H, CH_3 - $dmsO$), 6.39 (m, 2H, H2), 7.66 (m, 2H, H1), 7.90 (m, 2H, H3), 12.63 (s, 2H, N-H) ppm. UV-Vis (H_2O) [λ_{max} , nm (ϵ , $M^{-1} cm^{-1}$)]: 228 (1033), 300 (46).

[$Ru^{II}Cl_2(3,4-dmpzH)_2(dmsO)_2$], Ru5. This compound was prepared following a method analogous to that described for **Ru4** starting from [$Ru^{II}Cl_2(dmsO)_4$] (**P1**) (0.120 g, 0.25 mmol)

Chapter III

and 3,4-dimethylpyrazole (0.048 g, 0.50 mmol). Suitable crystals for X-ray diffraction were grown by slow evaporation of the mother liquor. Yield: 53 mg (41 %). Anal. Found (Calc.) for $C_{14}H_{28}N_4Cl_2O_2S_2Ru$: C, 32.13 (32.31); H, 5.47 (5.42); N, 10.35 (10.76) %. 1H -NMR (400 MHz, CD_2Cl_2 , 20 °C) = δ 1.95 (s, 6H, H5, H10), 2.22 (s, 6H, H9, H4), 3.19 (s, 12H, H11, H12, H13, H14), 7.62 (s, 2H, H3, H8), 11.98 (s, 2H, H2B, H4D) ppm. ^{13}C -NMR (400 MHz, CD_2Cl_2 , 20 °C) = δ 8.45 (5), 9.71 (4), 44.82 (6), 114.83 (2), 138.35 (2), 141.44 (1) ppm. For the NMR assignments we use the same labeling scheme as for the X-ray structures (Figure IV.2.3). IR (ν_{max} , cm^{-1}): ν 1092 (ν (S-O)), 1016 (ν (S-O)). $E_{1/2}$ (III/II) = 1.02 V vs. SCE (CH_2Cl_2 + 0.1 M TBAH). UV-Vis (H_2O) [λ_{max} , nm (ϵ , $M^{-1} cm^{-1}$): 238 (1476), 302 (102). ESI-MS (m/z): 485 $[RuCl(3,4-dmpzH)_2(dmsO)_2]^+$.

$[Ru^{II}Cl_2(3,5-dmpzH)_2(dmsO)_2]$, Ru6. This complex was prepared following a different procedure to that previously described in the literature.²⁹⁸

0.120 g (0.25 mmol) of $[Ru^{II}Cl_2(dmsO)_4]$ (**P1**) and 0.048 g (0.50 mmol) of 3,5-dimethylpyrazole were refluxed in 10 mL of methanol for 2 h. Afterwards, the volume of the solution was reduced to 1 mL and cooled at 0 °C. A yellow solid corresponding to **Ru6** was formed and was filtered on a frit, washed with diethyl ether and dried in vacuum. Yield: 55 mg (43 %). Anal. Exp. (calc) per $C_{14}H_{28}Cl_2N_4O_2S_2Ru$: C, 32.59 (32.31), N, 10.63 (10.76), H, 5.72 (5.42), S, 12.03 (12.32) %. 1H -NMR (400 MHz, CD_2Cl_2 , 20 °C) = δ 1.70 (s, 3H, H9), 2.12 (s, 3H, H4), 2.33 (s, 6H, H5, H10), 2.70 (s, 3H, H11), 2.86 (s, 3H, H14), 3.41 (s, 3H, H12), 3.77 (s, 3H, H13), 5.83 (s, 1H, H2), 5.90 (s, 1H, H7), 11.15 (s, 1H, H4A), 12.10 (s, 1H, H2A) ppm. $E_{1/2}$ (III/II) = 1.15 V vs. SCE (CH_2Cl_2 + 0.1 M TBAH). UV-Vis (MeOH) [λ_{max} , nm (ϵ , $M^{-1} cm^{-1}$): 364 (1472).

$[Ru^{II}Cl_2(trpy)(dmsO)]$ (P4). This complex was prepared through a modification of the method previously described in the literature.²⁹⁹

A 0.250 g (0.516 mmol) sample of $[Ru^{II}Cl_2(dmsO)_4]$ (**P1**) and 0.123 g (0.516 mmol) of 2,2':6',2''-terpyridine, *trpy*, were dissolved in 40 mL of absolute ethanol, and the resulting solution was refluxed for 2 h. A dark solid, corresponding to the mixture of *trans*- and *cis*- $[Ru^{II}Cl_2(dmsO)(trpy)]$ in a 1:0.6 ratio, was formed in solution and was filtered on a frit and washed with diethyl ether. A brown solid was obtained by reducing the volume of the mother liquor to 15 mL, and this solid corresponds to a mixture of *trans*- and *cis*- $[Ru^{II}Cl_2(trpy)(dmsO)]$ in a 0.4:1 ratio. Pure *cis*- $[Ru^{II}Cl_2(trpy)(dmsO)]$ was obtained as red crystals by slow evaporation of the solution at room temperature. Yield: 200.8 mg (80 %). $E_{1/2}$ (III/II): 0.69 (*trans*-), 0.88 (*cis*-) V vs. SCE (CH_2Cl_2 + 0.1 M TBAH).

***cis-* and *trans*-[Ru^{II}Cl(*pypz*-H)(*trpy*)](PF₆), **Ru7a** and **Ru7b**.**

Isomeric complexes **Ru7a** and **Ru7b** were obtained following three different synthetic routes, A-C, detailed below.

Route A

A 0.558 g (1.179 mmol) sample of [Ru^{II}Cl₂(*pypz*-H)(*dms*o)] complex (**P2**) and 0.275 g (1.155 mmol) of *trpy* were refluxed in 150 mL of methanol for 18 h. Afterwards, the solution was evaporated to dryness in a rotary evaporator and the residue redissolved in MeOH:NH₄OH (75:1). The mixture was cooled in an ice bath until a brown precipitate was formed, that was filtered on a frit and washed two times with cold MeOH:NH₄OH (75:1) mixture. At this point, the solid (PP1) and the filtrate (F1) were treated separately. Brown solid PP1 was purified through a recrystallization by dissolving it in a mixture of MeOH:HCl (adjusting the pH to < 2), followed by addition of 1 mL of a saturated NH₄PF₆ aqueous solution together with 100 mL of cold water under vigorous stirring. After cooling in an ice bath, pure **Ru7b** complex precipitated (267 mg, 34 % yield) that was filtered off and washed with cold H₂O and diethyl ether. On the other hand, filtrate F1 was reduced to dryness and purified by column chromatography (SiO₂, eluent MeOH:NH₄OH 30:1). The first orange fraction containing Ru(*trpy*)₂²⁺ was discarded together with a second purple fraction. Finally, a third brownish fraction containing the *cis*-isomer was obtained that was evaporated to dryness and redissolved in 10 mL of a MeOH:HCl mixture (pH<2). Then a saturated aqueous NH₄PF₆ solution was added and the resulting solution was cooled until precipitation. The fine crystalline precipitate was filtered off, washed twice with cold H₂O and diethyl ether and dried in vacuum obtaining 98.7 mg (13 % yield) of pure **Ru7a** complex.

A higher yield of **Ru7b** product can be obtained following the same synthetic procedure but using absolute ethanol instead of methanol as solvent, and maintaining the reflux throughout 48 h. Subsequent precipitation with aqueous saturated NH₄PF₆ solution and purification of the solid by column chromatography (Al₂O₃, eluent CH₂Cl₂:CH₃OH, 99:1 mixture) leads to the obtaining of pure **Ru7b** in 48 % yield.

Route B

A sample of [Ru^{III}Cl₃(*trpy*)] (**P3**, 0.1 g, 0.23 mmol) was added to a solution of LiCl (22 mg, 0.52 mmol) dissolved in 15 mL of EtOH:H₂O (9:1) under magnetic stirring. Then, NEt₃ (0.07 mL, 0.52 mmol) was added and the reaction mixture was stirred under N₂ atmosphere at room temperature for 30 min. Afterwards, *pypz*-H (0.033 g, 0.23 mmol) was added and the mixture

Chapter III

was refluxed for 2 h. The hot solution was then filtered off in a frit and the volume was reduced in a rotary evaporator. After addition of a saturated NH_4PF_6 aqueous solution a precipitate was formed which was filtered off and washed with cold water. This solid was purified by column chromatography (Al_2O_3 , eluent $\text{CH}_2\text{Cl}_2:\text{CH}_3\text{OH}$, 99:1 mixture) and a purple-reddish fraction, corresponding to complex **Ru7b**, was obtained (32 mg, 21 % yield) together with other secondary products.

Route C

A 150 mg (0.34 mmol) of complex $[\text{Ru}^{\text{II}}\text{Cl}_2(\text{trpy})(\text{dmsO})]$ (**P4**) and 49 mg (0.34 mmol) of *pypzH* were refluxed in 20 mL of absolute ethanol for 20 hours. After the reaction time, the mixture was cooled to room temperature and the volume was reduced. Afterwards, a saturated aqueous solution of NH_4PF_6 was added and a brown precipitate was formed, which was separated by filtration, washed with diethyl ether and dried in vacuum. This solid was purified by column chromatography (Al_2O_3 , eluent $\text{CH}_2\text{Cl}_2:\text{CH}_3\text{OH}$, 99:1 mixture), obtaining the pure **Ru7b** complex. Yield: 128 mg (57 %).

For Ru7a: $^1\text{H-NMR}$ (400 MHz, methanol- d_4 , 20 °C): δ 6.88 (ddd, 1H, H2, $^3J_{\text{H,H}} = 8.04, 6.66$ Hz, $^4J_{\text{H,H}} = 1.45$ Hz), 7.15 (ddd, 1H, H1, $^3J_{\text{H,H}} = 6.66$ Hz, $^4J_{\text{H,H}} = 1.33$ Hz, $^5J_{\text{H,H}} = 0.80$ Hz), 7.37 (ddd, 2H, H10, H22, $^3J_{\text{H,H}} = 7.53, 6.59$ Hz, $^4J_{\text{H,H}} = 1.31$ Hz), 7.53 (d, 1H, H7, $^3J_{\text{H,H}} = 2.89$ Hz), 7.65 (td, 1H, H3, $^3J_{\text{H,H}} = 7.98$ Hz, $^4J_{\text{H,H}} = 1.33$ Hz), 7.76 (ddd, 2H, H9, H23, $^3J_{\text{H,H}} = 6.59$ Hz, $^4J_{\text{H,H}} = 1.43$ Hz, $^5J_{\text{H,H}} = 0.71$ Hz), 7.92 (td, 2H, H11, H21, $^3J_{\text{H,H}} = 7.71$ Hz, $^4J_{\text{H,H}} = 1.43$ Hz), 8.08 (ddd, 1H, H4, $^3J_{\text{H,H}} = 7.98, ^4J_{\text{H,H}} = 1.45, ^5J_{\text{H,H}} = 0.80$ Hz), 8.12 (t, 1H, H16, $^3J_{\text{H,H}} = 8.06$ Hz), 8.38 (d, 1H, H8, $^3J_{\text{H,H}} = 2.89$ Hz), 8.50 (ddd, 2H, H12, H20, $^3J_{\text{H,H}} = 7.71$ Hz, $^4J_{\text{H,H}} = 1.13$ Hz, $^5J_{\text{H,H}} = 0.81$ Hz), 8.62 (d, 2H, H15, H17, $^3J_{\text{H,H}} = 8.06$ Hz) ppm. $^{13}\text{C-NMR}$ (400 MHz, methanol- d_4 , 20 °C): δ 106.0 (C7), 123.1 (C4), 123.6 (C15, C17), 124.6 (C12, C20), 125.3 (C2), 128.5 (C10, C22), 134.7 (C8), 134.9 (C16), 137.1 (C3), 138.1 (C11, C21), 152.7 (C1), 154.0 (C9, C23), 160.4 (C13, C19), 160.6 (C14, C18), 168.2 (C6), 168.3 (C5) ppm. For the NMR assignments we use the same labeling scheme shown in Figure IV.3.2. IR (ν_{max} , cm^{-1}): 3648, 3562, 1594, 1445, 1382, 838, 760. $E_{1/2}$ (III/II): 0.88 V vs. SCE ($\text{CH}_2\text{Cl}_2 + 0.1$ M TBAH). UV-Vis (CH_2Cl_2) [λ_{max} , nm (ϵ , $\text{M}^{-1} \text{cm}^{-1}$): 238 (1480), 276 (1163), 318 (1198).

For Ru7b: $^1\text{H-NMR}$ (400 MHz, methanol- d_4 , 20 °C): δ 7.09 (d, 1H, H7, $^3J_{\text{H,H}} = 2.84$ Hz), 7.32 (ddd, 2H, H10, H22, $^3J_{\text{H,H}} = 6.88, 6.57$ Hz, $^4J_{\text{H,H}} = 1.30$ Hz), 7.48 (d, 1H, H8, $^3J_{\text{H,H}} = 2.84$ Hz), 7.70 (ddd, 2H, H9, H23, $^3J_{\text{H,H}} = 6.57$ Hz, $^4J_{\text{H,H}} = 1.98$ Hz, $^5J_{\text{H,H}} = 0.72$ Hz), 7.81 (ddd, 1H, H2, $^3J_{\text{H,H}} = 6.54, 5.61$ Hz, $^4J_{\text{H,H}} = 1.4$ Hz), 7.91 (td, 2H, H11, H21, $^3J_{\text{H,H}} = 6.88$ Hz, $^4J_{\text{H,H}} = 1.98$ Hz), 8.10 (t, 1H, H16, $^3J_{\text{H,H}} = 8.10$ Hz), 8.23 (ddd, 1H, H3, $^3J_{\text{H,H}} = 7.78, 6.54$ Hz, $^4J_{\text{H,H}} = 1.46$ Hz), 8.36 (dd, 1H, H4, $^3J_{\text{H,H}} = 7.78$ Hz, $^4J_{\text{H,H}} = 1.41$ Hz), 8.48 (ddd, 2H, H12, H20, $^3J_{\text{H,H}} = 8.05$ Hz, $^4J_{\text{H,H}} = 1.30$ Hz, $^5J_{\text{H,H}} = 0.72$ Hz), 8.58 (d, H15,

H17, $^3J_{\text{H,H}} = 8.10$ Hz), 10.02 (ddd, 1H, H1, $^3J_{\text{H,H}} = 5.61$ Hz, $^4J_{\text{H,H}} = 1.46$ Hz, $^5J_{\text{H,H}} = 0.9$ Hz) ppm. ^{13}C -NMR (400 MHz, methanol- d_4 , 20 °C): δ 105.3 (C7), 123.2 (C4), 123.3 (C15, C17), 124.1 (C12, C20), 125.3 (C2), 128.3 (C10, C22), 134.2 (C8), 134.9 (C16), 137.9 (C11, C21), 138.0 (C3), 153.6 (C9, C23), 160.7 (C13, C19), 160.8 (C14, C18), 160.9 (C5, C6) ppm. Suitable crystals for X-ray diffraction were grown as brownish-purple needles by diffusion of diethyl ether into a CH_2Cl_2 solution of the pure complex. For the NMR assignments we use the same labeling scheme as for the X-ray structures (Figure IV.3.2). IR (ν max, cm^{-1}): 3800-3000 (w), 3200-2800 (m), 1628, 1445, 1386, 1062, 842, 760. $E_{1/2}$ (III/II): 0.80 V vs. SCE (CH_2Cl_2 + 0.1 M TBAH). UV-Vis (CH_2Cl_2) [λ_{max} , nm (ϵ , $\text{M}^{-1} \text{cm}^{-1}$): 236 (1477), 276 (1235), 322 (1146). ESI-MS (m/z): 514.9 [$\text{Ru}^{\text{II}}\text{Cl}(\text{trpy})(\text{pypz-H})$] $^+$.

[$\text{Ru}^{\text{II}}(\text{pypz-H})(\text{trpy})(\text{dmsO})](\text{PF}_6)_2$, Ru8.

Complex **Ru8** was obtained as minor product in the synthesis of complexes **Ru7a** and **Ru7b** when following routes A (synthesis carried out in absolute ethanol) and C. $E_{1/2}$ (III/II) = 1.48 V vs. SCE (CH_2Cl_2 + 0.1 M TBAH). Suitable crystals for X-ray diffraction of **Ru8** were grown as brown large needles.

[$\text{Ru}_2^{\text{II}}\text{Cl}(\text{trpy})_2(\mu\text{-Cl})(\mu\text{-pypz})](\text{PF}_6)$, Ru9

Complex **Ru9** was obtained as a minor product in the column chromatography carried out for the synthesis of complexes **Ru7a** and **Ru7b** by following route B, as a deep purple color fraction (12 mg, 5 % yield). $E_{1/2}$ (III-II/II-II): 0.49 V; $E_{1/2}$ (III-III/III-II): 0.96 V vs. SCE (phosphate buffer pH = 7).

For Ru9: ^1H -NMR (400 MHz, acetone- d_6 , 20 °C): δ 6.65 (td, 1H, H17, $^3J_{\text{H,H}} = 5.8$ Hz, $^4J_{\text{H,H}} = 1.48$ Hz), 7.04 (ddd, 1H, H16, $^3J_{\text{H,H}} = 5.68$ Hz, $^4J_{\text{H,H}} = 1.4$ Hz, $^5J_{\text{H,H}} = 0.76$ Hz), 7.54 (ddd, 2H, H2, H14, $^3J_{\text{H,H}} = 7.6$, 5.48 Hz, $^4J_{\text{H,H}} = 1.32$ Hz), 7.64 (td, 1H, H18, $^3J_{\text{H,H}} = 7.68$ Hz, $^4J_{\text{H,H}} = 1.4$ Hz), 7.65 (ddd, 2H, H25, H37, $^3J_{\text{H,H}} = 7.52$, 5.04 Hz, $^4J_{\text{H,H}} = 1.4$ Hz), 7.66 (t, 1H, H8, $^3J_{\text{H,H}} = 8.08$ Hz), 7.68 (d, 1H, H22, $^3J_{\text{H,H}} = 2.32$ Hz), 7.78 (td, 2H, H26, H36, $^3J_{\text{H,H}} = 7.68$ Hz, $^4J_{\text{H,H}} = 1.56$ Hz), 7.84 (td, 2H, H3, H13, $^3J_{\text{H,H}} = 7.76$ Hz, $^4J_{\text{H,H}} = 1.56$ Hz), 7.99 (t, 1H, H31, $^3J_{\text{H,H}} = 8.08$ Hz), 8.02 (ddd, 1H, H19, $^3J_{\text{H,H}} = 8.12$ Hz, $^4J_{\text{H,H}} = 1.44$ Hz, $^5J_{\text{H,H}} = 0.84$ Hz), 8.05 (ddd, 2H, H1, H15, $^3J_{\text{H,H}} = 5.44$ Hz, $^4J_{\text{H,H}} = 1.48$ Hz, $^5J_{\text{H,H}} = 0.72$ Hz), 8.26 (ddd, 2H, H27, H35, $^3J_{\text{H,H}} = 8.04$ Hz, $^4J_{\text{H,H}} = 1.32$ Hz, $^5J_{\text{H,H}} = 0.76$ Hz), 8.28 (d, 2H, H7, H9, $^3J_{\text{H,H}} = 8.04$ Hz), 8.36 (ddd, 2H, H4, H12, $^3J_{\text{H,H}} = 8.08$ Hz, $^4J_{\text{H,H}} = 1.20$ Hz, $^5J_{\text{H,H}} = 0.80$ Hz), 8.51 (d, 2H, H30, H32, $^3J_{\text{H,H}} = 8.08$ Hz), 8.80 (ddd, 2H, H24, H38, $^3J_{\text{H,H}} = 5.4$ Hz, $^4J_{\text{H,H}} = 1.48$ Hz, $^5J_{\text{H,H}} = 0.68$ Hz), 9.16 (d, 1H, H23, $^3J_{\text{H,H}} = 2.28$ Hz) ppm. ^{13}C -NMR (400 MHz, acetone- d_6 , 20 °C): δ 105.6 (C22), 120.5 (C19), 121.5 (C7, C9), 122.1 (C17), 122.9 (C27, C30, C32, C35), 123.9 (C4, C12), 127.3 (C25,

Chapter III

C37), 127.9 (C2, C14), 130.9 (C8), 133.2 (C31), 135.8 (C26, C36), 136.7 (C18), 137.0 (C3, C13), 143.6 (C23), 148.4 (C21), 152.2 (C16), 154.3 (C1, C15), 155.0 (C24, C38), 159.8 (C29, C33, C5, C11), 160.4 (C20), 161.2 (C28, C34), 162.7 (C6, C10) ppm. Suitable purple rhomboidal crystals for X-ray diffraction were grown by diffusion of diethyl ether into a CH₂Cl₂ solution of the pure complex. For the NMR assignments we use the same labeling scheme as for the X-ray structures (Figure IV.3.3). ESI-MS (m/z): 884.1 {[Ru^{II,III}Cl(trpy)₂(μ-Cl)(μ-pypz)]}⁺.

trans-[Ru^{II}(pypz-H)(trpy)(H₂O)](PF₆)₂, Ru10. 0.08 g of AgPF₆ (0.32 mmol) were added to a solution of **Ru7b** (0.1 g, 0.15 mmol) in 30 mL of H₂O, and the mixture was heated at reflux for 2 h in the absence of light. Then, the AgCl formed was filtered off through Celite. Afterwards, NH₄PF₆ (1 mL) was added to the filtrate and the volume reduced until a precipitate that corresponded to the **Ru10** aqua complex was formed, which was filtered on a filter, washed with cold water and diethyl ether and dried at vacuum. Yield: 0.040 g (40 %). ¹H-NMR (400 MHz, Methanol-d₄, 20 °C): δ 7.09 (d, 1H, H7, ³J_{H,H}= 2.94 Hz), 7.42 (ddd, 2H, H10, H22, ³J_{H,H}= 7.84, 5.53 Hz, ⁴J_{H,H}= 1.31 Hz), 7.53 (d, 1H, H8, ³J_{H,H}= 2.94 Hz), 7.78 (ddd, 2H, H9, H23, ³J_{H,H}= 5.53 Hz, ⁴J_{H,H}= 1.51 Hz, ⁵J_{H,H}= 0.76 Hz), 7.92 (ddd, 1H, H2, ³J_{H,H}= 7.66, 6.65 Hz, ⁴J_{H,H}= 1.44 Hz), 8.03 (ddd, 2H, H11, H21, ³J_{H,H}= 8.06, 7.84 Hz, ⁴J_{H,H}= 1.51 Hz), 8.25 (t, 1H, H16, ³J_{H,H}= 8.14 Hz), 8.33 (ddd, 1H, H3, ³J_{H,H}= 8.37, 7.66 Hz, ⁴J_{H,H}= 1.47 Hz), 8.47 (ddd, 1H, H4, ³J_{H,H}= 8.37 Hz, ⁴J_{H,H}= 1.44 Hz, ⁵J_{H,H}= 0.89 Hz), 8.58 (ddd, 2H, H12, H20, ³J_{H,H}= 8.06 Hz, ⁴J_{H,H}= 1.31 Hz, ⁵J_{H,H}= 0.76 Hz), 8.70 (d, 2H, H15, H17, ³J_{H,H}= 8.14 Hz), 9.48 (ddd, 1H, H1, ³J_{H,H}= 6.65 Hz, ⁴J_{H,H}= 1.47 Hz, ⁵J_{H,H}= 0.89 Hz) ppm. IR (ν_{max}, cm⁻¹): 3618, 3551, 1992, 1602, 1449, 820, 756. E_{1/2}(III/II): 0.26 V vs. SCE (phosphate buffer pH= 7). E_{1/2} (III/II): 0.40 V; E_{1/2} (IV/III): 0.69 V vs. SCE (phosphate buffer pH=7). UV-Vis (phosphate buffer pH= 7) [λ_{max}, nm (ε, M⁻¹ cm⁻¹): 230 (18800), 270 (16180), 315 (15060), 381 (3410), 460 (3654). For the NMR assignments we have used the numeration scheme in Figure IV.3.3.

[Ru^{II}(trpy)₂(μ-pypz)₂](PF₆)₂, Ru11

A single crystal of complex **Ru11** was obtained by treating **Ru7a** with AgPF₆ in H₂O at reflux for 2 h in the absence of light, after slow evaporation of the mother liquor.

III.2.4. Preparation of the heterogeneous systems

[Mn^{II}(OTf)₂(pypz-CH₂COOSiO₂)₂], SP@Mn8. SP (0.1 g) was added to a solution of **Mn8** (0.03 g, 0.037 mmol) in toluene (5 mL) and stirred at 35 °C for 6 days. The resulting product was centrifuged, washed with methanol (2 x 5 mL) and acetone (5 mL) and dried in a hot air oven at 110 °C. UV-Vis (MeOH) [λ_{max}, nm]: 248, 288.

[Ru^{II}Cl₂(dmsO)₂(pypz-CH₂COOSiO₂)], SP@Ru1. SP (0.1 g) was added to a solution of **Ru4** (0.05 g, 0.089 mmol) in EtOH:H₂O (7 mL, 6:1). Then, 1.5 equivalents of LiOH 4 M (0.133 mmol) were added and the dispersion was magnetically stirred at 50 °C for 1 h. Afterwards, the resulting dispersion was centrifuged, washed with MeOH (3 x 5 mL) and acetone (5 mL) and dried at vacuum. IR (ν_{\max} , cm⁻¹): 1699 (ν (C=O)_{st}). UV-Vis (MeOH) [λ_{\max} , nm]: 280, 378.

[Ru^{II}Cl₂(dmsO)₂(pypz-CH₂COOSiO₂@Fe₃O₄)], MSNP@Ru1. 0.025 g (0.045 mmol) of **Ru4** were added to a dispersion of **MSNP** (0.05 g) in EtOH:H₂O (7 mL, 6:1). Then, 1.5 equivalents of LiOH 4M (0.067 mmol) were added and the dispersion was mechanically stirred at room temperature for 4 h. Afterwards, the **MSNP@Ru1** were magnetically separated from the solution, washed with MeOH (3 x 5 mL) and acetone (5 mL) and dried at vacuum. IR (ν_{\max} , cm⁻¹): 1688 (ν (C=O)_{st}). UV-Vis (MeOH) [λ_{\max} , nm]: 278, 376.

III.3. Cytotoxicity assays

III.3.1. Tested compounds

Compounds and their ligands were first reconstituted in dmsO and later diluted with sterile and bidistilled water to a final concentration of 4 % dmsO and their concentration was determined using their extinction coefficients. The extinction coefficient of each manganese compound was calculated experimentally by measuring their absorbance at the wavelength where it has its maximum (λ_{\max}), i.e., 240 nm (**Mn1**), 276 nm (**Mn4**), 242 nm (**Mn5**), 282 nm (**Mn6**), 248 nm (**Mn7**), 278 nm (**Mn2** and **Mn8**) and 292 nm (**Mn10**), while for the ligands of compounds **Mn6-8**, **Mn1-Mn5**, and **Mn10** we used wavelengths of 278 nm, 276 nm, and 292 nm, respectively. A linear regression equation between absorbance at λ_{\max} (A_{\max}) and different compound concentrations was calculated. The extinction coefficients of compounds were 19082 (**Mn1**), 16291 (**Mn2**), 13353 (**Mn4**), 18186 (**Mn5**), 17526 (**Mn6**), 23274 (**Mn7**), 21380 (**Mn8**), and 23541 (**Mn10**) M⁻¹cm⁻¹. For the ligands pypz-H (**Mn1-5**), pypz-Me (**Mn6-7**), pypz-CH₂COOEt (**Mn8**) and (-)-L (**Mn10**) we used extinction coefficients of 12452, 6719, 6717, 3625, and 15467 M⁻¹cm⁻¹, respectively. The extinction coefficient of each ruthenium compound was calculated experimentally by measuring their absorbance at the wavelength where it has its maximum (λ_{\max}), i.e., 230 nm (**Ru4**), 238 nm (**Ru5**), 344 nm (**Ru6**), 286 nm (**P2**), 330 nm (**Ru12**), 336 nm (**Ru14**) and 340 nm (**Ru15**), while for the ligands pz-H, 3,4-dmpz-H, 3,5-dmpz-H, NO₂-pz-H, bpea and 9S3 we used wavelengths of 231 nm (for pz-H, 3,4-dmpz-H and 3,5-dmpz-H), 276 nm, 260 nm, 274 nm, respectively. A linear regression equation between absorbance at λ_{\max} (A_{\max}) and different compound concentrations was calculated. The extinction coefficients of compounds were 12692 (**Ru4**), 11938 (**Ru5**), 419 (**Ru6**), 10076 (**P2**), 4402 (**Ru12**), 5315

Chapter III

(Ru13) and 3336 (Ru14) $M^{-1}cm^{-1}$. For the ligands pz-H, 3,4-dmpz-H, 3,5-dmpz-H, NO_2 -pz-H, bpea and 9S3 we used extinction coefficients of 295, 2741, 662, 7048, 6866, and 208 $M^{-1}cm^{-1}$, respectively.

Stock solutions were then diluted to the desired final concentrations with sterile complete medium immediately before each experiment. Cisplatin (Pfizer, Spain) and carboplatin (Teva, Spain) were included as controls in these experiments.

III.3.2. Cell lines and culture conditions

NCI-H460 human lung cancer and OVCAR-8 human ovarian cancer cell lines were obtained from the National Cancer Institute-Frederick DCTD tumour cell line repository. MCF7, MDA-MB-231 and SK-BR-3 human breast cancer cells lines and CCD18-Co human colon fibroblasts were obtained from Celltec UB (Universitat de Barcelona, Spain).

The NCI-H460, OVCAR-8, MCF7 and MDA-MB-231 cells were routinely grown in RPMI, supplemented with 10 % fetal bovine serum (FBS), 50 U/mL penicillin, 50 μ g/mL streptomycin and 2 mM L-glutamine. The SK-BR-3 cells were grown in McCoy's 5A medium and the CCD-18Co in DMEM, in all cases supplemented with 10 % FBS, 50 U/mL penicillin, 50 μ g/mL streptomycin and 2 mM L-glutamine. The cells were used immediately after thawing and were routinely grown at 37 °C in a humidified atmosphere with 5 % CO_2 . All media and reagents used to culture the cell lines were from Lonza (Switzerland). Cells were maintained and propagated following established protocols and remained free of mycoplasma throughout the experiments.

III.3.3. Cell proliferation assays

Cells were seeded into 96-well plates at the appropriate density, i.e., 1500 for OVCAR-8; 1900 for NCI-H460; 4000 for MCF7; 2500 for MDA-MB-231; 10,000 for SK-BR-3 and 4000 for the non-tumor cell line CCD-18Co, cells per well. After 24 h of incubation, cells were treated for 72 h with various concentrations of the compounds. When indicated, the widely used ROS scavenger N-Acetyl-L-cysteine (NAC) (Sigma, St. Louis, MO, USA) was added to a final concentration of 5 mM. Cell viability was determined by the MTT method as previously described. The IC_{50} value corresponds to the concentration of the assayed compound required to inhibit cell proliferation by 50 % relative to untreated cells and, in each case, it was calculated by linear interpolation from the obtained growth curves. All data are reported as the mean \pm standard error (SE) of at least three independent experiments with three replicates in each.

III.3.4. Cell cycle phase analysis

Cell cycle phase analysis was performed by propidium iodide (PI) staining. NCI-H460 and OVCAR-8 cells (400,000 cells/100-mm dish) were treated with compound **Mn10** and its ligand (2 μM or 9 μM for NCI-H460 and 5 μM or 24 μM for OVCAR-8) for 72 hours. Cells were then harvested and fixed with 70 % ethanol for at least 1 hour at $-20\text{ }^{\circ}\text{C}$. Fixed cells were harvested by centrifugation and washed in cold PBS. These collected cells were resuspended in PBS ($1\text{-}2 \times 10^6/\text{mL}$) and treated with RNase A (100 $\mu\text{g}/\text{mL}$) and PI (40 $\mu\text{g}/\text{mL}$) (Molecular Probes, Eugene, OR, USA) at $37\text{ }^{\circ}\text{C}$ for 30 minutes prior to flow cytometric analysis. A minimum of 10,000 cells within the gated region were analyzed on a FACSCalibur flow cytometer (BD Biosciences, San Jose, CA, USA). Cell cycle distribution was analyzed using the FlowJo program (FreeStar, Ashland, OR, USA).

III.3.5. Flow cytometric analysis of ROS generation

ROS generation was determined by flow cytometry using the carboxy-20, 70-dichlorodihydrofluorescein diacetate probe (carboxy-H2DCFDA). Carboxy-H2DCFDA is oxidized to green fluorescent dichlorofluorescein (DCF) by ROS species. Cells were seeded in 6-well plates (70,000 cells/well) in phenol red-free RPMI 24 h prior to treatments. Cells were treated with different concentrations of compound **Mn10** and its ligand (2, 4.5 or 9 μM for NCI-H460 cells and 5, 12 or 24 μM for OVCAR-8 cells) for 48 or 72 hours at $37\text{ }^{\circ}\text{C}$. After treatments, cells were washed with PBS and incubated with 1 μM carboxy-H2DCFDA for NCI-H460 cells or 0.5 μM for OVCAR-8 cells in PBS for 30 minutes at $37\text{ }^{\circ}\text{C}$ in the dark. Then, cells were collected with phenol red-free trypsin and analyzed on a FACSCalibur flow cytometer. The geometric mean fluorescence intensity of 10,000 cells was established using CellQuest Pro software (Becton Dickinson).

III.3.6. Spectrophotometric and spectrofluorometric studies

Compound stability

Small amounts of freshly prepared individual compounds in dmsO 4 % were diluted in PBS, pH 7.4. The concentration of each compound in the final sample was 40 μM . The resulting solutions were monitored by collecting spectra at 0, 3, 24 and 48 hours at $25\text{ }^{\circ}\text{C}$ between 230 and 320 nm in a Perkin-Elmer Lambda BIO-20 UV-Vis spectrophotometer.

Chapter III

In vitro ROS generation

Generation of ROS species in vitro was measured by consumption of ascorbic acid (AA). Small amounts of compound **Mn10** and its ligand were dissolved in 4 % dmsO and diluted to a final concentration of 1 μ M with phosphate buffer pH= 7. The reaction was initiated by the addition of a solution of AA to a final concentration of 100 μ M. The disappearance of AA over time was followed by its UV absorbance at 265 nm using a Perkin-Elmer Lambda BIO-20 UV-Vis spectrophotometer.

Protein binding

UV-Vis spectra (between 230 and 320 nm) using a Perkin-Elmer Lambda BIO-20 UV-Vis spectrophotometer of 25 μ M of compound **Mn10** and its ligand were recorded before and after the addition of each model protein (chicken egg lysozyme, ribonuclease A and cytochrome C) at a stoichiometric ratio of 4:1 (metal/protein) at different times for a period of 48 h in the dark in PBS pH= 7.4.

III.3.7. DNA interaction analysis

DNA interaction was monitored by agarose gel electrophoresis. Stock solutions of the compound **Mn10** and its ligand were freshly prepared in milliQ water with 4 % dmsO. To investigate whether the presence of ROS could mediate the interaction of the compound with DNA, 1 μ L of H₂O₂ 30 % (w/v) was added to the reaction. The samples were prepared by mixing 0.5 μ L of supercoiled pUC18 DNA at a concentration of 0.5 μ g/ μ L (Thermo Scientific) with appropriate aliquots of the compound or ligand followed by dilution with TE buffer (10 mM Tris-HCl, pH= 7.6, 1 mM EDTA) to a final volume of 20 μ L. A sample of pUC18 DNA -without neither compound nor ligand was used as negative control. The samples were then incubated at 37 °C for 24 h and then 4 μ L of loading buffer (6x) (10 mM Tris-HCl, pH 7.6, 0.03 % bromophenol blue, 0.03 % xylene cyanol FF, 60 % glycerol, 60 mM EDTA) were added to each sample. The mixed solutions were loaded on a 0.8 % agarose gel in 0.5 x TBE buffer (89 mM Tris-borate, pH 8.3, 2 mM EDTA) and electrophoresis was carried out for 1 h and 10 min at 100 V. Gels were stained with a ethidium bromide (1 μ g/mL in TBE) for 15 min and the DNA bands were visualized under UV light. For comparison purposes, cisplatin effect was evaluated under the same experimental conditions.

III.3.8. Statistical analysis

All statistical analyses were performed with IBM SPSS Statistics 23 software for Windows (USA). Results were analysed using the Student's t test. P-values < 0.05 were considered statistically significant.

III.4. X-ray structure determination

The measurements were carried out on a BRUKER SMART APEX CCD using graphite monochromated Mo K α radiation ($\lambda = 0.71073 \text{ \AA}$) from an x-Ray Tube. Programs used: data collection, Smart;³⁰⁰ data reduction, Saint+;³⁰¹ absorption correction, SADABS.³⁰² Structure solution and refinement was done using SHELXTL.³⁰³ The structure was solved by direct methods and refined by full-matrix least-squares methods on F^2 . In all complexes the non-hydrogen atoms were refined anisotropically. For complexes **Mn1**, **Mn2**, **Mn3**, **Mn5**, **Mn6**, **Mn7**, **Mn8**, **Mn9**, **Ru1a**, **Ru1b**, **Ru5** and **Ru8**, all the H-atoms were placed in geometrically optimized positions and forced to ride on the atom to which they are attached, whereas for complexes **Mn4**, **Mn5**, **Ru7b**, **Ru9** and **Ru11**, some particular treatments were applied as described next. For complexes **Mn4** and **Ru7b**, the N-H hydrogen was located in the difference Fourier map and refined freely. Complex **Mn5** is a co-crystal consistent of an equimolar mixture of two isomeric molecules. For **Ru9**, the hydrogen of the different hydration water molecules present in the structure were not located on Fourier map, but were added in the empirical formula and derived values (e.g. formula weight, $F(000)$, etc), as in the case of **Mn4** which a considerable amount of electron density attributable to an ethyl ether disordered solvent molecule per asymmetric unit was removed with the SQUEEZE option of PLATON³⁰⁴. Those solvent molecules are, however, included in the reported chemical formula and derived values. Finally, regarding complex **Ru11** a considerable amount of electron density attributable to disordered solvent which could not be identified was removed with the SQUEEZE option of PLATON³⁰⁴. Those solvent molecules are, however, included in the reported chemical formula and derived values. The crystal was non-merohedrally twinned. The Twin law was calculated with the instruction TwinRotMat of PLATON³⁰⁴ which also generated the hkf15 files used to refine the structure.

The refinement parameters for all crystal structures solved are gathered in Table III.1:

Chapter III

Table III.1. Parameters for all crystal structures.

| Complex | Color | Solvent of crystallization | T (K) | θ range | Data collection | Number of reflections | Unique reflections [R(int)] |
|-------------|------------|---|--------|-----------------|--|-----------------------|-----------------------------|
| Mn1 | colorless | ethanol | 298(2) | 2.37 - 28.34° | full-sphere, ω and ϕ scans | 12727 | 2567 [0.1002] |
| Mn2 | colorless | THF | 298(2) | 2.329 - 28.369° | full-sphere, ω and ϕ scans | 15958 | 5985 [0.0769] |
| Mn3 | colorless | CH ₂ Cl ₂ | 298(2) | 2.03 - 28.30° | full-sphere, ω and ϕ scans | 40443 | 3467 [0.1204] |
| Mn4 | colorless | diethyl ether/ethanol | 100(2) | 2.15 - 28.46° | full-sphere, ω and ϕ scans | 20260 | 5745 [0.4239] |
| Mn5 | colorless | ethanol | 298(2) | 1.789 - 28.285° | full-sphere, ω and ϕ scans | 38802 | 6087 [0.0414] |
| Mn6 | colorless | CH ₃ CN | 142(2) | 1.518 - 28.228° | full-sphere, ω and ϕ scans | 10955 | 8273 [0.0816] |
| Mn7 | colorless | diethyl ether/thf | 130(2) | 1.455 - 28.282° | full-sphere, ω and ϕ scans | 9186 | 5471 [0.0853] |
| Mn8 | colorless | diethyl ether/CH ₂ Cl ₂ | 298(2) | 2.043 - 27.649° | full-sphere, ω and ϕ scans | 57987 | 8955 [0.0612] |
| Mn9 | dark green | ethanol | 293(2) | 2.19 - 28.33° | full-sphere, ω and ϕ scans | 24962 | 4154 [0.0826] |
| Ru1a | orange | diethyl ether/methanol | 143(2) | 2.343 - 28.391° | full-sphere, ω and ϕ scans | 31922 | 12040 [0.0438] |
| Ru1b | orange | ethanol/CH ₂ Cl ₂ | 100(2) | 2.301 - 28.294° | full-sphere, ω and ϕ scans | 35701 | 5635 [0.1050] |
| Ru2' | yellow | CHCl ₃ | 298(2) | 2.202 - 28.666° | full-sphere, ω and ϕ scans | 40751 | 6737 [0.0545] |
| Ru3 | colorless | CH ₂ Cl ₂ | 298(2) | 2.073 - 28.461° | full-sphere, ω | 11455 | 5491 [0.0699] |

| | | | | | | | |
|-------------|--------|---|--------|-----------------|--|-------|------------------|
| Ru5 | yellow | diethyl ether/methanol | 293(2) | 2.098 - 28.251° | and ϕ scans full-sphere, ω and ϕ scans | 31907 | 5147 [0.0462] |
| Ru7b | black | water | 298(2) | 2.461 - 28.426° | full-sphere, ω and ϕ scans | 21219 | 7288 [0.0458] |
| Ru8 | red | water | 100(2) | 2.073 - 28.506° | full-sphere, ω and ϕ scans | 46396 | 7628 [0.1877] |
| Ru9 | black | hexane/acetone | 298(2) | 2.1 - 28.3° | full-sphere, ω and ϕ scans | 66240 | 20358 [0.102] |
| Ru11 | brown | diethyl ether/ CH ₂ Cl ₂ | 193(2) | 1.659 - 28.285° | hemi-sphere, ω and ϕ scans | 8920 | 5850 [0.0685] |

III.5. Catalytic studies

III.5.1. Epoxidation of alkenes

III.5.1.1. Homogeneous phase

Mn-based catalysis

An anhydrous CH₃CN (1 mL) solution of alkene (250 μ mol), manganese catalyst (2.5 μ mol) and biphenyl (250 μ mol, internal standard) was prepared in a 5 mL flask and cooled in an ice bath. At this point, 39 % peracetic acid (500 μ mol) was added *via* syringe over 3 minutes under stirring. The reaction vessel was then taken out of the ice bath and allowed to progressively warm to RT. Each aliquot of the reaction taken for analysis was filtered through a basic alumina plug and was analysed in a Shimadzu GC-2010 gas chromatography apparatus equipped with an Astec CHIRALDEX G-TA column and a FID detector, and quantification was achieved from calibration curves.

Ru-based catalysis

The ruthenium catalyst (1.25 μ mol), alkene (125 μ mol) and PhI(OAc)₂ (250 μ mol) were stirred at room temperature in CH₂Cl₂ (2.5 mL) for 24 h. After addition of an internal standard, the sample was filtered through a basic alumina plug and quantified by GC analysis based on calibration curves for each substrate and epoxide.

Chapter III

III.5.1.2. Heterogeneous phase

In ionic liquid: solvent media

Manganese catalyst (2.5 μmol) and substrate (250 μmol) were dissolved in 2 mL of [bmim]PF₆:CH₃CN (1:1) (bmim= 1-butyl-3-methyl-imidazolium). 39 % peracetic acid (500 μmol) was added *via* syringe over 3 minutes at 0 °C. Afterwards the solution was stirred at RT for 3 h. After completion, CH₃CN was removed under vacuum and the resulting suspension was washed with diethylether (3 x 5 mL) to extract the epoxide (which was then analysed by GC after the addition of 250 μmol of biphenyl) and the oxidant by-products. The remaining mixture was washed with NaOH aqueous solution and dried in vacuum. A new load of substrate and oxidant dissolved in acetonitrile was then added and the mixture was left for an additional 3 h run. This procedure was repeated up to twelve times.

Based on silica-anchored catalysts

Alkene (2.2 μmol) and heterogenized manganese catalyst ($2.27 \cdot 10^{-4}$ μmol) were dissolved in 1 mL of anhydrous CH₃CN. The amount of heterogenized catalyst was calculated taking into account the functionalization of SP ($\text{mmol Mn} \cdot \text{g}^{-1}$). 39 % peracetic acid (4.54 μmol) was added *via* syringe over 3 minutes at 0 °C. Afterwards the solution was stirred for 3 or 24 h at RT. After completion, the resulting solution was centrifugated to separate the catalytic material from the reaction medium. An aliquot (100 μL) was taken from the solution, was filtered through a basic alumina plug and after the addition of an internal standard (biphenyl) the amount of the remaining substrate was quantified by GC analysis based on calibration curves. The catalytic heterogeneous system was washed with MeOH (3 x 5 mL) and acetone (2 x 5 mL) and was used in a subsequent catalytic run.

III.5.2. Hydration of nitriles

III.5.2.1. Homogeneous phase

The ruthenium catalyst (0.01 mmol), water (0.6 mL) and the corresponding nitrile (0.2 mmol) were introduced into a sealed tube and the reaction mixture was stirred at 100 °C for 20 h. The nitrile was extracted with chloroform containing an internal standard (biphenyl) to quantify the remaining substrate by GC. The identity and purity of the resulting amides was assessed by ¹H-NMR.

III.5.2.2. Heterogeneous phase

Nitrile (0.3 mmol) and heterogenized ruthenium catalyst (0.015 mmol) were dissolved in H₂O (1 mL) in a sealed tube and the reaction mixture was stirred at 100 °C for 20 h. The amount of heterogenized catalyst was calculated taking into account the functionalization of SP and MSNP (mmol Ru·g⁻¹). After completion, the resulting solution was centrifuged (in the case of SP support) or magnetically separated (in the case of MSNP support) to separate the catalytic material from the reaction medium. The catalytic heterogeneous system was washed with water (2 x 2 mL), and was used in a subsequent catalytic run. The aqueous phases were put together and the remaining substrate were extracted with chloroform (4 x 2 mL) containing an internal standard (biphenyl), was filtered through a basic alumina plug and the amount of the remaining nitrile was quantified by GC analysis based on calibration curves.

III.6. Additional instrumentation and measurements

FT-IR spectra were taken in a Mattson-Galaxy Satellite FT-IR spectrophotometer containing a MKII Golden Gate Single Reflection ATR System.

UV-Vis spectroscopy was performed on a Cary 50 Scan (Varian) UV-Vis spectrophotometer with 1 cm quartz cells.

Cyclic voltammetric (CV) and *differential pulse voltammetry (DPV)* experiments were performed in an IJ-Cambria IH-660 potentiostat using a three electrode cell. Glassy carbon electrode (3 mm diameter) from BAS was used as working electrode, platinum wire as auxiliary and SSCE as the reference electrode. All cyclic voltammograms presented in this work were recorded under nitrogen atmosphere unless explicitly mentioned. The complexes were dissolved in solvent containing the necessary amount of n-Bu₄NH⁺PF₆⁻ (TBAH) as supporting electrolyte to yield a 0.1 M ionic strength solution. All $E_{1/2}$ values reported in this work were estimated from cyclic voltammetric experiments as the average of the oxidative and reductive peak potentials $(E_{p,a} + E_{p,c})/2$, or directly from the DPV peak. Unless explicitly mentioned the concentration of the complexes was approximately 1 mM.

Elemental Analyses were performed using a CHNS-O Elemental Analyser EA-1108 from Fisons.

ESI-MS experiments were performed on a Navigator LC/MS chromatograph from Thermo Quest Finnigan, using acetonitrile as a mobile phase.

SEM images were recorded using a FE-SEM Hitachi, Japan, S-4100. Digital images were collected and processed by Quarz PCI program.

Chapter III

TEM images were recorded using a ZEISS EM910 equipped with a 4MP camera Gatan Orius SC 200 CCD.

For *metal content determination* a quadrupole-based inductively coupled plasma mass spectrometer system (ICP-MS, Agilent 7500c, Agilent Technologies, Tokyo, Japan) were used. This instrument is equipped with an octapole collision reaction cell. However, in this work, the collision reaction cell acts only as an ion focusing lens because it was not filled with any pressurized gas. Prior to measurements, sample were digested with HCl: HNO₃.

Thermogravimetric analysis (TGA) was performed under N₂ atmosphere with a 10 °C min⁻¹ heating rate from 30 °C to 700 °C.

NMR spectra were recorded on a 300 MHz and 400 MHz NMR spectrometer from Bruker. Chemical Shifts (δ) for ¹H and ¹³C were referred to internal solvent resonances.

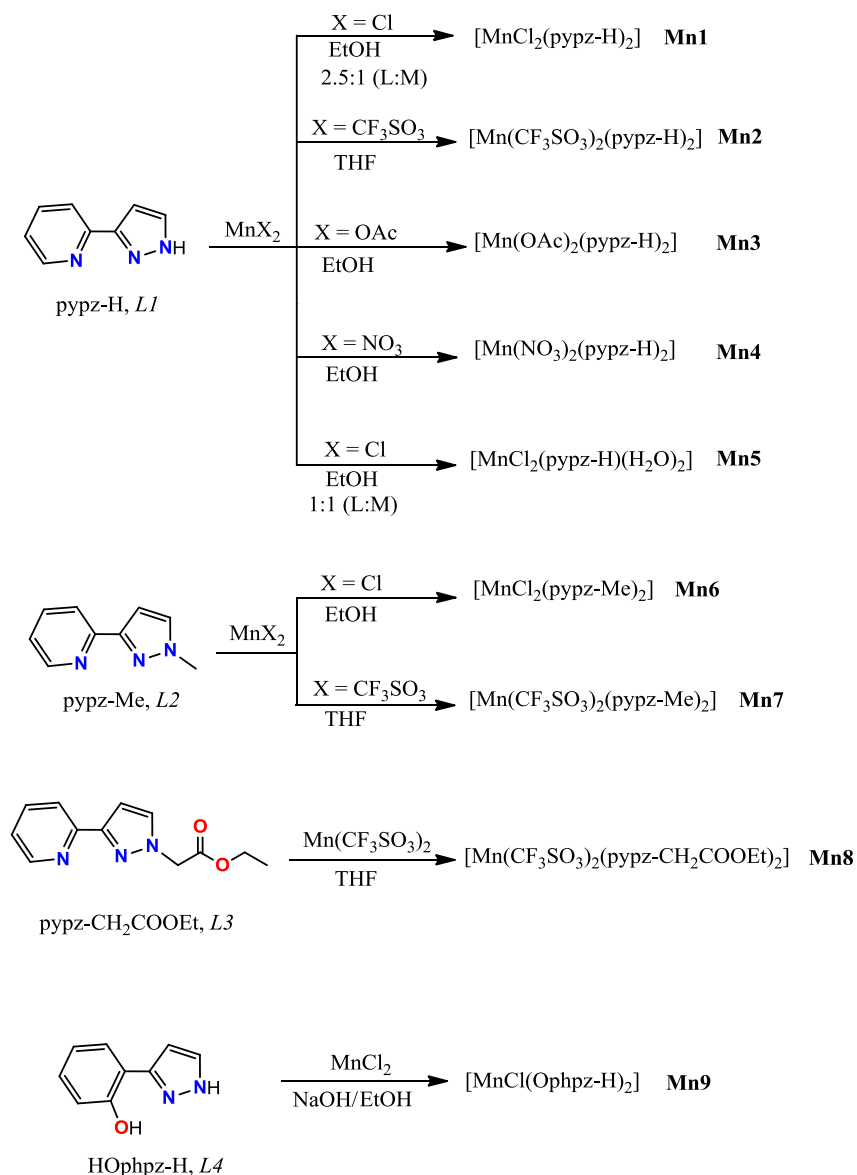
Catalytic experiments analyses were performed in a GC-2010 Gas Chromatograph from Shimadzu, equipped with an Astec CHIRALDEX G-TA Column (30 m x 0.25 mm diameter) incorporating a FID detector. All the product analyses in the catalytic experiments were performed based on calibration curves using biphenyl as internal standard.

Chapter IV. Results and discussion

IV.1. Reusable manganese complexes containing pyrazole-based ligands as catalysts for epoxidation reactions.

IV.1.1. Synthesis and Structure

The synthetic strategy followed for all the complexes described in this chapter, together with the ligands used, is outlined in Scheme IV.1.1. Different Mn(II) salts are used as starting materials and then the corresponding ligand is added stepwise for the preparation of complexes **Mn1-9**.



Scheme IV.1.1. Synthetic routes for the preparation of complexes **Mn1-9** and ligands used. The metal:ligand ratio was 1:2 unless specified otherwise.

When an ethanolic solution of ligand *pypz-H* is added to MnCl_2 dissolved in ethanol with a metal:ligand ratio 1:2.5, the complex $[\text{MnCl}_2(\text{pypz-H})_2]$, **Mn1**, is obtained in good yield and it can be crystallized by slow evaporation of the corresponding solution. However, when the

Chapter IV

metal:ligand ratio is 1:1 complex $[\text{MnCl}_2(\text{pypz-H})(\text{H}_2\text{O})_2]$, **Mn5**, containing only one unit of the bidentate ligand, is isolated. A metal:ligand ratio of 1:2 is used to obtain the mononuclear compounds $[\text{Mn}(\text{CF}_3\text{SO}_3)_2(\text{pypz-H})_2]$, **Mn2**, $[\text{Mn}(\text{OAc})_2(\text{pypz-H})_2]$, **Mn3**, and $[\text{Mn}(\text{NO}_3)_2(\text{pypz-H})_2]$, **Mn4**, starting from the corresponding Mn(II) salts. A similar strategy is used to obtain the complexes $[\text{MnCl}_2(\text{pypz-Me})_2]$, **Mn6**, and $[\text{Mn}(\text{CF}_3\text{SO}_3)_2(\text{pypz-Me})_2]$, **Mn7**, using in this case the pypz-Me ligand in a metal: ligand ratio 1:2. Compound $[\text{Mn}(\text{CF}_3\text{SO}_3)_2(\text{pypz-CH}_2\text{COOEt})_2]$, **Mn8**, is obtained in good yield when a THF solution of ligand *pypz-CH₂COOEt* is added to $\text{Mn}(\text{CF}_3\text{SO}_3)_2$ with the same metal:ligand ratio. Finally, the reaction of MnCl_2 with two equivalents of the *HOpmpz-H* ligand in the presence of NaOH results in the formation of the Mn(III) complex $[\text{MnCl}(\text{Opmpz-H})_2]$, **Mn9**. In this case, the deprotonation of the ligand upon coordination leads to the subsequent oxidation of the Mn center facilitated by the increased σ -donor capacity of the ligand.

The crystal structures of all complexes have been solved by X-ray diffraction analysis. Crystallographic data and selected bond distances and angles for compounds **Mn1-9** can be found in the Supporting Information section (Tables SIV.1.1 and SIV.1.2). ORTEP plots with the corresponding atom labels for the X-ray structures of all compounds are presented in Figures IV.1.1- IV.1.3.

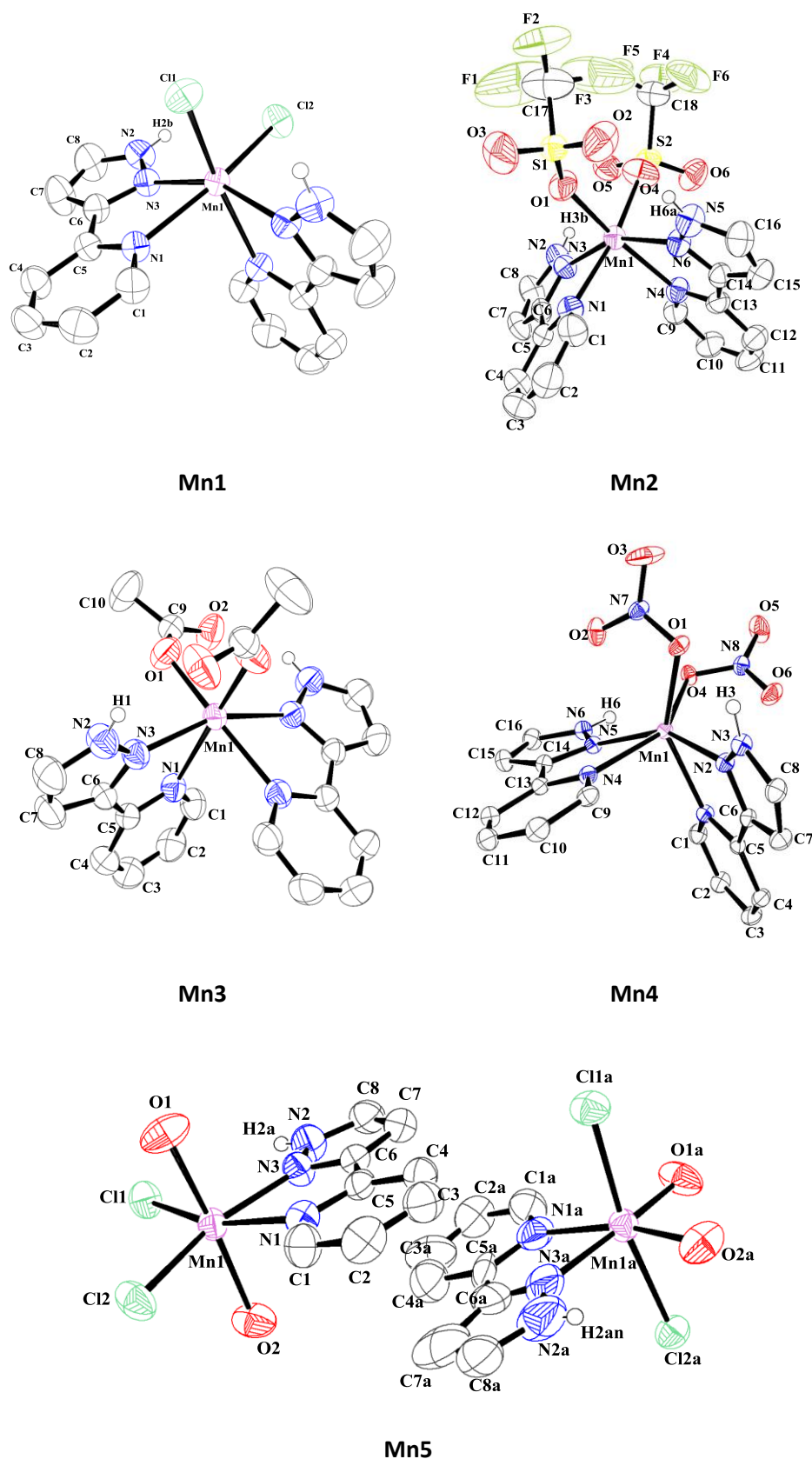


Figure IV.1.1. Ortep plots with the corresponding atom labels for the X-ray structures of compounds Mn1-Mn5, which contain the *pypz-H* ligand.

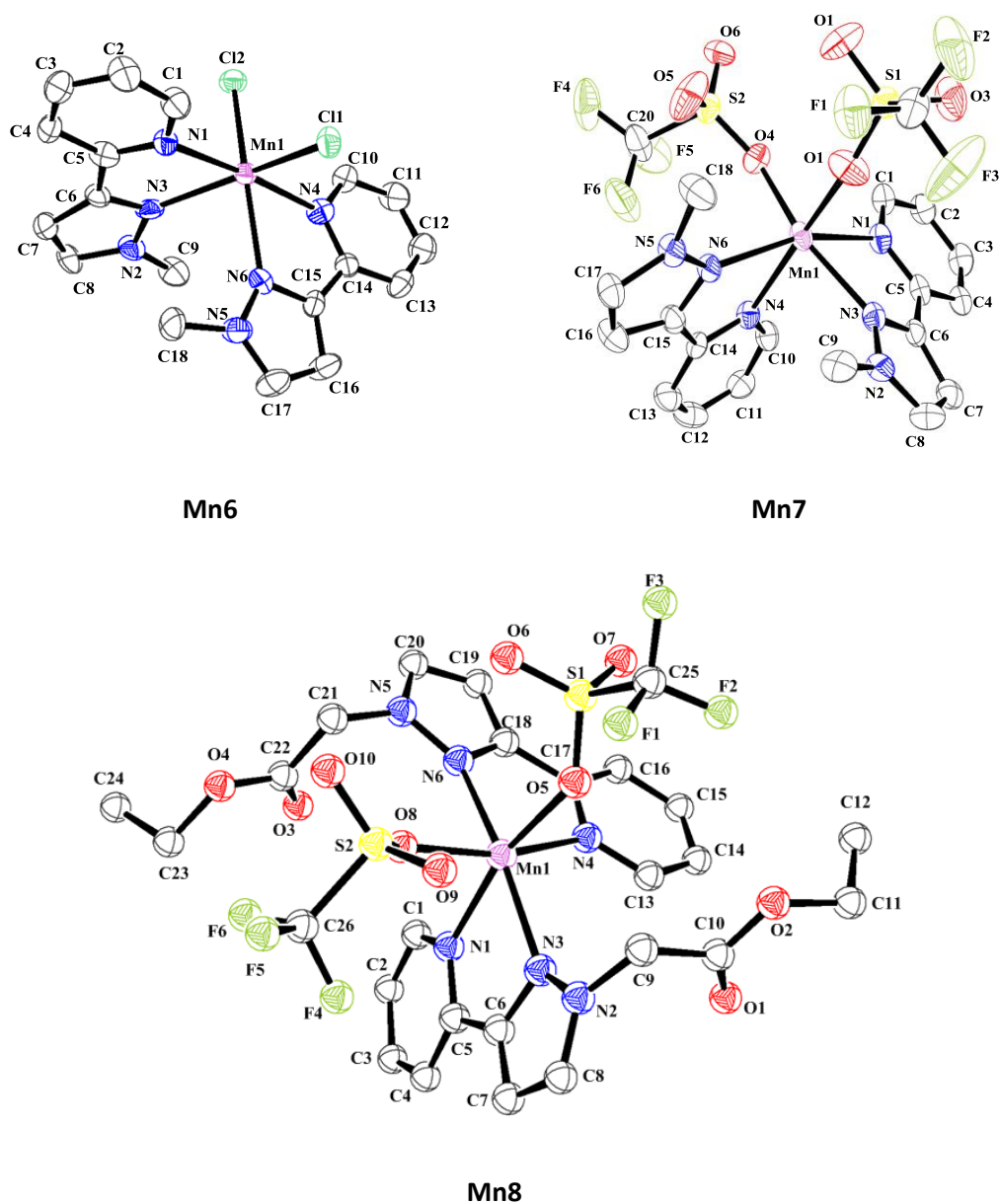


Figure IV.1.2. Ortep plots with the corresponding atom labels for the X-ray structures of compounds **Mn6** and **Mn7**, which contain the *pypz-Me* ligand, and **Mn8**, with the *pypz-CH₂COOEt* ligand.

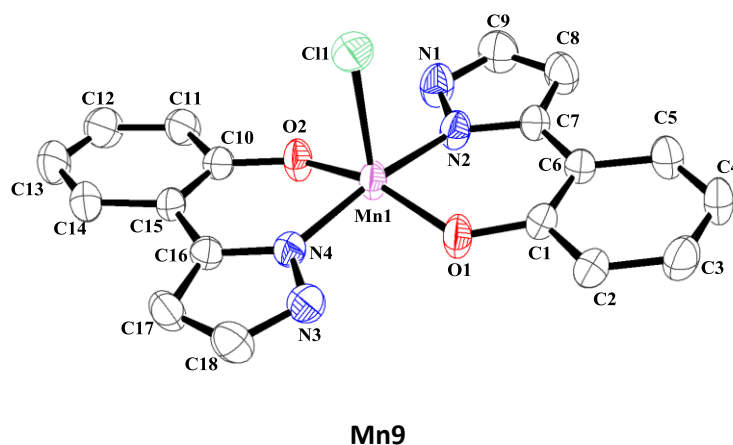


Figure IV.1.3. Ortep plot with the corresponding atom labels for the X-ray structure of compound **Mn9**, which presents the *Ophpz-H* ligand.

Crystal structures of mononuclear compounds **Mn1-4**, containing the *pypz-H* ligand, reveal in all cases a distorted octahedral geometry around the metal, where the Mn(II) ion is coordinated by four nitrogen atoms of two *pypz-H* ligands and two anionic monodentate ligands adopting a *cis* configuration. Compound **Mn3** is, to date, the first described mononuclear Mn(II) compound where acetate groups are acting as monodentate ligands adopting a *cis* configuration around the metal. It is noticeable that in the four complexes the respective anionic ligands (X) are situated *trans* to the pyridyl ring of each *pypz-H* ligand, which is consistent with the higher Lewis basicity of pyrazole as compared to pyridine then leading to thermodynamically more favourable pyridine-Mn-X *trans* diagonals. Mn-N bond lengths also manifest this *trans* influence since the average Mn-N_{pyridyl} bond distances for each compound (see Table SIV.1.2) are longer than the corresponding Mn-N_{pyrazole}, where two pyrazole rings are mutually in *trans* position. The Mn-Cl, Mn-O_{triflate}, Mn-O_{acetate} and Mn-O_{nitrate} bond distances in complexes **Mn1-4** are comparable to those found in similar Mn(II) compounds.³⁰⁵ Metal-ligand angles deviate significantly from the ideal value of 90° or 180° characteristic of a regular octahedron due to the spatially constrained nature of the *pypz-H* ligand coordinated to the metal (N_{pz}-Mn-N_{py}= 70.87°; 72.77°; 71.07°; 71.95° for **Mn1-Mn4** respectively); also, N_{pz}-Mn-N_{pz} bond angles are significantly less than 180°. This deviation is more significant for the nitrate compound **Mn4** that, in fact, presents a distorted geometry between octahedral and trigonal prismatic.

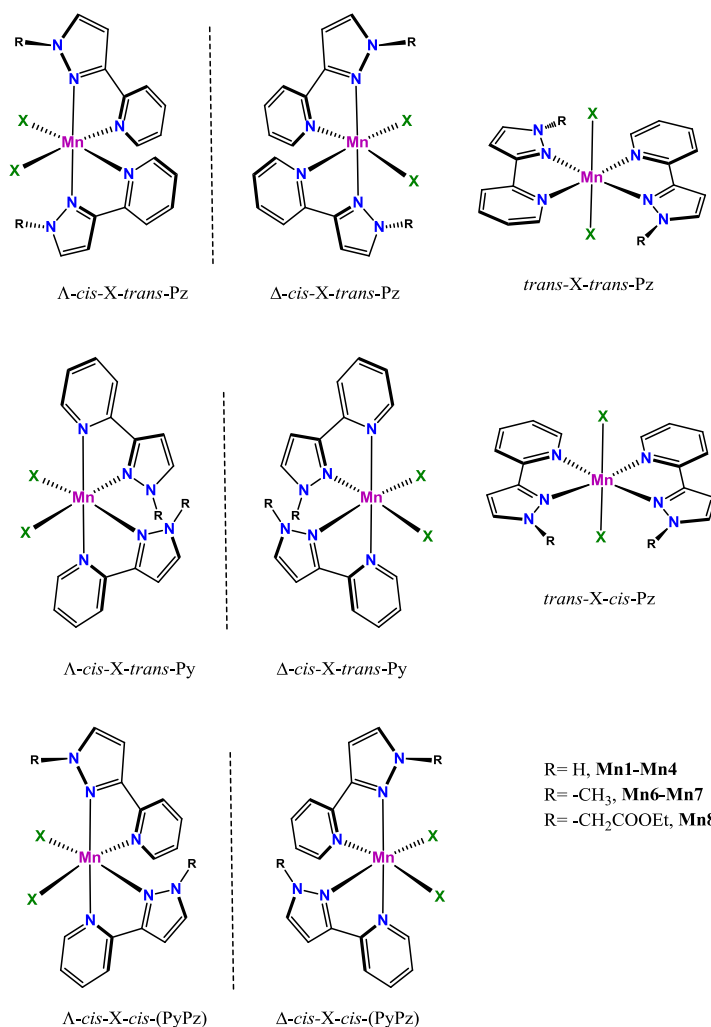
Also, weak intramolecular hydrogen bonding interactions are observed between the anionic X ligands and the pyrazolic hydrogen atoms. In complex **Mn1**, the H(2b)-Cl(1) bond distance is 3.148 Å (see Figure IV.1.1 for the numbering scheme). The triflate compound **Mn2** displays two strong intramolecular H-bonding between the non-coordinated oxygen atoms and the

Chapter IV

hydrogen atoms of the pyrazole ring (O(2)-H(6a) = 2.091 Å; O(5)-H(3b) = 2.120 Å) whereas for the acetate compound **Mn3**, a strong intramolecular H-bonding is present between the uncoordinated O(2) atom and H(1), 2.073 Å. For complex **Mn4**, the highly distorted geometry allows hydrogen-bonding interactions between the coordinated oxygen atoms and the closest pyrazolic hydrogen atoms (O(1)-H(3) = 2.786 Å; O(4)-H(6) = 2.721 Å).

Crystal structures of compounds **Mn6-Mn8** (Figure IV.1.2), containing in this case two units of the *pypz-Me* or the *pypz-CH₂COOEt* ligands, also reveal a distorted octahedral geometry around the metal, where Mn(II) ion is coordinated by four nitrogen atoms of two *pypz-R* ligands and by two anionic monodentate ligands adopting a *cis* configuration. The Mn-Cl and Mn-O_{triflate} bond distances are comparable to those found in similar Mn(II) compounds³⁰⁵ and also in complexes **Mn1-4**. Metal-ligand angles deviate significantly from the ideal value of 90° or 180° characteristic of a regular octahedron due to the spatially constrained nature of the *pypz-Me* or *pypz-CH₂COOEt* ligands coordinated to the metal: N(1)_{py}-Mn-N(3)_{pz} = 69.95°; N(4)_{py}-Mn-N(6)_{pz} = 70.4° (**Mn6**); N(1)_{py}-Mn-N(3)_{pz} = 73.0°; N(4)_{py}-Mn-N(6)_{pz} = 73.0° (**Mn7**); N(1)_{py}-Mn-N(3)_{pz} = 73.15°, N(4)_{py}-Mn-N(6)_{pz} = 73.45° (**Mn8**). Also, the *trans* N-Mn-N bond angles are significantly less than 180° (175.25° in **Mn6**, 160.3° in **Mn7** and 167.35° in **Mn8**). However, despite the similarity in the nature of the ligands and the overall structural parameters, different geometrical isomers are found for **Mn6** and **Mn7** in comparison with the rest of complexes. The structural factors that could have an influence in this distinctive behaviour are discussed next.

The spatial disposition of two *pypz-R* ligands and two monodentate ligands in an octahedral environment, as is the case of complexes **Mn1-4** and **Mn6-8**, could potentially lead to a set of eight different isomers (including three pairs of enantiomers, see Scheme IV.1.2). The nomenclature *trans* or *cis* for the isomers refers to the relative position of the two monodentate X ligands and also to the relative position of the pyridyl or pyrazolyl rings of the two *pypz-R* ligands in each case, as indicated in Scheme IV.1.2.



Scheme IV.1.2. Possible diastereoisomers for [MnX₂(pypz-R)₂] complexes (R = -H, -CH₃ or -CH₂COOEt), **Mn1-4** and **Mn6-8**.

As evidenced by the X-ray structures of the complexes (Figures IV.1.1 and IV.1.2), the enantiomeric pair Δ/Λ cis-X-trans-pz is the isomer obtained for the four complexes containing the *pypz-H* ligand, **Mn1-4**. The specificity towards this isomer can be interpreted in terms of the presence of the previously mentioned intramolecular H-bonds between the monodentate ligands (X) and the pyrazole H atoms in *cis* to each monodentate ligand, as will be described later (see Figure SIV.1.10). However, in complexes **Mn6-8**, where the pyrazolyl H atoms are not present, three different geometrical isomers can be found: the Δ/Λ cis-Cl-trans-py isomer for **Mn6**, the Δ/Λ cis-CF₃SO₃-cis-(PyPz) for **Mn7** and the Δ/Λ cis-CF₃SO₃-trans-pz isomer (as in the case of **Mn1-4**) for **Mn8**.

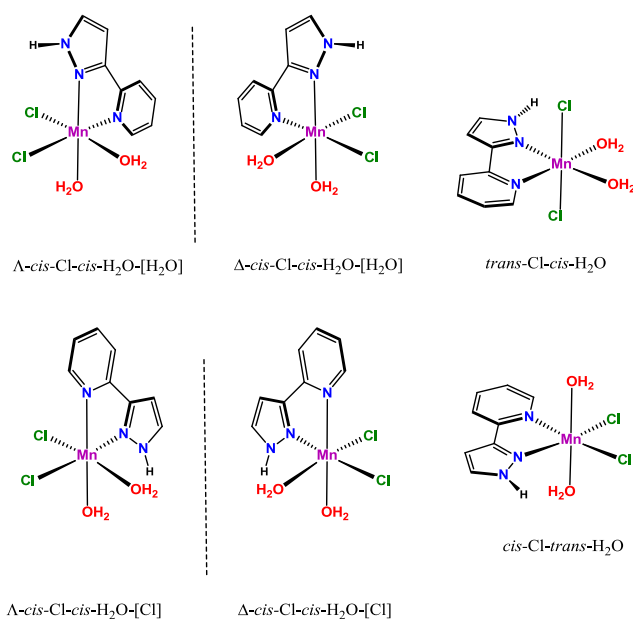
The preferential formation of the enantiomeric Δ/Λ cis-X-trans-py isomers in **Mn6** can be interpreted in terms of the presence of H-bonding involving the pyridyl rings of the *pypz-Me* ligands: two intramolecular H-bonds can be found between chlorido ligands and H atoms in position 2 of the pyridine rings (H1a-Cl2 = 2.762 Å, H10a-Cl1 = 2.733 Å). The electronic factors

Chapter IV

associated to the formation of such H-bonds are undoubtedly the main argument for the formation of this geometrical isomer because from a steric perspective it results in a highly hindered structure, with two methyl_{pz} groups directly facing the pyridyl ring of the other *pypz-Me* ligand thus resulting in an extremely distorted octahedral geometry (the corresponding *cis* bond angles are N1-Mn-N6 = 108.5° and N3-Mn-N4 = 105.2°, far above the ideal 90°). These kinds of interactions are determinant in the specificity towards an isomer in some compounds containing polypyridylic ligands.^{306,307} The obtaining of the Δ/Λ *cis-X-trans-pz* isomer in **Mn8** can be rationalized in similar terms: the two coordinated O atoms from triflate ligands interact with a methylene group from a -CH₂COOEt chain in *cis* (H9b-O5 = 2.425 Å; H21b-O8 = 2.411 Å). In this case, the length of the -CH₂COOEt chain allows the occurrence of additional H-bonds with the 2-pyridyl H atoms (H1a-O3 = 2.618 Å; H13a-O1 = 2.714 Å). Finally, in the case of complex **Mn7** the formation of the Δ/Λ *cis-X-cis*-(PyPz) isomer leads to the occurrence of only one intramolecular H-bonding between the coordinated oxygen atom of one triflate ligand and the H atom in 2 position of the pyridine ring situated in *cis* (H(1a)-O(4) = 2.615 Å). Such H-bonding is less energetic than the analogous H...Cl interaction found in **Mn6** and thus the steric arguments are in this case determinant preventing the formation of the Δ/Λ *cis-X-trans-py* isomer that would take benefit from the formation of two H-bonding interactions but that would in parallel set a methyl group and a pyridyl ring in a close, highly unfavourable *cis* location.

Regarding the rest of complexes, the X-ray structure of complex **Mn5** (Figure IV.1.1) is a co-crystal that contains two isomers: *trans*-Cl,*cis*-H₂O and *cis*-Cl,*trans*-H₂O (see Scheme IV.1.3) where two chlorido and two aqua ligands are mutually placed *trans* or *cis*, and π -stacking interactions between the *pypz-H* rings of the two isomers are present. Also, weak intramolecular H-bonding interactions take place between the hydrogen atoms of the *pypz-H* ligand and the monodentate Cl or H₂O ligands disposed in *cis* configuration and located at the equatorial plane defined by the *pypz-H* ligand (Npz-H...Cl, 3.094 Å, Npy-H...O H, 2.883 Å). These intramolecular hydrogen bonding interactions together with the spatially constrained nature of the *pypz-H* ligand coordinated to the metal are responsible for the distorted octahedral geometry observed around the Mn(II) ions (Npz-Mn(1)-Npy= 71.51°; Npz-Mn(1a)-Npy= 72.73°). Compound **Mn5** is the first reported co-crystal of Mn(II) containing Cl and H₂O ligands and also the first one containing a bidentate nitrogen ligand together with two Cl and two H₂O ligands; some compounds are described in the literature that contain Cl and H₂O ligands but together with two monodentate nitrogen ligands³⁰⁸ and, in all the cases, nitrogen ligands are arranged in *trans* position with respect to each other.

The spatial disposition of four monodentate ligands and one bidentate ligand in octahedral environment, as is the case of **Mn5**, could potentially lead to a set of six different stereoisomers (including two pairs of enantiomers), depicted in Scheme IV.1.3. The nomenclature *trans* or *cis* refers to the relative position of two identical monodentate ligands (Cl or H₂O) and, in the case of *cis,cis* isomers, the ligand indicated in brackets at the end is the one placed in *trans* with regard to the pyrazole ring.



Scheme IV.1.3. Possible diastereoisomers for complex **Mn5**.

As stated above, complex **Mn5** is attained as an equimolar mixture of the two *cis,trans* isomers depicted in Scheme IV.1.3 and this behaviour is most likely explained by supramolecular interactions taking place within the crystal. Weak intermolecular interactions such as hydrogen bonding and aryl-aryl stacking interactions play important roles in the creation of a variety of molecular architectures for molecular self-assembly and recognition.³⁰⁹ The geometries of ligands also influence the topologies of their metal complexes, especially for low-nuclearity coordination complexes.³¹⁰ In this context, the specificity towards the isomers formed in complex **Mn5** can be interpreted in terms of the presence of strong intermolecular H-bonding (O-H...Cl contacts around 2.3 Å) together with the above-mentioned π -stacking interactions between the pyridine and pyrazole rings that establish connections between the two isomers and favor their co-crystallization under the 1:1 ratio found. The resulting packing of this compound presents a compact structure made by alternate layers of the two different isomers, *trans*-Cl-*cis*-H₂O and *cis*-Cl-*trans*-H₂O (see Figure IV.1.4).

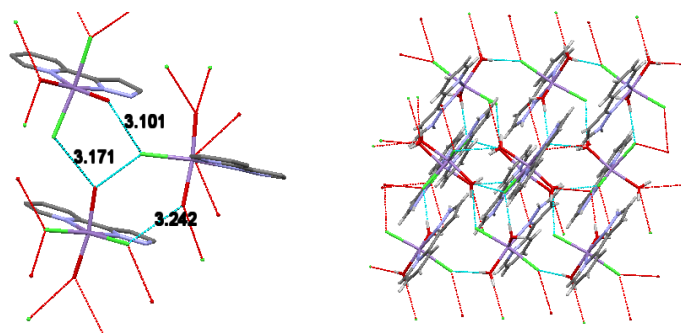
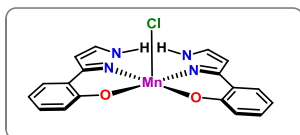


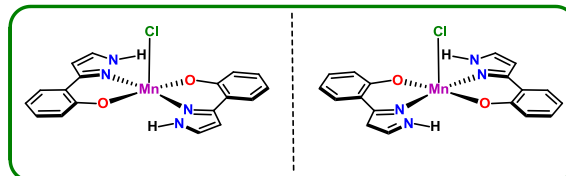
Figure IV.1.4. Intramolecular hydrogen bonding interactions and packing diagram for complex **Mn5**.

Finally, complex **Mn9** (Figure IV.1.3) can also be obtained as different isomers as depicted in Scheme IV.1.4, but the single *trans*-N-Mn-N isomer has been observed probably due, as is the case for complexes **Mn1-4**, to the presence of two H-bonding N-H...O interactions between the two Ophpz-H ligands that are not found in the rest of potential isomers.

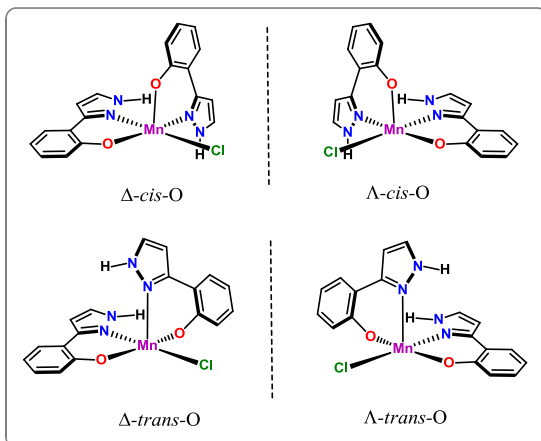
trans-N-Mn-O, apical Cl:



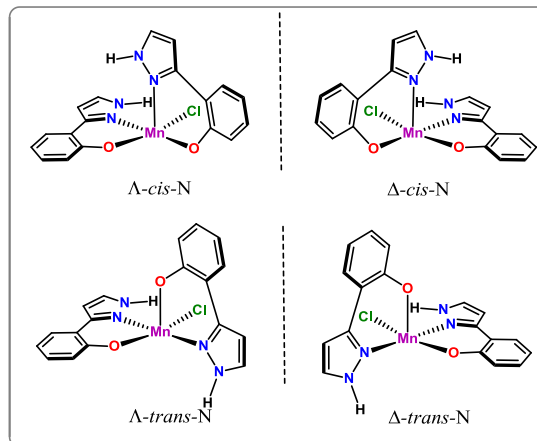
trans-N-Mn-N, apical Cl:



trans-Cl-Mn-N:



trans-Cl-Mn-O:



Scheme IV.1.4. Possible diastereoisomers for complex **Mn9**.

The geometry around the Mn(III) ion is a distorted square-pyramid with a τ index of 0.20 ($\tau = 0$ for a square-pyramid, and $\tau = 1$ for trigonal bipyramid),³¹¹ where the base is defined by the two bidentate ligands and the monodentate chloride ion occupies the apical position. The Mn-O and the Mn-N average bond lengths are 1.85 Å and 1.97 Å respectively and are shorter than the Mn-Cl bond (2.45 Å) which indicates that the chloride ion interacts with Mn(III) in a weaker way than the donor atoms from the hydroxyphenyl pyrazole ligands, as expected. However, the Mn-Cl bond is shorter than the analogous Mn-X distance found in a similar structure that

contains a Br⁻ ligand instead of Cl⁻, due to the smaller ionic radius and larger electronegativity of Cl⁻ when compared to Br⁻.^{312a} This fact is also reflected in the distortion of the coordination geometry, where the distance of the manganese(III) ion from the N₂O₂ mean plane is 0.242 Å (in the reported structure with a bromo ligand the distance of Mn with regard to the analogous plane is 0.337 Å). The average of the two intraligand O-Mn-N angles is slightly smaller than 90° (89.07°). The structure contains also intramolecular H-bonding interactions between the O atom of one *Ophpz-H* ligand and the pyrazole H atom of the other (Figures IV.1.3 and SIV.1.11). The packing of **Mn9**, organized in zig-zag ladder-like chains (Figure SIV.1.12), presents π -stacking interactions together with intermolecular H-bonding between Cl and the pyrazole N-H atoms, (N(1)-H(1)⋯Cl(1) = 3.207 Å). These interactions are stronger than in other compounds previously reported in the literature.³¹²

IV.1.2. Electrochemical properties

The redox potentials of complexes **Mn1-9** were determined by cyclic voltammetry (CV) and differential pulse voltammetry (DPV) in CH₃CN containing 0.1 M of n-Bu₄NPF₆ (TBAH) as supporting electrolyte using Ag/AgNO₃ as reference electrode. The voltammograms obtained are shown in Figures IV.1.5 and IV.1.6 and in the supporting information section (Figure SIV.1.13). The CV of complexes **Mn1** and **Mn5** (Figure IV.1.5) exhibit a one-electron quasi-reversible redox wave at potential values of $E_{1/2} = 0.63$ V (**Mn1**) and 0.66 V (**Mn5**) corresponding to the Mn(III)/Mn(II) system. In contrast, for compounds **Mn2**, **Mn3**, and **Mn4** the CV experiments do not display well defined redox processes and thus DPV experiments have been carried out to determine the potential values more precisely (Figure SIV.1.14), yielding $E_{1/2}$ values (in V) of 0.72 (**Mn2**), 0.74 (**Mn3**) and 0.73 (**Mn4**). As can be observed, triflate (**Mn2**), acetate (**Mn3**) and nitrate (**Mn4**) compounds are oxidized at higher potentials than the structurally similar chlorido complex **Mn1**, which can be explained in terms of the stronger electron-donating capacity of chlorido ligands compared to the above mentioned anions.

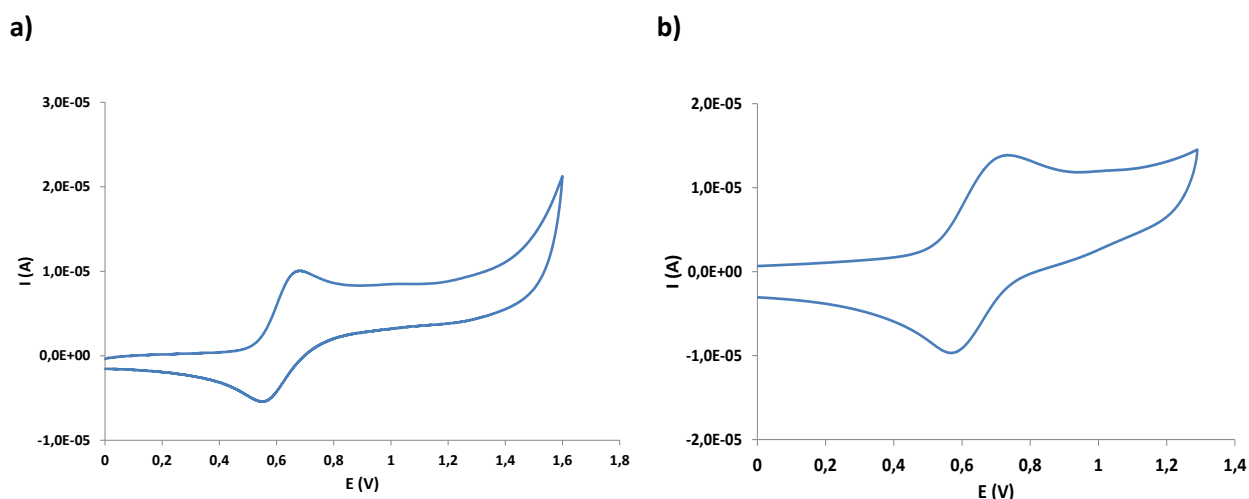


Figure IV.1.5. Cyclic voltammetry for complexes **Mn1** (a) and **Mn5** (b) in CH_3CN vs. Ag/AgNO_3 .

The CV and DPV obtained for complexes **Mn6-8**, containing substituted *pypz-R* ligands, are shown in Figure IV.1.6 and in the supporting information section (Figures SIV.1.13). The CV of **Mn6** (Figure IV.1.6) exhibits a one-electron quasi-reversible redox wave at a potential value of $E_{1/2} = 0.62$ V corresponding to the Mn(III)/Mn(II) system, whereas in the case of complexes **Mn7** and **Mn8** the CV experiments do not display well defined redox processes so DPV experiments have been done to determine the potential values more precisely (Figure SIV.1.14), showing $E_{1/2}$ values of 0.76 V for **Mn7** and 0.80 V for **Mn8**. These values are again higher than the corresponding to the chlorido complex **Mn6**, due to the stronger electron-donating capacity of chlorido ligands compared to the triflate anions present in **Mn7** and **Mn8** compounds, as was the case of complexes **Mn2-4** when compared to **Mn1**. However, when comparing the whole set of complexes, it can be observed that the Mn(III)/Mn(II) $E_{1/2}$ values are not significantly different for complexes leading an alkyl substituent on the *pypz-R* ligand when compared to the *pypz-H* complexes, and the geometrical isomer does not exert any substantial effect on the redox properties.

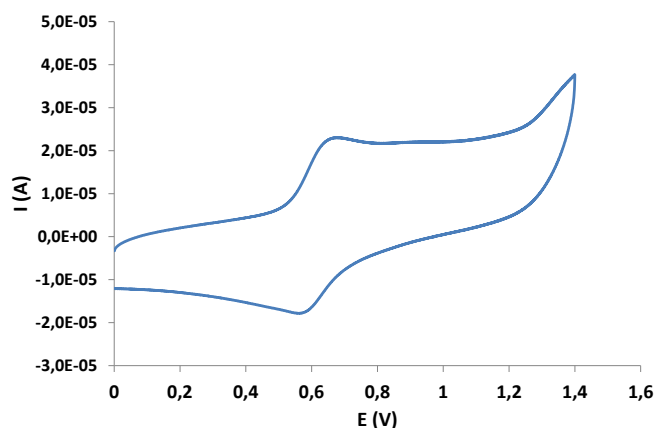


Figure IV.1.6. Cyclic voltammetry for complex **Mn6** in CH_3CN vs. Ag/AgNO_3 .

Regarding the pentacoordinated Mn(III) complex **Mn9**, an irreversible oxidation process is found at $E_{p,a} = 0.95$ V, which can be assigned to the Mn(IV/III) redox pair (Figure SIV.1.13). This assignment has been carried out on the basis of a bulk electrolysis (not shown) performed at an applied potential of 0.5 V after which the initial Mn(III) complex remains unchanged. We have not observed any wave corresponding to the Mn(III)/Mn(II) redox pair in the potential range from -0.6 to 1.5 V, indicating that the coordination of three anionic ligands to Mn highly destabilizes the Mn(II) oxidation state.

The monoelectronic nature of the wave was confirmed in compound **Mn1** by performing a bulk electrolysis of a 1 mM solution of the complex in acetonitrile at an applied potential of $E_{\text{app}} = 0.63$ V, which transfers one electron per molecule of complex and leads to the generation of $\{\text{Mn}^{\text{III}}\text{Cl}_2(\text{pypz-H})_2\}^+$ as attested by the CV obtained (Figure IV.1.7). However, the yield of Mn(III) species is only 83 % as judged by comparison between the intensities of the waves recorded before and after electrolysis, and two new irreversible oxidation waves appear at 0.8 and 1 V which, in the case of the latter, could tentatively be assigned to the oxidation of free chloride ions. The new wave at 0.8 V could be related to the presence of new Mn(II) species arising from substitution of Cl ligands by acetonitrile solvent, and the increase in the $E_{1/2}$ value with regard to the initial wave would be in accordance with the higher electron-withdrawing ability of CH_3CN when compared to chlorido.³¹³ The cyclic voltammetry obtained after back-electrolysis performed at 0.3 V shows an increase of the intensity of the Mn(III/II) redox wave but the initial species is not completely restored.

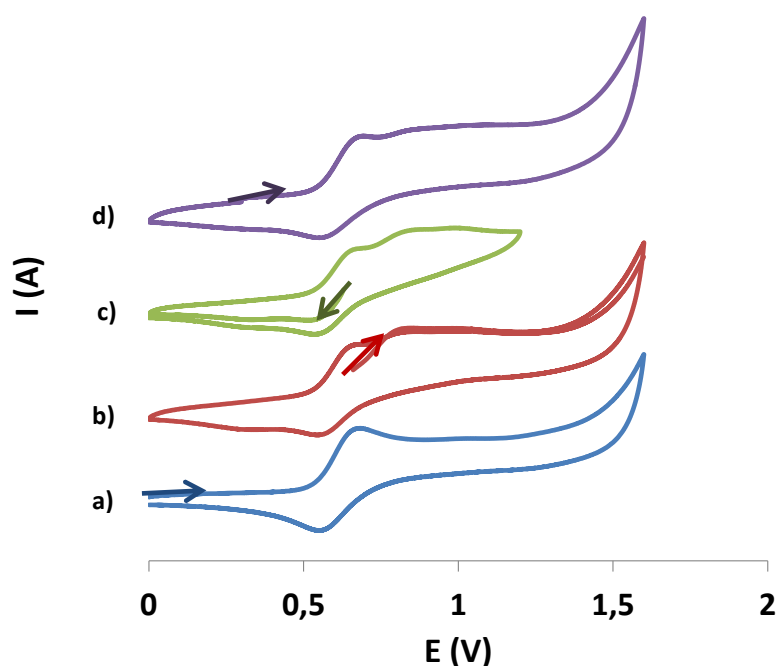


Figure IV.1.7. CV of a 1 mM acetonitrile solution containing 0.1 M TBAH of **Mn1** a) before electrolysis, b) and c) after electrolysis at 0.63 V, d) after back-electrolysis at 0.3 V. The initial scan direction is indicated by arrows in all cases.

The UV-Vis spectrum of the resulting oxidized compound was also performed (Figure SIV.1.15) and shows the same features than other Mn(III) complexes with nitrogen and chlorido based ligands described in the literature.^{313b,314}

IV.1.3. Catalytic olefin epoxidation in acetonitrile medium

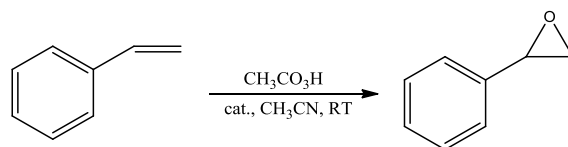
The catalytic activity of manganese compounds **Mn1-9** towards styrene epoxidation using peracetic acid (39 %) as oxidant in acetonitrile was investigated. Table IV.1.1 reports the conversion and selectivity values for the epoxide product in each case. No epoxidation occurred in the absence of catalyst, and olefin conversion values were below 5 % in the presence of different manganese salts. Hydrogen peroxide was also tested as oxidant but did not result in the formation of any epoxide and the decomposition of the oxidant dominated through catalase-like activity despite very extensive attempts to develop effective conditions similar to those previously reported.³¹⁵ For example, the use of a combination of H₂O₂ (50 % aqueous solution) and acetic acid at 0 °C (1:10 H₂O₂:AcOH ratio) gave very low conversion values (<10 %).

As we can see in Table IV.1.1, all the compounds show moderate conversion and selectivity values for styrene epoxide and in all cases benzaldehyde (4-19 % vs. epoxide) is detected as main side product.³¹⁶

The conversion values displayed by chlorido precatalysts with the *pypz-H* bidentate ligand, **Mn1** and **Mn5**, are higher than those presented by the triflate (**Mn2**), acetate (**Mn3**) or nitrate (**Mn4**) complexes. The differences observed can be explained by slower oxidation kinetics for the latter three compounds since the oxidation potential of the chlorido complexes ($E_{1/2} = 0.63$ V, **Mn1** and 0.66 V, **Mn5**) are significantly lower than those of complexes **Mn2-4** (above 0.7 V). Also, distinctive high-valent species are probably involved depending on the precatalyst used. Previous works³⁰⁶ demonstrated the remarkable differences in the oxidized species formed from structurally analogous chlorido and triflate Mn complexes containing bipyridyl ligands, where the high-valent species formed by oxidation of the chlorido complexes attained a higher oxidation state thanks to the presence of Cl ligands that remained coordinated after addition of the oxidant, and this was related to the better catalytic performance observed for these complexes when compared to the analogous triflate compounds. A similar picture can be postulated for the epoxidation mediated by complexes **Mn1-5**.

Chapter IV

Table IV.1.1. Catalytic epoxidation of styrene by **Mn1-9** compounds using PAA as oxidant.^a Conversion (conv.) and selectivity (sel.) values are given in %.



| Entry | compound | conv. | sel. ^b |
|-------|--|-------|-------------------|
| 1 | [MnCl ₂ (pypz-H) ₂], Mn1 | 47 | 60 |
| 2 | [Mn(CF ₃ SO ₃) ₂ (pypz-H) ₂], Mn2 | 22 | 30 |
| 3 | [Mn(CH ₃ CO ₂) ₂ (pypz-H) ₂], Mn3 | 26 | 55 |
| 4 | [Mn(NO ₃) ₂ (pypz-H) ₂], Mn4 | 24 | 61 |
| 5 | [MnCl ₂ (pypz-H)(H ₂ O) ₂], Mn5 | 51 | 47 |
| 6 | [MnCl ₂ (pypz-Me) ₂], Mn6 | 12 | >99 |
| 7 | [Mn(CF ₃ SO ₃) ₂ (pypz-Me) ₂], Mn7 | 10 | >99 |
| 8 | [Mn(CF ₃ SO ₃) ₂ (pypz-CH ₂ COOEt) ₂], Mn8 | 21 | 58 |
| 9 | [MnCl(Ophpz-H) ₂], Mn9 | 34 | 50 |

^a**Conditions:** catalyst (2.5 μmol), substrate (250 μmol), CH₃CN (1 mL). Peracetic acid 39 % (500 μmol) added in 3 minutes at 0 °C, then 3 hours of reaction at RT. ^bSelectivity for epoxide (sel.): [Yield/Conversion] x 100.

It is worth to notice that the replacement of the pyrazolic-*H* by the -*CH*₃ moiety as in the case of the chlorocomplex **Mn6** leads to a notable decrease of the conversion when compared to its analogous **Mn1** complex (12 and 47 % of conversion respectively), though in parallel with a remarkable increase in the selectivity. A similar effect can be observed for related triflate complexes (entries 2 and 7). On the other hand, when comparing analogous complexes with substituted *pypz-R* ligands and different monodentate X ligands, the conversion value achieved in the epoxidation of styrene for **Mn6** is only slightly higher than that displayed by its analogous triflate **Mn7** complex, in contrast with the difference observed between complexes **Mn1** and **Mn2** explained above. Moreover, compound **Mn8**, with triflate and *pypz-CH*₂COOEt ligands, shows better performance than **Mn6** and **Mn7** complexes. These evidences indicate that other factors than redox potential must be taken into account, and the N-substitution of the *pypz* ligand seems in general to worsen the catalytic activity. This effect could arise either

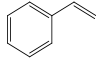
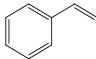
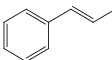
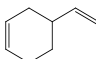
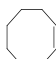
from the higher electron density of the alkylated *pypz-R* ligands, or from a structural influence that would hinder the decoordination of the X ligands making it more sluggish. The different geometrical isomer in **Mn6** and **Mn7** could also have some influence since it might condition the approach of the alkene substrate to the active intermediate species upon decoordination of the monodentate X ligands.

Finally, the activity of complex **Mn9** towards the styrene epoxidation is also moderate despite its pentacoordinated nature that in principle should favour the approach of the substrate towards the active site. This fact could be due to the strongly coordinating and electron-donor ability of the anionic phenolate moieties that would increase the stability of a putative high-valent metal-oxo intermediate hence decreasing its reactivity and leading to a lower conversion of substrate, as has been observed with other Mn(III) compounds.³¹⁶ In the case of **Mn9** complex, the main factors affecting the reactivity seem to be the nature of the ligands and the coordination environment rather than the oxidation state of the initial precatalyst.

In order to further rationalize the catalytic behaviour of the complexes, compounds **Mn1**, **Mn5** and **Mn6-9** (which present different number and types of bidentate ligands, different isomers, coordination environments, and Mn oxidation state) have been tested in the epoxidation of other olefins. Table IV.1.2 reports the conversion and the selectivity values obtained for the corresponding epoxide products.

Chapter IV

Table IV.1.2. Catalytic epoxidation of different alkenes with compounds **Mn1**, **Mn5** and **Mn6-9**, using peracetic acid as oxidant.^a Conversion (conv.) and selectivity (sel.) values are given in %.

| Entry | Complex Substrate | Mn1 | | Mn5 | | Mn6 | | Mn7 | | Mn8 | | Mn9 | |
|-------|---|-------|----------------------------|-------|----------------------------|-------|-----------------------------|-------|-----------------------------|-------|-----------------------------|-------|----------------------------|
| | | conv. | sel. ^b | conv. | sel. | conv. | sel. | conv. | sel. | conv. | sel. | conv. | sel. |
| 1 |  | 47 | 60 | 51 | 47 | 12 | >99 | 10 | >99 | 21 | 58 | 34 | 50 |
| 2 |  | 41 | 89 [85/15] ^c | 33 | 68 [80/20] ^c | 31 | 89 [30/70] ^c | 28 | 92 [56/44] ^c | 30 | 98 [1/99] ^c | 61 | 84 [85/15] ^c |
| 3 |  | 61 | >99 | 47 | 58 | 41 | 72 | 37 | 67 | 55 | 57 | 87 | 85 |
| 4 |  | >99 | 92 [100/0] ^d | 80 | 90 [100/0] ^d | 66 | >99 [100/0] ^d | 62 | >99 [100/0] ^d | 91 | >99 [100/0] ^d | >99 | 63 [100/0] ^d |
| 5 |  | >99 | >99 | 86 | >99 | 80 | >99 | 82 | >99 | 85 | 85 | 98 | >99 |

^a**Conditions:** catalyst (2.5 μmol), substrate (250 μmol), CH_3CN (1 mL). Peracetic acid 39% (500 μmol) added in 3 minutes at 0 °C, then 3 hours of reaction at RT. ^bSelectivity for epoxide (sel.): [Yield/Conversion] x 100. ^cRatio [% *cis* epoxide/ % *trans* epoxide]. ^dRatio [% ring epoxide/ % vinyl epoxide].

As can be observed in Table IV.1.2, moderate conversion values are obtained in general for the three aromatic olefins tested (entries 1-3) whereas the six catalysts display better performances when epoxidizing the aliphatic cyclooctene and 4-vinylcyclohex-1-ene substrates (entries 4 and 5). Moderate to high selectivity values for the corresponding epoxides are observed in all cases, with formation of minor amounts of the corresponding aldehyde, alcohol or/and ketone.

The improved performance observed for the most electron-rich aliphatic substrates suggests that an electrophilic active species could be responsible for the attack at the alkene position. This is also in agreement with the catalysts leading specifically to the epoxidation of the ring alkene position at the 4-vinylcyclohex-1-ene substrate. The epoxidation of this olefin with manganese complexes has been only scarcely studied^{140,155} and the results indicate that either a mixture of the two possible regioisomers or the corresponding diepoxide are formed. To the best of our knowledge, the total epoxidation of the alkene ring position has never been reported with manganese compounds.

Concerning the epoxidation of the aromatic substrates (entries 1-3), it is interesting to observe the increased conversion of compound **Mn9** with regard to the rest of complexes in the epoxidation of *cis* and *trans*- β -methylstyrene, which could be caused by the hexacoordinated nature of the latter precatalysts that presumably leads to an increased steric encumbrance (the pyramidal complex **Mn9** probably provides a faster route for the approach of the substrate). However, for styrene, as described earlier, the best performances are shown by the *pypz-H* complexes **Mn1** and **Mn5**, followed by the pyramidal **Mn9** complex and with the compounds containing the alkylated *pypz-R* ligands displaying the worse conversion degrees. This behaviour seems to indicate that, in the case of styrene, electronic factors dominate over the steric encumbrance and consequently the most electron-rich complexes **Mn6-8** (with alkylated *pypz-R* ligands) and **Mn9** (containing the anionic *Ophpz-H* ligand), lead to lower conversion degrees compared to the *pypz-H* **Mn1** and **Mn5** compounds. As mentioned above, slower kinetics for the decoordination of the monodentate X ligands due to steric factors can also be invoked to explain the lower activity of complexes **Mn6-8**.

On the other hand, the epoxidation of the aliphatic substrates (entries 4 and 5) manifests both types of effects. Considering structural factors, we should expect complex **Mn9** to be the best catalyst and, indeed, it displays excellent performance for both aliphatic substrates. However, the octahedral complex **Mn1** presents an equal activity, followed by complexes **Mn5** and **Mn8**, and then by compounds **Mn6** and **Mn7**. Firstly, if we compare the two octahedral *pypz-H* complexes **Mn1** and **Mn5**, the lower performance displayed by **Mn5** is rather explained by electronic factors as a less electrophilic active species is expected for this catalyst that contains only one electron-acceptor *pypz-H* ligand, differently to the bis(*pypz-H*) complex **Mn1**. In contrast, the complete conversion attained by complex **Mn9** evidences a structural influence since one would expect a poorly electrophilic intermediate for this catalyst containing two anionic *Ophpz-H* ligands, as discussed above for the aromatic substrates. Secondly, we should expect a relatively poor activity for complex **Mn8** (containing the *pypz-CH₂COOEt* ligand) arising from both electronic and structural factors, as is the case of complexes **Mn6** and **Mn7**. However, triflate compound **Mn8** performs in general better than the other two *pypz-R* complexes, and these results could also be explained on the basis of both electronic and structural arguments, invoking favourable interactions exerted by the the CH_2COOEt substituents thanks to the overall spatial arrangement in the high-valent metal-oxo intermediates. In this context, it is important to bear in mind the type of environment close to the Mn=O active group where the olefin will approach, and substituents in **Mn8** might play a role by exerting Van der Waals or H-bonding interactions that could favour the substrate

Chapter IV

approach. As mentioned above, the three *pypz-R* compounds are isolated under different geometrical isomers and, in the case of complex **Mn8**, both CH₂COOEt arms would be close to the vacant sites left after decoordination of the triflate ligands, a fact that could explain in part its improved performance with regard to **Mn6** and **Mn7**.

Regarding the oxidation of *cis*- β -methylstyrene, the selectivity for the epoxide is high in all cases, but it is not stereospecific since a certain amount of *trans*-epoxide (between 15 and 99 %, depending on the catalyst) is produced. This behaviour is similar to that displayed by Mn(salen) catalysts bearing chlorido as counterion/axial ligand,³¹⁷ but it is different to [MnCl₂(L)₂], with L= pinene-bipyridylic ligand,^{306,137} where only *cis*-epoxide is produced. This results suggest in our compounds the presence of a long-lived free substrate radical during the oxygen transfer process^{139a} where the C-C bond rotation leading to *cis/trans* isomerization in the intermediate species formed is faster than the closure of the ring (Scheme I.13).

It is surprising this variance in *cis/trans* selectivity when complex **Mn1** is compared to the structurally analogous [MnCl₂(L)₂], where the only difference is the presence of a second pyridyl ring instead of pyrazolyl in the bidentate ligand. It is clear that the pyrazole ring must have a distinctive electronic and/or structural influence in the stabilization of the intermediate radical species formed. The differences in the reaction pathway arising from the distinctive nature of a bipyridyl and *pypz* ligands have been analysed through DFT calculations and will be described later in this chapter. Moreover, it seems clear that the occurrence of different structural isomers in the compounds tested, together with electronic factors, must have a distinctive influence in the stabilization of the intermediate species formed and consequently in the different *cis/trans* selectivity values observed in Table IV.1.2.

In order to obtain more information about the formation of high-valent species in acetonitrile, we carried out UV-Vis spectroscopic measurements on compounds **Mn1** and **Mn9** to observe their evolution after addition of peracetic acid and styrene. The procedure consisted on adding 2 equivalents of peracetic acid and, after 15 minutes, 10 equivalents of styrene, and monitoring the UV-Vis spectrum periodically (see below). The oxidant was initially added at a temperature of -10 °C to slow down the reaction in the case of **Mn1**, but for **Mn9** the temperature had to be increased to 25 °C due to solubility problems.

The different UV-Vis spectra registered are gathered in Figure IV.1.8. In the case of complex **Mn1**, the initial colourless solution changed to brown with the addition of peracetic acid at -10 °C and a new band appeared in the visible region at 570 nm with a strong increase of the absorbance below 490 nm (Figure IV.1.8A). This band suggests the formation of Mn(III)

species,³¹⁴ as also stated by the ESI-MS experiments described later. After 15 minutes evolving to room temperature the spectrum is unchanged. Subsequent addition of styrene (10 equivalents) induces a change in the spectrum, reducing this species to low-valent manganese (II) species.

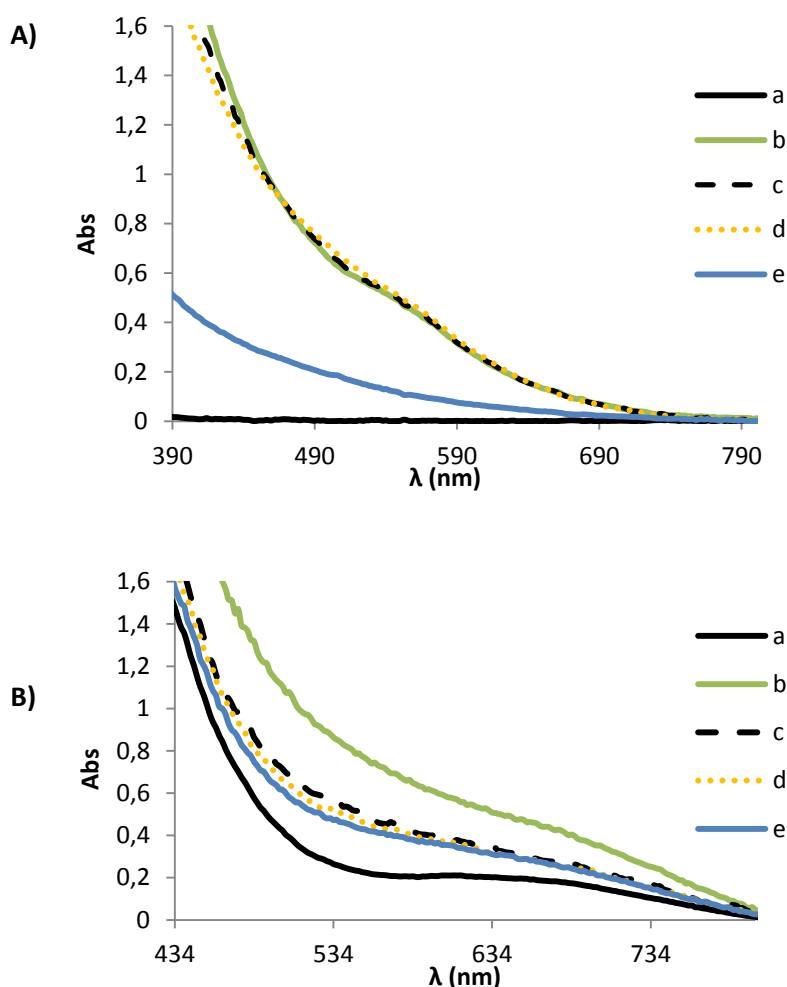


Figure IV.1.8. A) Evolution of UV-Vis spectrum of complex **Mn1** in CH₃CN (1.4 mM), upon addition of 2 eq. of peracetic acid at -10 °C and 10 eq. of styrene substrate at 15 °C: (a) initial, (b) 1 minute after addition of PAA, (c) 15 minutes after addition of PAA (addition of styrene at this point), (d) 1 hour after addition of styrene (e) 20 hours after addition of styrene; B) Evolution of UV-Vis spectrum of complex **Mn9** in CH₃CN (1.4 mM), upon addition of 2 eq. of PAA at 25 °C and 10 eq. of styrene substrate at 25 °C: (a) initial, (b) 1 minute after addition of PAA, (c) 15 minutes after addition of PAA (addition of styrene at this point), (d) 1 hour after addition of styrene (e) 20 hours after addition of styrene.

A similar experiment has been performed with **Mn9** (Figure IV.1.8B), but at an initial temperature of 25 °C. When 2 eq. of peracetic acid were added to an acetonitrile solution containing the Mn(III) compound, the initial dark green colour turned to greenish-brown, and the band at 636 nm was initially shifted to 680 nm. After 15 minutes, a decrease of the overall absorbance was observed, indicating that lower temperatures would be necessary to avoid degradation under these experimental conditions. This latest spectrum can be attributed to a

Chapter IV

new Mn(III) species arising from oxidant and solvent coordination as evidenced by the ESI-MS spectrum of the solution (see below). At this point, styrene is added but no further changes are observed in the UV-Vis spectra. It must be noticed that the catalytic experiments previously described have been carried out using a large excess of oxidant, thus allowing the catalytic activity for both complexes.

Electrospray mass spectra were recorded in positive detection mode for both complexes after addition of two equivalents of peracetic at 0 °C (Figure SIV.1.16). In the starting solution (still without oxidant), ions at m/z 457.2 for **Mn1** and 372.9 for **Mn9** were detected, corresponding to $[\text{MnCl}_2(\text{pypz-H})_2] \cdot \text{H}_2\text{O} \cdot \text{Na}^+$ and $[\text{Mn}(\text{Ophpz-H})_2]^+$ respectively. After addition of PAA new peaks appear that, in the case of compound **Mn1**, may be attributed to different cationic species of Mn(II), Mn(III) and oxo-bridged binuclear manganese (III) compounds. In the case of **Mn9** only mononuclear cationic species of Mn(III) have been detected.

In addition to the species mentioned above, it should be noted that other high-valent mononuclear oxo or peroxy manganese species could be involved as catalytic active species, as has previously been reported in the epoxidation reaction with peracids.^{154h,318} Also, several types of reactive intermediates including *cis*- $\text{Mn}^{\text{IV}}(\text{O})_2$ and *trans*- $\text{Mn}^{\text{V}}(\text{O})_2$,^{319,320} have been proposed in the literature for Mn-catalysed organic oxidations. These intermediate species might be transiently formed upon addition of oxidant, but they are not spectroscopically observable, or they are present in a too low concentration to be detected in the experimental conditions tested.

IV.1.4. Computational studies on the epoxidation of *cis* olefins

DFT calculations have been carried out to unravel the origin of the about 15 % of *cis* \rightarrow *trans* isomerization in the epoxidation of *cis*- β -methyl styrene with complex **Mn1** in comparison with the total stereoselectivity for the *cis*-epoxide observed with $[\text{MnCl}_2(\text{L})]$ (L = SPAN ligands)^{138c} or $[\text{MnCl}_2(\text{L})_2]$ (L = bipyridylic ligands).¹³⁷ Starting with the catalytic, high oxidation active species $[\text{Mn}^{\text{IV}}(\text{O})_2]$ generated from the precatalyst **Mn1**, Figure IV.1.9 displays the reaction profiles leading to *cis* and *trans* epoxides.

The initial ground state of complex **Mn1** is a doublet. Then it switches to quadruplet after the formation of the biradical species **II**. The reaction pathway follows the typical scheme for such epoxidations, with two steps that require overcoming low barriers for system **Mn1**. Once the intermediate radical species **II**_{*cis*} is formed, the direct closure of the ring (**II**_{*cis*} \rightarrow **III**_{*cis*}) requires overcoming a barrier of 2.0 Kcal/mol, a value slightly higher than the 1.0 Kcal/mol

corresponding to the barrier of the $cis \rightarrow trans$ isomerization, $\text{II}_{cis} \rightarrow \text{II}_{trans}$. However, the closure of the ring after isomerization through the subsequent transition state $\text{II}_{trans} \rightarrow \text{III}_{trans}$, requires 0.6 kcal/mol more than the closing transition state $\text{II}_{cis} \rightarrow \text{III}_{cis}$ leading to *cis* epoxide. This explains why there is some degree of $cis \rightarrow trans$ isomerization although at the end the *cis* epoxidized product is the main product obtained experimentally despite being 1.1 Kcal/mol less stable.

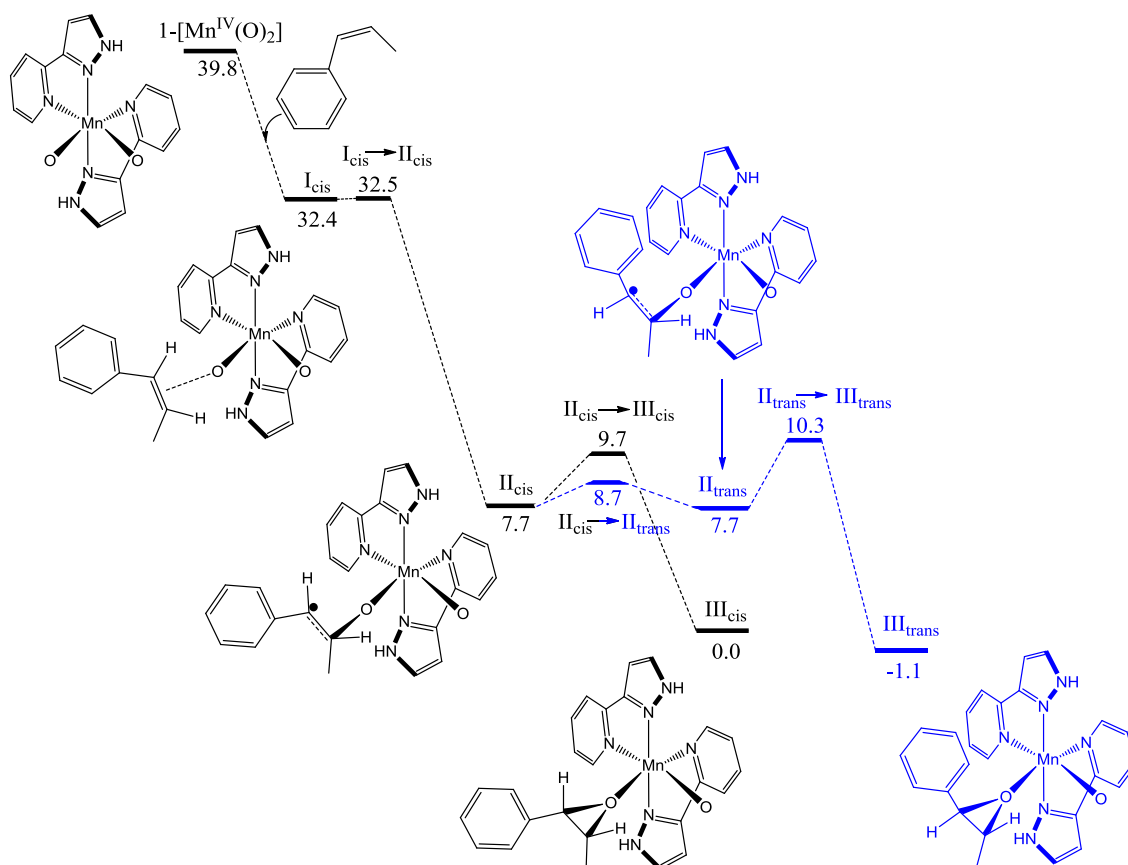


Figure IV.1.9. Reaction pathway for the epoxidation of the *cis*- β -methylstyrene substrate by the catalyst **Mn1** (Gibbs energies in Kcal mol⁻¹).

As discussed before, the stereoselectivity observed in catalyst **Mn1** is different to that found in catalysts with non-pyrazolic based ligands. To explore the origin of this difference we have calculated the reaction mechanism for some complexes bearing non-pyrazolic ligands (complexes **2** and **3**, Figure SIV.1.17), and also for complex **1**, where we have substituted the NH groups of catalyst **Mn1** by CH₂, to discuss the role of potential H-bonds involving the NH groups. In all cases, the reaction profile is quite similar (see Table IV.1.3), although some differences are observed. If we focus the discussion on the stereoselectivity of the reaction, we have to analyze the reaction pathways starting from II_{cis} . For complex **1** the energy barriers of the reactions $\text{II}_{cis} \rightarrow \text{III}_{cis}$ and $\text{II}_{cis} \rightarrow \text{II}_{trans}$ are very low, 0.5 and 0.3 Kcal/mol respectively. On the

Chapter IV

other hand, the $\text{II}_{trans} \rightarrow \text{III}_{trans}$ process has to surpass a barrier of 3.2 Kcal/mol. Overall, for **1**, application of the Curtin-Hammett principle leads to the conclusion that the *cis* product formation will be more favored in this case than for **Mn1**. To compare the role of pyridyl and pyrazole based ligands, we envisaged calculations with complexes **2** and **3**, which experimentally have demonstrated to give selective *cis* epoxidation from *cis* substrates. Bearing in mind the previously reported SPAN based system **2** (see Figure SIV.1.17),^{138c} we found a relative instability of the II_{cis} species that would not favor the *cis* \rightarrow *trans* isomerization but the direct closure of the *cis* epoxide ring through a barrierless step ($\text{II}_{cis} \rightarrow \text{III}_{cis}$), i.e., the key results to point out are that the barrier of the isomerization $\text{II}_{cis} \rightarrow \text{II}_{trans}$ is 2.0 Kcal/mol higher in energy than the closure of the *cis* epoxide, exactly the opposite with respect to the situation found in **Mn1**. Consequently, for catalyst **2**, II_{trans} is not formed and the reaction is completely stereoselective. To find a reason for the higher reactivity of **2** as compared to **Mn1** in the $\text{II}_{cis} \rightarrow \text{III}_{cis}$ process, we looked at the NBO charges of intermediate II_{cis} and we found only slight differences. For instance, the negative charge of the oxygen atom attacking the C atom to close the ring is 0.03 electrons more negative in **2**. Even though this slightly different charge can make a difference, we think that the main reason for the larger reactivity of the $\text{II}_{cis} \rightarrow \text{III}_{cis}$ process in **2** has to be ascribed to the different O...C distance in II_{cis} that will be transformed into a O-C bond in III_{cis} . This distance is nearly 0.3 Å shorter for complex **2** (see Figure SIV.1.17), with respect to complex **Mn1**.

Table IV.1.3. Reaction coordinate energies (in Kcal mol⁻¹) for epoxidation of *cis*- β -methylstyrene with catalysts **Mn1**, **1**, **2** and **3**.

| Cat | [Mn ^{IV} O ₂] | I _{cis} | I _{cis} -II _{cis} | II _{cis} | II _{cis} -III _{cis} | II _{cis} -III _{cis} barrier | III _{cis} | II _{cis} - II _{trans} | II _{cis} -II _{trans} barrier | II _{trans} | II _{trans} - III _{trans} | II _{trans} -III _{trans} barrier | III _{trans} |
|------------|------------------------------------|------------------|-------------------------------------|-------------------|---------------------------------------|--|--------------------|--|---|---------------------|---|--|----------------------|
| Mn1 | 39.8 | 32.4 | 32.5 | 7.7 | 9.7 | 2 | 0.0 | 8.7 | 1 | 7.7 | 10.3 | 2.6 | -1.1 |
| 1 | 35.6 | 30.6 | 33.9 | 9.2 | 9.7 | 0.5 | 0.0 | 9.5 | 0.3 | 8.0 | 11.2 | 3.2 | -2.5 |
| 2 | 33.4 | 31.3 | 32.0 | 7.5 | 8.8 | 1.3 | 0.0 | 10.8 | 3.3 | 5.6 | 6.9 | 1.3 | -1.0 |
| 3 | 37.8 | 31.5 | 32.2 | 8.4 | 10.1 | 1.7 | 0.0 | 13.2 | 4.8 | 6.9 | 7.0 | 0.1 | -2.8 |

On the other hand, the use of a bipyridyl ligand in **3** (see Figure SIV.1.17) instead of five-membered rings like in systems **Mn1** and **1**, and with added sterical hindrance due to the presence of a pinene group in each bipyridine, confirms that the formation of *trans* epoxides was not possible because $\text{II}_{cis} \rightarrow \text{II}_{trans}$ transition state is 3.1 Kcal/mol higher in energy with respect

to the closure of the *cis* epoxide through the **II_{cis}-III_{cis}** pathway and thus, no competition is likely.

Further calculations on the epoxidation of the 4-vinylcyclohex-1-ene substrate by **Mn1**-[Mn^{IV}(O)₂] confirmed the complete selectivity towards the alkene epoxidation at the ring position that was found experimentally. Indeed, the first barrier of the reaction pathway, which would be equivalent to the **I_{cis}-II_{cis}** step displayed in Figure IV.1.9 for the *cis*- β -methylstyrene substrate, is located 1.8 Kcal/mol higher in energy for the terminal epoxidation than for the ring epoxidation.

IV.1.5. Catalytic olefin epoxidation in different media. Reusability of catalysts in ionic liquid:CH₃CN.

We have also tested the performance of precatalysts **Mn1**, **Mn5** and **Mn9** in different media to the above described acetonitrile. Current research has been going on in trying to find new solvents with low environmental impact.² The need to develop sustainable oxidation processes led us to test the effect of different clean solvents as ionic liquids (IL) or glycerol on the epoxidation of alkenes using the above-mentioned compounds as catalysts.

First of all, the suitability of using an ionic liquid as solvent or co-solvent was evaluated with the commercial ionic liquid [bmim]PF₆. We have investigated the catalytic performance of complex **Mn1** in ionic liquid media using different IL:acetonitrile ratios, with *trans*- β -methylstyrene as substrate, and the results are displayed in Table IV.1.4.

Table IV.1.4. Optimization of the procedure for the epoxidation of *trans*- β -methylstyrene substrate in ionic liquid:solvent media with **Mn1** as catalyst. Conditions: *trans*- β -methylstyrene (250 μ mol), catalyst (2.5 μ mol), peracetic acid (500 μ mol), RT, 3h. Conversion (conv.) and selectivity (sel.) values are given in % and were evaluated by GC analysis with biphenyl as internal standard.

| Entry | [bmim]PF ₆ /solvent ratio | Solvent | conv. | sel. |
|-------|--------------------------------------|--------------------|-------|------|
| 1 | 1/0 | - | 99 | <10 |
| 2 | 1/0.5 | CH ₃ CN | 90 | 43 |
| 3 | 1/1 | CH ₃ CN | 85 | 96 |

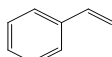
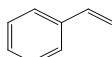
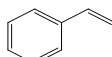
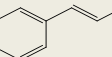
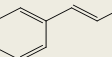
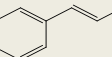
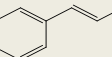



In pure ionic liquid (entry 1 in Table IV.1.4) quantitative olefin conversions are obtained, but with low selectivity values, presumably due to the hydrolysis and/or overoxidation of the corresponding epoxide.³²¹ In general, better performances (in terms of conversion and selectivity) are obtained in presence of IL:CH₃CN 1:1 ([bmim]PF₆:acetonitrile ratios) (entry 3),

Chapter IV

and these conditions were chosen for subsequent catalytic tests carried out in a mixture of solvent and ionic liquid.

The results obtained for the catalytic tests performed with complexes **Mn1**, **Mn5** and **Mn9** using different solvents are gathered in Table IV.1.5. The substrates chosen for this study were *cis* and *trans*- β -methylstyrene, and cyclooctene. As was the case for the catalytic experiments performed in acetonitrile, no epoxidation occurred in the absence of catalyst or in the presence of Mn salts in any case. The results obtained in pure acetonitrile, discussed previously, are included for purposes of comparison

Table IV.1.5. Epoxidation tests performed with complexes **Mn1**, **Mn5** and **Mn9** in different media.^a Conversion (conv.) and selectivity (sel.) values are given in %.

| Entry | Substrate | Solvent | [MnCl ₂ (pypz-H) ₂], Mn1 | | [MnCl ₂ (H ₂ O) ₂ (pypz-H)], Mn5 | | [MnCl(Ophpz-H) ₂], Mn9 | |
|-------|---|---|--|-------------------|--|-----------------|---------------------------------------|-----------------|
| | | | conv. | sel. ^b | conv. | sel. | conv. | sel. |
| 1 |  | CH ₃ CN | 41 | 89 ^c | 33 | 68 ^c | 61 | 84 ^c |
| 2 |  | [bmim]PF ₆ :CH ₃ CN | 80 | 80 ^d | 43 | 70 ^d | 65 | 80 ^d |
| 3 |  | glycerol | 73 | 57 ^e | 38 | 32 ^e | 76 | 25 ^e |
| 4 |  | CH ₃ CN | 61 | >99 | 47 | 58 | 87 | 85 |
| 5 |  | [bmim]PF ₆ | 99 | <10 | 76 | 14 | 97 | <10 |
| 6 |  | [bmim]PF ₆ :CH ₃ CN | 85 | 96 | 54 | 83 | 82 | 97 |
| 7 |  | glycerol | 86 | 38 | 71 | 20 | 90 | 17 |
| 8 |  | CH ₃ CN | >99 | >99 | 86 | >99 | 98 | 99 |
| 9 |  | [bmim]PF ₆ :CH ₃ CN | >99 | >99 | 73 | >99 | 99 | 97 |
| 10 |  | glycerol | 64 | 76 | 69 | 69 | 74 | 98 |

^a**Conditions:** catalyst (2.5 μ mol), substrate (250 μ mol), Solvent (2 mL). Peracetic acid 39% (500 μ mol) added in 3 minutes at 0 °C, then 3 hours of reaction at RT. When using [bmim]PF₆:CH₃CN mixtures the ratio was 1:1 in all cases. ^bSelectivity for epoxide (sel.): [Yield/Conversion] x 100. ^c15 % of *trans* epoxide isomer has been obtained for catalysts **Mn1** and **Mn9**, whereas it was of 20 % for **Mn5**. ^d<5 % of *trans* epoxide isomer has been obtained for all catalysts. ^e100 % of *cis* epoxide has been obtained.

As can be observed (comparing for instance entries 1/2, 4/6 or 8/9) the selectivity for the epoxide product is well maintained in IL:CH₃CN 1:1 mixture when compared to acetonitrile with only a slight decrease in some cases, but it is important to note that the presence of the ionic liquid exerts a significant stabilizing effect on our catalysts, and the conversions are improved particularly for complex **Mn1**, whereas are well maintained at moderate to high values for the case of complexes **Mn5** and **Mn9**. The ionic liquids have been described to have

a variety of distinctive effects in catalysis (being in some cases directly involved in the catalytic path) and, in our case, we can postulate a stabilizing effect arising from electrostatic or π -cation interactions between the bmim^+ cation and the aromatic rings of the ligands in the intermediate Mn species.³²² However, the presence of acetonitrile is essential to achieve good selectivities for the epoxide product (see entry 5), and a possible reason is that it could inhibit the mechanism of hydrolysis in a similar way to other coordinating base species which block the access of the epoxide to the acidic metal centre inhibiting the hydrolysis and consequently increasing the selectivity for the corresponding epoxide.³²³

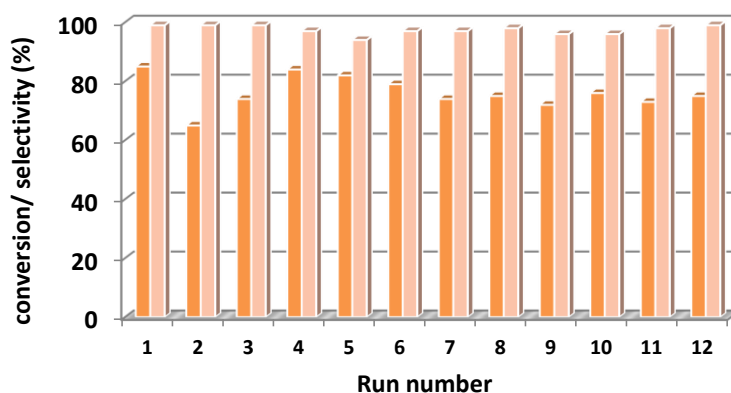
On the other hand, the reaction in glycerol leads to an increase in the conversion values for the methylstyrene substrates with regard to acetonitrile (compare entries 1 and 3, or 4 and 7) but in the case of cyclooctene only a moderate conversion is attained. Also, the selectivity values for the corresponding epoxides are moderate to low, probably due to the hydrolysis of the epoxide as described previously for the IL:acetonitrile systems.⁴ In the case of cyclooctene the selectivity values in glycerol are higher than for the two methylstyrene substrates but, although a decrease in the selectivity was observed for the latter, a total stereospecificity was observed for the *cis* epoxide in the epoxidation of *cis*- β -methylstyrene mediated by the complexes synthesized. In this context, these preliminary results are promising for the use of glycerol as a green solvent in oxidation processes using peracetic acid as oxidant. As we have previously reported, the performance of compound **Mn1** as catalyst in these media is better than the one displayed by compound **Mn5**, which corroborates again the role of pyrazolic ligands in the modulation of the catalytic activity.

Based in the above results, the recyclability of the **Mn1** and **Mn9** catalytic systems was investigated in $[\text{bmim}]\text{PF}_6:\text{CH}_3\text{CN}$ medium and the results obtained for both catalysts are displayed in Figure IV.1.10 and in Figures SIV.1.19 and SIV.1.20. One can observe that the catalysts maintain an excellent performance through up to 12 runs in all cases. The selectivity towards the epoxide product is also well maintained and the conversion values are near 100 % for *trans*- β -methylstyrene (Figure IV.1.10) and cyclooctene (Figure SIV.1.20), and close to 90 % for *cis*- β -methylstyrene (Figure SIV.1.19). In this latest case, the selectivity for the *cis* epoxide is maintained through all the runs and this value is higher than in acetonitrile solvent (< 5 % of *trans* epoxide isomer has been obtained for catalyst **Mn1** and < 10 % for catalyst **Mn9**, whereas in acetonitrile this value was around 15 %). The overall turnover numbers for the obtaining of the respective epoxides are; 914 (complex **Mn1**) and 1033 (complex **Mn9**) for *trans*- β -methylstyrene; 1190 (complex **Mn1**) for cyclooctene; 915 (complex **Mn1**) and 880 (complex **Mn9**) for *cis*- β -methylstyrene. It is worth to notice the good stabilizing effect of the

Chapter IV

ionic liquid on the catalysts that allows their reuse without loss of activity and keeping excellent selectivity values.

a)



b)

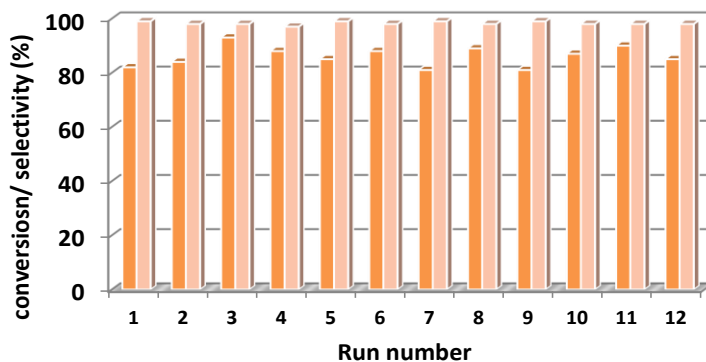


Figure IV.1.10. Conversion (orange bars) and selectivity (pink bars) values obtained throughout consecutive reuses of complex **Mn1** (a) and complex **Mn9** (b) in the epoxidation of *trans*- β -methylstyrene in [bmim]PF₆:CH₃CN (see text for experimental conditions).

To the best of our knowledge, these systems constitute one of the most effective and stable epoxidation systems based on the reutilization of manganese compounds and the first example of Mn(II) and Mn(III) complexes with pyrazole-based ligands tested under such conditions.

IV.1.6. Heterogenization of complex [Mn(CF₃SO₃)₂(pypz-CH₂COOEt)₂] onto a SiO₂ support.

IV.1.6.1. Immobilization of complex Mn8

The immobilization method used for the heterogeneization of [Mn(CF₃SO₃)₂(pypz-CH₂COOEt)₂] (**Mn8**) is based on covalent binding formed between the modified pyridine-pyrazole ligand containing an ethyl ester group and the silica particles and, consequently, a strong interaction

between the catalyst and the support is achieved. In order to create this covalent bond, the *pypz-H* ligand was first functionalized with an ethyl acetate group to generate the *pypz-CH₂COOEt* ligand. The anchoring to the surface of silica particles will be carried out through the subsequent hydrolysis of the terminal ester group of the ligand to generate the corresponding carboxylic acid, which will be able to form covalent C-O-Si bonds at the surface of the silica particles.

Silica mesoporous particles (SP) with mean diameter of aprox. 200 nm and surface area of 886 m²/g were chosen as heterogeneous support. The immobilization of the complex onto the SP surface was performed through the attachment of the previously synthesized **Mn8** complex (that bears two units of the *pypz-CH₂COOEt* ligand), by simply stirring a toluene solution of the complex and SP at 35 °C for 6 days (Figure IV.1.11). The resulting **SP@Mn8** modified silica was centrifuged, washed with methanol and acetone and dried at air.

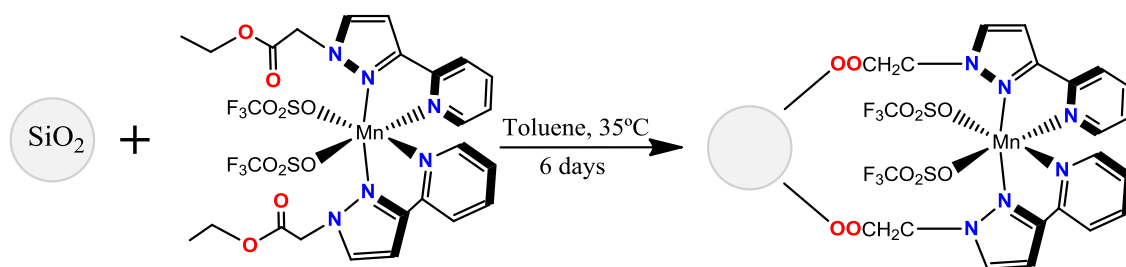


Figure IV.1.11. Synthetic strategy for the immobilization of **Mn8** onto silica particles (SP).

However, under the synthetic conditions described above, a considerable low yield of the compound attached onto SP (quantified through ICP-AES spectroscopy as described later) was obtained. This fact, could probably be due to the incomplete hydrolysis of the ester moiety to the corresponding carboxylic acid. Other conditions (such as the use of protic solvents, heating the solution at temperatures above 35 °C or the addition of little amounts of base) have been tried but the complex was unstable in such conditions.

IV.1.6.2. Characterization of the functionalized support

The heterogeneous support was characterized by spectroscopic techniques. The UV-Vis spectrum obtained for a suspension of **SP@Mn8** in methanol was compared with that of the homogeneous compound **Mn8**, confirming that the immobilized species is indeed complex **Mn8** based on the similarity of the respective spectra (Figure IV.1.12). The complex exhibits ligand-based π - π^* bands below 300 nm.

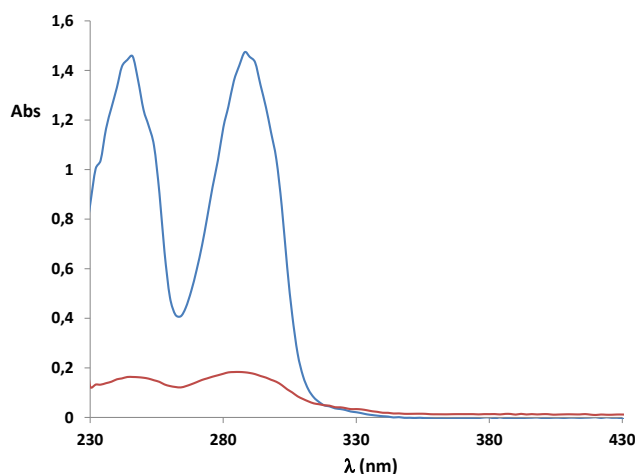



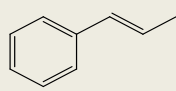
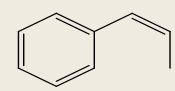
Figure IV.1.12. UV-vis spectrum for homogeneous complex **Mn8** (blue) and heterogeneous **SP@Mn8** catalyst (red) in MeOH.

The amount of catalyst anchored onto the silica support was determined by atomic emission (ICP-AES) spectroscopy, and $2.5 \cdot 10^{-5}$ % Mn (g Mn/ 100g of SiO₂) was detected.

IV.1.6.3. Catalytic activity in olefin epoxidation

The catalytic activity of **SP@Mn8** was evaluated in epoxidation of alkenes in CH₃CN, under the same conditions used with the analogous homogeneous complex **Mn8**. Cyclooctene, *trans*- β -methylstyrene and *cis*- β -methylstyrene were used as test substrates. Table IV.1.6 shows the preliminary results obtained.

Table IV.1.6. Epoxidation tests performed with heterogeneous complex **SP@Mn8** in CH₃CN.^a Conversion (conv.) and selectivity (sel.) values are given in %.

| Substrate |  |  |  | | | |
|-----------|---|--|---|------|-------|------|
| Time (h) | conv. | sel. ^b | conv. | sel. | conv. | sel. |
| 3 | 43 | >99 | 0 | - | 0 | - |
| 24 | 62 | >99 | 15 | >99 | 15 | >99 |

^a**Conditions:** alkene (2.2 μ mol), catalyst ($2.27 \cdot 10^{-4}$ μ mol), CH₃CN (1 mL). Peracetic acid 39 % (4.54 μ mol) added in 3 minutes at 0 °C, then 3 or 24 hours of reaction at RT. ^bSelectivity for epoxide (sel.): [Yield/Conversion] x 100. A blank experiment using unfunctionalized silica yielded 10 % of conversion. This value has been subtracted from the results shown above.

As can be observed in Table IV.1.6, low conversion values were obtained for the aromatic substrates, whereas moderate conversion were achieved for cyclooctene with an excellent selectivity towards the epoxide product, in all cases. Longer reaction times were evaluated in

the heterogeneous system as kinetics are expected to be much slower due to the higher difficulty of the substrates to reach the anchored catalyst and also to the low amount of catalyst used.

The recyclability of the heterogeneous **SP@Mn8** catalyst was studied towards the epoxidation of cyclooctene at RT for 3 h. The performances of four consecutive reuses of the catalytic system are displayed in Figure IV.1.13.

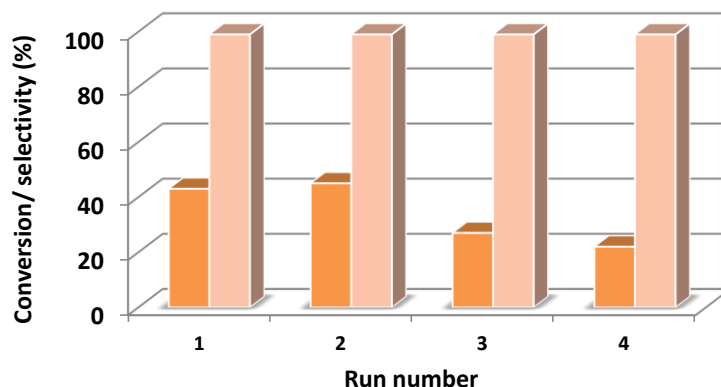


Figure IV.1.13. Conversion (orange bars) and selectivity (pink bars) values obtained throughout consecutive reuses of heterogeneous **SP@Mn8** in the epoxidation of cyclooctene in CH_3CN (see text for experimental conditions).

The heterogeneous complex shows a slight decrease of the conversion values along the successive runs but an excellent selectivity for the epoxide product is maintained. The TON values obtained are excellent (4330, 4500, 2660, 2160 for runs 1-4 respectively, with an overall TON above 13600). As mentioned in the introduction, the control of the activity in heterogeneous catalytic systems is not easy since active sites are placed in a microporous environment that often causes diffusion control of the catalyzed reaction and thus reduces both activity and selectivity degree. In this case, the conversions are indeed lower than those presented by the analogous homogeneous system but keeping an excellent selectivity.

In summary, in this chapter we have synthesized and fully characterized a family of new manganese(II) and manganese(III) complexes containing pyrazole-based ligands. The redox properties of all complexes have been studied and several different redox processes are found in all cases.

All complexes have been studied as precatalysts in the epoxidation of some alkenes using peracetic acid as oxidant, displaying in general moderate to excellent conversion and

Chapter IV

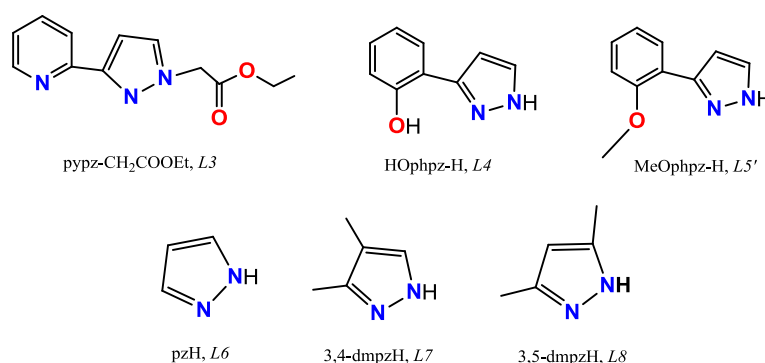
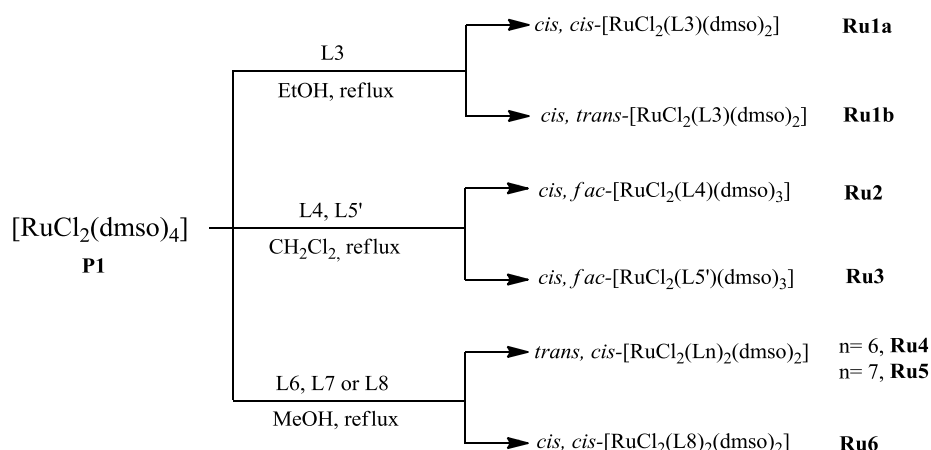
selectivity values, with the best results obtained for aliphatic substrates. A certain degree of *cis* → *trans* isomerization has been evidenced in the epoxidation of *cis* olefins, in accordance with the computational calculations performed on these systems. Chlorido complexes **Mn1**, **Mn5** and **Mn9** have also been investigated in epoxidation catalysis carried out in other media such as glycerol and ionic liquid:solvent medium. In the latter all catalysts show a remarkable effectiveness and selectivity for the epoxide product. Also, an excellent degree of reusability in the epoxidation of some alkenes in this medium has been observed for catalysts **Mn1** and **Mn9**, which were found to be robust and recyclable catalytic systems that can be reused without loss of activity and keeping high conversion and selectivity values after twelve cycles.

Also, we have successfully heterogenized complex **Mn8** onto silica particles leading to the **SP@Mn8** heterogeneous catalyst which has been characterized by UV-Vis and ICP-AES spectroscopic techniques. Preliminary studies in epoxidation of alkenes in acetonitrile has been carried out using **SP@Mn8**, under the same conditions used with the analogous homogeneous complex **Mn8**. Its recyclability has been studied towards the epoxidation of cyclooctene for four consecutive reuses, showing a slight decrease of the conversion values along the successive runs but keeping an excellent selectivity towards the epoxide product.

IV.2. Ru(II) complexes containing dmsO and pyrazolyl ligands as catalysts for nitrile hydration.

IV.2.1. Synthesis and structure

The synthetic strategy followed for the preparation of ruthenium(II) complexes **Ru1-Ru6** is outlined in Scheme IV.2.1. Reaction of equimolar amounts of $[\text{RuCl}_2(\text{dmsO})_4]$ (**P1**) and the bidentate *pypz-CH₂COOEt* ligand, *L3*, in absolute ethanol at reflux under nitrogen atmosphere and in the absence of light gives a mixture of the *cis,cis* and *cis,trans* isomers for complex **Ru1** (where the nomenclature refers to the one-to-one position of Cl and dmsO ligands respectively) in 1:0.5 ratio. Although this mixture couldn't be purified, an alternative synthesis in dichloromethane led to the sole *cis,trans-Ru1b* isomer that was obtained in a very low yield together with a certain amount of the starting **P1** complex.



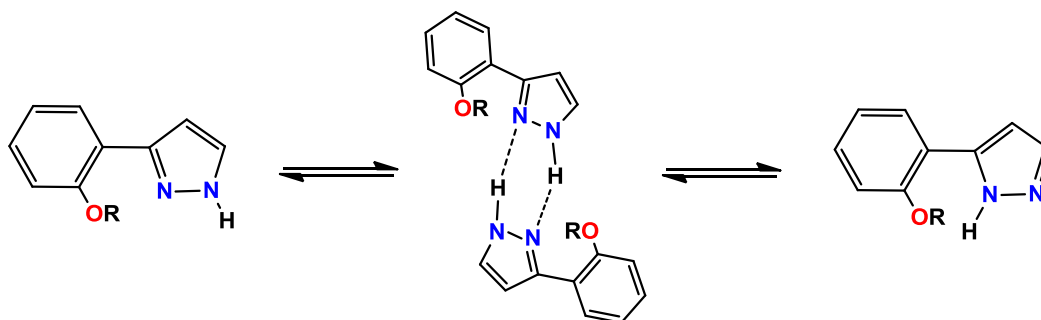
Scheme IV.2.1. Synthetic strategy for **Ru1-Ru6** compounds and ligands used.

On the other hand, the reaction of $[\text{RuCl}_2(\text{dmsO})_4]$ (**P1**) with equimolar amounts of the bidentate ligands *HOphpz-H*, *L4*, or *MeOphpz-H*, *L5'*, in CH_2Cl_2 at reflux leads respectively to compounds *cis, fac-Ru2* and *cis, fac-Ru3*, where the term *cis* indicates again the relative position of two Cl ligands and *fac* refers to the facial disposition of the three dmsO ligands (see below for a discussion on the geometrial isomers obtained). The synthesis of complex **Ru2** also

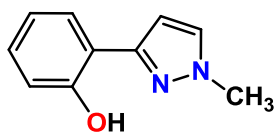
Chapter IV

leads to the generation of a secondary product, **Ru2'**, that contains two units of the *L4* ligand (see SI). In all cases, ligands *L4* and *L5'* coordinate in a monodentate fashion through the outer pyrazolyl N atom thanks to the tautomeric capability of the pyrazolyl proton³²⁴ (see Scheme IV.2.2A). This is consistent with the well-known tautomerism of diazoles via intermolecular proton transfer^{324b,325} or with the behaviour displayed by other similar ruthenium compounds found in the literature,³²⁶ and might lead to a more stable conformation that prevents the coordination of *L4* and *L5'* in a chelate manner.

A



B



Scheme IV.2.2. A, Tautomerization of the ligands 3(5)-(2'-hydroxyphenyl)pyrazole, *L4* (R= H), and 3-(2-methoxyphenyl)-1H-pyrazole, *L5'* (R= CH₃). B, ligand 2-(1-methyl-1H-pyrazol-3-yl)phenol, *L5*.

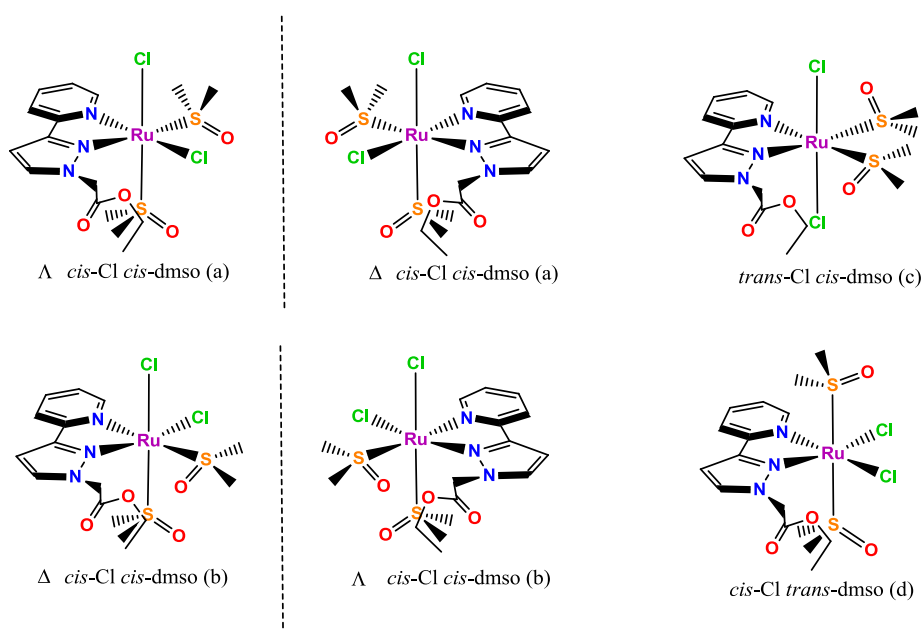
Despite many efforts have been done to obtain the bidentate *L4* and *L5'* compounds we could only observe the monodentate coordination in ruthenium(II) complexes **Ru2**, **Ru2'** and **Ru3**. We also tried to coordinate ligand *L5* (Scheme IV.2.2B), which cannot undergo the tautomerization process, using the same reaction conditions than for the coordination of ligands *L4* and *L5'* but no reaction occurred in this case, thus indicating that bidentate coordination is not favoured for this phenolate-type of ligands, as is also the case for monodentate O-coordination through the phenolate moiety.

Finally, the reaction of [RuCl₂(dmsO)₄] (**P1**) and the monodentate ligands pzH, *L6*, 3,4-dmpzH, *L7*, or 3,5-dmpzH, *L8*, in 1:2 ratio at reflux under inert atmosphere and in the absence of light produces respectively the complexes *trans,cis*-**Ru4**, *trans,cis*-**Ru5** and *cis,cis*-**Ru6** (the nomenclature *cis* or *trans* refers again to the relative position of Cl and dmsO ligands respectively). Note that compound **Ru4** has been previously described in the literature²⁹⁷ and

compound **Ru6** has been obtained earlier in our group,²⁹⁸ but in this chapter we present a new synthetic method for both complexes.

Structural analysis

The substitution of two dmsoligands in $[\text{RuCl}_2(\text{dmsol})_4]$ by the unsymmetrical bidentate ligand **L3**, generating complexes **Ru1a** and **Ru1b**, can potentially lead to the formation of six different stereoisomers (including two pairs of enantiomers) which are depicted in Scheme IV.2.3.



Scheme IV.2.3. Possible stereoisomers for complex **Ru1**.

In the case of compound **Ru1** two geometrical isomers, Λ/Δ *cis*-Cl *cis*-dmsol (**Ru1a**) and the *cis*-Cl,*trans*-dmsol (**Ru1b**) have been detected in 1:2 ratio respectively when the reaction is performed in ethanol, either when the reaction is limited to 15' or it is extended up to 24 h, whereas only the *cis,trans*-**Ru1b** isomer is obtained in dichloromethane but in an incomplete reaction. In general, the preference towards the formation of a specific isomer in Ru(II) complexes can be explained taking into account the following structural and electronic factors:

- Ru(II) is a d^6 ion, it forms strong bonds with N-donor ligands and these cannot be exchanged in solution with other coordinated ligands, thus minimizing the geometrical reorganization after their coordination.
- The existence of strong intramolecular interactions as hydrogen bonding.
- The steric hindrance caused by bulky substituents at the ligands.

Chapter IV

- The synergistic π -donor and π -acceptor effects among π -donor and π -acceptor ligands mutually placed in *trans*.

In the case of **Ru1** compound, the mixture of isomers obtained seem to be a balance between electronic and structural factors. Firstly, the *cis*-Cl,*cis*-dmsO (a) and (b) isomers (Scheme IV.2.3) seem to be energetically favoured thanks to the occurrence of a *trans* Cl-Ru-dmsO layout that takes advantage of the synergistic effect of a π -donor (Cl) and a π -acceptor (dmsO) placed in *trans* and, indeed, the *cis,cis* isomer (b) was obtained specifically in the synthesis of the analogous complex containing the related *pypz-H* ligand,^{107c,184a} also favoured by the occurrence of H-bonding interactions between the equatorial dmsO ligand and the N_{pz}-H proton. However, in the case of **Ru1** complexes, the pendant ethylester arm in the *pypz* ligand prevents the formation of hydrogen bonds and, additionally, provides a high degree of steric hindrance that probably difficults the coplanar disposition of the *L3* ligand together with one dmsO and one Cl ligands. Thus, the *cis*-Cl,*trans*-dmsO isomer (d), which is probably favoured only by steric factors, is formed exclusively in dichloromethane, where the reaction temperature wouldn't allow to surpass the energetic barrier leading to the *cis*-Cl,*cis*-dmsO (a), and is still obtained as major product in ethanol, together with the *cis,cis*-**Ru1a** isomer.

The crystal structure of complexes **Ru1a** and **Ru1b** have been solved by X-ray diffraction analysis. Figure IV.2.1 displays the ORTEP diagram corresponding to their molecular structures whereas selected bond parameters as well as the main crystallographic data can be found in the supporting information (Tables SIV.2.1 and SIV.2.2).

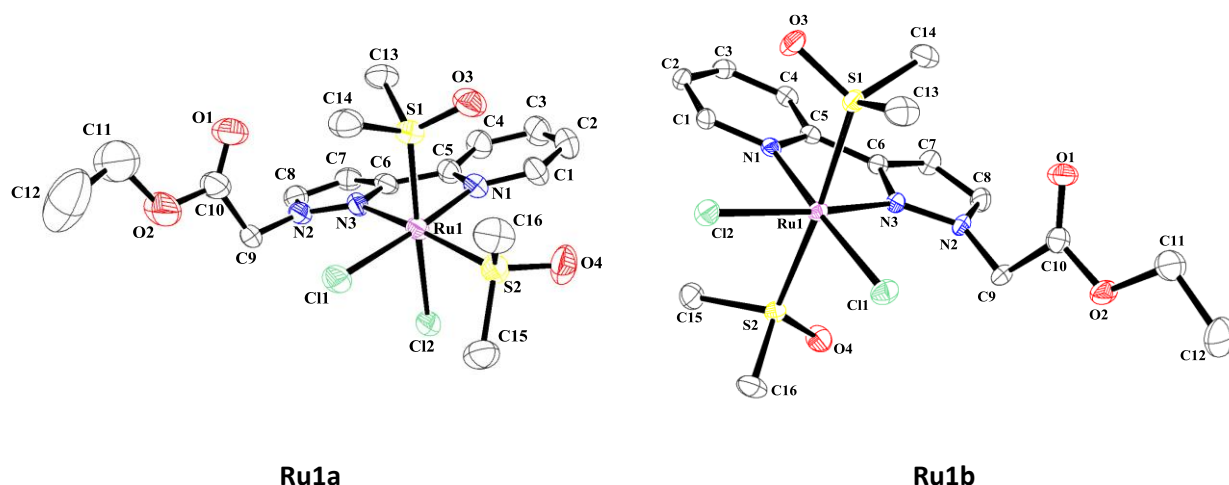
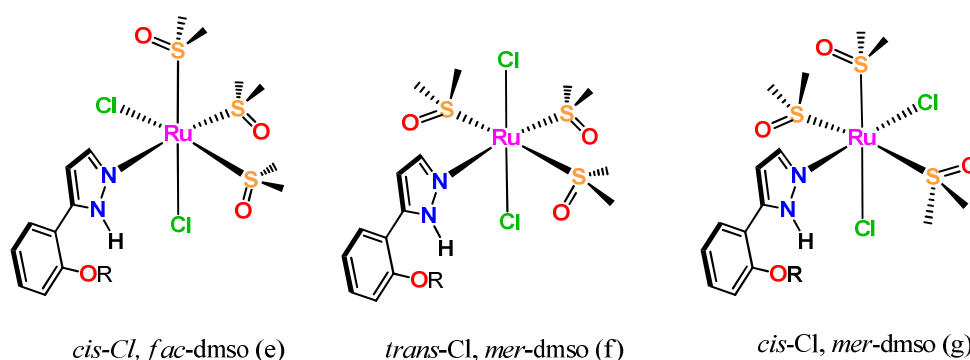


Figure IV.2.1. ORTEP plots and labeling schemes for complex **Ru1a** and **Ru1b**.

The X-ray structure shows that the Ru metal center adopts an octahedral distorted type of coordination in both cases, where the the *pypz* ligand acts in a bidentate fashion and the other coordination sites are occupied by two chlorido ligands in *cis* and two dmsos in *cis* (**Ru1a**) or *trans* (**Ru1b**). All bond distances are within the expected values for this type of complexes.^{107c,108c,112c,184a,327} It is interesting to note that in complex **Ru1a**, where the pyrazolyl ring has a dmsos ligand in *trans* position, the Ru-N_{pz} bond length (2.116 Å) is larger than the analogous distance observed for complex **Ru1b** (2.069 Å), where a Cl ligand is located in *trans*, evidencing the *trans* influence of dmsos respect to the chlorido ligand.

The chelate N(1)-Ru(1)-N(3) angle is 77.4(2)° for **Ru1a** and 78.18(11)° for **Ru1b**, showing the geometrical restrictions imposed by the bidentate *pypz*-CH₂COOEt ligand, which is considered to define the equatorial plane of the structure; as a consequence of this, the rest of the equatorial angles are larger than the 90° expected for an ideal octahedral geometry. In the case of **Ru1a**, the presence of a bulky dmsos ligand in the equatorial plane forces a further enlargement of the N1-Ru-S2 bond angle (99.5°) with regard to the equivalent angle in **Ru1b** (N1-Ru-Cl = 93.8°), which is concomitant to a lower N_{pz}-Ru-Cl angle in **Ru1a** (97.8°, vs. 99.1° in **Ru1b**) and thus provokes an approach of the pendant ethylester arm to the equatorial Cl ligand in *cis* for **Ru1a**. This fact could be the origin of a distinctive behaviour in NMR spectroscopy between the two isomers, as will be discussed later.

For compounds **Ru2** and **Ru3**, containing each of them a monodentate pyrazolate ligand (L4 or L5') together with three dmsos and two Cl ligands, only three different isomers can be obtained, which are displayed in Scheme IV.2.4:



Scheme IV.2.4. Possible stereoisomers for complexes **Ru2** (R= H) and **Ru3** (R= -CH₃).

Among the three potential isomers, the occurrence of only monodentate ligands will probably make steric hindrance a less determining factor in the preference for a specific geometrical isomer. However, from an electronic perspective, the *cis*-Cl,*fac*-dmsos isomer (e) is presumably the most favoured thermodynamically thanks to the occurrence of two Cl-Ru-dmsos *trans* axis

Chapter IV

and, indeed, complexes **Ru2** and **Ru3** are obtained exclusively under this isomeric form, as confirmed by different techniques (see below). An X-ray diffraction structure could be obtained for complex **Ru3**, which is shown in Figure IV.2.2. A packing diagram of the structure, together with selected bond parameters and crystallographic data can be found in the supporting information.

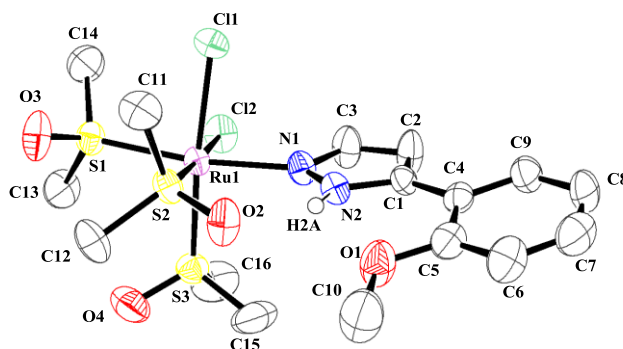
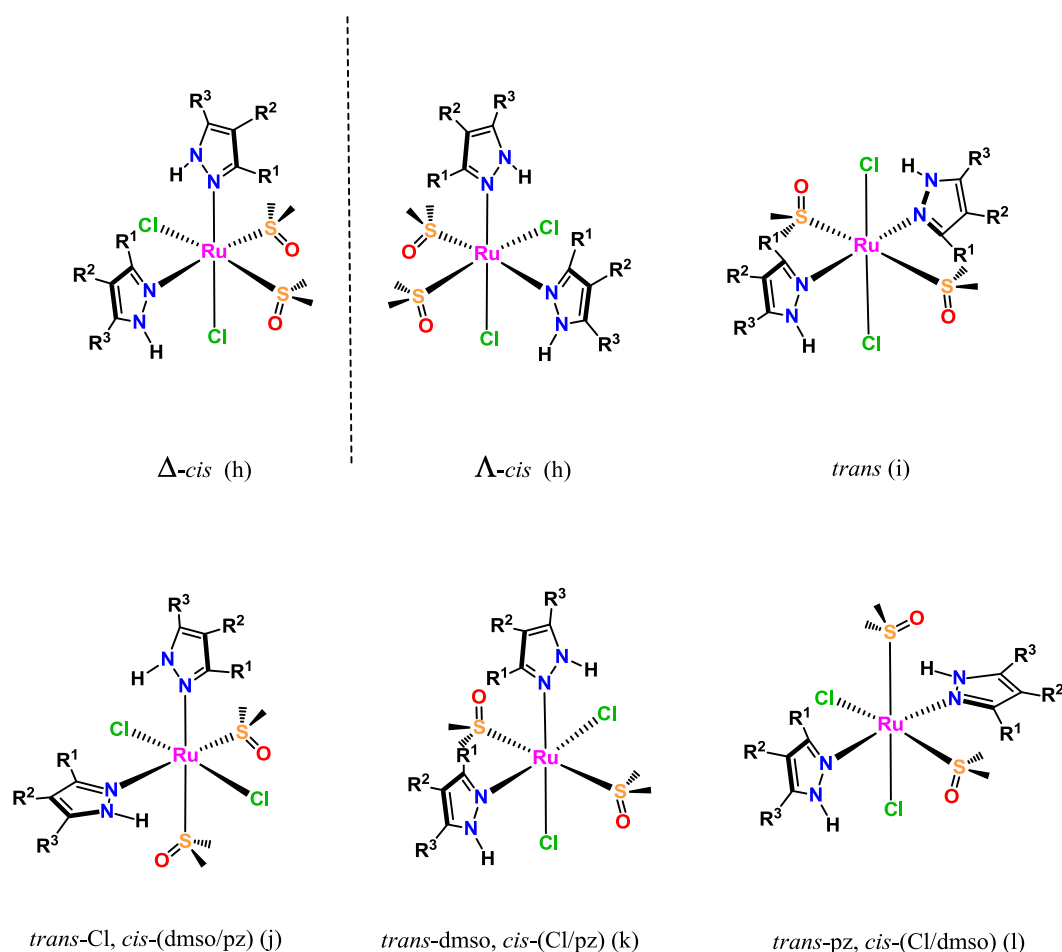


Figure IV.2.2. ORTEP plot and labeling scheme for compound **Ru3**.

Complex **Ru3** also presents a distorted octahedral geometry, with two strong H-bonding interactions that take place between N_{pz} -H(2) (which is now bonded to the inner N_{pz} atom as a consequence of the tautomerization process in $L5'$) and oxygen atoms in the structure: on one hand, the oxygen atom of the dmsoligand in *cis* ($H(2)\cdots O(2) = 1.954 \text{ \AA}$) and on the other hand the methoxy oxygen atom of the ligand $L5'$ itself ($H(2)\cdots O(1) = 2.102 \text{ \AA}$).

Finally, six different isomers (including two pairs of enantiomers, see Scheme IV.2.5) can be formed in the synthesis of compounds **Ru4-6** (and also **Ru2'**, obtained as secondary product in the synthesis of **Ru2** as described above), which bear three pairs of different monodentate ligands.



Scheme IV.2.5. Possible stereoisomers for compounds **Ru2'** ($R^1 = R^2 = \text{H}$; $R^3 = -\text{pH}$), **Ru4** ($R^1 = R^2 = R^3 = \text{H}$), **Ru5** ($R^1 = \text{H}$; $R^2 = R^3 = -\text{CH}_3$) and **Ru6** ($R^1 = -\text{CH}_3$; $R^2 = \text{H}$, $R^3 = -\text{CH}_3$).

In this case, as described above for the geometrical isomers depicted in Scheme IV.2.5), we cannot expect structural factors to address a marked preference for a specific isomer. Nevertheless, electronic factors are neither determinant in this case since different geometrical isomers have been found experimentally. Thus, for complex **Ru6** the main isomer obtained was the most asymmetric enantiomeric pair (h) whereas for **Ru2'**, **Ru4** and **Ru5** the trans-Cl isomer (j) is formed preferentially. It is worth mentioning that the alternative syntheses followed for the preparation of complexes **Ru4** and **Ru6** (with shorter reaction times than the procedures previously reported^{297,298} lead to the same isomer than the formerly obtained in both cases. A crystal structure could be obtained for compound **Ru5** which reveals an octahedral distorted type of coordination. The corresponding ORTEP diagram is shown in Figure IV.2.3.

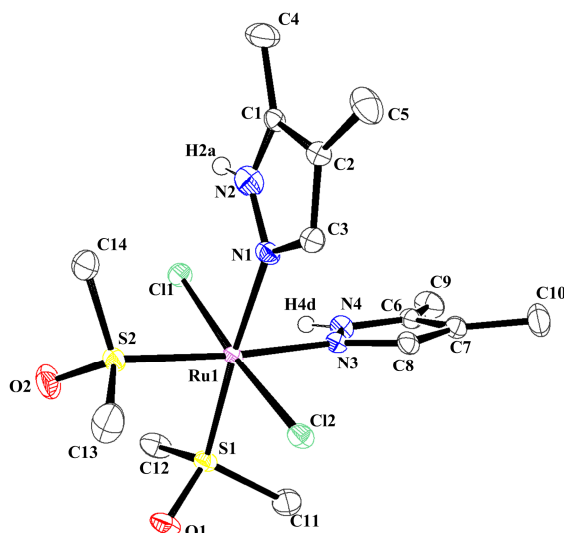


Figure IV.2.3. ORTEP plot and labeling scheme for compound **Ru5**.

Four intramolecular H-bonds are formed between the monodentate Cl ligands and the H_{pz} placed in *cis* ($H(4D)\cdots Cl(1)$, 2.780 Å; $H(2A)\cdots Cl(1)$, 2.552 Å), and between chlorido and the protons in the 5th position of the pyrazolyl ring ($H(3A)\cdots Cl(2)$, 2.812 Å; $H(8A)\cdots Cl(2)$, 2.849 Å) (see Figures SIV.2.10-SIV.2.12).

As a general trend, the Ru metal centers adopt an octahedrally distorted type of coordination with the corresponding pyrazolyl ring of each ligand coordinated in *trans* with respect to a dmsoligand in most cases. The exception is complex **Ru1b**, where steric hindrance seem to be determinant to destabilize the *cis,cis* isomer **Ru1a**.

IV.2.2. Spectroscopic properties

The IR spectra for all complexes (Figures SIV.2.5-SIV.2.9) show bands around 1090-1110 cm^{-1} that can be assigned to the $\nu(S=O)$ stretching, and the absence of any significant vibration in the 930-920 cm^{-1} range indicates a sulfur-bonded dmsoligand complex,^{327a,106c,328} as confirmed by the X-ray structures obtained. The S-coordination increases the S-O bond order and thus the stretching band appears at higher wavenumbers with respect to that shown by free dmsoligand (1050 cm^{-1}).^{106a}

The one-dimensional (1D) and two-dimensional (2D) NMR spectra of complexes **Ru1-Ru6** were registered in CDCl_3 , CD_2Cl_2 or acetone- d_6 and are presented in Figure IV.2.4 and in the Supporting Information (Figures SIV.2.15- SIV.2.21). The resonances found for all complexes are consistent with the structures obtained in the solid state. The complexes exhibit two sets of signals: one in the aromatic region corresponding to the rings of the N-donor ligands and

the N-donor ligands and the other one in the aliphatic region assigned to the methyl groups of the bonded dmsO ligands, to the methylene and ethyl groups of the aliphatic chain of the pyrazole N-substituted in complex **Ru1**, and to the pyrazole methyl groups of complexes **Ru5-6**. In all cases, the resonances of the aromatic region are easily identified through the COSY and NOESY spectra.

Compound **Ru1a** has been obtained together with **Ru1b** and the assignment of the different resonances has been made by comparison with the spectrum of pure **Ru1b** (see Figure IV.2.4). **Ru1a** is an asymmetric molecule and it generates four different methyl resonances for the dmsO ligands (see Figure IV.2.5 for details of some significant regions of the spectrum). The resonances at lower chemical shift (2.49 and 3.19 ppm) display a cross coupling in the COSY spectrum and are assigned to the spatially close C14 and C16 methyl groups (see Figure IV.2. for the numbering scheme used). On the other hand, the resonances of C13 and C15 methyl groups (found respectively at 3.51 and 3.61 ppm) are influenced by the deshielding effect of the close N-pyrazole and chlorido ligands. In the aromatic region, the H(1)_{py} is easily identified at 9.88 ppm due to the deshielding effect exerted by the oxygen atom of the equatorial dmsO ligand. In contrast, in complex **Ru1b** a symmetry plane makes the two dmsO ligands magnetically equivalent and thus only two signals at 3.01 and 3.16 ppm are observed, that are assigned respectively to C14+C15 and C13+C16 methyl groups again on the basis of the deshielding effect exerted by the two close chlorido ligands over the latter.

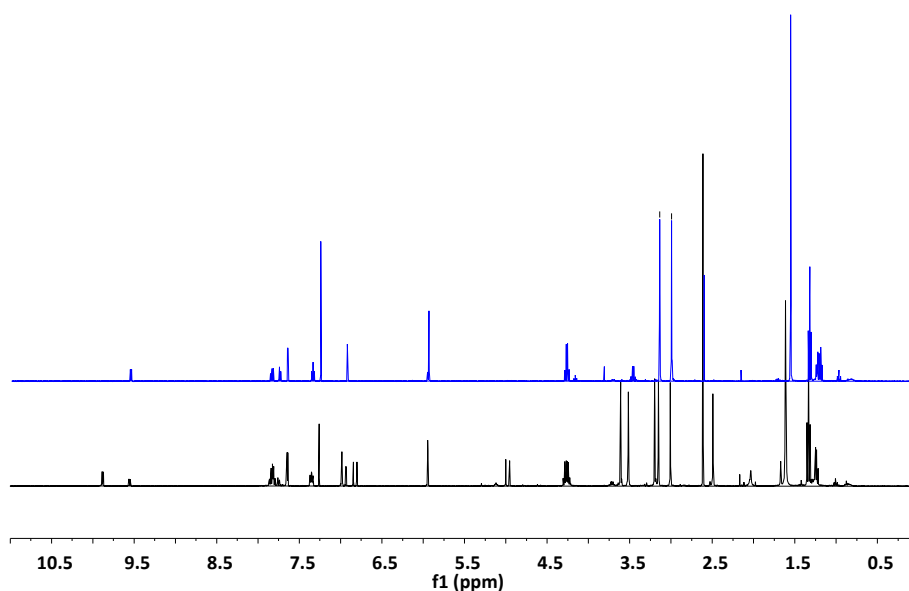


Figure IV.2.4. Black, $^1\text{H-NMR}$ spectrum (400 MHz, CDCl_3) of an isomeric mixture of **Ru1a** and **Ru1b** in a 1:0.5 ratio. Blue, $^1\text{H-NMR}$ spectrum of the pure complex **Ru1b** at the same scale to facilitate the identification of the **Ru1a** signals.

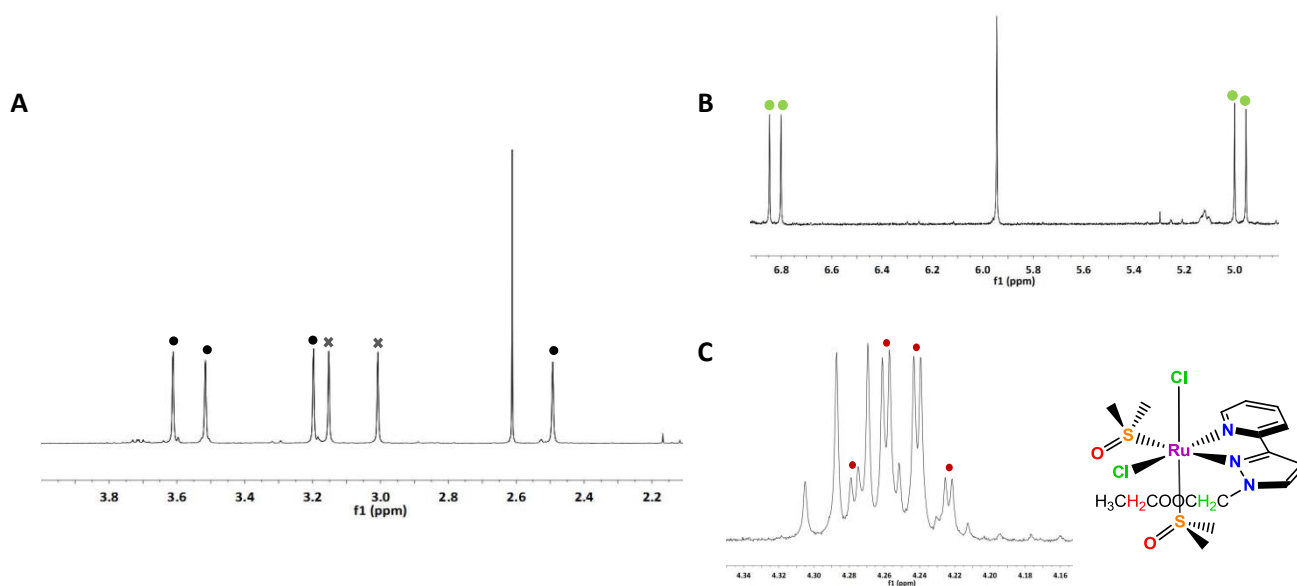


Figure IV.2.5. Different regions of the ^1H -NMR spectrum of an isomeric mixture of **Ru1a** and **Ru1b** in a 1:0.5 ratio, 400 MHz, CDCl_3 . The figure shows some examples of the high asymmetry of the **Ru1a** molecule: A) four methyl dmsol signals (black dots), whereas only two dmsol signals for **Ru1b** isomer (grey crosses); B) signals of the methylene protons (green dots), and C) signals which correspond to the aliphatic chain of the terminal ester group (red dots).

The resonances of the pendant ethylester arm also show significant differences between the two complexes. In the symmetric **Ru1b** the ethyl group displays a typical triplet+quadruplet set of signals and a singlet is observed at 5.95 ppm for the two protons of the methylene C9 group. However, in **Ru1a** two close quadruplet signals are observed for the H11 ethyl protons and the two methylene H9 and H9' protons appear as doublets at significantly different chemical shift (see Figure IV.2.5 B and C). This behaviour manifests a distinct magnetic environment of the two H atoms bonded to a specific carbon atom, and the occurrence of this phenomenon only in **Ru1a** could be related to the smaller bond angle between the pyrazolyl ring and the Cl1 ligand in *cis* due to the steric hindrance exerted by the equatorial dmsol ligand, as described previously in the structural description. This would allow stronger H-bonding interactions involving the pendant ethylester arm and the chlorido ligand, consequently restricting its free rotation and providing such different magnetic environments for two H atoms located at the same C atom.

Compounds **Ru2** and **Ru3** present simpler spectra due to the occurrence of only one N-donor ligand. Their ^1H -NMR spectra show three resonances corresponding to three pairs of magnetically equivalent dmsol methyl groups (Figures SIV.2.7 and SIV.2.8).

Compounds **Ru4-6**, which contain two dmsol, two monodentate Cl ligands and two pyrazolyl derivatives, show different behaviours in ^1H -NMR arising from the distinct geometrical isomers

found. Complexes **Ru4** and **Ru5** are symmetrical and display a singlet corresponding to the four dmsO methyl groups at 3.14 and 3.19 ppm respectively, and **Ru5** also displays two additional singlets at 1.95 and 2.22 ppm corresponding respectively to the methyl groups at positions 4 and 3 of the pyrazole ligand. Finally, complex **Ru6** is the most asymmetric molecule and consequently it displays eight different resonances, four corresponding to the methyl dmsO signals and the other four assigned to the pyrazole methyl groups at positions 3 and 5.

The UV-Vis spectra of complexes **Ru1-Ru6** have been registered in dichloromethane, water or methanol and are displayed in the Supporting Information (Figure SIV.2.13). The spectral features of complexes are presented in the experimental section and in Table IV.2.1. The complexes exhibit very intense ligand based π - π^* bands below 300 nm and relatively intense bands above 300 nm mainly due to $d\pi$ - π^* MLCT transitions.³²⁹

Table IV.2.1. UV-Vis spectroscopic features in CH₂Cl₂ (**Ru1**, as a mixture of isomers **Ru1a** and **Ru1b**), MeOH (**Ru2**, **Ru3** and **Ru6**) and in H₂O (**Ru4-5**).

| Compound | λ_{max} , nm (ϵ , M ⁻¹ ·cm ⁻¹) |
|---|--|
| [RuCl ₂ (pypzCH ₂ COOEt)(dmsO) ₂], Ru1 | 278 (579), 376 (152) |
| [RuCl ₂ (HOphpz-H)(dmsO) ₃], Ru2 | 302 (17593), 358 (1731) |
| [RuCl ₂ (MeOphpz-H)(dmsO) ₃], Ru3 | 358 (725) |
| [RuCl ₂ (pz-H) ₂ (dmsO) ₂], Ru4 | 228 (1033), 300 (46) |
| [RuCl ₂ (3,4-dmpz-H) ₂ (dmsO) ₂], Ru5 | 238 (1476), 302 (102) |
| [RuCl ₂ (3,5-dmpz-H) ₂ (dmsO) ₂], Ru6 | 364 (1472) |

In general, the lower aromatic character of the monodentate R₂-pz-H ligands (where R= H or CH₃, ligands *L6-L8* in Scheme IV.2.1) when compared to bidentate *pypz-R*₁ (R= CH₂COOEt), *L3*, involves ligand orbitals of higher energy for the former and, consequently, provokes a blue-shift of the $d\pi$ - π^* bands for complexes **Ru4-6** when compared to **Ru1**. The intraligand π - π^* bands are also affected in a similar manner and, for complex **Ru6**, these bands are sufficiently blue-shifted as to be out of the solvent range. It is striking to see that complex **Ru3**, which contains an ether O-CH₃ substituent in the aromatic ring, displays $d\pi$ - π^* absorptions above 300 nm whereas the analogous complex **Ru2**, which contains a phenol ring, shows only bands below the 300 nm corresponding to π - π^* absorptions that display high molar extinction coefficients.

IV.2.3. Electrochemical properties and linkage isomerization

The redox properties of complexes **Ru1-5** have been determined by CV experiments and the corresponding voltammograms are displayed in the Supporting Information (Figure SIV.2.14). Table IV.2.2 contains the electrochemical data of all complexes. In the case of complex **Ru1a**, a dmsO linkage isomerization process takes place upon Ru(II)→Ru(III) oxidation, due to the increased hard Lewis acid character of the oxidized Ru(III) ion, that displays more affinity for the O-bonded dmsO acting as a harder Lewis base (see below). The anodic and cathodic peak potential values corresponding respectively to the Ru-S and Ru-O forms are also given in Table IV.2.2.

Table IV.2.2. Electrochemical data (CH₂Cl₂ + 0.1M TBAH vs. SCE) for complexes **Ru1-Ru6**.

| Compound | $E_{1/2}$ (III/II) (V) | E_{pa} (V) | | E_{pc} (V) | |
|--|------------------------|--|--|--|--|
| | | [Ru ^{II} -S → Ru ^{III} -S] | [Ru ^{III} -O → Ru ^{II} -O] | [Ru ^{III} -O → Ru ^{II} -O] | [Ru ^{II} -S → Ru ^{III} -S] |
| [RuCl ₂ (pypzCH ₂ COOEt)(dmsO) ₂], Ru1a | 1.14 | 1.18 | | 0.38 | |
| [RuCl ₂ (pypzCH ₂ COOEt)(dmsO) ₂], Ru1b | 0.96 | | | | |
| [RuCl ₂ (HOphpz-H)(dmsO) ₃], Ru2 | | 1.60 | | | |
| [RuCl ₂ (MeOphpz-H)(dmsO) ₃], Ru3 | | 1.65 | | 0.7 | |
| [RuCl ₂ (pz-H) ₂ (dmsO) ₂], Ru4 | 1.08 | | | | |
| [RuCl ₂ (3,4-dmpz-H) ₂ (dmsO) ₂], Ru5 | 1.02 | | | | |
| [RuCl ₂ (3,5-dmpz-H) ₂ (dmsO) ₂], Ru6 | 1.15 | | | | |

Complexes **Ru1a** and **Ru1b**, containing the bidentate *pypz-CH₂COOEt* ligand, exhibit two different behaviours. The latter shows a reversible monoelectronic Ru(III/II) redox wave at $E_{1/2}$ values of 0.96 V vs. SCE, whereas the former shows an electrochemically irreversible process at $E_{pa} = 1.18$ V with a cathodic peak at $E_{pc} = 0.38$ V, suggesting the occurrence of a quasi-quantitative dmsO ligand linkage isomerization process. Consequently, a comparison between the two compounds can be done only on the basis of the anodic E_{pa} values, which are 1.18 and 1.00 V for compounds **Ru1a** and **Ru1b** respectively. The slight increase in the [Ru^{II}-S → Ru^{III}-S] oxidation potential value for complex **Ru1a** in comparison to **Ru1b** could be related to the non-favorable *trans* disposition of the dmsO ligands in **Ru1b**, that could lower their π-acceptor ability thus making the complex slightly easier to be oxidized. On the other hand, the dmsO linkage isomerization that takes place for **Ru1a** could be favoured by the steric encumbrance

exerted by the equatorial dmso ligand that, upon Ru-S→Ru-O isomerization, would place its methyl dmso groups in a less hindered position, further away from the metal center.

As mentioned above, the **Ru1a** complex undergoes a dmso linkage isomerization process. This can be illustrated by the cyclic voltammogram of a **Ru1** isomeric mixture in CH₃CN at a scan rate of 0.1 V and starting the potential scanning at $E_{init}=0$ V (see Figure IV.2.6). The CV shows an anodic peak at $E_{pa}=1.2$ V vs. SCE which corresponds to the oxidation of Ru^{II}(dmso-S) species to Ru^{III}(dmso-S) (the notation dmso-S indicates that the dimethylsulfoxide ligand is coordinated to ruthenium via the sulfur atom). This species undergoes a fast linkage isomerism forming Ru^{III}(dmso-O) (see Scheme IV.2.6). Upon back-scanning to low potential, the isomerized species undergoes reduction at $E_{pc}=0.38$ V to form Ru^{II}(dmso-O) and then rearranges restoring the initial complex. This shift to lower potential values (0.38 vs. 1.1 V) for the O-coordinated dmso complex is due to the lower electron-withdrawing ability of the O-coordinated dmso, then making the upper oxidation states of Ru more accessible.

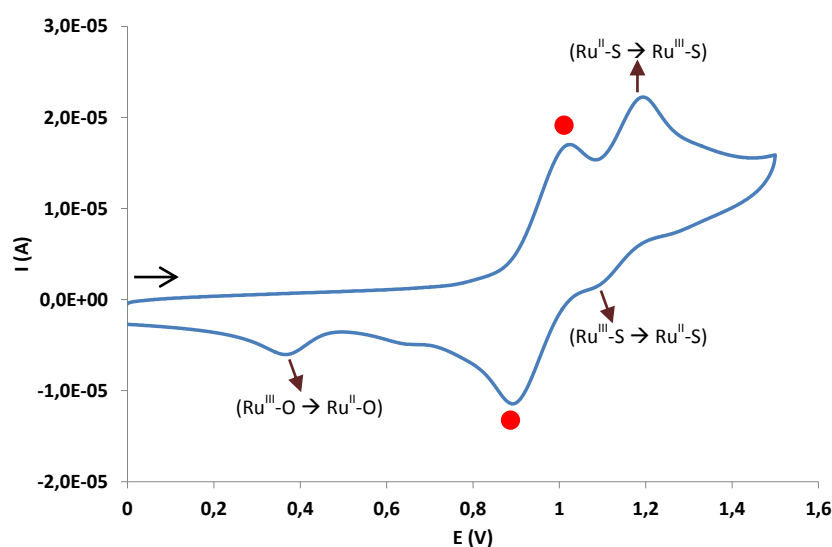
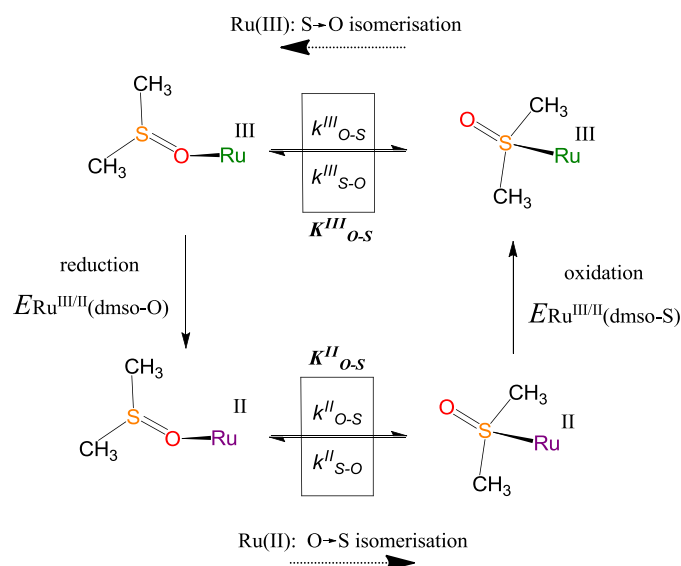


Figure IV.2.6. CV of complex **Ru1** (as a mixture of isomers **Ru1a** and **Ru1b**) performed in CH₃CN (TBAH 0.1 M) vs. SCE starting the scanning potential at $E_{init}=0$ V. Red dots indicate the anodic and cathodic peaks of isomer **Ru1b** which does not present dmso linkage isomerization process.



Scheme IV.2.6. Electron transfer and linkage isomerization processes observed for Ru-dmsO complexes.

The isomerization process becomes more evident by starting the potential scanning at $E_{init} = 1.6$ V and applying an equilibration time of 1 minute prior the cathodic scan (see Figure IV.2.7).

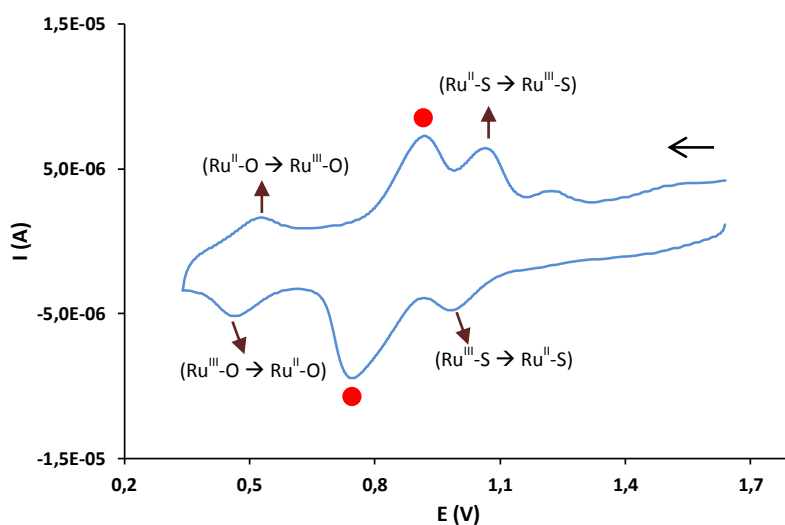


Figure IV.2.7. CV of complex **Ru1** (as a mixture of isomers **Ru1a** and **Ru1b**) performed in CH_3CN (TBAH 0.1 M) vs. SCE starting the scanning potential at $E_{init} = 1.6$ V. Red dots indicate the anodic and cathodic peaks of isomer **Ru1b** which does not present dmsO linkage isomerization process.

A thorough kinetic study has been carried out on the linkage isomerization using an isomeric mixture of complexes **Ru1a** and **Ru1b**, following the method described in the literature^{327b,330} that is detailed below.

The scan rates directly influence the intensity of waves of the cyclic voltammograms and this dependence provides information about the participation of chemical reactions coupled to electrochemical processes (as is the example of dmsO linkage isomerization shown in Scheme

IV.2.6), allowing the determination of the corresponding rates and equilibrium constants. To do so, cyclic voltammograms at different scan rates, starting the potential scanning from the lower and upper points of the CV range, has been performed for complex **Ru1** in CH₃CN. The set of formulas used are gathered in Table SIV.2.3.

The equilibrium constant for the Ru^{III}-O \rightleftharpoons Ru^{III}-S reaction (K^{III}_{O-S}) can be obtained from cyclic voltammograms recorded through starting the potential scanning from the upper E_{init} values (1.6 V with 1 minute of equilibration time at the initial potential, see Figure IV.2.8) and applying eq. 1 (Table SIV.2.3). Plotting the ratio i_{c1}/i_{c2} vs. v^{-1} and extrapolating v to infinity in order to obtain the intercept values (Figure SIV.2.23) results in $K^{III}_{O-S} = 0.14$ (see Table IV.2.3).

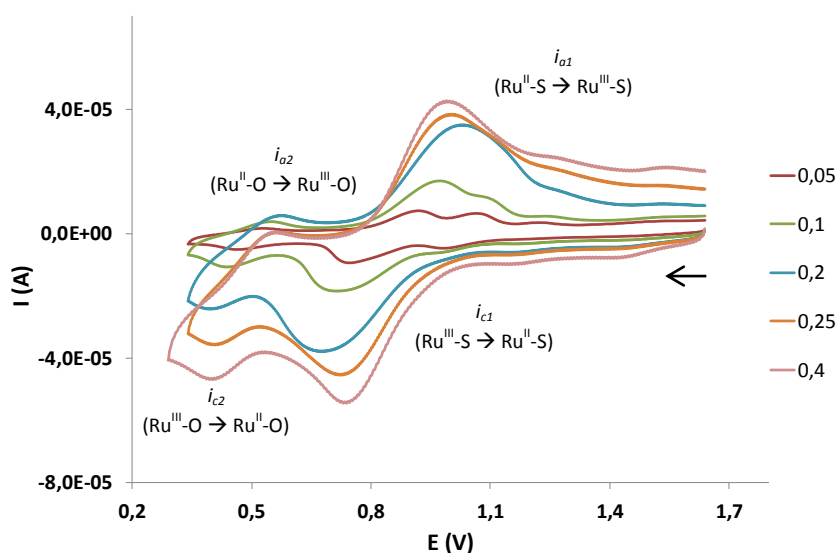


Figure IV.2.8. CV of complex **Ru1** (as a mixture of isomers **Ru1a** and **Ru1b**) performed in CH₃CN (TBAH 0.1 M) vs. SCE starting the scanning potential at $E_{init} = 1.2$ V, at scan rates between 0.05 and 0.4 V·s⁻¹, applying an equilibration time of 1 min.

The kinetic isomerization constants (k^{III}_{O-S} and k^{III}_{S-O}) are calculated by plotting $v^{1/2}$ vs. the i_d/i_k ratio (eq. 2, Table SIV.2.3), where i_k represents the measured peak current (i_{c1}) and i_d the corresponding diffusional current in the absence of a chemical reaction (i_{o1}). The i_k and i_d values were obtained respectively from the cyclic voltammograms performed through reverse (Figure IV.2.8) and direct (Figure SIV.2.22) scan potentials. From the value of the slope obtained (Figure SIV.2.24), and considering that $K^{III}_{O-S} = k^{III}_{O-S}/k^{III}_{S-O}$, the following kinetic constants can be calculated: $k^{III}_{O-S} = 5.41 \times 10^{-2} \text{ s}^{-1}$ and $k^{III}_{S-O} = 3.8 \times 10^{-1} \text{ s}^{-1}$.

With the equilibrium constant K^{III}_{O-S} and assuming that $E^\circ = E_{1/2}$ or E_{pa} for each linkage isomer, eq. 3 (Table SIV.2.3) can be used to calculate the equilibrium constant for the Ru^{II}-O \rightleftharpoons Ru^{II}-S

Chapter IV

process in the Ru(II) oxidation state, k''_{O-S} , resulting in $K''_{O-S} = 7.75 \times 10^6$. Finally, the kinetic isomerization constants in the Ru(II) oxidation state can be calculated from eq. 4 in Table SIV.2.3 and the linear fit of the corresponding plots (Figure SIV.2.25) yield $k''_{O-S} = 6.0 \times 10^{-3} \text{ s}^{-1}$ and $k''_{S-O} = 7.7 \times 10^{-9} \text{ s}^{-1}$.

Table IV.2.3. Thermodynamic and kinetic parameters for the linkage isomerization in complex **Ru1a**, together with related Ru-dmso complexes.^a

| Entry | Compound | K'''_{O-S} | k'''_{O-S} (s^{-1}) | k'''_{S-O} (s^{-1}) | K''_{O-S} | k''_{O-S} (s^{-1}) | k''_{S-O} (s^{-1}) |
|-------|---|--------------|-------------------------------------|-------------------------------------|----------------------|------------------------------------|------------------------------------|
| 1 | <i>cis,cis</i> -[RuCl ₂ (pypz-CH ₂ COOEt)(dmso) ₂], Ru1a | 0.14 | $5.41 \cdot 10^{-2}$ | $3.8 \cdot 10^{-1}$ | $7.75 \cdot 10^6$ | $6.0 \cdot 10^{-3}$ | $7.7 \cdot 10^{-9}$ |
| 2 | <i>cis,cis</i> -[RuCl ₂ (pypz-H)(dmso-S) ₂] (ref 327b) | 1.39 | $1.76 \cdot 10^{-1}$ | $1.26 \cdot 10^{-1}$ | $1.34 \cdot 10^{12}$ | $1.1 \cdot 10^{-1}$ | $8.2 \cdot 10^{-14}$ |
| 3 | <i>cis,cis</i> -[RuCl ₂ (H3p)(dmso-S) ₂] (ref 112c) | 1.7 | $2.8 \cdot 10^{-1}$ | $1.7 \cdot 10^{-1}$ | $5.2 \cdot 10^{11}$ | $4.9 \cdot 10^{-1}$ | $9.3 \cdot 10^{-14}$ |
| 4 | <i>trans,cis</i> -[RuCl ₂ (H3p)(dmso-S) ₂] (ref 112c) | 0.27 | $5.7 \cdot 10^{-2}$ | $2.2 \cdot 10^{-1}$ | $5.3 \cdot 10^8$ | $8.7 \cdot 10^{-2}$ | $1.6 \cdot 10^{-10}$ |
| 5 | <i>trans,cis</i> -[RuCl ₂ (bpp)(dmso-S) ₂] ⁻ (ref 107c) | 0.26 | $1.7 \cdot 10^{-2}$ | $6.5 \cdot 10^{-2}$ | $6.5 \cdot 10^9$ | $1.3 \cdot 10^{-1}$ | $2.1 \cdot 10^{-11}$ |
| 6 | <i>out</i> -[Ru(L ²)(trpy)(dmso-S)] ⁺ (ref 331) | 0.13 | $7.7 \cdot 10^{-2}$ | $6.0 \cdot 10^{-1}$ | $5.5 \cdot 10^8$ | $2.5 \cdot 10^{-1}$ | $4.6 \cdot 10^{-10}$ |
| 7 | <i>cis, fac</i> -[RuCl ₂ (CH ₃ -pz-H)(dmso-S) ₃] (ref 327b) | 0.036 | $1.9 \cdot 10^{-2}$ | $5.3 \cdot 10^{-1}$ | $1.53 \cdot 10^{12}$ | $7.2 \cdot 10^{-2}$ | $4.7 \cdot 10^{-14}$ |

^aH3p is 5-phenyl-3-(2-pyridyl)-1H-pyrazole, L² is 5-phenyl-3-(pyridin-2-yl)pyrazolate and bpp is 3,5-(2-pyridyl)pyrazolate.^{327b}

As can be observed in Table IV.2.3, the values of K''_{O-S} obtained for all complexes are very high indicating that, in Ru(II) redox state, the dmso ligand displays a high preference to be bound to the metal through the S atom. However, the value displayed by complex **Ru1a** is markedly lower to that shown by the related complex in entry 2, for which the bidentate ligand is pypz-H, with no pendant ethylester arm. This indicates that the thermodynamic stability of **Ru1a** is lower, in accordance with that stated above in the description of the synthetic procedure, where the *trans*-dmso isomer **Ru1b** is the major product obtained either in EtOH or dichloromethane as solvent. The steric encumbrance exerted by the *pypz-CH₂COOEt* ligand makes complex **Ru1a** the least stable of the whole series gathered in Table IV.2.3, even below the complexes in entries 4 and 5, which display a *trans*-Cl layout.

In the Ru(III) state, the K'''_{O-S} values evidence that, for complex **Ru1a**, the Ru-O bound form is dominant in sharp contrast with the structurally related *cis,cis* complexes in entries 2 and 3, thus evidencing a relatively low thermodynamic stability also for the oxidized form of the complex, as could be expected from the smaller radius of the Ru(III) ion that enhances the overall steric hindrance around the metal center. This is in accordance with the CVs registered

for the complex, where the cathodic peak corresponding to the $\text{Ru}^{\text{III}}\text{-S} \rightarrow \text{Ru}^{\text{II}}\text{-S}$ reduction process is only hardly observed.

Regarding the kinetic constants, **Ru1a** presents a higher $\text{Ru-S} \rightarrow \text{Ru-O}$ isomerization rate than that displayed by most of the complexes in Table IV.2.3, even in the Ru(II) oxidation state. A major number of π -acceptor ligands is a factor that seems to favour the $\text{Ru-S} \rightarrow \text{Ru-O}$ isomerization after generation of the Ru(III) species^{327b} but, in the case of **Ru1a**, the number of pyridyl or dmsoligands coordinated to the metal is the same as for complexes in entries 2-5. The electron-withdrawing character of the ethylester substituent at the pyrazolyl ring could play a role similar to that of π -acceptor ligands. However, steric influence, which would prevent the ligands to approach the Ru metal center upon oxidation and thus would lower the amount of electron density given to the metal, can also be considered.

On the other hand, complexes **Ru2** and **Ru3**, which contain three dmsoligands, two monodentate Cl and one monodentate phenol-pyrazole based ligand, exhibit electrochemically irreversible Ru(III)/Ru(II) redox processes at E_{pa} value of 1.60 V and 1.65 V respectively. In the case of **Ru2**, the irreversible nature of the wave probably indicates that the complex is degraded after oxidation. In contrast, **Ru3** exhibits a cathodic peak at $E_{pc} = 0.7$ V which indicates that a dmsolinkage isomerization process is taking place after Ru(II) to Ru(III) oxidation. Such linkage isomerization process has been evidenced by performing cyclic voltammograms at different scan rates. A detail of the cathodic peaks observed in the CV obtained at four different scan rates are shown in Figure IV.2.9:

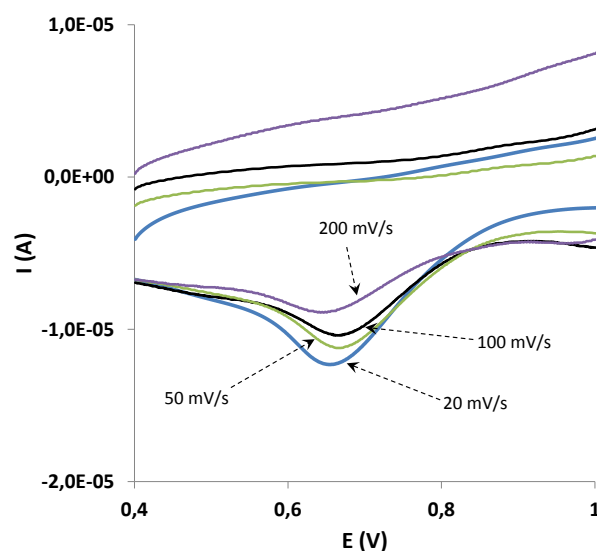


Figure IV.2.9. Intensity of the cathodic $\text{Ru}^{\text{III}}\text{-O} \rightarrow \text{Ru}^{\text{II}}\text{-O}$ peak at different scan rates.

Chapter IV

As can be observed in Figure IV.2.9, lower scan rates lead to an increased cathodic intensity of the peak, which is consistent with the isomerized Ru(III)-O being formed in higher amount throughout the cathodic scan timescale.

Pyrazole-based complexes **Ru4-6** show chemically and electrochemically reversible Ru(III/II) redox processes with similar $E_{1/2}$ values (1.08, 1.02 and 1.15 V respectively). It is interesting to note that among complexes **Ru5** and **Ru6**, which contain dimethyl-substituted pyrazole rings, compound **Ru5** shows a lower potential value. This fact could be explained in terms of geometrical stability. Both complexes are different isomers and **Ru5** contains the two strong σ -donor Cl ligands in an unfavorable *trans* disposition. This geometry probably diminishes the overall electron density given to the metal and thus could stabilize better a higher oxidation state of ruthenium (Ru(II) \rightarrow Ru(III)), decreasing the oxidation potential values. In **Ru6**, the structure is energetically stable thanks to the synergistic π -donor and π -acceptor effects of *trans* Cl and dmsol ligands, and also to the relative *trans* disposition of pyrazolyl rings and dmsol.

IV.2.4. Catalytic hydration of nitriles

We have checked all complexes in the catalytic hydration process of different nitriles under neutral conditions using water as solvent. The catalytic conditions were initially optimised testing the isomeric mixture of complex **Ru1** at different catalyst:substrate ratios and at different temperatures, using benzonitrile as substrate, as shown in Table IV.2.4. As could be expected, better conversion values were obtained in a 5:100 cat:substrate ratio at 100 °C, and these were the conditions chosen for the rest of the catalytic tests.

Table IV.2.4. Optimization of the catalytic hydration conditions for complex **Ru1** using benzonitrile as substrate.

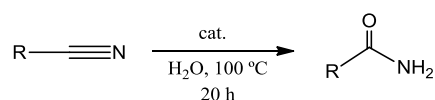
| Entry | t (h) | T (°C) | cat: subs (ratio) | conv. (%) |
|-------|-------|--------|-------------------|-----------|
| 1 | 20 | 80 | 1:100 | 38 |
| 2 | 20 | 80 | 5:100 | 71 |
| 3 | 20 | 100 | 1:100 | 46 |
| 4 | 20 | 100 | 5:100 | 88 |

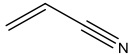
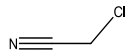
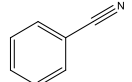
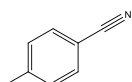
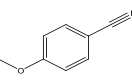
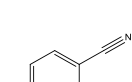
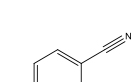
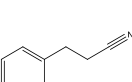
To evaluate the overall catalytic performance, the remaining substrate has been quantified through GC chromatography with biphenyl as the internal standard, and the hydrolysis products have been analyzed by NMR spectroscopy and compared to pure samples of the corresponding amide and acid derivatives. Conversion and selectivity values for *cis*, *cis*- and *cis*,

trans-[RuCl₂(pypz-CH₂COOEt)(dmsO)₂] as a mixture of isomers, **Ru1**, [RuCl₂(HOphpz-H)(dmsO)₃], **Ru2**, [RuCl₂(MeOphpz-H)(dmsO)₃], **Ru3**, [RuCl₂(pz-H)₂(dmsO)₂], **Ru4**, [RuCl₂(3,4-dmpzH)₂(dmsO)₂], **Ru5**, and [RuCl₂(3,5-dmpzH)₂(dmsO)₂], **Ru6**, are summarized in Table IV.1.2, together with the conditions used in the catalysis.

Firstly, blank experiments (without catalyst) were carried out by keeping the substrates in water at 100 °C for 20 h. In all cases, the nitrile was quantitatively recovered except for the aliphatic substrate chloroacetonitrile, where a conversion around 45 % was achieved. However, no traces of the amide product were found after the blank test.

Table IV.2.5. Catalytic hydration of nitriles to amides in water mediated by compounds **Ru1-6**.^a Conversion (conv.) and selectivity (sel.) values are given in %.



| Entry | Complex Substrate | Ru1 | | Ru2 | | Ru3 | | Ru4 | | Ru5 | | Ru6 | |
|-------|---|-------|-------------------|-------|------|-------|------|-------|------|-------|------|-------|------|
| | | conv. | sel. ^b | conv. | sel. | conv. | sel. | conv. | sel. | conv. | sel. | conv. | sel. |
| 1 |  | 55 | 23 | 56 | ~3 | 70 | 71 | 70 | 84 | 68 | 69 | 86 | 80 |
| 2 |  | 60 | 80 | 71 | >99 | 82 | >99 | 83 | >99 | 86 | >99 | 86 | 80 |
| 3 |  | 88 | 88 | 99 | 80 | 98 | 68 | >99 | 90 | >99 | 90 | >99 | >99 |
| 4 |  | 14 | 67 | 98 | 63 | 29 | 39 | 54 | 50 | 84 | 61 | 97 | 57 |
| 5 |  | 33 | 68 | 62 | 77 | 33 | 29 | 54 | 48 | 21 | 8 | 66 | 13 |
| 6 |  | 34 | >99 | 97 | 56 | 68 | 62 | >99 | 76 | >99 | 83 | >99 | 70 |
| 7 |  | 17 | 16 | 57 | >99 | 26 | 98 | 40 | 66 | 67 | 76 | 54 | 79 |
| 8 |  | 6 | - | 60 | - | 36 | - | 42 | - | 47 | - | 62 | - |

^a**Conditions:** Reactions performed at 100 °C in H₂O and in a [Substrate]:[Ru] ratio= 100:5 (see experimental section for details). Time: 20 h reaction. ^bSelectivity for the amide (sel.) = (amide yield/substrate conversion) x 100, determined by ¹H-NMR analysis of the reaction mixture.

Chapter IV

As we can observe in Table IV.2.5 all complexes were found to be active towards nitrile hydration, with low-moderate to high conversion values. Among all the substrates tested, aromatic substrates (entries 3-7) show in general better activities and this is in accordance with the general mechanism currently accepted in the metal-mediated hydration of nitriles, which begins with a substitution process at the catalyst where a ligand is replaced by the corresponding nitrile in the metal coordination environment and a subsequent nucleophilic attack of water (or hydroxo anions) on the nitrile carbon atom takes place (see introduction, section I.3.3.3).^{184a} Then, the electronic properties of the substrates influence the extent of the hydration reactions and consequently the more activated nitriles, bearing electron-withdrawing substituents, are expected to show the best results. However, some differences can be observed within the bench of aromatic substrates: benzonitrile (entry 3) displays the best results whereas p-benzonitrile and 4-methoxybenzonitrile (entries 4 and 5) are in general less active, probably due to the presence of an electron-donating group at the ring. On the other hand, halide substituted benzonitriles (entries 6 and 7) are also expected to display good performances thanks to the electron-withdrawing character of the halide substituents (inductive effect). However, for p-chlorobenzonitrile (entry 7) the performance is clearly lowered for all catalysts, indicating that a deactivating effect, probably caused by the resonance delocalization of the Cl lone pairs throughout the aromatic system, is taking place (the same resonance effect is expected to be much less significant for the smaller fluoride substituent and, indeed, the results obtained for p-fluorobenzonitrile are comparable to that displayed by benzonitrile except for catalysts **Ru1** and **Ru3**, for which structural factors at the catalysts might play a role, as will be discussed later).

Regarding the aliphatic substrates (entries 1, 2 and 8 in Table IV.2.5), the most activated 2-chloroacetonitrile (entry 2) displays the best conversion and selectivity values, followed by acrylonitrile (entry 1) and finally 3-phenylpropanenitrile (entry 8). For 2-chloroacetonitrile, a considerable degree of substrate conversion was also obtained in blank experiments though in this latest case the amide product was not obtained. In the catalytic tests performed with **Ru1-6** the interaction of a given catalyst with 2-chloroacetonitrile must present faster kinetics as high selectivities for the amide product are shown in all cases. Note the activating effect that Cl substituents have on this aliphatic substrate, in contrast with the above-described p-chlorobenzonitrile.

The hydration of acrylonitrile (entry 1) is particularly interesting for the industrial applications of the acrylamide product. The best results are obtained with this substrate for catalysts **Ru3-**

Ru6, with conversion and selectivity values above ~70%. In the case of **Ru1**, high acid product amounts (above 75 %) have been detected.

On the other hand, the electronic characteristics of the ligands in the catalyst influence the ability of the metal to activate the nitrile substrate: a high electron-withdrawing character of the ligands will drive the metal to a stronger activation of the coordinated nitrile substrate, making it more susceptible to a water (or hydroxo) nucleophilic attack. This would be in accordance with complexes **Ru2-3**, which contain three highly π -acceptor dmsO ligands, displaying better conversions than the rest of catalysts tested, which contain only two coordinated dmsO (this has been evidenced in the activity shown by analogous complexes previously described, which contain bidentate and monodentate pyrazolyl ligands).^{184a} However, whereas catalyst **Ru2** is among the most active complexes of Table IV.2.5 (together with complexes **Ru4-6**), **Ru3** displays lower activity, particularly for the substrates of entries 4-8. This could be explained in terms of structural restrictions arising from the methylated *MeOphpz-H* ligand in **Ru3**, that would hinder the approach of the bulkier substrates of entries 4-8. This steric effect would still have some influence (though in a much lesser extent) in catalyst **Ru2** since it displays overall performance comparable or even slightly worse to that of complexes **Ru4-Ru6**, and this cannot be explained only by electronic arguments as the latter compounds contain only two π -acceptor dmsO ligands.

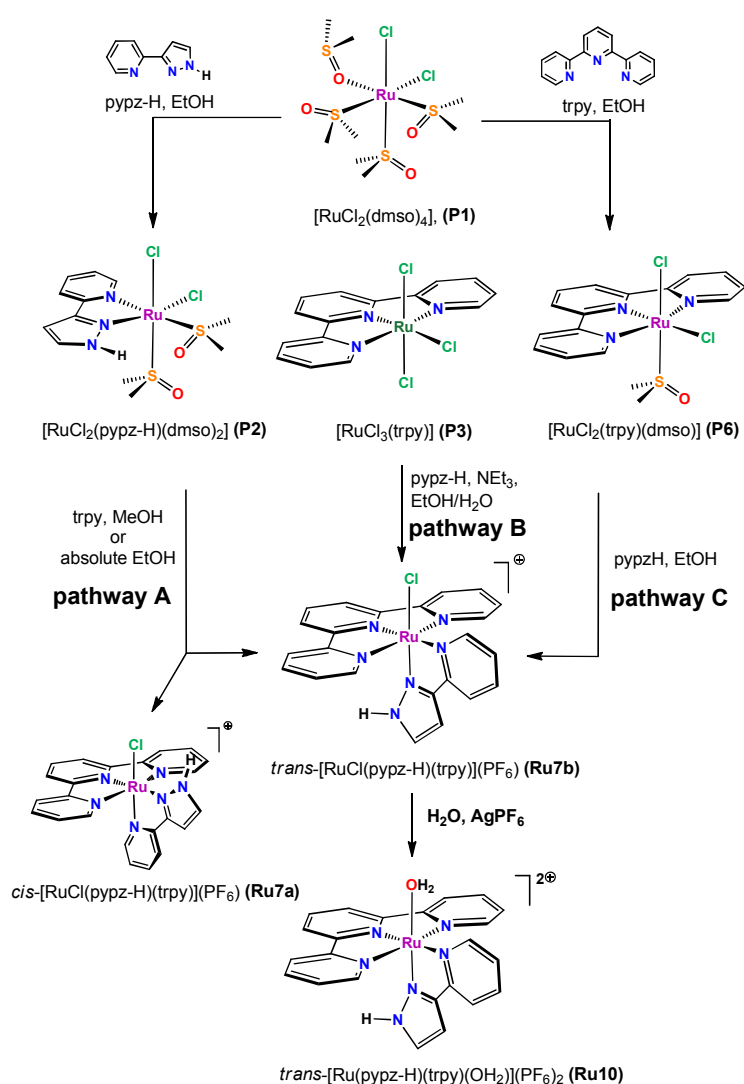
Finally, the isomeric mixture **Ru1** leads to the lower conversion values, in particular for substrates of entries 4-8, despite containing also two dmsO ligands. This could be explained, on one hand, by the steric encumbrance exerted by the pendant ethylester arm and, on the other hand, by the lower flexibility of a putative intermediate species containing the chelate *pypz-CH₂COOEt* ligand, in contrast with the rest of complexes that contain only monodentate ligands. Also, the occurrence of a higher number of potentially labile sites in complexes **Ru2-6** can be considered as the involvement of parallel mechanisms, involving the decoordination of dmsO but also of monodentate pyrazolyl ligands cannot be ruled out.

In conclusion, the catalytic activity in the hydration of nitriles is in general governed by the electronic factors of the substrates, with the more activated nitriles showing better overall performances, but steric factors are also manifested in the case of catalysts **Ru1** and **Ru3**, which display lower activity for the bulkier substrates. Complexes **Ru4-Ru6** display in general excellent performances despite containing only two π -acceptor dmsO ligands.

IV.3. Ru(II) complexes containing trpy and pyridylpyrazole ligands as catalysts for epoxidation of alkenes.

IV.3.1. Synthesis and structure

Three synthetic pathways were followed for the preparation of the Ru(II) compounds *cis* and *trans*-[Ru^{II}Cl(trpy)(pypz-H)](PF₆) (**Ru7a** and **Ru7b** respectively) and *trans*-[Ru^{II}(trpy)(pypz-H)(OH₂)](PF₆)₂, **Ru10**, which are outlined in Scheme IV.3.1 (the nomenclature *trans* and *cis* for complexes refers to the relative position of the monodentate ligand with regard to the pyrazole ring of the *pypz-H* ligand, see below). Different complexes, *cis*(Cl),*cis*(S)-[Ru^{II}Cl₂(pypz-H)(dmsO)₂],¹⁸⁴ **P2**, [Ru^{III}Cl₃(trpy)],²⁹⁶ **P3** and [Ru^{II}Cl₂(trpy)(dmsO)],²⁹⁹ **P6**, were used as starting products depending on the synthetic strategy (pathways A, B or C) used. Compounds **P2** and **P6** were first obtained by reaction of [Ru^{II}Cl₂(dmsO)₄] (**P1**) with *pypz-H* or *trpy* ligand respectively, in EtOH at reflux.



Scheme IV.3.1. Schematic pathways for the synthesis of the Ru(II)-chlorido compounds **Ru7a** and **Ru7b** and the aqua-complex **Ru10** (other minor products were obtained in the different synthesis but are not displayed, see text for details).

In pathway A, **P2** reacts with equimolar amounts of commercial *trpy* ligand in methanol at reflux (18 h) to generate a mixture of Ru(II)-Cl isomeric compounds, *cis* and *trans*-[Ru^{II}Cl(*pypz*-H)(*trpy*)](PF₆), **Ru7a** and **Ru7b**, in a 4:1 ratio, which are separated and purified through crystallization and by column chromatography. The use of absolute ethanol instead methanol as solvent, along with a longer reflux time (up to 48 h), leads to an increased final yield of the pure *trans*-isomer **Ru7b** (see the experimental section). In pathway B, equimolar amounts of [Ru^{III}Cl₃(*trpy*)], **P3**, and the bidentate *pypz*-H ligand in EtOH:H₂O (9:1) in the presence of Et₃N (1.2 equivalents, used as reducing agent), resulted in the substitution of two chlorido ligands in **P3** to generate the Ru(II) complex **Ru7b** as a single *trans*-isomer together with other secondary products, among which the dimeric species [Ru₂^{II}Cl(*trpy*)₂(μ-Cl)(μ-*pypz*)](PF₆), **Ru9**, that contains a deprotonated *pypz*⁻ bridging ligand. Finally in pathway C, **P6** reacts with equimolar amounts of *pypz*-H ligand in EtOH at reflux for 20 h and leads to the major formation of **Ru7b** compound isolated after chromatography. In both pathways A and C, the formation of the *dms*o-complex *trans*-[Ru^{II}(*pypz*-H)(*trpy*)(*dms*o)](PF₆)₂, **Ru8**, as a minor product was also observed. Treatment of the *trans*-[Ru^{II}Cl(*pypz*-H)(*trpy*)](PF₆) **Ru7b** complex with Ag⁺ generates the corresponding aqua compound, *trans*-[Ru^{II}(*pypz*-H)(*trpy*)(OH₂)](PF₆)₂, **Ru10**. Finally, treatment of the *cis*-[Ru^{II}Cl(*pypz*-H)(*trpy*)](PF₆) **Ru7a** complex with Ag⁺ generates a minor product which corresponds to the dimeric species [Ru₂^{II}(*trpy*)₂(μ-*pypz*)₂](PF₆)₂, **Ru11**.

In all the synthetic pathways, the obtaining of the *trans* isomer **Ru7b** is favored versus the *cis* **Ru7a** isomer. This fact could in principle be due to both steric and electronic effects. From a structural point of view, the proximity of the pyridilic N-H proton to the central pyridine ring of the *trpy* ligand placed in a relative *cis* disposition in the case of the **Ru7a** isomer (see Figure IV.3.1) could increase the steric hindrance when compared to **Ru7b**, where this position is occupied by the smaller pyrazolyl ring. This would be in accordance with the *cis:trans* ratio obtained in previous works for the analogous chlorido complexes containing the *pypz*-Me ligand, with a pyridilic N-CH₃ group instead of N-H (see Figure SIV.3.8 in the supporting information): this additional methyl group would sterically hamper the formation of the *trans* isomer and, indeed, the *pypz*-Me complexes are isolated in a roughly 1:1 isomeric ratio.³³² However, the *trans* isomer was again clearly favoured in the case of another family of complexes containing the NHC carbene CN-Me ligand³³³ (Figure SIV.3.8) with an isolated *cis:trans* ratio of 1:4, despite that the steric encumbrance is almost identical to that of the *pypz*-Me complexes. For carbene CN-Me complexes, electronic factors related to the particularly strong σ-donor capacity of the carbene NHC rings seem to be determinant in the preference for the *trans* isomer (probably exerting as distinctive *trans* effect during the

Chapter IV

coordination step), and a similar argument could be invoked in the case of complexes **Ru7a** and **Ru7b** since we expect the pyrazolyl ring in *pypz-H* to have an increased sigma-donor character thanks to the relative acidity of the N-H proton.

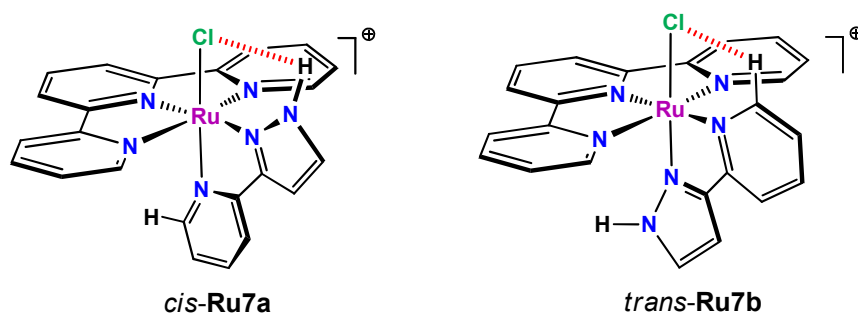


Figure IV.3.1. Hydrogen bond formation (red dashed line) between the Cl ligand and the pyrazolic N-H proton (*cis*-**Ru7a**) or the pyridylic H(1) proton (*trans*-**Ru7b**).

It is interesting to note that the hydrogen bond formed between the N-H and the close chlorido ligand in the case of the *cis* isomer **Ru7a** will probably increase the N-H acidic character and thus enhance the coordinative ability (due to a higher Lewis basicity) of this negatively charged N_{pz} atom upon deprotonation, which could explain the formation of the dimeric by-product species **Ru9** and **Ru11** (see below). As can be observed in the corresponding X-ray structures (Figure IV.3.3), both structures involve *cis* precursor moieties, and this could also explain in part the lower amount of *cis* isomer **Ru7a** obtained in the synthesis.

The crystal structures of compound *trans*-[Ru^{II}Cl(trpy)(*pypz-H*)](PF₆), **Ru7b**, and that of the minor products *trans*-[Ru^{II}(*pypz-H*)(trpy)(dmsO)](PF₆)₂, **Ru8**, [Ru₂^{II}Cl(trpy)₂(μ-Cl)(μ-*pypz*)](PF₆), **Ru9**, and [Ru₂^{II}(trpy)₂(μ-*pypz*)₂](PF₆)₂, **Ru11**, have been solved by X-ray diffraction analysis from a single crystal. Figures IV.3.2 and IV.3.3 display the molecular structures for the compounds, whereas the main crystallographic data and selected bond distances and angles can be found in the Supporting Information section (Tables SIV.3.1 and SIV.3.2).

The structure of **Ru7b** (Figure IV.3.2) shows that the Ru metal center adopts an octahedral distorted type of coordination where the *trpy* ligand is bonded in a meridional manner and the *pypz-H* ligand acts in a bidentate fashion. The sixth coordination site is occupied by the chlorido ligand placed in *trans* respect to the pyrazole ring. All bond distances and angles are within the expected values for this type of complexes.^{332,328}

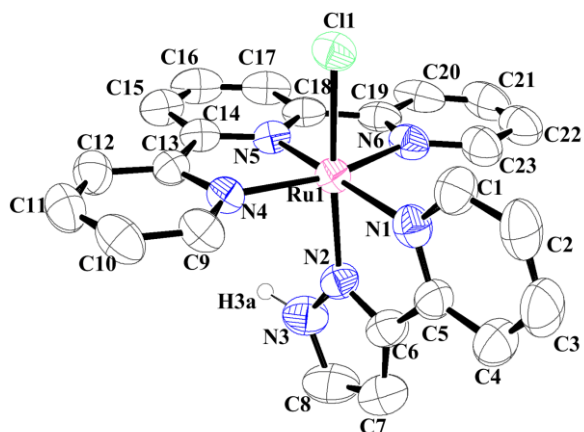
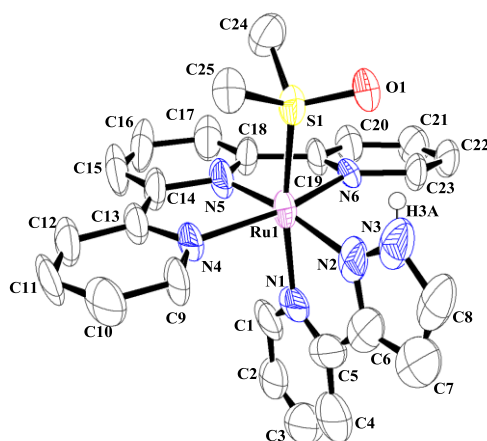
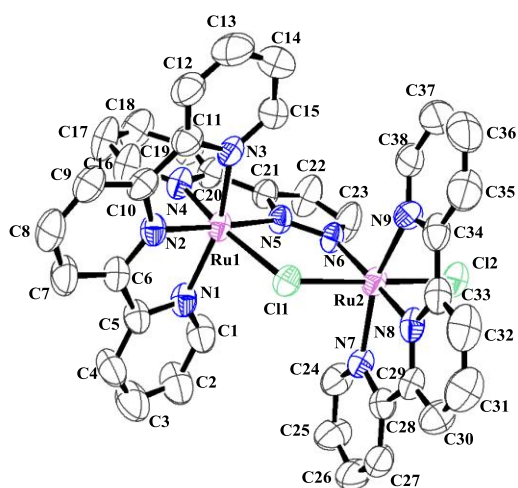


Figure IV.3.2. ORTEP plot and labeling scheme for the cationic moiety in the X-ray structure of complex **Ru7b**.

a)



b)



c)

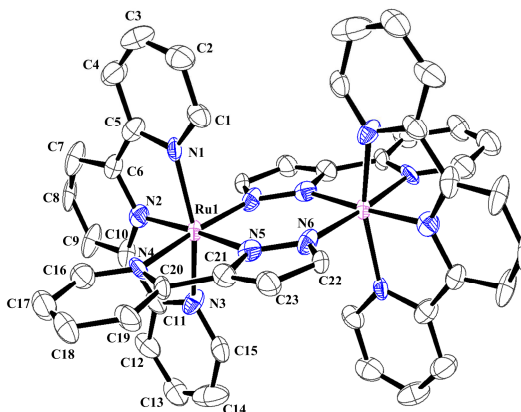


Figure IV.3.3. ORTEP plots and labeling schemes for the cationic moieties in the X-ray structures of complexes **Ru8** (a), **Ru9** (b) and **Ru11** (c) isolated as minor products during the synthesis of the chloro compounds **Ru7a** and **Ru7b**.

In the case of the side-product **Ru8**, the ruthenium metal center also adopts an octahedral distorted type of coordination similar to that described for **Ru7b**, but the sixth coordination site is occupied by the dmsoligand that displays a hydrogen bonding interaction between the O(1) of the dmsoligand and the pyrazolic proton N-H (2.339 Å).

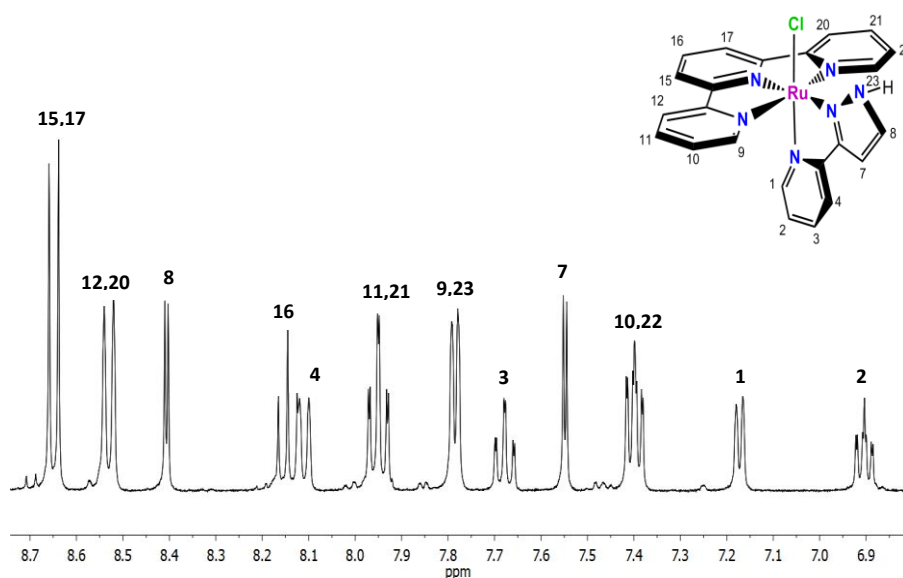
Regarding the dimeric compounds **Ru9** and **Ru11**, their structures show again distorted octahedral geometries around the metal centers, where the *trpy* ligands are also bonded in a meridional manner and the deprotonated pyrazole rings of the corresponding *pypz-H* ligands are bridging two ruthenium centers. In the case of **Ru9**, the structure is asymmetrical and shows two Ru(*trpy*) centers connected by a deprotonated *pypz⁻* ligand and by a bridging chlorido. The structure can be observed as a merge of a mononuclear *cis* **Ru7a** unit (corresponding to Ru1 in Figure IV.3.3b) and a reduced form of [Ru^{III}Cl₃(*trpy*)], used as starting material in route B, after decoordination of one chlorido ligand (precursor of Ru2). The formation of **Ru9** is probably favoured by the presence, in the reaction medium of pathway B, of the reducing agent NEt₃ that can also act as a base, presumably assisting the deprotonation of the incipiently formed **Ru7a** compound and thus increasing the coordinating ability of the deprotonated N_{pz} atom, as mentioned earlier. On the other hand, **Ru11** displays a symmetric cation with an inversion center, and each ruthenium is coordinated by one terpyridine ligand and by two bridging *pypz⁻* ligands. Again, the *trpy* and *pypz⁻* arrangement around each Ru metal center corresponds to that of a *cis* isomer thus reinforcing the hypothesis of the easy deprotonation of the pyrazolic proton in **Ru7a** then lowering the yield obtained with respect to the *trans* **Ru7b** isomer.

IV.3.2. Spectroscopic properties

The IR spectra of compound **Ru7** (as a mixture of isomers *cis* and *trans*, **Ru7a** and **Ru7b** respectively) and **Ru10** (Figure SIV.3.1) show bands around 3600-3400, 3090 and 1412-1389 cm^{-1} , that can be respectively assigned to $\nu_{\text{N-H}}$, $\nu_{\text{C-H}}$ and $\nu_{\text{C=N}}$ stretching modes of the polypyridylic ligands. In the case of **Ru10**, the spectrum displays an additional peak over 3350 cm^{-1} which corresponds to the $\nu_{\text{O-H}}$ stretching of the aqua ligand.

The one-dimensional (1D) and two-dimensional (2D) NMR spectra of compounds **Ru7a**, **Ru7b**, **Ru9** and **Ru10** were recorded in methanol- d_4 and are presented in Figures IV.3.4- IV.3.5 and in the supporting information (Figures SIV.3.4-SIV.3.7). The resonances for the complexes, all of them found in the aromatic region, are consistent with the solid-state structures determined through X-ray diffraction for **Ru7b** and **Ru9**. The combination of 1D and 2D NMR spectra allows to identifying all the resonances for the complexes. The most interesting feature of the spectra of chloro-complexes **Ru7a** and **Ru7b** (Figure IV.3.4) is the deshielding effect exerted by the chlorido ligand over the pyridilic H(1) of the bidentate ligand in the *trans* isomer **Ru7b** ($\delta = 10.0$ ppm) with regard to **Ru7a**, where H(1) is influenced by the aromatic π electron density then appearing upfield with regard to **Ru7b** ($\delta = 7.2$ ppm). This is an evidence of the spatially close Cl ligand to H(1) in the case of the *trans* isomer. For the *trans* Ru-OH₂ **Ru10** complex (Figure IV.3.5) the deshielding effect of the H₂O ligand over H(1) is not as strong as that observed in the corresponding chlorido complex **Ru7a**, thus leading to a lower chemical shift ($\delta = 9.4$ ppm).

a)



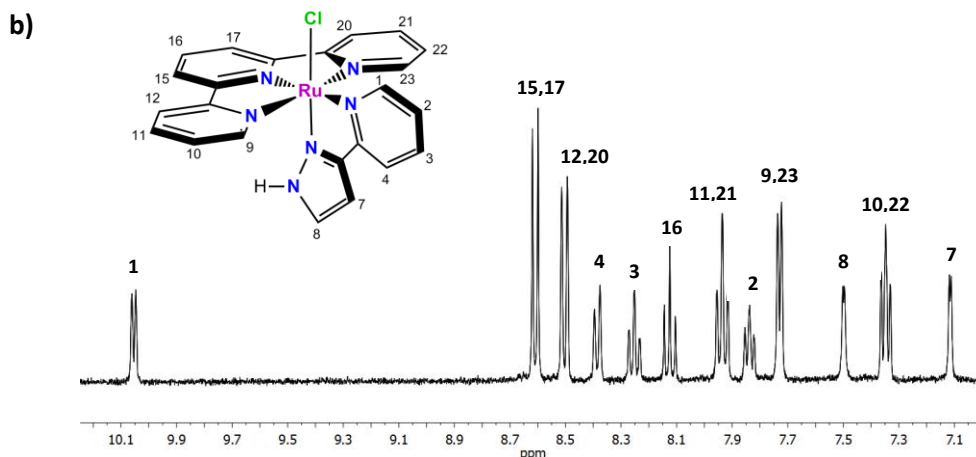


Figure IV.3.4. ^1H -NMR spectra of complexes a) **Ru7a** and b) **Ru7b** in methanol- d_4

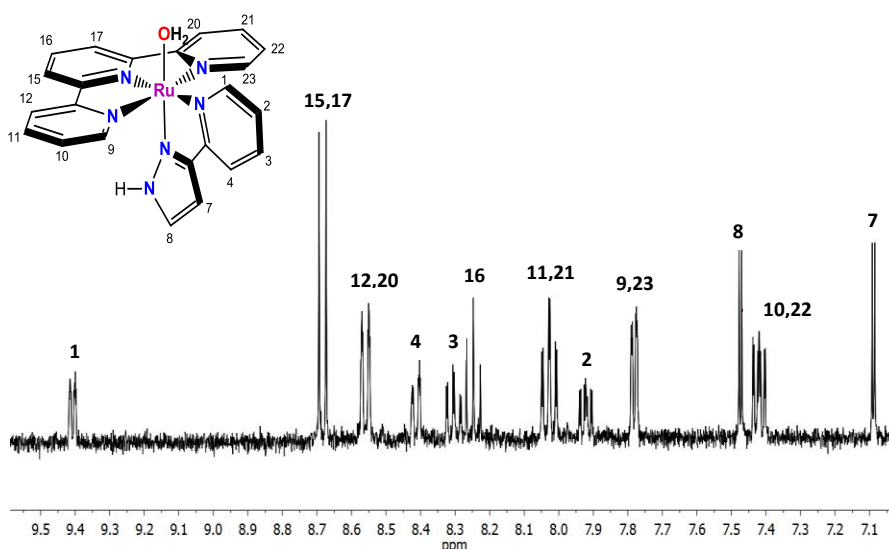


Figure IV.3.5. ^1H -NMR spectrum of complex **Ru10** in methanol- d_4 .

The UV-Vis spectra of complexes **Ru7a**, **Ru7b** and **Ru10** registered in CH_2Cl_2 or aqueous phosphate buffer are displayed in Figure IV.3.6. The complexes exhibit ligand based $\pi\text{-}\pi^*$ bands below 350 nm and relatively intense bands above 350 nm assigned mainly to $d\pi\text{-}\pi^*$ transitions due to a series of MLCT transitions. For the Ru-Cl complexes the MLCT bands are shifted to the red with regard to the Ru- OH_2 due to the relative destabilization of the $d\pi(\text{Ru})$ levels provoked by the chloro ligand. A similar MLCT maximum wavelength values are observed for other complexes described in the literature.³³²⁻³³⁴

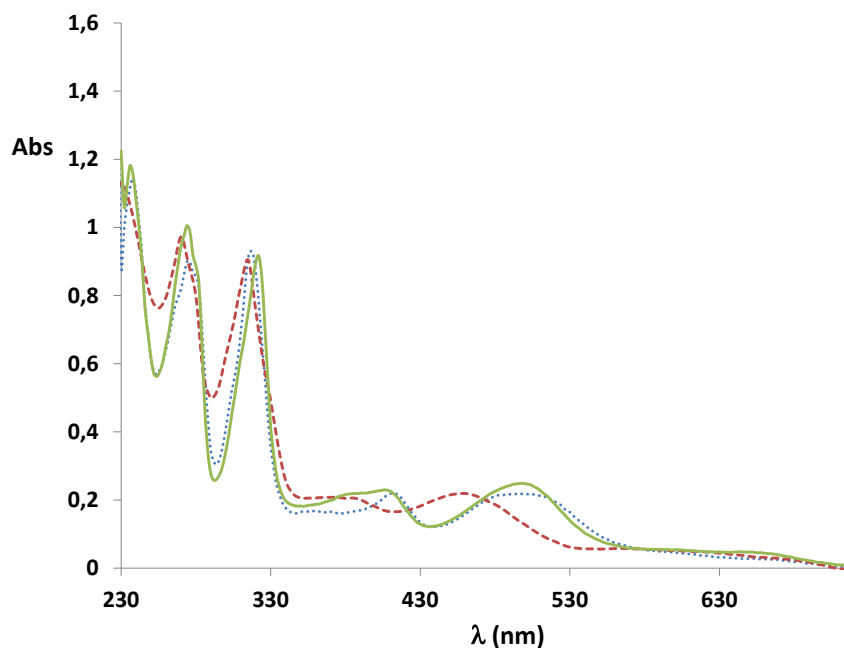


Figure IV.3.6. UV-Vis spectra of **Ru7a** (solid line), **Ru7b** (dotted line) in CH_2Cl_2 and **Ru10** (dashed line) in phosphate buffer (pH= 7).

IV.3.3. Electrochemical properties

The redox properties of chlorido complexes **Ru7a** and **Ru7b**, the dmsu complex **Ru8**, the dimeric complex **Ru9** and the aqua complex **Ru10** were investigated by means of cyclic voltammetry (CV) and differential pulse voltammetry (DPV). Figure IV.3.7 shows the CVs of **Ru7a** and **Ru7b** registered in dichloromethane, and IV.3.8 displays the DPV of **Ru10** in aqueous medium. CV and DPVs experiments for complexes **Ru8** and **Ru9** performed in CH_2Cl_2 are shown in the supporting information (Figures SIV.3.2 and SIV.3.3).

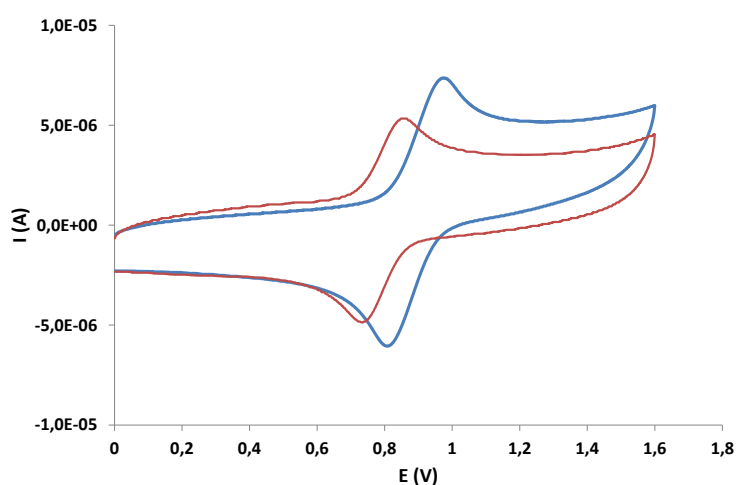


Figure IV.3.7. CV for complex **Ru7a** (blue) and **Ru7b** (red) registered in CH_2Cl_2 vs. SCE.

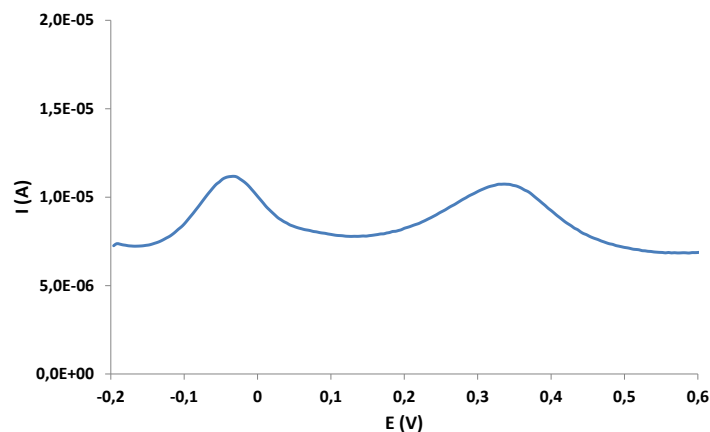


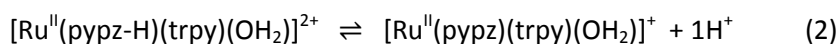
Figure IV.3.8. DPV of complex **Ru10** in phosphate buffer (pH adjusted to 11.8) vs. SCE.

Chlorido complexes **Ru7a** and **Ru7b** exhibit a reversible one electron Ru(III)/Ru(II) redox process at $E_{1/2} = 0.88$ V and $E_{1/2} = 0.80$ V vs. SCE, respectively (Figure IV.3.7). Despite presenting the same coordination environment, higher potential values are obtained for the *cis* chlorido complex **Ru7a** (0.88 V) when compared to the analogous *trans* **Ru7b** (0.80 V). This behaviour is distinct to that shown by the analogous *pypz-Me* complexes,³³² where the two chlorido isomers display almost identical $E_{1/2}$ values, but is related to the redox properties of the above-mentioned carbene CN-Me complexes³³³, where the two isomers present redox couples with values that differ in around 100 mV. In the case of complexes **Ru7a** and **Ru7b** the redox behaviour evidences that the oxidation state (III) is affected by the relative coordination of the pyridylpyrazole ligand to the ruthenium, leading to a greater stabilization of Ru(III) when the pyrazolyl ring is placed in *trans* respect to the σ -donor chlorido ligand.

On the other hand, the aqua complex **Ru10** exhibits two reversible redox processes at $E_{1/2} = -0.03$ V and 0.34 V vs. SCE in aqueous phosphate buffer at pH= 11.8, corresponding to the one electron Ru(III)/Ru(II) and Ru(IV/III) redox couples, as we have confirmed through the Pourbaix diagram (see below).

The redox potentials for the Ru-aqua complexes are pH dependent, due to the capacity of the coordinated aqua and pyrazolylic (PzH) ligands to exchange protons (equations (2) and (3)):

$$pK_a(\text{Ru}^{\text{II}})_1$$



$$pK_a(\text{Ru}^{\text{II}})_2$$



When the Ru(II) form is oxidized, the higher Lewis acidity of the upper oxidation state leads to the parallel deprotonation of one or more of the ligands, originating a pH-dependence of the $E_{1/2}$ values. Such dependence is represented under the form of Pourbaix diagrams, and that corresponding to complex **Ru10** is displayed in Figure IV.3.9. The diagram shows several pH-potential regions arising from the multiple protonation sites in the complex. The changes in the slope correspond to the pKa values of the Ru(II) or Ru(III) species, and are indicated with vertical lines in each case.

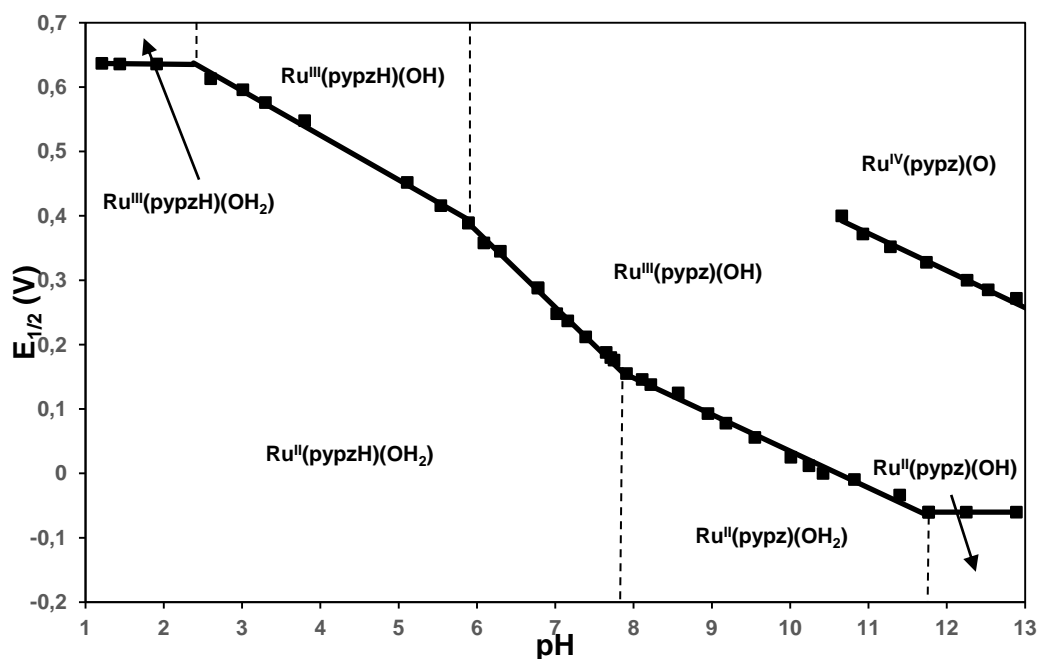
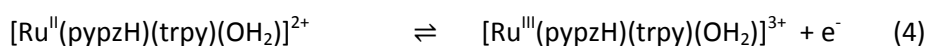


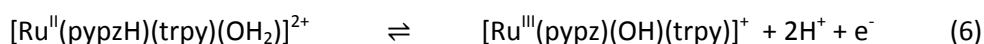
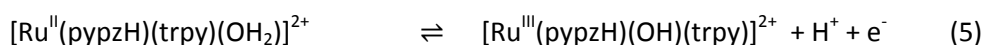
Figure IV.3.9. Pourbaix diagram for complex **Ru10**. The pH-potential regions of stability and the proton composition for the different redox species are indicated. The pKa of each species is represented with a dashed vertical line.

Under acidic conditions only one electrochemically quasireversible wave is observed corresponding to the Ru(III/II) couple; for pH values below 2.4, the potential is not pH-dependent and the wave observed at $E_{1/2}=0.64$ V corresponds to the simple one-electron oxidation process displayed in equation 4:

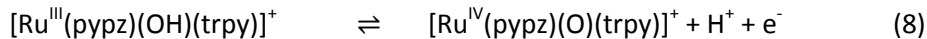
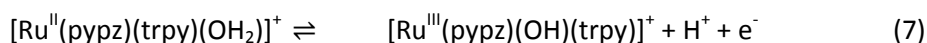
Chapter IV



Within the pH range 2.4 – 5.9 approximately, the potential decreases ~69 mV per pH unit, whereas in the pH range 5.9 - 7.9 this decrease is of 118 mV. These variations are consistent with the processes shown in equations 5 and 6, respectively:



At basic pH two redox processes can be detected. For instance, at pH= 11.8 two reversible redox processes at $E_{1/2} = -0.03$ V and 0.34 V are observed. The first wave is assigned to the Ru(III)/Ru(II) couple and the second to the Ru(IV)/Ru(III) redox pair (equations 7 and 8):



As mentioned above, the changes in the slope indicated by the vertical lines in the Pourbaix diagram correspond to the pKa values of the Ru(II) and Ru(III) species. In the case of **Ru10**, the pKa values for Ru(II) are $\text{pKa}(\text{Ru}^{\text{II}})_1 = 7.9$ and $\text{pKa}(\text{Ru}^{\text{II}})_2 = 11.8$, corresponding to the protonation/deprotonation of the pyrazole ring and the aqua ligand respectively. In the case of Ru(III), the values of $\text{pKa}(\text{Ru}^{\text{III}})_1 = 2.5$ and $\text{pKa}(\text{Ru}^{\text{III}})_2 = 6$ can be assigned to the aqua ligand and pyrazole ring, respectively. As can be observed, the oxidation to Ru(III) and the subsequent increase of the Lewis acid character has a notably higher influence on the pKa value of the aqua ligand, which is directly coordinated to the Ru metal center, than on that of the pyrazolyl ligand.

Table IV.3.1 shows the comparison of the redox potential of the Ru-OH₂ complex **Ru10** with others previously reported in the literature.^{332,335,336}

Table IV.3.1. pKa and electrochemical data (pH= 7, $E_{1/2}$ in V vs. SCE) for aqua complexes described in this work and others for purposes of comparison.

| entry | compound | $E_{1/2}$ (III/II) | $E_{1/2}$ (IV/III) | pK _a (II) | pK _a (III) | ref |
|-------|---|--------------------|--------------------|------------------------|-----------------------|-----|
| 1 | Ru10 | 0.26 | 0.61 ^a | 11.8(7.9) ^b | 2.5(5.9) ^b | c |
| 2 | <i>trans</i> -[Ru(trpy)(pypz-Me)(OH ₂)] ²⁺ | 0.39 | 0.57 | 10.1 | 0.95 | 332 |
| 3 | [Ru(trpy)(bpy)(OH ₂)] ²⁺ | 0.49 | 0.62 | 9.7 | 1.7 | 335 |
| 4 | [Ru(trpy)(acac)(OH ₂)] ⁺ | 0.19 | 0.56 | 11.2 | 5.2 | 336 |

^aValue estimated from extrapolation of the (IV/III) trace in the Pourbaix diagram to pH = 7. ^bIn parentheses, pKa value corresponding to the deprotonation of the pyrazolyl ligand. ^cThis work.

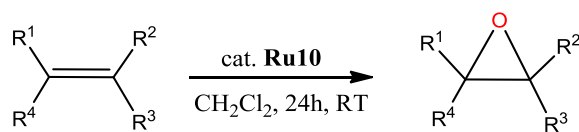
The redox potential of the couple Ru(III/II) in **Ru10** is lower than that displayed by the analogous *trans*-[Ru^{II}(trpy)(pypz-Me)(OH₂)]²⁺ and [Ru(trpy)(bpy)(OH₂)]²⁺ complexes (entries 2 and 3), which is in accordance with the higher electron-donor character of the *pypz-H* ligand with regard to *pypz-Me* or *bpy*. In this line, the substitution of the bidentate ligands in entries 1-3 by a strong σ -donor anionic ligand such as acetylacetonate (*acac*) produces a stabilization of the Ru(III) oxidation state and thus a strong decrease of the III/II couple to values below to that observed in **Ru10**, which bears the neutral *pypz-H* ligand. However, the IV/III couple is much less affected by the different bidentate ligands present (in the case of complex **Ru10** the $E_{1/2}$ (IV/III) wave is not observed in the Pourbaix diagram but it could be estimated to be around 0.61 V). Regarding the pKa values, complex **Ru10** presents the highest pKa(II) value (11.8) followed by that displayed by the *acac* complex in entry 4. This is in accordance with the anionic nature of *acac* and of the *pypz*⁻ ligand (that is deprotonated at this pH value) which are strong σ -donor and thus make the Ru metal center and the coordinated aqua ligand less acidic.

IV.3.4. Catalytic epoxidation of alkenes

The catalytic activity of the ruthenium aqua complex *trans* **Ru10** was checked in the epoxidation of different alkenes in dichloromethane and using iodobenzene diacetate as oxidant, with a catalyst:substrate:oxidant ratio of 1:100:200. No epoxidation occurred in the absence of catalyst. Table IV.3.2 reports the conversion and selectivity values for the epoxide product in each case.

Chapter IV

Table IV.3.2. Ru-catalyzed alkene epoxidation mediated by complex **Ru10**.^a Conversion (conv.) and selectivity (sel.) values are given in %.



| Entry | Complex | Ru10 | |
|-------|-----------|-------|-----------------------------|
| | Substrate | conv. | sel. ^b |
| 1 | | 69 | >99 |
| 2 | | 90 | >99 [78/22] ^c |
| 3 | | 86 | 82 |
| 4 | | >99 | >99 [100/0] ^d |
| 5 | | 94 | >99 |
| 6 | | 66 | >99 |

^aConditions: **Ru10**:subs:PhI(OAc)₂ (catalyst/substrate/oxidant) ratio of 1:100:200 in CH₂Cl₂, 24 h at RT. ^bSelectivity for epoxide (sel.): [Yield/conversion] x 100. ^cRatio [% *cis* epoxide/ % *trans* epoxide]. ^dRatio [% ring epoxide/ % vinyl epoxide].

As can be observed in Table IV.3.2, in general moderate to high conversions and good selectivity values for the corresponding epoxides (with benzaldehyde identified as the main byproduct) are obtained for all the substrates tested. Both aliphatic and aromatic alkenes are efficiently epoxidized and, among the aromatic ones (entries 1-3), styrene (entry 1) displays a slightly lower conversion degree. This would be in accordance with the involvement of an electrophilic active species that would display better reactivity towards the alkyl-substituted β -methylstyrenes (entries 2 and 3) than for styrene. The conversion trend within aliphatic olefins (entries 4-6) would also be in accordance with the occurrence of such electrophilic active species, achieving slightly lower conversion values for the monosubstituted 1-octene substrate (entry 6) when compared to the alkyl-disubstituted cyclic olefins.

Within the epoxidation area a particularly interesting reaction is the stereoselective epoxidation of *cis*-alkenes.^{166,192b,337} The *cis* \rightarrow *trans* isomerization in epoxidation processes involving *cis* alkenes is a common phenomenon due to the higher thermodynamic stability of the *trans* epoxides. To undergo such isomerization, a rotation around the C-C bond is required involving the presence of a relatively long-lived free substrate radical during the oxygen

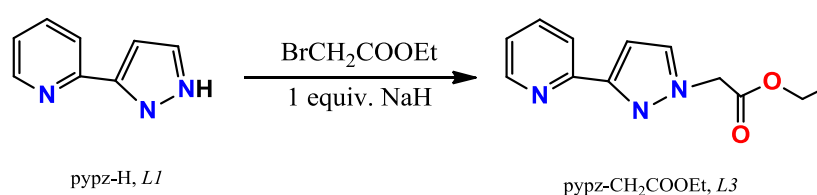
transfer process (see introduction, Scheme I.13). The activity of **Ru10** with regard to the epoxidation of *cis*- β -methylstyrene shows 78 % of *cis*-epoxide and 22 % of *trans*-epoxide, and this fact must be caused by the involvement of a relatively stable radical species in the catalytic cycle that undergoes isomerization to the most thermodynamic stable *trans* isomer. It is interesting to compare the activity of complex **Ru10** with regard to the previously reported *trans*-[Ru(trpy)(pypz-Me)(OH₂)]²⁺, for which the isomerization to the *trans*-epoxide is inexistent. Taking into account that both catalysts present similar redox behaviour (with two clearly separated monoelectronic redox processes) their different stereoselectivity could be related to structural factors associated to the presence of the additional methyl group which could hinder the *cis* \rightarrow *trans* rotation of the intermediate species in the catalytic cycle.

Regarding the 4-vinylcyclohexene substrate, **Ru10** is specific towards the ring oxidation, again in agreement with the formation of an electrophilic catalytic species that would preferentially epoxidize the disubstituted ring double bond.

IV.4. Heterogenization of complex $[\text{RuCl}_2(\text{pypz-CH}_2\text{COOEt})(\text{dmsO})_2]$. Evaluation of the catalytic activity in the hydration of nitriles.

IV.4.1. Strategies for the immobilization of Ru complexes

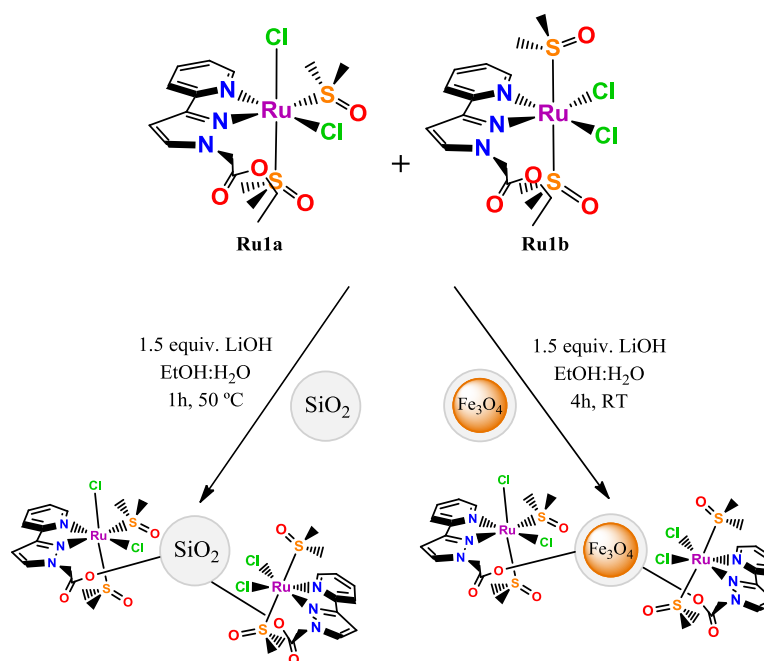
The immobilization method used for the heterogenization of $[\text{Ru}^{\text{II}}\text{Cl}_2(\text{pypz-CH}_2\text{COOEt})(\text{dmsO})_2]$ (**Ru1**, as a mixture of isomers **Ru1a** and **Ru1b**, see section IV.2) described in this chapter is based in the formation of hybrid materials in which the support and the heterogenized compound are linked by a chemical bond. A covalent binding is formed between the modified pyridine-pyrazole ligand containing an ethyl ester group (Scheme IV.4.1) and the surface of different types of silica particles, through the hydrolysis of the terminal ester group.



Scheme IV.4.1. Modification of the *pypz-H* ligand by the introduction of a terminal ester group, *pypz-CH₂COOEt*.

In this chapter, two different SiO_2 supports were used: commercial silica mesoporous particles (SP) and silica-coated Fe_3O_4 magnetic nanoparticles (MSNP), with mean diameters of aprox. 200 nm and 20 nm, respectively. The main physical parameters for both types of support are shown in Table 1, and full characterization of MSNP particles can be found elsewhere.²⁸⁸

The strategy followed for the immobilization of complex **Ru1** consists in the reaction of molecular complex with SP or MSNP particles as is shown in Scheme 2. In the case of the SP material, an EtOH:H₂O mixture (6:1) was used to solubilize the complex **Ru1** and afterwards the SP was added to the solution together with 1.5 equivalents of LiOH in aqueous solution. The resulting dispersion was heated at 50 °C and stirred for one hour. The resulting heterogeneous system **SP@Ru1** was centrifuged, washed and dried at vacuum. The yellow color of the final solid indicates that the complex was successfully attached to the silica surface. For MSNP, a similar procedure was used with the difference that it was mechanically stirred at room temperature for 4 h. The brown-reddish color of the MSNP does not allow to see the yellow color of complex **Ru1** attached onto the silica surface, but further experiments confirmed its presence. To the best of our knowledge, this is the first example of a dmsO ruthenium complex immobilized and fully characterized (see below) onto silica supports including magnetic particles.



Scheme IV.4.2. Synthetic strategies for the immobilization of complex **Ru1** (as mixture of isomers **Ru1a** and **Ru1b**) onto SP (grey spheres) and MSNP (orange-core and grey-shell spheres).

IV.4.2. Characterization of supports

The different techniques used for the characterization of the supports described below correspond to both **SP@Ru1** and **MSNP@Ru1** particles, except for the physical parameters which are given for the naked silica and MSNP supports.

IV.4.2.1. Physical parameters of the silica supports used

The physical parameters were measured on the various silica supports prior to the attachment of the complex or ligand and are summarized in Table IV.4.1. As can be observed, the core-shell MSNP is not a mesoporous material (does not have pores on the surface) in contrast with SP. The specific surface areas (S_{BET}) of the supports are quite different, with SP having a value around ten times as much than MSNP. Finally, MSNP contain around 24.3 % of Fe.

Table IV.4.1. Physical parameters of the different supports used.

| Support | Particle size (nm) | Pore | | S_{BET} | % Fe |
|---------|--------------------|-----------------------------------|-----------|------------------|-------|
| | | Volume (cm^3/g) | Size (nm) | | |
| SP | ~200 | 0.002 | 4 | 886 | - |
| MSNP | ~20 | - | - | 80.3 | 24.29 |

Chapter IV

IV.4.2.2. Atomic Emission Spectroscopy (ICP-AES)

From the ICP-AES experiments, the amount of **Ru1** complex covalently anchored to the supports was obtained. The results are shown in Table IV.4.2.

Table IV.4.2. Amount of Ru anchored in the different supports.

| Support | Average Ru(%) ^a | Ru(mmol/g silica) |
|---------|----------------------------|-------------------|
| SP | 3.08 | 0.305 |
| MSNP | 1.32 | 0.131 |

^a % g Ru/100 g support

As can be observed in Table IV.4.2, a lower amount of Ru was anchored onto the MSNP support probably due to the incomplete hydrolysis of the ester groups since milder reaction conditions have been used to hydrolyze the ethyl groups of the ester ligand.

IV.4.2.3. SEM images

Scanning electron microscopy (SEM) was performed on the two supports after functionalization, and the images obtained are displayed in Figure IV.4.1. As can be observed, both supports maintain their particle size and morphology after the attachment process. Figure SIV.4.1 shows the SEM images obtained for supports SP and MSNP before anchoring the complex (MSNP particles had been synthesized and fully characterized by the group of Dr. Josep Ros from UAB).²⁸⁸ The resolution of the MSNP are not as good as for SP because of aggregation phenomena.

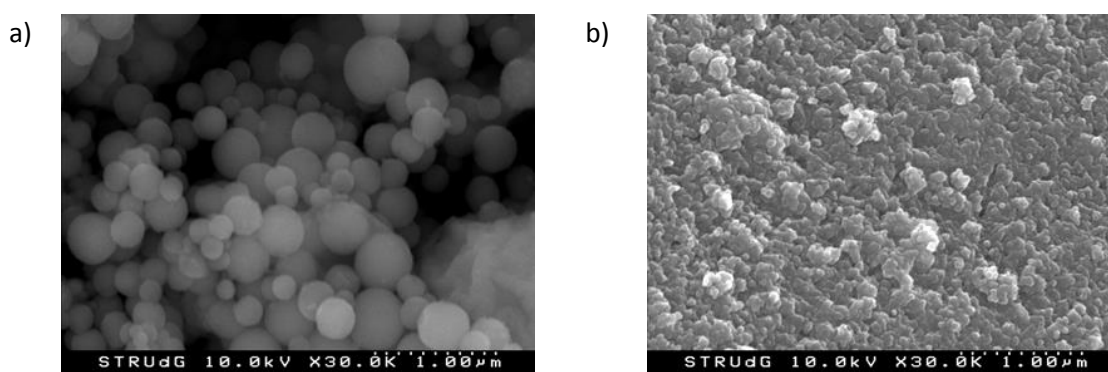


Figure IV.4.1. SEM images of a) SP and b) MSNP after the anchoring of the Ru complex.

IV.4.2.4. TEM images

Transmission electron microscopy (TEM) was performed on the two different supports after functionalization, and the images obtained are displayed in Figure IV.4.2. This technique gave better resolution for magnetic nanoparticles MSNP, where the Fe_3O_4 core and the SiO_2 shell can be observed (Figure IV.4.2b, black and grey zones respectively). Also, TEM images for the SP and MSNP supports before anchoring the complex were registered and the images are shown in Figure SIV.4.2. As can be observed, both supports maintain their particle size and morphology after the attachment process.

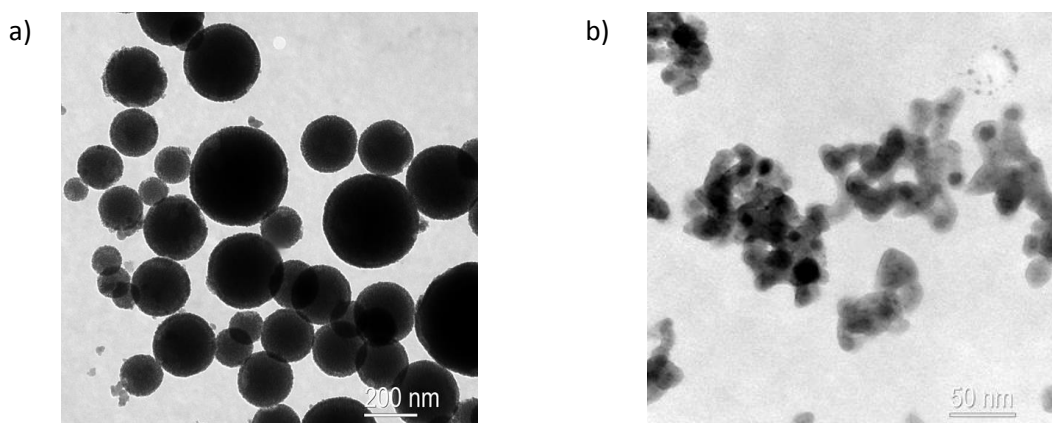


Figure IV.4.2. TEM images of a) SP and b) MSNP after the anchoring of the Ru complex.

IV.4.2.5. Thermal studies (TGA)

Thermogravimetric profiles have been registered for the naked SP support and for the two (**SP@Ru1** and **MSNP@Ru1**) supports after anchoring the Ru complex, and the results obtained are shown in Figure IV.4.3. In all cases, the supports present an initial weight loss at temperatures below 150 °C, corresponding to the evaporation of adsorbed solvent. At higher temperatures, the weight loss for both heterogeneous materials corresponds to the release of the Ru complex. For **SP@Ru1** the weight loss was 17.1 %, whereas it was of 7.3 % for MSNP.

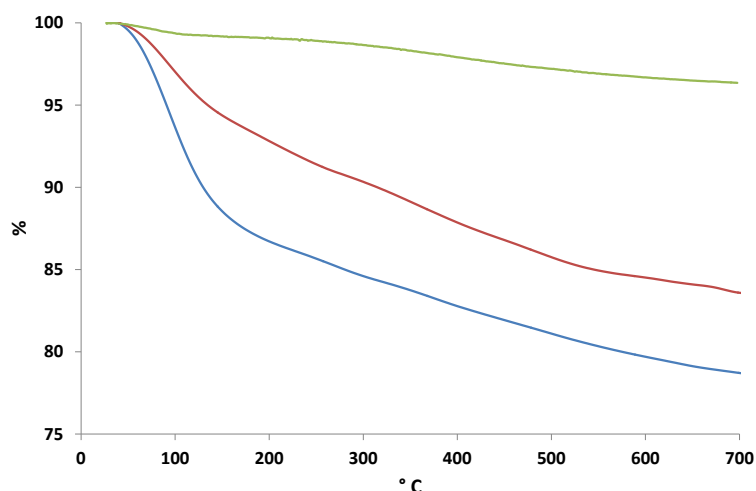


Figure IV.4.3. Thermogravimetric profiles of naked SP support (green), SP@Ru1 (blue) and MSNP@Ru1 (red).

IV.4.2.6. X-ray Photoelectron Spectroscopy (XPS)

The X-ray Photoelectron Spectroscopy (XPS) technique relies upon the photoelectric effect. An electron in an atom of a solid may absorb an incident photon and so gain sufficient energy to leave the confines of that atom's potential well. Although photoelectrons are produced wherever X-rays penetrate, only those within a few nanometres of the surface can actually escape the solid completely and thus carry information about their origins in their kinetic energy. Given the fixed energies of core energy levels in atoms, the net energy of a photoelectron is also fixed and a binding energy of its origin can be determined. For a given element, the energies of the core levels do not vary a great deal, so each element has a characteristic "fingerprint" spectrum.³³⁸

The XPS survey spectra have been registered for **SP@Ru1** and **MSNP@Ru1**, and the corresponding overall spectra are shown in Figure IV.4.4 and in the supporting information (Figures SIV.4.3 and SIV.4.4 respectively). Peaks corresponding to C, Si, O and Ru are clearly observed for both samples, with a strong signal near 530 eV which corresponds to the 1s orbital from the oxygen atoms of the silica, together with two weak signals identified as C 1s (~282-290 eV) and Si 2p (~103 eV) (see Figure IV.4.4a and Figure SIV.4.3).³³⁹ A third weak signal at ~280.85 eV for **SP@Ru1** and ~280.5 eV for **MSNP@Ru1** was identified as the Ru(3d_{5/2}) orbital, confirming the ruthenium (II) oxidation state. This signal is in close proximity to the C 1s signal (Figure IV.4.4b) and a deconvolution of the overall signal has been performed for both samples (Figures SIV.4.3 and SIV.4.4 in the supporting information). The Ru(3d_{5/2}) value is similar to that reported for other Ru(II) complexes found in the literature.³⁴⁰

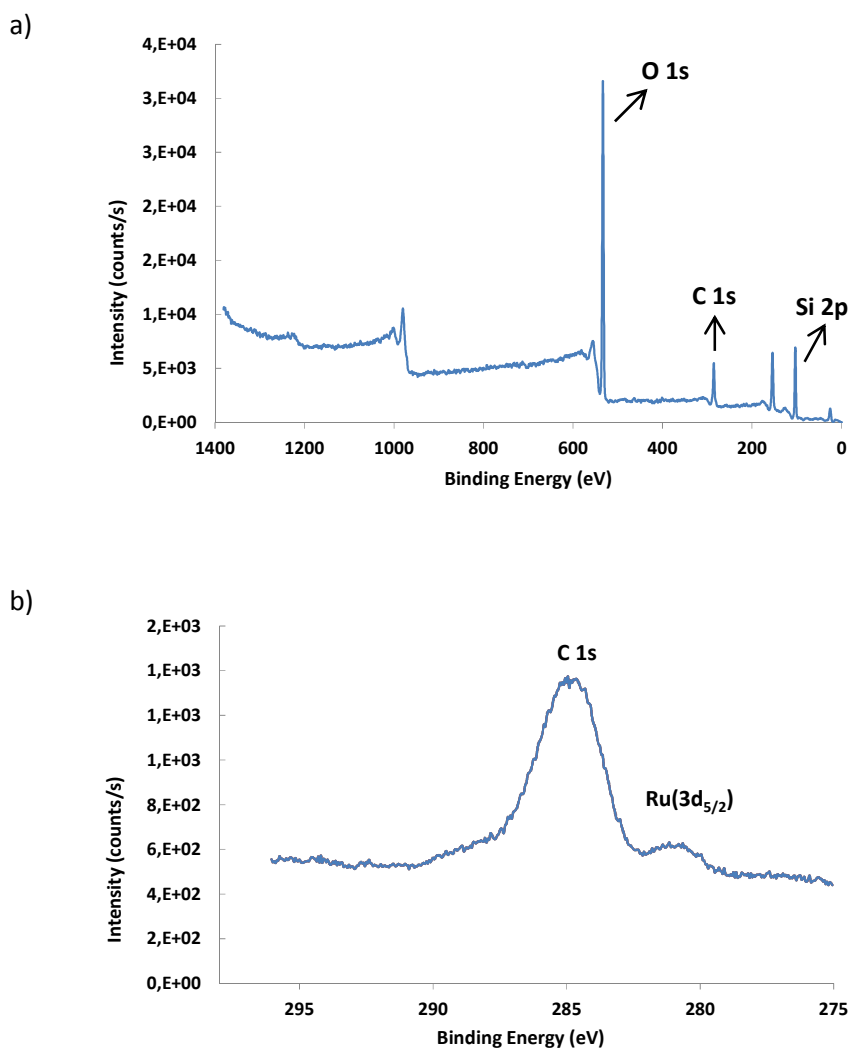


Figure IV.4.4. XPS survey scans of **SP@Ru1**: a) overall XPS spectra and b) C 1s signal together with Ru(3d_{5/2}) band.

IV.4.2.7. Spectroscopic properties

Both heterogeneous systems **SP@Ru1** and **MSNP@Ru1** have been characterized through IR and UV-Vis spectroscopies. Figure IV.4.5a displays the IR spectra for SP and **SP@Ru1** and, as can be observed in the inset, the modified silica **SP@Ru1** shows bands around 1702 cm⁻¹ that can be assigned to $\nu(\text{C-O})$ stretching modes of the supported *pypz-CH₂COOEt* ligand. In a similar way, **MSNP@Ru1** (Figure IV.4.5b) displays the analogous $\nu(\text{C-O})$ band at 1695 cm⁻¹.

Chapter IV

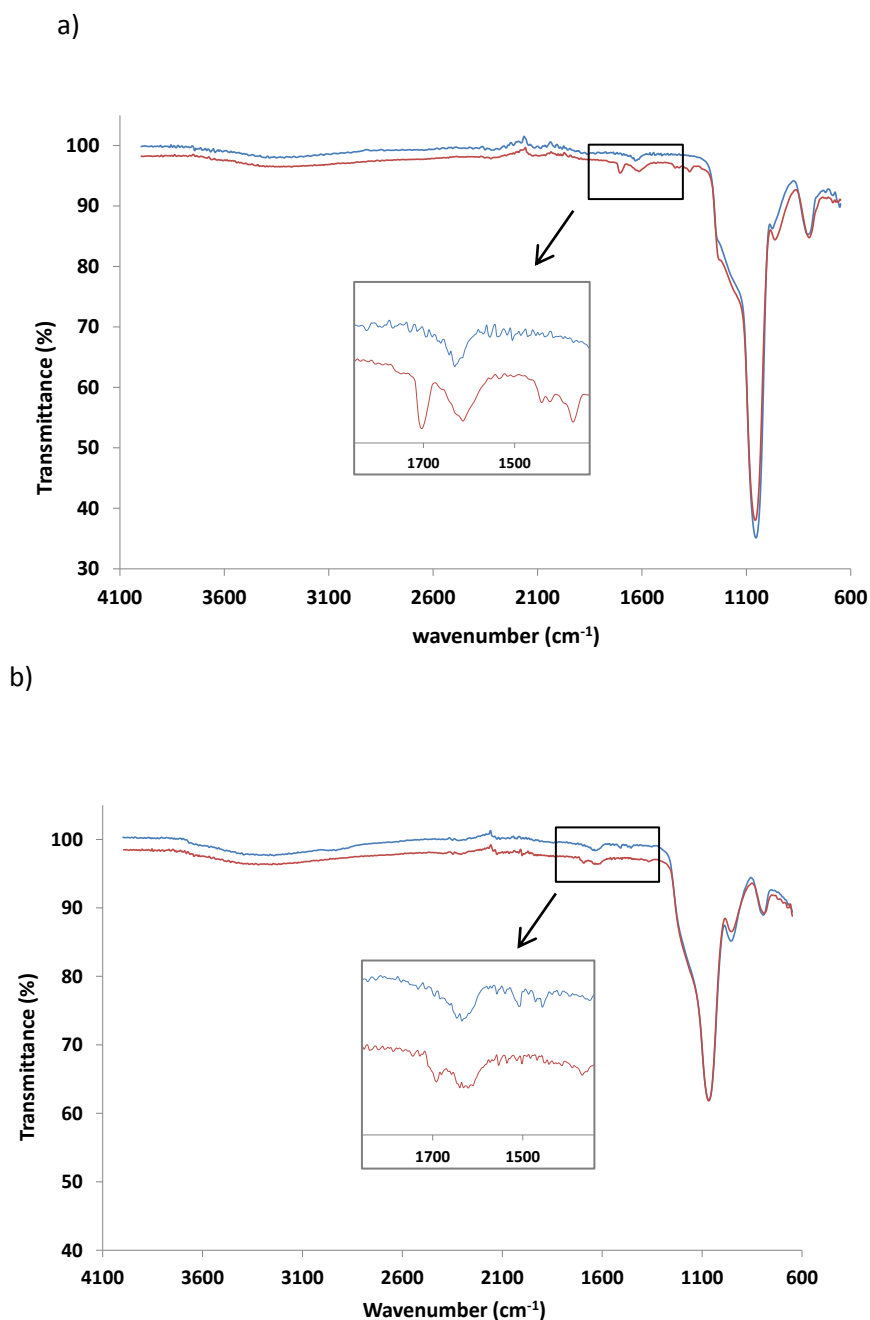


Figure IV.4.5. IR spectra of a) **SP@Ru1** and b) **MSNP@Ru1**. Blanks of SP and MSNP respectively are represented in blue, and the heterogeneous complex in red lines.

The UV-Vis spectra for **SP@Ru1** and **MSNP@Ru1** have been registered on a suspension of the heterogeneous support in dichloromethane and are displayed in Figure IV.4.6, together with the UV-Vis spectrum of the homogeneous complex **Ru1** and those of SP and MSNP naked supports. The anchored complex exhibits ligand based π - π^* bands below 350 nm and relatively intense bands above 350 nm mainly due to $d\pi(\text{Ru})$ - $\pi^*(\text{L})$ MLCT transitions³²⁹ that are similar to those obtained for the homogeneous complex **Ru1**. We can then assert that the anchored **Ru1** complex is analogous to that previously synthesized in solution.

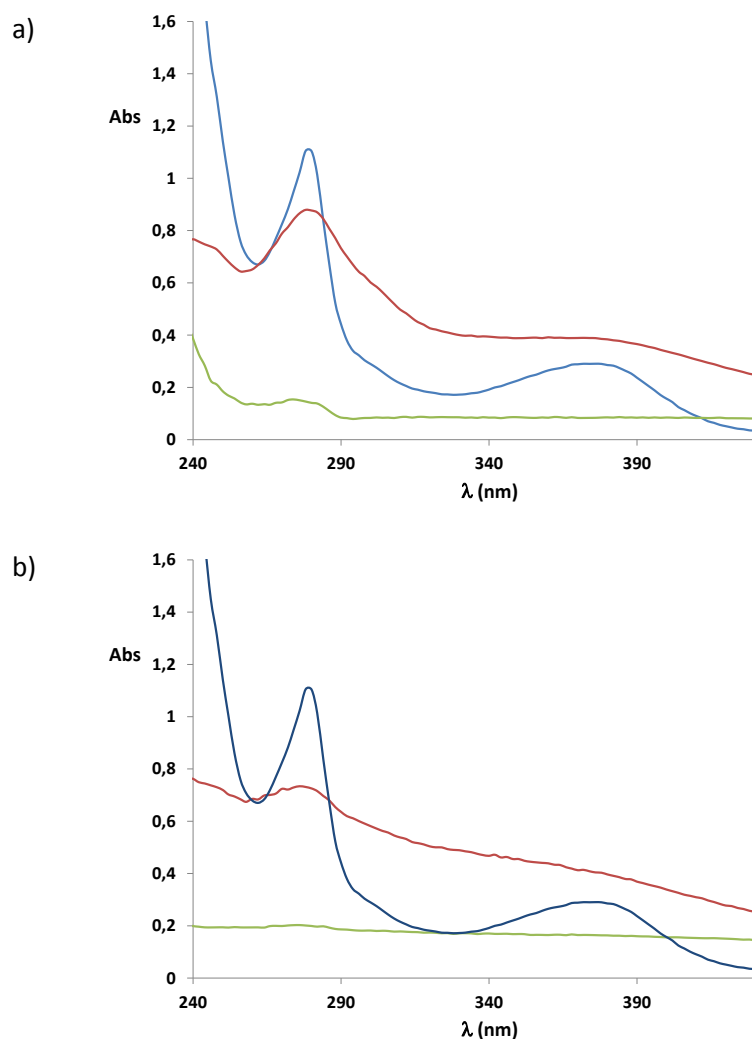


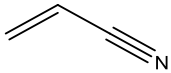
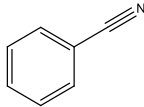
Figure IV.4.6. UV-Vis spectra (red lines) for a) **SP@Ru1** and b) **MSNP@Ru1**. In each figure, spectra of the corresponding naked SP and MSNP supports are depicted in green and that of complex **Ru1** in blue.

IV.4.3. Catalytic hydration of nitriles

The catalytic activity of the heterogeneous systems **SP@Ru1** and **MSNP@Ru1** was tested in the hydration of benzonitrile and acrylonitrile under neutral conditions using water as solvent at 100 °C. The experimental conditions used were analogous to that used in homogeneous catalysis (catalyst:substrate, 5:100). Conversion and selectivity values obtained with the heterogeneized systems, together with the values attained with $[\text{RuCl}_2(\text{dmsO})_2(\text{pypz-CH}_2\text{COOEt})]$, **Ru1**, are gathered in Table IV.4.3. A blank experiment using naked SP and MSNP yielded 10 and 17 % of amide respectively. This value has been subtracted from the results shown in Table IV.4.3.

Chapter IV

Table IV.4.3. Ru-catalyzed hydration of nitriles to amides in water using homogeneous complex Ru1 and the heterogenized systems **SP@Ru1** and **MSNP@Ru1**.^a Conversion (conv.) and selectivity (sel.) values are given in %.

| Complex | Ru1 | | SP@Ru1 | | MSNP@Ru1 | |
|---|-------|-------------------|--------|------|----------|------|
| | conv. | sel. ^b | conv. | sel. | conv. | sel. |
|  | 55 | 23 | >99 | 72 | >99 | 83 |
|  | 88 | 88 | 85 | 83 | >99 | 88 |

^a**Conditions:** Reactions performed at 100 °C in H₂O (3 mL) and in a [Substrate]:[Ru] ratio= 100:5. Time: 20 h reaction. ^bSelectivity for the amide is determined by ¹H-NMR analysis of the reaction mixture. Selectivity (sel.) = (amide yield/substrate conversion) x 100.

It is interesting to note that both heterogenized catalysts showed better performances in terms of conversion and selectivity values than the homogeneous counterpart, with an outstanding improvement for the less activated acrylonitrile substrate. This could be explained by the fact that the SP and MSNP supports might play a certain role in the catalytic pathway, perhaps diminishing the catalyst-self deactivation pathways.

For practical applications the life-time of a catalyst and its level of reusability are very important factors. In this sense, and based on the results shown above, the recyclability of the heterogeneous systems **SP@Ru1** and **MSNP@Ru1** was investigated. In all cases, after the first run the reaction mixture was cooled and the catalyst was recovered by centrifugation (in the case of SP support) or magnetically (in the case of MSNP support), washed with water and introduced in the reaction flask with a new load of substrate under the same experimental conditions.

The results obtained for both heterogeneous systems throughout several consecutive runs using benzonitrile and acrylonitrile as substrates are shown in Figures IV.4.7 and IV.4.8 respectively.

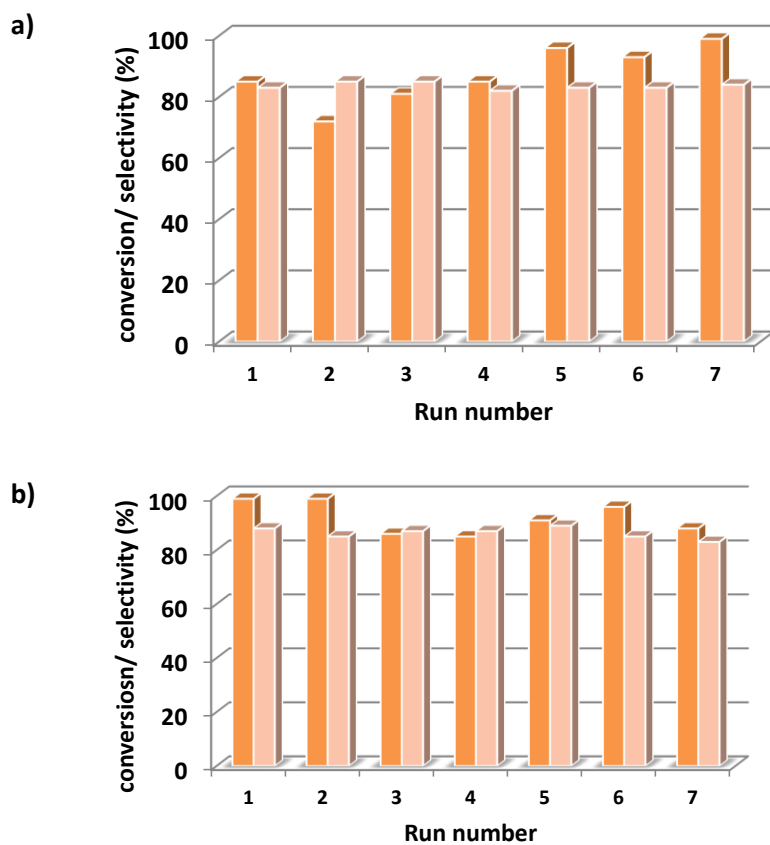


Figure IV.4.7. Conversion (orange bars) and selectivity (pink bars) values obtained throughout consecutive reuses of **SP@Ru1** (a) and **MSNP@Ru1** (b) in the hydration of benzonitrile to benzamide in water (see text for experimental conditions).

Chapter IV

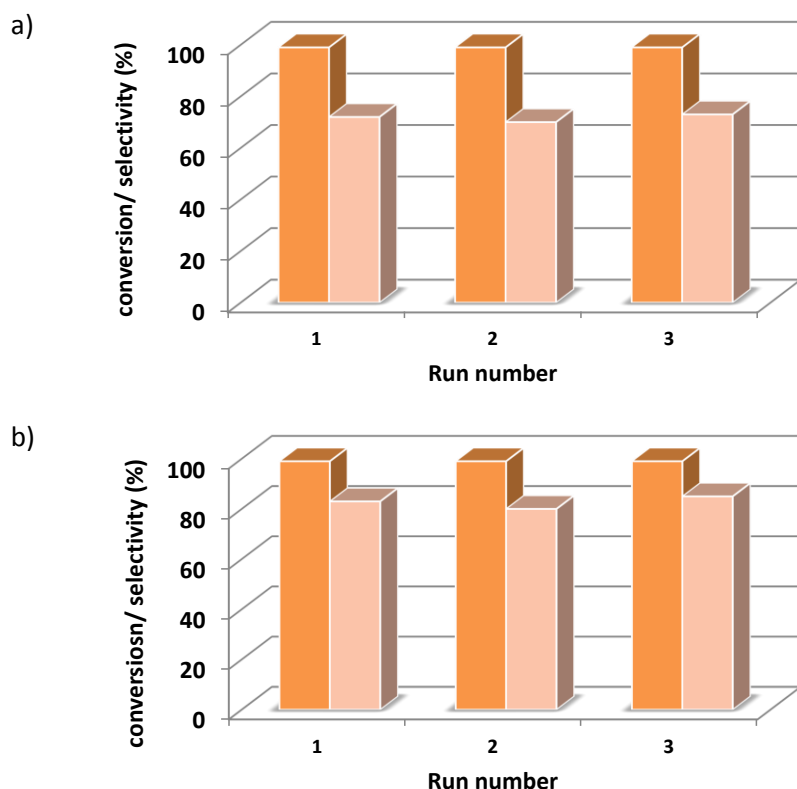


Figure IV.4.8. Conversion (orange bars) and selectivity (pink bars) values obtained throughout consecutive reuses of **SP@Ru1** (a) and **MSNP@Ru1** (b) in the hydration of acrylonitrile to acrylamide in water (see text for experimental conditions).

One can observe that the catalysts maintain an excellent performance through all the runs, with conversion values above 75 % for benzonitrile and close to 95 % for acrylonitrile when using both heterogeneous systems. The selectivity towards the amide product is also well maintained in similar values to that found for the first run in all cases: for benzonitrile, the average selectivity values are 85 % and 90 % for **SP@Ru1** and **MSNP@Ru1** respectively, whereas in acrylonitrile the SP-based catalyst displays a slightly lower value (~ 70 %) than the **MSNP** (~80 %).

The overall turnover numbers obtained with **SP@Ru1** are 102 for benzonitrile and 43 for acrylonitrile, whereas for **MSNP@Ru1** are 111 and 49 respectively.

In view of these results, the reutilization of **SP@Ru1** and **MSNP@Ru1** systems in the hydration of both benzonitrile and acrylonitrile has demonstrated a good effectiveness, keeping high conversion and selectivity values through all the runs. In the case of the nanoparticles, the magnetic core allows us to attract and remove them from the reaction medium by a magnet, facilitating the reusability of the material.

IV.5. Biological application of some manganese and ruthenium complexes. Evaluation of the activity against tumoral cells.

IV.5.1. Manganese complexes

As it has been exposed in Chapter 1, manganese-based complexes may be valuable antitumor agents though they have been only scarcely studied for such purpose. Mn complexes have potentially fewer side effects and are more environment-friendly compared to other metals. Moreover, some factors such as hydrophobicity (that may help cellular uptake) the presence of chelating ligands (that would control the reactivity towards different biomolecules, and the interaction with them through hydrogen bonding or intercalation) or the occurrence of good leaving groups (which provide vacant sites for metal-interaction with target molecules) would seem to be essential requirements for the cytotoxic activity of Mn complexes.

In previous works, we have studied the coordination of some nitrogen-based ligands such as pyridines,^{138c} bipyridine^{25b,137} and pyrazoles³⁴¹ to manganese ions together with their characterisation and catalytic behaviour in epoxidation reactions. We thought that manganese complexes containing these N-chelating ligands and chloride, triflate or nitrate as labile ligands could show good cytotoxicity against certain cell lines, as has been observed with the α -[Ru(azpy)₂Cl₂] compound, which contains the same type of ligands.²³⁷ These manganese complexes would accomplish most of the aforementioned requirements for anticancer activity and then could be a promising alternative to the current *precious metal* based compounds. Moreover, slight modifications on the ligands such as alkylation at the acidic positions could enhance their hydrophobicity and inertness, thus potentially improving their activity.

The manganese compounds studied in this chapter for this purpose are those with general formula [MnX₂(pypz-H)₂] (X= Cl, **Mn1**; CF₃SO₃, **Mn2**; NO₃, **Mn4**), and complexes [MnCl₂(H₂O)₂(pypz-H)] (**Mn5**), [MnX₂(pypz-Me)₂] (X= Cl, **Mn6**; CF₃SO₃, **Mn7**) and [Mn(CF₃SO₃)₂(pypz-CH₂COOEt)₂] (**Mn8**), which have been fully described and characterized in section IV.1, together with compound [Mn(CF₃SO₃)₂(-)-L)₂] (**Mn10**, see Figure IV.5.1) that was previously synthesized in our group.^{25b,137}

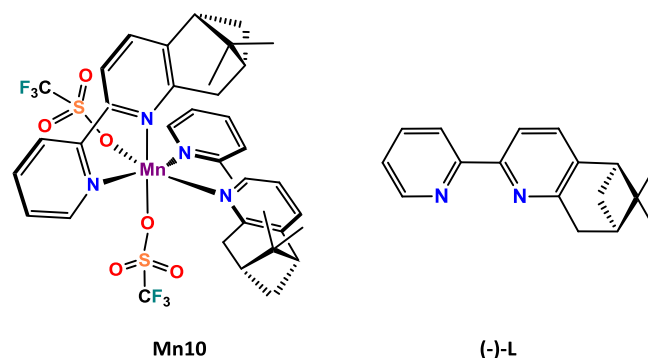


Figure IV.5.1. Structure of complex $[\text{Mn}(\text{CF}_3\text{SO}_3)_2((\text{-})\text{-L})_2]$ (**Mn10**) and the ligand (-)-pinene[5,6]bipyridine ((-)-L).

IV.5.1.1. Stability tests

Before the cytotoxicity measurements, the stability of all the compounds in physiological conditions was tested by monitoring the changes in their UV-Vis spectra after a period of 72 h (Figure SIV.5.1 displays the spectra registered in PBS at pH= 7.4 for complexes **Mn6-10** as representative examples), and no significant changes from the initial spectrum were observed, thus indicating that the compounds are stable in PBS at pH= 7.4. The potential decoordination of N-donor ligands wouldn't lead to significant changes in the maximum absorbance wavelengths given the featureless UV-Vis spectra of free Mn ions but, in parallel, we should expect a considerable drop in the absorbance due to the lower extinction coefficient of the free ligands with respect to the complexes that is not observed experimentally. In order to study the occurrence of rapid changes that could take place in the complexes shortly after solubilization (and that would not be observed in the UV-Vis spectra due to the need of longer times for the preparation of solutions with exact concentrations), some VC experiments were carried out with compounds **Mn6-8** in aqueous solution containing a mixture of NaCl and KCl (0.103 and 0.0049 M respectively) as electrolyte support, which mimics the concentration of these ions in the PBS medium used for UV-Vis spectroscopy. Complexes were dissolved in the NaCl/KCl aqueous solution (1 mg/2 mL) and then their cyclic voltammograms were recorded immediately (Figure IV.5.2 displays the CV obtained for complex **Mn7**). After 30 minutes, little amounts of p-toluene sulfonic acid were added to the solution causing the shift of the redox wave towards upper potential values. The subsequent addition of NaOH shifted the cyclic wave back to lower potentials. This pH dependence of the redox potential presumably indicates the presence of an aqua-complex generated upon substitution of one or two monodentate ligands by water medium within the first few seconds after solubilization. The new species is stable for several days as discussed earlier from UV-Vis experiments.

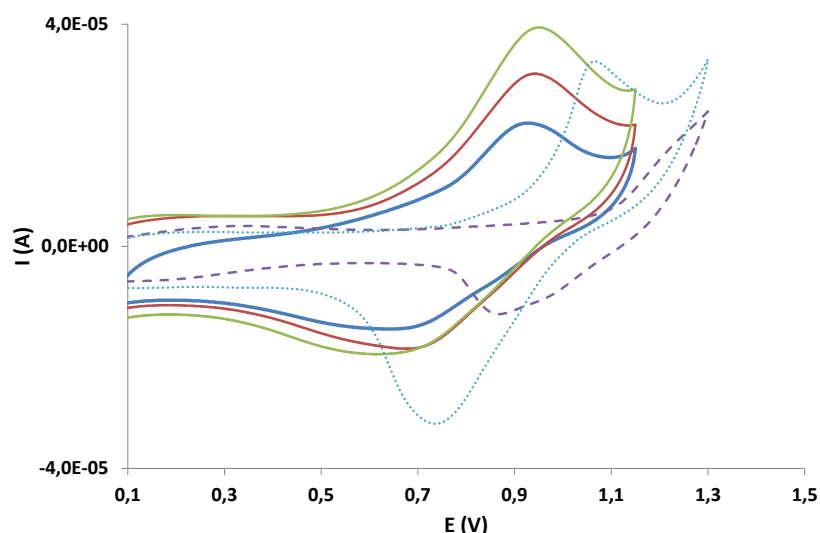


Figure IV.5.2. VC of compound **Mn7** in $\text{H}_2\text{O} + 0.103 \text{ M NaCl}/0.0049 \text{ M KCl}$ vs. SCE. The solid lines correspond to the voltammograms registered after complex solubilization at different times (blue, 25 s; red, 7 min; green, 30 min). The purple dashed line corresponds to the CV obtained after addition of p-toluene sulfonic acid, whereas that recorded after addition of NaOH is displayed as a blue dotted line.

The behaviour displayed by **Mn7** was parallel to that shown by complexes **Mn6** and **Mn8** in the same medium. Other media such as 0.1 M solutions of NH_4PF_6 or $\text{Na}(\text{CF}_3\text{SO}_3)$ were also used (the latest to test the influence of extra triflate anions on the substitution kinetics in the case of complex **Mn8**, that contains triflate as monodentate ligands), leading to similar results (Figure SIV.5.2).

IV.5.1.2. Cytotoxicity assays

The cytotoxic effect of the manganese compounds, containing pyridine-pyrazole (**Mn1-2** and **Mn4-8**) and (-)-pinene[5,6]bipyridine (**Mn10**) ligands, together with different monodentate labile ligands was evaluated in two human cancer cell lines, NCI-H460 and OVCAR-8, after 72 h of exposure to them. Each ligand was also evaluated to discern the role of the manganese moiety on the cytotoxic effect. All the tested compounds exhibited cytotoxic effects in a dose-dependent manner. Table IV.5.1 shows the corresponding IC_{50} values.

Chapter IV

Table IV.5.1. IC₅₀* values (μM) of tested ligands and compounds **Mn1-2**, **Mn4-8** and **Mn10** on the indicated cell lines.

| Compound | NCI-H460 | OVCAR-8 |
|--|------------|-------------|
| [MnCl ₂ (pypz-H) ₂], Mn1 | 124.7±2.6 | 373.1±62.7 |
| [Mn(CF ₃ SO ₃) ₂ (pypz-H) ₂], Mn2 | 189.2±29.2 | 492.4± 93.4 |
| [Mn(NO ₃) ₂ (pypz-H) ₂], Mn4 | 157.2±32.1 | >600.00 |
| [MnCl ₂ (H ₂ O) ₂ (pypz-H)], Mn5 | 132.2±23.5 | 413.1±45.8 |
| [MnCl ₂ (pypz-Me) ₂], Mn6 | 160.8±20.2 | >600.00 |
| [Mn(CF ₃ SO ₃) ₂ (pypz-Me) ₂], Mn7 | 94.3±10.9 | 318.3±53.0 |
| [Mn(CF ₃ SO ₃) ₂ (pypz-CH ₂ COOEt) ₂], Mn8 | 51.3±7.2 | 212.5±37.5 |
| [Mn(CF ₃ SO ₃) ₂ ((-)-L) ₂], Mn10 | 1.7±0.4 | 4,7±0,4 |
| (-)-L | 3.3±0.1 | 15.9±3.8 |
| pypz-Me | >600.00 | >600.00 |
| pypz-CH ₂ COOEt | 160.5±21.3 | >600.00 |
| pypz-H | >600.00 | >600.00 |
| Cisplatin | 1.0±0.1 | 6.9±1.2 |
| Carboplatin | 12.8±2.2 | 110.0±4.2 |

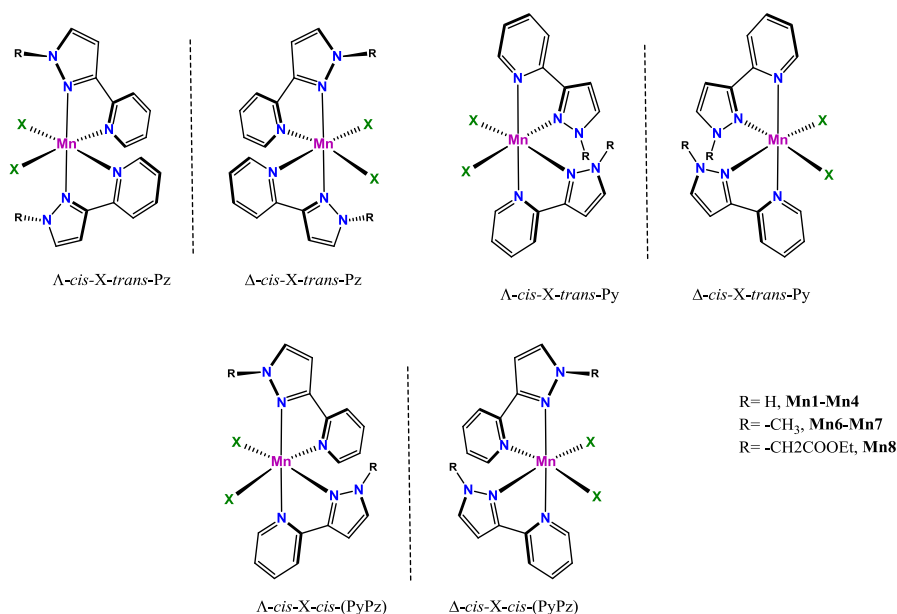
*IC₅₀ values correspond to the concentrations of each compound or its ligands that are required to inhibit cell proliferation by 50 %. Data are presented as mean ± SE of at least three independent experiments conducted in triplicate.

Among the compounds containing pyridine-pyrazole ligands, **Mn7** and **Mn8** are cytotoxic for both cells lines, whereas none of the corresponding *pypz-R* ligands displays significant activity (only a minor effect could be observed in the case of ligand *pypz-CH₂COOEt* on NCI-H460 cell line). Compound **Mn10**, containing the pinene-bipyridine ligand (-)-L, presents a remarkable cytotoxicity that is of the same order of magnitude than that shown by cisplatin for both cell lines and between 10- and 22-fold higher than that of carboplatin for NCI-H460 and OVCAR-8, respectively. In all cases manganese complexes have higher biological activity than their free ligands, confirming that the antitumor activities of pyrazolyl and bipyridyl ligands can be

enhanced by coordinating the corresponding ligand to manganese. In general, the NCI-H460 cell line is more sensitive to the action of compounds than the OVCAR-8 cell line.

Similar to other ruthenium²³⁷ and platinum compounds,³⁴² the *cis*-coordinated labile groups in our complexes could be crucial for the good values obtained in the cytotoxic results, as it seems to be a key factor for the coordination of the metal to DNA.³⁴³ The selectivity toward these bases appears to result from both electronic and steric effects.³⁴⁴ The nature of N-R groups (CH₂COOEt, H or Me) seems also to be important in the activity shown by the different complexes with pyrazolic ligands: as a general trend, complexes containing the less polar alkylated *pypz-Me* and *pypz-CH₂COOEt* ligands display better activities than those containing *pypz-H*, in consistency with hydrophobicity being a favourable requirement for cytotoxic activity as mentioned earlier. An additional influence of the N-R groups over the activity could arise from the potential H-bonding interactions that the R substituents on the pyrazole ring may present around the vacant site after removal of the leaving groups. If we compare, for instance, compounds **Mn6-Mn8**, we can observe that manganese compound **Mn8**, which shows the *cis-X-trans-pz* geometry (see Scheme IV.5.1), places the two N-CH₂COOEt groups of the N-pyrazole ligands in *cis* to each monodentate labile group, a fact that could favour a best accessibility or interaction through hydrogen bonding with some biomolecules approaching the vacant sites; in the case of complex **Mn7**, only one N-CH₃ group is in *cis* to the labile positions and for complex **Mn6** these N-CH₃ groups are situated *trans*- to these groups, thus exerting low influence. Complexes **Mn1**, **Mn2** and **Mn4** display the same *cis-X-trans-pz* geometry than complex **Mn8** and, consequently, the geometrical isomer itself is not a determinant factor for cytotoxicity. Nevertheless, the geometry determines the spatial disposition of the N-R substituents which seems to be important in the antiproliferative activity of the pyrazolic complexes, with a certain contribution of the polarity of the substituents on the ligands as the more polar N-H groups instead of N-R organic substituents seem to slightly worsen the cytotoxicity activity.

Chapter IV



Scheme IV.5.1. Diastereoisomers obtained for [MnX₂(pypz-R)₂] complexes (R = -H, -CH₃ or -CH₂COOEt), **Mn1-4** and **Mn6-8**.

Compound **Mn10**, which contains the more apolar ligand (-)-L and that presents pyridine rings in *cis* to the labile positions, exhibits increased activity. In concordance with the results obtained for the series of pyrazole ligands described above, we can assert that an overall increase in the hydrophobicity of the compounds seems to have certain importance since compounds **Mn7** and **Mn8**, and particularly **Mn10** exhibit the highest cytotoxic effect. However, an additional influence of the leaving group can be also postulated here, as these three compounds contain triflates as monodentate anionic ligands. The presence of triflate seems to have a positive influence on the cytotoxicity activity when comparing for instance compounds **Mn6** and **Mn7**, with the chloro compounds **Mn6** displaying lower activity. This fact could be related to an easier dissociation of the triflate groups that could facilitate the coordination of the metal ion to target molecules.

Taking into account the higher antiproliferative effect of compound **Mn10**, and the remarkable difference with respect to the rest of the compounds containing pyrazole ligands, we further investigated its cytotoxicity on a panel of breast tumour cell lines (MCF7, SK-BR-3 and MDA-MB-231) as well as on the CC18-Co non-tumour cell line (Table IV.5.2). Compound **Mn10** is twice more cytotoxic than its ligand on the three breast cancer cell lines representatives of tumours ER⁺ PR⁺ (MCF7), Her2⁺ (SK-BR-3) and triple negative (MDA-MB-231). At the same time, it is clearly selective for cancer cells because its IC₅₀ value for the non-tumour cell line CC18-Co is higher than 30 μM.

Table IV.5.2. IC₅₀^a values (μM) of compound **Mn10** and its ligand on the indicated cell lines.

| Cell line | Compound Mn10 | (-)-L |
|------------|---------------|----------|
| MCF7 | 5.4±0.4 | 11.9±1.9 |
| MDA-MB-231 | 7.5±1.1 | 15.5±0.3 |
| SK-BR-3 | 15.1±1.6 | 27.1±1.7 |
| CCD-18Co | >30 | >30 |

^a IC₅₀ values correspond to the concentrations of each compound or its ligands that are required to inhibit cell proliferation by 50 %. Data are presented as mean ± SE of at least three independent experiments conducted in triplicate.

Provided the interesting results of compound **Mn10** we further characterized how its antiproliferative effect may be exerted.

IV.5.1.2.1. Analysis of compound Mn10 treatment on the cell cycle phase distribution

The effect of **Mn10** on the OVCAR-8 and NCI-H460 cell cycle phase distribution has been investigated by flow cytometry. For comparison, the effect of its ligand was also analyzed. After 72 h of exposure to compound **Mn10** or to its ligand, it can be observed only a minor accumulation on the G₀/G₁ cell cycle phase (see Figure SIV.5.5) compared to that of untreated growing cells in OVCAR-8 and in NCI-H460 cells (Table IV.5.3).

Chapter IV

Table IV.5.3. Effects of compound **Mn10** and its ligand at the indicated concentrations on the OVCAR-8 and NCI-H460 cell cycle phase distribution after treatment for 72 h. Untreated OVCAR-8 and NCI-H460 cells were used as control.

| OVCAR-8 ^a | Control | Mn10 | | (-)-L | |
|----------------------|---------|-----------|------------|-----------|------------|
| | | 5 μ M | 24 μ M | 5 μ M | 24 μ M |
| G0/G1 | 52.9 | 58.2 | 64.7 | 58.8 | 63.6 |
| S | 30.1 | 27.3 | 21.5 | 27.0 | 24.0 |
| G2/M | 15.8 | 14.1 | 11.8 | 13.5 | 10.9 |

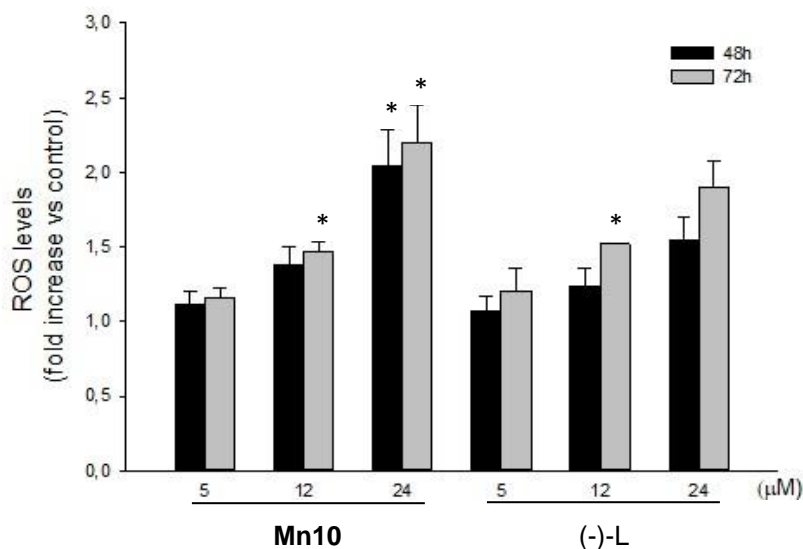
| NCI-H460 ^a | Control | Mn10 | | (-)-L | |
|-----------------------|---------|-----------|-----------|-----------|-----------|
| | | 2 μ M | 9 μ M | 2 μ M | 9 μ M |
| G0/G1 | 65.7 | 62.4 | 72.2 | 60.9 | 71.5 |
| S | 20.6 | 22.1 | 16.8 | 25.4 | 18.4 |
| G2/M | 13.8 | 15.3 | 10.4 | 13.6 | 9.8 |

^a Treated cells were permeabilized and stained with PI. Cell DNA content was analyzed by flow cytometry. Data are representative of three independent assays. Values were analyzed from 10,000 total events.

IV.5.1.2.2. ROS generation triggered by compound Mn10

To determine whether ROS play an important role in the antiproliferative effect induced by compound **Mn10**, we investigated by flow cytometry whether the treatment with this compound increased the levels of ROS in OVCAR-8 and NCI-H460 cells. Cells were treated for 48 or 72 h with compound **Mn10** at different concentrations and then labelled with carboxy-H2DCFDA, which is oxidized to green fluorescent dichlorofluorescein in presence of ROS thus allowing quantification (see Chapter 3, experimental section). For comparison, the effect of the ligand was also analyzed. As it is observed in Figure IV.5.3, the ROS levels increase with time and concentration in both cell lines either with the compound **Mn10** or its ligand. The effect of compound **Mn10** is higher than that of the ligand and, in the NCI-H460 cell line, the ROS production is enhanced compared to OVCAR-8.

(A) OVCAR-8



(B) NCI-H460

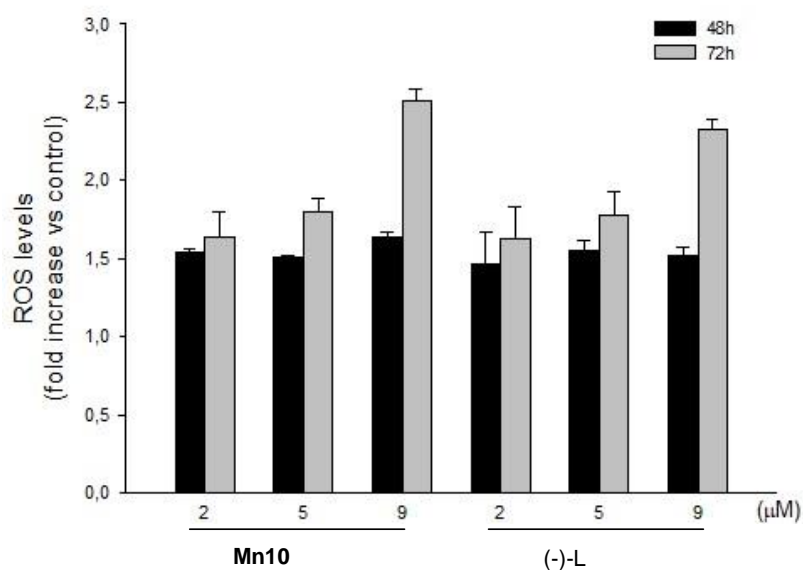


Figure IV.5.3. ROS production triggered by compound **Mn10** and its ligand in OVCAR-8 (A) and NCI-H460 (B) cell lines. Cells were treated for 48 and 72 h with the compound or (-)-L and generation of ROS was measured by flow cytometry after labelling with carboxy-H2DCFDA (see the text for more details). ROS levels are indicated as fold-increase vs. control (non-treated cells). Values were analyzed from 10,000 total events. Data are presented as mean \pm SE of at least three independent experiments. Differences versus untreated cells were considered significant at * $p < 0.05$.

Further, we investigated whether the increase of ROS could explain the antiproliferative effect of compound **Mn10**. We measured cellular viability, using the MTT assay, of NCI-H460 cell line treated with different concentrations of compound **Mn10** or its ligand in the presence and absence of the reducing agent N-acetyl cysteine (NAC). This reducing agent counteracts the

Chapter IV

ROS production in the cells. Figure IV.5.4 shows that the presence of NAC reduces the antiproliferative effect of compound **Mn10** at all the concentrations assayed. We also investigated whether compound **Mn10** was able to generate ROS in vitro evaluating its ability to consume ascorbic acid. The results were negative, indicating that the compound does not produce ROS by itself. This result seems to indicate that compound **Mn10** increases intracellular ROS concentration by affecting those enzymes that control the homeostasis of ROS.

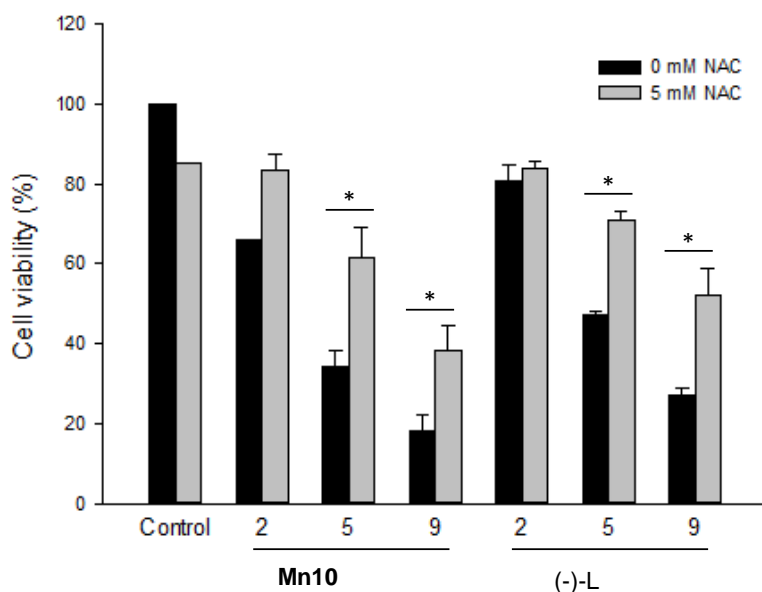


Figure IV.5.4. Cellular viability of NCI-H460 cells after treatment with compound **Mn10** and its ligand in the presence and absence of N-acetyl cysteine (NAC). Cellular viability was measured by the MTT assay. Data are presented as mean \pm SE of at least three independent experiments. Differences in the cell viability values of cells with and without NAC treatment were considered significant at * $p < 0.05$.

IV.5.1.2.3. Binding of compound **Mn10** to proteins and DNA

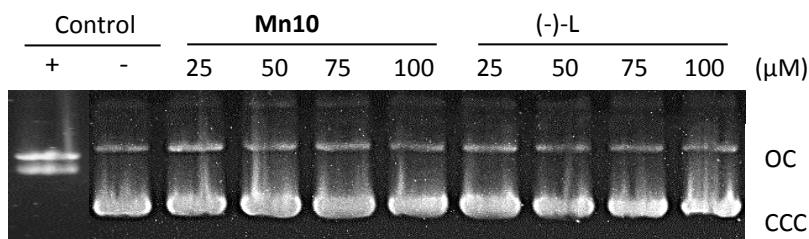
We tested the ability of compound **Mn10** to interact with protein models and DNA. Protein interaction of compound **Mn10** and its ligand was tested using three different protein models: chicken egg lysozyme, human pancreatic ribonuclease and cytochrome C, by following the changes in the complex UV-Vis spectra after the addition of the protein at different times for a period of 48 h (metal:protein molar ratio 4:1). In any case the spectrum of compound **Mn10**, which displays a maximum at 292 nm, was changed (Figure SIV.5.3) indicating that compound **Mn10** does not interact with these model proteins.

To test the ability of **Mn10** and its ligand to interact with DNA, three different concentrations of the compound and its ligand were incubated with DNA (plasmid pUC18) at 37 °C for 24 h and the effects were analysed in an agarose gel electrophoresis. The results are shown in Figure IV.5.5A. As can be observed, neither the ligand nor the compound are able to interact

with DNA since at all the concentrations assayed the bands observed, corresponding to the supercoiled form (CCC) and circular nicked form (OC), are identical to those of the negative control (plasmid pUC18 alone). In contrast, cisplatin, the positive control, promotes the described effect on DNA i.e., the migration of the CCC form decreases until it co-migrates with relaxed (OC form) to reach the coalescence point.³⁴⁵ Taking into account the results of ROS generation by **Mn10** we performed the same assay of DNA interaction in the presence of H₂O₂. It can be observed (Figure IV.5.5B) that, in the presence of H₂O₂, increasing concentrations of **Mn10** from 25 to 100 μM are able to change the ratio of the CCC to OC form of DNA and at 75 μM concentration it is also observed the appearance of a band corresponding to the linear form of plasmid pUC18 (L) that is formed when both DNA strands are broken. Finally, at 100 μM, degradation of DNA is clearly produced. In contrast, the ligand does not have any effect in the DNA topology even at the maximum concentration assayed when compared with the negative control (plasmid pUC18 alone). Thus, we can conclude that in the presence of ROS compound **Mn10** cuts the DNA and promotes its degradation presenting a different behaviour from that observed for cisplatin in this assay. Provided that compound **Mn10** and its ligand trigger ROS generation, the fact that the latter does not cut the DNA may explain the higher antiproliferative effect of the compound. This result confirms that ligand coordination enhances the cytotoxic properties.

Chapter IV

A)



B)

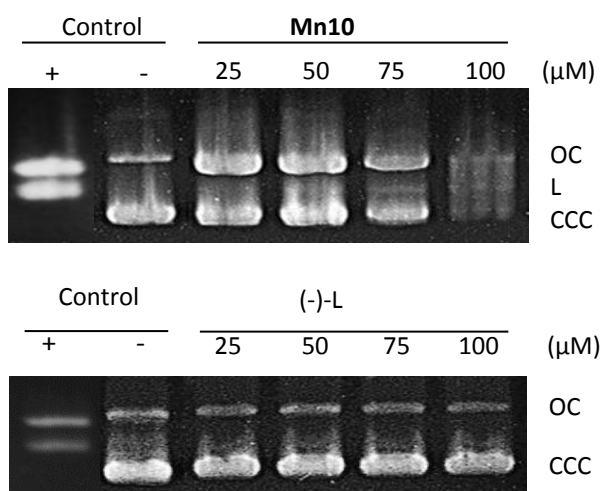


Figure IV.5.5. Agarose gel electrophoresis of pUC18 plasmid DNA treated with different concentrations (indicated in μM) of compound **Mn10** and its ligand in the absence (A) and presence (B) of H_2O_2 . (A) From left to right, lane 1, cisplatin (positive control), lane 2 plasmid pUC18 alone (negative control), lanes 3–6 increasing amounts of compound **Mn10** and lanes 7–10 increasing amounts of ligand (–)-L; (B) From left to right in both gels (Mn10 and (–)-L), lane 1 cisplatin (positive control), lane 2 plasmid pUC18 alone (negative control), lanes 3–6 increasing amounts of compound Mn10 or its ligand ((–)-L). OC = open circular form; CCC = covalently closed circular form; L = linear form.

IV.5.2. Ruthenium complexes

The ruthenium compounds studied in this chapter for this purpose are **Ru4–6**, with general formula $[\text{RuCl}_2(\text{L})_2(\text{dmsO})_2]$ (L= pz-H (**Ru4**), 3,4-dmpz-H (**Ru5**), 3,5-dmpz-H (**Ru6**)), which have been fully described and characterized in Chapter 5, together with compounds $[\text{RuCl}_2(\text{pypz-H})(\text{dmsO})_2]$ (**P2**), $[\text{RuCl}_2(\text{bpea})(\text{dmsO})]$ (**Ru12**),^{106c} $[\text{RuCl}_2(\text{NO}_2\text{-pzH})(\text{dmsO})_3]$ (**Ru13**)^{184b} and $[\text{RuCl}(\text{pypz-H})(9\text{S3})]\text{Cl}$ (**Ru14**),³⁴⁶ that were previously synthesized in our group (see Figure IV.5.6).

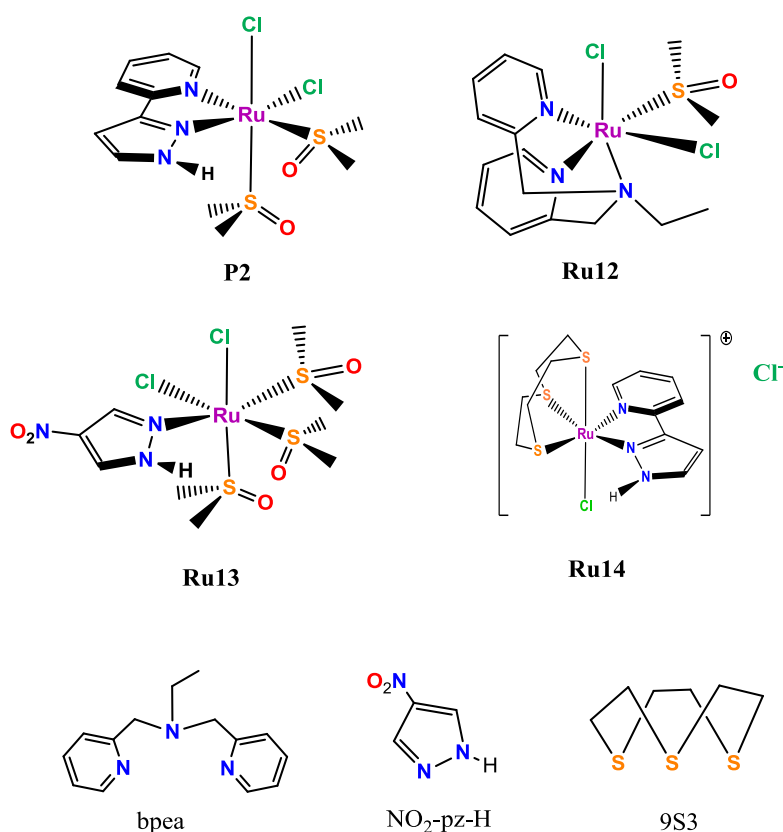


Figure IV.5.6. Structures of complexes $[\text{RuCl}_2(\text{pypz-H})(\text{dmsO})_2]$ (**P2**), $[\text{RuCl}_2(\text{bpea})(\text{dmsO})]$ (**Ru12**), $[\text{RuCl}_2(\text{NO}_2\text{-pzH})(\text{dmsO})_3]$ (**Ru13**), $[\text{RuCl}(\text{pypz-H})(9\text{S3})]\text{Cl}$ (**Ru14**) and the free ligands *N,N*-bis(pyridin-3-yl)methanamine (bpea), 4-nitro-1*H*-pyrazole ($\text{NO}_2\text{-pz-H}$) and 1,4,7-trithionane (9S3).

IV.5.2.1. Stability tests

Before the cytotoxicity measurements, the stability of all the compounds in physiological conditions was tested by monitoring the changes in their UV-Vis spectra after a period of 72 h (see SI, Figure SIV.5.4). For complex **Ru14**, a rapid substitution of the chlorido ligand by water or another component of the working medium takes place immediately after solubilization in aqueous media as evidenced by previously in our group³⁴⁶ and, after that, its UV-Vis spectra did not experiment any further change for 72 h. In overall, all the compounds were stable in PBS/complete medium at pH 7.4.

IV.5.2.2. Cytotoxicity assays

As described earlier for Mn complexes, the cytotoxic effect of the above-mentioned ruthenium compounds was evaluated in two human cancer cell lines, NCI-H460 and OVCAR-8, after 72 h of exposure to them. Each ligand was also evaluated to discern the role of the ruthenium moiety on the cytotoxic effect. All the tested compounds exhibited cytotoxic effects in a dose-dependent manner. Table IV.5.4 shows the corresponding IC_{50} values.

Chapter IV

Table IV.5.4. IC₅₀* values (μM) of tested ligands and compounds **Ru4-6**, **P2** and **Ru12-14** on the indicated cell lines.

| Compound | NCI-H460 | OVCAR-8 |
|--|------------|------------|
| [RuCl ₂ (pz-H) ₂ (dmsO) ₂], Ru4 | 308.0±31.6 | 338.0±31.6 |
| [RuCl ₂ (3,4-dmpz-H) ₂ (dmsO) ₂], Ru5 | 125.5±32.7 | 203.6±50.0 |
| [RuCl ₂ (3,5-dmpz-H) ₂ (dmsO) ₂], Ru6 | 187.0±50.5 | 215.6±48.0 |
| [RuCl ₂ (pypz-H)(dmsO) ₂], P2 | 370.7±21.0 | 532.3±35.5 |
| [RuCl ₂ (bpea)(dmsO)], Ru12 | 325.0±38.5 | >600.00 |
| [RuCl ₂ (NO ₂ -pz-H)(dmsO) ₃], Ru13 | >600.00 | >600.00 |
| [RuCl(pypz-H)(9S3)], Ru14 | 149.0±31.1 | 234.2±46.5 |
| pz-H | >600.00 | >600.00 |
| 3,4-dmpz-H | >600.00 | >600.00 |
| 3,5-dmpz-H | >600.00 | >600.00 |
| bpea | 48,6±20.0 | 108.7±15.0 |
| pypz-H | >600,00 | >600.00 |
| NO ₂ -pz-H | >600.00 | >600.00 |
| 9S3 | >600.00 | >600.00 |
| Carboplatin | 12.8±2.2 | 110.0±4.2 |

*IC₅₀ values correspond to the concentrations of each compound or its ligands that are required to inhibit cell proliferation by 50 %. Data are presented as mean ± SE of at least three independent experiments conducted in triplicate.

As it can be observed in Table IV.5.4, all compounds show in general higher cytotoxicities towards the NCI-H460 than for the OVCAR-8 cell lines, as is also the case for Mn complexes (see Table IV.5.1). However, although they are active for both cancer cell lines tested, the IC₅₀ values obtained are rather high when compared to those presented by carboplatin or other ruthenium compounds previously described in the literature.³⁴⁷ On the other hand, as a general trend the IC₅₀ values of the free ligands are higher than those presented by the ruthenium complexes tested, thus indicating that the presence of metal is necessary to achieve

cytotoxicity, except for the case of the *bpea* ligand, which presents lower IC_{50} values for both cell lines and therefore higher cytotoxicity than the corresponding complex **Ru12**. For the OVCAR-8 cell line, the IC_{50} value obtained for *bpea* is similar to the one presented by carboplatin. This result is interesting as the majority of the clinical therapeutic treatments against the human ovarian cancer are based in the administration of platinum-based complexes.

The possible binding to DNA of complexes **Ru5-6**, which in general present the lowest IC_{50} values among all the compounds tested, together with the free *bpea* ligand, was studied by incubating them with plasmid pUC18 at 37 °C for 24 h and the effects were analysed in an agarose gel electrophoresis. Neither the ligand nor the compounds were able to interact with DNA since at all the concentrations assayed the bands observed are identical to those of the negative control (plasmid pUC18 alone, see Figure IV.5.7).

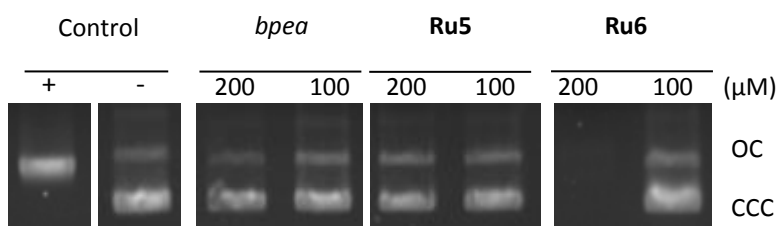


Figure IV.5.7. Agarose gel electrophoresis of pUC18 plasmid DNA treated with different concentrations (indicated in μ M) of compounds Ru5-6 and ligand *bpea*. From left to right, lane 1, cisplatin (positive control), lane 2 plasmid pUC18 alone (negative control), lanes 3–8 indicated concentrations of *bpea* and complexes Ru5 and Ru6. OC = open circular form; CCC = covalently closed circular form.

IV.5.3. Summary

For all the manganese compounds assayed, complexes have higher biological activity than their free ligands, confirming that the antitumor activities of pyrazole and bipyridine ligands can be enhanced by coordinating the corresponding ligand to manganese. Among all the characteristics of the ligands, their hydrophobic character seems to be critical to enable them with antiproliferative activities. Compound **Mn10** has been chosen since it presents a higher hydrophobic character than the rest of the compounds containing pyrazole ligands. The cytotoxicity of this compound in vitro is of the same order of magnitude than that shown by cisplatin for both cell lines and even higher than that of carboplatin. We show that compound **Mn10** inhibits the proliferation of cancer cells by triggering the generation of reactive oxygen species and by binding to DNA.

Chapter IV

Although the IC_{50} values obtained for all the ruthenium compounds tested in this work were too high to do a further investigation about their mechanisms of action, these results prompted us to keep investigating about these kind of complexes in order to obtain new ruthenium complexes with higher cytotoxicities than those found in the literature.

Surprisingly, the *bpea* ligand showed a remarkable cytotoxicity against both cancer cell lines tested (NCI-460 and OVCAR-8), specially towards the human cancer cell line OVCAR-8.

Chapter V. Conclusions

This PhD Thesis collects the synthesis and thorough study of new Mn and Ru compounds containing N-donor ligands as catalysts in important transformations as epoxidation of alkenes and nitrile hydration reactions. The immobilization of these compounds onto different silica supports as well as the use of different solvent media allow the reutilization of the catalysts in the mentioned processes. Also, this work provides novel potential chemotherapeutic agents against two human cancer cell lines, OVCAR-8 and NCI-H460. The most important conclusions arising from the present work are summarized below:

Regarding manganese complexes

- New manganese complexes containing the bidentate ligands 2-(3-pyrazolyl)pyridine, *pypz-H*, 2-(1-methyl-3-pyrazolyl)pyridine, *pypz-Me*, 2-(1H-pyrazol-3-yl)phenol, *HOphpz-H*, and 3-(2-pyridyl)-1-(pyrazolyl)acetic acid ethylester, *pypz-CH₂COOEt*, have been synthesized and thoroughly characterized by analytical, structural and electrochemical techniques. The complexes prepared are: $[\text{Mn}^{\text{II}}\text{X}_2(\text{pypz-H})_2]$ ($\text{X} = \text{Cl}^-$, **Mn1**; CF_3SO_3 , **Mn2**; OAc , **Mn3**; NO_3 , **Mn4**), $[\text{Mn}^{\text{II}}\text{Cl}_2(\text{pypz-H})(\text{H}_2\text{O})_2]$ (**Mn5**), $[\text{Mn}^{\text{II}}\text{X}_2(\text{pypz-Me})_2]$ ($\text{X} = \text{Cl}^-$, **Mn6**; CF_3SO_3 , **Mn7**), $[\text{Mn}^{\text{II}}(\text{CF}_3\text{SO}_3)_2(\text{pypz-CH}_2\text{COOEt})_2]$ (**Mn8**) and $[\text{Mn}^{\text{III}}\text{Cl}(\text{Ophpz-H})_2]$ (**Mn9**).
- The X-ray structures for complexes **Mn1-8** display hexacoordinated Mn(II) ions, with distorted octahedral geometry around the metal. Among these, complexes **Mn1-4**, bearing two units of the *pypz-H* ligand, are obtained in all cases as the Δ/Λ *cis-X-trans*-py isomer, which seems to be energetically favoured thanks to H-bonding interactions involving the pyrazolic H atoms and the monodentate ligands. In contrast, for manganese complexes with *pypz-Me* or *pypz-CH₂COOEt* ligands other H-bonding interactions, along with steric factors, lead to obtaining different diastereoisomers: Δ/Λ *cis-Cl-trans-py* for **Mn6**, Δ/Λ *cis-CF₃SO₃-cis-(PyPz)* for **Mn7** and Δ/Λ *cis-CF₃SO₃-trans-pz* for **Mn8**. Complex **Mn5**, containing one unit of the *pypz-H* ligand, is the first co-crystal consisting of two isomers of a hexacoordinated Mn(II) species, *trans-Cl-cis-H₂O* and *cis-Cl-trans-H₂O*. Finally, complex **Mn9**, containing two *Ophpz-H*⁻ and one chlorido ligand, displays a penta-coordinated Mn(III) environment and has been obtained as a single isomer.
- The redox properties of all complexes have been studied by cyclic voltammetry (CV) and differential pulse voltammetry (DPV) experiments in CH₃CN. Complexes **Mn1-8** exhibit one-electron Mn(III/II) redox processes and, among those containing the *pypz-H* ligand, the triflate (**Mn2**), acetate (**Mn3**) and nitrate (**Mn4**) compounds are oxidized at higher potentials than the structurally similar chlorido complex **Mn1** and the bis-Cl bis-

H₂O compound **Mn5**, which can be explained in terms of the stronger electron-donating capacity of chlorido ligands compared to the above mentioned anions. A similar behaviour has been observed for **Mn6-8** containing the substituted *pypz-R* ligands, where the redox potential values presented by the triflate complexes **Mn7** and **Mn8** are again higher than that of the chlorido **Mn6** complex. These results have shown that neither the geometric isomer nor the type of substituent on the pyrazole ring (H, Me or CH₂COOEt) exert any substantial effect on the redox properties of these compounds.

- Finally, complex **Mn9** shows an irreversible oxidation process which can be assigned to the Mn(IV/III) redox pair. The Mn(III/II) redox pair has not been observed in the potential range from -0.6 to 1.5 V, indicating that the coordination of three anionic ligands to Mn highly destabilizes the Mn(II) oxidation state.
- All the manganese complexes synthesized have been tested as precatalysts in styrene epoxidation in acetonitrile medium using peracetic acid as oxidant. Among the six-coordinated complexes **Mn1-5**, containing the *pypz-H* ligand, an increased performance in the oxidation of this substrate is observed for the chlorido complexes **Mn1** and **Mn5** with respect to triflate, acetate and nitrate compounds. This reveals the role of the monodentate ligands in the catalytic activity observed, which can arise from distinctive intermediate species or from faster oxidation kinetics due to the higher electron donating ability of Cl ligands in the case of **Mn1**. For pyrazole-substituted complexes **Mn6-8**, worse conversion values were obtained probably due to steric factors which can slow the kinetics for the decoordination of the monodentate ligands, and also to electronic effects arising from the increased electron-donor character of the substituents at the *pypz-R* ligands. Finally, the pentacoordinated Mn(III) complex **Mn9** also shows moderate performance, probably due to the relative stabilization of a high-valent intermediate species by the electron-donor character of phenolate and chlorido anionic ligands.
 - Other aromatic and aliphatic substrates were tested with complexes **Mn1**, **Mn5** and **Mn6-9** with better conversion values obtained for aliphatic olefins in all cases, suggesting the involvement of a catalytic electrophilic active species. This is in agreement with the 4-vinylcyclohex-1-ene substrate being epoxidized specifically at the more electron-rich ring position with all catalysts

- The epoxidation of aromatic substrates with complexes **Mn1**, **Mn5** and **Mn6-9** evidences the influence of structural factors in the epoxidation of *cis*- and *trans*- β -methylstyrene, for which the pentacoordinated catalyst **Mn9** displays the best conversion values, in contrast to that observed for styrene. In the case of aliphatic substrates, both electronic and steric factors are manifested: on one hand, electronic factors can explain the better performance displayed by compound **Mn1**, containing two pyrazolic ligands, in comparison to that presented by **Mn5**, with only one pyrazolic ligand and for which a less electrophilic active species can be expected. However, structural factors must be determinant in the excellent conversion and selectivity values displayed by the pentacoordinated complex **Mn9**, where a poorly electrophilic active species will be presumably formed. These results highlight the crucial role that pyrazolic ligands seem to have in the fine tuning of the intermediate species formed during oxidative catalysis.
- Regarding the selectivity in the epoxidation of *cis*- β -methylstyrene, moderate to high percentages of epoxide are obtained, but with a certain degree of *cis* to *trans* isomerization, which suggest the presence of a long-lived free substrate radical during the oxygen transfer process. These results are in agreement with computational calculations performed on complex **Mn1**, which predict a lower barrier for the closure of the *cis* epoxide than for the isomerization step, but with a small overall energy difference ($0.6 \text{ Kcal}\cdot\text{mol}^{-1}$) that explains the partial formation of the thermodynamically more stable *trans* epoxide.
- The catalytic olefin epoxidation in different solvents (glycerol, IL:CH₃CN and IL) has been studied, using the chlorido complexes **Mn1**, **Mn5** and **Mn9** as catalysts using peracetic acid as oxidant. The epoxidation in an ionic liquid:solvent medium, [bmim]PF₆:CH₃CN, shows a remarkable effectiveness and selectivity for the epoxide product, but the presence of acetonitrile is essential to achieve good performances. A possible reason is that it could inhibit the hydrolysis and/or overoxidation of the product. Also, an excellent degree of reusability in the epoxidation of some alkenes in this medium has been observed for catalysts **Mn1** and **Mn6** without loss of activity and keeping high conversion and selectivity values after twelve cycles. When glycerol is used as solvent, the selectivity values for the corresponding epoxides are moderate to low, with only moderate conversion degrees.

Chapter V

- Complex **Mn8** has been successfully immobilized onto a silica support and the new functionalized silica has been characterized by spectroscopic techniques (UV-Vis, ICP-AES). The heterogeneous catalytic activity has been tested with regard to the epoxidation of some alkenes using peracetic acid as oxidant, and its reutilization allowed the effective recyclability of this catalytic system through several consecutive runs.
- Manganese compounds **Mn1-9** together with complex $[\text{Mn}^{\text{II}}(\text{CF}_3\text{SO}_3)_2((-)\text{-pinene}[5,6]\text{bipyridine})_2]$ (**Mn10**), previously synthesized in our group, have been studied as potential antitumor agents. Pyrazolic complexes **Mn7** and **Mn8**, and mainly the bipyridyl complex **Mn10**, show a remarkable antiproliferative activity against different human tumour cell lines, OVCAR-8 and NCI-H460. The overall hydrophobic nature of the compounds seems to be a determinant factor in their cytotoxic effect since complexes **Mn7** and **Mn8** (bearing the apolar –Me and –CH₂COOEt substituents at the bidentate ligands) and complex **Mn10** (which contains the pinene-bipyridine ligand) are better than the rest of complexes which contain the more polar *pypz-H* ligand. The geometrical isomer of the complexes is not a determinant factor on the cytotoxicity. The occurrence of triflate as monodentate anionic ligand, as is the case of complexes **Mn7**, **Mn8** and **Mn10**, seems also to have a positive influence on the cytotoxic activity. The antitumor activity displayed by **Mn10** is of the same order of magnitude than that of cisplatin, and kills the cancer cells by generating ROS species that enable it to cut the DNA.

Regarding ruthenium complexes

- New ruthenium(II) dmsO complexes containing the bidentate ligands 3-(2-pyridyl)-1-(pyrazolyl)acetic acid ethylester, *pypz-CH₂COOEt*, 2-(1H-pyrazol-3-yl)phenol, *HOphpz-H*, and 3-(2-methoxyphenyl)pyrazole, *MeOphpz-H*, and the monodentate ligand 3,4-dimethyl pyrazole, *3,4-dmpzH*, have been synthesized and thoroughly characterized by analytical, structural, spectroscopic and electrochemical techniques. The complexes prepared are: *cis,cis*-[RuCl₂(*pypz-CH₂COOEt*)(dmsO)₂] (**Ru1a**), *cis,trans*-[RuCl₂(*pypz-CH₂COOEt*)(dmsO)₂] (**Ru1b**), *cis,trans*-[RuCl₂(*HOphpz-H*)(dmsO)₃] (**Ru2**), *cis,cis*-[RuCl₂(*HOphpz-H*)(dmsO)₂] (**Ru2'**), *cis,trans*-[RuCl₂(*MeOphpz-H*)(dmsO)₃] (**Ru3**) and *cis,cis*-[RuCl₂(*3,4-dmpzH*)(dmsO)₂] (**Ru5**).
- Isomeric complexes **Ru1a** and **Ru1b** are obtained from the same reaction mixture in a 1:2 ratio when using ethanol as reaction solvent, whereas isomerically pure **Ru1b** is

produced in dichloromethane, indicating that the *cis,cis* geometrical isomer is not energetically favoured.

- The crystal structures of all complexes (except for **Ru2**) have been solved by X-ray diffraction analysis and in all cases the Ru metal center adopts an octahedrally distorted type of coordination. The characterization in solution is consistent with the structures obtained in the solid state. The compounds have been mostly obtained as a single geometrical isomer and this can be rationalized taking into account structural and electronic factors as hydrogen bonding and synergistic electronic effects among ligands.
- The redox properties of complexes **Ru1-Ru5** have been investigated. Complexes **Ru1a** and **Ru1b**, containing the *pypz-CH₂COOEt* ligand, exhibit two different behaviours. **Ru1b** shows a reversible monoelectronic Ru(III)/Ru(II) redox wave, whereas **Ru1a** shows an electrochemically irreversible oxidation process due to a quasi-quantitative Ru-S → Ru-O dmsO ligand linkage isomerization in parallel with the oxidation of the Ru^{II}(dmsO-S) species to Ru^{III}(dmsO-O). **Ru2** and **Ru3** exhibit an electrochemically irreversible (III/II) redox process and, in the case of **Ru3**, a certain degree of dmsO linkage isomerization has also been observed. **Ru4-6** show chemically and electrochemically reversible Ru(III/II) redox processes.
- The isomerization process for complex **Ru1a** has been studied through scan rate dependent cyclic voltammograms and the kinetic and equilibrium constants for linkage isomerization have been calculated. The values obtained allow concluding that, in Ru(II) redox state, the dmsO ligand displays a high preference to be bound to the metal through the S atom but this preference is lower than that displayed by similar complexes previously described. Steric hindrance arising from the presence of a bulky ethylester substituent at the *pypz-R* ligand seems to be determinant for the relatively lower thermodynamically stability of **Ru1a** in its Ru(II) form, which is consistent with the lower yield obtained for this complex in the synthesis. In oxidation state (III), the dmsO ligand displays a higher preference to be bound to the metal through the O atom than that shown by other related *cis,cis* complexes.
- The nitrile hydration catalysis has been evaluated for complexes **Ru1-Ru6** under neutral conditions in water as solvent using different nitrile substrates and low-moderate to high conversion and selectivity values were observed. The more activated nitriles show in general better performances, but steric factors worsen the activity in

the case of catalysts **Ru1** and **Ru3**, which display lower conversion values for the bulkier substrates.

- Complex **Ru1** (as a mixture of isomers **Ru1a** and **Ru1b**) has been successfully immobilized onto silica particles (SP) and magnetic silica nanoparticles (MSNP). These heterogeneous systems **SP@Ru1** and **MSNP@Ru1** have been fully characterized by ICP-AES, IR, UV-Vis, SEM, TEM, TGA and XPS, confirming the presence of Ru(II) and the ligand *pypz-CH₂COOSi*~ anchored in both materials.
- The catalytic activity of the heterogeneous systems **SP@Ru1** and **MSNP@Ru1** was tested in the hydration of benzonitrile and acrylonitrile under neutral conditions using water as solvent. Both heterogeneous systems showed better performances in terms of conversion and selectivity values than the homogeneous counterparts. Also, their recyclability was investigated throughout several consecutive runs, showing a good effectiveness and keeping high conversion and selectivity values through all the runs.
- Three new ruthenium(II) compounds containing the tridentate 2,2':6,2''-terpyridine, *trpy*, and the bidentate ligand 2-(3-pyrazolyl)pyridine, *pypz-H*, ligands have been synthesized and fully characterized through analytical, structural, spectroscopic and electrochemical techniques: *cis* and *trans*-[Ru^{II}Cl(*pypz-H*)(*trpy*)](PF₆), **Ru7a** and **Ru7b**, and *trans*-[Ru^{II}(*pypz-H*)(*trpy*)(OH₂)](PF₆)₂, **Ru10**. Other minor products (*trans*-[Ru^{II}(*pypz-H*)(*trpy*)(dmsO)](PF₆)₂, **Ru8**; [Ru₂^{II}Cl(*trpy*)₂(μ-Cl)(μ-*pypz*)](PF₆), **Ru9**; and [Ru₂^{II}(*trpy*)₂(μ-*pypz*)₂](PF₆)₂, **Ru11**, were obtained and characterized in different extent.
- Regarding the two isomers obtained, *cis* and *trans*, **Ru7a** and **Ru7b**, the latter is the most favored one probably due to steric and electronic effects. The aqua complex **Ru10** was easily obtained after refluxing the chlorido complex **Ru7b** in water in the presence of Ag⁺.
- The crystal structures of compound *trans*-[Ru^{II}Cl(*trpy*)(*pypz-H*)](PF₆), **Ru7b**, and that of the minor products *trans*-[Ru^{II}(*pypz-H*)(*trpy*)(dmsO)](PF₆)₂, **Ru8**, [Ru₂^{II}Cl(*trpy*)₂(μ-Cl)(μ-*pypz*)](PF₆), **Ru9**, and [Ru₂^{II}(*trpy*)₂(μ-*pypz*)₂](PF₆)₂, **Ru11**, display an octahedral distorted type of coordination around the Ru metal center with the *trpy* ligand bonded in a meridional manner. In the case of **Ru7b** and **Ru8** the *pypz-H* ligand acts in a bidentate fashion and the sixth coordination site is occupied by the chlorido or dmsO ligand, placed in *trans* respect to the corresponding pyrazole ring. In the case of the dimeric compounds, the deprotonated pyrazole rings of the corresponding *pypz-H* ligands are bridging two ruthenium centers.

- The electrochemical properties of **Ru7a** and **Ru7b** have been investigated. Both complexes exhibit a reversible one electron Ru(III)/Ru(II) redox process, with the *cis*-complex **Ru7a** exhibiting a higher redox potential than that of the *trans*-complex **Ru7b**. This behaviour evidences that the oxidation state (III) is affected by the relative coordination of the pyridylpyrazole ligand to the ruthenium, leading to a greater stabilization of Ru(III) when the pyrazolyl ring is placed in *trans* respect to the σ -donor chlorido ligand.
- The redox characterization of the Ru-aqua complex **Ru10** showed the occurrence of a two-electron (IV/II) redox process. The Pourbaix diagram obtained indicates that two deprotonation processes can take place, which take place at the *pypz-H* and aqua ligands. The redox potential of the Ru(III/II) couple in **Ru10** is lower than that displayed by the analogous *trans*-[Ru^{II}(trpy)(pypz-Me)(OH₂)]⁺² and [Ru(trpy)(bpy)(OH₂)]²⁺ complexes, which is in accordance with the higher electron-donor character of the *pypz-H* ligand with regard to *pypz-Me* or *bpy*. The pKa values for the aqua-complex **Ru10** are also higher than those of the above-mentioned *trpy* complexes, and this is in accordance with the anionic nature of the *pypz*⁻ ligand which is a strong σ -donor and thus make the Ru metal center and the coordinated aqua ligand less acidic.
 - Compound **Ru10** was tested in the epoxidation of different alkenes, showing good conversion and selectivity values for both aliphatic and aromatic substrates. Regarding the *cis*- β -methylstyrene, a certain isomerization to the *trans*-epoxide has been observed, in contrast to the previously reported *trans*-[Ru(trpy)(pypz-Me)(OH₂)]²⁺, for which the isomerization to the *trans*-epoxide is inexistent. Taking into account that both catalysts present similar redox behaviour (with two clearly separated monoelectronic redox processes) their different stereoselectivity could be related to structural factors associated to the presence of the additional methyl group which could hinder the *cis* \rightarrow *trans* rotation of the intermediate species in the catalytic cycle.
 - Regarding the 4-vinylcyclohexene substrate, **Ru10** is specific towards the ring oxidation, in agreement with the formation of an electrophilic catalytic species that would preferably epoxidize the disubstituted ring double bond.
- Complexes **Ru4-6**, together with compounds [RuCl₂(pypz-H)(dmsO)₂] (**P2**), [RuCl₂(bpea)(dmsO)] (**Ru12**), [RuCl₂(NO₂-pzH)(dmsO)₃] (**Ru13**) and [RuCl(pypz-H)(9S3)]Cl (**Ru14**), previously synthesized in our group, were studied as potential antitumor

Chapter V

agents through the study of *in vitro* cytotoxicity against human cancer cell lines, OVCAR-8 and NCI-H460. Although they are active for both cancer cell lines tested, the IC_{50} values obtained are rather high when compared to those presented by carboplatin or other ruthenium compounds previously described in the literature. As a general trend, the IC_{50} values of the free ligands are higher than those presented by the ruthenium complexes tested, thus indicating that the presence of metal is necessary to achieve cytotoxicity, except for the case of the *bpea* ligand, which presents lower IC_{50} values (and therefore higher cytotoxicity) than the corresponding complex **Ru12** for both cell lines. For the OVCAR-8 cell line, the IC_{50} value obtained for *bpea* is similar to the one presented by carboplatin. This result is interesting as the majority of the clinical therapeutic treatments against the human ovarian cancer are based in the administration of platinum-based complexes. Neither the ligand nor the compounds were able to interact with DNA.

Chapter VI. References

- ¹ a) Anastas, P. T. and Warner, J. C. *Green Chemistry: Theory and Practice*. Oxford University Press: Oxford, U.K., **1998**; b) Lancaster, M. in Clark, J. H., Macquarrie, D. J. (eds.) *Handbook of Green Chemistry and Technology*,. Blackwell Publishing: Abingdon (U.K), **2002**; c) Lancaster, M. *Green Chemistry: An Introductory Text*. RSC: London, **2002**; d) Poliakoff, M., Fitzpatrick, J. M., Farren, T. R. and Anastas, P. T. *Science* **2002**, 297(5582), 807-810; e) Anastas, P. T., Kirchhoff, M. *Acc. Chem. Res.* **2002**, 35(9), 686-694; f) Sheldon, R. A. *Green Chem.* **2005**, 7(5), 267-278; g) Sheldon, R. A., Arends, I. W. C. E. and Hanefeld, U. *Green Chemistry and Catalysis*. Wiley-VCH: Weinheim (Germany), **2007**.
- ² a) Capello, C., Fischer, U. and Hungerbühler, K. *Green Chem.* **2007**, 9(9), 927-934; b) García-Marín, H., Van der Toorn, J. C., Mayoral, J. A., García, J. I. and Arends, I. W. C. E. *Green Chem.* **2009**, 11(10), 1605-1609.
- ³ a) Tavor, D., Sheviev, O., Dlugy, C. and Wolfson, A. *Can. J. Chem.* **2010**, 88(4), 305-308; b) Francos, J. and Cadierno V. *Green Chem.* **2010**, 12(9), 1552-1555; c) Balieu, S., El Zein, A., De Sousa, R., Jérôme F., Tatibouët, A., Gatard, S., Pouilloux, Y., Barrault, J., Rollin P. and Bouquillon, S. *Adv. Synth. Catal.* **2010**, 352(11-12), 1826-1833; d) Díaz-Álvarez, A. E., Francos, J., Lastra-Barreira, B., Crochet, P. and Cadierno, V. *Chem. Commun.* **2011**, 47(22), 6208-6227; e) Gu, Y. and Jérôme, F. *Green Chem.* **2010**, 12(7), 1127-1138; f) García, J. I., García-Marín, H., Mayoral, J. A. and Pérez, P. *Green Chem.* **2010**, 12(3), 426-434.
- ⁴ García-Marín, H., Van der Toorn, J. C., Mayoral, J. A., García J. I. and Arends, I. W.C. E. *J. Mol. Cat. A* **2011**, 334(1-2), 83-88.
- ⁵ a) Li, C.-J. *Chem. Rev.* **2005**, 105(8), 3095-3166; b) Li, C.-J. and Chan, T. H. *Comprehensive Organic Reactions in Aqueous Media*. Wiley-VCH: Weinheim (Germany), **2007**; c) Lindström, U. *Organic Reactions in water*. Blackwell Publishing: Oxford (U.K.), **2007**; d) Kerton, F. M. *Alternatives Solvents for Green Chemistry*. RSC Publishing: Cambridge (U.K.), **2009**; e) Skouta, R. *Green Chem. Lett. Rev.* **2009**, 2(3), 121-156; f) Anastas, O. T. and Li, C.-J. *Handbook of Green Chemistry*. Wiley-VCH: Weinheim (Germany), **2010**.
- ⁶ a) Centi, G. and Perathoner, S. *Methods and Tools of Sustainable Industrial Chemistry: Catalysis*, in Cavani, F., Centi, G., Perathoner, S. and Trifiró, F. (eds.) *Sustainable Industrial Chemistry*. Wiley-VCH: Weinheim (Germany), **2009**; b) Plechkova, N. V. and Seddon, K. R. *Chem. Soc. Rev.* **2008**, 37(1), 123-150.
- ⁷ Cornils, B. *Applied homogeneous catalysis with organometallic compounds: a comprehensive handbook in three volumes* (2nd ed.). Wiley-VCH: Weinheim (Germany), **2002**.
- ⁸ a) Ertl, G. *Handbook of heterogeneous catalysis* (2nd ed.). Wiley-VCH, John Wiley distributor: Weinheim (Germany), **2008**; b) Anastas, P. *Handbook of green chemistry*. Wiley-VCH: Weinheim (Germany), **2009**.
- ⁹ a) Gladysz, J. *Chem. Rev.* **2002**, 102(10), 3215-3216; b) Bell, A. T. *Science* **2003**, 299(5613), 1688-1691; c) Schlögl, R. and Abd Hamid, S. B. *Angew. Chem. Int. Ed.* **2004**, 116(13), 1656-1667; d) Thomas, J. M. and

Chapter VI

Thomas, W. J. *Principles and practice of heterogeneous catalysis* (2n ed.). Wiley-VCH: Weinheim (Germany), **2015**.

¹⁰ Francàs, L. *Ruthenium complexes with polynucleating ligands and their capacity to catalytically oxidize water to dioxygen*, Universitat Autònoma de Barcelona, **2011**. <<http://hdl.handle.net/10803/83973>>

¹¹ a) Cozzi, F. *Adv. Synth. Catal.* **2006**, 348(12-13), 1367-1390; b) Dioso, B. M. L., Vankelecom, I. F. J. and Jacobs, P. A. *Adv. Synth. Catal.* **2006**, 348(12-13), 1413-1446; c) Lu, J. and Toy, P. H. *Chem. Rev.* **2009**, 109(2), 815-838.

¹² a) Sheldon, R. A. and van Bekkum, H. *Fine Chemicals through Heterogeneous Catalysis*. Wiley-VCH: Weinheim (Germany), **2001**; b) Sheldon, R. A. *Chem. Commun.* **2008**, 0(29), 3352-3365.

¹³ a) Meille, V. *Appl. Catal. A-Gen* **2006**, 315, 1-17; b) Campanati, M., Fornasari, G. and Vaccari, A. *Catal. Today* **2003**, 77(4), 299-314.

¹⁴ a) McMorn, P. and Hutchings, G., *J. Chem. Soc. Rev.* **2004**, 33(2), 108-122; b) Thomas, J. M., Raja, R. and Lewis, D. W. *Angew. Chem. Int. Ed.* **2005**, 44(40), 6456-6482; c) Dal Santo, V., Liguori, F., Pirovano, C. and Guidotti, M. *Molecules* **2010**, 15(6), 3829-3856.

¹⁵ Ferrer, I. *Development of new reusable materials based on Ru complexes with catalytic activity for olefin epoxidation and nitrile hydration*, Universitat de Girona, **2015**. <<http://hdl.handle.net/10803/322785>>

¹⁶ Gheorghiu, C. C., Salinas-Martínez de Lecea, C. and Román-Martínez, C. M. *Ap. Cat. A: Gen* **2014**, 478, 194-203.

¹⁷ a) Barbaro, P. and Liguori, F. *Chem. Rev.* **2009**, 109(2), 515-529; b) Shaughnessy, K. H. *Chem. Rev.* **2009**, 109(2), 643-710.

¹⁸ a) Parton, R. F., Vankelecom, I. F. J., Casselman, M. J. A., Bezaukhanova, C. P., Uytterhoeven, J. B. and Jacobs, P. A. *Nature* **1994**, 370, 541-544; b) Knops-Gerrits, P.-P., de Vos, D., Thibault-Starzyk, F. and Jacobs, P. A. *Nature* **1994**, 369, 543-546; c) Mori, K., Kagohara, K. and Yamashite, H. *J. Phys. Chem. C* **2008**, 112(7), 2593-2600; d) Le, C.-H., Lin, H.-C., Cheng, S.-H., Lin, T.-S. and Mou, C.-Y. *J. Phys. Chem. C* **2009**, 113(36), 16058-16069.

¹⁹ Dupont, J., de Souza, R. F. and Suarez, P. A. *Chem. Rev.* **2002**, 102(10), 3667-3692; b) Freemantle, M. *Chem. Eng. News* **2001**, 79(1), 21-25.

²⁰ a) Mutin, P. H., Guerrero, G. and Vioux, A. *J. Mater. Chem.* **2005**, 15(35-36), 3761-3768; b) Ribeiro, S. M., Serra, A. C. and Rocha Gonsalves A. *Tetrahedron* **2007**, 63(33), 7885-7981; c) Sayah, R., Framery, E. and Dufaud, V. *Green Chem.* **2009**, 11(10), 1694-1702; d) Stamatis, A., Giasafaki, D., Christoforidis, K. C., Deligiannakis, Y. and Louludi, M. *J. Mol. Catal. A: Chem.* **2010**, 319(1-2), 58-65.

²¹ Ranke, J., Stolte, S., Störmann, R., Arning, J. and Jastorff, B. *Chem. Rev.* **2007**, 107(6), 2183-2206.

- ²² Liu, Y., Zhang, H.-J., Lu, Y., Cai, Y.-Q. and Liu, X.-L. *Green Chem.* **2007**, 9(10), 1114-1119.
- ²³ Wilkes, J. S. *J. Mol. Catal. A: Chem.* **2004**, 214, 11-17.
- ²⁴ a) Hagiwara, R. and Ito, Y. *Fluorine Chem.* **2000**, 105(2), 221-227; b) Huddleston, J. G., Visser, A. E., Reichert, W. M., Willauer, H. D., Broker, G. A. and Rogers, R. D. *Green Chem.* **2001**, 3(4), 156-164.
- ²⁵ a) Ho, K.-P., Wong, W.-L., Lee, L. Y. S., Lam, K.-M., Chan, T. H. and Wong, K.-Y. *Chem. Asian. J.* **2010**, 5(9), 1970-1973; b) Rich, J., Manrique, E., Molton, F., Duboc, C., Collomb, M.-N., Rodríguez, M. and Romero, I. *Eur. J. Inorg. Chem.* **2014**, 2014(16), 2663-2670.
- ²⁶ a) de Bellefon, C., Pollet, E. and Grenouillet, P. *J. Mol. Catal.* **1999**, 145(1-2), 121-126; b) Böhm, V. P. W. and Herrman, W. A. *Chem. Eur. J.* **2000**, 6(6), 1017-1025; c) Rogers, D. R. and Seddon, K. R. *Science* **2003**, 302(5646), 792-793; d) Nakashima, K., Kubota, F., Maruyama, T. and Goto, M. *Ind. Eng. Chem. Res.* **2005**, 44(12), 4368-4372.
- ²⁷ Coma, A. and Garcia, H. *Adv. Synth. Catal.* **2006**, 348(12-13), 1391-1412.
- ²⁸ Blümel, J. *Coord. Chem. Rev.* **2008**, 252(21-22), 2410-2423.
- ²⁹ Bergbreiter, D. E. *Chem. Rev.* **2002**, 102(10), 3345-3384.
- ³⁰ a) Sodhi, R. K., Paul, S. and Clark, J. H. *Green Chem.* **2012**, 14(6), 1649-1656; b) Zucca, P. and Sanjust, E. *Molecules* **2014**, 19(9), 14139-14194.
- ³¹ Zukal, A., Opanasenko, M., Rubes, M., Nachtigall, P. and Jagiello, J. *Cat. Today* **2015**, 243, 69-75.
- ³² a) Maeda, K., Teramura, K., Lu, D., Takata, T., Saito, N., Inoue, Y. and Domen, K. *Nature* **2006**, 440, 295; b) Qiu, X., Miyauchi, M., Yu, H., Ire, H. and Hashimoto, K. *J. Am. Chem. Soc.* **2010**, 132(43), 15259-15267.
- ³³ a) Sirimanne, P., Winther-Jensen, B., Weerasinghe, H. and Cheng, Y. *Thin Solid Films* **2010**, 518(10), 2871-2875; b) Krebs, F. and Biancardo, M. *Sol. Energ. Mat. Sol. C* **2006**, 90(2), 142-165.
- ³⁴ Francàs, L., Sala, X., Benet-Buchholz, J., Escriche, L. and Llobet, A. *Chem. Sus. Chem.* **2009**, 2(4), 321-329.
- ³⁵ Satterfield, C. N. *Heterogeneous Catalysis in Industrial Practice: Catalyst Preparation and Manufacture* (2nd ed). Krieger Publishing Co.: Malabar (USA), **1996**, pp. 87-129.
- ³⁶ Huirache, R., Nava, R., Peza, C. L., Lara, J., Alonso, G., Pawlec, B. and Rivera, E. M. *Materials* **2013**, 6(9), 4139-4167.
- ³⁷ Ameta, K. L. and Penoni, A. *Heterogeneous Catalysis: A Versatile Tool for the Synthesis of Bioactive Heterocycles*. CRC Press Taylor & Francis Group, LLC: Boca Raton (USA), **2015**, pp. 134.
- ³⁸ a) Wang, Z., Xiao, P., Shen, N. and He, B. *Colloids Surf. A Physicochem. Eng. Asp.* **2006**, 276(1-3), 116-121; b) Shätz, A., Hager, M. and Reiser, O. *Adv. Funct. Mater.* **2009**, 19(13), 2109-2115; c) Schmid, G.

Chapter VI

Nanoparticles: From Theory to Application. Wiley-VCH: Weheim (Germany), **2010**; d) Lim, C. W. and Lee, I. S. *Nano Today* **2010**, 5(5), 412-434; e) Polshettiwar, V. and Varma, R. S. *Green Chem.* **2010**, 12(5), 743-754; f) Zhang, F., Jin, J., Zhong, X., Li, S., Niu, J., Li, R. and Ma, J. *Green Chem.* **2011**, 13(5), 1238-1242; g) Polshettiwar, V., Luque, R., Fihri, A., Zhu, H., Bouhrara, M. and Basset, J. M. *Chem. Rev.* **2011**, 111(5), 3036-3075; h) Deng, J., Mo, L. P., Zhao, F. Y., Hou, L. L., Yang, L. and Zhang, Z. H. *Green Chem.* **2011**, 13(9), 2576-2584; i) Mondai, J., Sen, T. and Bhaumik, A. *Dalton Trans.* **2012**, 41(20), 6173-6181; j) Liu, Y. H., Deng, J., Gao, J. W. and Zhang, Z. H. *Adv. Synth. Catal.* **2012**, 354(2-3), 441-447; k) Li, P. H., Li, B. L., An, Z. M., Mo, L. P., Cui, Z. S. and Zhang, Z. H. *Adv. Synth. Catal.* **2013**, 355(14-15), 2952-2959; l) Ma, F. P., Li, P. H., Li, B. L., Mo, L. P., Liu, N., Kang, H. J., Liu, Y. N. and Zhang, Z. H. *Appl. Catal. A Gen.* **2013**, 457, 34-41; m) Lu, J., Li, X. T., Ma, E. Q., Mo, L. P. and Zhang, Z. H. *ChemCatChem* **2014**, 6(10), 2854-2859.

³⁹ a) Shylesh, S., Schünemann, V. and Thiel, W. R. *Angew. Chem. Int. Ed.* **2010**, 49(20), 3428-3459; b) Vaquer, L., Riente, P., Sala, X., Janast, S., Benet-Buchholz, J., Llobet, A. and Pericàs, M. A. *Catal. Sci. Technol.* **2013**, 3(3), 706-714.

⁴⁰ a) Zoreh, N., Hosseini, S. H., Pourjavadi, A. and Bennet, C. *RSC Adv.* **2014**, 4(91), 50047-50055; b) Safari, J. and Javadian, L. *RSC Adv.* **2014**, 4(90), 48973-48979; c) Keypour, H., Balali, M., Haghdoost, M. M. and Bagherzadeh, M. *RSC Adv.* **2015**, 5(66), 53349-53356.

⁴¹ Zhu, C. L., Zhang, M. L., Qiao, Y. J., Xiao, G., Zhang, F. and Chen, Y. J. *J. Phys. Chem. C* **2010**, 114(39), 16229-16235.

⁴² a) Lyon, J. L., Fleming, D. A., Stone, M. B., Schiffer, P. and Williams, M. E. *Nano Lett.* **2004**, 4(4), 719-723; b) Li, Y., Wu, J. S., Qi, D. W., Xu, X. Q., Deng, C. H., Yang, P. Y. and Zhuang, X. M. *Chem. Commun.* **2008**, 5, 564-566; c) Yang, P. P., Quan, Z. W., Hou, Z. Y., Li, C. X., Kang, X. J., Cheng, Z. Y. and Lin, J. *Biomaterials* **2009**, 30(27), 4786-4850; d) Zhang, M., Wu, Y. P., Feng, X. Z., He, X. W., Chen, L. X. and Zhang, Y. K. *J. Mater. Chem.*, **2010**, 20(28), 5835-5842; e) Liu, S. S., Chen, H. M., Lu, X. H., Deng, C. H., Zhang, X. M. and Yang, P. Y. *Angew. Chem. Int. Ed.* **2010**, 49(41), 7557-7561; f) Won, Y. H., Aboagye, D., Jang, H. S., Jitianu, A. and Stanciu, L. A. *J. Mater. Chem.* **2010**, 20(24), 5030-5034.

⁴³ a) García-Garrido, S. E., Francos, J., Cadierno, V., Basset, J.-M. and Polshettiwar, V. *Chem. Sus. Chem.* **2011**, 4(1), 104-111; b) Baig, R. B. N. and Varma, R. S. *Chem. Commun.* **2012**, 48(50), 6220-6222.

⁴⁴ a) Sheldon, R. A. and Kochi, J. K. *Metal Catalyzed Oxidation of Organic Compounds*. Academic Press: New York (USA), **1981**; b) Gamez, P., Aubel, P. G., Driessen, W. L. and Reedjik, J. *Chem. Soc. Rev.* **2001**, 30(6), 376-385; c) Meunier, B. *Biomimetic Oxidations Catalyzed by Transition Metal Complexes*. Imperial College Press: London (UK), **2000**.

⁴⁵ a) Ko, S. Y., Lee, A. W. M., Masamune, S., Reed, L. A., Sharpless, K. B. and Walker, F. J. *Science* **1983**, 220(4600), 949-951; b) Nicolaou, K. C., Winssinger, N., Pastor, J., Ninkovic, S., Sarabia, F., He, Y., Vourloumis, D., Yang, Z., Li, T., Giannakakou, P. and Hamel, E. *Nature* **1997**, 387, 268-272; c) Gagnon, S.

D., in Mark, H. F., Bikales, N. M., Overberger, C. G., Menges, G. and Kroschwitz J. I. (eds.) *Encyclopedia of Polymer Science and Engineering* (2n ed.). John Wiley & Sons: New York (USA), **1985**, vol. 6, p. 273-307; d) Darensbourg, D. J., Mackiewicz, R. M., Phelps, A. L. and Billodeaux, D. R. *Acc. Chem. Res.* **2004**, 37(11), 836-844; e) Jacobsen, E. N. in Ojima, I. (ed.) *Catalytic Asymmetric Synthesis*. VCH Publishers: New York (USA), **1993**, p. 229; f) De Faveri, G., Ilyashenko, G. and Watkinson, M. *Chem. Soc. Rev.* **2011**, 40(3), 1722-1760.

⁴⁶ a) Zabicky, J. (ed.) *The Chemistry of Amides*. Wiley-Interscience: New York (USA), **1970**; b) Acrylamide is one of the most important commodity chemicals and is used in coagulators, soil conditioners, and stock additives for paper treatment and paper sizing, and for adhesives, paint, and petroleum recovering agents. Hydration of acrylonitrile, by using copper or enzymatic catalysis, produces annually more than 2×10^5 tons of acrylamide, representing the main route for the manufacture of this chemical. See, for example: Yamada, H. and Kobayashi, M. *Biosci. Biotechnol. Biochem.* **1996**, 60(9), 1391-1400; c) Greenberg, A., Breneman, C. M. and Liebman, J. F. (eds.) *The Amide Linkage: Structural Significance in Chemistry, Biochemistry and Materials Science*. Wiley: New York (USA), **2000**; d) Johansson, I. in *Kirk-Othmer Encyclopedia of Chemical Technology* (5th ed.). Wiley: New York (USA), **2004**, Vol. 2.

⁴⁷ a) Amides also have pharmacological interest. See, for example: Rivara, S., Lodola, A., Mor, M., Bedini, A., Spadoni, G., Lucini, V., Pannacci, M., Frascini, F., Scaglione, F., Ochoa Sanchez, R., Gobbi, G. and Tarzia, G. *J. Med. Chem.* **2007**, 50(26), 6618-6626; b) Bhattacharya, A., Scott, B. P., Nasser, N., Ao, H., Maher, M. P., Dubin, A. E., Swanson, D. M., Shankley, M. P., Wickenden, A. D. and Chaplan, S. R. *J. Pharmacol. Exp. Ther.* **2007**, 323(2), 665-674.

⁴⁸ Bäckwall, J. E. *Modern Oxidation Methods*. Wiley-VCH: Weinheim (Germany), **2004**.

⁴⁹ Spero, G. B., Thompson, J. L., Magerlein, B. J., Hanze, A. R., Murray, H. C., Sebek, O. K. and Hogg, J. A. *J. Am. Chem. Soc.* **1956**, 78(23), 6213-6214.

⁵⁰ a) Smith, J. G. *Synthesis* **1984**, 8, 629-656; b) Jacobsen, E. N. *Acc. Chem. Res.* **2000**, 33(6), 421-431; c) de Vries, E. J. and Janssen, D. B. *Curr. Opin. Biotechnol.* **2003**, 14(4), 414-420; d) Muzart, J. *Eur. J. Org. Chem.* **2011**, 25, 4717-4741.

⁵¹ Rao, A. S. *Comprehensive Organic Synthesis*, Trost, B. M., Fleming, I., Pattenden, G. (eds.). Pergamon: Oxford (UK), **1991**, pp. 358-375.

⁵² Denmark, S. E. and Wu, Z. *Synlett.* **1999**, 11, 1787-1794.

⁵³ Jacobsen, E. N. *Coord. Chem. Rev.* **1995**, 140, 189-214.

⁵⁴ Noyori, R., Aoki, M. and Sato, K. *Chem. Commun.* **2003**, 16, 1977-1986.

⁵⁵ a) Swern, D. (ed.) *Organic Peroxides*. John Wiley & Sons: New York (USA), **1970**, Vol. 1, p. 654; b) Murphy, A., Dubois, G., Stack, T. D. P. *J. Am. Chem. Soc.* **2003**, 125(18), 5250-5251.

Chapter VI

- ⁵⁶ a) Banfi, S., Montanari, F., Quici, S., Barkanova, S. V., Kaliya, O. L., Kopranenkov, V. N. and Lukyanets, E. A. *Tetrahedron Lett.* **1995**, 36(13), 2317-2320; b) Dubois, G., Murphy, A., Stack, T. D. P. *Org. Lett.* **2003**, 5(14), 2469-2472.
- ⁵⁷ a) Lugo-Mas, O., Dey, A., Xu, L., Davin, S. D., Benedict, J., Kaminsky, W., Hodgson, K. O., Hedman, B., Solomon, E. I. and Kovacs, J. A. *J. Am. Chem. Soc.* **2006**, 128(34), 11211-11221; b) Kovacs, J. A. *Chem. Rev.* **2004**, 104(2), 825-848.
- ⁵⁸ a) Endo, I., Nojiri, M., Tsujimura, M., Nakasako, M., Nagashima, S., Yohda, M. and Odaka, M. *J. Inorg. Biochem.* **2001**, 83(4), 247-253; b) Li, B., Su, J. and Tao, J. *Org. Process Res. Dev.* **2011**, 15(1), 291-293.
- ⁵⁹ a) Stein, M. and Breit, B. *Angew. Chem. Int. Ed.* **2013**, 52(8), 2231-2234; b) Reeves, J. T., Tan, Z., Marsini, M. A., Han, Z. S., Xu, Y., Reeves, D. C., Lee, H., Lu, B. Z. and Senanayake, C. H. *Adv. Synth. Catal.* **2013**, 355(1), 47-52; c) Werkmesister, S., Bornschein, C., Junge, K. and Beller, M. *Chem. Eur. J.* **2013**, 19(14), 4437-4440.
- ⁶⁰ a) Dopp, D. and Dopp, H. in *Methoden Org. Chem. (Houben Weyl)*. Thieme Verlag: Stuttgart (Germany), **1985**, vol. E5(2), pp. 1024; b) Bailey, P. D., Mills, T. J., Pettercrew, R., Price, R. A. in Katritzky, A. R. and Taylor, R. R. J. K. (eds.) *Comprehensive Organic Functional Group Transformations II*. Elsevier: Oxford (UK), **2005**, Vol. 5, pp. 201; c) Montalbetti, C. A. G. N. and Falque, V. *Tetrahedron*, **2005**, 61(46), 10827-10852.
- ⁶¹ Valeur, E. and Bradley, M. *Chem. Soc. Rev.* **2009**, 38(2), 606-631.
- ⁶² Allen, C. L. and Williams, J. J. M. *Chem. Soc. Rev.* **2011**, 40(7), 3405-3415.
- ⁶³ a) Pattabiraman, V. R. and Bode, J. W. *Nature* **2011**, 480(7378), 471-479; b) Singh, C., Kumar, V., Sharma, U., Kumar, N. and Singh, B. *Curr. Org. Synth.* **2013**, 10(2), 241-264.
- ⁶⁴ Moorthy, J. N. and Singhal, N. *J. Org. Chem.* **2005**, 70(5), 1926-1929.
- ⁶⁵ a) Kornblum, N. and Singaram, S. *J. Org. Chem.* **1976**, 44(25), 4727-4729; b) Katritzky, A. R., Pilarski, B. and Urogdi, L. *Synthesis* **1989**, 12, 949-950.
- ⁶⁶ a) Kobayashi, M. and Shimizu, S. *Curr. Opin. Chem. Biol.* **2000**, 4(1), 95-102; b) Prasad, S. S. and Bhalla, T. C. *Biotechnol. Adv.* **2010**, 28(6), 725-741.
- ⁶⁷ Tao, J. and Xu, J.-H. *Curr. Opin. Chem. Biol.* **2009**, 13(1), 43-50.
- ⁶⁸ Chiswell, B., McKenzie, E. D. and Lindoy, L. F. *Comprehensive Coordination Chemistry*, Wilkinson, G. (ed.). Pergamon: Oxford (UK), **1987**, vol. 4, Ch 41.
- ⁶⁹ a) Ganguly, S., Karmakar, S., Pal, C. K. and Chakravorty, A. *Inorg. Chem.* **1999**, 38(8), 5984-5987; b) Saha, A., Majumdar, P. and Goswami, S. *Dalton Trans.* **2000**, 11, 1703-1708.

- ⁷⁰ a) Greenwood, N. N. and Earnshaw, A. *Chemistry of the elements*. Elsevier Butterworth Heinemann: Oxford (UK), **1997**, 2nd ed., Ch 24; b) Cotton, F. A., Wilkinson, G., Murillo, C. A. and Bochmann, M. *Advanced Inorganic Chemistry* (6th ed.). John Wiley & Sons: New York (USA), **1999**, Ch 17.
- ⁷¹ Lah, S. and Chun, H. *Inorg. Chem.* **1997**, 36(9), 1782-1785.
- ⁷² Dube, K. S. and Harrop, T. C. *Dalton Trans.* **2011**, 40(29), 7496-7498.
- ⁷³ Deroche, A., Morgenstern-Baradau, I., Cesario, M., Guilhem, J., Keita, B., Nadjo, L. and Houée-Levin, C. *J. Am. Chem. Soc.* **1996**, 118(19), 4567-4573.
- ⁷⁴ Darensbourg, D. J. and Frantz, E. B. *Dalton Trans.* **2008**, 0(37) 5031-5036.
- ⁷⁵ Romain, S., Baffert, C., Duboc, C., Leprêtre, J.-C., Deronzier, A. and Collomb, M.-N. *Inorg. Chem.* **2009**, 48(7), 3125-3131.
- ⁷⁶ Romain, S., Duboc, C., Neese, F., Rivière, E., Hanton, L. R., Blackman, A. G., Philouze, C., Laprêtre, J.-C., Deronzier, A. and Collomb, M.-N. *Chem. Eur. J.*, **2009** 15(4), 980-988.
- ⁷⁷ a) Griffith, W. P. *Chem. Soc. Rev.* **1992**, 21(3), 179-185; b) Bruneau, C. *Ruthenium catalysts and fine chemistry*. Springer-Verlag: Berlin (Germany), **2004**.
- ⁷⁸ a) Meyer, T. J. *Pure Appl. Chem.* **1990**, 62(6), 1003-1009; b) Qu, P., Thompson, D. W. and Meyer, G. J. *Langmuir* **2000**, 16(10), 4662-4671; c) Butler, J., George, M., Schoonover, J., Dattelbaum, D. and Meyer, T. *Coord. Chem. Rev.* **2007**, 251(3-4), 492-514.
- ⁷⁹ a) Meyer, T. J. and Huynh, M. H. V. *Inorg. Chem.* **2003**, 42(25), 8140-8160; b) Seok, W. K. and Meyer, T. J. *Inorg. Chem.* **2005**, 44(11), 3931-3941; c) Goeltz, J. C., Hanson, C. J. and Kubiak, C. P. *Inorg. Chem.* **2009**, 48(11), 4763-4767.
- ⁸⁰ Ley, S. V., Norman, J., Griffith, W. P. and Marsden, S. P. *Synthesis* **1994**, 7, 639-666.
- ⁸¹ a) Whittall, I. R., McDonagh, A. M., Humphrey, M. G. and Samoc, M. *Adv. Organomet. Chem.* **1999**, 43, 349-405; b) Coe, B. J. *Acc. Chem. Res.* **2006**, 39(6), 383-393; c) Green, K., Cifuentes, M., Corkery, T., Samoc, M. and Humphrey, M. *Angew. Chem. Int. Ed.* **2009**, 48(42), 7867-7870; d) Coe, B. J. *Coord. Chem. Rev.* **2013**, 257(9-10), 1438-1458.
- ⁸² a) Desplanches, C., Ruiz, E. and Alvarez, S. *Eur. J. Inorg. Chem.* **2003**, 2003, 9, 1756-1760; b) Mikuiya, M., Yoshioka, D. and Handa, M. *Coord. Chem. Rev.* **2006**, 250(17-18), 2194-2211; c) Wang, D., Yang, H.-Q., Wu, G.-H., Hou, X.-F. and Yang, J.-H. *Inorg. Chem. Commun.* **2014**, 46, 241-243; d) Upadhyay, A., Rajpurohit, J., Singh, M. K., Dubey, R., Srivastava, A. K., Kumar, A., Rajaraman, G. and Shanmugam, M. *Chem. Eur. J.* **2014**, 20(20), 6061-6070.
- ⁸³ a) Fillaut, J., Andriès, J., Marwaha, R. D., Lanoë, P., Lohio, O., Toupet, L. and Williams, G. J. *J. Organomet. Chem.* **2008**, 693(2), 228-234; b) Kizaki, T., Abe, T., Matsumoto, T. and Ogo, S. *Chem. Lett.*

Chapter VI

2010, 39(2), 128-129; c) Chen, X.-M., Wu, G.-H., Chen, J.-M., Jiang, Y.-Q., Chen, G.-N., Oyama, M., X., Chen and Wang, X.-R. *Biosens. Bioelectron.* **2010**, 26(2), 872-876.

⁸⁴ a) Aquino, M. A. *Coord. Chem. Rev.* **1998**, 170(1), 141-202; b) Yoshida, J., Watanabe, G., Kazikawa, K., Kawabata, Y. and Yuge, H. *Inorg. Chem.* **2014**, 52(19), 11042-11050.

⁸⁵ a) Bergamo, A. and Sava, G. *Dalton Trans.* **2007**, 0, 1267-1272; b) Silva, D. D. O. *Anticancer Agents Med. Chem.* **2010**, 10(4), 312-323; c) Ji, L., Zheng, W., Lin, Y., Wang, X., Lü, S., Hao, X., Luo, Q., Li, X., Yang, L. and Wang, F. *Eur. J. Med. Chem.* **2014**, 77, 110-120.

⁸⁶ a) Vos, J. G. and Kelly, J. M. *Dalton Trans.* **2006**, 41, 4869-4883; b) Zhang, S., Ding, Y. and Wei, H. *Molecules* **2014**, 19(8), 11933-11987.

⁸⁷ a) Xie, P.-H., Hou, Y.-J., Wei, T.-X., Zang, B.-W., Cao, Y. and Huang, C.-H. *Inorg. Chim. Acta* **2000**, 308(1-2), 73-79; b) Chen, C., Pootrakulchote, N., Wu, S., Wang, M., Li, J., Tsai, J., Wu, C., Zakeeruddin, S. M. and Grätzel, M. *J. Phys. Chem. C* **2009**, 113(48), 20752-20757; c) Yin, J.-F., Velayudham, M., Bhattacharya, D., Lin, H.-C. and Lu, K.-L. *Coord. Chem. Rev.* **2012**, 256(23-24), 3008-3035; d) Kurzeev, S. A., Medved'ko, A. V., Grinberg, V. A., Kozyukhin, S. A., Emets, V. V., Sadovnikov, A. A., Baranchikov, A. E., Ivanov, V. K., Andreev, V. N. and Nizhnikovskii, E. A. *J. Rus. Inorg. Chem.* **2014**, 59(7), 658-664.

⁸⁸ a) Barigelletti, F. and Flamigni, L. *Chem. Soc. Rev.* **2000**, 29(1), 1-12; b) Belser, P., De Cola, L., Hartl, F., Adamo, V., Bozic, B., Chriqui, Y., Iyer, V. M., Jukes, R. T. F., Kühni, J., Querol, M., Roma, S. and Salluce, N. *Adv. Funct. Mater.* **2006**, 16(2), 195-208; c) Mishra, L., Yadaw, A. K. and Govil, G. *Indian J. Chem. Sect. A: Inorg., Bioinorg., Phys., Theor. Anal. Chem.*, **2003**, 42A, 1797-1814; d) Newkome, G. R., Cho, T. J., Moorefield, C. N., Mohapatra, P. P. and Godínez, L. A. *Chem. Eur. J.* **2004**, 10(6), 1493-1500.

⁸⁹ a) Delaney, S., Pascaly, M., Bhattacharya, O. K., Han, K. and Barton, J. K. *Inorg. Chem.* **2002**, 41(7), 1966-1974; b) Zhang, Q., Liu, J., Liu, J., Zhang, P., Ren, X., Liu, Y., Huang, Y. and Ji, L. *J. Inorg. Biochem.* **2004**, 98(8), 1405-1412; c) Zhang, Q., Liu, J., Ren, X. and Zhang, O. *Transit. Metal. Chem.* **2005**, 30(3), 285-289; d) Tan, L., Zhang, S., Liu, X. and Xiao, T. *Aust. J. Chem.* **2008**, 61(9), 725-731; e) Liu, Y., Liang, Z., Li, Z., Zeng, C., Yao, J., Huang, H. and Wu, F. *Biometals* **2010**, 23(4), 739-752; f) He, X., Zeng, L., Yang, G., Xie, L., Sun, X. and Tan, L. *Inorg. Chim. Acta* **2013**, 408, 9-17.

⁹⁰ a) Ding, F., Sun, Y.-G., Verpoort, F., Dragutan, V. and Dragutan, I. *J. Mol. Cat. A-Chem.* **2014**, 386, 86-94; b) Chan, K.-H., Guan, X., Lo, V. K.-Y. and Che, C.-M. *Angew. Chem. Int. Ed.* **2014**, 53(11), 2982-2987.

⁹¹ a) Hemelaere, R., Calijo, F., Mauduit, M., Carreaux, F. and Carboni, B. *Eur. J. Org. Chem.* **2014**, 16, 3328-3333; b) Ascic, E., Ohm, R. G., Petersen, R., Hansen, M. R., Hansen, C. L., Madsen, D., Tanner, D. and Nielsen, T. E. *Chem. Eur. J.* **2014**, 20(12), 3297-3300.

⁹² Bokare, A. D. and Cho, W. I. *J. Haz. Mat.* **2014**, 275, 121-135.

- ⁹³ a) Pagliaro, M., Campestrini, S. and Ciriminna, R. *Chem. Soc. Rev.* **2005**, 34(10), 837-845; b) Bagh, B., McKinty, A. M., Lough, A. J. and Stephan, D. W. *Dalton Trans.* **2014**, 43(34), 12842-12850; c) Aguiló, J., Francàs, L., Hiu, H. J., Bofill, R., Garcia-Anton, J., Benet-Buchholz, J., Llobet, A., Escriche, L. and Sala, X. *Cat. Sci. Tech.* **2014**, 4(1), 190-199.
- ⁹⁴ Fernandez-Zumel, M. A., Kiefer, G., Thommes, K., Scopetelli, R. and Severin, K. *Eur. J. Inorg. Chem.* **2010**, 23, 3596-3601.
- ⁹⁵ a) Siffert, N. and Bühl, M. *J. Am. Chem. Soc.* **2010**, 132(23), 8056-8070; b) Duman, S. and Özkar, S. *Int. J. Hyd. Ener.* **2013**, 38(1), 180-187.
- ⁹⁶ a) Aydemir, M., Meric, N. and Baysal, A. *J. Organomet. Chem.* **2012**, 720, 38-45; b) Anitha, P., Manikandan, R., Endo, A., Hashimoto, T. and Viswanatamurhi, P. *Spec. Acta Part A: Mol. Biomol. Spect.* **2012**, 99, 174-180; c) Zheng, L., Wu, F., Li, Y.-Y., Dong, Z.-R. and Gao, J.-X. *J. Organomet. Chem.* **2014**, 762, 34-39; d) Aydemir, M., Ocak, Y. S., Rafikova, K., Kystaubayeva, N., Kayan, C., Zazybin, A., Ok, F., Baysal, A. and Temel, H. *Appl. Organomet. Chem.*, **2014**, 28(6), 396-404.
- ⁹⁷ a) Mandal, S., Samanta, S., Mondal, T. K. and Goswami, S. *Organometallics* **2012**, 31(15), 5282-5293; b) Reddy, M. C. and Jeganmohan, M. *Org. Lett.* **2014**, 16(18), 4866-4869.
- ⁹⁸ a) Mangold, S. L., O'Leary, D. J. and Grubbs, R. H. *J. Am. Chem. Soc.* **2014**, 136(35), 12469-12478; b) Hartung, J., Dornan, P. K. and Grubbs, R. H. *J. Am. Chem. Soc.* **2014**, 136(37), 13029-13037; c) Antonucci, A., Basseti, M., Bruneau, C., Dixneuf, P. H. and Pasquini, C. *Organometallics*, **2010**, 29(20), 4524-4531.
- ⁹⁹ van Leeuwen, P. W. N. M. *Homogeneous Catalysis: Understanding the Art*. Springer: Netherlands, **2004**.
- ¹⁰⁰ a) Brandt, W. W., Dwyer, F. P. and Gyarfas, E. C. *Chem. Rev.* **1954**, 54(6), 959-1017; b) Dwyer, F. P. and Mellor, D. P. *Chelating Agents and Metal Chelates*. Academic Press: New York (USA), **1964**.
- ¹⁰¹ a) Durham, B., Caspar, J. V., Nagle, J. K. and Meyer, T. J. *J. Am. Chem. Soc.* **1982**, 104(18), 4803-4810; b) Pugh, J. R., Bruce, M. R. M., Sullivan, B. P. and Meyer, T. J. *Inorg. Chem.* **1991**, 30(1), 86-91.
- ¹⁰² Dovletoglou, A., Adeyemi, S. A. and Meyer, T. J. *Inorg. Chem.* **1996**, 35(14), 4120-4127.
- ¹⁰³ Costentin, C., Robert, M. and Saveant, J.-M. *Chem. Rev.* **2010**, 110(12), PR1-PR40.
- ¹⁰⁴ a) Takeuchi, K. J., Thompson, M. S., Pipes, D. W. and Meyer, T. J. *Inorg. Chem.* **1984**, 23(13), 1845-1851; b) Roecker, L., Kutner, W., Gilbert, J. A., Simmons, M., Murray, R. W. and Meyer, T. J. *Inorg. Chem.* **1985**, 24(23), 3784-3791; c) Suen, H. F., Wilson, S. W., Pomerantz, M. and Walsh, J. K. *Inorg. Chem.* **1989**, 28(4), 786-791; d) Llobet, A. *Inorg. Chim. Acta* **1994**, 221(1-2), 125-131.
- ¹⁰⁵ a) Lindquist, I. and Einarsson, P. *Acta Chem. Scand.* **1959**, 13, 420-424; b) Cotton, F. A. and Elder, R. C. *J. Am. Chem. Soc.* **1960**, 82(12), 2986-2991; c) Cotton, F. A. and Francis, R. J. *Inorg. Nucl. Chem.* **1961**, 17(1-2), 62-68.

Chapter VI

¹⁰⁶ a) Evans, I. P., Spencer, A. and Wilkinson, G. *J. Chem. Soc, Dalton Trans.* **1973**, 2, 204-209; b) Alessio, E., Mestroni, G., Nardin, G., Attia, W. M., Calligaris, M., Sava, G. and Zorzet, S. *Inorg. Chem.* **1988**, 27(23), 4099-4106; c) Alessio, E. *Chem. Rev.* **2004**, 104(9), 4203-4242; d) Mola, J., Romero, I., Rodríguez, M., Bozoglian, F., Poater, A., Sola, M., Parella, T., Benet-Buchholz, J., Fontrodona, X. and Llobet, A. *Inorg. Chem.* **2007**, 46(25), 10707-10716.

¹⁰⁷ a) Khan, M. M. T., Mohiuddin, R., Vancheesan, S. and Swamy, B. *Ind. J. Chem. Section A: Inorg., Phys., Theor.&Anal.* **1981**, 204, 564; b) van der Drift, R. C., Sprengers, J. W., Bouwman, E., Mul, W. P., Kooijman, H., Spek, A. L. and Drent, E. *Eur. J. Inorg. Chem.* **2002**, 8, 2147-2155; c) Sens, C., Rodríguez, M., Romero, I., Llobet, A., Parella, T., Sullivan, B. P. and Benet-Buchholz, J. *Inorg. Chem.* **2003**, 42(6), 2040-2048; d) Shan, N., Adams, H. and Thomas, J. A. *Inorg. Chim. Acta* **2006**, 359(3), 759-765; e) Martínez, R., Ramón, D. J. and Yus, M. *Eur. J. Org. Chem.* **2007**, 10, 1599-1605; f) Wang, L., Duan, L., Stewart, B., Pu, M., Liu, J., Privalov, T. and Sun, L. *J. Am. Chem. Soc.* **2012**, 134(45), 18868-18880; g) Bolyog-Nagy, E., Udvardy, A., Joó, F. and Kathó, A. *Tetrahedron Lett.* **2014**, 55(26), 3615-3617.

¹⁰⁸ a) Sava, G., Gagliardi, R., Bergamo, A., Alessio, E. and Mestroni, G. *Anticancer Res.* **1999**, 19(2A), 969-972; b) Bergamo, A., Stucco, G., Gava, B., Cocchietto, M., Alessio, E., Serli, B., Iengo, E. and Sava, G. *J. Pharm. And Exp. Therap.* **2003**, 305(2), 725-732; c) Bratsos, I., Simonin, C., Zangranado, E., T., Gianferrara, Bergamo, A. and Alessio, E. *Dalton Trans.* **2011**, 40, 9533-9543; d) David, S., Perkins, R. S., Fronczek, F. R., Kasiri, S., Mandal, S. S. and Srivastava, R. S. *J. Inorg. Biochem.* **2012**, 111, 33-39; e) Alagesan, M., Bhuvanesh, N. S. P. and Dharmaraj, N. *Dalton Trans.* **2014**, 43, 6087-6099.

¹⁰⁹ a) Sava, G., Pacor, S., Mestroni, G. and Alessio, E. *Clin. Exp. Met.* **1992**, 10(4), 273-280; b) Mestroni, G., Alessio, E., Sava, G., Pacor, S., Coluccia, M., Boccarelli, A. *Metal-based drugs* **1994**, 1, 41-63; c) Alessio, E., Iengo, E., Zorzet, S., Bergamo, A., Coluccia, Boccarelli, M., A. and Sava, G. *J. Inorg. Biochem.* **2000**, 79(1-4), 173-177; d) Alessio, E., Mestroni, G., Bergamo, A. and Sava, G. *Curr. Top. Med. Chem.* **2004**, 4(15), 1525-1533; e) Brastos, L., Jedner, S., Gianferrara, T. and Alessio, E. *Chimia* **2007**, 61(11), 692-697.

¹¹⁰ a) Alessio, E., Macchi, M., Heath, S. L. and Marzilli, L. G. *Inorg. Chem.* **1997**, 36(24), 5614-5623; b) Heseck, D., Inoue, Y., Everit, S. R. L., Ishida, H., Kunieda, M. and Drew, M. G. B. *Chem. Commun.* **1999**, 5, 403-404; c) Malik, Robinson, K. Z., S. D. and Steed, J. W. *Polyhedron* **2000**, 19(13), 1589-1592.

¹¹¹ a) Ashton, P. R., Ballardini, R., Balzani, V., Credi, A., Dress, K. R., Ishow, E., Cornelis, J., Kocian, O., Preece, J. A., Spencer, N., Stoddart, J. F., Venturi, M. and Wenger, S. *Chem. Eur. J.* **2000**, 6(19), 3558-3574; b) Ballardini, R., Balzani, V., Credi, A., Gandolfi, M. T. and Venturi, M. *Int. J. Photoen.* **2001**, 3(2), 63-77; c) Baranoff, E., Collin, J. P., Furusho, J., Furusho, Y., Laemmel, A. C. and Sauvage, J. P. *Inorg. Chem.* **2002**, 41(5), 1215-1222.

¹¹² a) Smith, M. K., Gibson, J. A., Young, C. G., Broomhead, J. A., Junk, P. C. and Keene, F. R. *Eur. J. Inorg. Chem.* **2000**, 6, 1365-1370; b) Kato, M., Takayanagi, T., Fujihara, T. and Nagasawa, A. *Inorg. Chim. Acta*

2009, 362(4), 1199-1203; c) Roeser, S., Maji, S., Benet-Buchholz, J., Pons, J. and Llobet, A. *Eur. J. Inorg. Chem.* **2013**, 2, 232-240; d) Jin, Y. and Rack, J. J. *Isr. J. Chem.* **2013**, 53(5), 280-287.

¹¹³ Alessio, E., Bolle, M., Milani, B., Mestroni, G., Faleschini, P., Geremia, S. and Calligaris, M. *Inorg. Chem.* **1995**, 34(19), 4716-4721.

¹¹⁴ Pearson, R. G. *J. Chem. Educ.* **1968**, 45(10), 643.

¹¹⁵ a) Bruijninx, P. C. A., van Koten, G. and Gebbink, R. J. M. K. *Chem. Soc. Rev.* **2008**, 37(12), 2716-2744; b) Crabtree, R. H. *Oxidation Catalysis by Transition Metal Complexes, in Encyclopedia of Inorganic and Bioinorganic Chemistry*. John Wiley & Sons: New York (USA), **2011**.

¹¹⁶ Lippard, S. J. and Berg, J. M. *Principles of Bioinorganic Chemistry*. University of Science Books: Mill Valley (USA), **1994**.

¹¹⁷ Gómez, L. *Bioinspired iron and manganese catalyst for the effective and selective oxidation of alkanes and alkenes*, Universitat de Girona, **2010**. <<http://hdl.handle.net/10803/8056>>

¹¹⁸ a) Pecoraro, V. L. (ed.) *Manganese Redox Enzymes*. VCH Publisher: New York (USA), **1992**; b) Luo, J. *Manganese Superoxide Dismutase (MnSOD), B-180 Medical Laboratories Free Radical and Radiation Biology Program*. The University of Iowa: Iowa City (USA), **2001**.

¹¹⁹ Miller, A.-F. *FEBS Letters* **2012**, 586(5), 585-595.

¹²⁰ Riley, D. P. *Chem. Rev.* **1999**, 99(9), 2573-2587.

¹²¹ Dismukes, G. C. and van Willigen, R. T. *Manganese: The Oxygen-Evolving Complex & Models, in Encyclopedia of Inorganic and Bioinorganic Chemistry*. John Wiley & Sons: New York (USA), **2011**.

¹²² a) Zouni, A., Witt, H.-T., Kern, J., Fromme, P., Krauss, N., Saenger, W. and Orth, P. *Nature* **2001**, 409, 739-743; b) Loll, B., Kern, J., Saenger, W., Zouni, A. and Biesiadka, J. *Nature* **2005**, 438, 1040-1044; c) Suga, M., Akita, F., Hirata, K., Ueno, G., Murakami, H., Nakajima, Y., Shimizu, T., Yamashita, K., Yamamoto, M., Ago, H. and Shen, J.-R. *Nature* **2015**, 517(7532), 99-103.

¹²³ Waldo, G. S. and Penner-Hahn, J. E. *Biochemistry* **1995**, 34(5), 1507-1512.

¹²⁴ a) Kono, Y. and Fridovich, I. *Biol. Chem.* **1983**, 258, 6015-6019; b) Allgood, G. S. and Perry, J. J. *J. Bacteriol.* **1986**, 168(2), 563-567.

¹²⁵ a) Antonyuk, S. V., Melik-Adamyanyan, V. R., Popov, A. N., Lamzin, V. S., Hempstead, P. D., Harrison, P. M., Artymiuk, P. J. and Barynin, V. V. *Crystallography Reports* **2000**, 45(1), 105-116; b) Barynin, V. V., Whittaker, M. M., Antonyuk, S. V., Lamzin, V. S., Harrison, P. M., Artymiuk, P. J. and Whittaker, J. W. *Structure* **2001**, 9(8), 725-738.

¹²⁶ a) Ghanotakis, D. F. and Yocum, C. F. *Annu. Rev. Plant Physiol. Plant. Mol. Biol.* **1990**, 41, 255-276; b) J. W. Whittaker *Arch. Biochem. Biophys.* **2012**, 525(2), 111-120.

Chapter VI

- ¹²⁷ Wu, A. J., Penner-Hahn, J. E. and Pecoraro, V. L. *Chem. Rev.* **2004**, 104(2), 903-938.
- ¹²⁸ a) Mathur, P., Crowder, M. and Dismukes, G. C. *J. Am. Chem. Soc.* **1987**, 109(17), 5227-5233; b) Sakiyama, H., Okawa, H. and Suzuki, M. *J. Chem. Soc., Dalton Trans.*, **1993**, 24, 3823-3825; c) Wieghardt, K., Bossek, U., Nuber, B., Weiss, J., Bonvoisin, J., Corbella, M., Vitols, S. E. and Girerd, J. J. *J. Am. Chem. Soc.* **1988**, 110(22), 7398-7411; d) Bossek, U., Weyermüller, T., Wieghardt, K., Nuber, B. and Weiss, J. *J. Am. Chem. Soc.* **1990**, 112(17), 6387-6388; e) Higuchi, C., Sakiyama, H., Okawa, H. and Fenton, D. E. *J. Chem. Soc., Dalton Trans.* **1995**, 4015-4020; f) Dismukes, G. C. *Chem. Rev.* **1996**, 96(7), 2909-2926; g) Palopoli, C., Bruzzo, N., Hureau, C., Ladeira, S., Murgida, D. and Signorella, S. *Inorg. Chem.* **2011**, 50(18), 8973-8983.
- ¹²⁹ Meunier, B., de Visser, S. P. and Shaik, S. *Chem. Rev.* **2004**, 104(9), 3947-3980.
- ¹³⁰ a) Ayougou, K., Bill, E., Charnock, J. M., Garner, C. D., Mandon, D., Trautwein, A. X., Weiss, R., Winkler, H. *Angew. Chem. Int. Ed. Engl.* **1995**, 34(3), 343-346; b) Song, W. J., Seo, M. S., George, S. D., Otha, T., Song, R., Kang, M.-J., Tosha, T., Kitagawa, T., Solomon, E. I. and Nam, W. *J. Am. Chem. Soc.* **2007**, 129(5), 1268-1277.
- ¹³¹ Tabushi, I., Kodera, M. and Yokoyama, M. *J. Am. Chem. Soc.* **1985**, 107(15), 4466-4473.
- ¹³² a) Sono, M., Roach, M. P., Coulter, E. D. and Dawson, J. H. *Chem. Rev.* **1996**, 96(7), 2841-2887; b) Bernadou, J. and Meunier, B. *Adv. Synth. Catal.* **2004**, 346(4), 171-184; c) Groves, J. T. *Cytochrome P450: Structure, Mechanism and Biochemistry*, Ortiz de Montellano, P. R. (ed.). Kluwer Academic/Plenum Publishers: New York (USA), **2005**, 3rd ed., Ch 1.
- ¹³³ Meunier, B. *Chem. Rev.* **1992**, 92(6), 1411-1456.
- ¹³⁴ a) Groves, J. T. *J. Inorg. Biochem.* **2006**, 100(4), 434-447; b) Nam, W. *Acc. Chem. Res.* **2007**, 40(7), 522-531; c) de Oliveira, F. T., Chanda, A., Banerjee, D., Shan, X., Monda, S., Que Jr., L., Bominaar, E. L., Münck, E. and Collins, T. J. *Science* **2007**, 315(5813), 835-838.
- ¹³⁵ a) Costas, M. *Coord. Chem. Rev.* **2011**, 255(23-24), 2912-2932; b) Shaik, S., Cohen, S., Wang, Y., Chen, H., Kumar, D., Thiel, W. *Chem. Rev.* **2010**, 110(2), 949-1017; c) Lee, J. Y., Lee, Y.-M., Kotani, H., Nam, W. and Fukuzumi, S. *Chem. Commun.* **2009**, 6, 704-706; d) Lanucara, F. and Crestoni, M. E. *Chem. Eur. J.* **2011**, 17(43), 12092-12100.
- ¹³⁶ a) Gómez, M., Muller, G. and Rocamora, M. *Coord. Chem. Rev.* **1999**, 193-195, 769-835; b) Hargaden, G. C. and Guiry, P. J. *Chem. Rev.* **2009**, 109(6), 2505-2550.
- ¹³⁷ Rich, J., Rodríguez, M., Romero, I., Vaquer, L., Sala, X., Llobet, A., Corbella, M., Collomb, M.-N. and Fontrodona, X. *Dalton Trans.* **2009**, 38, 8117-8126.
- ¹³⁸ a) von Zelewsky, A. and Mamula, O. *J. Chem. Soc., Dalton Trans.* **2000**, 219-231; b) Chelucci, G. and Thummel, R. P. *Chem. Rev.* **2002**, 102(9), 3129-3170; c) Rich, J., Rodríguez, M., Romero, I., Fontrodona,

X., van Leeuwen, P. W. N. M, Freixa, Z., Sala, X., Poater, A. and Solà, M. *Eur. J. Inorg. Chem.* **2013**, 7, 1213-1224.

¹³⁹ a) Palucki, M., Finney, M. S., Pospisil, P. J., Güler, M. L., Ishida, T. and Jacobsen, E. N. *J. Am. Chem. Soc.* **1998**, 120(5), 948-954; b) Katsuky, T. *Adv. Synth. Catal.* **2002**, 344(2), 131-147; c) Cozzi, P. G. *Chem. Soc. Rev.* **2004**, 33(7), 410-421.

¹⁴⁰ Garcia-Bosch, I., Company, A., Fontrodona, X., Ribas, X. and Costas, M. *Org. Lett.*, **2008**, 10(11), 2095-2098.

¹⁴¹ Hage, R., Iburg, J. E., Kerschner, J., Koek, J. H., Lempers, E. L. M., Martens, R. J., Racherla, U. S., Russell, S. W., Swarthoff, T., van Vliet, M. R. P., Warnaar, J. B., van der Wolf, L. and Krijnen, B. *Nature* **1994**, 369, 637-639.

¹⁴² a) Nehru, K., Kim, S. J., Kim, I. Y., Seo, M. S., Kim, Y., Kim, S.-J., Kim, J. and Nam, W. *Chem. Commun.* **2007**, 44, 4623-4625; b) Saravanan, N. and Palaniandavar, M. *Inorg. Chim. Acta* **2012**, 385, 100-111; c) Murphy, A., Pace, A. and Stack, T. D. *Org. Lett.* **2004**, 6(18), 3119-3122; d) Goldsmith, C. R. and Jiang, W. *Inorg. Chim. Acta* **2012**, 384, 340-344; e) Murphy, A. and Stack, T. D. *J. Mol. Cat. A: Chem.* **2006**, 251(1-2), 78-88.

¹⁴³ Terry, J.T. and Stack, T. D. P. *J. Am. Chem. Soc.* **2008**, 130(14), 4945-4953.

¹⁴⁴ a) McGarrigle, E. M. and Gilheany, D. G. *Chem. Rev.* **2005**, 105(5), 1563-1602; b) Sibbons, K. F., Shastri, K. and Watkinson, M. *Dalton Trans.* **2006**, 5, 645-661.

¹⁴⁵ a) Guilmet, E. and Meunier, B. *Tetrahedron Lett.* **1980**, 21(46), 4449-4450; b) Meunier, B., Guimet, E., De Carvalho, M. E. and Poilblanc, R. *J. Am. Chem. Soc.* **1984**, 106(22), 6668-6676.

¹⁴⁶ Samsel, E. G., Srinivasan, K. and Kochi, J. K. *J. Am. Chem. Soc.* **1985**, 107(25), 7606-7617.

¹⁴⁷ Srinivasan, K., Michaud, P. and Kochi, J. K. *J. Am. Chem. Soc.* **1986**, 108(9), 2309-2320.

¹⁴⁸ Irie, R., Noda, K., Ito, Y., Matsumoto, N. and Katsuki, T. *Tetrahedron Lett.* **1990**, 31(50), 7345-7348.

¹⁴⁹ Zhang, W., Loebach, J. L., Wilson, S. R. and Jacobsen, E. N. *J. Am. Chem. Soc.* **1990**, 112(7), 2801-2803.

¹⁵⁰ a) Irie, R., Noda, K., Ito, Y. and Katsuki, T. *Tetrahedron Lett.* **1991**, 32(8), 1055-1058; b) Hosoya, N., Irie, R. and Katsuki, T. *Synlett* **1993**, 4, 261-263; c) Sasaki, H., Irie, R. and Katsuki, T. *Synlett* **1994**, 5, 356-358.

¹⁵¹ a) Lee, N. H., Muci, A. R. and Jacobsen, E. N. *Tetrahedron Lett.* **1991**, 32(38), 5055-5058; b) Deng, L. and Jacobsen, E. N. *J. Org. Chem.* **1992**, 57(15), 4320-4323; c) Larrow, J. F., Jacobsen, E. N., Gao, Y., Hong, Y., Nie, X. and Zepp, C. M. *J. Org. Chem.* **1994**, 59(7), 1939-1942.

¹⁵² Palucki, M., Pospisil, P. J., Zhang, W. and Jacobsen, E. N. *J. Am. Chem. Soc.*, **1994**, 116(20), 9333-9334.

Chapter VI

¹⁵³ a) Bernardo, K., Robert, A., Dahan, G. and Meunier, B. *New J. Chem.* **1995**, 19, 129-131; b) Bernardo, K., Leppard, S., Robert, A., Commenges, G., Dahan, F. and Meunier, B. *Inorg. Chem.* **1996**, 35(2), 387-396.

¹⁵⁴ a) de Vos, D. E. and Bein, T. *J. Organomet. Chem.* **1996**, 1-2, 195-200; b) de Vos, D. E., Sels, B. F., Reynaers, M., Rao, Y. V. S. and Jacobs, P. A. *Tetrahedron Lett.* **1998**, 39(20), 3221-3224; c) Berkessel, A. and Sklorz, C. A. *Tetrahedron Lett.* **1999**, 40(45), 7965-7968; d) Saisaha, P. *Manganese catalysed oxidations with hydrogen peroxide: applications and mechanistic insights*, University of Groningen, **2012**. <<http://hdl.handle.net/11370/ade98d10-3f3d-42e1-bc01-83d85f386f45>>; e) Guillemot, G., Neuburger, M. and Pfaltz, A. *Chem.-Eur. J.* **2007**, 13(32), 8960-8970; f) Gómez, L., Garcia-Bosch, I., Company, A., Sala, X., Fontrodona, X., Ribas, X. and Costas, M. *Dalton Trans.* **2007**, 5539-5545; g) Wu, M., Wang, B., Wang, S., Xia, C. and Sun, W. *Org. Lett.* **2009**, 11(16), 3622-3625; h) Ottenbacher, R. V., Bryliakov, K. P. and Talsi, E. P. *Inorg. Chem.* **2010**, 49(18), 8620-8628; i) Ottenbacher, R. V., Bryliakov, K. P. and Talsi, E. P. *Adv. Synth. Catal.* **2011**, 353(6), 885-889; j) Wang, B., Miao, C., Wang, S., Kühn, F. E., Xia, C. and Sun, W. *J. Organomet. Chem.* **2012**, 715, 9-12; k) Garcia-Bosch, I., Gomez, L., Polo, A., Ribas, X. and Costas, M. *Adv. Synth. Catal.* **2012**, 354(1), 65-70; l) Lyakin, O. Y., Ottenbacher, R. V., Bryliakov, K. P. and Talsi, E. P. *ACS Catal.* **2012**, 2(6), 1196-1202; m) Maity, N. C., Bera, P. K., Ghosh, D., Abdi, S. H. R., Kureshy, R. I., Khan, N. H., Bajaj, H. C. and Suresh, E. *Catal. Sci. Technol.* **2014**, 4(1), 208-217; n) Shen, D., Qiu, B., Xu, D., Miao, C., Xia, C. and Sun, W. *Org. Lett.* **2016**, 18(3), 372-375.

¹⁵⁵ Kang, B., Kim, M., Lee, J., Do, Y. and Chang, S. *J. Org. Chem.* **2006**, 71(18), 6721-6727.

¹⁵⁶ Ilyashenko, G., Sale, D., Motevalli, M. and Watkinson, M. *J. Mol. Catal. A: Chem.* **2008**, 1-2, 296, 1-8.

¹⁵⁷ Murahashi, S.-L. and Komiyama, N. *Ruthenium in Organic Synthesis*. Wiley-VCH: Weinheim (Germany), **2004**.

¹⁵⁸ a) Meyer, T. J. *J. Electrochem. Soc.* **1984**, 131(7), 221C; b) Masllorens, E., Rodríguez, M., Romero, I., Roglans, A., Parella, T., Benet-Buchholz, J., Poyatos, M. and Llobet, A. *J. Am. Chem. Soc.* **2006**, 128(16), 5306-5307; c) Dakkach, M., Atlamsani, A., Parella, T., Fontrodona, X., Romero, I. and Rodríguez, M. *Inorg. Chem.* **2013**, 52(9), 5077-5087.

¹⁵⁹ Keene, F. R. *Coord. Chem. Rev.* **1999**, 187(1), 121-149.

¹⁶⁰ Hudlicky, M. *Oxidations in Organic Chemistry*. ACS Monograph: Washington (USA), **1990**, Vol. 186.

¹⁶¹ Barf, G. A. and Sheldon, R. A. *J. Mol. Catal. A: Chem.* **1995**, 98, 143-146.

¹⁶² Chatterjee, D. *Coord. Chem. Rev.* **2008**, 252(1-2), 176-198.

¹⁶³ Bailey, A. J., Griffith, W. P., White, A. J. P. and Williams, D. J. *J. Chem. Soc., Chem. Commun.* **1994**, 16, 1833-1834.

¹⁶⁴ Fung, W.-H., Yu, W.-Y. and Che, C.-M. *J. Org. Chem.* **1998**, 63(22), 7715-7726.

- ¹⁶⁵ a) Groves, J. T. and Stern, M. K. *J. Am. Chem. Soc.* **1987**, 109(12), 3812-3814; b) Castellino, A. J. and Bruice, T. C. *J. Am. Chem. Soc.*, **1988**, 110(1), 158-162; c) Castellino, A. J. and Bruice, T. C. *J. Am. Chem. Soc.* **1988**, 110(22), 7512-7519; d) Groves, J. T. and Stern, M. K. *J. Am. Chem. Soc.* **1988**, 110(26), 8628-8638.
- ¹⁶⁶ Chatterjee, D. *J. Mol. Cat. A: Chem.* **2009**, 310(1-2), 174-179.
- ¹⁶⁷ Balavoine, G., Eskenazi, C., Meunier, F. and Rivière, H. *Tetrahedron Lett.* **1984**, 25(30), 3187-3190.
- ¹⁶⁸ Chatterjee, D., Sengupta, A. and Mitra, A. *Polyhedron* **2007**, 26(1), 178-183.
- ¹⁶⁹ Sala, X., Santana, N., Serrano, I., Plantalech, E., Romero, I., Rodríguez, M., Llobet, A., Jansat, S., Gómez, M. and Fontrodona, X. *Eur. J. Inorg. Chem.* **2007**, 33, 5207-5214.
- ¹⁷⁰ Serrano, I., Sala, X., Plantalech, E., Rodríguez, M., Romero, I., Jansat, S., Gómez, M., Parella, T., Sidjayacoumar, Stoeckli-Evans, H., Solans, X., Font-Bardia, M., Vidjayacoumar, B. and Llobet, A. *Inorg. Chem.* **2007**, 46(13), 5381-5389.
- ¹⁷¹ Diamond, S.E., Grant, B., Tom, G. M. and Taube, H. *Tetrahedron Lett.* **1974**, 15(46), 4025-4028.
- ¹⁷² a) Murahashi, S.-I., Sasao, S., Saito, E. and Naota, T. *J. Org. Chem.* **1992**, 57(9), 2521-2523; b) Murahashi, S.-I., Sasao, S., Saito, E. and Naota, T. *Tetrahedron*, **1993**, 49(39), 8805-8826; c) Murahashi, S.-I. and Naota, T. *Bull. Chem. Soc. Jpn* **1996**, 69, 1805-1824; d) Murahashi, S.-I. and Takaya, H. *Acc. Chem. Res.* **2000**, 33(4), 225-233.
- ¹⁷³ a) Yu Kukushkin, V. and Pombeiro, A. J. L. *Chem. Rev.* **2002**, 102(5), 1771-1802; b) Katz, N. E., Fagalde, F., Lis de Katz, N. D., Mellace, M. G., Romero, I., Llobet, A. and Benet-Buchholz, J. *Eur. J. Inorg. Chem.* **2005**, 15, 3019-3023; c) Yu Kukushkin, V. and Pombeiro, A. J. L. *Inorg. Chim. Acta* **2005**, 358(1), 1-21; d) Mola, J., Pujol, D., Rodríguez, M., Romero, I., Sala, X., Katz, N. E., Parella, T., Benet-Buchholz, J., Fontrodona, X. and Llobet, A. *Aus. J. Chem.* **2009**, 62(12), 1675-1683.
- ¹⁷⁴ a) Fung, W. K., Huang, X., Man, M. L., Ng, S. M., Hung, M. Y., Lin, Z. and Lau, C. P. *J. Am. Chem. Soc.* **2003**, 125(38), 11539-11544; b) Lau, C. P., Ng, S. M., Jia, G. and Lin, Z. *Coord. Chem. Rev.* **2007**, 251(17-20), 2223-2237.
- ¹⁷⁵ a) O'Connor, J. M. and Casey, C. P. *Chem. Rev.* **1987**, 87(2), 307-318; b) Cadierno, V., Díez, J., Gamasa, M. P., Gimeno, J. and Lastra, E. *Coord. Chem. Rev.* **1999**, 193-195, 147-205; c) Zargarian, D. *Coord. Chem. Rev.* **2000**, 233-234, 157-176.
- ¹⁷⁶ Leung, C. W., Zheng, W., Wang, D., Ng, S. M., Yeung, C. H., Zhou, Z., Lin, Z. and Lau, C. P. *Organometallics* **2007**, 26(8), 1924-1933.
- ¹⁷⁷ a) Oshiki, T., Yamashita, H., Sawada, K., Utsunomiya, M., Takahashi, K. and Takai, K. *Organometallics* **2005**, 24(26), 6287-6290; b) Oshiki, T., Hyodo, I. and Ishizuka, A. *J. Synth. Org. Chem. Jpn* **2010**, 68(1), 41-51; c) Muranaka, M., Hyodo, I., Okumura, W. and Oshiki, T. *Catal. Today*, **2011**, 164(1), 552-555.

Chapter VI

¹⁷⁸ a) Borovik, A. S. *Acc. Chem. Res.* **2005**, 38(1), 54-61; b) Ikariya, T., Murata, K. and Noyori, R. *Org. Biomol. Chem.* **2006**, 4(3), 393-406; c) Grotjahn, D. B. *Dalton Trans.* **2008**, 46, 6497-6508; d) Ikariya, T. and Gridnev, I. D. *Top. Catal.* **2010**, 53(13-14), 894-901.

¹⁷⁹ Smejkaln, T. and Breit, B. *Organometallics* **2007**, 26(9), 2461-2464.

¹⁸⁰ García-Álvarez, R., Díez, J., Crochet, P. and Cadierno, V. *Organometallics* **2010**, 29(17), 3955-3965.

¹⁸¹ a) Phillips, A. D., Gonsalvi, L., Romerosa, A., Vizza, F. and Peruzzini, M. *Coord. Chem. Rev.* **2004**, 248(11-12), 955-993; b) Zablocka, M., Hameau, A., Caminade, A.-M. and Majoral, J.-P. *Adv. Synth. Catal.* **2010**, 352(14-15), 2341-2358; c) Gonsalvi, L. and Peruzzini, M. *Catal. Met. Complexes* **2011**, 37, 183-212.

¹⁸² a) Cadierno, V., Francos, J. and Gimeno, J. *Chem. Eur. J.* **2008**, 14(22), 6601-6605; b) Cadierno, V., Díez, J., Francos, J. and Gimeno, J. *Chem. Eur. J.* **2010**, 16(32), 9808-9817; c) García-Álvarez, R., Díez, J., Crochet, P. and Cadierno, V. *Organometallics* **2011**, 30(20), 5442-5451; d) García-Álvarez, R., Crochet, P. and Cadierno, V. *Green. Chem.* **2013**, 15(1), 46-66.

¹⁸³ García-Álvarez, R., Zablocka, M., Crochet, P., Duhayon, C., Mayoral, J.-P. and Cadierno, V. *Green Chem.* **2013**, 15(9), 2447-2456.

¹⁸⁴ a) Ferrer, I., Rich, J., Fontrodona, X., Rodríguez, M. and Romero, I. *Dalton Trans.* **2013**, 42(37), 13461-13469; b) Ferrer, I., Fontrodona, X., Rodríguez, M. and Romero, I. *Dalton Trans.* **2016**, 45(7), 3163-3174.

¹⁸⁵ a) Sels, B. F., Villa, A. L., Hoegaerts, D., De Vos, D. E. and Pierre, A. J. *Topics Cat.* **2000**, 13, 223-229; b) Lou, L.-L., Yu, K., Ding, F., Zhou, W., Peng, X. and Liu, S. *Tetrahedron Lett.* **2006**, 47(37), 6513-6516; c) Alkordi, M. H., Liu, Y., Larsen, R. W., Eubank, J. F. and Eddaoudi, M. *J. Am. Chem. Soc.* **2008**, 130(38), 12639-12641; d) Faria, A. L., Mac Leod, T. O. C., Barros, V. R. P. and Assis, M. D. *J. Braz. Chem. Soc.* **2009**, 20(5), 895-906.

¹⁸⁶ a) Parton, R. F., Neys, P. E., Jacobs, P. A., Sosa, R. C. and Rouxhet, P. G. *J. Catal.* **1996**, 164(2), 341-346; b) Zucca, O., Sollai, F., Garau, A., Rescigno, A. and Sanjust, E. *J. Mol. Catal. A: Chem.* **2009**, 306(1-2), 89-96; c) Halma, M., Castro, K. A. D. de F., Prévot, V., Forano, C., Wypych, F. and S. *J. Mol. Catal. A: Chem.* **2009**, 310(1-2), 42-50.

¹⁸⁷ Ballesteros, R., Fajardo, M., Sierra, I. and del Hierro, I. *J. Mol. Catal. A: Chem.* **2009**, 310(1-2), 83-92; b) Ballesteros, R., Pérez, Y., Fajardo, M., Sierra, I. and del Hierro, I. *Micro. and Meso. Mat.* **2008**, 116(1-3), 452-460.

¹⁸⁸ Luque, R., Badamali, S. K., Clarck, J. H., Fleming, M. and Macquarrie, D. J. *Appl. Catal. A: Gen.* **2008**, 341(1-2), 154-159.

¹⁸⁹ a) Haas, G. R. and Kolis, J. W. *Organometallics* **1998**, 17(20), 4454-4460; b) Deubel, D. V., Sundermeyer, J. R. and Frenking, G. *J. Am. Chem. Soc.* **2000**, 122(41), 10101-10108; c) Buffon, R. and Schuchardt, U. *J. Braz. Chem. Soc.* **2003**, 14(3), 347-353.

- ¹⁹⁰ Maurya, M. R., Kumar, A. and Pessoa, J. C. *Coord. Chem. Rev.* **2011**, 255(19-20), 2315-2344.
- ¹⁹¹ a) Sels, B. F., de Vos, D. E., Buntix, M. and Jacobs, P. A. *J. Catal.* **2003**, 216(1-2), 288-297; b) Le, Y., Yang, X., Dai, W.-L., Gao, R. and Fan, D. *Cat. Commun.* **2008**, 9(9), 1838-1841; c) Sofia, L. T. A., Krishnan, A., Sankar, M., Raj, N. K., Manikandan, P., Rajamohanam, P. R. and Ajithkumar, R. G. *J. Phys. Chem. C* **2009**, 113(50), 21114-21122; d) Amini, M., Haghdoost, M. M. and Bagherzadeh, M. *Coord. Chem. Rev.* **2014**, 268, 83-100.
- ¹⁹² a) Nestler, O. and Severin, K. *Org. Lett.* **2001**, 3(24), 3907-3909; b) Kobayashi, S. and Sugiura, M. *Adv. Synth. Catal.* **2006**, 348(12-13), 1496-1504; c) Che, C.-M. and Huang, J. -S. *Chem. Commun.* **2009**, 27, 3996-4015.
- ¹⁹³ a) Tsang, S. C., Caps, V., Paraskevas, I., Chadwick, D. and Thompsett, D. *Angew. Chem. Int. Ed.* **2004**, 43(42), 5645-5649; b) Guin, D., Baruwati, B. and Manorama, S. V. *Org. Lett.* **2007**, 9(7), 1419-1421; c) Jacinto, M. J., Santos, O. H. C. F., Jardim, R. F., Landers, R. and Rossi, L. M. *Appl. Catal. A: Gen.* **2009**, 360(2), 177-182; d) Rossi, L. M., Cosata, N. J. S., Silva, F. P. and Wojcieszak, R. *Green Chem.* **2014**, 16(6), 2906-2933.
- ¹⁹⁴ Kamonsatikul, C., Khamnaen, T., Phiriyawirut, P., Charoenchaidet, S. and Somsook, E. *Catal. Commun.* **2012**, 26, 1-5.
- ¹⁹⁵ Shi, F., Tse, M. K., Pohl, M.-M., Brückner, A., Zhang, S. and Beller, M. *Angew. Chem. Int. Ed.* **2007**, 46(46), 8866-8868.
- ¹⁹⁶ a) Ligtenbarg, A.G.J., Hage, R. and Feringa, B. L. *Coord. Chem. Rev.* **2003**, 237(1-2), 89-101; b) Bolm, C. *Coord. Chem. Rev.* **2003**, 237(1-2), 245-256.
- ¹⁹⁷ Maurya, M. R., Saklani, H., Kumar, A. and Chand, S. *Catal. Lett.* **2004**, 93(1-2), 121-127.
- ¹⁹⁸ Maurya, M. R. and Sikarwar, S. *Catal. Commun.* **2007**, 8(12), 2017-2024.
- ¹⁹⁹ El-Qisiari, A. L., Qaseer, H. A. and Henry, P. M. *Tetrahedron Lett.* **2002**, 43(23), 4229-4231.
- ²⁰⁰ Severeys, A., De Vos, D. E. and Jacobs, P. A. *Green Chem.* **2002**, 4(4), 380-384.
- ²⁰¹ Song, C. E. and Roh, E. J. *Chem. Commun.* **2000**, 10, 837-838.
- ²⁰² Smith, K., Liu, S. and El-Hiti, G. A. *Catal. Lett.* **2004**, 2-3, 98, 95-101.
- ²⁰³ a) Li, Z. and Xia, C.-G. *Tetrahedron Lett.* **2003**, 44(10), 2069-2071; b) Li, Z., Xia, C.-G. and Ji, M. *Appl. Catal. A: General* **2003**, 252(1), 17-21; c) Li, Z. and Xia, C.-G. *J. Mol. Catal. A: Chem.* **2004**, 214(1), 95-101.
- ²⁰⁴ a) Liu, Y., Zhang, H.-J., Lu, Y., He, X.-S., Wang, X. and Ding, X. *J. Mol. Catal. A: Chem.* **2010**, 287(1-2), 80-86; b) Tan, R., Yin, D., Yu, N., Zhao, H. and Yin, D. *J. Catal.* **2009**, 263(2), 284-291; c) Teixeira, J., Silva, A. R., Branco, L. C., Afonso, C. A. M. and Freire, C. *Inorg. Chim. Acta* **2010**, 363(13), 3321-3329.
- ²⁰⁵ Tong, K.-H., Wong, K.-Y. and Chan, T. H. *Org. Lett.* **2003**, 5(19), 3423-3425.

Chapter VI

- ²⁰⁶ Pinto, L. D., Dupont, J., de Souza, R. F. and Bernardo-Gusamo, K. *Catal. Commun.* **2008**, 9(1), 135-139.
- ²⁰⁷ Zhang, Z., Li, H., Liu, Y. and Ye, Y. *Synth. React. Inorg. Met. Org. Nano Met. Chem.* **2009**, 39(3), 144-148.
- ²⁰⁸ a) Cooke, P. R. and Lindsay Smith, J. R. *Tetrahedron Lett.* **1992**, 33(19), 2737-2740; b) Cooke, P. R. and Lindsay Smith, J. R. *J. Chem. Soc. Perkin Trans. 1* **1994**, 14, 1913-1923; c) Vinhado, F. S., Cynthia, M. C., Prado-Manso, H. C. and Iamamoto, Y. *J. Mol. Catal. A: Chem.* **2001**, 174(1-2), 279-288; d) Sacco, H. C., Iamamoto, Y. and Lindsay Smith, J. R. *J. Chem. Soc. Perkin Trans. 2* **2001**, 2, 181-190; e) Ferreira, A. D. Q., Vinhado, F. S. and Iamamoto, Y. *J. Mol. Catal. A: Chem.* **2006**, 243(1), 111-119.
- ²⁰⁹ a) Van der Made, A. W., Smeets, J. W. H., Nolte, R. J. M. and Drenth, W. *J. Chem. Soc., Chem. Commun.* **1983**, 21, 1204-1206; b) Iamamoto, Y., Ciuffi, K. J., Sacco, H. C., Prado, C. M. C., de Moraes, M. and Nascimento, O. R. *J. Mol. Catal.* **1994**, 88(2), 167-176.
- ²¹⁰ a) Salavati-Niasari, M. *Transition Met. Chem.* **2008**, 33(4), 443-452; b) Salavati-Niasari, M., Salimi, Z., Bazarganipour, M. and Davar, F. *Inorg. Chim. Acta* **2009**, 362, 3715-3724.
- ²¹¹ a) Riollet, V., Quadrelli, E. A., Copéret, C., Basset, J.-M., Andersen, R. A., Köhler, K., Böttcher, R.-M. and Herdtweck, E. *Chem. Eur. J.* **2005**, 11(24), 7358-7365; b) Luts, T. and Papp, H. *Kinetics and Catalysis* **2007**, 48(1), 176-182; c) Chaigon, J., Stiriba, S.-E., Lloret, F., Yuste, C., Pilet, G., Bonneviot, L., Albela, B. and Castro, I. *Dalton Trans.* **2014**, 43, 9704-9713; d) Sadeghzadeh, S. M., Daneshfar, F. and Malekzadeh, M. *Chin. J. Chem.* **2014**, 32(4), 349-355; e) Sadeghzadeh, S. M. and Malekzadeh, M. *J. Mol. Liq.* **2015**, 202, 46-51; f) Bagherzadeh, M. and Mortazavi-Manesh, A. *RSC Adv.* **2016**, 6(47), 41551-41560.
- ²¹² Khalil, T. A., Chaabene, S. B., Boujday, S. and Bergaoui, L. *IOSR J. Appl. Chem.* **2015**, 8(1), 36-46.
- ²¹³ a) Tu, X., Fu, X., Hu, X. and Li, Y. *Inorg. Chem. Commun.* **2010**, 13(3), 404-407; b) Raj, J., Herzoga, G., Manning, M., Volcke, C., MacCraith, B. D., Ballantyne, S., Thompson, M. and Arrigan, D. W. M. *Biosens. Bioelectron.* **2009**, 24(8), 2654-2658; c) Battha, D., Stadden, E., Hashem, E., Sparrow, I. J. G. and Emmerson, G. D. *J. Immunol. Methods* **2010**, 362(1-2), 121-126; d) Aissaoui, N., Landoulsi, J., Bergaoui, L., Boujday, S. and Lambert, J.-F. *Enzyme Microb. Technol.* **2013**, 52(6-7), 336-343.
- ²¹⁴ Mimoun, H., Mignard, M., Brechot, P. and Saussine, L. *J. Am. Chem. Soc.* **1986**, 108(13), 3711-3718.
- ²¹⁵ a) Campelj, S., Makovec, D. and Drogenik, M. *J. Magn. Magn. Mater.* **2009**, 321(10), 1346-1350; b) Bagherzadeh, M. and Mortazavi-Manesh, A. *J. Coord. Chem.* **2015**, 68(13), 2347-2360.
- ²¹⁶ Tada, M., Muratsugu, S., Kinoshita, M., Sasalo, T. and Iwasawa, Y. *J. Am. Chem. Soc.* **2010**, 132(2), 713-724.
- ²¹⁷ Pappotiou, F., Karidi, K., Garoufis, A. and Louloudi, M. *Polyhedron* **2013**, 52, 634-638.

- ²¹⁸ a) Ferrer, I., Fontrodona, X., Roig, A., Rodríguez, M. and Romero, I. *Chem. Eur. J.* **2017**, 23(17), 4096-4107; b) Dakkach, M., López, M. I., Romero, I., Rodríguez, M., Atlamsani, A., Parella, T., Fontrodona, X. and Llobet, A. *Inorg. Chem.* **2010**, 49(15), 7072-7079.
- ²¹⁹ Ishizuka, A., Yoshiaki, N. and Oshiki, T. *Chem. Lett.* **2009**, 38(4), 360-361.
- ²²⁰ Subramanian, T. and Pitchumani, K. *Catal. Commun.* **2012**, 29, 109-113.
- ²²¹ a) Kim, A. Y., Bae, J. S., Park, S., Park, S. and Park, K. H. *Catal. Lett.* **2011**, 141, 685-690; b) Shimizu, K., Imaiida, N., Sawabe, K. and Satshuma, A. *Appl. Catal. A* **2012**, 421-422, 114; c) Sherbow, T. J., Downs, E. L., Sayler, R. I., Razink, J. J., Juliette, J. J. and Tyler, D. R. *ACS Catal.* **2014**, 4(9), 3096-3104.
- ²²² Liu, Y.-M., He, L., Wang, M.-M., Cao, Y., He, H.-Y. and Fan, K.-N. *Chem. Sus. Chem.* **2012**, 5(8), 1392-1396.
- ²²³ a) Kumar, S. and Das, P. *New J. Chem.* **2013**, 37(10), 2987-2990; b) Matsuoka, A., Isogawa, T., Morioka, Y., Knappett, B. R., Wheatley, A. E. H., Saito, S. and Naka, H. *RSC Adv.* **2015**, 5(16), 12152-12160.
- ²²⁴ Kurata, T., Tamuro, A., Murata, Y., Nagashima, S., Okano, T. and Ohfuchi, K. *Jpn. Kokai Tokkyo Koho, JP 48054021*, **1973**.
- ²²⁵ Mizuno, T. *Jpn. Kokai Tokkyo Koho, JP 2005170821*, **2005**.
- ²²⁶ Oshiki, T. and Ishizuka, A. *Jpn. Kokai Tokkyo Koho, JP 2009214099*, **2009**.
- ²²⁷ a) Yamaguchi, K., M. Matsushita and N. Mizuno *Angew. Chem. Int. Ed.*, **2004**, 43, 1576-1580; b) Yamaguchi, K. and Mizuno, N. *Synlett*, **2010**, 2365-2382.
- ²²⁸ a) V. Polshettiwar and Varma, R. S. *Chem. Eur. J.* **2009**, 15(7), 1582-1586; b) Baig, R. B. N. and Varma, R. S. *Green Chem.* **2013**, 15(2), 398-417.
- ²²⁹ Woo, H., Lee, K., Park, S. and Park, K. H. *Molecules* **2014**, 19(1), 699-712.
- ²³⁰ Gawande, M. B., Branco, P. S., Nogueira, I. D., Ghumman, C. A. A., Bundaleski, N., Santos, A., Teodoro, O. M. N. D. and Luque, R. *Green Chem.* **2013**, 15(3), 682-689.
- ²³¹ García-Álvarez, R., Francos, J., Tomás-Mendivil, E., Crochet, P. and Cadierno, V. J. *Organomet. Chem.*, **2014**, 771, 93-104.
- ²³² Rafique, S., Idress, M., Nasim, A., Akbar, H. and Athar, A. *Biotechnol. Mol. Biol. Rev.* **2010**, 5(2), 38-45.
- ²³³ Rosenberg, B., VanCamp, L., Trosko, J. E. and Mansour, V. H. *Nature* **1969**, 222, 385-386.
- ²³⁴ a) Jamieson, E. R. and Lippard, S. J. *Chem. Rev.* **1999**, 99(9), 2467-2498; b) Cohen, S. M. and Lippard, S. J. *Prog. Nucleic Acid Res. Mol. Biol.*, **2001**, 67, 93-130; c) Choy, H. *Expert Rev. Anticancer Ther.* **2006**, 6(7), 973-982; d) Eckardt, J. R., Bentsion, D. L., Lipatov, O. N., Polyakov, L. S., MacKintosh, F. R., Karlin, D.

Chapter VI

A., Baker, G. S. and Breitz, H. B. *J. Clin. Oncol.* **2009**, 26(12), 2046-2051; e) Wheate, N. J., Walker, S., Craig, G. E. and Oun, R. *Dalton Trans.* **2010**, 39, 8113-8127; f) Olszewski, U. and Hamilton, G. *Anti-Cancer Agents Med. Chem.* **2010**, 13(10), 293-301.

²³⁵ a) Boerner, L. J. K. and Zaleski, J. M. *Curr. Opin. Chem. Biol.* **2005**, 9(2), 135-144; b) Ott, I. and Gust, R. *Arch. Pharm.* **2007**, 340(3), 117-126.

²³⁶ a) Keppler, B. K., Berger, M. R. and Heim, M. E. *Cancer Treat. Rev.* **1990**, 17, 261-277; b) Köpf-Maier, P. *Eur. J. Clin. Pharmacol.* **1994**, 47(1), 1-16; c) Köpf-Maier, P. *Anticancer Res.* **1999**, 19(1), 493-504; d) Sava, G., Zorzet, S., Turrin, C., Vita, E., Soranzo, M., Zabucchi, G., Cocchietto, M., Bergamo, A., DiGiovine, S., Pezzoni, G., Sartor, L. and Garbisa, S. *Clin. Cancer Res.* **2003**, 9, 1898-1905; e) Gust, R., Ott, I., Posselt, D. and Sommer, K. *J. Med. Chem.* **2004**, 47(24), 5837-5846; g) Hartinger, C. G., Jakupec, Zorbas-Seifried, M. A., S., Groessi, M., Egger, A., Berger, W., Zorbas, H., Dyson, P. J. and Keppler, B. K. *Chem. Biodivers.* **2008**, 5(10), 2140-2155; h) Gasser, G., Ott, I. and Metzler-Nolte, N. *Organometallic Anticancer Compounds. J. Med. Chem.* **2011**, 54(1), 3-25.

²³⁷ Velders, A. H., Kooijman, H., Spek, A. L., Haasnoot, J. G., De Vos, D. and Reedijk, J. *Inorg. Chem.* **2000**, 39(14), 2966-2967.

²³⁸ Dash, S. K., Chattopadhyay, S., Ghosh, T., Tripathy, S., Das, S., Das, D. and Roy, S. *Oncology* **2013**, ID 709269.

²³⁹ Wesselborg, S., Engels, I. H., Rossmann, E., Los, M. and Schulze-Osthoff, K. *Blood* **1999**, 93(9), 3053-3063.

²⁴⁰ Basu, A. and Miura, A. *Int. J. Mol. Med.* **2002**, 10(1), 541-545.

²⁴¹ a) Brambilla, C., Ferrari, L., Passoni, P. and Bonadonna, G. *Cancer Treat. Rev.* **1993**, 19, 3-9; b) Robson, H., Meyer, S., Shalet, S. M., Anderson, E., Roberts, S. and Eden, O. B. *Med. Pediatr. Oncol.* **2002**, 39(6), 573-580; c) Zhang, C. X. and Lippard, S. J. *Curr. Opin. Chem. Biol.* **2003**, 7(4), 481-489; d) Markman, M. *Exp. Opin. Drug. Saf.* **2003**, 2(6), 597-607; e) Barnes, K. R. and Lippard, S. J. *Met. Ions. Biol. Syst.* **2004**, 42, 143-177; e) Stordal, B., Pavlakis, N. and Davey, R. *Cancer Treat. Rev.* **2007**, 33(4), 347-357; f) Zhang, L., Zhang, Y., Huang, P. Y., Xu, F., Peng, P. J. and Guan, Z. Z. *Cancer Chemother. Pharmacol.* **2008**, 61(1), 33-38; g) Ansari, K. I., Mishra, B. P. and Mandal, S. S. *Biochim. Biophys. Acta* **2008**, 1779(1), 66-73; h) Tan, C.-P., Lu, Y.-Y., Ji, L.-N. and Mao, Z.-W. *Metallomics* **2014**, 6(5), 978-995.

²⁴² a) Amaravadi, R. K., Lippincott-Shwartz, J., Yin, X. M., Weiss, W. A., Takebe, N., DiPaola, R. S., Lotze, M. T. and White, E. *Clin. Cancer Res.* **2011**, 17(4), 654-666; b) Liu, E. Y. and Ryan, K. M. *J. Cell. Sci.* **2012**, 125(10), 2349-2358.

²⁴³ a) Kondo, Y. and Kondo, S. *Autophagy* **2006**, 2(2), 85-90; b) Shen, H. M. and Codogno, P. *Autophagy* **2011**, 7(5), 457-465.

- ²⁴⁴ a) Moretti, L., Yang, E. S., Kim, K. W. and Lu, B. *Drug Resist. Updat.* **2007**, 10(4-5), 135-143; b) Mathew, R., Karantza-Wadsworth, V. and White, E. *Nat. Rev. Cancer* **2007**, 7(12), 961-967.
- ²⁴⁵ Galluzi, L., Vitale, I., Abrams, J. M., Alnemri, E. S., Baehrecke, E. H., Blagosklonny, M. V., Dawson, T. M., Dawson, V. L., El-Deiry, W. S., Fulda, S., Gottfried, E., Green, D. R., Hengartner, M. O., Kepp, O., Knight, R. A., Kumar, S., Lipton, S. A., Lu, X., Madeo, F., Malorni, W., Mehlen, P., Nuñez, G., Peter, M. E., Piacentini, M., Rubinsztein, D. C., Shi, Y., Simon, H. U., Vandenabeele, P., White, E., Yuan, J., Zhivotovs.ky, B., Melino, G. and Kroemer, G. *Cell Death Differ.* **2012**, 19, 107-120.
- ²⁴⁶ a) Galluzzi, L., Maiuri, M. C., Vitale, I., Zischka, H., Castedo, M., Zitvogel, L. and Kroemer, G. *Cell Death Diff.* **2007**, 14(7), 1237-1243; b) Kroemer, G., Galluzzi, L., Vandenabeele, P., Abrams, J., Alnemri, E. S., Baehrecke, E. H., Blagosklonny, M. V., El-Deiry, W. S., Golstein, P., Green, D. R., Hengartner, M., Knight, R. A., Kumar, S., Lipton, S. A., Malorni, W., Nuñez, G., Peter, M. E., Tschopp, J., Yuan, J., Piacentini, M., Zhivotovs.ky, B. and Melino, G. *Cell Death Diff.* **2009**, 16(1), 3-11.
- ²⁴⁷ a) Degterev, A. and Yuan, J. *Nat. Rev. Mol. Cell. Biol.* **2008**, 9(5), 378-390; b) Hitomi, J., Christofferson, D. E., Ng, A., Yao, J., Degterev, A., Xavier, R. J. and Yuan, J. *Cell* **2008**, 135(7), 1311-1323; c) Linkermann, A., Green, D. R. *N. Eng. J. Med.* **2014**, 5, 370(5), 455-465.
- ²⁴⁸ Eskelinen, E. L. *Curr. Opin. Pharmacol.* **2011**, 11(4), 294-300.
- ²⁴⁹ Bergamo, A. and Sava, G. *Dalton Trans.*, **2011**, 40, 7817-7823.
- ²⁵⁰ Kostova, L. *Anti-Cancer Agents Med. Chem.* **2009**, 9(8), 827-842.
- ²⁵¹ Chitambar, C. R. *Future Med. Chem.* **2012**, 4(10), 1257-1272.
- ²⁵² Pabla, N. and Dong, Z. *Kidney Int.* **2008**, 73(9), 994-1007.
- ²⁵³ Kalinowska-Lis, U., Ochocki, J. and Matlawska-Wasowska, K. *Coord. Chem. Rev.* **2008**, 252(12-14), 1328-1345.
- ²⁵⁴ a) Skander, M., Retailleau, P., Bourrié, B., Schio, L., Mailliet, P. and Marinetti, A. *J. Med. Chem.* **2010**, 53(5), 2146-2154; b) Chtchigrovskiy, M., Eloy, L., Jullien, H., Saker, L., Ségal-Bendirdjian, E., Poupon, J., Bombard, S., Cresteil, T., Retailleau, P. and Marinetti, A. *J. Med. Chem.* **2013**, 56(5), 2074-2086.
- ²⁵⁵ a) Kaludjerovic, G. N., Miljkovic, D., Momcilovi, M., Djinic, V. M., Mostarica Stojkovic, M., Sabo, T. J. and Trajkovic, V. *Int. J. Cancer* **2005**, 116(3), 479-486; b) Maksimovic-Ivanic, D., Miljatovic, S., Mirkov, I., Stosic-Grujicic, S., Miljkovic, D., Sabi, T. J., Trajkovic, V. and Kaludjerovic G. N. *Metallomics* **2012**, 4(11), 1155-1159.
- ²⁵⁶ a) Min, Y., Li, J., Liu, F., Yeow, E. K. and Xing, B. *Angew. Chem. Int. Ed.* **2014**, 53(4), 1012-1216; b) Müller, P., Schröder, B., Parkinson, J. A., Kratochwill, N. A., Coxall, R. A., Parkin, A., Parsons, S. and Sadler, P. J. *Angew. Chem. Int. Ed.* **2003**, 42(3), 335-339.

Chapter VI

- ²⁵⁷ Dasari, S. and Tchounwou, P. B. *Eur. J. Pharmacol.* **2014**, 740, 364-378.
- ²⁵⁸ a) Scolaro, C., Bergamo, A., Brescacin, L., Delfino, R., Cocchietto, M., Laurency, G., Geldbach, T. J., Sava, G. and Dyson, P. J. *J. Med. Chem.* **2005**, 48(12), 4161-4171; b) Kapitza, S., Pongratz, M., Jakupec, M. A., Heffeter, P., Berger, W., Lackinger, L., Keppler, B. K. and Marian, B. *J. Cancer Res. Clin. Oncol.* **2005**, 131(2), 101-110; c) Ang, W. H., Daldini, E., Scolaro, C., Scopelliti, R., Juillerat-Jeannerat, L. and Dyson, P. J. *Inorg. Chem.* **2006**, 45(22), 9006-9013; d) Scolaro, C., Geldbach, T. J., Rochat, S., Dorcier, A., Gossens, C., Bergamo, A., Cocchietto, M., Tavernelli, I., Sava, G., Rothlisberger, U. and Dyson, P. J. *Organometallics* **2006**, 25(3), 756-765; e) Bugarcic, T., Nováková, O., Halámiková, A., Zerkánková, L., Vrána, O., Kaspárková, J., Habtemariam, A., Parsons, S., Sadler, P. J. and Brabec, V. *J. Med. Chem.* **2008**, 51(17), 5310-5319; f) Chen, T. F., Liu, Y. A., Zheng, W. J., Liu, J. and Wong, Y. S. *Inorg. Chem.* **2010**, 49(14), 6366-6368; g) Ang, W. H., Casini, A., Sava, G. and Dyson, P. J. *J. Organomet. Chem.* **2011**, 696(5), 989-998.
- ²⁵⁹ Page, S. *Education in Chemistry RSC*, **2012**, 26-29.
- ²⁶⁰ Herman, A., Tanski, J. M., Tibbetts, M. F. and Anderson, C. M. *Inorg. Chem.* **2008**, 47(1), 274-280.
- ²⁶¹ Therrien, B., Ang, W. H., Chérioux, F., Vieille-Petit, L., Juillerat-Jeanneret, L., Süß-Fink, G. and Dyson, P. J. *J. Cluster Sci.* **2007**, 18(3), 741-752.
- ²⁶² Hotze, A. C. G., van der Geer, E. P. L., Kooijman, H., Spek, A. L., Haasnoot, J. G. and Reedik, J. *Eur. J. Inorg. Chem.* **2005**, 13, 2648-2657.
- ²⁶³ Therrien, B., Süß-Fink, G., Govindaswamy, P., Renfrew, A. K. and Dyson, P. J. *Angew. Chem. Int. Ed.* **2008**, 47(20), 3773-3776.
- ²⁶⁴ Süß-Fink, G. *Dalton Trans.* **2010**, 39, 1673-1688.
- ²⁶⁵ Kisova, A., Zerkánková, L., Habtemariam, A., Sadler, P. J., Brabec, V. and Kasparkova, J. *Mol. Pharm.* **2012**, 9(3), 694-694.
- ²⁶⁶ Pierroz, V., Joshi, T., Leonidova, A., Mari, C., Schur, J., Ott, I., Spiccia, L., Ferrari, S. and Gasser, G. *J. Am. Chem. Soc.* **2012**, 134(50), 20376-20387.
- ²⁶⁷ Qian, C., Wang, J. Q., Song, C. L., Wang, L. L., Ji, L. N. and Chao, H. *Metallomics* **2013**, 5(7), 844-854.
- ²⁶⁸ Yadav, A., Janaratne, T., Krishnan, A., Singhal, S. S., Yadav, S., Dayoub, A. S., Hawkins, D. L., Awasthi, S. and MacDonnell, F. M. *Mol. Cancer. Ther.* **2013**, 12(5), 643-653.
- ²⁶⁹ a) Messori, L., Orioli, P., Vullo, D., Alessio, E. and Iengo, E. *Eur. J. Biochem.* **2000**, 267(4), 1206-1213; b) Bergamo, A., Messori, L., Piccioli, F., Cocchietto, M. and Sava, G. *Invest. New Drugs* **2003**, V21, 401-411; c) Sava, G., Frausin, F., Cocchietto, M., Vita, F., Podda, E., Spessotto, P., Furlani, A., Scarcia, V. and Zabucchi, G. *Eur. J. Cancer* **2004**, 40(9), 1383-1396; d) Ravera, M., Baracco, S., Cassino, C., Colangelo, D., Bagni, G., Sava, G. and Osella, D. *J. Inorg. Biochem.* **2004**, 98(6), 984-1174; e) Frausin, F., Scarcia, V.,

Cocchieto, M., Furlani, A., Serli, B., Alessio, E. and Sava, G. *J. Pharmacol. Exp. Ther.* **2005**, 313(1), 227-233.

²⁷⁰ Brabec, V. and Novakova, O. *Drug Resist. Updates* **2006**, 9(3), 111-122.

²⁷¹ Vargiu, A. V., Robertazzi, A., Magistrato, A., Ruggerone, P. and Carloni, P. *J. Phys. Chem.* **2008**, 112(14), 4401-4409.

²⁷² a) Ansari, K. I., Grant, J. D., Kasiri, S., Woldemariam, G., Shrestha, B. and Mandal, S. S. *J. Inorg. Biochem.* **2009**, 103(5), 818-826; b) Li, M. X., Chen, C. L., Zhang, D., Niu, J. Y. and Ji, B. S. *Eur. J. Med. Chem.* **2010**, 45(7), 3169-3177; c) Zhou, D.-F., Chen, Q.-Y., Qi, Y., Fu, H.-Ji., Li, Z., Zhao, K.-D. and Gao, J. *Inorg. Chem.* **2011**, 50(15), 6929-6937; d) Zhang, F., Lin, Q.-Y., Zheng, X.-L., Zhang, L.-L., Yang, Q. and Gu, J.-Y. *J. Fluoresc.* **2012**, 22(5), 1395-1406; e) Pereira, T. A., Teixeira da Silva, G. E., Hernández, R. B., Forti, F. L. and Espósito, B. P. *Biometals* **2013**, 26(3), 439-446; f) Liu, J., Guo, W., Li, Li, J., X., Geng, J., Chen, Q. and Gao, J. *Int. J. Mol. Med.* **2015**, 35(3), 607-616.

²⁷³ a) Ronconi, L. and Sadler, P. J. *Coord. Chem. Rev.* **2007**, 251(13-14), 1633-1648; b) Fulda, S., Galluzzi, L. and Kroemer, G. *Nat. Rev. Drug Discovery* **2010**, 9(6), 447-464.

²⁷⁴ a) Hoye, A. T., Davoren, J. E., Wipf, P., Fink, M. P. and Kagan, V. E. *Acc. Chem. Res.* **2008**, 41(1), 87-97; b) Muscella, A., Calabriso, N., Fanizzi, E. P., Pascali, S. A. D., Urso, L., Ciccarese, A., Migoni, D. and Marsigliante, S. *Br. J. Pharmacol.* **2008**, 153(1), 34-41; c) Ansari, K. I., Kasiri, S., Grant, J. D. and Mandal, S. S. *Dalton Trans.*, **2009**, 8525-8531.

²⁷⁵ Camara, K. S., Lesnefsky, E. J. and Stowe, D. F. *Antioxid. Redox. Signaling* **2010**, 13(3), 279-347.

²⁷⁶ a) Monteith, G. R., Andrew, D. M., Faddy, H. M. and Robert-Thomson, S. K. *Nat. Rev. Cancer* **2007**, 8(7), 519-529; b) Frezza, C. and Gottlieb, E. *Semin. Cancer Biol.* **2009**, 19(4), 4-15.

²⁷⁷ a) Aschner, M., Ruilarte, T. R., Schneider, J. S. and Zhang, W. *Toxicol. Appl. Pharmacol.* **2007**, 221(2), 131-147; b) Calzolari, A., Oliviero, I., Deaglio, S., Mariani, G., Biffoni, M., Sposi, N. M., Malavasi, F., Peschle, C. and Testa, U. *Blood Cells, Mol. Dis.*, **2007**, 39(1), 82-91.

²⁷⁸ Sciot, R. P., Eyken, V. and Desmet, V. J. *Histopathology* **1990**, 16(1), 59-62.

²⁷⁹ a) Chen, Q. Y., Zhou, D. F., Huang, J., Guo, W. J. and Gao, J. *J. Inorg. Biochem.* **2010**, 104(11), 1141-1149.

²⁸⁰ López-Lázaro, M. *Cancer Lett.* **2007**, 252(1), 1-8.

²⁸¹ Schumacker, P. T. *Cancer Cell* **2006**, 10(3), 175-176.

²⁸² a) Bhat, S. S., Kumbharm, A. S., Lönnecke, P. and Hey-Hawkins, E. *Inorg. Chem.* **2010**, 49(11), 4843-4853; b) Abu-Youssef, M. A. M., Soliman, S. M., Langer, V., Gohar, Y. M., Hasanen, A. A., Makhyoun, M. A., Zaky, A. H. and Öhrström, L. R. *Inorg. Chem.* **2010**, 49(14), 9788-9797.

Chapter VI

- ²⁸³ Allardyce, C. S. and Dyson, P. J. *Platinum Metals Rev.* **2001**, 45(2), 62-69.
- ²⁸⁴ a) Sava, G., Pacor, S., Mestroni, G. and Alessio, E. *Anticancer Drugs* **1992**, 3(1), 25-31; b) Bacac, M., Hotze, A. C. G., van der Schilden, K., Haasnoot, J. G., Pacor, S., Alessio, E., Sava, G. and Reedijk, J. J. *Inorg. Biochem.* **2004**, 98(2), 402-412.
- ²⁸⁵ a) Gava, B., Zorzet, P., Spessotto, P., Cocchietto, M. and Sava, G. *J. Pharmacol. Exp. Ther.* **2006**, 317(1), 284-291; b) Antonarakis, E. S. and Emadi, A. *Cancer Chemoth. Pharm.* **2010**, 66(1), 1-9.
- ²⁸⁶ a) Iengo, E., Mestroni, G., Geremia, S., Calligaris, M. and Alessio, E. *J. Chem. Soc., Dalton Trans.* **1999**, 19, 3361-3371; b) Serli, B., Iengo, E., Gianferrari, T., Zangrando, E. and Alessio, E. *Metal-Based Drugs* **2001**, 8(1), 9-18; c) Velderes, A. H., Bergamo, A., Alessio, E., Zangrando, E., Haasnoot, J. G., Casarsa, C., Cocchietto, M., Zozet, S. and Sava, G. *J. Med. Chem.* **2004**, 47(7), 1110-1119; d) Groessl, M., Reisner, E., Hartinger, C. G., Eichinger, R., Semenova, O., Timerbaev, A. R., Jakupec, M. A., Arion, V. B. and Keppler, B. K. *J. Med. Chem.* **2007**, 50(9), 2185-2193; e) Hudej, R., Miklavcic, D., Cemazar, M., Todorovic, V., Sersa, G., Bergamo, A., Sava, G., Martincic, A., Scancar, J., Keppler, B. K. and Turel, I. *J. Memb. Biol.* **2014**, 247(12), 1239-1251.
- ²⁸⁷ Hartinger, C. G., Zorbas-Seifried, S., Jakupec, M. A., Kynast, B., Zorbas, H. and Keppler, B. K. *J. Inorg. Biochem.* **2006**, 100(5-6), 891-904.
- ²⁸⁸ Lu, C.Y., Puig, T., Obradors, X., Ricart, S. and Ros, J. *RSC Adv.* **2016**, 6(91), 88762-88769.
- ²⁸⁹ Brunner, H. and Scheck, T. *Chem. Ber.* **1992**, 125(3), 701-709.
- ²⁹⁰ Huckel, W. and Bretschneider, H. *Chem. Ber.* **1937**, 70(8), 2024-2026.
- ²⁹¹ Thiel, W. R., Angstl, M. and Priermeier, T. *Chem. Ber.* **1994**, 127(12), 2373-2379.
- ²⁹² Pal, S., Chan, M. K. and Armstrong, W. H. *J. Am. Chem. Soc.* **1992**, 114(16), 6398-6406.
- ²⁹³ Catalán, J., Fabero, F., Claramunt, R. M., Santa María, M. D., Foces-Foces, M. C., Hernández, F., Martínez-Ripoll, M., Elguero, J. and Sastre, R. *J. Am. Chem. Soc.* **1992**, 114(13), 5039-5048.
- ²⁹⁴ Seubert, C. K., Sun, Y. and Thiel, W. R. *Dalton Trans.* **2009**, 4971-4977.
- ²⁹⁵ Inada, Y., Nakano, Y., Inamo, M. and Funashashi, S. *Inorg. Chem.* **2000**, 39(21), 4793-4801.
- ²⁹⁶ Sullivan, B. P., Calvert, J. M. and Meyer, T. J. *Inorg. Chem.* **1980**, 19(5), 1404-1407.
- ²⁹⁷ a) Taqui Khan, M. M., Roy, P. S., Venkatasubramanian, K. and Khan, N. H. *Inorg. Chim. Acta* **1990**, 176(1), 49-55; b) Iengo, E., Zangrando, E., Baiutti, E., Munini, F. and Alessio, E. *Eur. J. Inorg. Chem.* **2005**, 6, 1019-1031.
- ²⁹⁸ Serrano, I. "Síntesi i caracterització de nous complexos de ruteni contenint lligands quirals. Aplicacions en catàlisi asimètrica", Universitat de Girona, **2008**. <<http://hdl.handle.net/10803/8050>>

- ²⁹⁹ Ziessel, R., Grosshenny, V., Hissler, M. and Stroh, C. *Inorg. Chem.* **2004**, 43(14), 4262-4271.
- ³⁰⁰ Bruker Advanced X-raySolutions. SMART: Version 5.631, **1997-2002**.
- ³⁰¹ Bruker Advanced X-raySolutions. SAINT +, Version 6.361, **2001**.
- ³⁰² a) Sheldrick, G. M. *Empirical Absorption Correction Program*, Universität Göttingen, **1996**; b) Bruker Advanced X-raySolutions. SADABS Version 2.10, **2001**.
- ³⁰³ a) Sheldrick, G. M. *Program for Crystal Structure Refinement*, Universität Göttingen, **1997**; b) Bruker Advanced X-raySolutions. SHELXTL Version 6.14, **2000-2003**.
- ³⁰⁴ Spek, A. L. (**2009**). Acta Cryst. D65, 148-155 PLATON, A Multipurpose Crystallographic Tool, Utrecht University, Utrecht, The Netherlands.
- ³⁰⁵ a) McCann, S., McCann, M., Casey, R. M. T., Jackman, M., Devereux, M. and McKee, V. *Inorg. Chim. Acta* **1998**, 279(1), 24-29; b) Chen, C., Zhu, H., Huang, D., Wen, T., Liu, Q., Liao, D. and Cui, J. *Inorg. Chim. Acta* **2001**, 320(1-2), 159-166; c) Smith, J. A., Galán-Masacrós, Clérac, J. R., Sun, J.-S., Ouyang, X. and Dunbar, K. R. *Polyhedron* **2001**, 20(11-14), 1727-1734; d) Baffert, C., Romero, I., Pécaut, J., Llobet, A., Deronzier, A. and Collomb, M.-N. *Inorg. Chim. Acta* **2004**, 357(12), 3430-3436; e) Zou, R.-Q., Liu, C.-S., Shi, X.-S., Bu, X.-H. and Ribas, J. *Cryst. Eng. Comm.* **2005**, 7(118), 722-727; f) van Gorkum, R., Buda, F., Kooijman, H., Spek, A. L., Bouwman, E. and Reedijk, J. *Eur. J. Inorg. Chem.* **2005**, 11, 2255-2261.
- ³⁰⁶ Rich, J., Manrique, E., Molton, F., Duboc, C., Collomb, M.-N., Rodríguez, M. and Romero, I. *Eur. J. Inorg. Chem.* **2014**, 16, 2663-2670.
- ³⁰⁷ a) Sala, X., Poater, A., von Zelewsky, A., Parella, T., Fontrodona, X., Romero, I., Solà, M., Rodríguez, M. and Llobet, A. *Inorg. Chem.* **2008**, 47(18), 8016-8024. b) Rodríguez, M., Romero, I., Llobet, A., Deronzier, A., Biner, M., Parella, T. and Stoeckli-Evans, H. *Inorg. Chem.* **2001**, 40(17), 4150-4156.
- ³⁰⁸ a) Karthikeyan, M., Karthikeyan, S. and Manimaran, B. *Acta Cryst. Sect. E* **2011**, 67(Pt 10), m1367; b) Hachula, B., Pedras, M., Petak, D., Nowak, M., Kusz, J. and Borek, J. *Acta Cryst. Sect. C* **2009**, 65(Pt 6), m215-m218; c) Kruszynski, R., Bartczak, T. J., Adamczyk, A., Czakis-Sulikowska, D. and Kaluzna, J. *Acta Cryst. Sect. E* **2001**, 57(Pt 5), m183-m185.
- ³⁰⁹ Lehn, J. M. *Supramolecular Chemistry*. VCH: Weinheim (Germany), **1995**.
- ³¹⁰ Bu, X. H., Tong, M. L., Chang, H. C., Kitagawa, S. and Batten, S. R. *Angew. Chem., Int. Ed.* **2004**, 43(2), 192-195.
- ³¹¹ Addison, A.W., Rao, T. N., Reedijk, J., Rijn, J. V. and Verschoor, G. C. *Dalton Trans.* **1984**, 7, 1349-1356.
- ³¹² a) Viciano-Chumillas, M., Giménez-Marqués, M., Tanase, S., Evangelisti, M., Mutikainen, I., Turpeinen, U., Smits, J. M. M., de Gelder, R., de Jongh, L. J. and Reedijk, J. *J. Phys. Chem. C* **2008**, 112(51), 20525-

Chapter VI

20534; b) Viciano-Chumillas, M., Tanase, S., Mutikainen, I., Turpeinen, U., de Jongh, L. J. and Reedijk, J. *Dalton Trans.* **2009**, 36, 7445-7453.

³¹³ a) Romero, I., Collomb, M.-N., Deronzier, A., Llobet, A., Perret, E., Pecaut, J., Le Pape, L. and Latour, J. *M. Eur. J. Inorg. Chem.* **2001**, 1, 69-72; b) Hureau, C., Blondin, G., Charlot, M.-F., Philouze, C., Nierlich, M., Césarío, M. and Anxolabéhère-Mallart, E. *Inorg. Chem.* **2005**, 44(10), 3669–3683.

³¹⁴ a) Dingle, R. *Acta Chem. Scand.* **1966**, 20(1), 33-44; b) Davis, T. S., Fackler, J. P. and Weeks, M. J. *Inorg. Chem.* **1968**, 7(3), 1994-2002; c) Pascaly, M., Duda, M., Rompel, A., Sift, B. H., Meyer-Klaucke, W. and Krebs, B. *Inorg. Chim. Acta* **1999**, 291(1-2), 289-299; d) Triller, M. U., Pursche, D., Hsieh, W.-Y., Pecoraro, V. L., Rompel, A. and Krebs, B. *Inorg. Chem.* **2003**, 42(20), 6274-6283; e) Mantell, C., Chen, H. Y., Crabtree, R. H., Brudvig, G. V., Pecaut, J., Collomb, M.-N. and Duboc, C. *Chem. Phys. Chem.* **2005**, 6(3), 541-546.

³¹⁵ Cussó, O., Garcia-Bosch, I., Font, D., Ribas, X., Lloret-Fillol, J. and Costas, M. *Org. Lett.* **2013**, 15(24), 6158-6161.

³¹⁶ Sankaralingam, M. and Palaniandavar, M. *Dalton Trans.* **2014**, 43, 538-550.

³¹⁷ a) Adam, W., Roschmann, K. J., Saha-Möller, C. R. and Seebach, D. J. *J. Am. Chem. Soc.* **2002**, 124(18), 5068-5073; b) Park, S.-E., Song, W. J., Ryu, Y. O., Lim, M. H., Song, R., Kim, K. M. and Nam, W. J. *J. Inorg. Biochem.* **2005**, 99(2), 424-431.

³¹⁸ Lee, S. H., Xu, L., Park, B. K., Mironov, Y. V., Kim, S. H., Song, Y. J., Kim, C., Kim, Y. and Kim, S.-J. *Chem. Eur. J.* **2010**, 16(15), 4678-4685.

³¹⁹ a) Yin, G., Buchalova, M., Danby, A. M., Perkins, C.M., Kitko, D., Carter, J. D., Scheper, W. M. and Busch, D. H. *J. Am. Chem. Soc.* **2005**, 127(49), 17170-17171; b) Yin, G., Danby, A. M., Kitko, D., Carter, J. D., Scheper, W. M. and Busch, D. H. *J. Am. Chem. Soc.* **2008**, 130(48), 16245-16253.

³²⁰ a) Jin, N., Ibrahim, M., Spiro, T. G. and Groves, J. T. *J. Am. Chem. Soc.* **2007**, 129(41), 12416-12417; b) Liu, W. and Groves, J. T. *J. Am. Chem. Soc.* **2010**, 132(37), 12847-12849.

³²¹ Ferbert, M., Montilla, F., Galindo, A., Moyano, R., Pastor, A. and Alvarez, E. *Dalton Trans.* **2011**, 40, 5210-5219.

³²² a) Ma, J. C. and Dougherty, D. A. *Chem. Rev.* **1997**, 97(5), 1303-1324; b) Hanke, C. G., Johansson, A., Harper, J. B. and Lynden-Bell, R. M. *Chem. Phys. Lett.* **2003**, 374(1-2), 85-90; c) Olivier-Bourbigou, H., Magna, L. and Morvan, D. *Appl. Catal. A* **2010**, 373(1-2), 1-56; d) Pârvulescu, V. I. and Hardadre, C. *Chem. Rev.* **2007**, 107(6), 2615-2665.

³²³ a) Rudolph, J., Reddy, K. L., Chiang, J. P. and Sharpless, K. B. *J. Am. Chem. Soc.* **1997**, 119(26), 6189-6190; b) Adolfsson, H., Converso, A. and Sharpless, K. B. *Tetrahedron Lett.* **1999**, 40(21), 3991-3994.

- ³²⁴ a) Jaronczyk, M., Dobrowolski, J. Cz. and Mazurek, A. P. *J. Mol. Struct-Theochem* **2004**, 673(1-3), 17-28; b) Claramunt, R. M., Ángeles García, M., López, C., Trofimenko, S., Yap, G. P. A., Alkorta, I. and Elguero, J. *Magn. Reson. Chem.* **2005**, 43(1), 89-91 and references cited therein; c) Alkorta, I. and Elguero, J. *J. Chil. Chem. Soc.* **2015**, 60, 2966-2970.
- ³²⁵ a) Cornago, P., Cabildo, P., Claramunt, R. M., Bouissane, L., Pinilla, E., Torres, M. R. and Elguero, J. *New. J. Chem.* **2009**, 33(1), 125-135.
- ³²⁶ Díez, J., Gimeno, J., Merino, I., Rubio, E. and Suárez, F. J. *Inorg. Chem.* **2011**, 50(11), 4868-4881.
- ³²⁷ Ferrer, I., Fontrodona, X., Rodríguez, M. and Romero, I. *Dalton Trans.* **2016**, 45, 3163-3171.
- ³²⁸ Sens, C., Rodríguez, M., Romero, I., Parella, T., Benet-Buchholz, J. and Llobet, A. *Inorg. Chem.* **2003**, 42(25), 8385-8394.
- ³²⁹ Balzani, V., Juris, A. and Vetry, M. *Chem. Rev.* **1996**, 96(2), 759-834.
- ³³⁰ Nicholson, R. S. and Shain, I. *Anal Chem.* **1964**, 36(4), 706-723.
- ³³¹ Benet-Buchholz, J., Comba, P., Llobet, A., Roeser, S., Vadivelu, P. and Wiesner, S. *Dalton Trans.* **2010**, 39, 3315-3320.
- ³³² Dakkach, M., López, I., Romero, I., Rodríguez, M., Atlamsani, A., Parella, T., Fontrodona, X. and Llobet, A. *Inorg. Chem.* **2010**, 49(15), 7072-079.
- ³³³ Dakkach, M., Atlamsani, A., Parella, T., Fontrodona, X., Romero, I. and Rodríguez, M. *Inorg. Chem.* **2013**, 52(9), 507-5087.
- ³³⁴ Roeser, S., Farràs, P., Bozoglian, F., Martínez-Belmonte, M., Benet-Buchholz, J. and Llobet, A. *ChemSusChem* **2011**, 4(2), 197-207.
- ³³⁵ Binstead, R. A. and Meyer, T. J. *J. Am. Chem. Soc.* **1987**, 109(11), 3287-3297.
- ³³⁶ Bessel, C. A., Leising, R. A. and Takeuchi, K. J. *J. Chem. Soc; Chem. Commun.* **1991**, 17, 883-835.
- ³³⁷ a) Barf, G. A. and Sheldon, R. A. *J. Mol. Catal. A: Chem.* **1995**, 102(1), 23-39; b) Tse, M. K., Döbler, C., Bhor, S., Klawonn, M., Mägerleins, W., Hugl, H. and Beller, M. *Angew. Chem. Int. Ed.* **2004**, 43(39), 5255-5260; c) Tse, M. K., Bhor, S., Klawonn, M., Anilkumar, G., Jiao, H., Spannenberg, A., Döbler, C., Mägerlein, W., Hugl, H. and Beller, M. *Chem. Eur. J.* **2006**, 12(7), 1875-1888; d) Mägerlein, W., Dreisbach, C., Hugl, H., Tse, K., Klawonn, M., Bhor, S. and Beller, M. *Catal. Today* **2007**, 121(1-2), 140-150; e) Benet-Buchholz, J., Comba, P., Llobet, A., Roeser, S., Vadivelu, P., Wadepoh, H. and Wiesner, S. *Dalton Trans.* **2009**, 5910-5923; f) Chowdhure, A. D., Das, A., Irshad, K., Mobin, S. M. and Lahiri, G. K. *Inorg. Chem.* **2011**, 50(5), 1775-1785.
- ³³⁸ Smith, R. *Platinum Metals Rev.* **2009**, 53(2), 55-56.

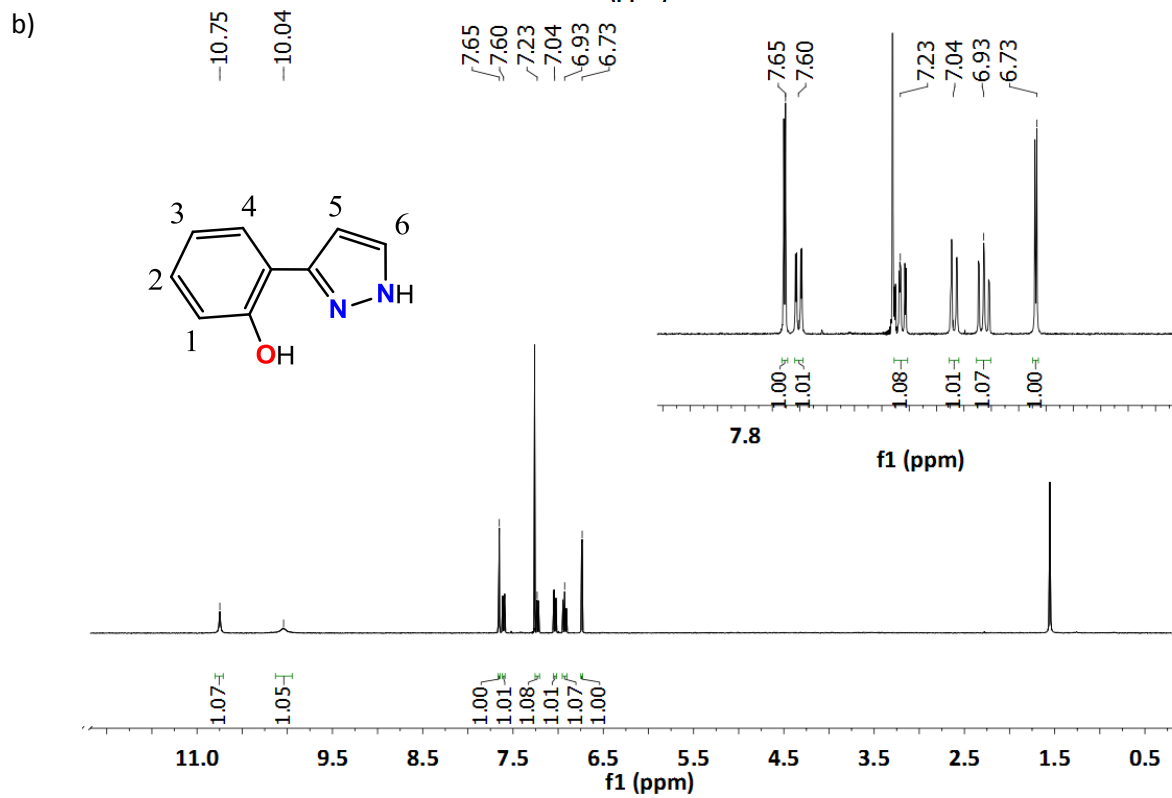
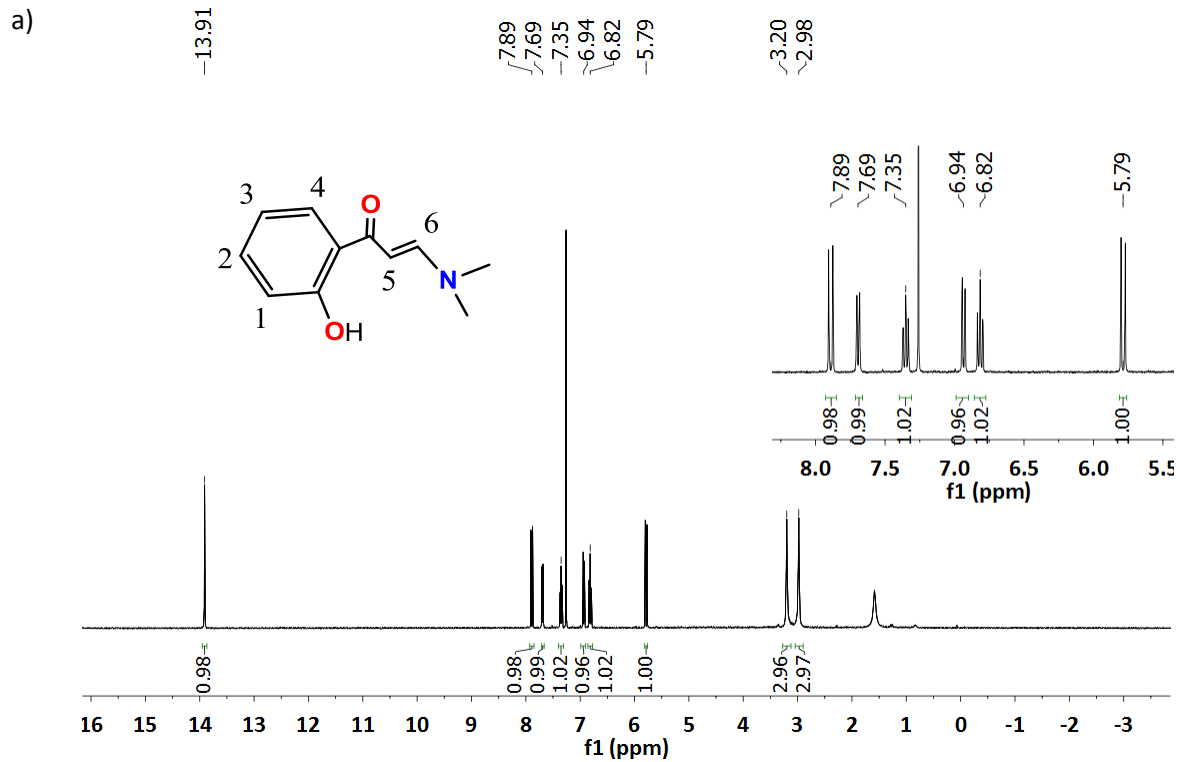
Chapter VI

- ³³⁹ Hanif, M. A. "Characterization of Pd nanoparticles and of silica-supported Pd-catalysts for the Suzuki-Miyaura reaction", *Queen's University*, **2014**. <<http://hdl.handle.net/1974/12513>>
- ³⁴⁰ Morgan, D. J. *Surf. Interface. Anal.* **2015**, 47(11), 1072-1079.
- ³⁴¹ Manrique, E., Poater, A., Fontrodona, X., Solà, M., Rodríguez, M. and Romero, I. *Dalton Trans.* **2015**, 17529-17543.
- ³⁴² Novakova, O., Kasparkova, J., Vrana, O., van Vliet, P. M., Reedijk, J. and Brabec, V. *Biochemistry* **1995**, 34(38), 12369-12378.
- ³⁴³ Hotze, A. C. G., Velders, A. H., Ugozzoli, F., Biagini-Cingi, M., Manotti-Lanfredi, A. M., Haasnoot, J. G. and Reedijk, J. *Inorg. Chem.* **2000**, 39(17), 3838-3844.
- ³⁴⁴ Liu, Z. and Sadler, P. J. *Acc. Chem. Res.* **2014**, 47(4), 1174-1185.
- ³⁴⁵ Yadav, P. N., Beveridge, R. E., Blay, J., Boyd, A. R., Chojnacka, M. W., Decken, A., Deshpande, A. A., Gardiner, M. G., Hambley, T. W., Hughes, M. J., Jolly, L., Lavangie, J. A., MacInnis, T. D., McFarland, S. A., New, E. J. and Gossage, R. A. *Med. Chem. Commun.* **2011**, 2(4), 274-277.
- ³⁴⁶ Lopes, P. "New ruthenium complexes containing N- or/and S-donor type of ligands as catalysts for nitrile hydration". TFG
- ³⁴⁷ Frasca, D., Ciampa, J., Emerson, J., Umans, R. S. and Clarke, M. J. *Metal Based Drugs*, **1996**, 3(6), 197-209.

ANNEX. Suporting information

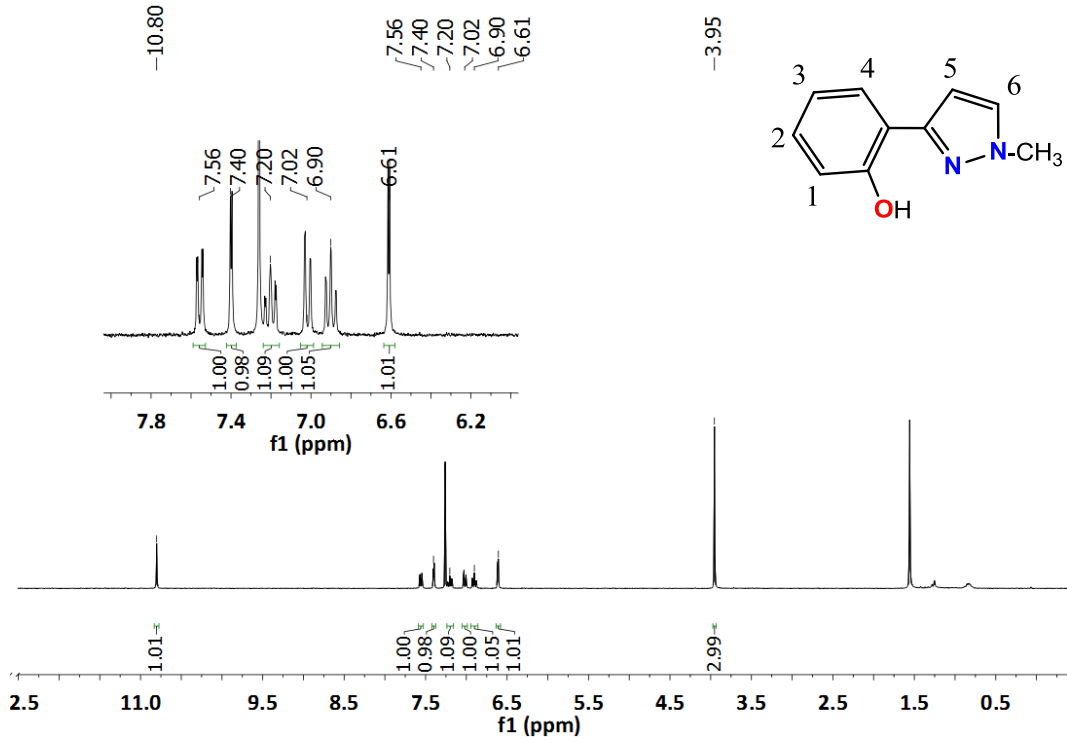
ANNEX. Supporting Information

Chapter 3

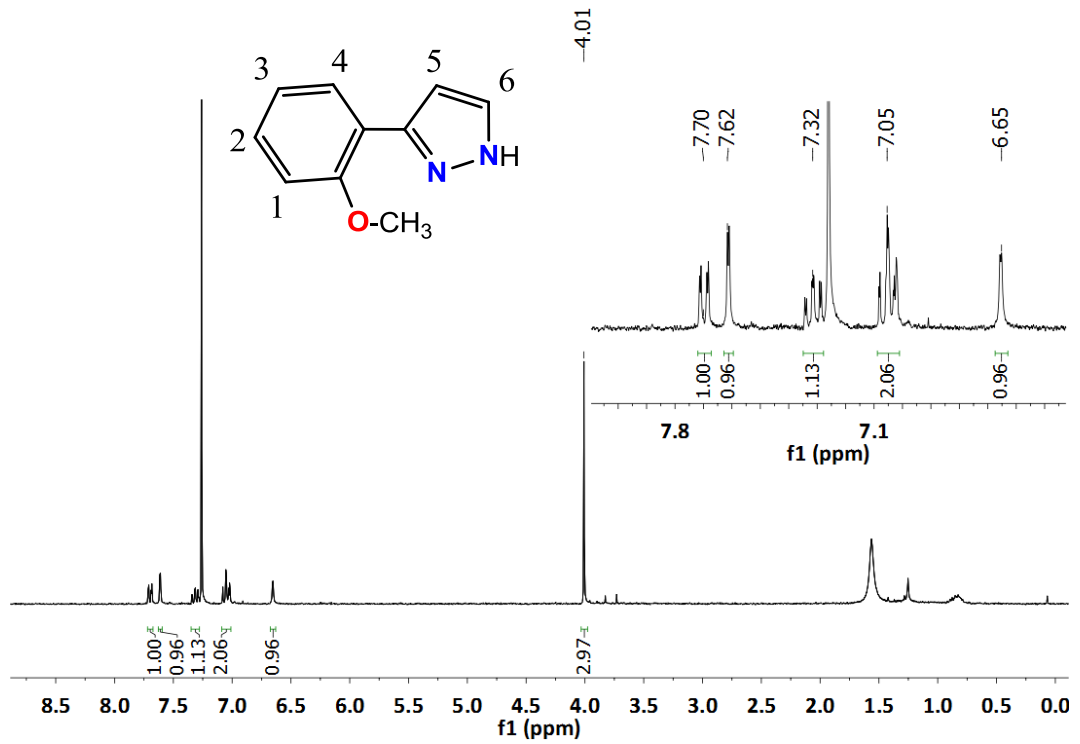


Annex

c)



d)



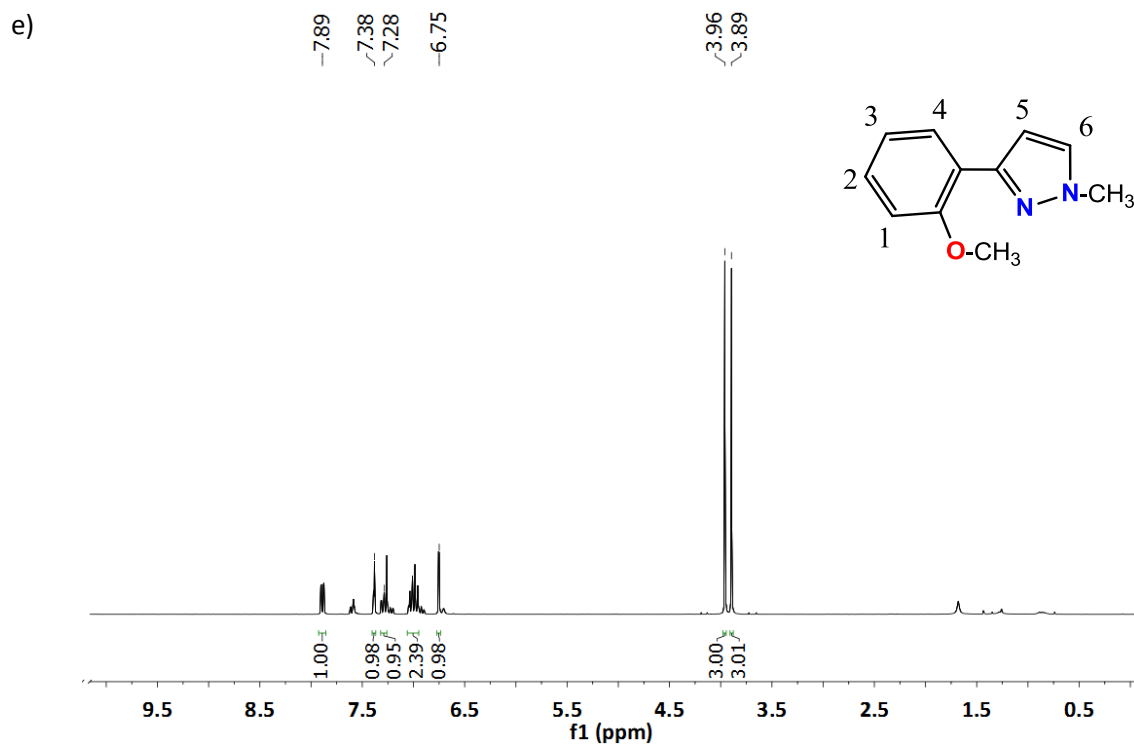


Figure SIII.1. ¹H-NMR in CDCl₃ of *L* (a), *L4* (b), *L5* (c), *L5'* (d) and *L5''* (e).

Chapter 4

Table SIV.1.1. Crystallographic data for complexes **Mn1-Mn9**.

| | Mn1 | Mn2 | Mn3 | Mn4 | Mn5 | Mn6 | Mn7 | Mn8 | Mn9 |
|--|--|---|---|---|--|--|---|--|---|
| Empirical formula | C ₁₆ H ₁₄ Cl ₂ MnN ₆ | C ₁₈ H ₁₄ F ₆ MnN ₆ O ₆ S ₂ | C ₂₄ H ₂₈ MnN ₆ O ₈ | C ₁₆ H ₁₄ MnN ₈ O ₆ | C ₈ H ₁₁ Cl ₂ MnN ₃ O ₂ | C ₁₈ H ₁₈ Cl ₂ MnN ₆ | C ₂₀ H ₁₈ F ₆ MnN ₆ O ₆ S ₂ | C ₂₇ H ₂₈ F ₆ MnN ₆ O ₁₀ S ₂ Cl ₂ | C ₁₈ H ₁₄ ClMnN ₄ O ₂ |
| Formula weight | 416.17 | 643.41 | 583.46 | 543.41 | 307.04 | 444.22 | 671.46 | 900.51 | 408.72 |
| Crystal system | Monoclinic | Triclinic | Orthorhombic | Monoclinic | Monoclinic | Triclinic | Monoclinic | Monoclinic | Monoclinic |
| Space group | C2/c | P -1 | Pbcn | P21/c | P21/c | P -1 | C 2/c | P 21/c | P2(1)/c |
| a/Å | 10.562(2) | 9.879(2) | 13.439(3) | 12.558(17) | 11.642(2) | 7.916(7) | 22.475(6) | 11.577(2) | 12.183(4) |
| b/Å | 14.818(3) | 10.616(3) | 10.422(3) | 11.881(16) | 19.420(4) | 13.457(12) | 9.064(3) | 20.847(4) | 7.422(3) |
| c/Å | 13.274(3) | 13.434(3) | 20.069(5) | 19.294(18) | 11.223(2) | 18.745(16) | 29.523(9) | 16.274(3) | 18.732(7) |
| α/° | 90 | 86.091(5) | 90 | 90 | 90 | 90.535(17) | 90 | 90 | 90 |
| β/° | 91.500(4) | 83.134(5) | 90 | 95.143(2) | 102.100(4) | 92.560(15) | 108.499(7) | 101.281(3) | 96.061(6) |
| γ/° | 90 | 62.804(4) | 90 | 90 | 90 | 94.308(16) | 90 | 90 | 90 |
| V/Å³ | 2076.8(8) | 1244.5(5) | 2811(12) | 2382(5) | 2480.8(9) | 1989(3) | 5704(3) | 3851.6(12) | 1684.3(11) |
| Formula units per cell | 4 | 2 | 4 | 4 | 8 | 4 | 8 | 4 | 4 |
| T/K | 298(2) | 298(2) | 298(2) | 100(2) | 298(2) | 142(2) | 130(2) | 298(2) | 293(2) |
| ρ_{calc}/Mgm⁻³ | 1.331 | 1.717 | 1.379 | 1.308 | 1.644 | 1.483 | 1.564 | 1.553 | 1.612 |
| μ/mm⁻¹ | 0.903 | 0.791 | 0.525 | 0.624 | 1.483 | 0.948 | 0.694 | 0.677 | 0.964 |
| Reflections collected/unique | 12727/2567 | 15958/5985 | 40443/3467 | 20260/5745 | 38802/6087 | 10955/8273 | 9186/5471 | 57987/8955 | 24962/4154 |
| R(int) | 0.1002 | 0.0769 | 0.1204 | 0.4239 | 0.0414 | 0.0816 | 0.0853 | 0.0612 | 0.0826 |
| Final R indices, [I>2σ(I)] | R ₁ = 0.0492, wR ² = 0.1126 | R ₁ = 0.0801, wR ² =0.1309 | R ₁ = 0.0468, wR ² = 0.1022 | R ₁ = 0.1355, wR ² = 0.2408 | R ₁ = 0.0686, wR ² = 0.1611 | R ₁ = 0.1261; wR ² =0.3026 | R ₁ = 0.0788; wR ² =0.1488 | R ₁ = 0.0722; wR ² =0.1834 | R ₁ = 0.0475, wR ² = 0.0953 |
| R indices [all data] | R ₁ = 0.0686, wR ² = 0.1227 | R ₁ = 0.1438, wR ² = 0.1566 | R ₁ = 0.0900, wR ² = 0.1223 | R ₁ = 0.3981, wR ² = 0.3067 | R ₁ = 0.0856, wR ² = 0.1705 | R ₁ = 0.2115, wR ² = 0.3645 | R ₁ = 0.1798, wR ² = 0.1874 | R ₁ = 0.1213, wR ² = 0.2196 | R ₁ = 0.0877, wR ² = 0.1093 |

Table SIV.1.2. Selected bond lengths (Å) and angles (°) for Mn1-Mn9.

| Mn1 | | | |
|----------------------------|------------|--|---------------------------------|
| Mn—Cl(1) | 2.4768(8) | Cl(1)—Mn—Cl(1) | 97.95(4) |
| Mn—N(1) _{py} | 2.351(2) | N(1) _{py} —Mn—N(2) _{pz} or N(1) _{py} —Mn—N(3) _{pz} | 70.87(7) |
| Mn—N(3) _{pz} | 2.236(2) | N(1) _{py} —Mn—N(1) _{py} N(3) _{pz} —Mn—N(3) _{pz} | 86.20(10) 157.15(12) |
| Mn2 | | | |
| Mn—O(1) | 2.172(3) | O(4)—Mn—O(1) | 89.31(15) |
| Mn—O(4) | 2.155(4) | N(1) _{py} —Mn—N(3) _{pz} | 73.13(14) |
| Mn—N(1) _{py} | 2.288(4) | N(1) _{py} —Mn—N(4) _{py} | 90.83(15) |
| Mn—N(4) _{py} | 2.312(4) | | |
| Mn—N(3) _{pz} | 2.230(4) | N(3) _{pz} —Mn—N(6) _{pz} | 155.37(15) |
| Mn—N(6) _{pz} | 2.212(4) | | |
| Mn3 | | | |
| Mn—O(1) | 2.1262(18) | O(1)—Mn—O(1) | 94.61(11) |
| Mn—N(1) _{py} | 2.3381(19) | N(1) _{py} —Mn—N(3) _{pz} | 71.08(7) |
| Mn—N(3) _{pz} | 2.2616(18) | N(1) _{py} —Mn—N(1) _{py} N(3) _{pz} —Mn—N(3) _{pz} | 82.39(9) 159.59(9) |
| Mn4 | | | |
| Mn—O(1) | 2.2230(19) | O(4)—Mn—O(1) | 79.70(7) |
| Mn—O(4) | 2.2465(18) | N(1) _{py} —Mn—N(3) _{pz} | 71.95(8) |
| Mn—N(1) _{py} | 2.269(2) | N(1) _{py} —Mn—N(4) _{py} | 94.52(8) |
| Mn—N(4) _{py} | 2.310(2) | | |
| Mn—N(3) _{pz} | 2.272(2) | N(3) _{pz} —Mn—N(6) _{pz} | 150.74(8) |
| Mn—N(6) _{pz} | 2.281(2) | | |
| Mn5 | | | |
| Mn(1)—Cl(1) | 2.4751(15) | O(2)—Mn(1)—O(1) | 170.63 (10) |
| Mn(1)—Cl(2) | 2.5013(15) | O(1a)—Mn(1a)—O(2a) | 101.04 (13) |
| Mn(1)—O(1) | 2.218(3) | Cl(1)—Mn(1)—Cl(2) | 105.23(5) |
| Mn(1)—O(2) | 2.202(3) | Cl(1a)—Mn(1a)—Cl(2a) | 170.65 (5) |
| Mn(1)—N(1) _{py} | 2.301(4) | N(1) _{py} —Mn(1)—N(3) _{pz} | 71.52 (14) |
| Mn(1)—N(3) _{pz} | 2.258(4) | N(1a) _{py} —Mn(1a)—N(3a) _{pz} | 72.7 (2) |
| Mn(1a)—Cl(1a) | 2.5235(15) | O(1)—Mn(1)—N(1) _{py} | 88.85 (14) |
| Mn(1a)—Cl(2a) | 2.5945(14) | Cl(1a)—Mn(1a)—N(1a) _{py} | 92.27 (12) |
| Mn(1a)—O(1a) | 2.151(3) | O(1)—Mn(1)—N(3) _{pz} | 90.58 (13) |
| Mn(1a)—O(2a) | 2.174(3) | Cl(1a)—Mn(1a)—N(3) _{pz} | 97.83 (15) |
| Mn(1a)—N(1a) _{py} | 2.242(5) | Cl(1)—Mn(1)—N(3) _{pz} | 89.75 (11) |
| Mn(1a)—N(3a) _{pz} | 2.241(5) | O(2a)—Mn(1a)—N(3a) _{pz} | 91.5 (2) |
| Mn6 | | | |
| Mn—Cl(1) | 2.4715(4) | Cl(1)—Mn—Cl(2) | 104.095(11) |
| Mn—Cl(2) | 2.483(3) | N(4) _{py} —Mn—Cl(2) | 91.505(19) |
| Mn—N(1) _{py} | 2.3485(9) | N(3) _{pz} —Mn—N(6) _{pz} | 81.35(3) |
| Mn—N(4) _{py} | 2.3565(10) | N(1) _{py} —Mn—N(3) _{pz} | 69.95(3) |
| Mn—N(3) _{pz} | 2.351(8) | N(1) _{py} —Mn—N(4) _{py} | 175.25(3) |
| Mn—N(6) _{pz} | 2.316(9) | N(4) _{py} —Mn—N(6) _{pz} N(1) _{py} —Mn—Cl(1) | 70.4(3) 90.2(2) |
| Mn7 | | | |
| Mn—O(1) | 2.176(4) | O(4)—Mn—O(1) | 95.10(18) |
| Mn—O(4) | 2.161(5) | N(1) _{py} —Mn—N(3) _{pz} | 73.0(2) |
| Mn—N(1) _{py} | 2.255(6) | N(1) _{py} —Mn—N(4) _{py} | 88.79(19) |
| Mn—N(4) _{py} | 2.321(5) | N(3) _{pz} —Mn—N(6) _{pz} | 99.0(2) |
| Mn—N(3) _{pz} | 2.232(6) | N(3) _{pz} —Mn—N(4) _{py} | 87.29(18) |
| Mn—N(6) _{pz} | 2.230(6) | N(4) _{py} —Mn—N(6) _{pz} N(6) _{pz} —Mn—O(4) O(1)—Mn—N(1) _{py} | 73.0(2) 98.1(2) 99.60(19) |
| Mn8 | | | |
| Mn—O(5) | 2.149(3) | O(5)—Mn—O(8) | 92.63(13) |
| Mn—O(8) | 2.130(3) | N(1) _{py} —Mn—N(3) _{pz} | 73.15(12) |
| Mn—N(1) _{py} | 2.252(4) | N(1) _{py} —Mn—N(4) _{py} | 89.89(13) |
| Mn—N(4) _{py} | 2.235(4) | N(3) _{pz} —Mn—N(6) _{pz} | 167.35(12) |

Annex

| | | | |
|-----------------------|------------|---|------------|
| Mn—N(3) _{pz} | 2.254(3) | N(3) _{pz} —Mn—N(4) _{py} | 102.16(13) |
| Mn—N(6) _{pz} | 2.272(2) | N(4) _{py} —Mn—N(6) _{pz} | 73.45(12) |
| | | N(6) _{pz} —Mn—O(5) | 96.58(2) |
| | | O(8)—Mn—N(1) _{py} | 93.11(13) |
| Mn9 | | | |
| Mn—Cl(1) | 2.4515(12) | Cl(1)—Mn—O(2) | 98.39(7) |
| Mn—O(1) | 1.8522(19) | Cl(1)—Mn—N(2) _{pz} | 93.14(8) |
| Mn—O(2) | 1.8481(19) | Cl(1)—Mn—O(1) | 102.56(7) |
| Mn—N(2) _{pz} | 1.976(2) | O(1)—Mn—O(2) | 159.05(10) |
| Mn—N(4) _{pz} | 1.970(2) | O(1)—Mn—N(2) | 88.77(9) |
| | | O(2)—Mn—N(4) _{pz} | 89.37(9) |

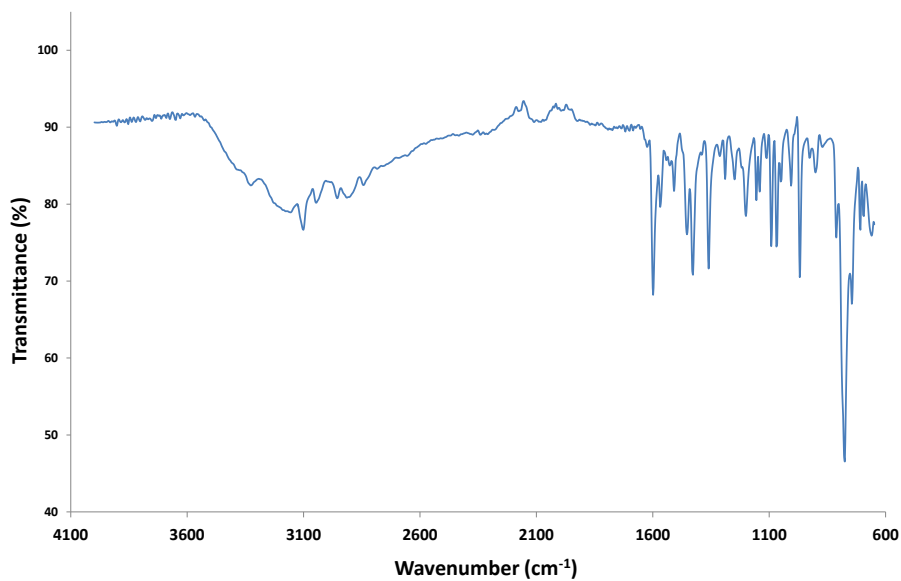


Figure SIV.1.2. FTIR spectra of Mn1.

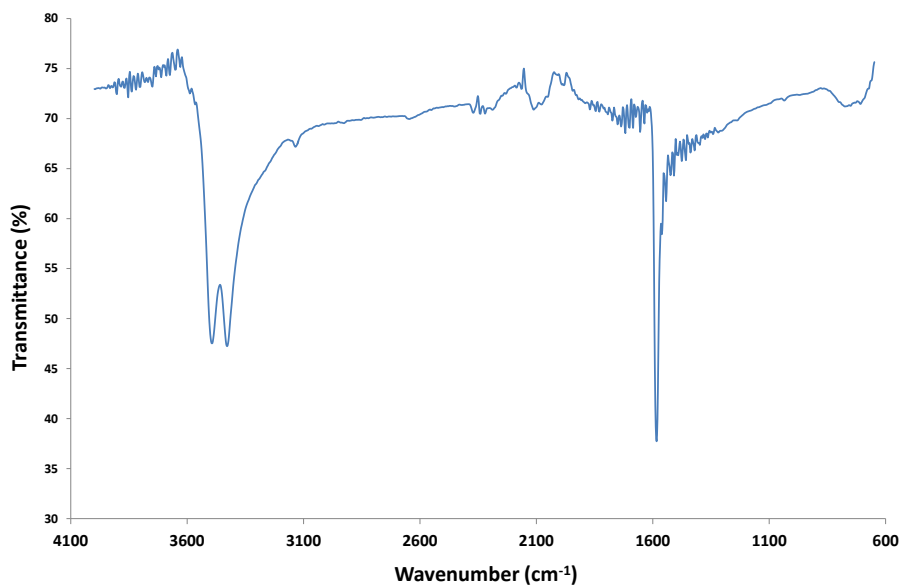


Figure SIV.1.3. FTIR spectra of Mn2.

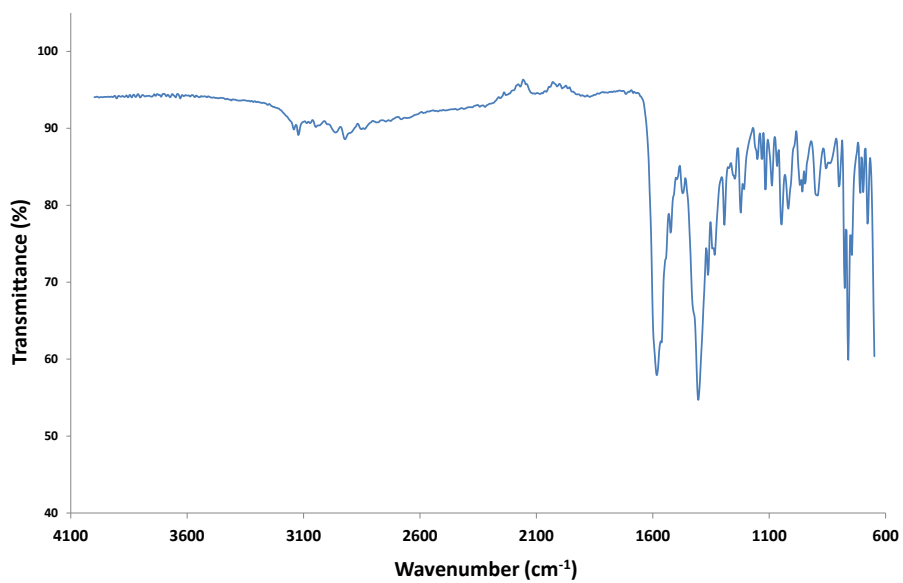


Figure SIV.1.4. FTIR spectra of Mn3.

Annex

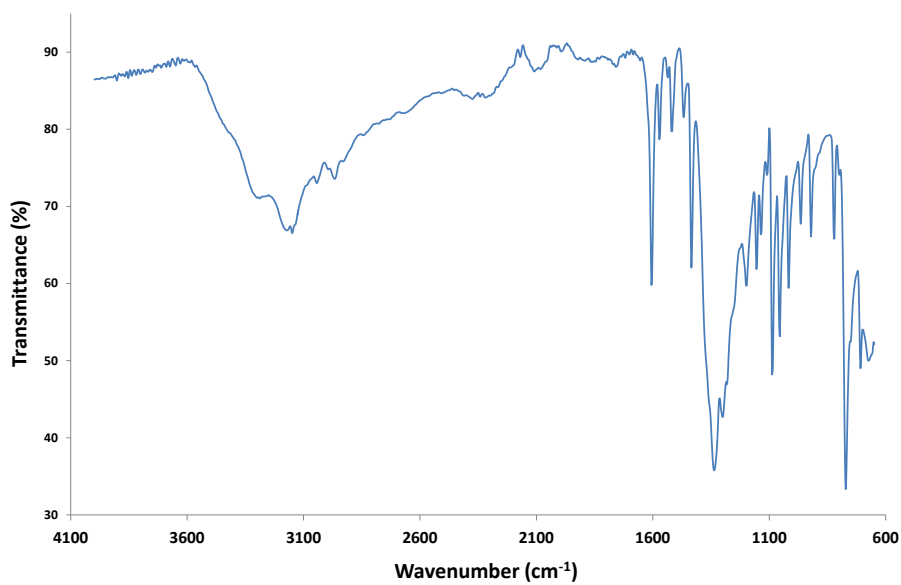


Figure SIV.1.5. FTIR spectra of Mn4.

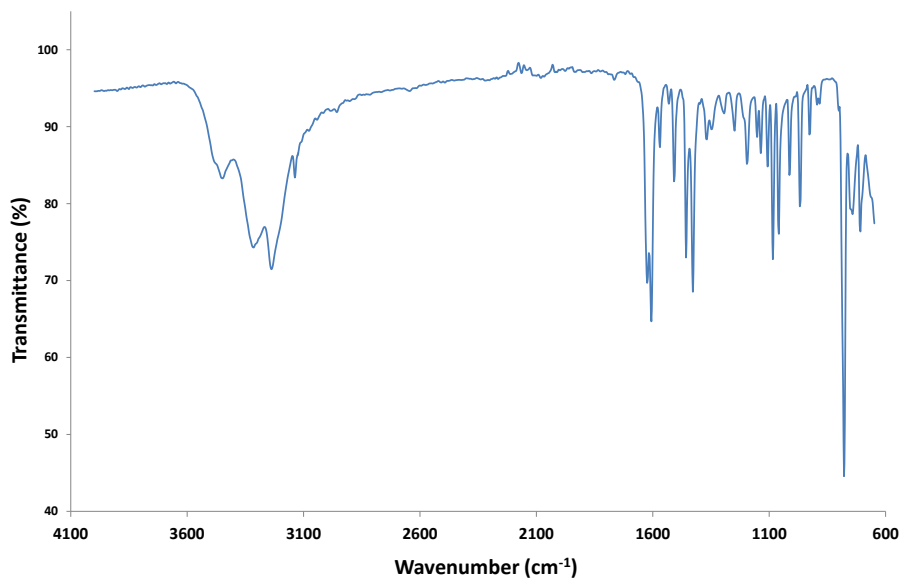


Figure SIV.1.6. FTIR spectra of Mn5.

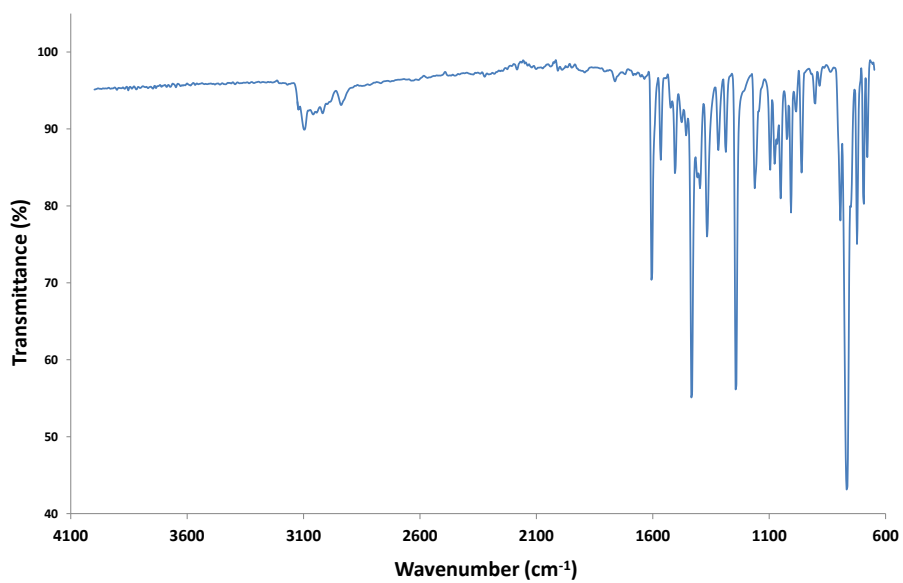


Figure SIV.1.7. FTIR spectra of Mn6.

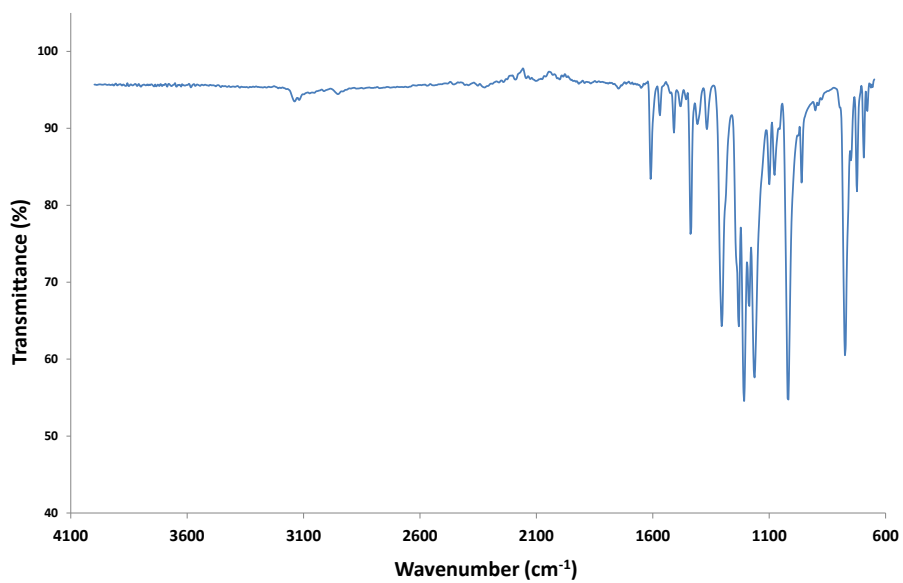


Figure SIV.1.8. FTIR spectra of Mn7.

Annex

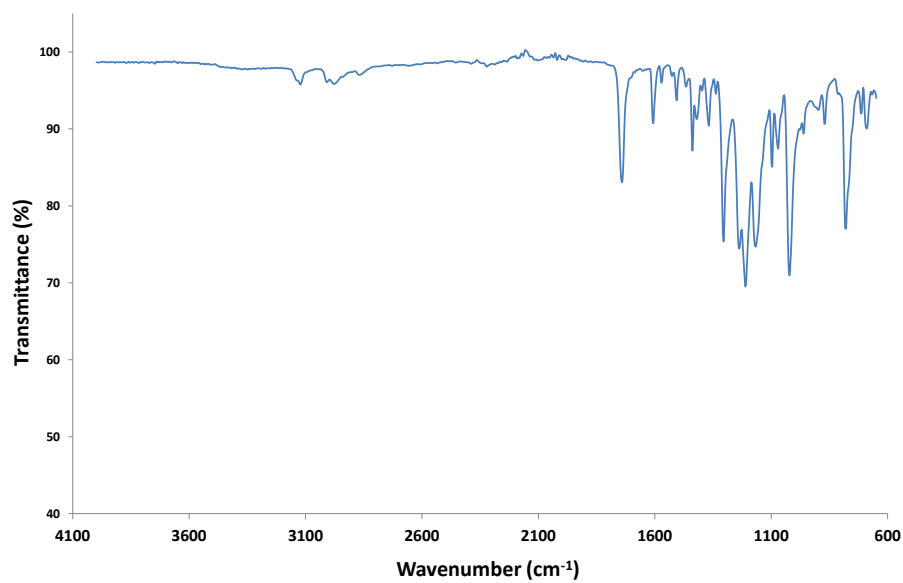


Figure SIV.1.9. FTIR spectra of Mn8.

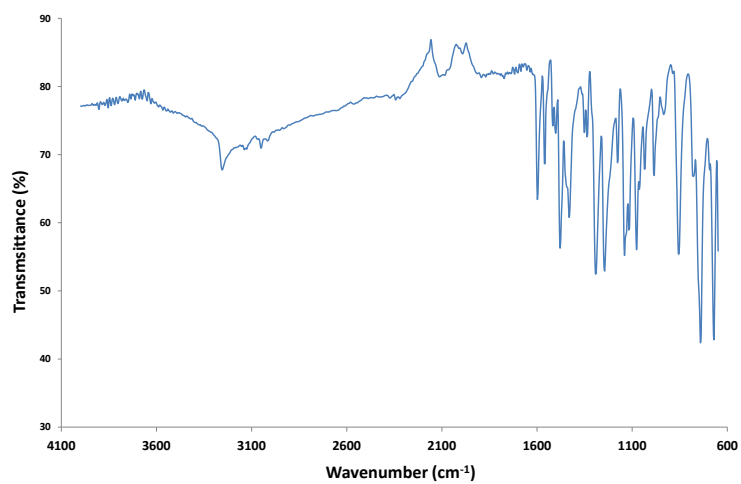


Figure SIV.1.10. FTIR spectra of Mn9.

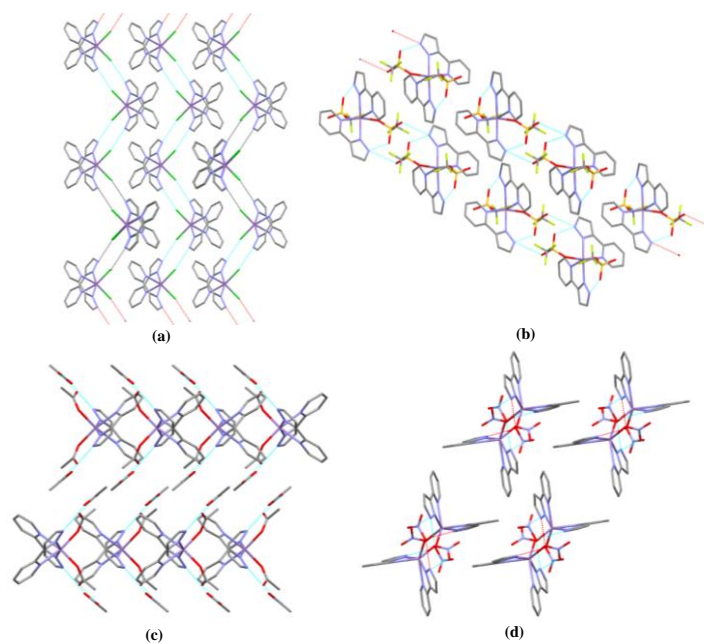


Figure SIV.1.10. Packing diagram for the structures of **Mn1** (a), **Mn2** (b), **Mn3** (c) and **Mn4** (d). The intermolecular H-bonding interactions are depicted in pale blue color.

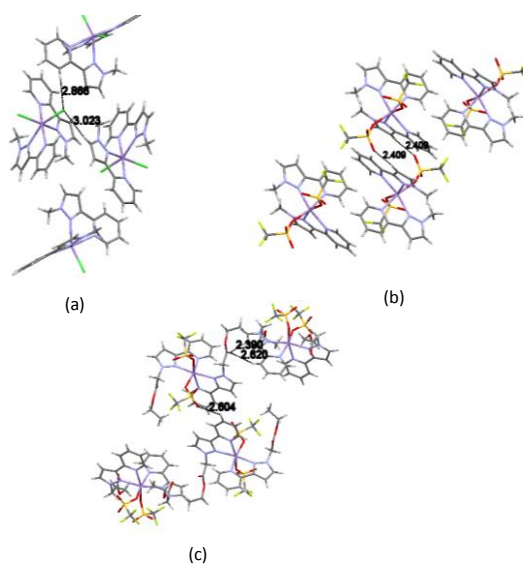


Figure SIV.1.11. Packing diagram for complexes **Mn6** (a), **Mn7** (b) and **Mn8** (c).

Annex

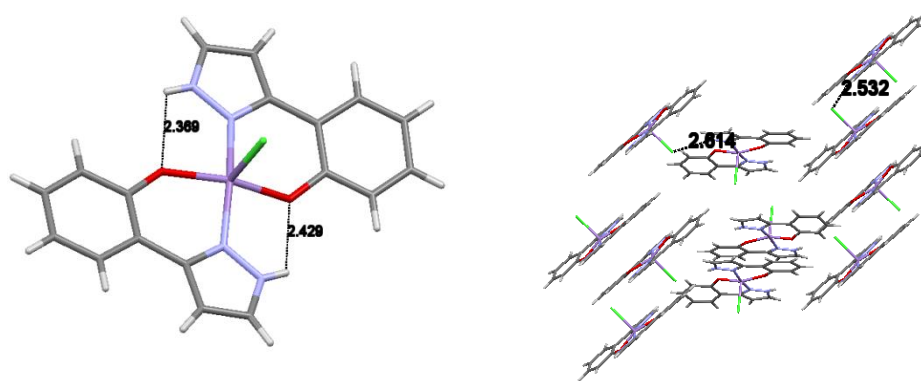


Figure SIV.1.12. Intramolecular hydrogen bonding interactions and packing diagram for complex **Mn9**.

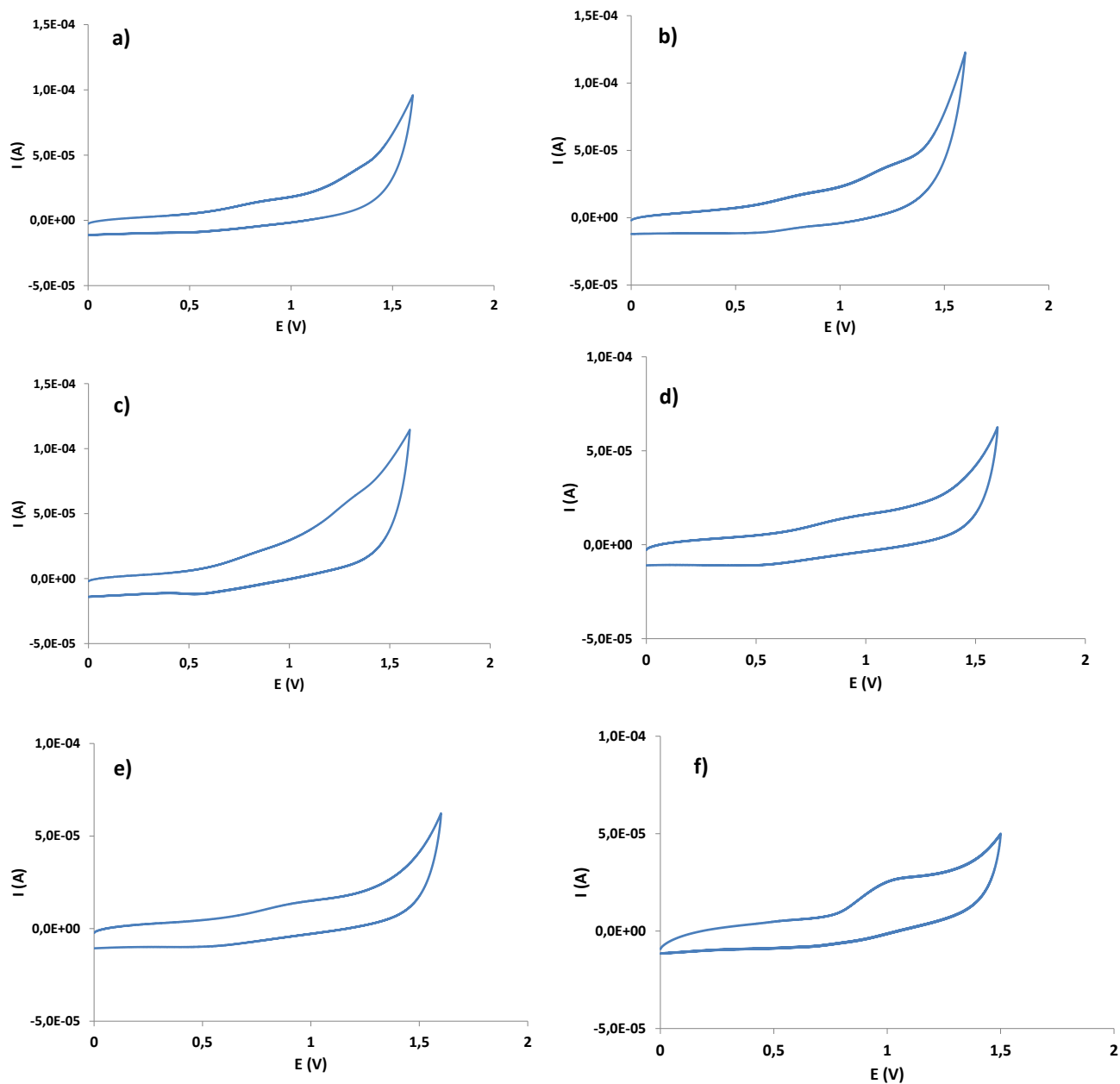


Figure SIV.1.13. Cyclic voltammetry of **Mn2-4** and **Mn7-8** compounds (**Mn2** (a), 2 mM; **Mn3** (b), 1 mM; **Mn4** (c), 1 mM; **Mn7** (d), 1 mM; **Mn8** (e), 1 mM and **Mn9** (f) 1 mM). Experiments have been performed in CH_3CN containing, 0.1 M of $n\text{-Bu}_4\text{NPF}_6$ (TBAH) using a graphite working electrode (3 mm diameter) and Ag/AgNO_3 as reference electrode; scan rate: 200mV/s.

Annex

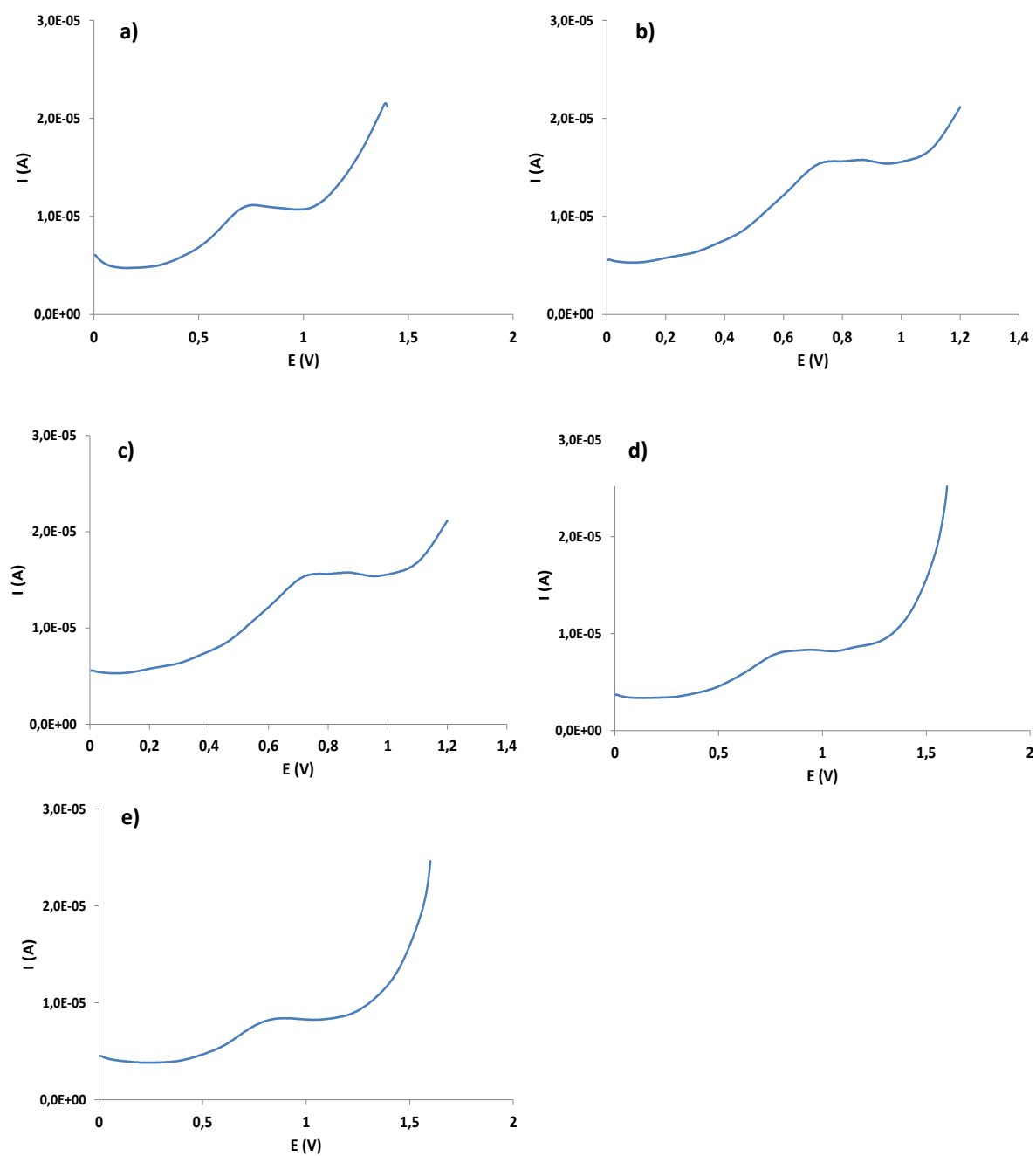


Figure SIV.1.14. DPV of **Mn2-4** and **Mn7-8** compounds (**Mn2** (a), 2 mM; **Mn3** (b), 1 mM; **Mn4** (c), 1 mM; **Mn7** (d), 1 mM; **Mn8** (e), 1 mM). Experiments have been performed in CH_3CN containing, 0.1 M of $n\text{-Bu}_4\text{NPF}_6$ (TBAH) using a graphite working electrode (3 mm diameter); scan rate: 100mV/s.

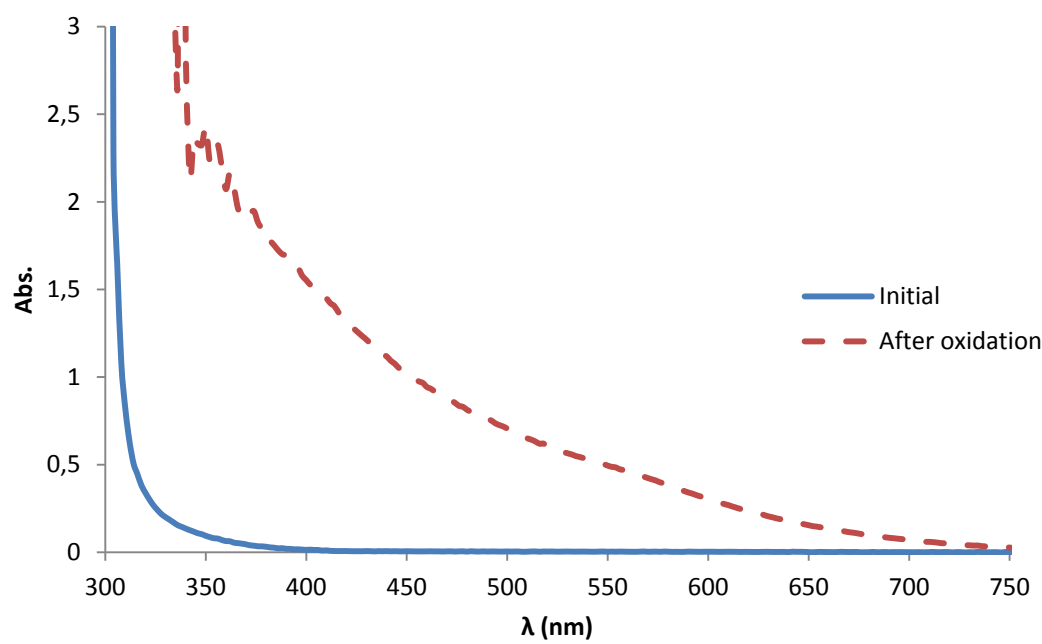
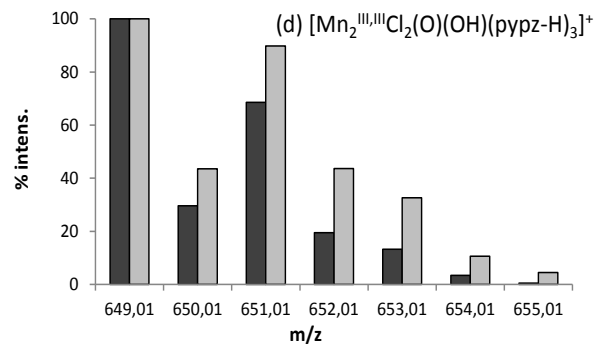
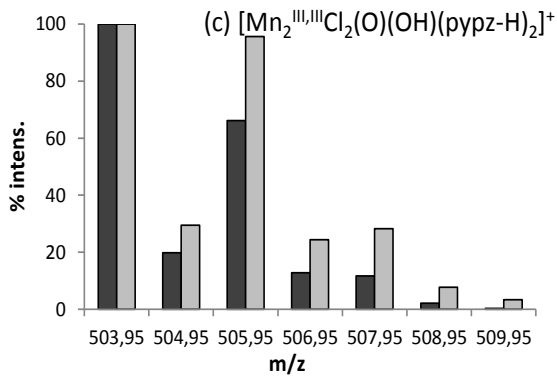
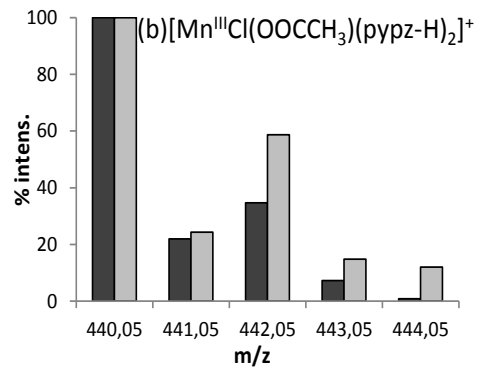
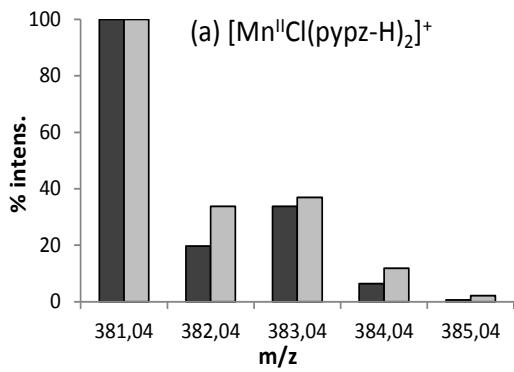
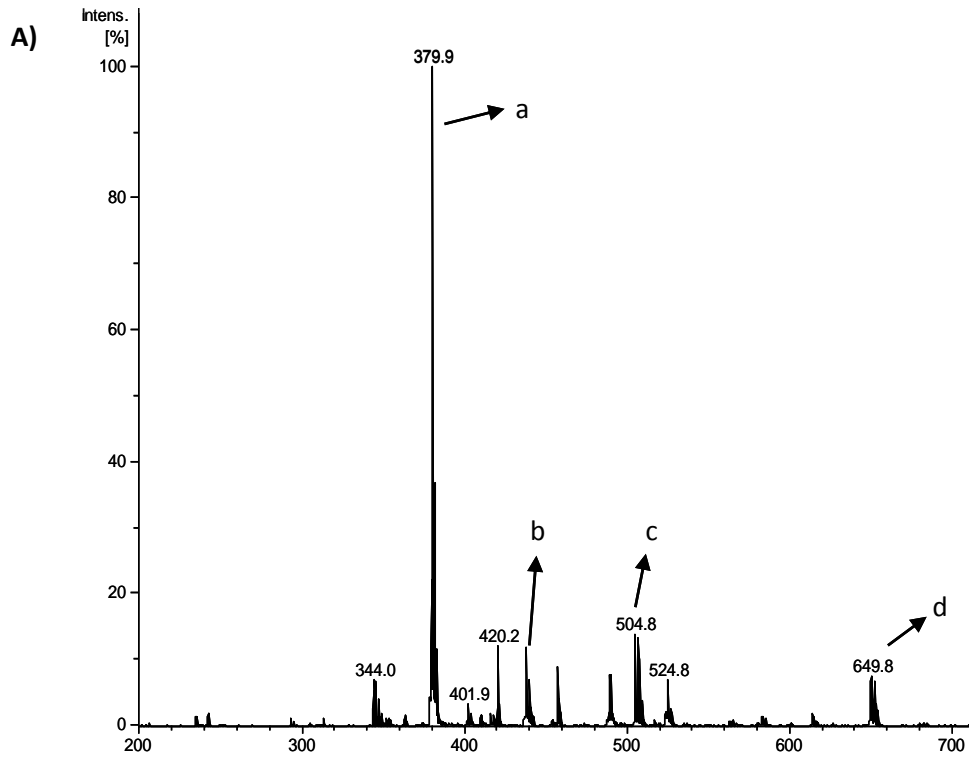


Figure SIV.1.15. UV-vis spectra for complex **Mn1** and for the species formed after exhaustive oxidation.

Annex



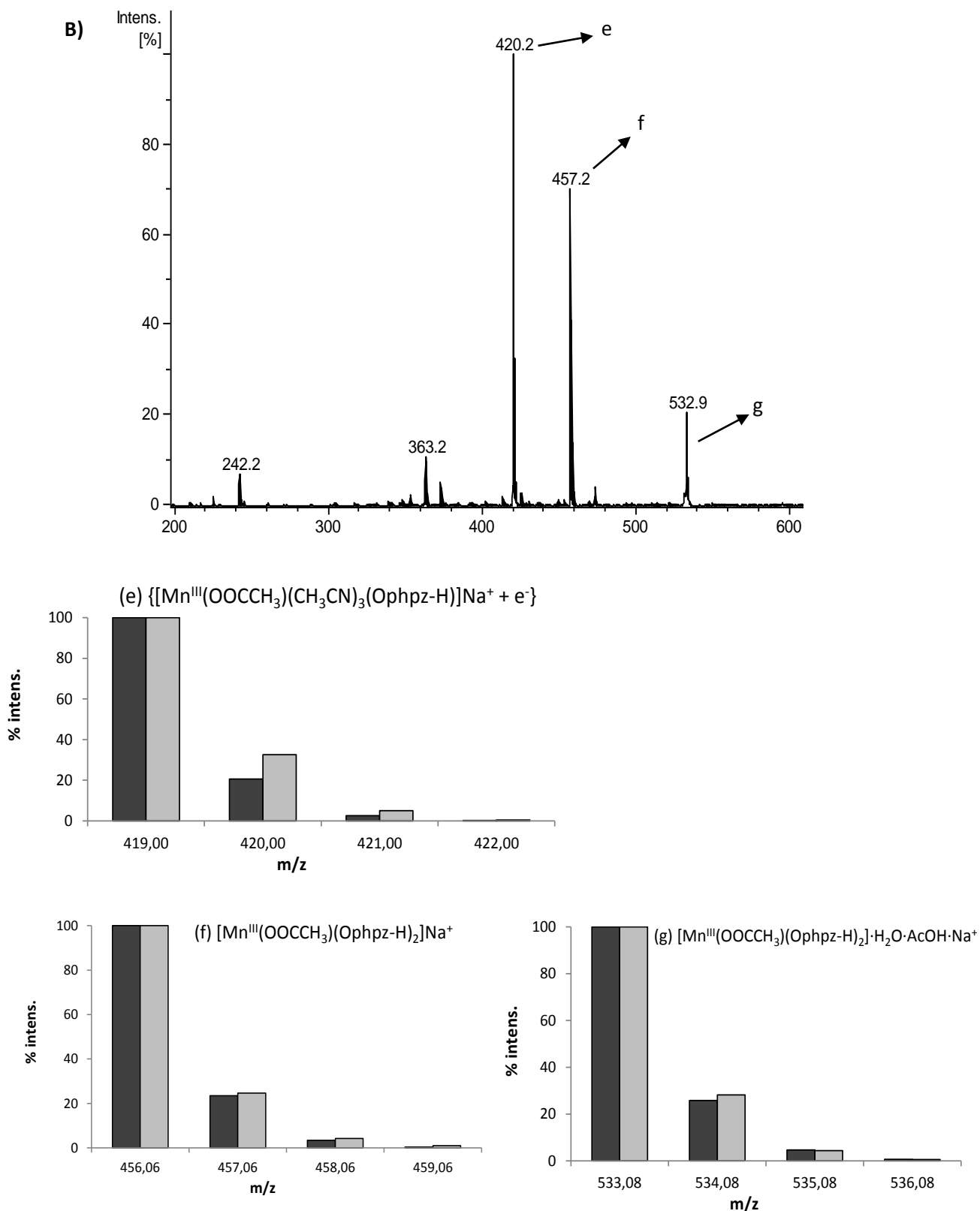


Figure SIV.1.16. ESI-MS spectrum formed after addition of 2 eq of peracetic acid to a solution of complexes A) **Mn1** and B) **Mn9** in CH_3CN at 0°C (2.5mM) together with the corresponding simulations of some selected peaks (experimental values, black bars; simulated, grey bars).

Annex

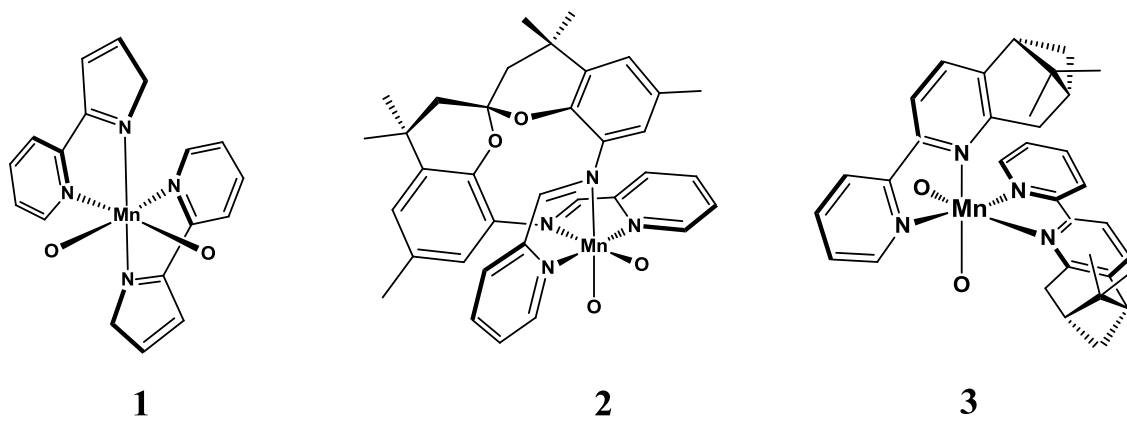


Figure SIV.1.17. Lewis structures of catalysts 1-3.

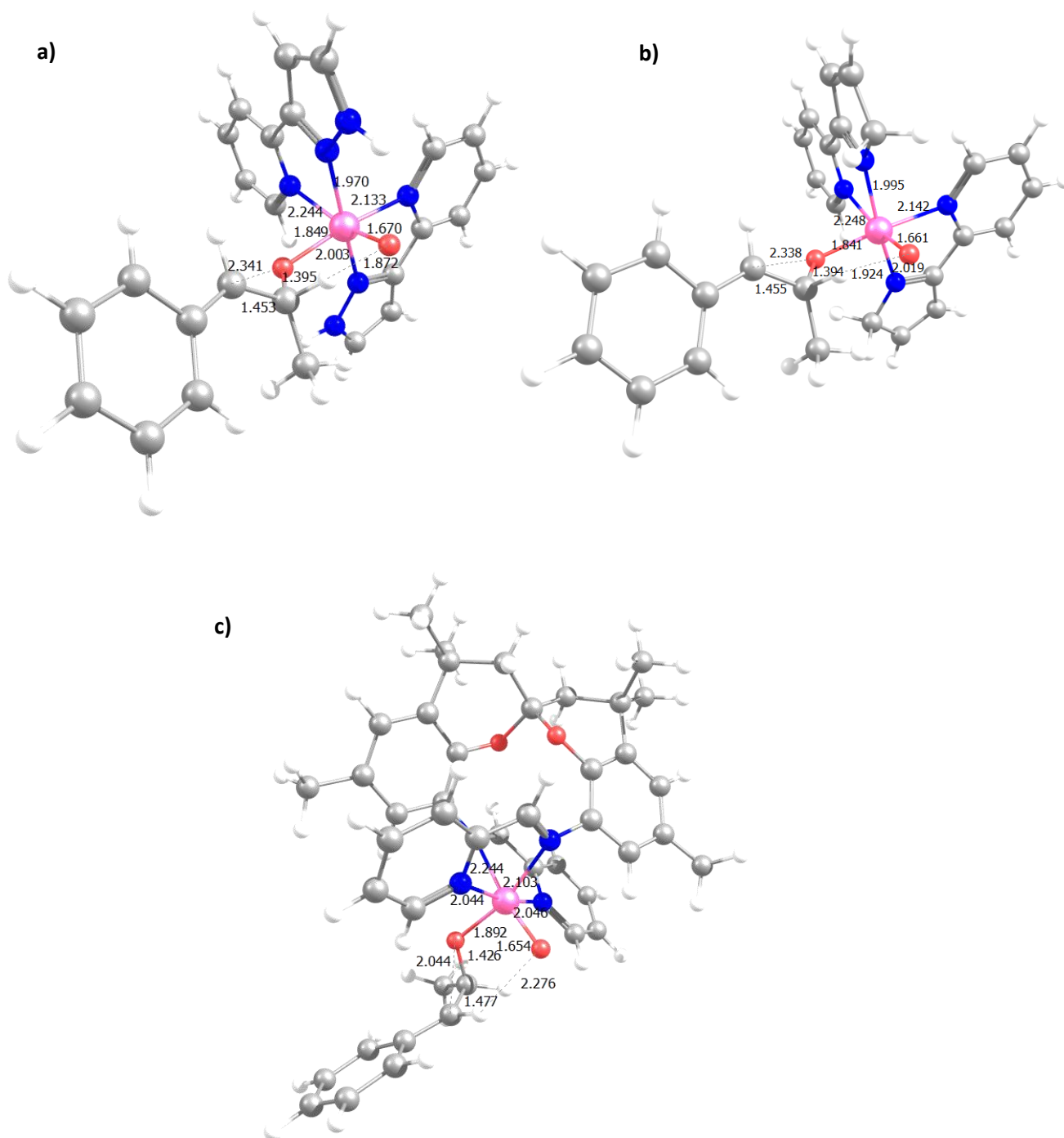


Figure SIV.1.18. Molecular structures of intermediates lics of catalysts a) **Mn1**, b) **2** and c) **3** (distances in Å).

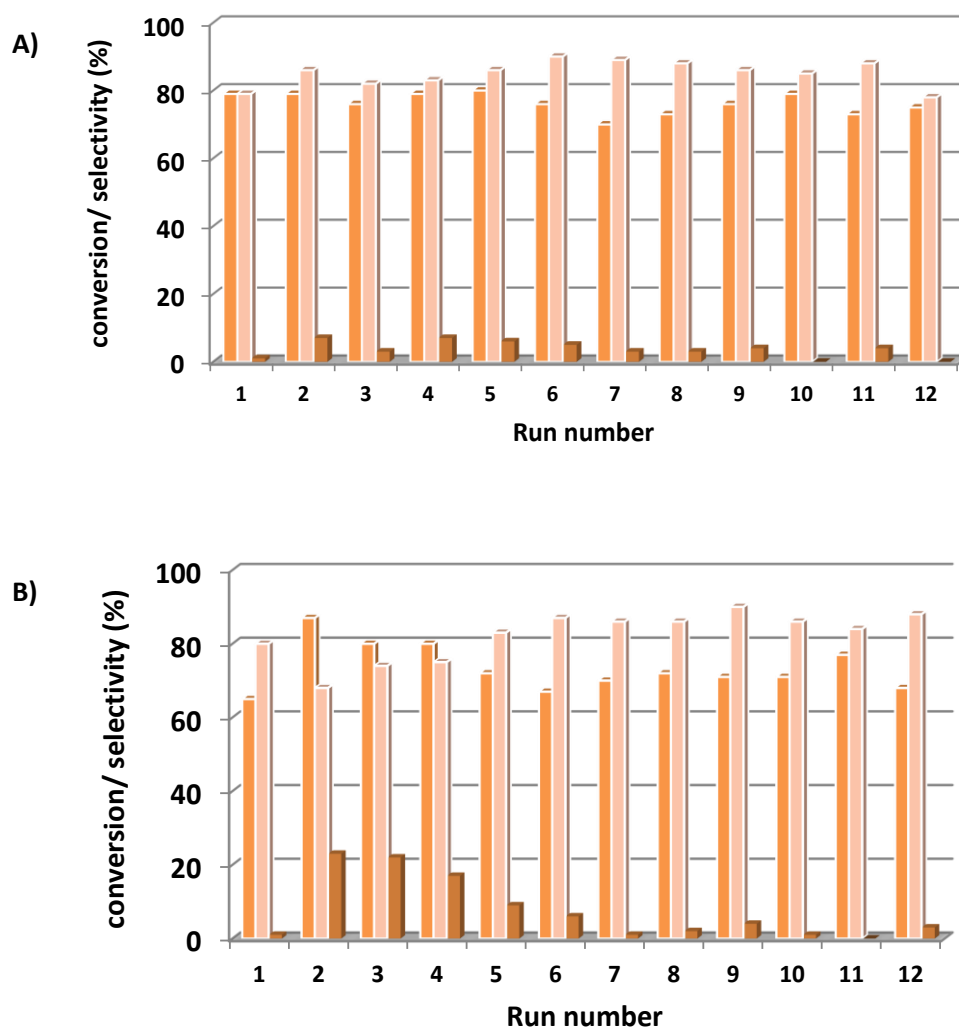


Figure SIV.1.19. Conversion (orange bars) and selectivity (pink bars) values obtained throughout consecutive reuses of complex **Mn1** (A) and complex **Mn9** (B) in the epoxidation of *cis*- β -methylstyrene in [bmim]PF₆:CH₃CN (see text for experimental conditions).

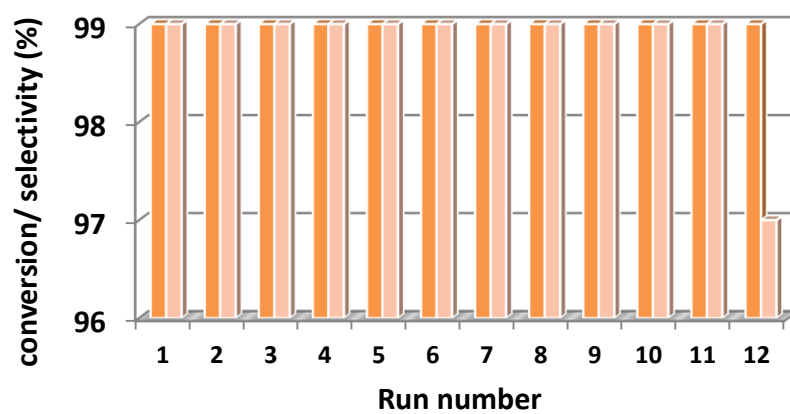


Figure SIV.1.20. Conversion (orange bars) and selectivity (pink bars) values obtained throughout consecutive reuses of complex **Mn1** in the epoxidation of cyclooctene in [bmim]PF₆:CH₃CN (see text for experimental conditions).

Chapter 5

Synthesis and characterization of complex $[\text{RuCl}_2(\text{HOphpzH})_2(\text{dmsO})_2]$ ($\text{Ru2}'$)*Synthesis and structure*

The substitution of two dmsO ligands in $[\text{RuCl}_2(\text{dmsO})_4]$ by *L4* acting as monodentate ligands leads to the formation of compound $[\text{RuCl}_2(\text{HOphpzH})_2(\text{dmsO})_2]$, $\text{Ru2}'$, that can present six different isomers (including two pairs of enantiomers) as depicted in Scheme IV.1.2. The crystal structure of compound $\text{Ru2}'$ (Figure SIV.2.1, left) reveals the nature of the complex as the *trans*-Cl, *cis*-(dmsO/pz) geometric isomer (j, Scheme IV.1.2). The *trans* disposition of the Cl ligands, despite being unfavorable in energetic terms (two strong σ -donor ligands in *trans*), favors the H-bond formation in both equatorial and axial planes between the chlorido ligands and the hydrogen atoms of the pyrazolic ligands. The hydrogen bonding interactions take place between the monodentate Cl ligands with the hydrogen of the pyrazolyl ligands in *cis* ($\text{N}_{\text{pz}}\text{-H}(3\text{A})\cdots\text{Cl}(1)$, 2.470 Å; $\text{N}_{\text{pz}}\text{-H}(1\text{B})\cdots\text{Cl}(2)$, 2.457 Å), and with the protons in the 5th position of each pyrazolyl ring ($\text{H}(10\text{A})\cdots\text{Cl}(2)$, 2.882 Å; $\text{H}(1\text{A})\cdots\text{Cl}(1)$, 2.848 Å), see Figure SIV.2.1 (right).

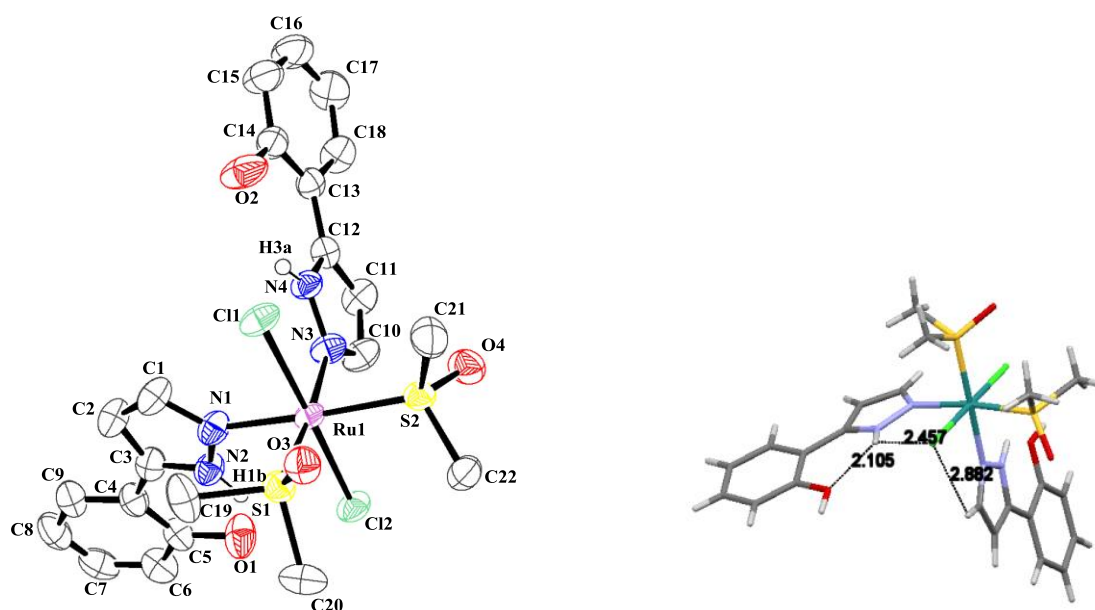


Figure SIV.2.1. Left, ortep plot and labeling scheme for the X-ray diffraction of compound $\text{Ru2}'$. Right, detail of the intramolecular H-bonding interactions taking place.

Electrochemical properties

The cyclic voltammetry registered in acetonitrile for complex **Ru2'** (Figure SIV.2.2) presents two irreversible redox processes at $E_{pa} = 1.31$ V (Ru(II→III)) and $E_{pa} = 1.59$ V (oxidation process associated with the ligand).

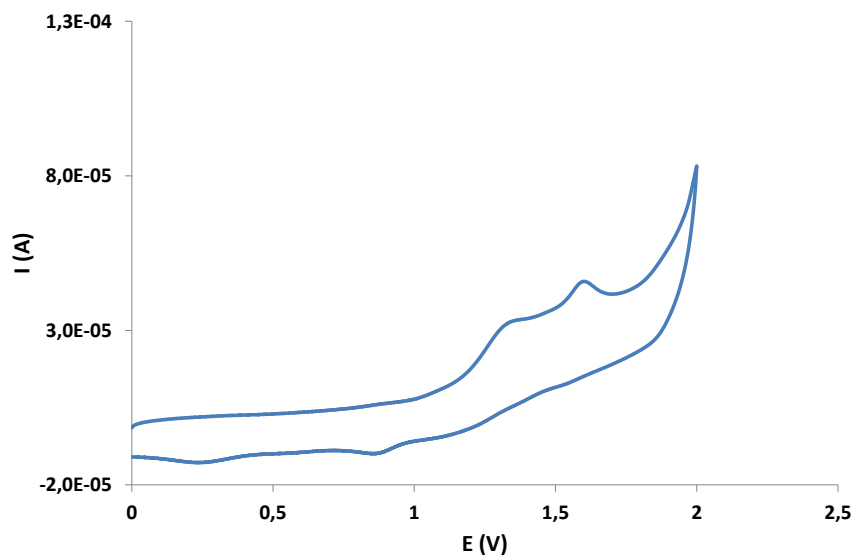


Figure SIV.2.2. CV of complex **Ru2'** in $\text{CH}_3\text{CN} + 0.1$ M TBAH.

Spectroscopic properties

The UV-Vis spectrum for complex **Ru2'** has been performed in MeOH (Figure SIV.2.3). The complex exhibits relatively intense bands between 250 and 300 nm assigned to $d\pi-\pi^*$ MLCT.

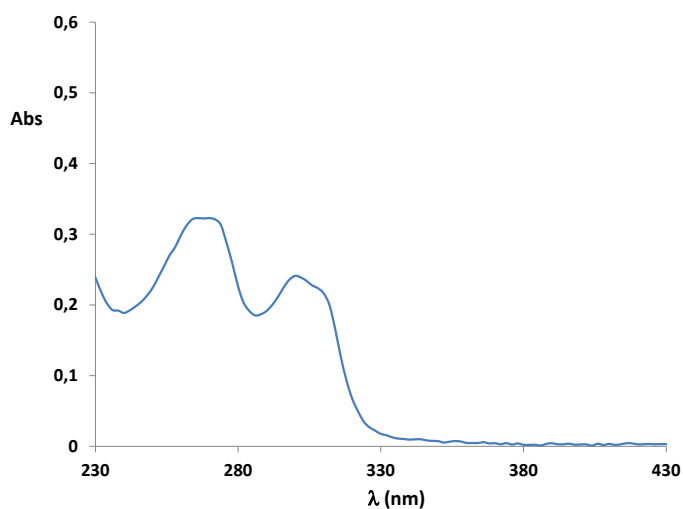
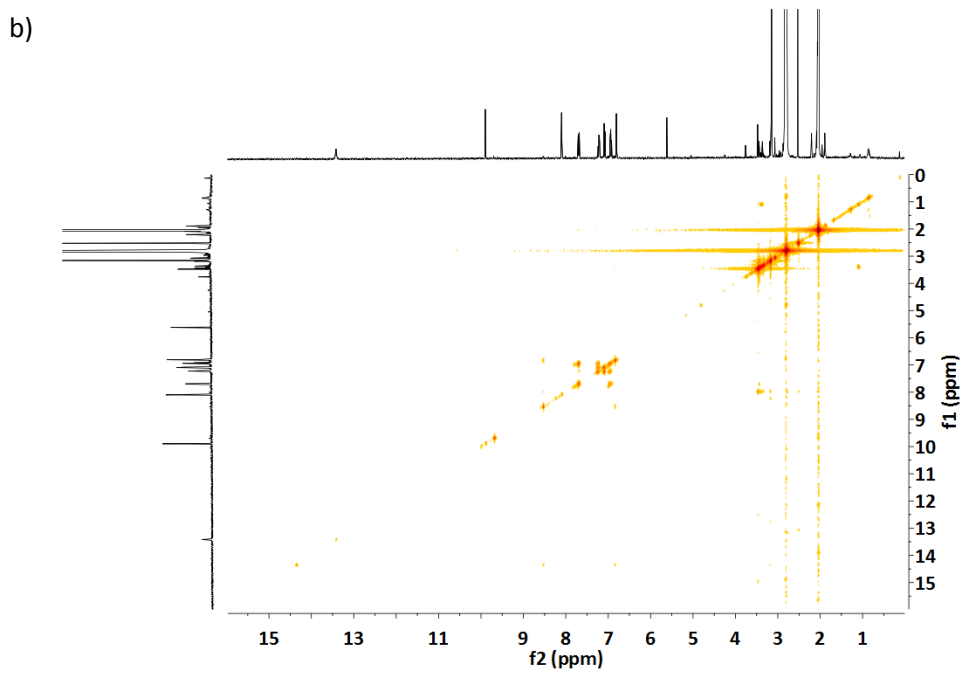
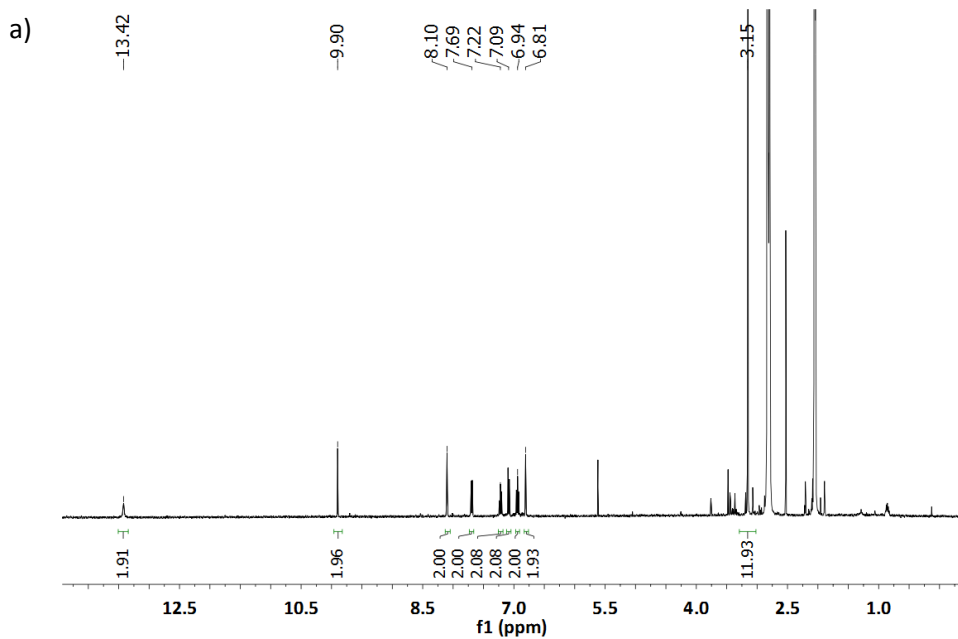


Figure SIV.2.3. UV-Vis spectra of a 0.1 mM solution of complex **Ru2'** in MeOH.

Annex

The 1D and 2D NMR spectra (^1H -NMR, COSY and NOESY) were registered in acetone- d_6 (Figure SIV.2.4). Complex **Ru2'** presents a C2 symmetry axis that interconverts all the identical ligands, so the two HOphpz-H and the two dmsol ligands show magnetically equivalent signals.



c)

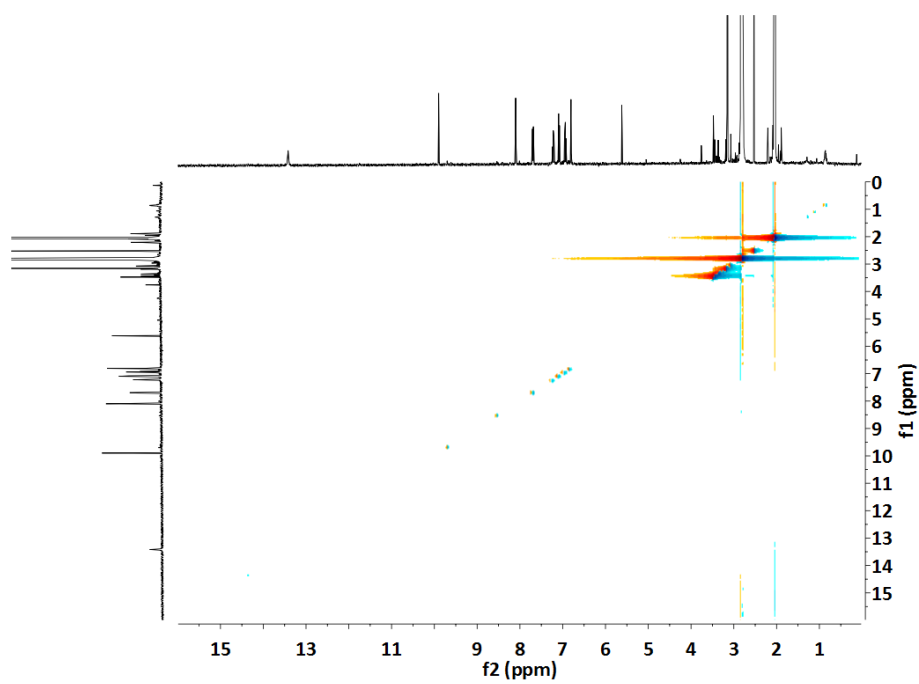


Figure SIV.2.4. NMR of Ru2', 400 MHz, acetone-d₆: a) ¹H-NMR; b) COSY; c) NOESY.

Annex

Table SIV.2.1. Crystallographic data for complexes Ru1-3 and Ru5.

| | Ru1a | Ru1b | Ru2 | Ru3 | Ru5 |
|--|---|---|---|---|---|
| Empirical formula | C ₁₈ H ₃₁ Cl ₂ N ₃ O ₅ | C ₁₆ H ₂₅ Cl ₂ N ₃ O ₄ | C ₂₂ H ₂₈ Cl ₂ N ₄ O ₄ | C ₁₆ H ₂₈ Cl ₂ N ₂ O ₄ | C ₁₄ H ₂₈ Cl ₂ N ₄ O ₂ |
| Formula weight | 605.55 | 559.48 | 648.57 | 580.55 | 520.49 |
| Crystal system | Monoclinic | Monoclinic | Orthorhombic | Triclinic | Monoclinic |
| Space group | P21 | P21/n | Pna21 | P -1 | P21/c |
| a/Å | 8.2315(12) | 9.405(2) | 24.517(8) | 8.089(3) | 10.168(2) |
| b/Å | 25.635(4) | 17.702(4) | 14.093(5) | 10.670(4) | 11.447(2) |
| c/Å | 12.3938(18) | 13.828(3) | 7.813(2) | 14.557(5) | 18.887(3) |
| α/° | 90 | 90 | 90 | 69.903(7) | 90 |
| β/° | 107.335(2) | 95.678(4) | 90 | 85.921(7) | 107.348(9) |
| γ/° | 90 | 90 | 90 | 86.309(6) | 90 |
| V/Å³ | 2496.5(6) | 2291.0(9) | 2699.6(15) | 1175.9(8) | 2098.3(7) |
| Formula units per cell | 4 | 4 | 4 | 2 | 4 |
| T/K | 143(2) | 100(2) | 298(2) | 298(2) | 293(2) |
| ρ_{calc}/Mgm⁻³ | 1.611 | 1.622 | 1.596 | 1.640 | 1.648 |
| μ/mm⁻¹ | 1.043 | 1.126 | 0.969 | 1.184 | 1.217 |
| Reflections collected/unique | 31922/12040 | 35701/5635 | 40751/6737 | 11455/5491 | 31907/5147 |
| R(int) | 0.0438 | 0.1050 | 0.0545 | 0.0699 | 0.0462 |
| Final indices, [I>2σ(I)] | R ₁ = 0.0442, wR ² = 0.1051 | R ₁ = 0.0440, wR ² =0.0871 | R ₁ = 0.0401, wR ² = 0.0776 | R ₁ = 0.0576, wR ² =0.1157 | R ₁ = 0.0342; wR ² =0.0775 |
| R indices [all data] | R ₁ = 0.0504, wR ² = 0.1051 | R ₁ = 0.0721, wR ² = 0.0983 | R ₁ = 0.0552, wR ² = 0.0834 | R ₁ = 0.1161, wR ² =0.1383 | R ₁ = 0.0389, wR ² =0.0795 |

Table SIV.2.2. Selected bond lengths (Å) and angles (°) for Ru1-3 and Ru5.

| Ru1a | | | |
|-----------------------|------------|---|------------|
| Ru—Cl(1) | 2.4271(16) | Cl(1)—Ru—Cl(2) | 91.02(6) |
| Ru—Cl(2) | 2.4403(16) | N(1) _{py} —Ru—N(3) _{pz} | 77.4(2) |
| Ru—N(1) _{py} | 2.102(5) | N(1) _{py} —Ru—Cl(1) | 175.16(16) |
| Ru—N(3) _{pz} | 2.117(5) | N(1) _{py} —Ru—Cl(2) | 89.04(15) |
| Ru—S(1) | 2.2428(17) | N(1) _{py} —Ru—S(1) | 86.71(15) |
| Ru—S(2) | 2.4271(16) | N(1) _{py} —Ru—S(2) | 98.33(16) |
| | | N(3) _{pz} —Ru—Cl(1) | 97.75(14) |
| | | N(3) _{pz} —Ru—Cl(2) | 83.95(14) |
| | | N(3) _{pz} —Ru—S(1) | 93.69(14) |
| | | N(3) _{pz} —Ru—S(2) | 170.27(15) |
| | | S(1)—Ru—S(2) | 94.82(7) |
| | | S(1)—Ru—Cl(1) | 93.09(6) |
| | | S(1)—Ru—Cl(2) | 175.51(7) |
| | | S(2)—Ru—Cl(1) | 86.51(7) |
| | | S(2)—Ru—Cl(2) | 87.24(7) |
| Ru1b | | | |
| Ru—Cl(1) | 2.4244(10) | Cl(1)—Ru—Cl(2) | 88.89(4) |
| Ru—Cl(2) | 2.4128(10) | N(1) _{py} —Ru—N(3) _{pz} | 78.18(11) |
| Ru—N(1) _{py} | 2.071(3) | N(1) _{py} —Ru—Cl(1) | 177.13(8) |
| Ru—N(3) _{pz} | 2.069(3) | N(1) _{py} —Ru—Cl(2) | 93.91(8) |
| Ru—S(1) | 2.3101(11) | N(1) _{py} —Ru—S(1) | 86.04(8) |
| Ru—S(2) | 2.3027(11) | N(1) _{py} —Ru—S(2) | 91.75(8) |
| | | N(3) _{pz} —Ru—Cl(1) | 99.14(8) |
| | | N(3) _{pz} —Ru—Cl(2) | 171.94(8) |
| | | N(3) _{pz} —Ru—S(1) | 92.96(8) |
| | | N(3) _{pz} —Ru—S(2) | 90.57(8) |
| | | S(1)—Ru—S(2) | 175.37(3) |
| | | S(1)—Ru—Cl(1) | 93.13(3) |
| | | S(1)—Ru—Cl(2) | 87.24(3) |
| | | S(2)—Ru—Cl(1) | 89.27(3) |
| | | S(2)—Ru—Cl(2) | 88.85(3) |
| Ru2 | | | |
| Ru—Cl(1) | 2.3959(14) | Cl(1)—Ru—Cl(2) | 177.57(5) |
| Ru—Cl(2) | 2.4145(13) | N(2) _{pz} —Ru—N(4) _{pz} | 84.03(18) |
| Ru—S(1) | 2.2435(14) | N(2) _{pz} —Ru—Cl(1) | 88.59(13) |
| Ru—S(2) | 2.2489(15) | N(2) _{pz} —Ru—Cl(2) | 89.30(12) |
| Ru—N(2) _{pz} | 2.115(5) | N(2) _{pz} —Ru—S(1) | 92.90(12) |
| Ru—N(4) _{pz} | 2.116(4) | N(2) _{pz} —Ru—S(2) | 172.68(12) |
| | | N(4) _{pz} —Ru—Cl(1) | 89.64(11) |
| | | N(4) _{pz} —Ru—Cl(2) | 88.94(11) |
| | | N(4) _{pz} —Ru—S(1) | 174.97(12) |
| | | N(4) _{pz} —Ru—S(2) | 88.88(13) |
| | | S(1)—Ru—S(2) | 94.30(5) |
| | | S(1)—Ru—Cl(2) | 95.02(5) |
| | | S(1)—Ru—Cl(1) | 86.30(12) |
| | | S(2)—Ru—Cl(1) | 93.19(5) |
| | | S(2)—Ru—Cl(2) | 88.75(5) |
| Ru3 | | | |
| Ru—Cl(1) | 2.4264(16) | Cl(1)—Ru—Cl(2) | 88.13(6) |
| Ru—Cl(2) | 2.4256(16) | Cl(1)—Ru—N(1) _{pz} | 84.44(13) |
| Ru—S(1) | 2.2779(16) | Cl(2)—Ru—N(1) _{pz} | 88.29(13) |
| Ru—S(2) | 2.2941(17) | Cl(1)—Ru—S(1) | 90.39(6) |
| Ru—S(3) | 2.2662(17) | Cl(1)—Ru—S(2) | 88.73(6) |
| Ru—N(1) _{pz} | 2.138(5) | Cl(1)—Ru—S(3) | 175.36(6) |
| | | Cl(2)—Ru—S(1) | 177.58(6) |
| | | Cl(2)—Ru—S(2) | 85.22(6) |
| | | Cl(2)—Ru—S(3) | 90.72(6) |
| | | S(1)—Ru—S(2) | 92.84(6) |
| | | S(1)—Ru—S(3) | 90.91(6) |
| | | S(1)—Ru—N(1) _{pz} | 93.47(13) |

| | | | |
|-----------------------------|-----------|---|------------|
| | | S(2)—Ru—N(1)_{pz} | 170.72(13) |
| | | S(3)—Ru—N(1)_{pz} | 91.04(14) |
| Ru5 | | | |
| Ru—Cl(1) | 2.4140(7) | Cl(1)—Ru—Cl(2) | 175.46(2) |
| Ru—Cl(2) | 2.4045(7) | N(1)_{pz}—Ru—N(3)_{pz} | 84.83(8) |
| Ru—N(1)_{pz} | 2.122(2) | N(1)_{pz}—Ru—Cl(1) | 88.27(6) |
| Ru—N(3)_{pz} | 2.115(2) | N(1)_{pz}—Ru—Cl(2) | 88.79(6) |
| Ru—S(1) | 2.2348(7) | N(1)_{pz}—Ru—S(1) | 175.29(6) |
| Ru—S(2) | 2.2443(7) | N(1)_{pz}—Ru—S(2) | 92.51(6) |
| | | N(3)_{pz}—Ru—Cl(1) | 88.00(6) |
| | | N(3)_{pz}—Ru—Cl(2) | 88.28(6) |
| | | N(3)_{pz}—Ru—S(1) | 93.94(6) |
| | | N(3)_{pz}—Ru—S(2) | 175.55(6) |
| | | S(1)—Ru—S(2) | 89.00(3) |
| | | S(1)—Ru—Cl(1) | 96.23(2) |
| | | S(1)—Ru—Cl(2) | 86.63(2) |
| | | S(2)—Ru—Cl(1) | 88.35(3) |
| | | S(2)—Ru—Cl(2) | 95.24(3) |

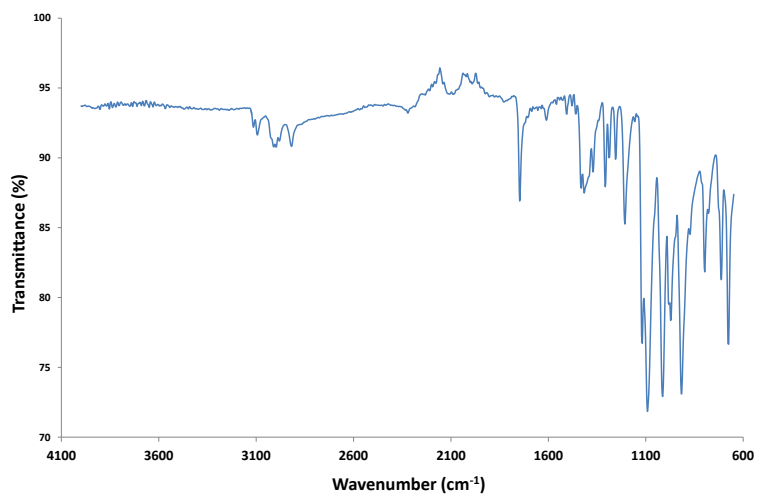


Figure SIV.2.5. FTIR spectra of **Ru1b**.

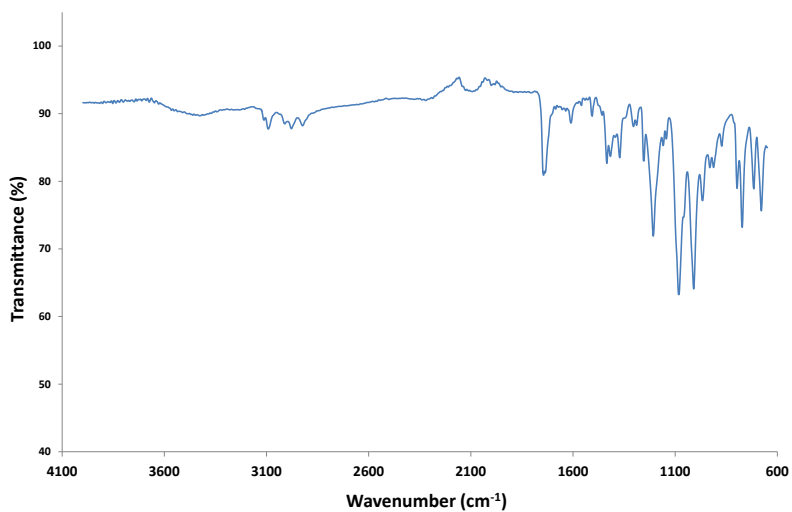


Figure SIV.2.6. FTIR spectra of a mixture of **Ru1a** and **Ru1b** isomers.

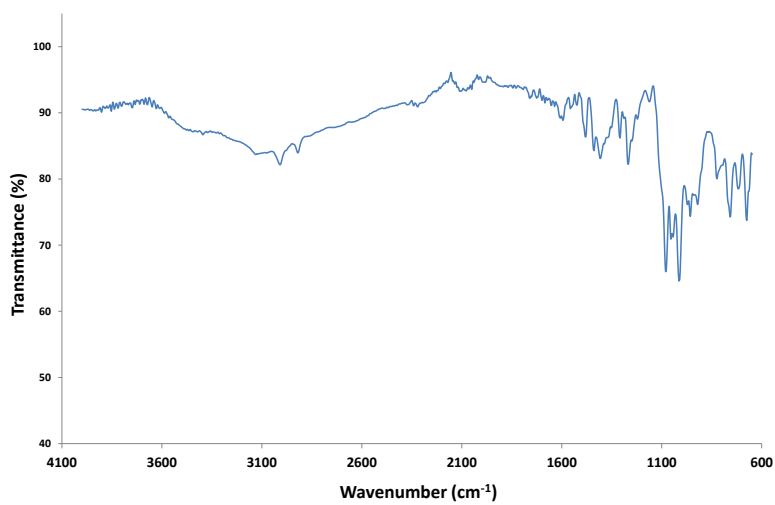


Figure SIV.2.7. FTIR spectra of **Ru2**.

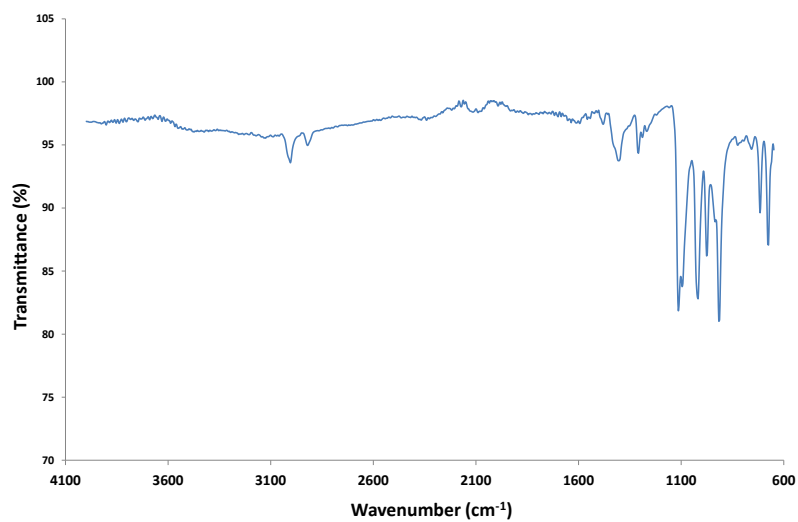


Figure SIV.2.8. FTIR spectra of Ru3.

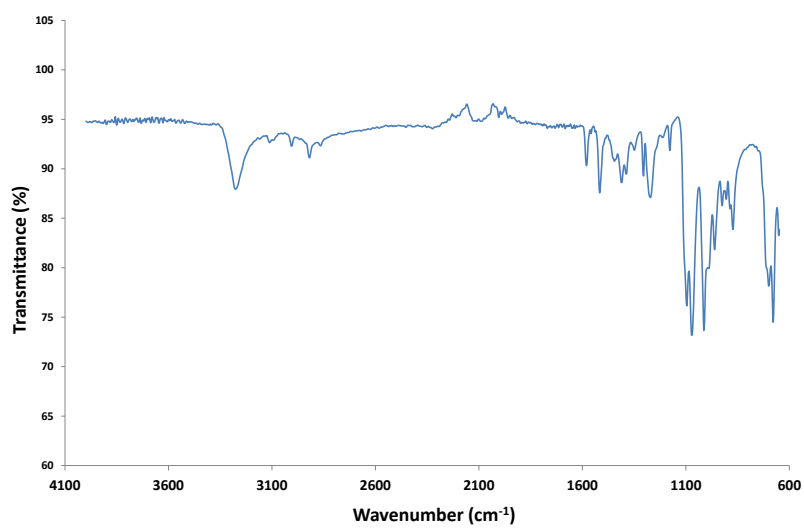


Figure SIV.2.9. FTIR spectra of Ru5.

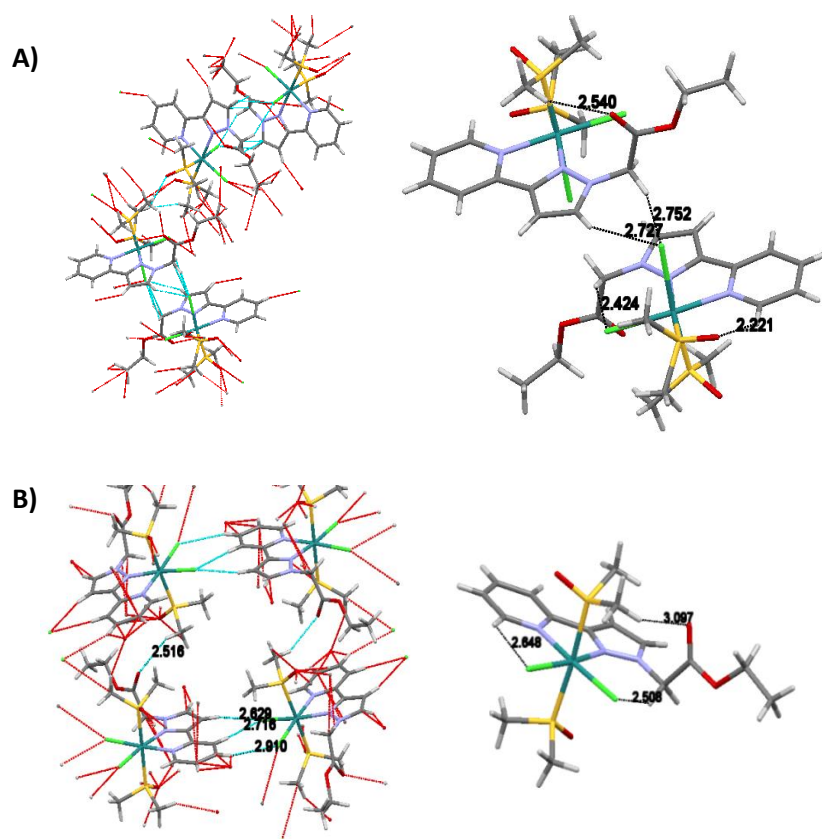


Figure SIV.2.10. Intermolecular and intramolecular hydrogen-bonding interactions and packing diagram for complex **Ru1**, A) Λ/Δ *cis*-Cl *cis*-dmso isomer (a) (**Ru1a**) and B) *cis*-Cl *trans*-dmso isomer (d) (**Ru1b**).

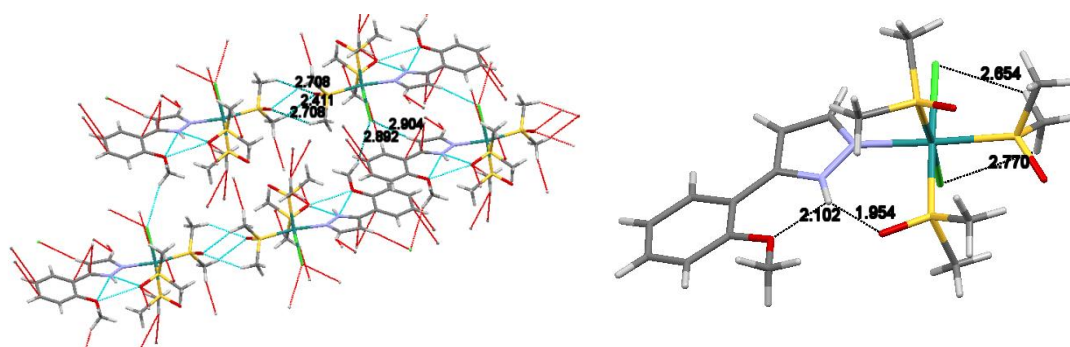


Figure SIV.2.11. Intermolecular and intramolecular hydrogen-bonding interactions and packing diagram for complex **Ru3**.

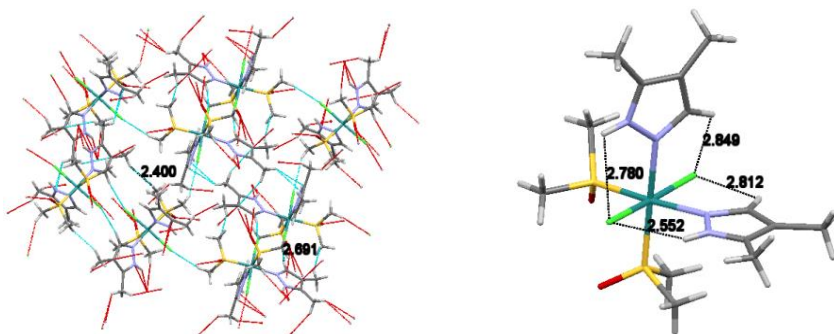
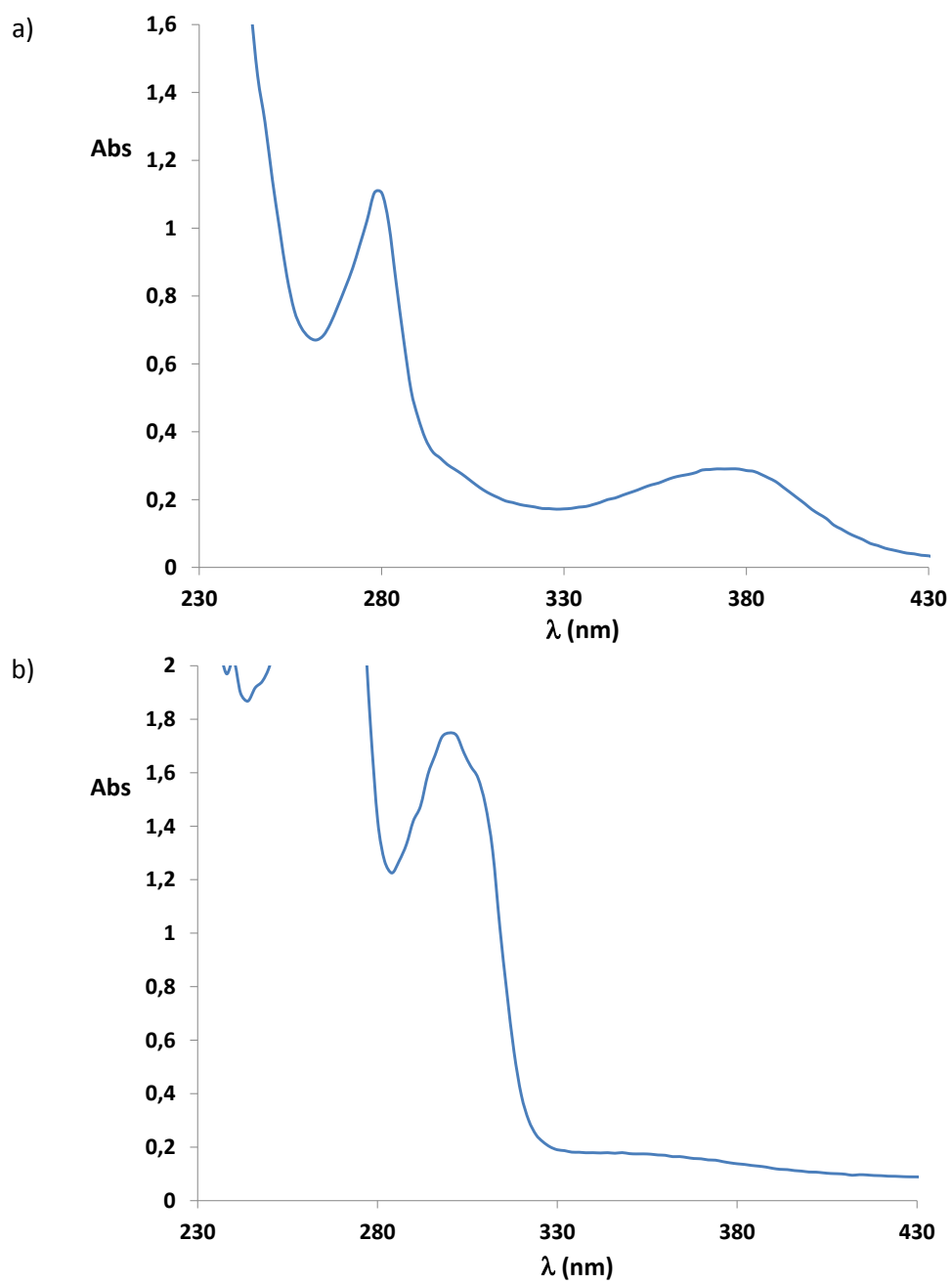
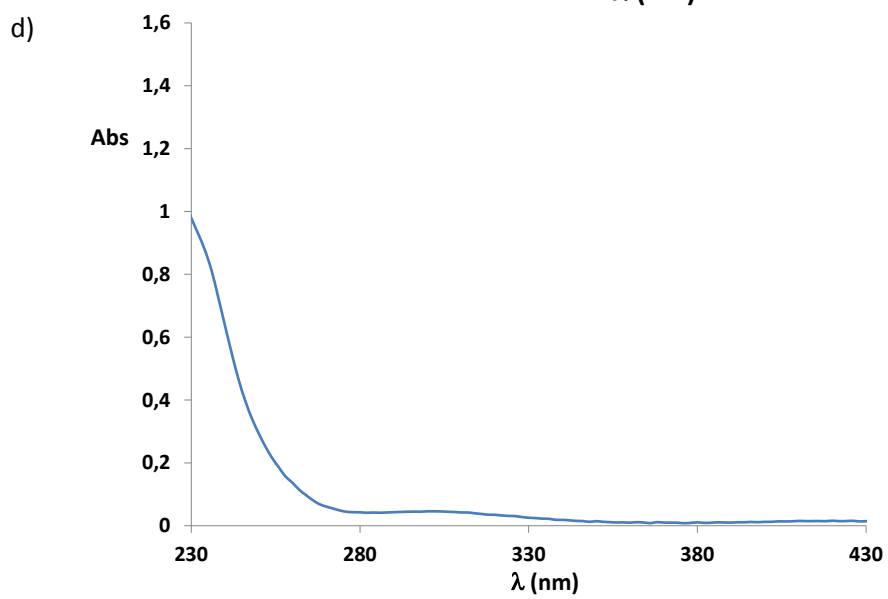
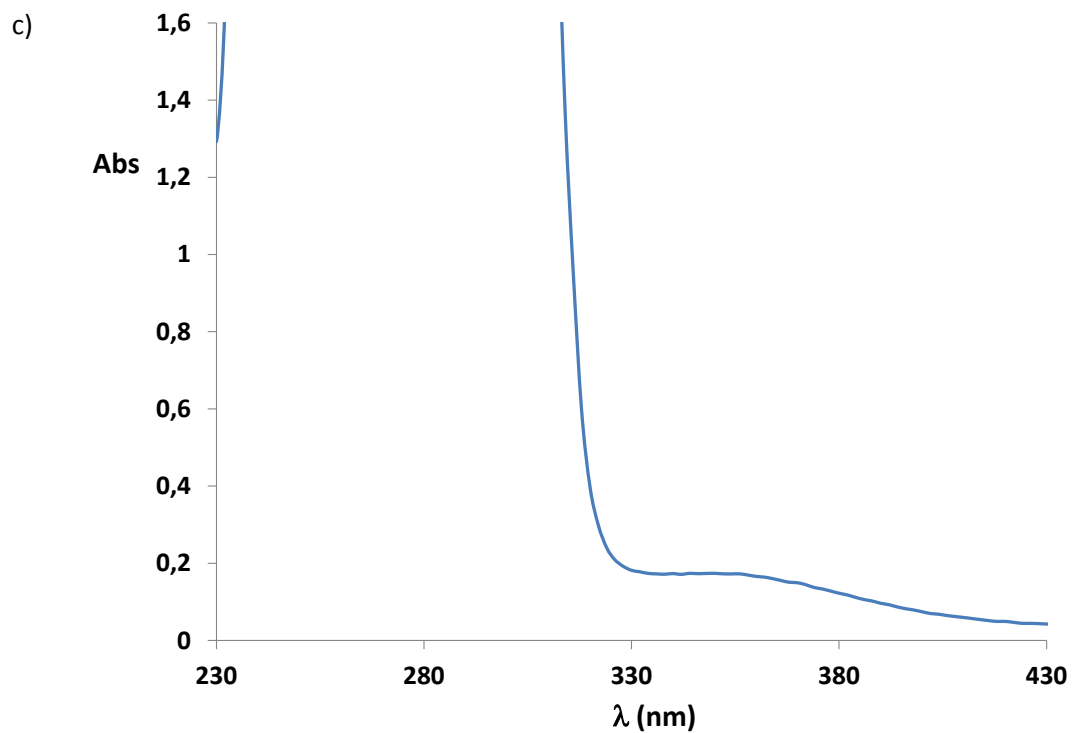


Figure SIV.2.12. Intermolecular and intramolecular hydrogen-bonding interactions and packing diagram for complex Ru5.





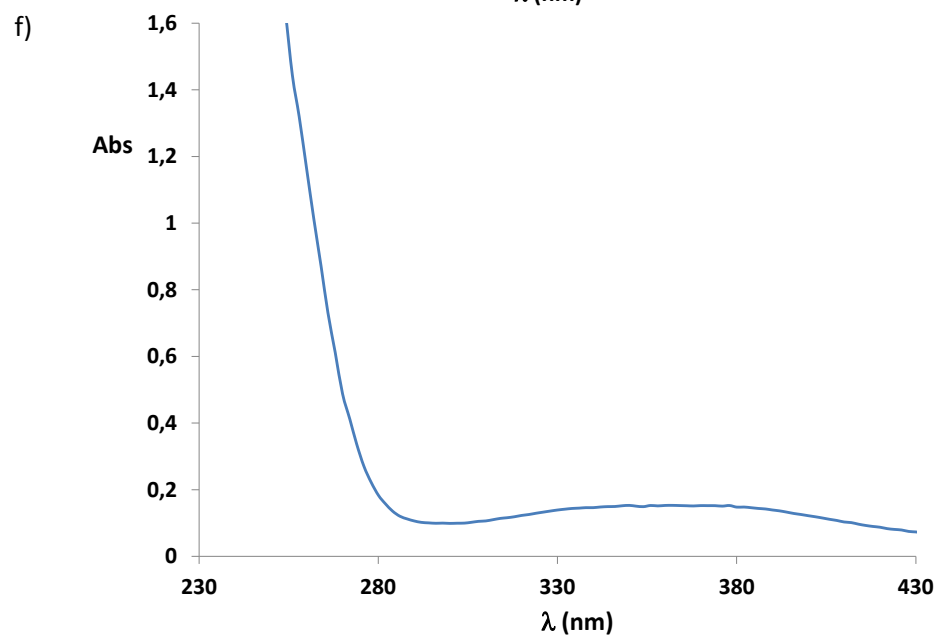
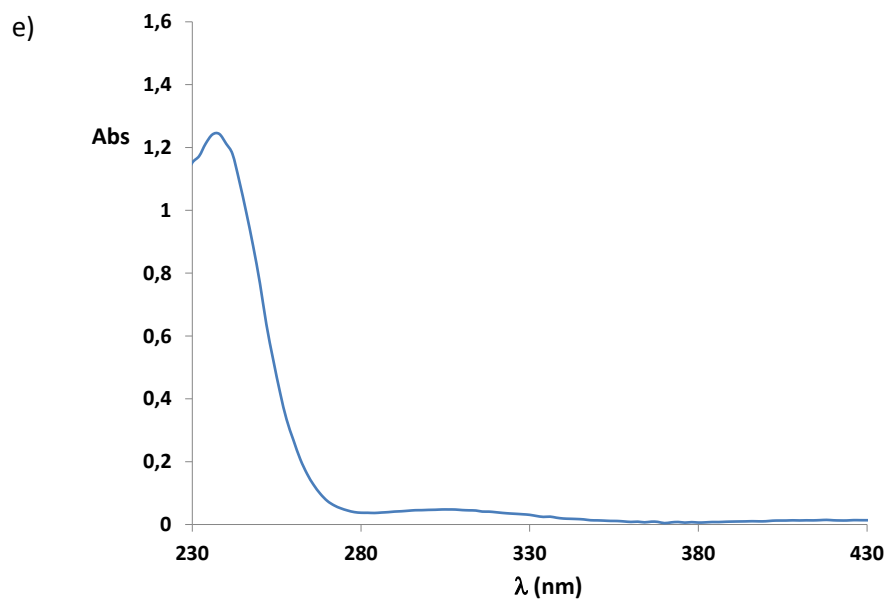
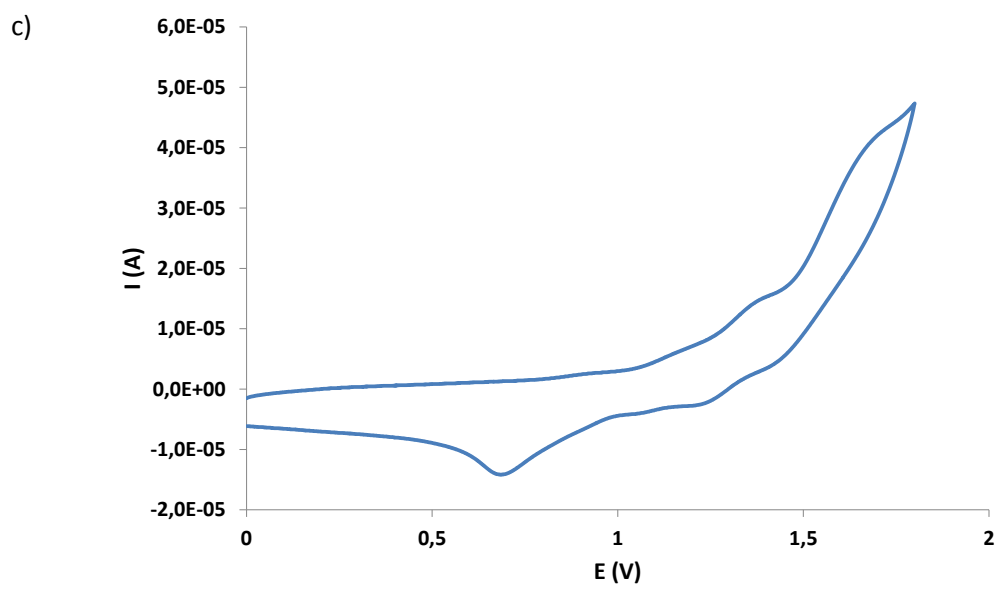
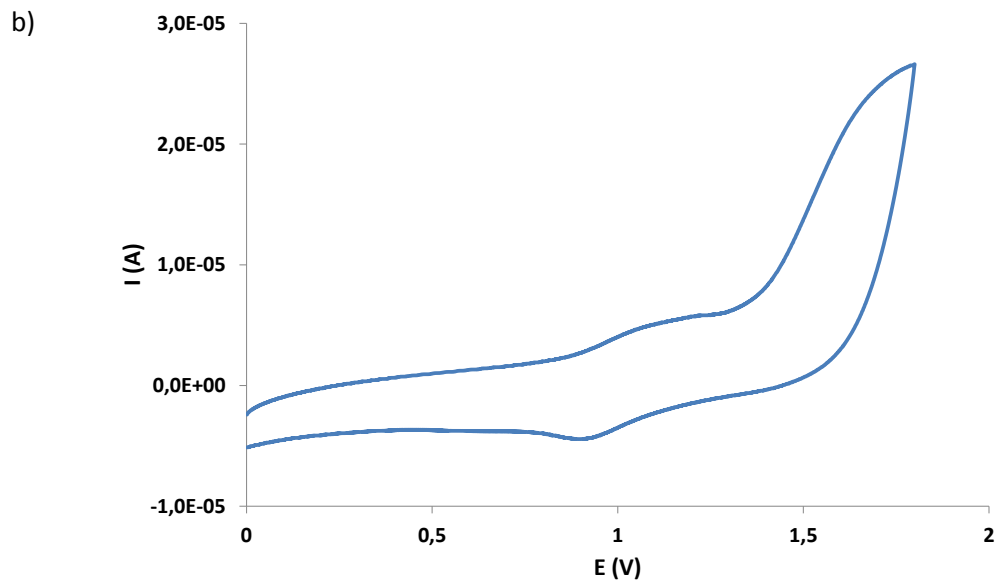
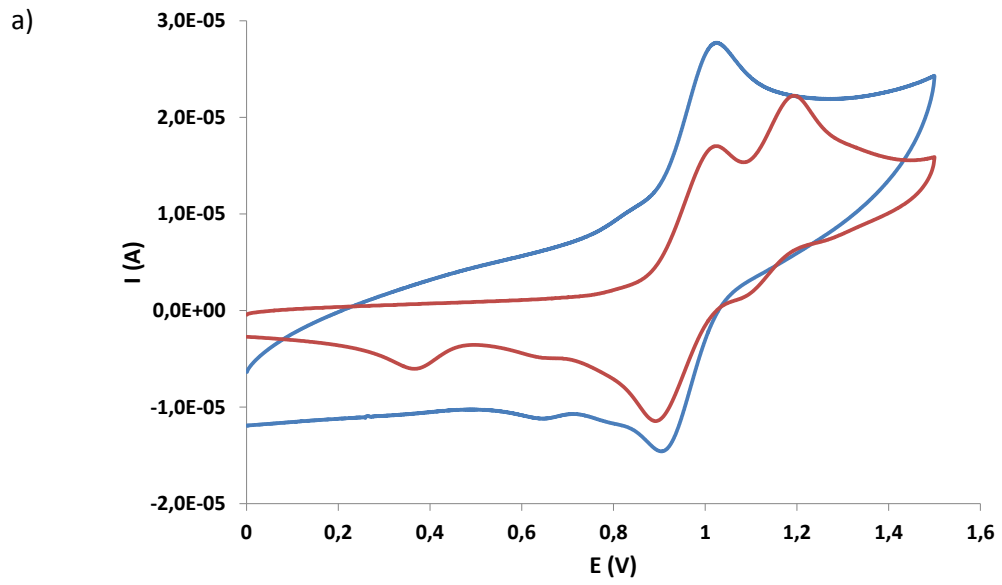


Figure SIV.2.13. UV-Vis spectra of complexes a) **Ru1** (0.2 mM in CH₂Cl₂), b) **Ru2** (0.1 mM in MeOH), c) **Ru3** (0.1 mM in CH₂Cl₂), d) **Ru4** (0.1 mM in H₂O), e) **Ru5** (0.1 mM in H₂O) and f) **Ru6** (0.2 mM in MeOH).



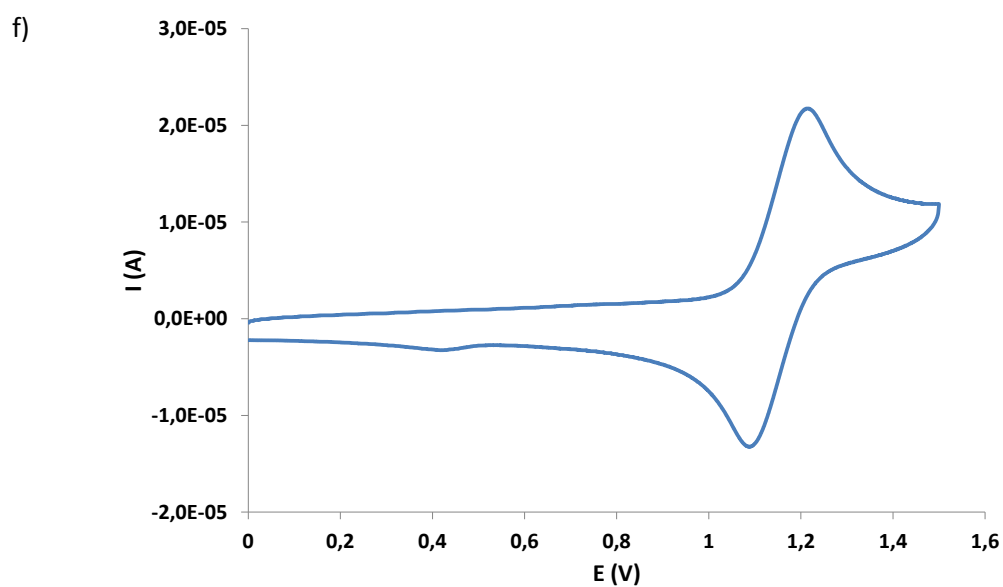
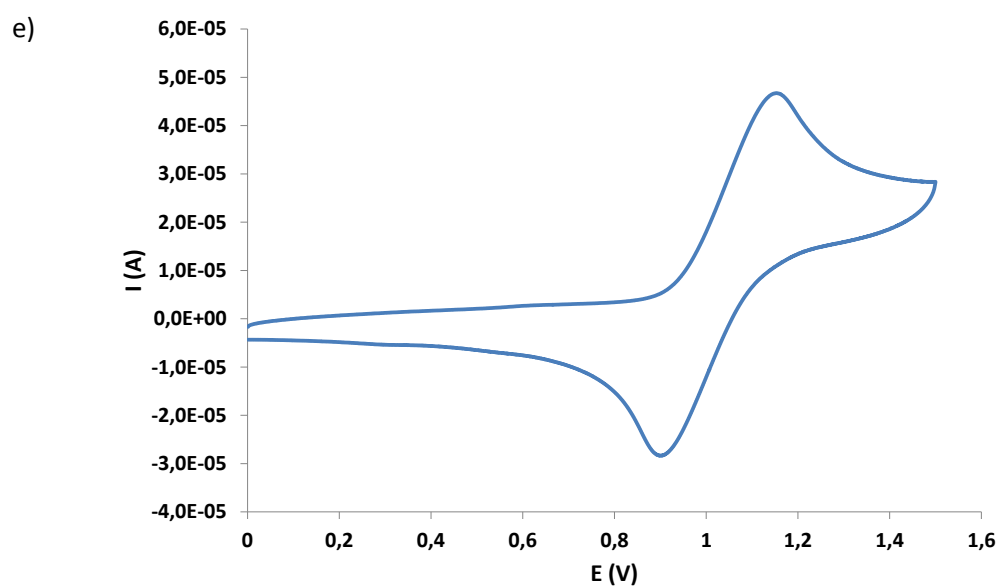
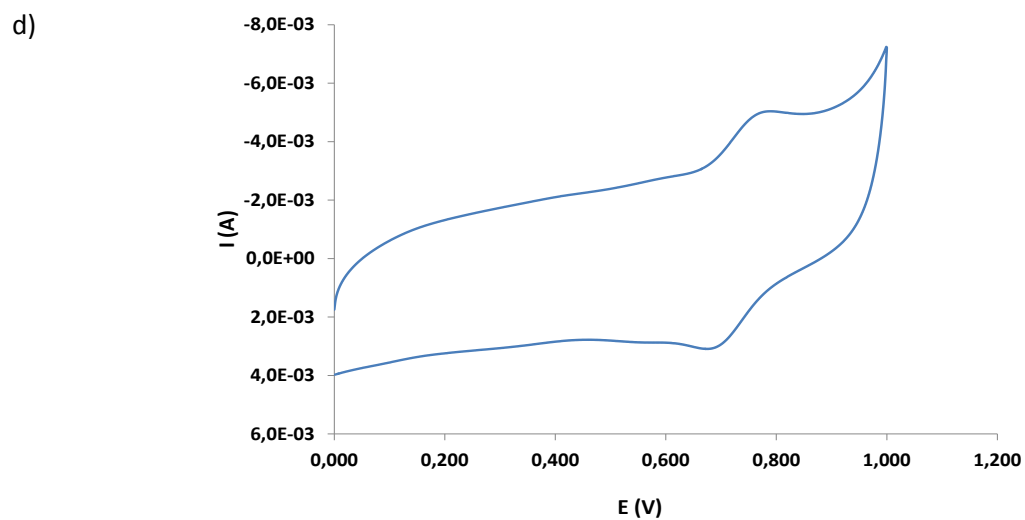
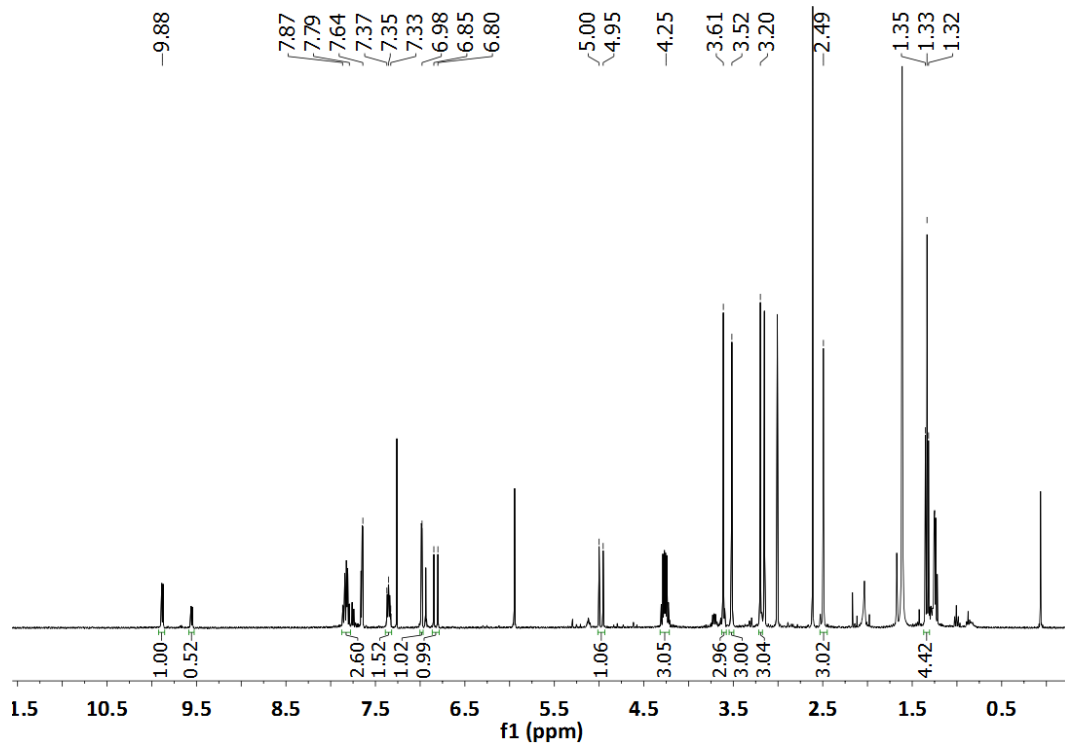
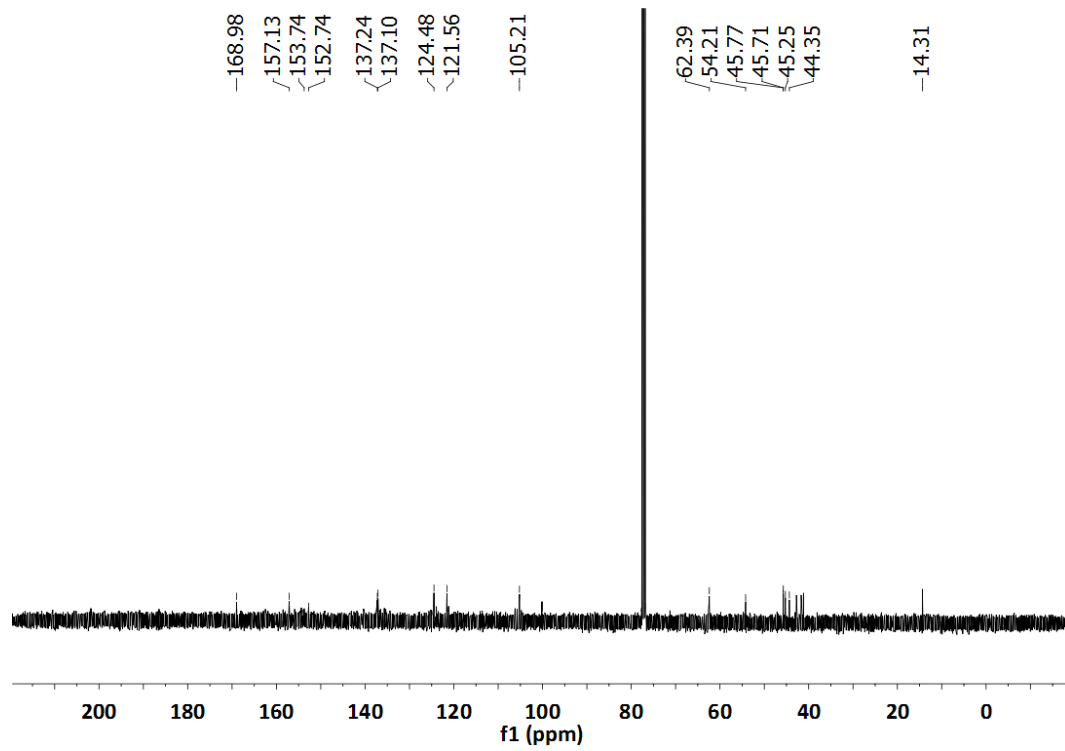


Figure SIV.2.14. Cyclic voltammograms in CH_2Cl_2 vs. SCE of a) **Ru1** (pure isomer **Ru1b** (blue) and the mixture of isomers **Ru1a** and **Ru1b** (red), b) **Ru2**, c) **Ru3** d) **Ru4**, e) **Ru5** and f) **Ru6**.

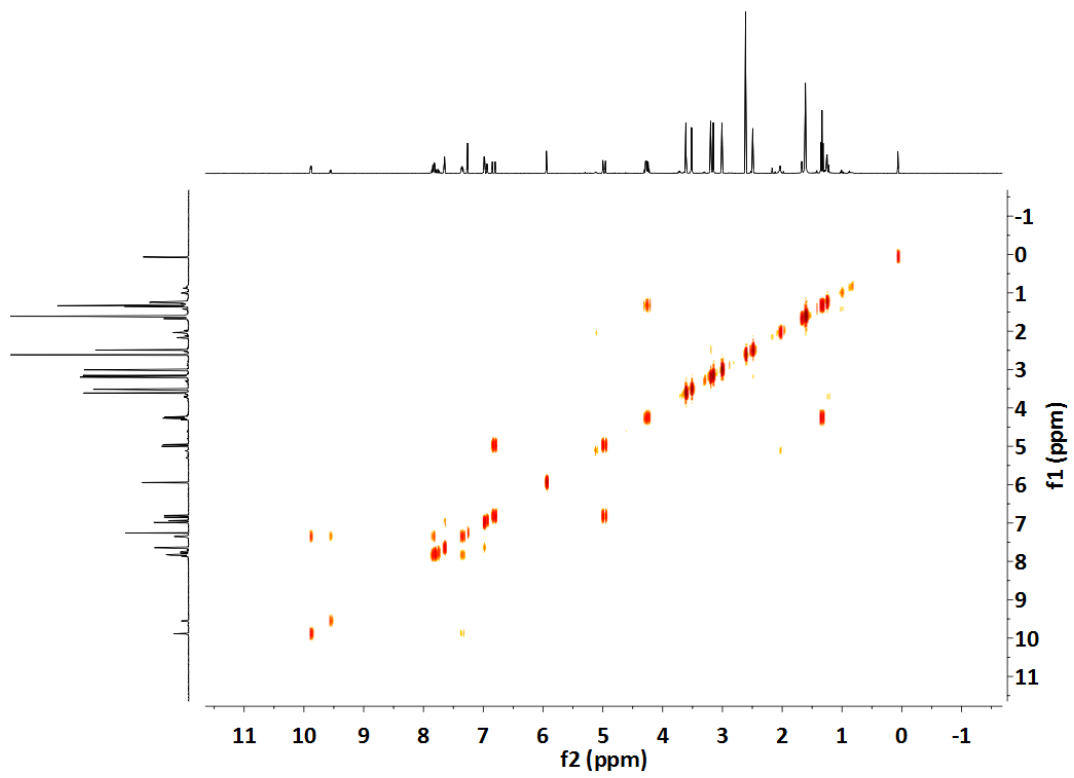
a)



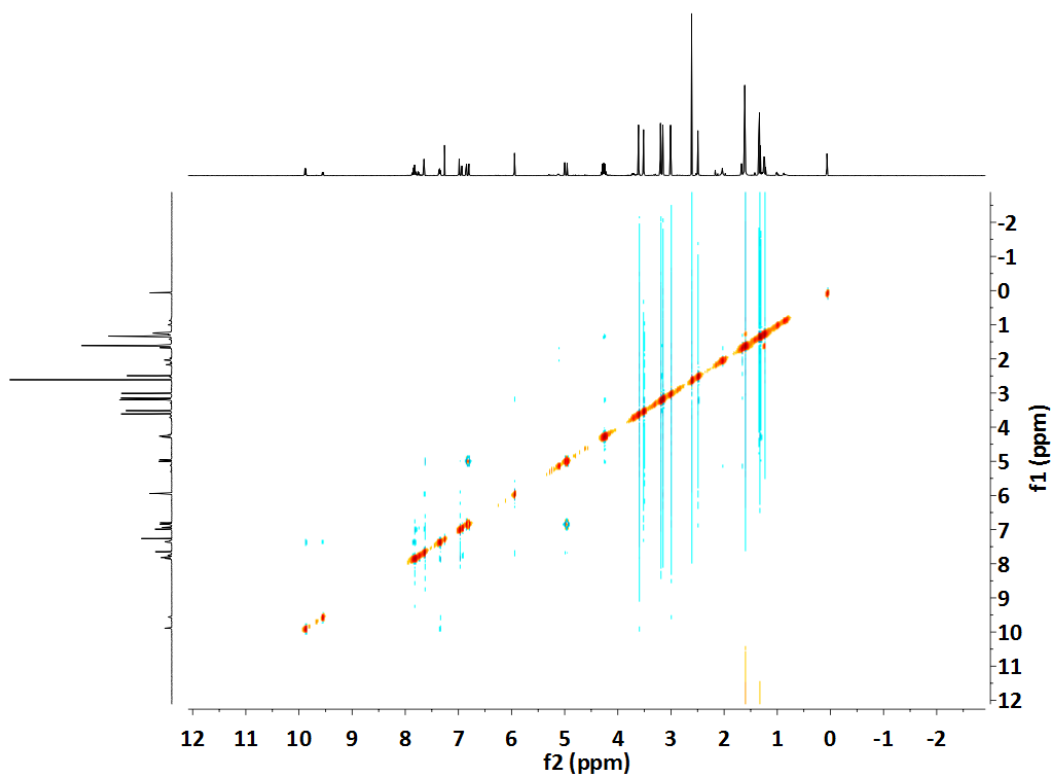
b)



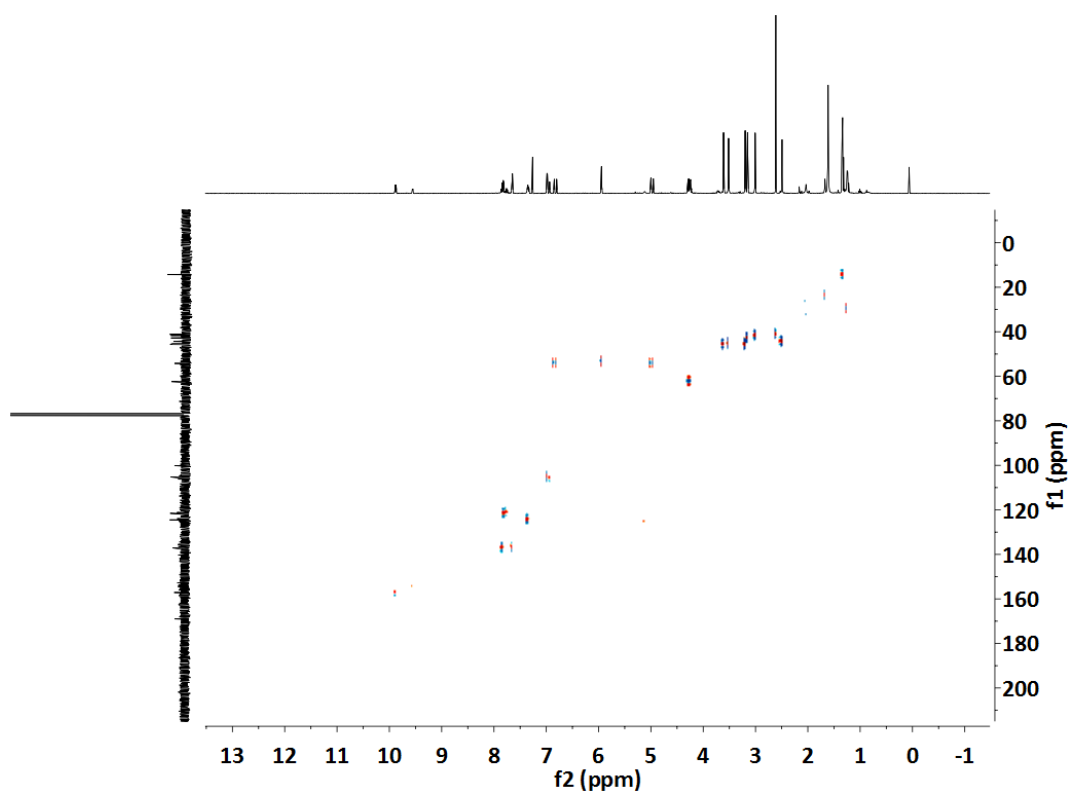
c)



d)



e)



f)

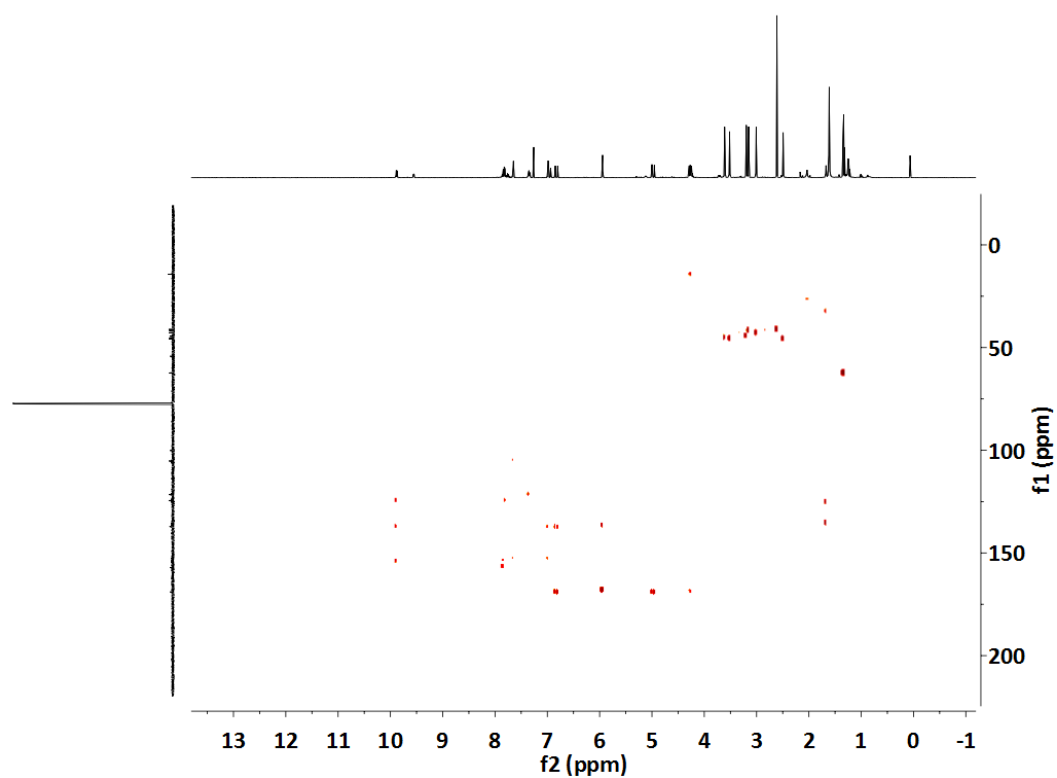
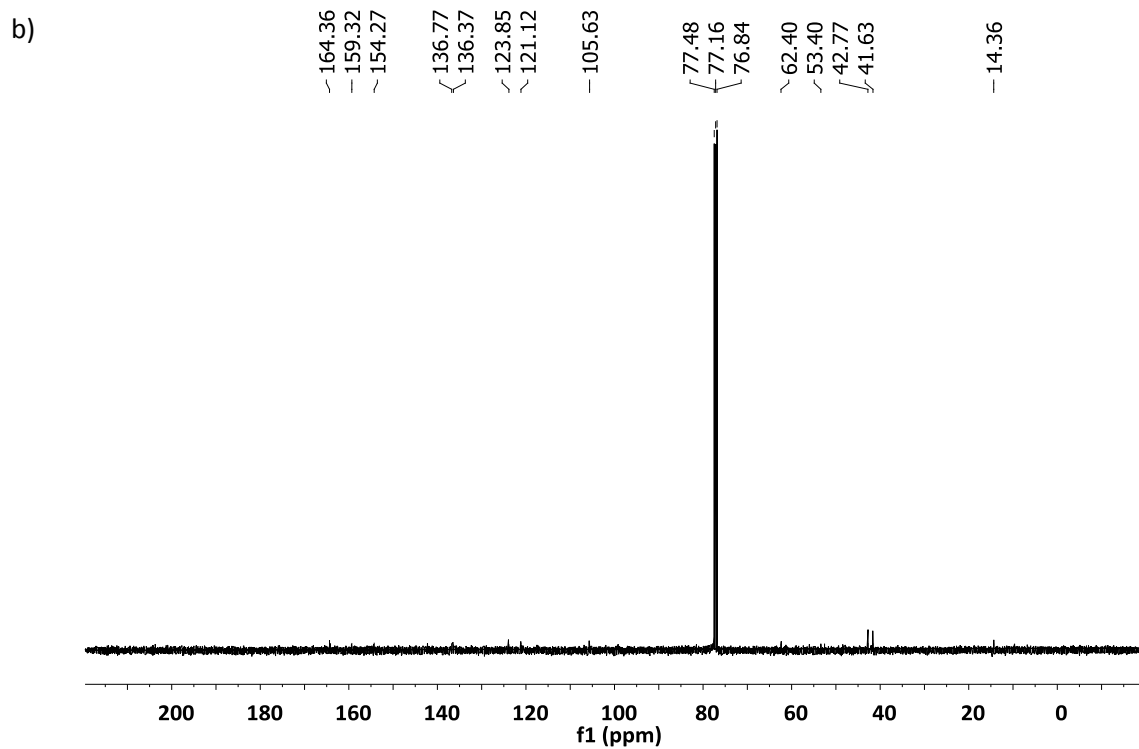
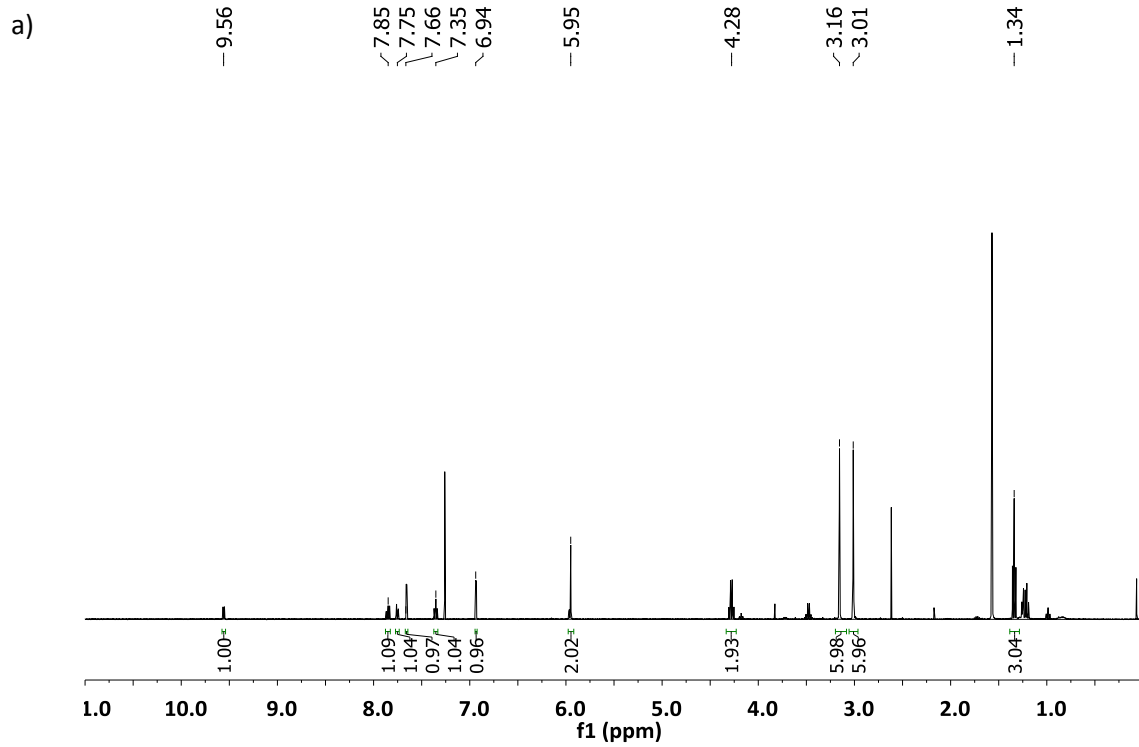
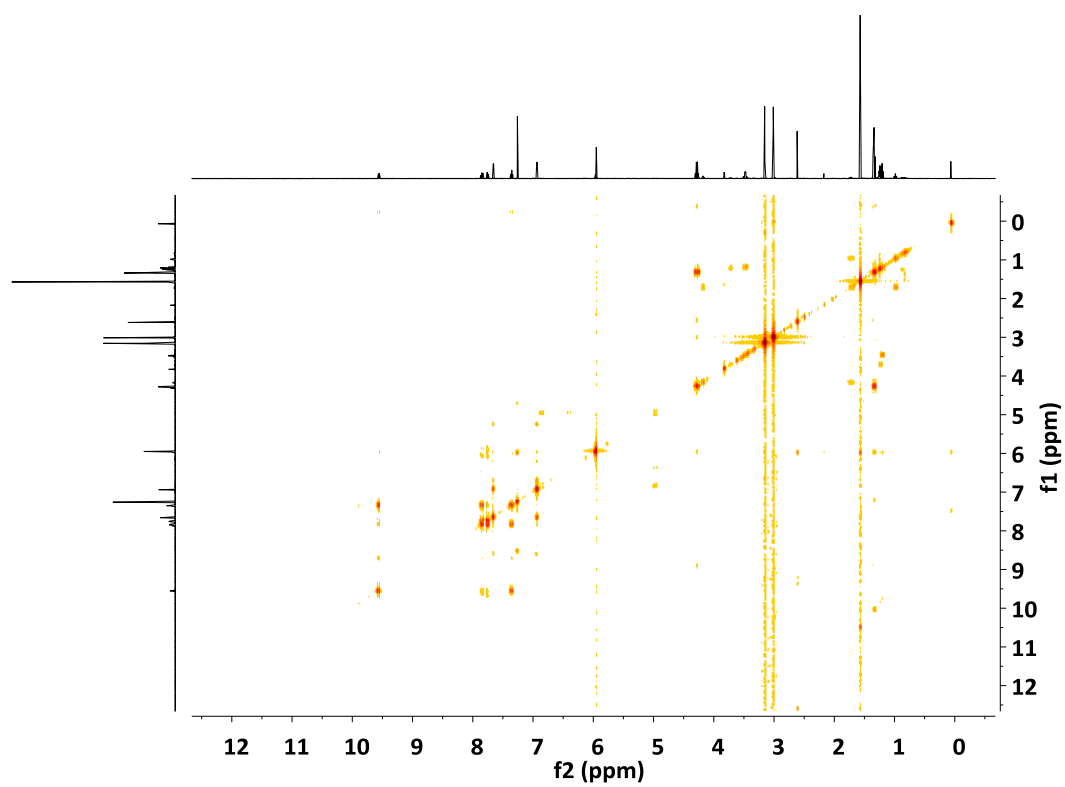


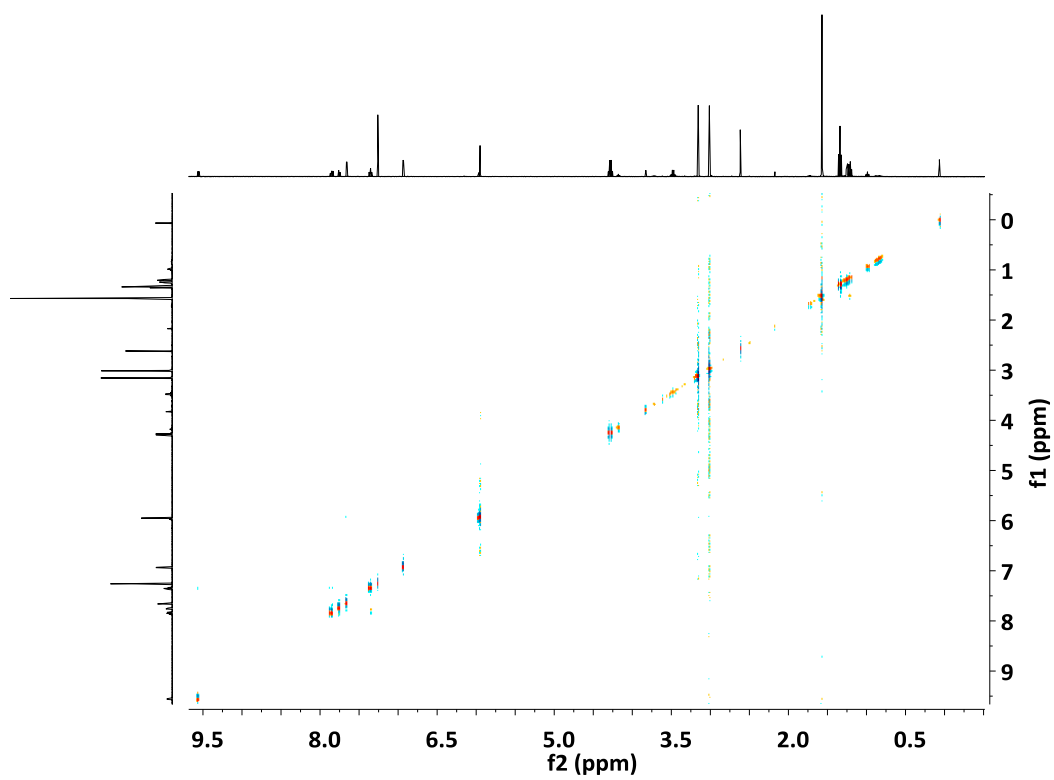
Figure SIV.2.15. NMR of **Ru1a**, as mixture of isomers **Ru1a** and **Ru1b** (1: 0.5), 400 MHz, CDCl_3 : a) ^1H -NMR; b) ^{13}C -NMR; c) COESY; d) NOESY; e) ^1H - ^{13}C HSQC; f) ^1H - ^{13}C HMBC.



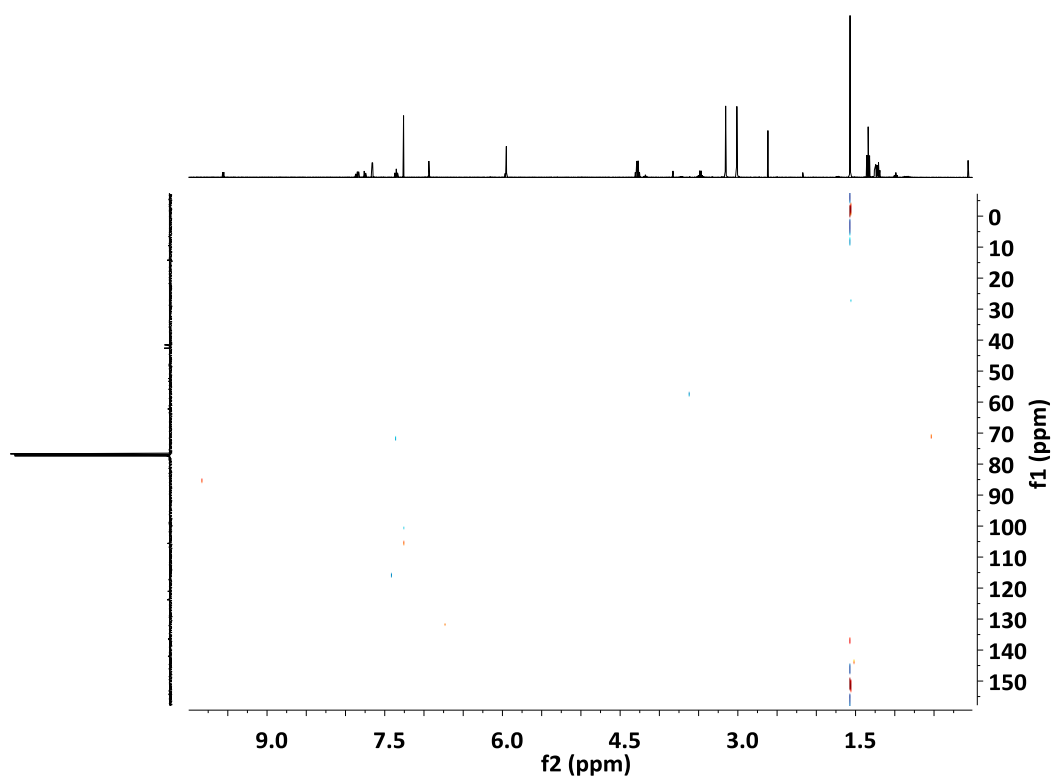
c)



d)



e)



f)

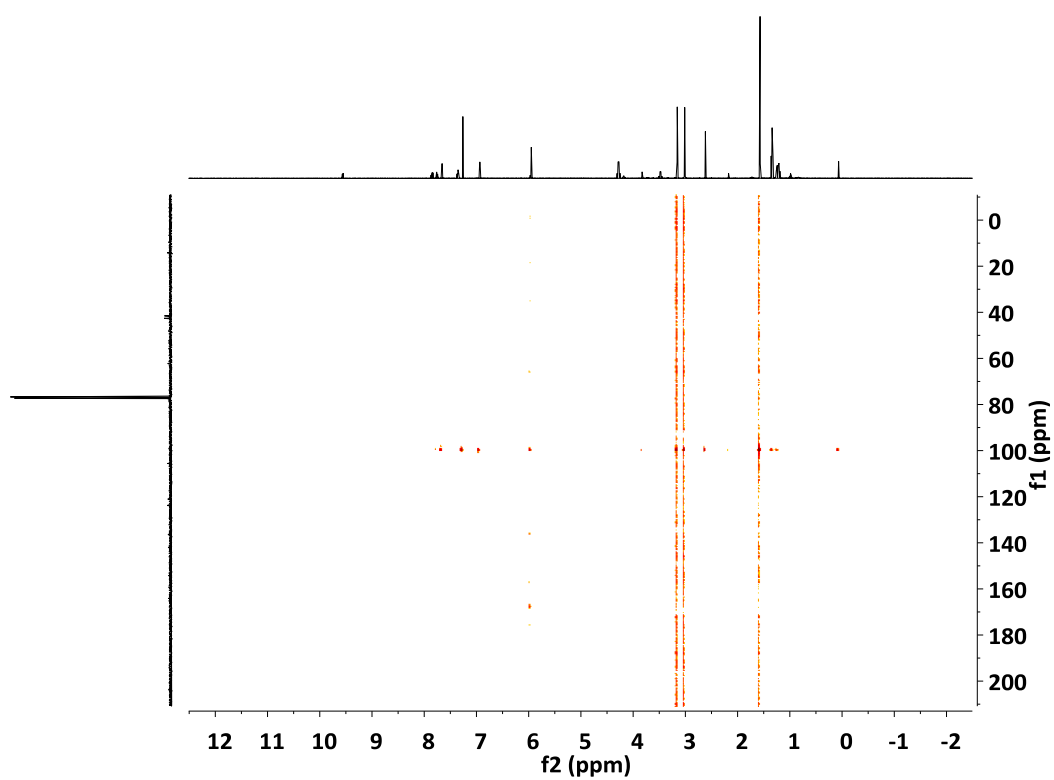
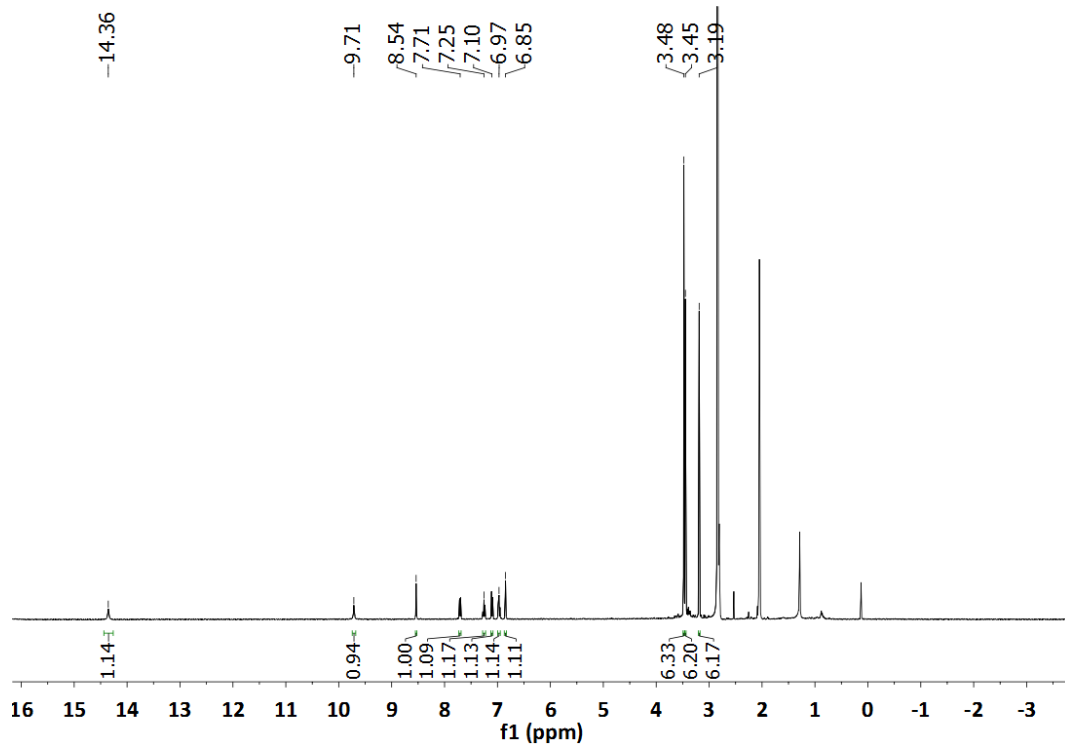
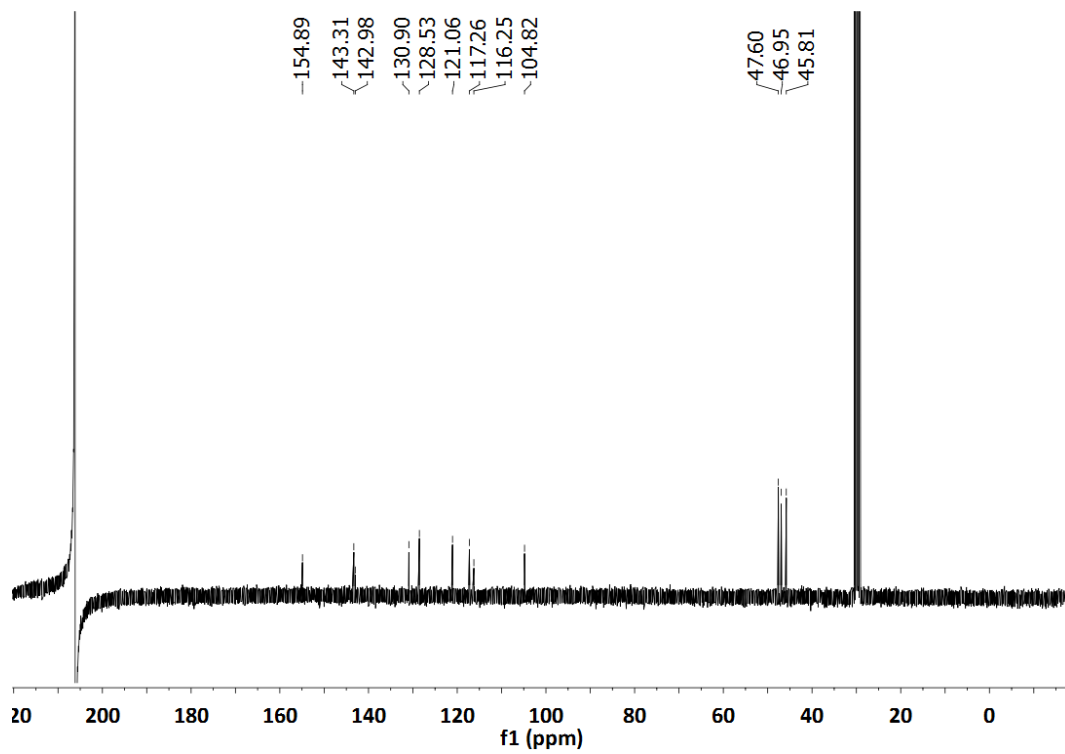


Figure SIV.2.16. NMR of **Ru1b**, 400 MHz, CDCl_3 : a) ^1H -NMR; b) ^{13}C -NMR; c) COESY; d) NOESY; e) ^1H - ^{13}C HSQC; f) ^1H - ^{13}C HMBC.

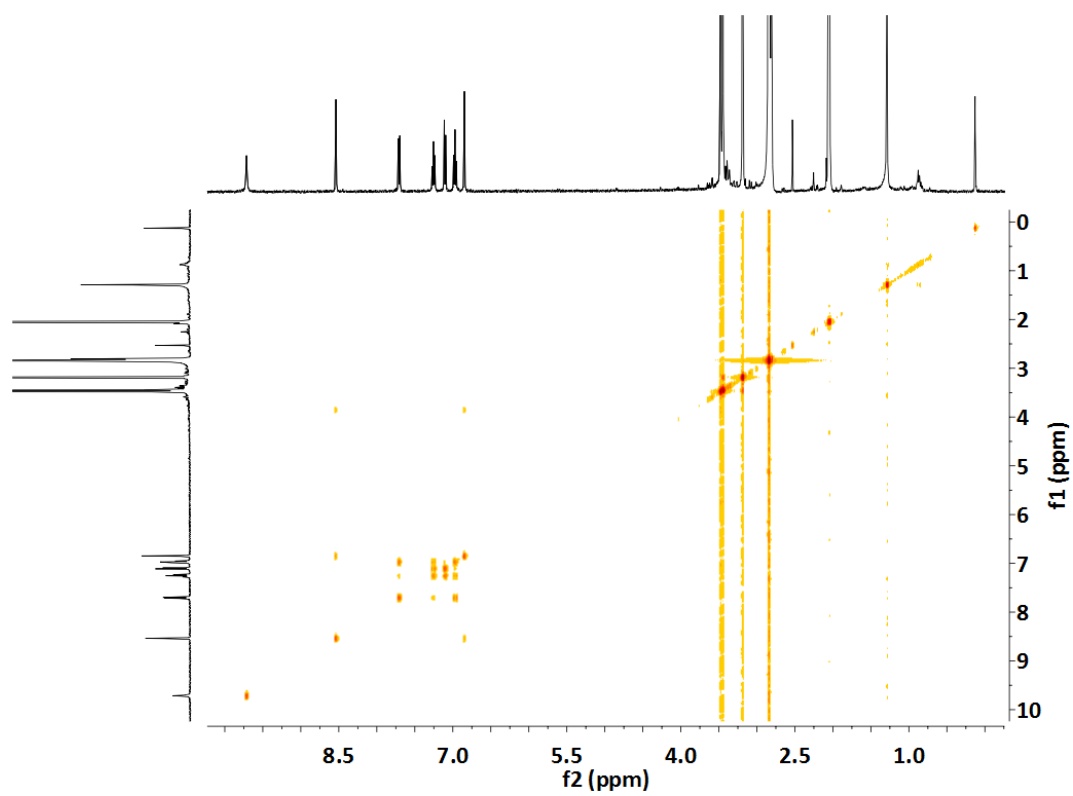
a)



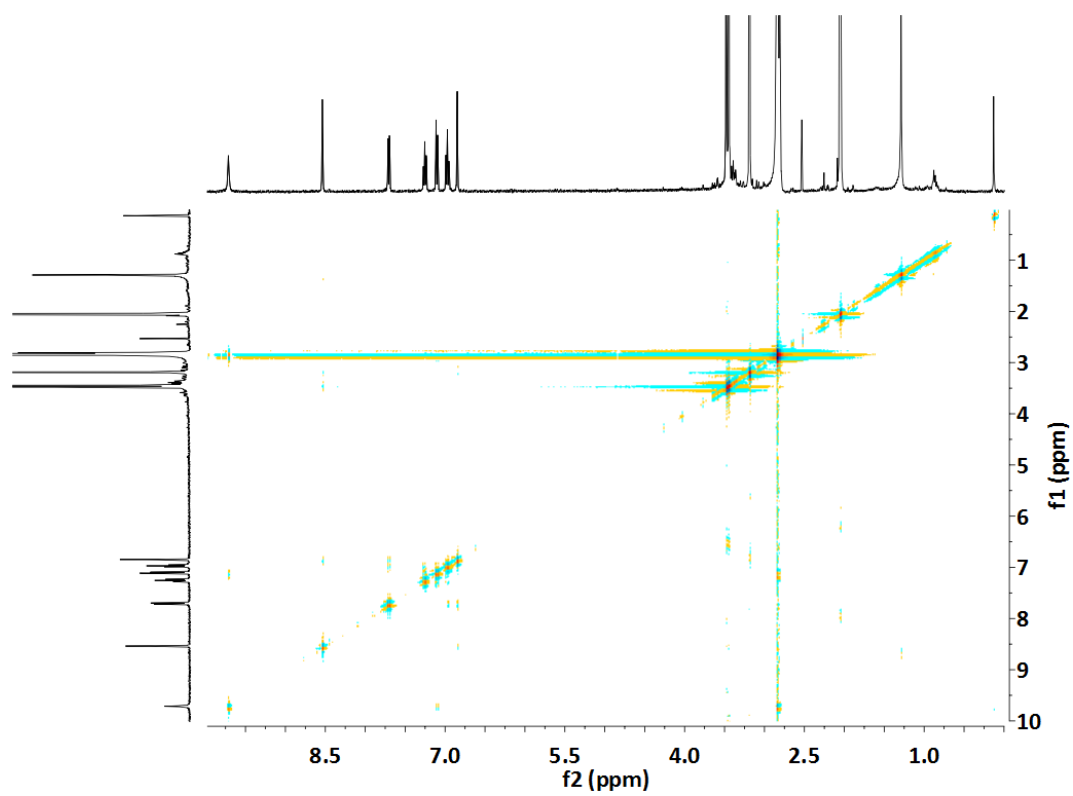
b)



c)



d)



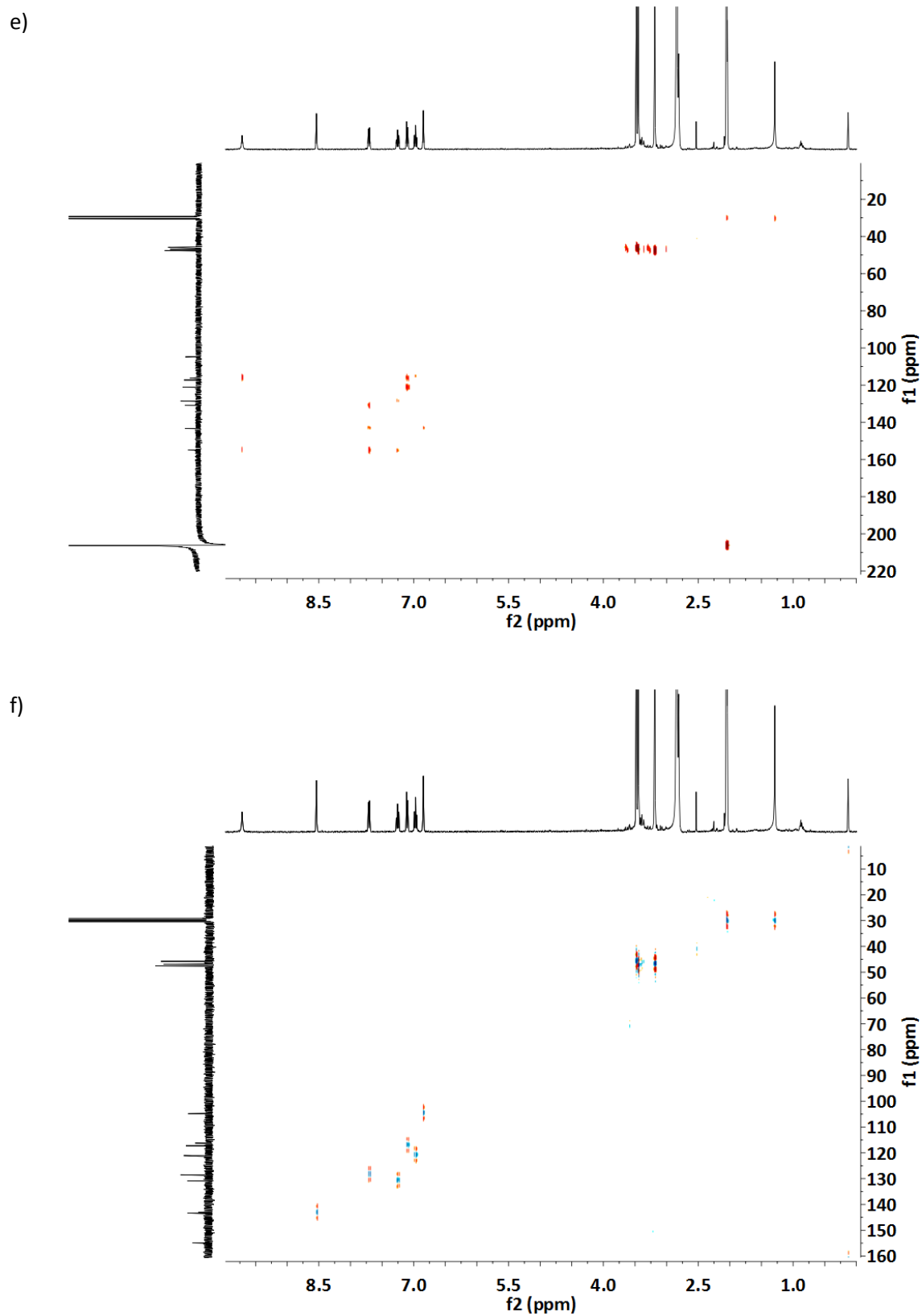
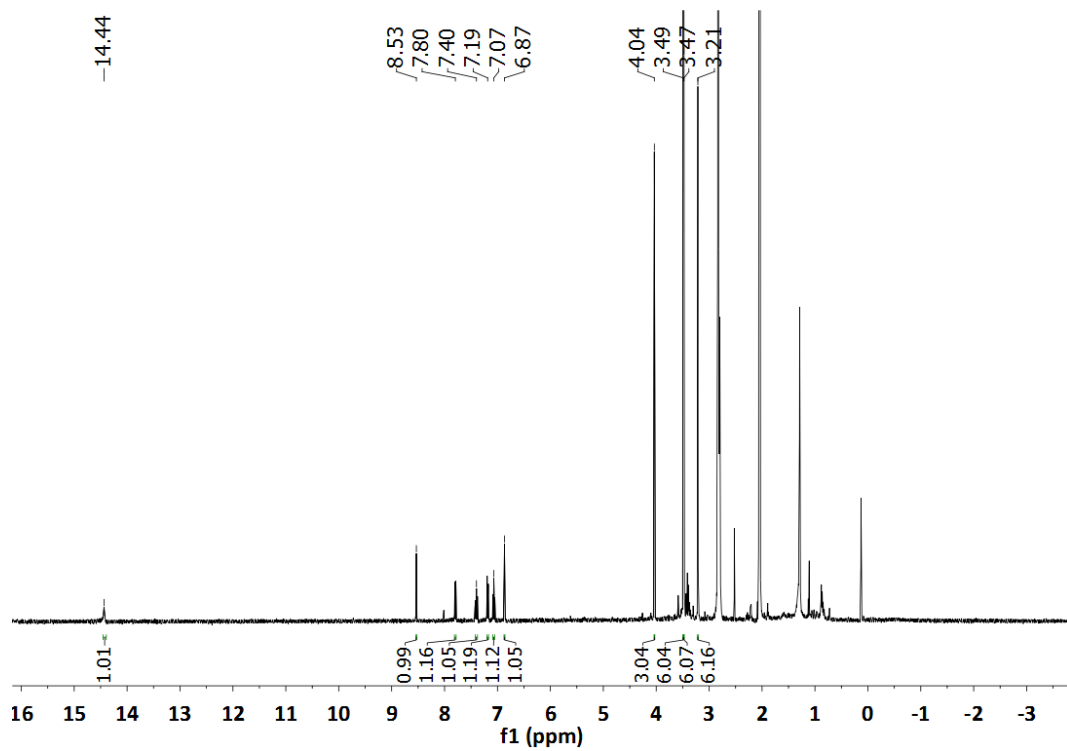
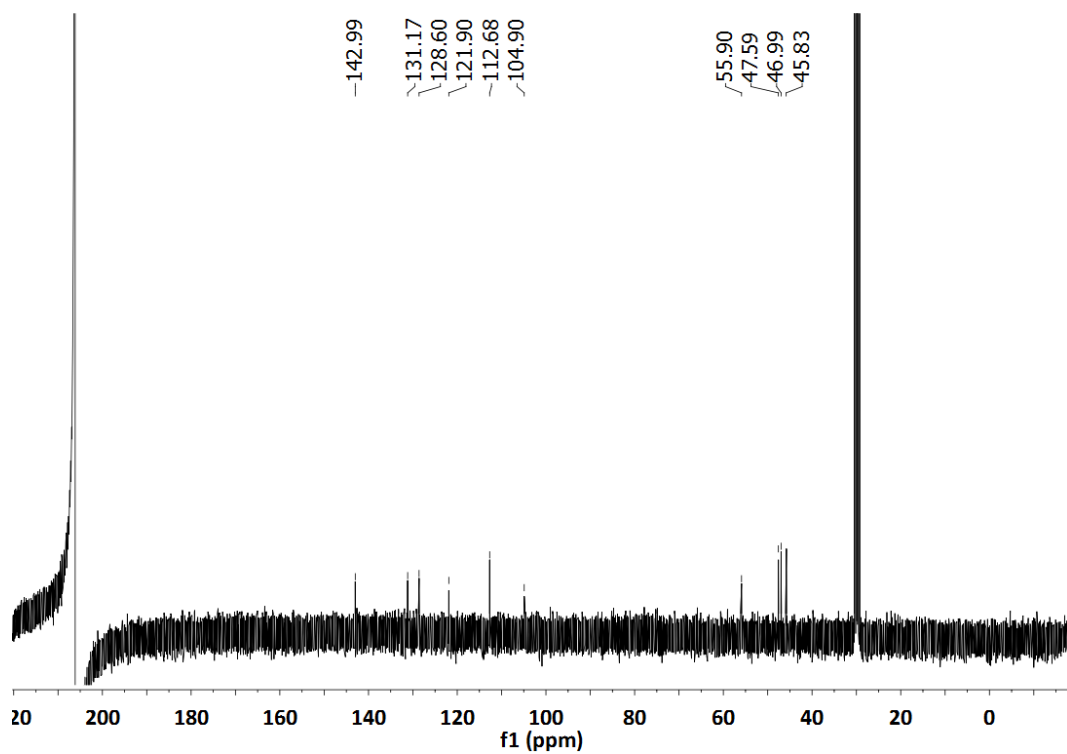


Figure SIV.2.17. NMR of **Ru2**, 400 MHz, acetone- d_6 : a) ^1H -NMR; b) ^{13}C -NMR; c) COESY; d) NOESY; e) ^1H - ^{13}C HSQC; f) ^1H - ^{13}C HMBC.

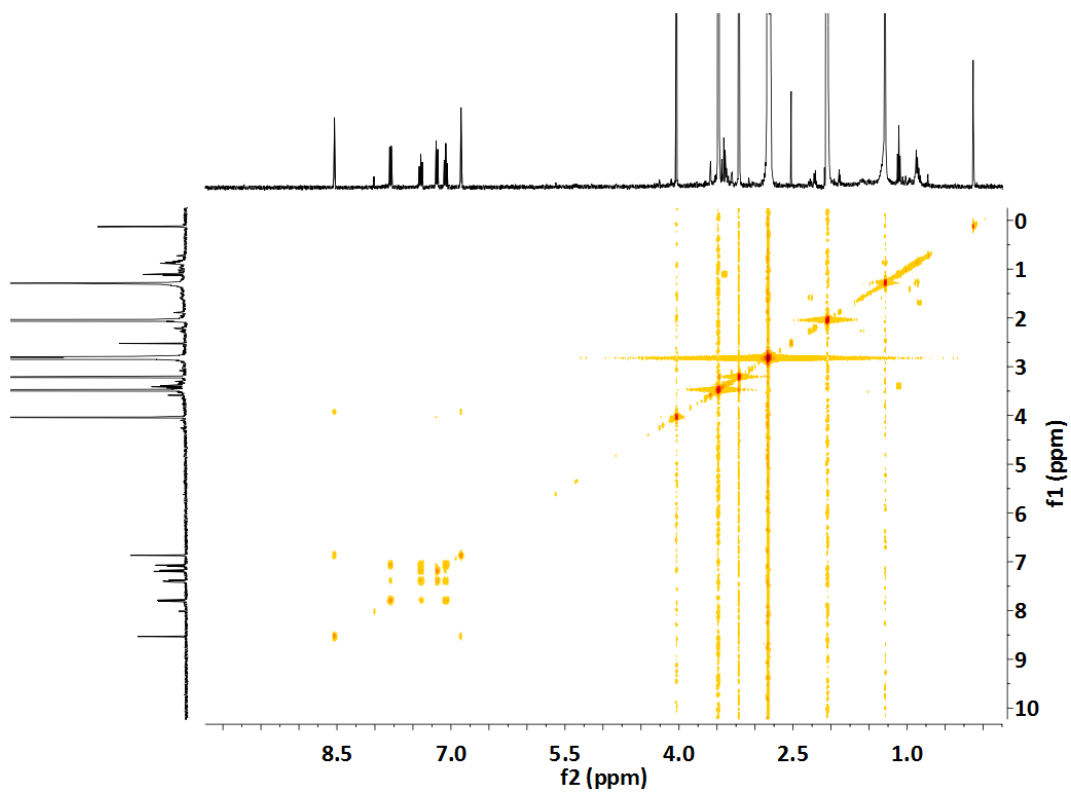
a)



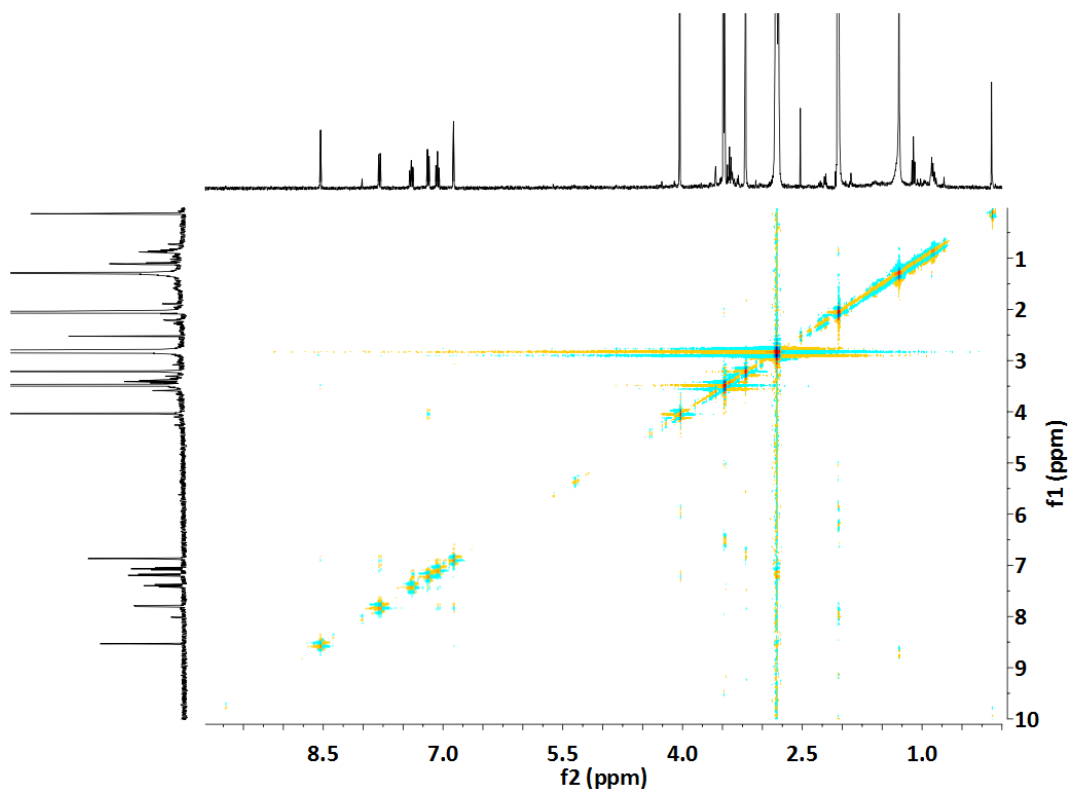
b)



c)



d)



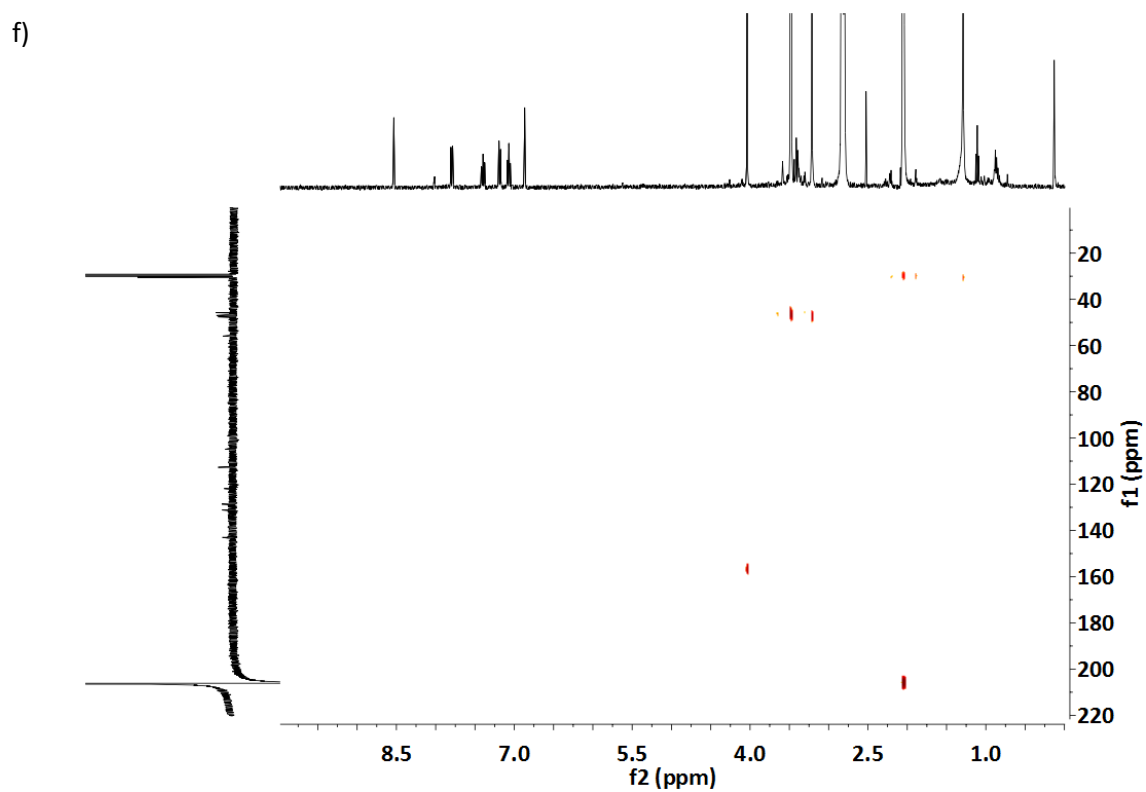
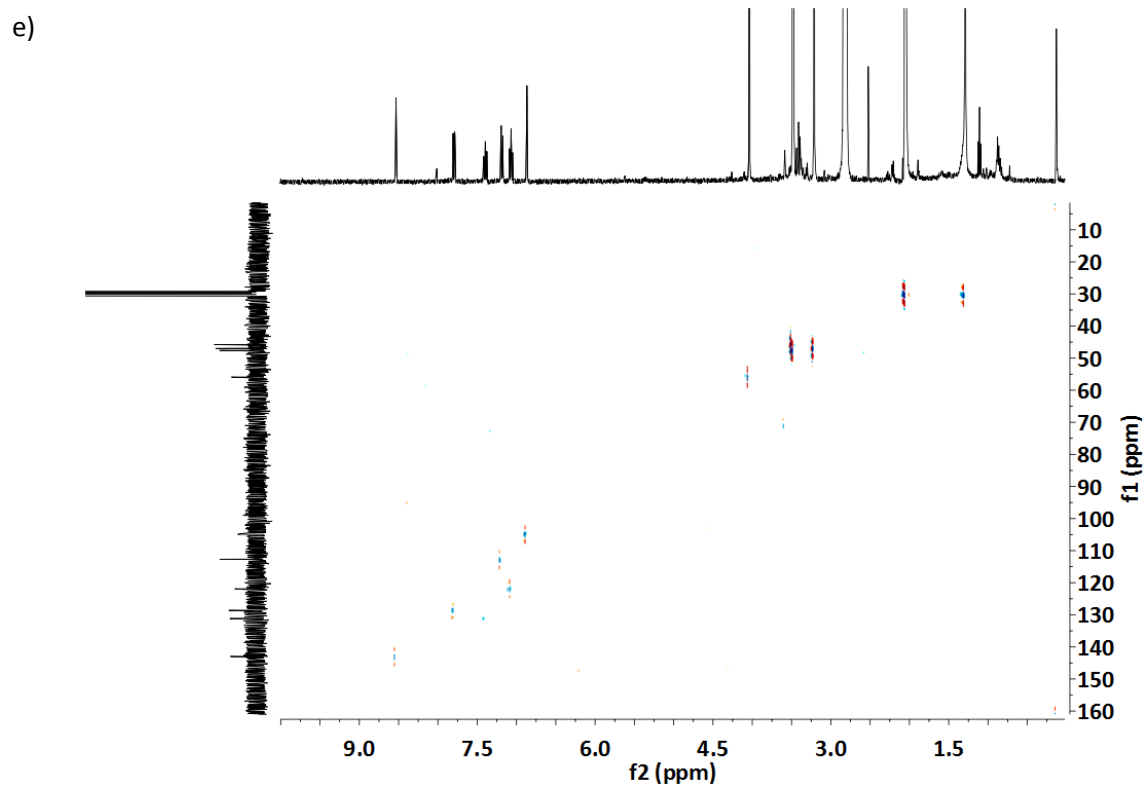


Figure SIV.2.18. NMR of **Ru3**, 400 MHz, acetone- d_6 : a) ^1H -NMR; b) ^{13}C -NMR; c) COESY; d) NOESY; e) ^1H - ^{13}C HSQC; f) ^1H - ^{13}C HMBC.

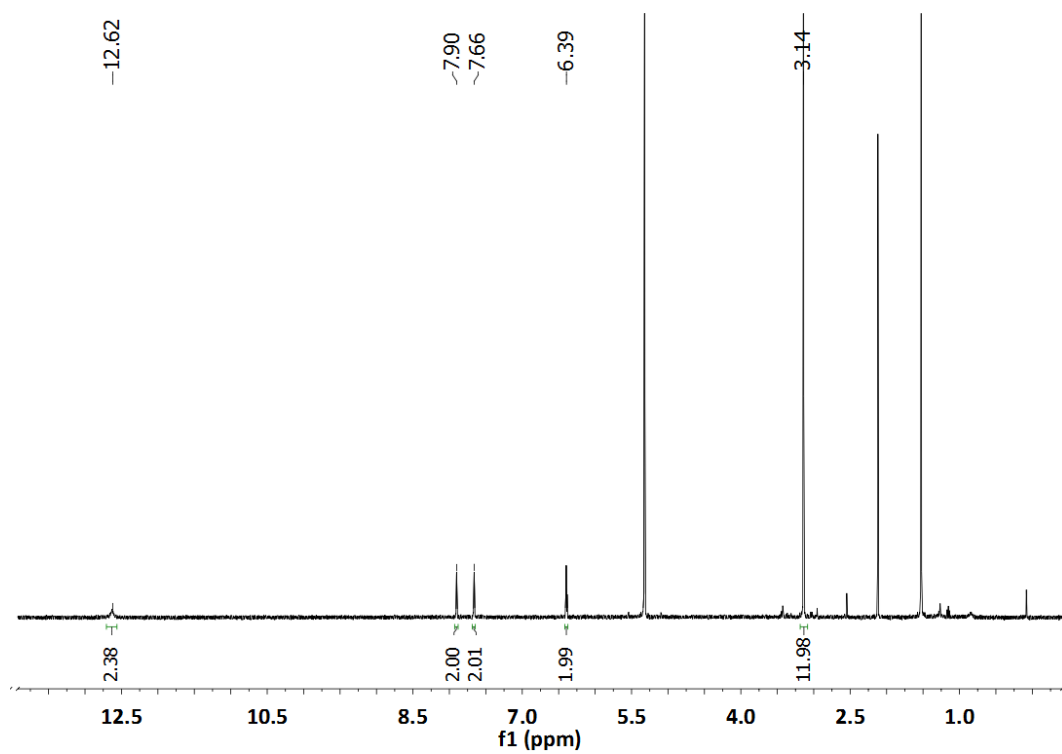
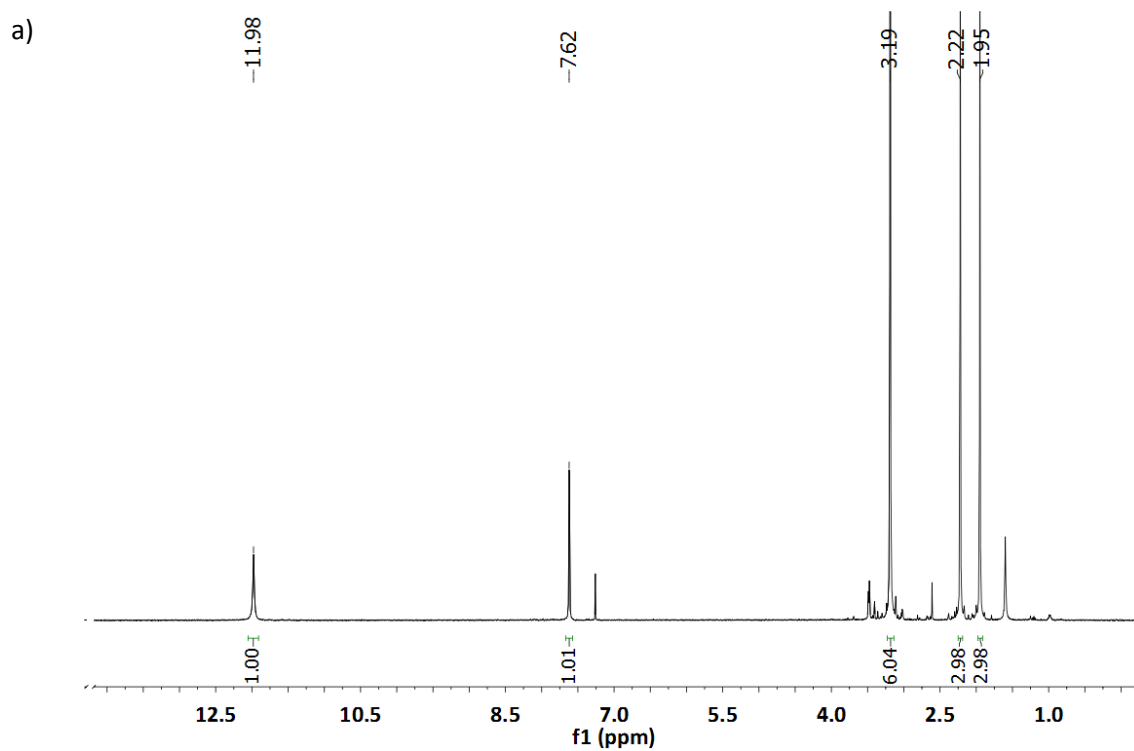
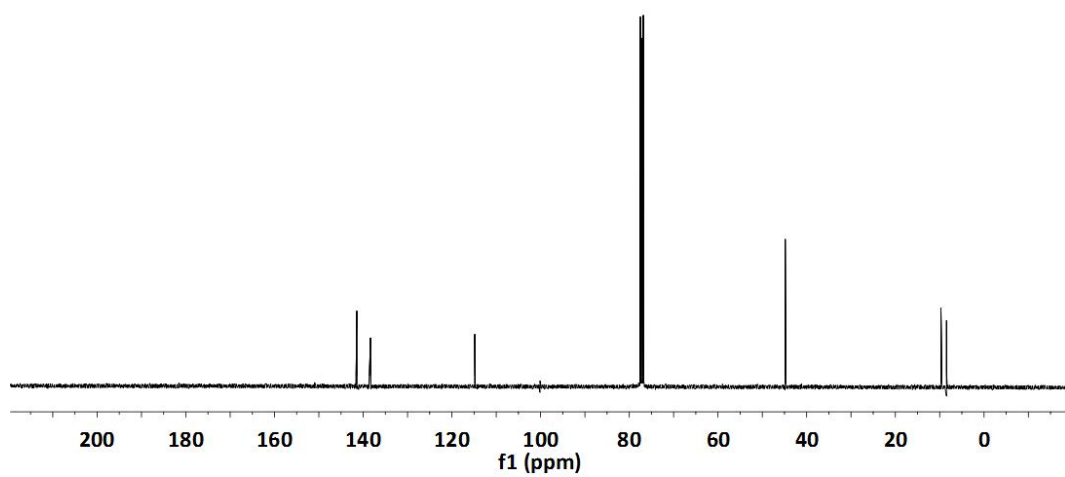


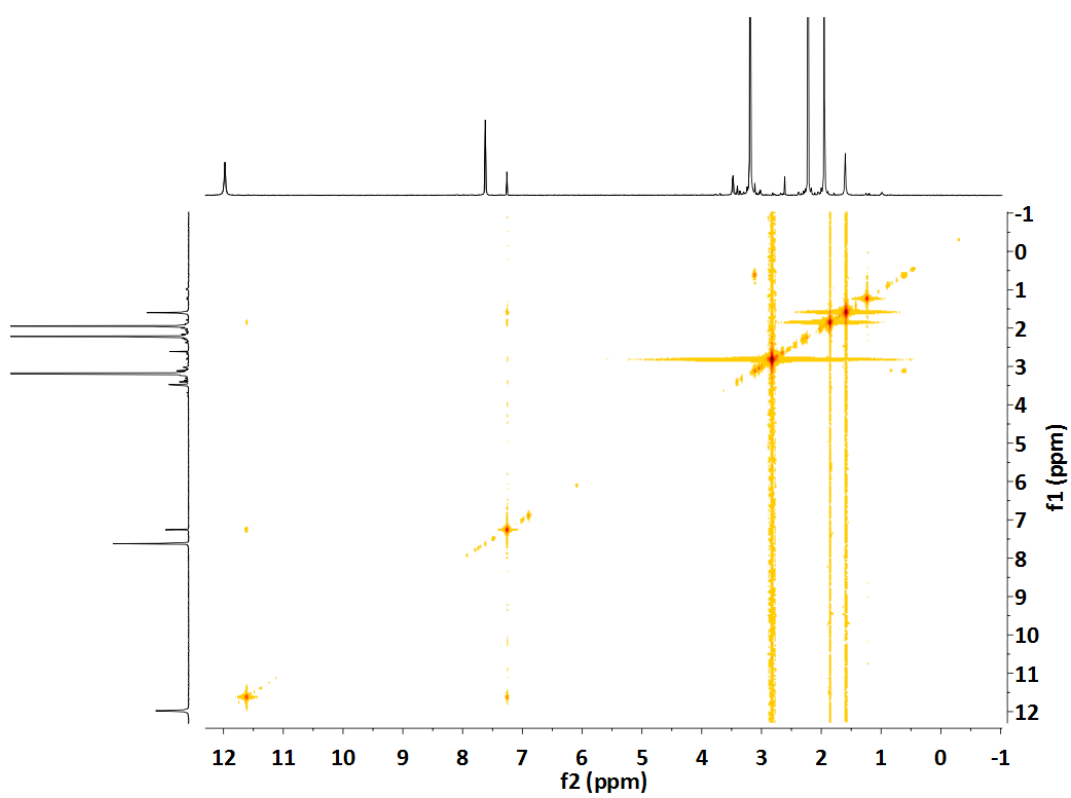
Figure SIV.2.19. $^1\text{H-NMR}$ of Ru4, 400 MHz, CD_2Cl_2 .



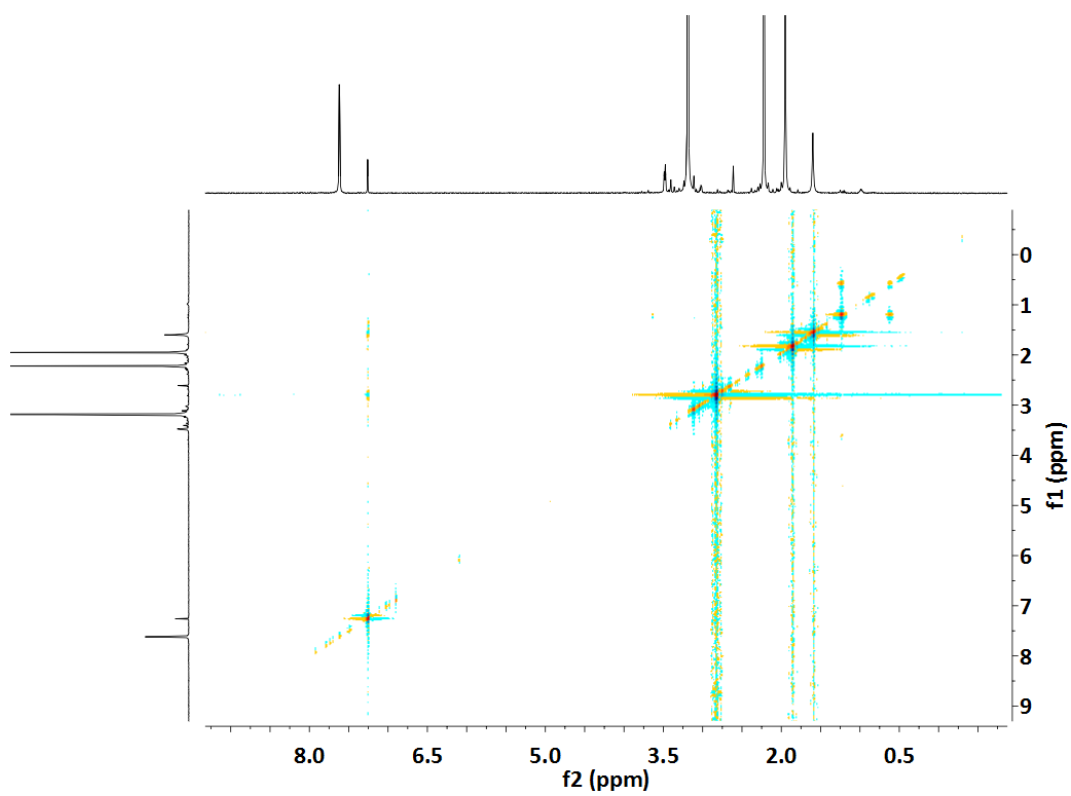
b)



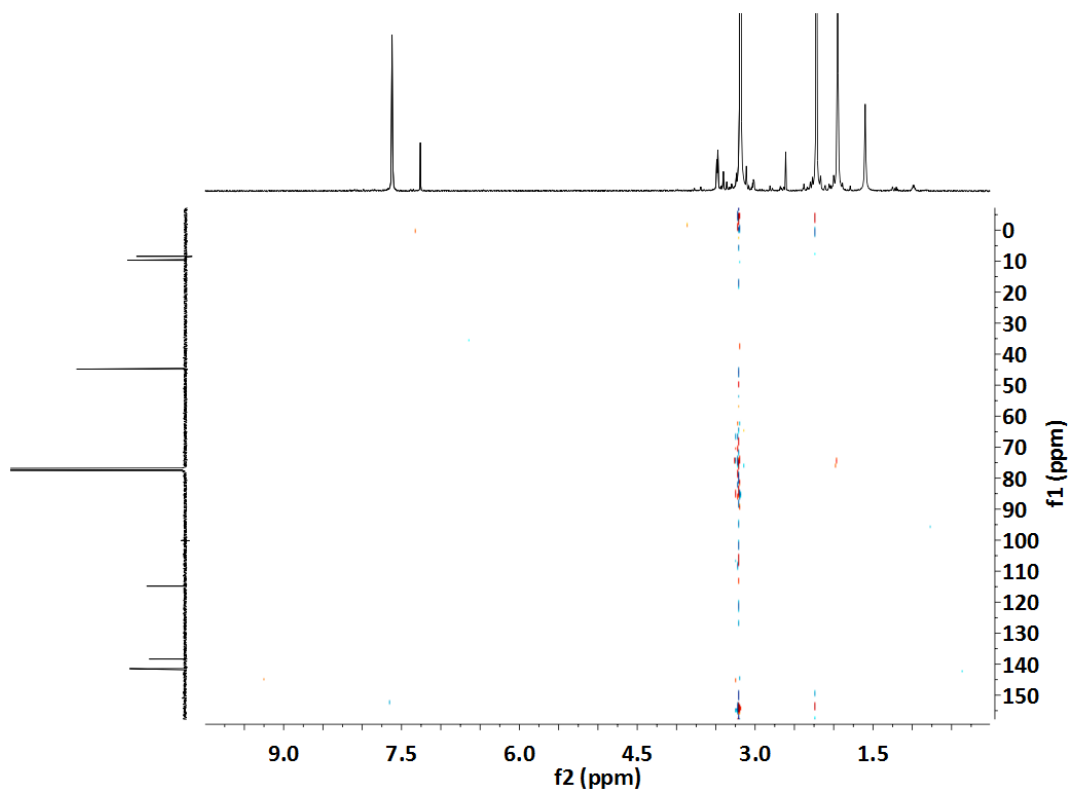
c)



d)



e)



f)

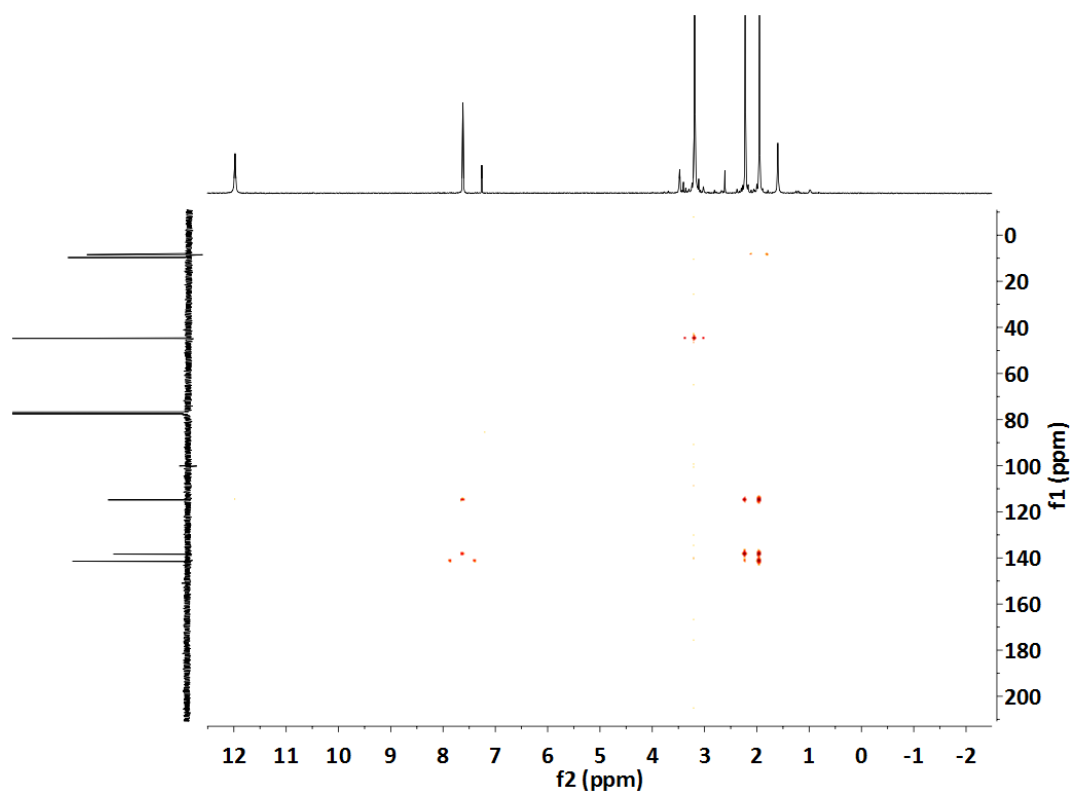


Figure SIV.2.20. NMR of Ru5, 400 MHz, CDCl₃: a) ¹H-NMR; b) ¹³C-NMR; c) COESY; d) NOESY; e) ¹H-¹³C HSQC; f) ¹H-¹³C HMBC.

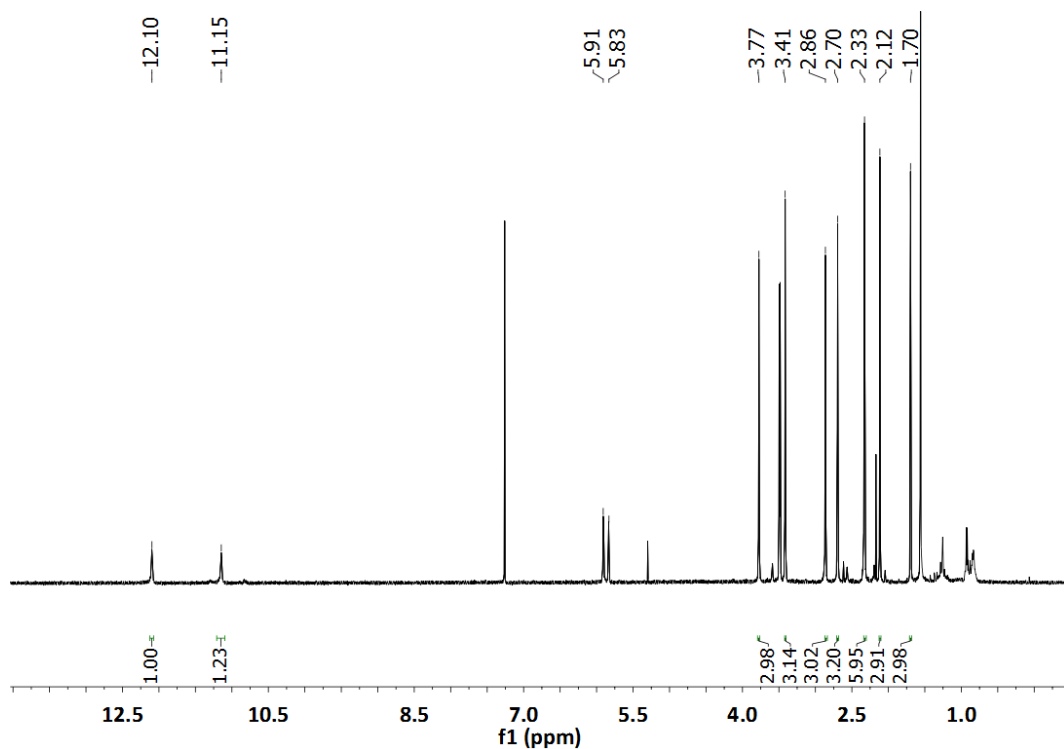


Figure SIV.2.21. ¹H-NMR of Ru6, 400 MHz, CDCl₃.

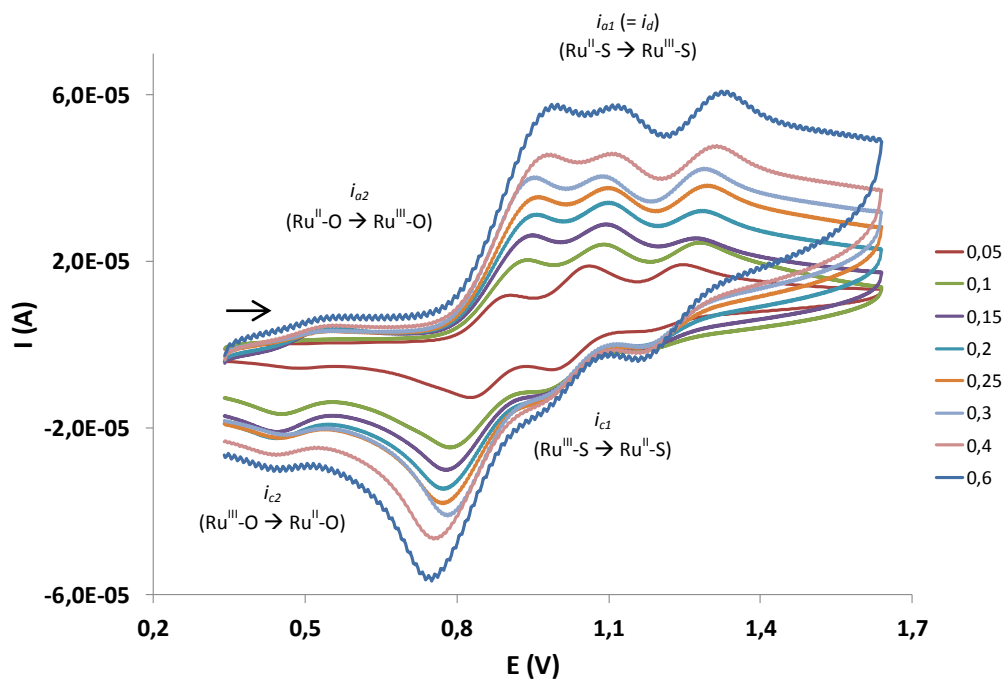


Figure SIV.2.22. CV of complex **Ru1a** registered in CH_3CN (TBAH, 0.1 M) vs SCE starting at $E_{\text{init}} = 0.3$ V and scanning towards increasing potential values at scan rates between 0.05 and 0.6 V/s (equilibration time = 2 s).

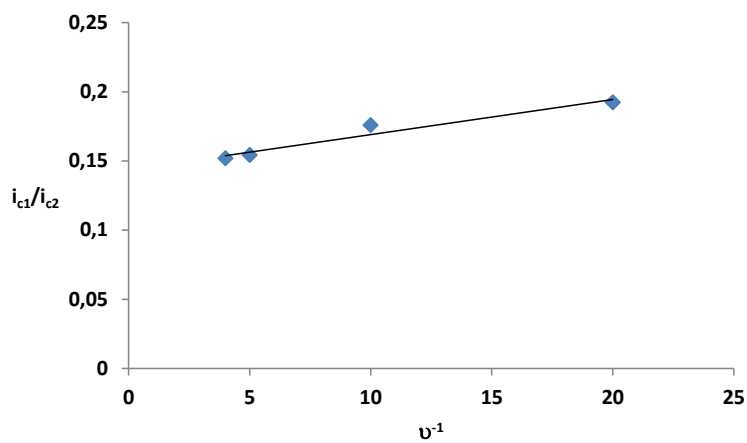


Figure SIV.2.23. Plot of i_{c1}/i_{c2} vs. v^{-1} to obtain K_{O-S}^{III} for complex **Ru1a**.

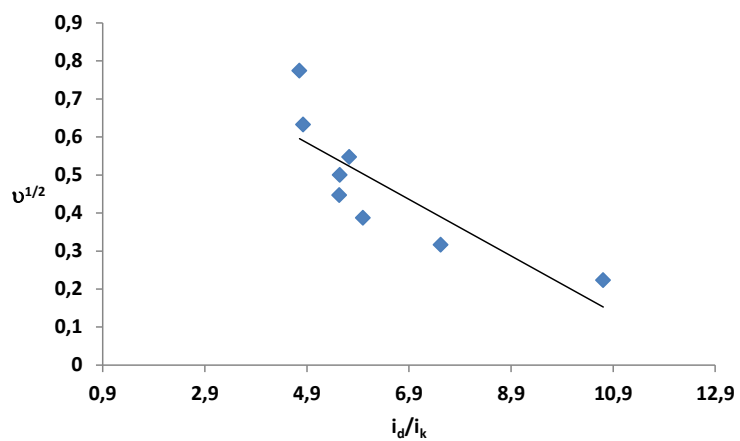


Figure SIV.2.24. Plot of $v^{1/2}$ vs. i_d/i_k to obtain k'''_{O-S} and k'''_{S-O} for complex Ru1a.

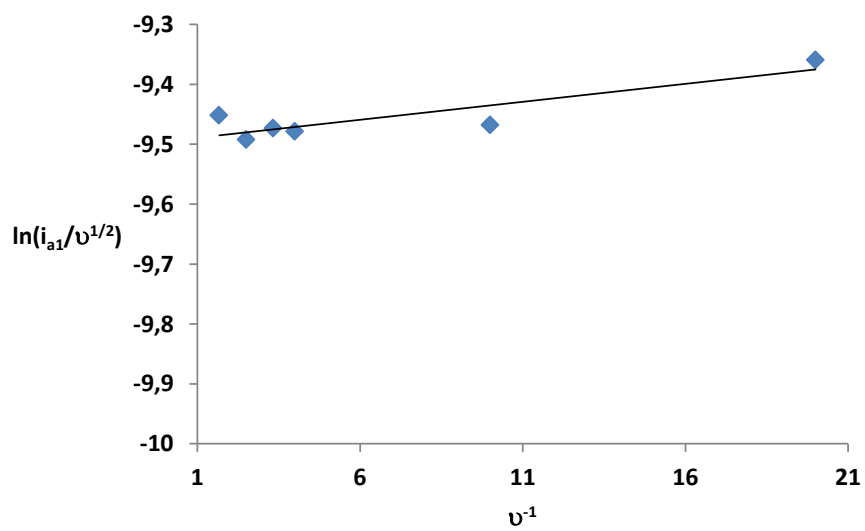


Figure SIV.2.25. Plot of $\ln(i_{a1}/v^{1/2})$ vs. v^{-1} to obtain k''_{O-S} for complex Ru1a.

Table SIV.2.3. Formulas used for the calculation of rate (k) and equilibrium (K) constants.

| Equations | Description of parameters |
|---|---|
| $\frac{i_{c1}}{i_{c2}} = a \cdot \frac{1}{v} + K_{O-S}^{III}$ <p style="text-align: center;">(eq. 1)</p> | <p>i_c = cathodic peak intensity (A)</p> <p>$a = RT/nF$, with:</p> <p>R = Boltzmann constant (J/(K·mol))</p> <p>T = temperature (K)</p> <p>n = number of exchanged electrons</p> <p>F = Faraday constant (A·s/mol)</p> <p>v = scan rate (V/s)</p> <p>K = equilibrium constant</p> |
| $\sqrt{v} = \frac{1}{\frac{0.471}{K_{O-S}^{III}} \cdot \sqrt{\frac{nFl}{RT}}} \cdot \frac{i_d}{i_k} - \frac{1.02}{\frac{0.471}{K_{O-S}^{III}} \cdot \sqrt{\frac{nFl}{RT}}}$ <p style="text-align: center;">(eq. 2)</p> | <p>i_d = diffusional current in the absence of a chemical reaction (= i_{a1})</p> <p>i_k = measured peak current (= i_{c1})</p> <p>$l = k_{O-S}^{III} + k_{S-O}^{III}$</p> |
| $K^{II} = K^{III} + e^{\frac{F}{RT}(E_{Ru-S}^0 - E_{Ru-O}^0)}$ <p style="text-align: center;">(eq. 3)</p> | <p>E^0 = standard potential</p> |
| $\ln\left(\frac{i_{a1}}{\sqrt{v}}\right) = k_{O-S}^{II} \cdot \frac{1}{v} + b$ <p style="text-align: center;">(eq. 4)</p> | |

Chapter 6

Table SIV.3.1. Crystallographic data for complexes **Ru7b-9** and **Ru11**.

| | Ru7b | Ru8 | Ru9 | Ru11 |
|--|---|---|---|--|
| Empirical formula | C ₂₇ H ₂₇ Cl ₁ N ₆ O ₁ F ₆ P ₁ Ru ₁ | C ₂₅ H ₂₄ S ₁ N ₆ O ₁ F ₁₂ P ₂ Ru ₁ | C ₇₉ H ₆₆ Cl ₄ N ₁₈ F ₁₂ P ₂ O ₃ Ru ₄ | C ₄₆ H ₃₄ N ₁₂ F ₁₂ P ₂ Ru ₂ |
| Formula weight | 733.03 | 847.57 | 2151.51 | 1246.93 |
| Crystal system | Triclinic | Monoclinic | Triclinic | Triclinic |
| Space group | P-1 | C 2/c | P-1 | P-1 |
| a/Å | 10.503(10) | 22.793(10) | 13.019(2) | 8.731(6) |
| b/Å | 11.377(11) | 10.889(6) | 18.411(3) | 12.835(8) |
| c/Å | 13.781(13) | 24.907(11) | 18.677(3) | 12.943(8) |
| α/° | 69.045(14) | 90 | 83(3) | 71.468(11) |
| β/° | 86.516(16) | 92.581(10) | 81.185(3) | 89.272(10) |
| γ/° | 85.950(16) | 90 | 71.846(3) | 86.629(12) |
| V/Å³ | 1533(3) | 6175(5) | 4190.3(13) | 1372.8(15) |
| Formula units per cell | 2 | 8 | 2 | 1 |
| T/K | 298(2) | 100(2) | 298(2) | 193(2) |
| ρ_{calc}/Mgm⁻³ | 1.588 | 1.823 | 1.705 | 1.508 |
| μ/mm⁻¹ | 0.719 | 0.785 | 0.960 | 0.692 |
| Reflections collected/unique | 21219/7288 | 46396/7628 | 66240/20358 | 8920/5850 |
| R(int) | 0.0458 | 0.1877 | 0.102 | 0.0685 |
| Final R indices, [I>2σ(I)] | R ₁ = 0.0722, wR ² = 0.2019 | R ₁ = 0.1108, wR ² =0.2751 | R ₁ = 0.0582, wR ² = 0.1127 | R ₁ = 0.1231, wR ² =0.3154 |
| R indices [all data] | R ₁ = 0.0881, wR ² = 0.2221 | R ₁ = 0.2364, wR ² = 0.3585 | R ₁ = 0.1598, wR ² = 0.1477 | R ₁ = 0.1399, wR ² =0.3304 |

Table SIV.3.2. Selected bond lengths (Å) and angles (°) for Ru7b-9 and Ru11.

| Ru7b | | | |
|-----------------------|------------|---|------------|
| Ru—Cl(1) | 2.396(3) | Cl(1)—Ru—N(1) _{py} | 94.14(13) |
| Ru—N(1) _{py} | 2.103(5) | N(1) _{py} —Ru—N(2) _{pz} | 77.03(17) |
| Ru—N(2) _{pz} | 2.040(5) | N(1) _{py} —Ru—N(4) | 104.61(17) |
| Ru—N(4) | 2.076(4) | N(1) _{py} —Ru—N(5) | 174.38(15) |
| Ru—N(5) | 1.952(4) | N(1) _{py} —Ru—N(6) | 95.99(18) |
| Ru—N(6) | 2.081(4) | N(2) _{pz} —Ru—N(4) | 91.48(16) |
| | | N(2) _{pz} —Ru—N(5) | 99.34(16) |
| | | N(2) _{pz} —Ru—N(6) | 92.38(17) |
| | | N(2) _{pz} —Ru—Cl(1) | 170.82(12) |
| | | N(5)—Ru—N(4) | 79.61(17) |
| | | N(5)—Ru—N(6) | 79.78(18) |
| | | N(5)—Ru—Cl(1) | 89.66(12) |
| | | N(4)—Ru—N(6) | 159.38(18) |
| | | N(4)—Ru—Cl(1) | 88.33(11) |
| | | N(6)—Ru—Cl(1) | 91.00(12) |
| Ru8 | | | |
| Ru—S(1) | 2.267(3) | S(1)—Ru—N(1) | 95.7(3) |
| Ru—N(1) _{py} | 2.084(8) | N(1)—Ru—N(2) | 80.1(4) |
| Ru—N(2) _{pz} | 1.987(9) | N(1)—Ru—N(4) _{py} | 89.6(3) |
| Ru—N(3) | 2.077(7) | N(1)—Ru—N(3) | 159.6(4) |
| Ru—N(4) | 2.121(11) | N(1)—Ru—N(6) _{pz} | 98.3(4) |
| Ru—N(6) | 2.044(10) | N(2)—Ru—N(4) _{py} | 92.6(5) |
| | | N(2)—Ru—N(3) | 79.7(3) |
| | | N(2)—Ru—N(6) _{pz} | 170.8(4) |
| | | N(2)—Ru—Cl(1) | 90.57(8) |
| | | N(3)—Ru—N(4) _{py} | 88.0(3) |
| | | N(3)—Ru—N(6) _{pz} | 101.1(3) |
| | | N(3)—Ru—S(1) | 89.9(2) |
| | | N(4) _{py} —Ru—N(6) _{pz} | 89.27(3) |
| | | N(4) _{py} —Ru—S(1) | 170.1(3) |
| | | N(6) _{pz} —Ru—S(1) | 92.6(3) |
| Ru9 | | | |
| Ru(1)—Cl(1) | 2.4189(15) | N(2)—Ru(1)—N(5) | 174.4(2) |
| Ru(1)—N(1) | 2.062(5) | N(2)—Ru(1)—N(4) | 95.8(2) |
| Ru(1)—N(2) | 1.962(4) | N(5)—Ru(1)—N(4) | 78.67(19) |
| Ru(1)—N(3) | 2.073(5) | N(2)—Ru(1)—N(1) | 79.69(19) |
| Ru(1)—N(4) | 2.056(5) | N(5)—Ru(1)—N(1) | 99.59(18) |
| Ru(1)—N(5) | 2.037(4) | N(4)—Ru(1)—N(1) | 91.4(2) |
| Ru(2)—Cl(1) | | N(2)—Ru(1)—N(3) | 78.9(2) |
| | | N(5)—Ru(1)—N(3) | 101.77(19) |
| | | N(4)—Ru(1)—N(3) | 91.04(19) |
| | | N(1)—Ru(1)—N(3) | 158.57(19) |
| | | N(8)—Ru(2)—N(9) | 79.7(2) |
| | | N(8)—Ru(2)—N(7) | 78.8(2) |
| | | N(9)—Ru(2)—N(7) | 158.2(2) |
| | | N(8)—Ru(2)—N(6) | 177.33(18) |
| | | N(9)—Ru(2)—N(6) | 100.6(2) |
| | | N(7)—Ru(2)—N(6) | 100.99(19) |
| | | N(2)—Ru(1)—Cl(1) | 98.12(15) |
| | | N(5)—Ru(1)—Cl(1) | 87.41(14) |
| | | N(4)—Ru(1)—Cl(1) | 165.95(14) |
| | | N(1)—Ru(1)—Cl(1) | 89.07(14) |
| | | N(3)—Ru(1)—Cl(1) | 93.66(13) |
| | | N(8)—Ru(2)—Cl(2) | 93.40(14) |
| | | N(9)—Ru(2)—Cl(2) | 88.55(14) |
| | | N(7)—Ru(2)—Cl(2) | 88.85(13) |
| | | N(6)—Ru(2)—Cl(2) | 89.26(13) |
| | | N(8)—Ru(2)—Cl(1) | 88.07(14) |
| | | N(9)—Ru(2)—Cl(1) | 90.66(14) |
| | | N(7)—Ru(2)—Cl(1) | 92.49(13) |

| | | | |
|-------------------|-----------|--------------------------|-----------|
| | | N(6)—Ru(2)—Cl(1) | 89.27(13) |
| | | Cl(2)—Ru(2)—Cl(1) | 178.17(6) |
| Ru11 | | | |
| Ru(1)—N(1) | 2.055(10) | N(2)—Ru(1)—N(1) | 79.2(4) |
| Ru(1)—N(2) | 1.964(10) | N(2)—Ru(1)—N(3) | 80.7(4) |
| Ru(1)—N(3) | 2.067(9) | N(1)—Ru(1)—N(3) | 160.0(4) |
| Ru(1)—N(4) | 2.074(10) | N(2)—Ru(1)—N(4) | 94.2(4) |
| Ru(1)—N(5) | 2.085(11) | N(1)—Ru(1)—N(4) | 87.6(4) |
| Ru(1)—N(6) | 2.097(10) | N(3)—Ru(1)—N(4) | 93.4(4) |
| | | N(2)—Ru(1)—N(5) | 172.4(4) |
| | | N(1)—Ru(1)—N(5) | 101.9(4) |
| | | N(3)—Ru(1)—N(5) | 97.9(4) |
| | | N(4)—Ru(1)—N(5) | 78.5(4) |
| | | N(2)—Ru(2)—N(6) | 89.8(4) |
| | | N(1)—Ru(2)—N(6) | 91.6(4) |
| | | N(3)—Ru(2)—N(6) | 88.7(3) |
| | | N(4)—Ru(2)—N(6) | 175.8(4) |
| | | N(5)—Ru(2)—N(6) | 97.7(4) |

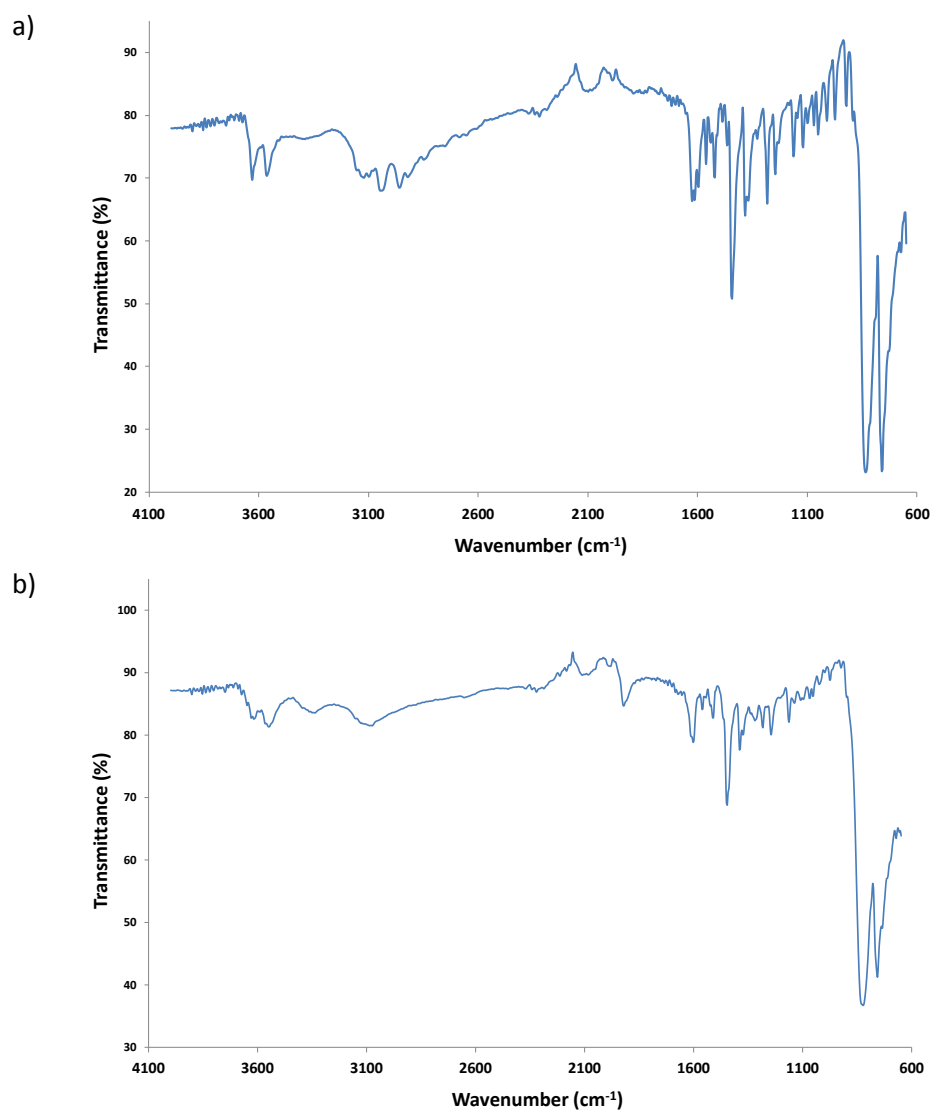


Figure SIV.3.1. FTIR spectra of a mixture of the chlorido complexes **Ru7a** and **Ru7b** (a), and the *trans* aqua complex **Ru10** (b).

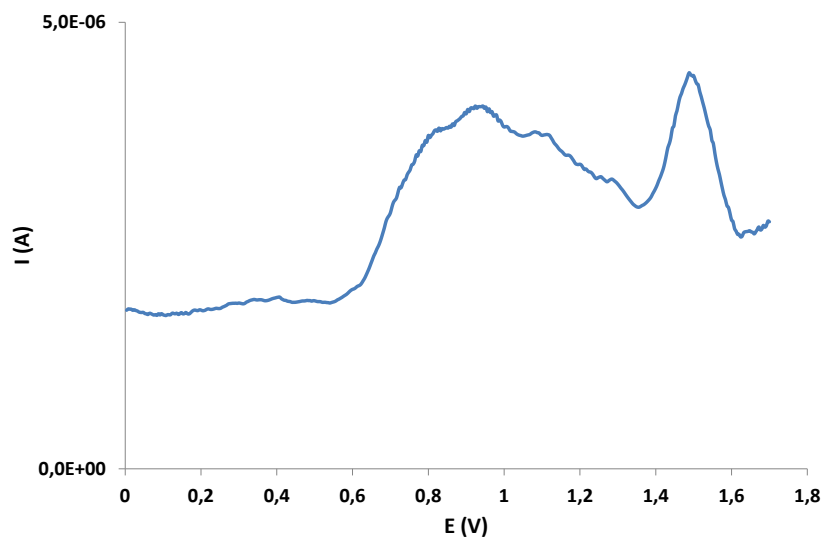


Figure SIV.3.2. DPV experiment for dmsol complex **Ru8** ($\text{CH}_2\text{Cl}_2 + 0.1 \text{ M TBAH vs. SCE}$).

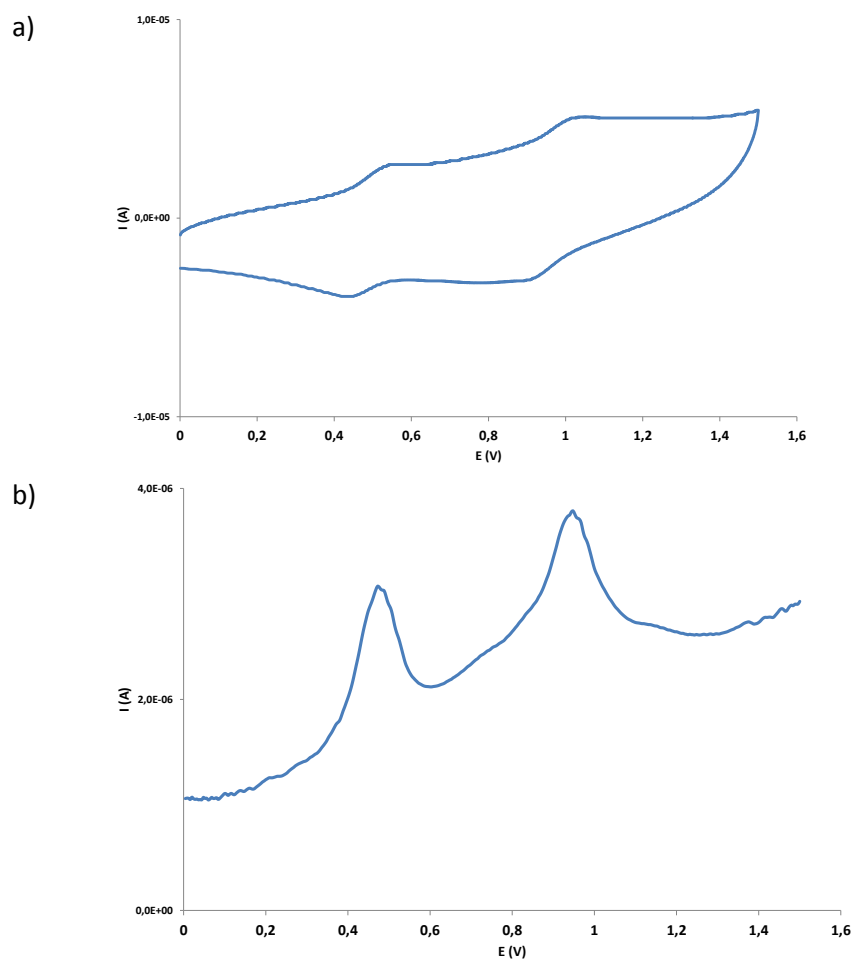
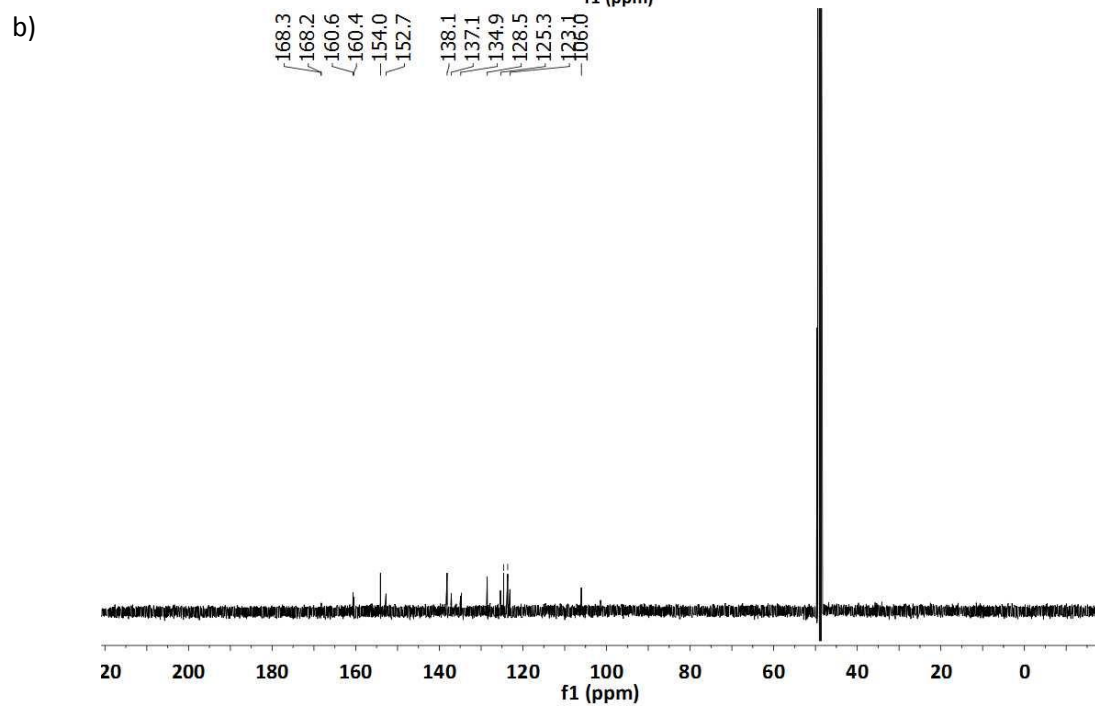
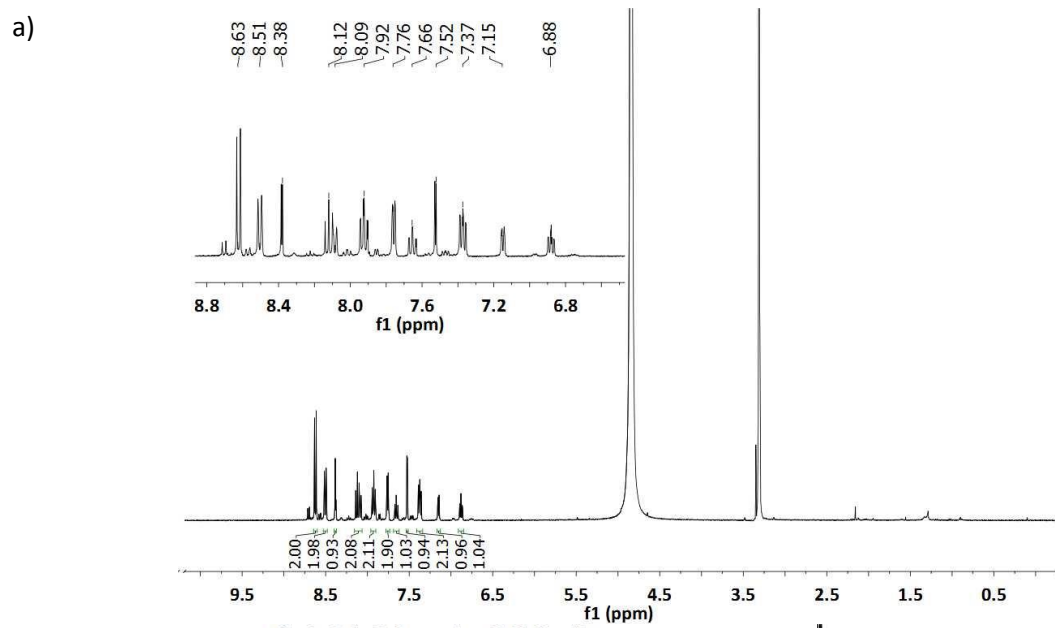
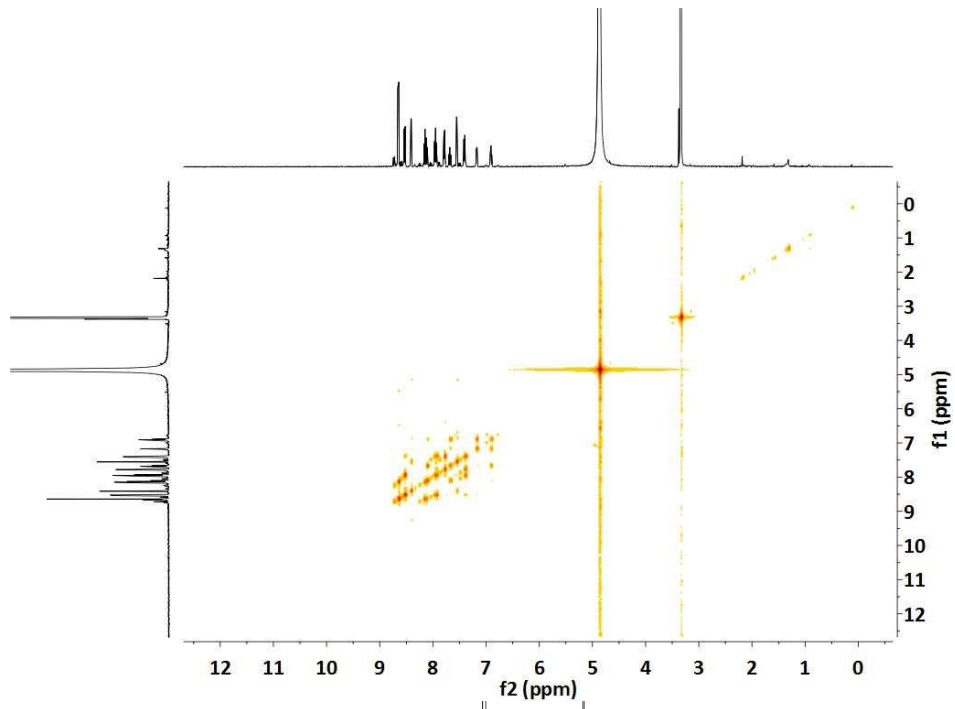


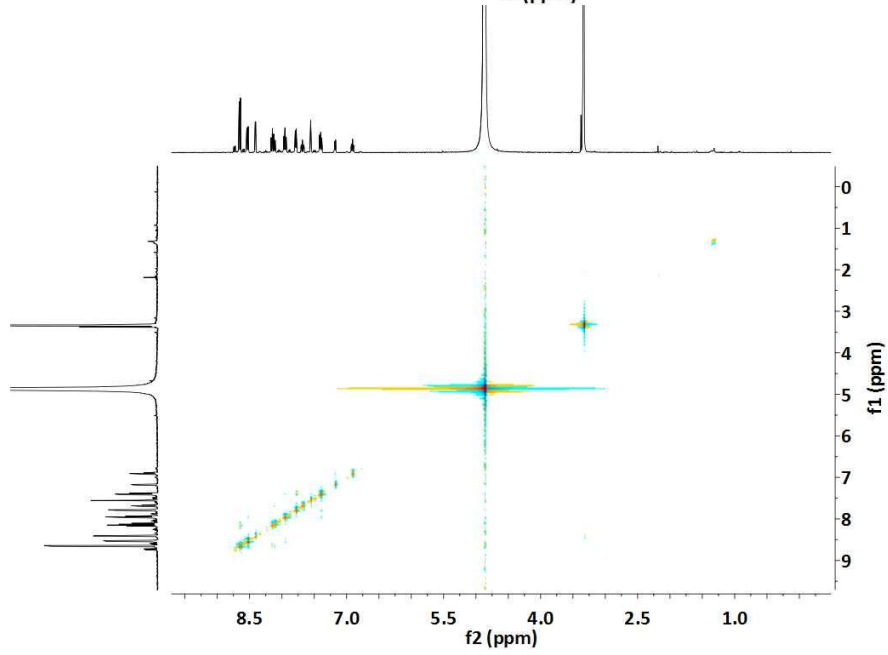
Figure SIV.3.3. VC (a) and DPV experiment (b) for the dimeric complex **Ru9** ($\text{CH}_2\text{Cl}_2 + 0.1 \text{ M TBAH vs. SCE}$).



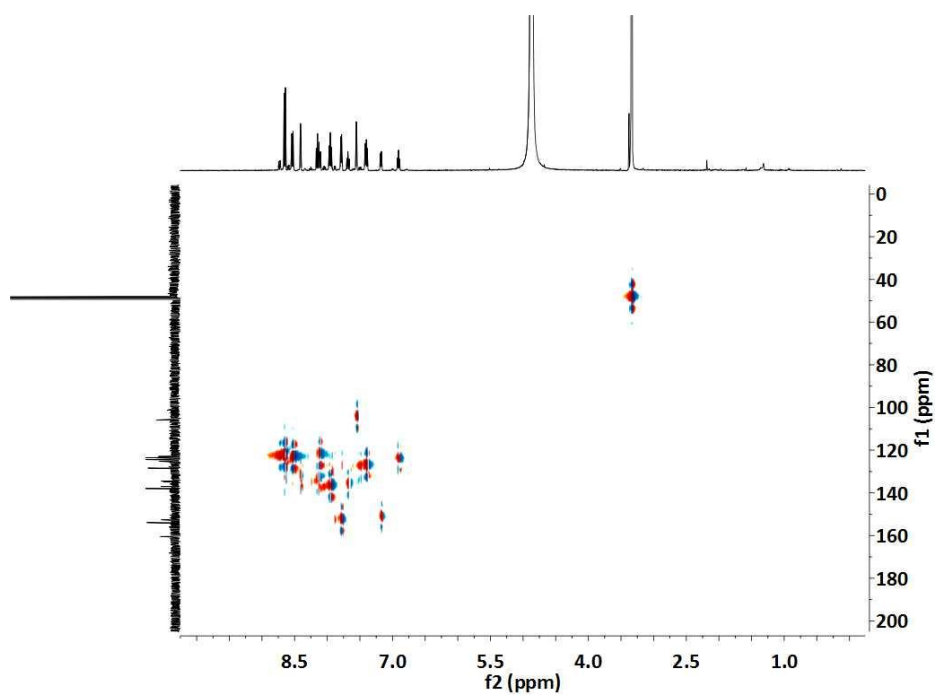
c)



d)



e)



f)

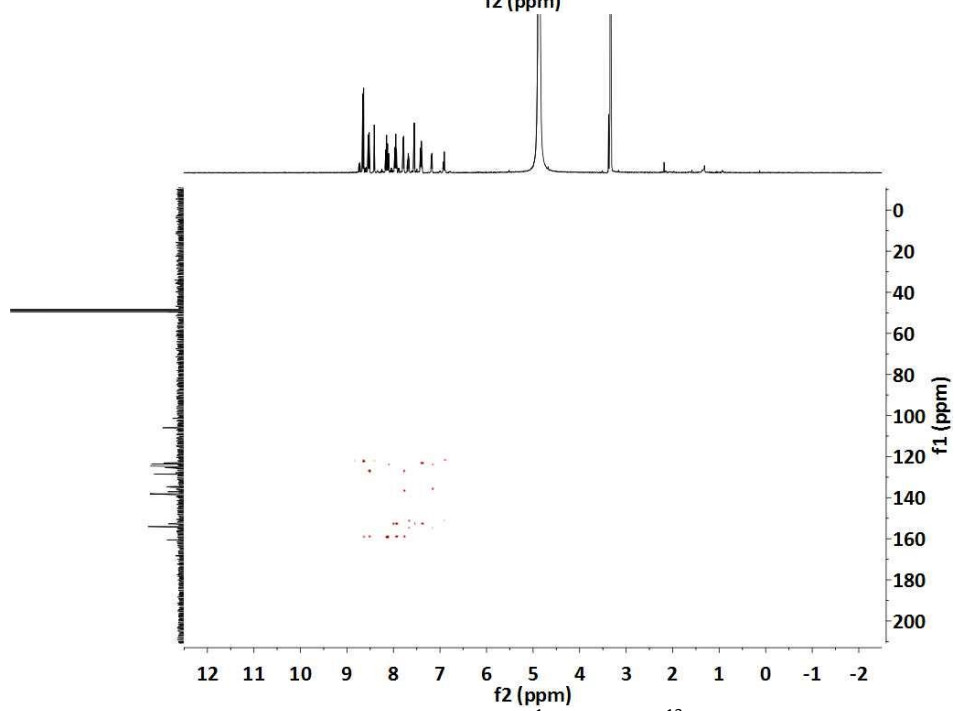
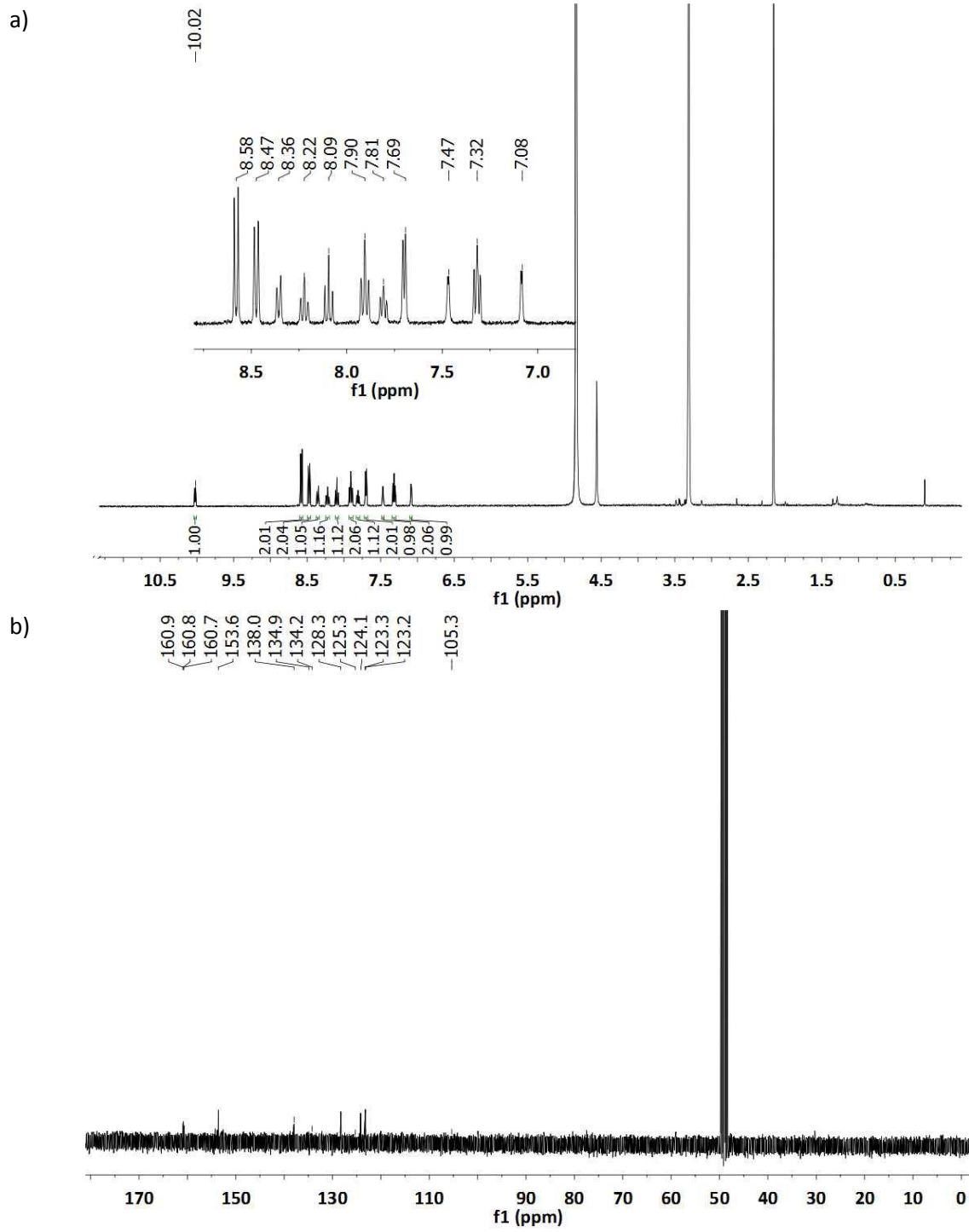
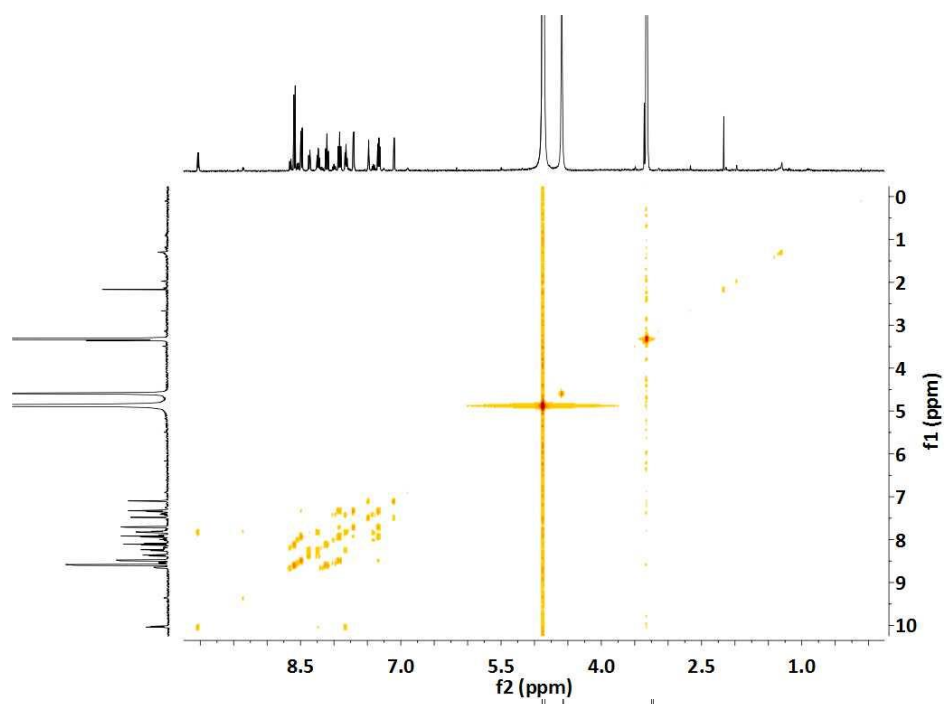


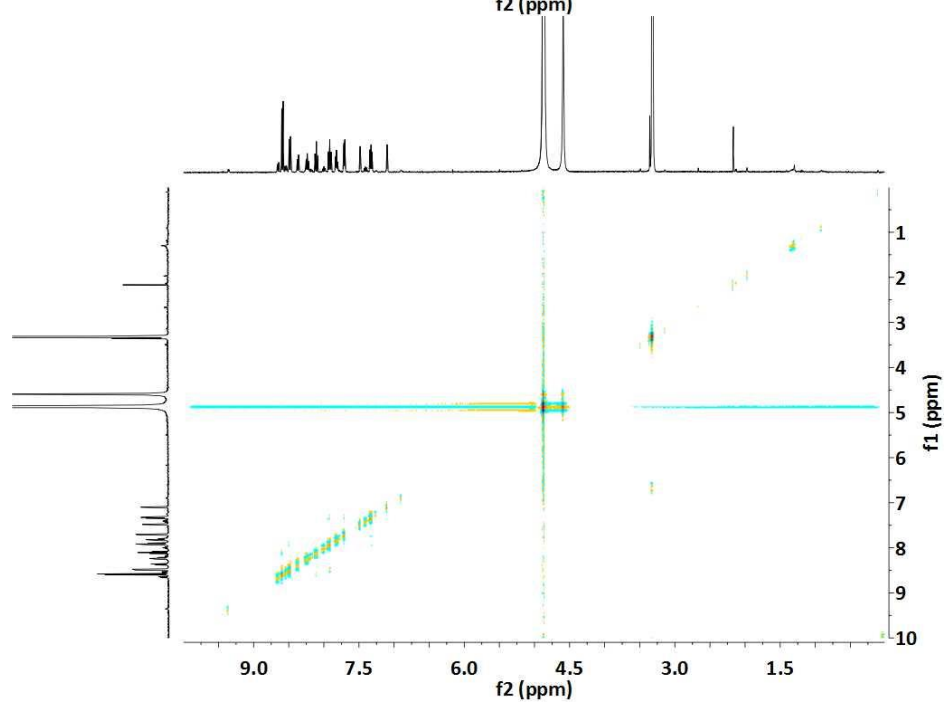
Figure SIV.3.4. NMR of **Ru7a**, 400 MHz, methanol- d_5 : a) ^1H -NMR; b) ^{13}C -NMR; c) COESY; d) NOESY; e) ^1H - ^{13}C HSQC; f) ^1H - ^{13}C HMBC.

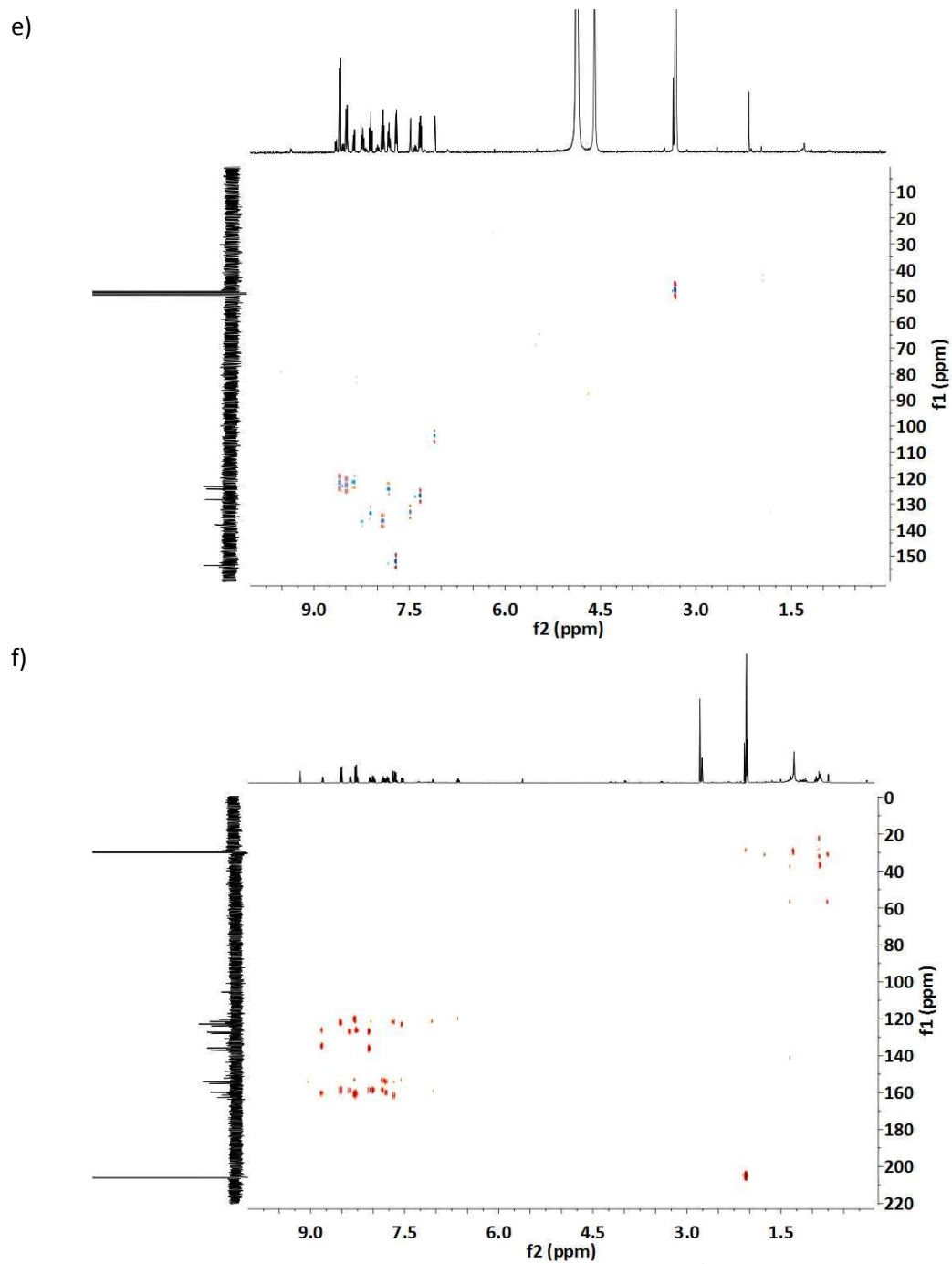


c)

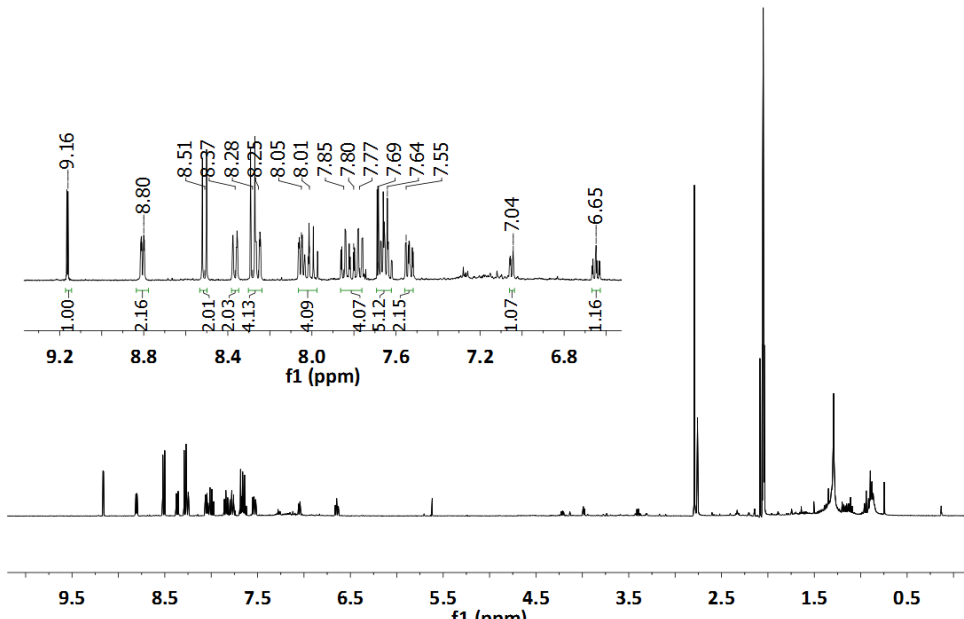


d)

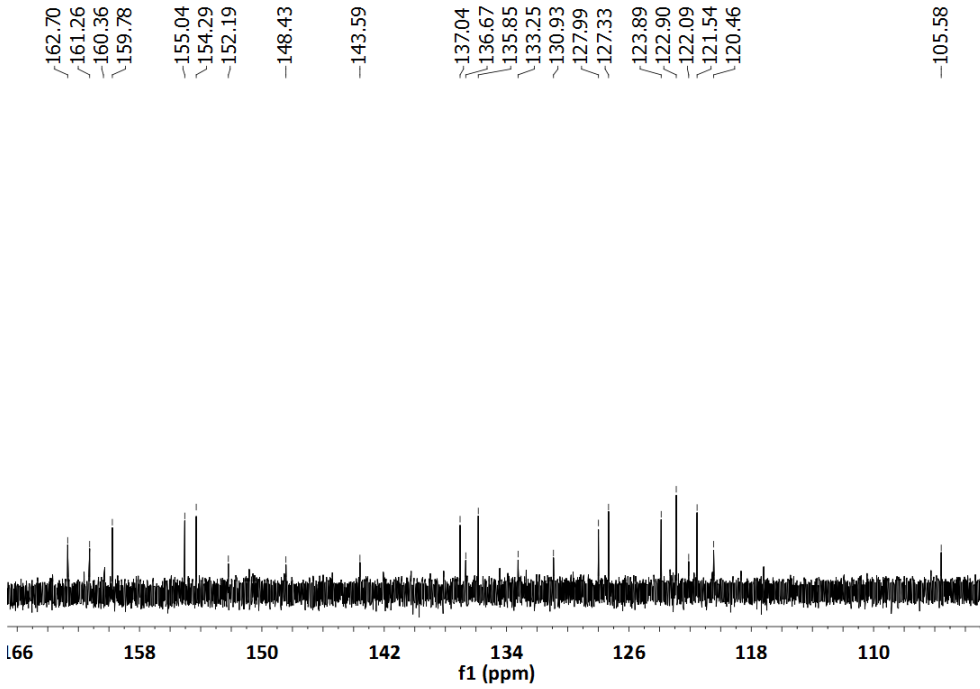




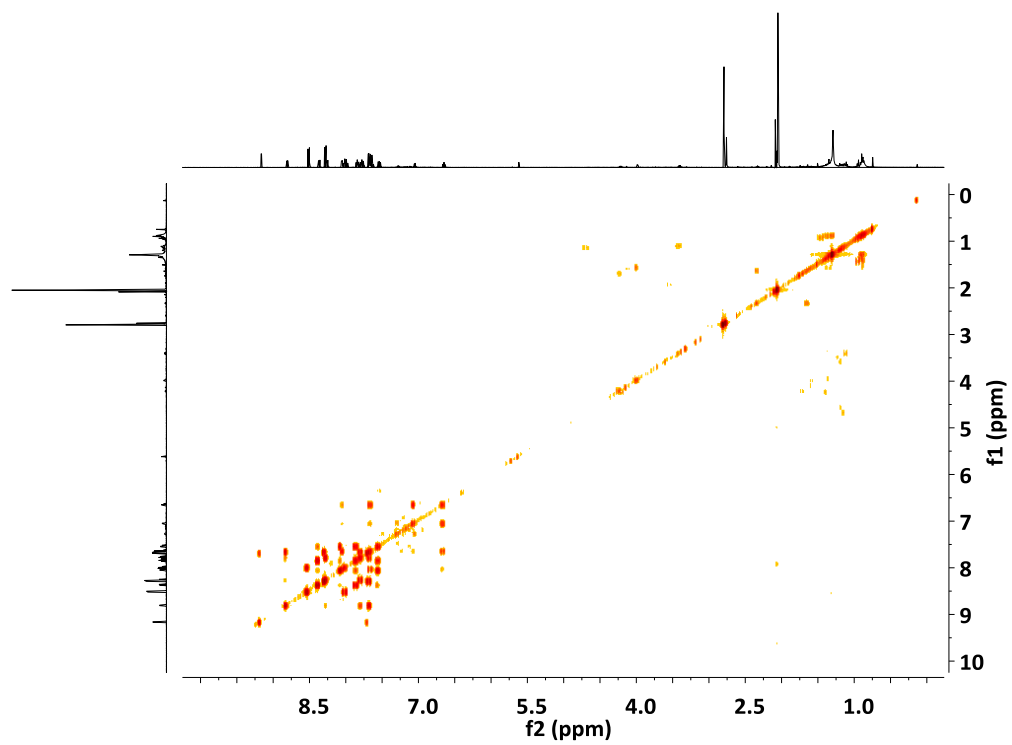
a)



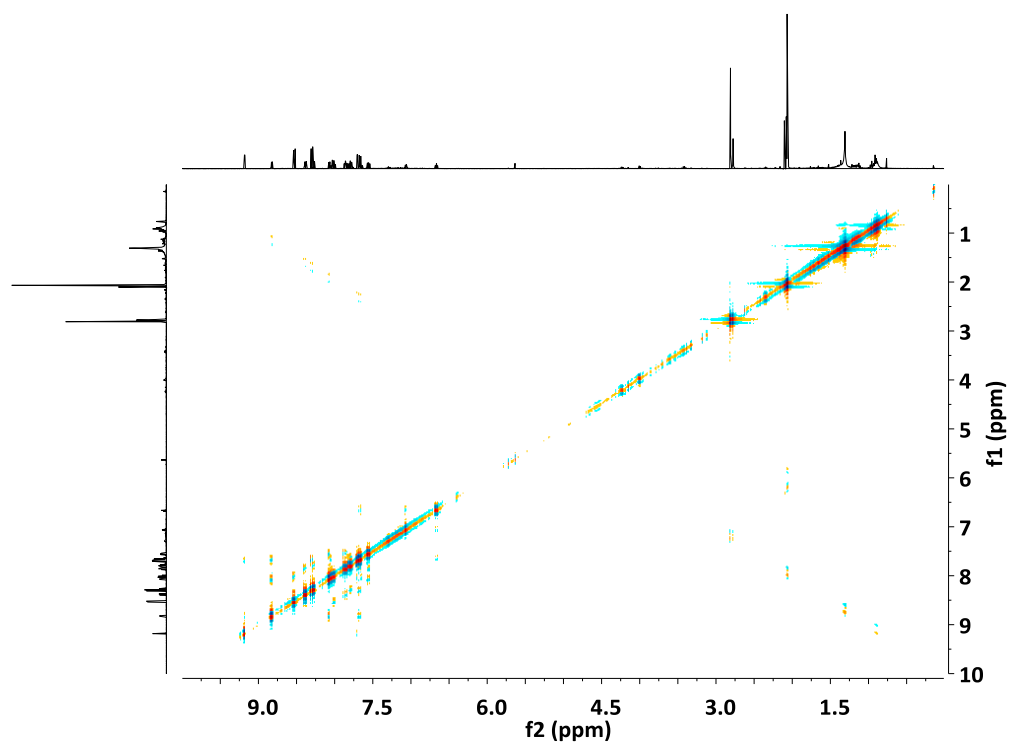
b)



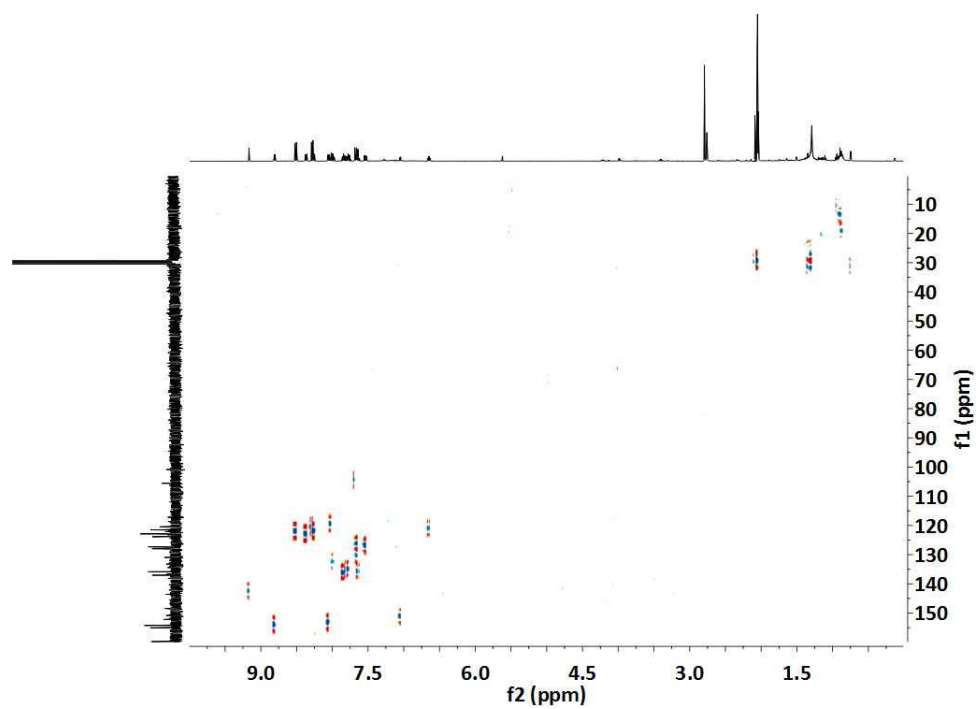
c)



d)



e)



f)

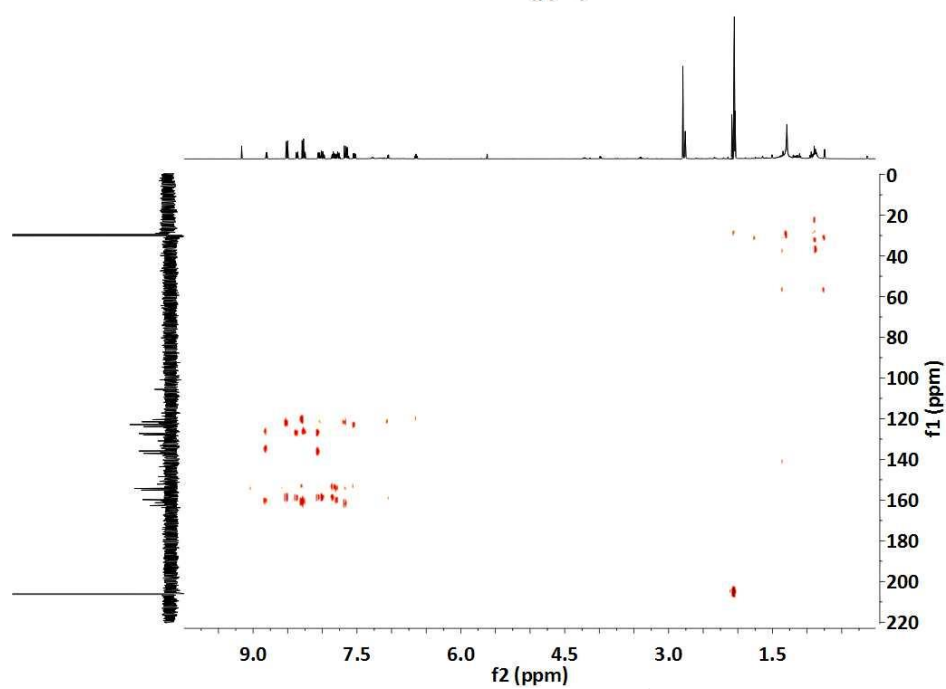


Figure SIV.3.6. NMR of **Ru9**, 400 MHz, acetone- d_6 : a) ^1H -NMR; b) ^{13}C -NMR; c) COESY; d) NOESY; e) ^1H - ^{13}C HSQC; f) ^1H - ^{13}C HMBC.

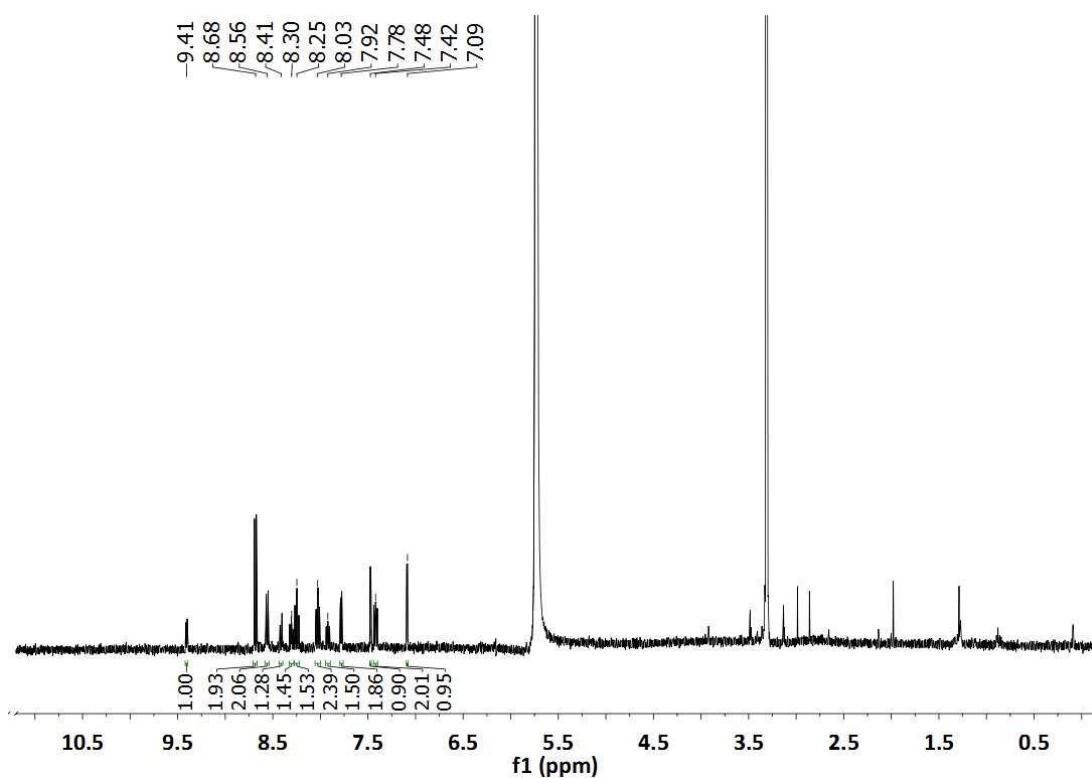


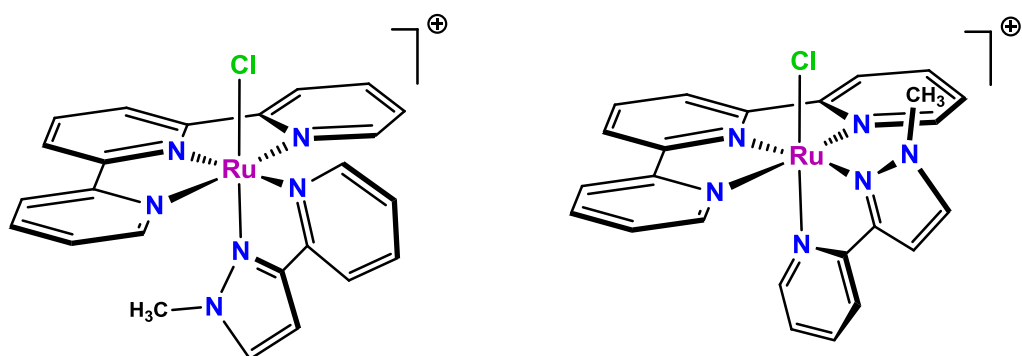
Figure SIV.3.7. $^1\text{H-NMR}$ of Ru10, 400 MHz, methanol- d_5 .

$$E_{1/2} = E_{1/2}^{\circ} - 0.059 (m/n) \text{ pH}$$

- $E_{1/2}$: half wave redox potential at a given pH
 $E_{1/2}^{\circ}$: half wave redox potential at standard conditions
 m: number of transferred protons
 n: number of transferred electrons

Equation SIV.3.9. Relation between potential and pH in the Nernst equation.

(a)



(b)

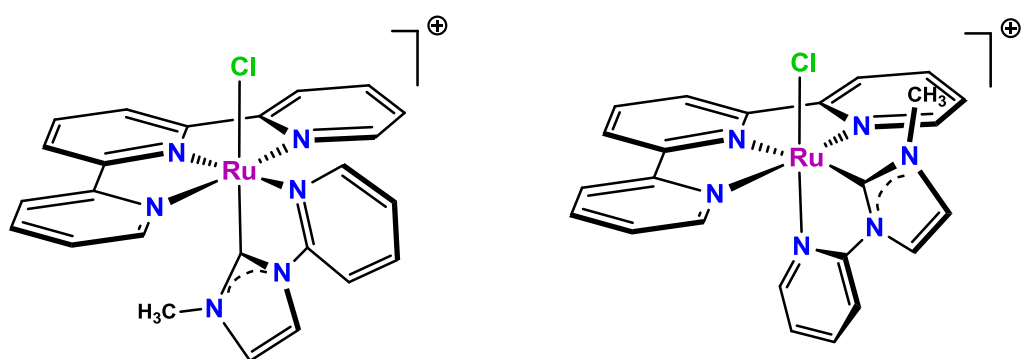


Figure SIV.3.8. Schematic structures for the *cis* and *trans* isomers of complexes (a) $[\text{RuCl}(\text{pypz-Me})(\text{trpy})]^+$ and (b) $[\text{RuCl}(\text{CN-Me})(\text{trpy})]^+$.

Chapter 7

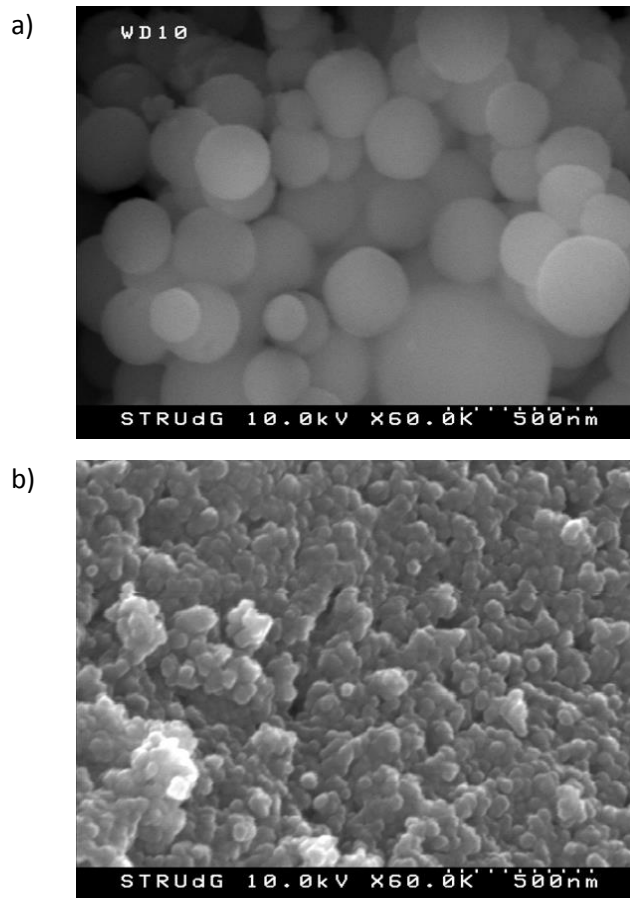
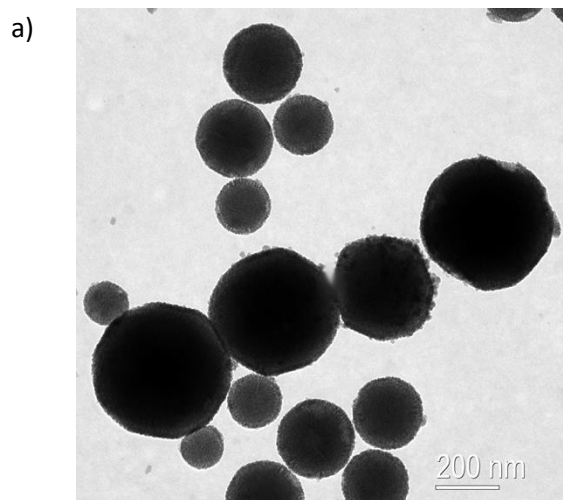


Figure SIV.4.1. SEM images of a) SP and b) MSNP before the anchoring of the Ru complex. Notice that for magnetic nanoparticles (b) the resolution is not as good as for the SP caused for aggregation.



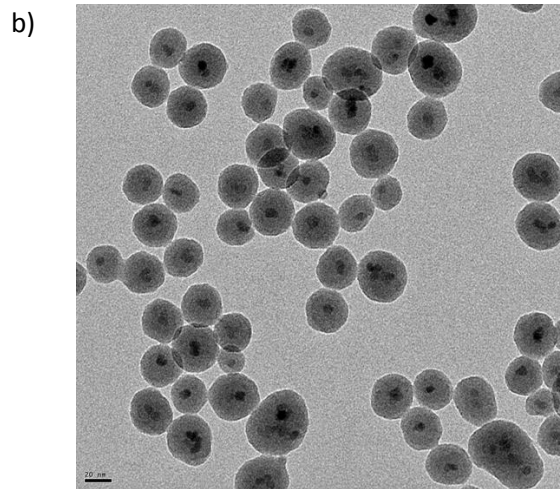
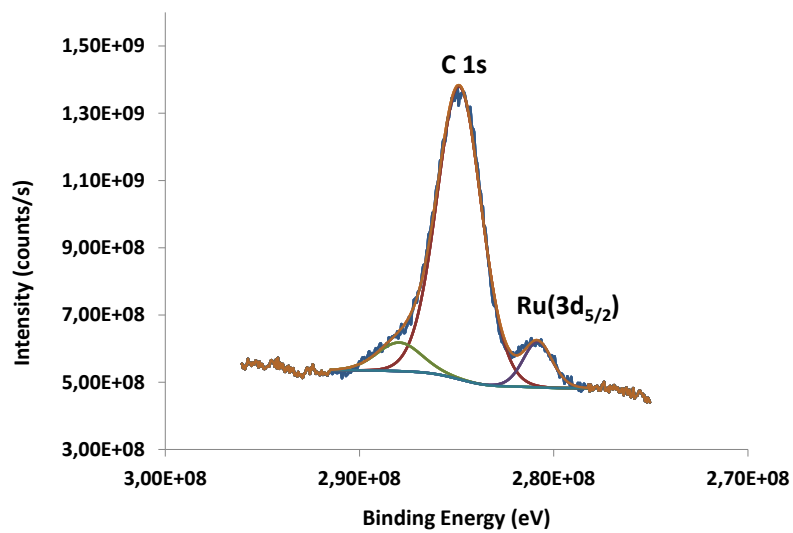
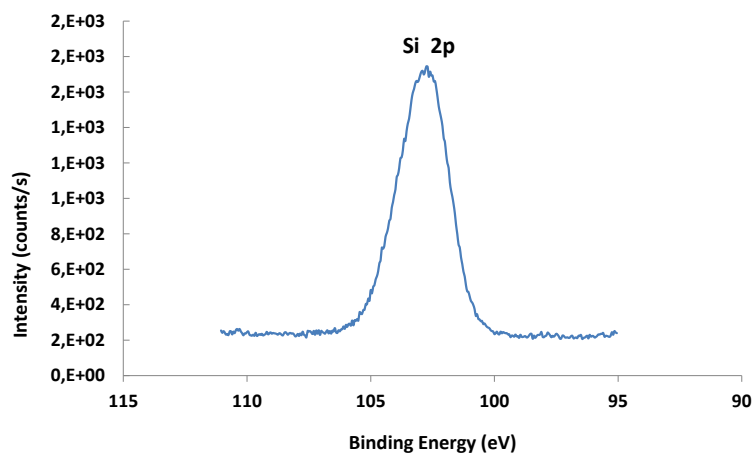


Figure SIV.4.2. TEM images of a) SP and b) MSNP before the anchoring of the Ru complex (Image (b) was obtained by the group of Dr. Josep Ros from ICMA B).

a)



b)



c)

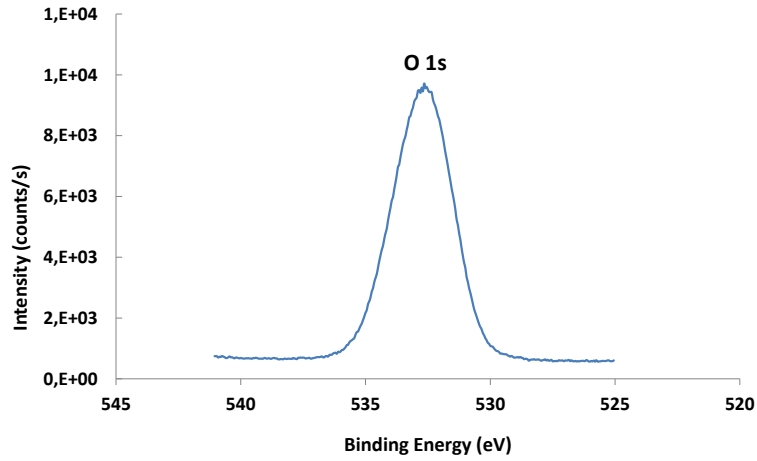
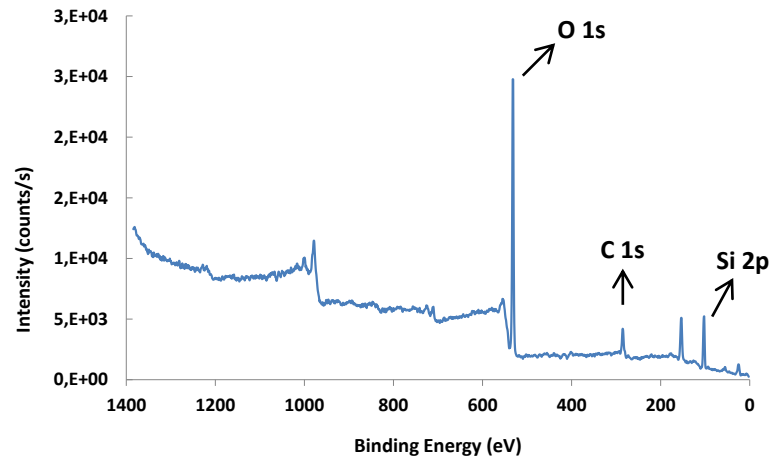
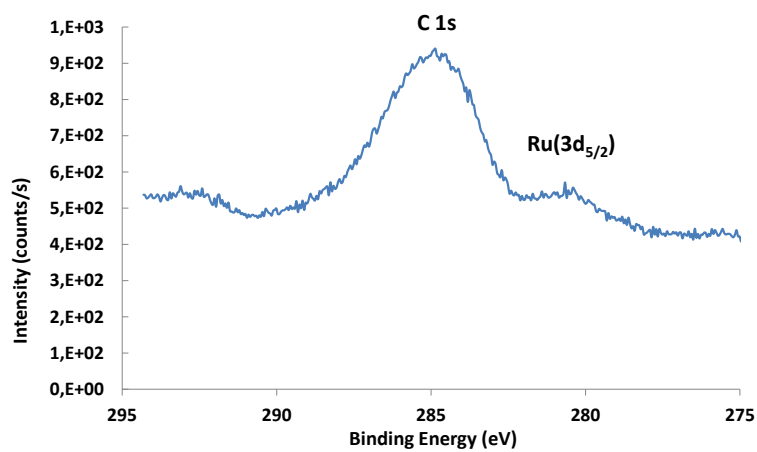


Figure SIV.4.3. XPS survey scans of **SP@Ru1**: a) deconvoluted XPS spectra for C 1s and Ru ($3d_{5/2}$) signals, b) Si 2p signal and c) O 1s signal.

a)



b)



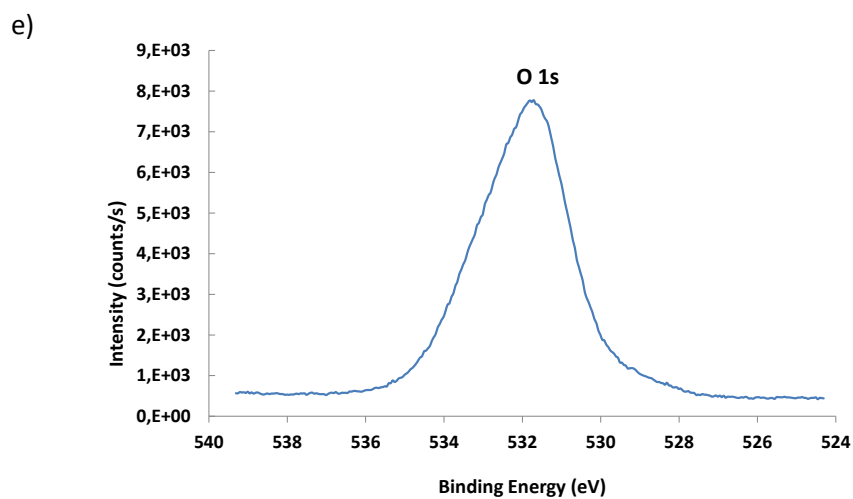
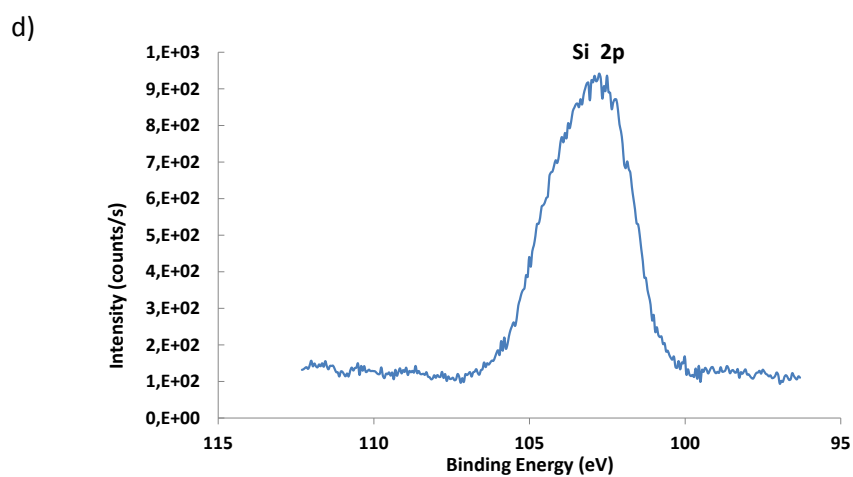
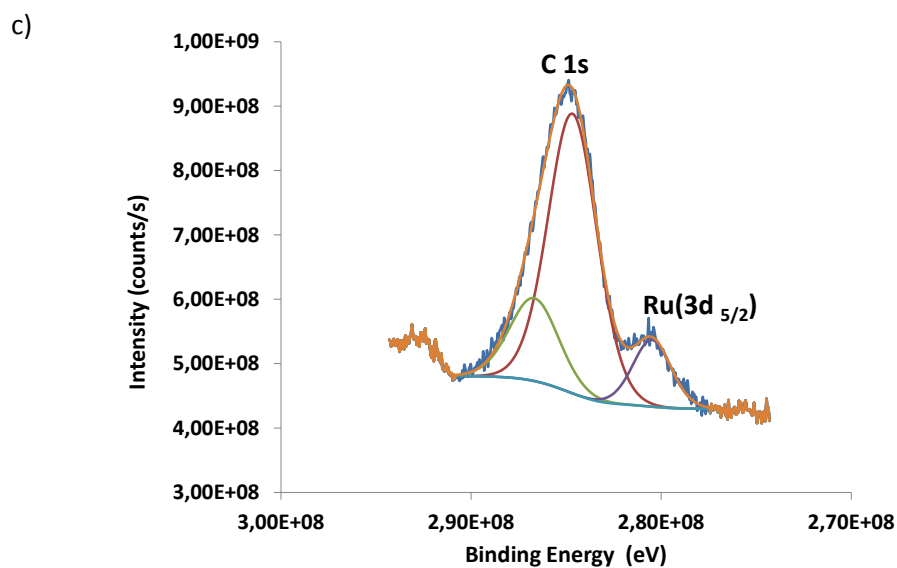
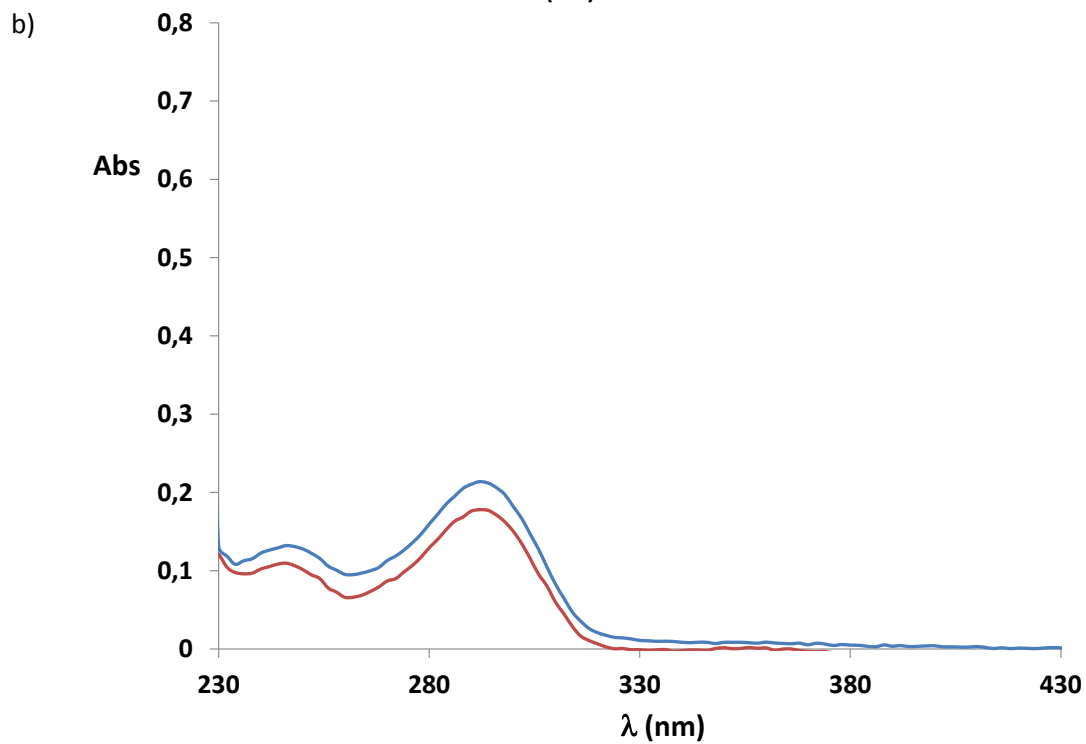
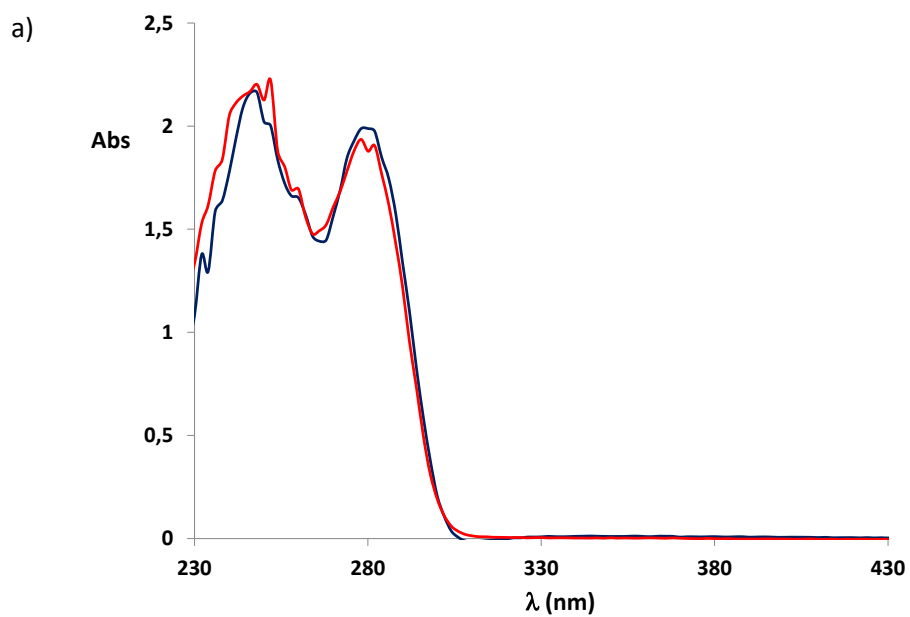


Figure SIV.4.4. XPS survey scans of **MSNP@Ru1**: a) overall XPS spectra, b) C 1s and Ru ($3d_{5/2}$) signals, c) deconvoluted XPS spectra for C 1s and Ru ($3d_{5/2}$) signals, d) Si 2p signal and e) O 1s signal.

Chapter 8



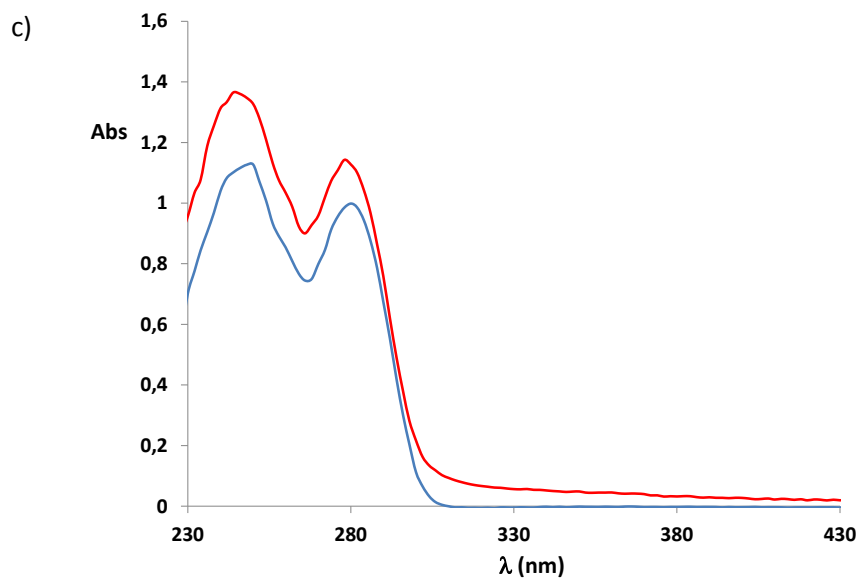
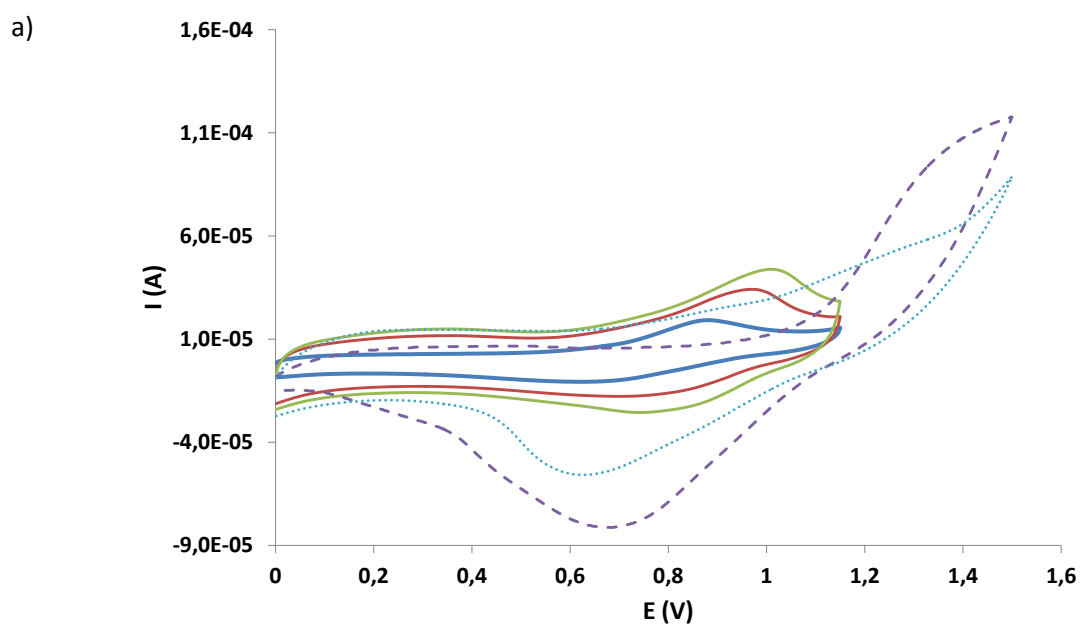
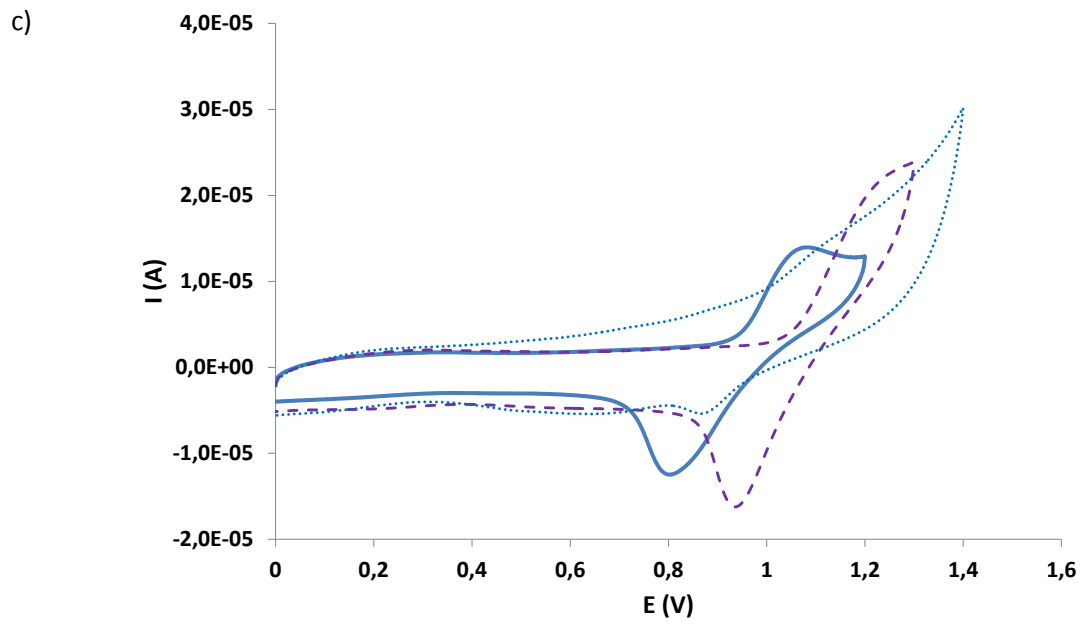
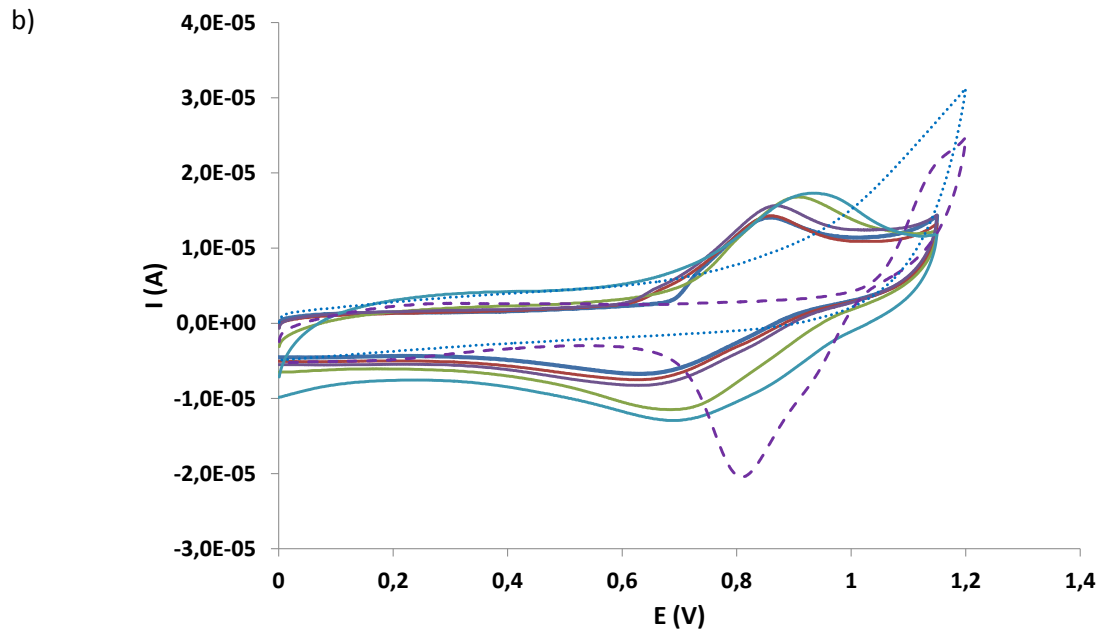
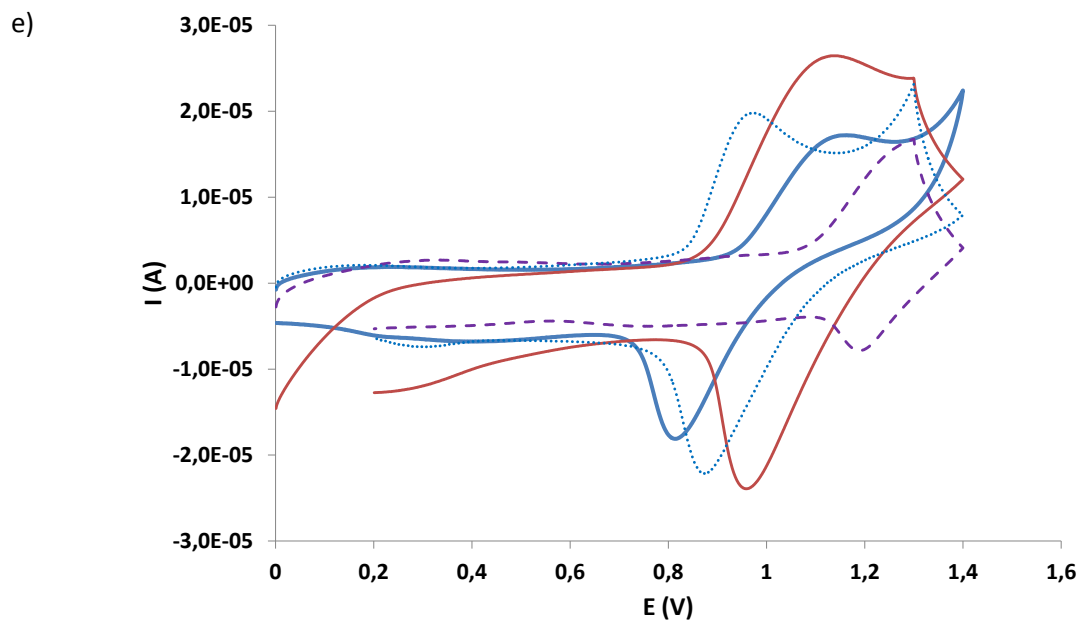
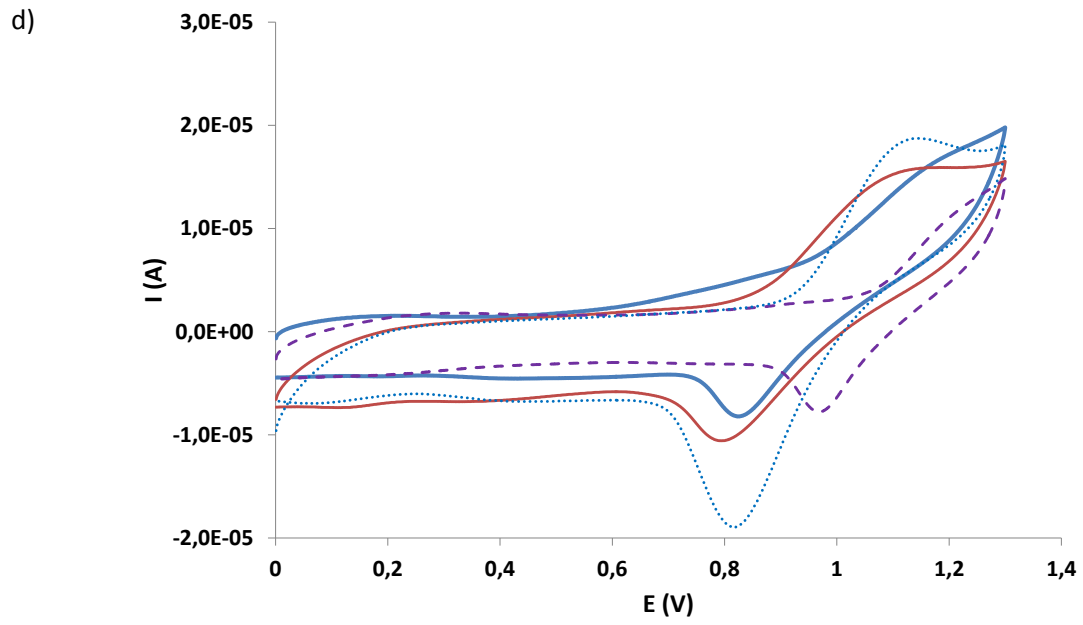


Figure SIV.5.1. UV-Vis spectra registered in PBS of complexes a) Mn6, b) Mn7 and c) Mn8. Blue lines correspond to the initial spectrum registered and red lines after 72 h.







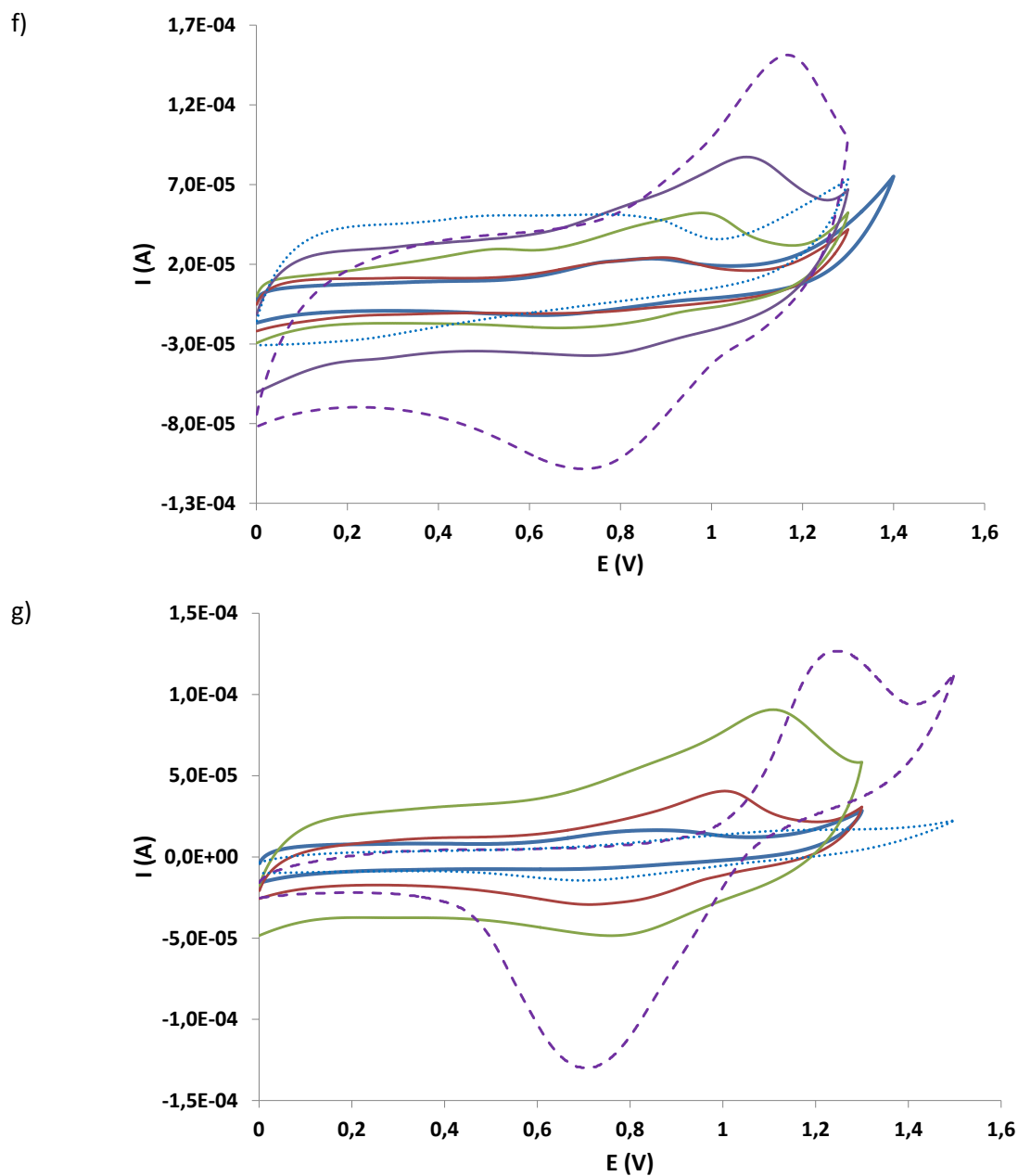


Figure SIV.5.2. a) **Mn6** and b) **Mn8** in $\text{H}_2\text{O} + 0.103 \text{ M NaCl}/0.0049 \text{ M KCl}$; c) **Mn6**, d) **Mn7** and e) **Mn8** in $\text{H}_2\text{O} + 0.1 \text{ M NH}_4\text{PF}_6$; f) **Mn7** and g) **Mn8** in $\text{H}_2\text{O} + 0.1 \text{ M Na(OSO}_2\text{CF}_3)$ vs. SCE. The solid lines correspond to the voltammograms registered after complex solubilization at different times. The purple dashed line corresponds to the CV obtained after addition of p-toluene sulfonic acid, whereas that recorded after addition of NaOH is displayed as a blue dotted line.

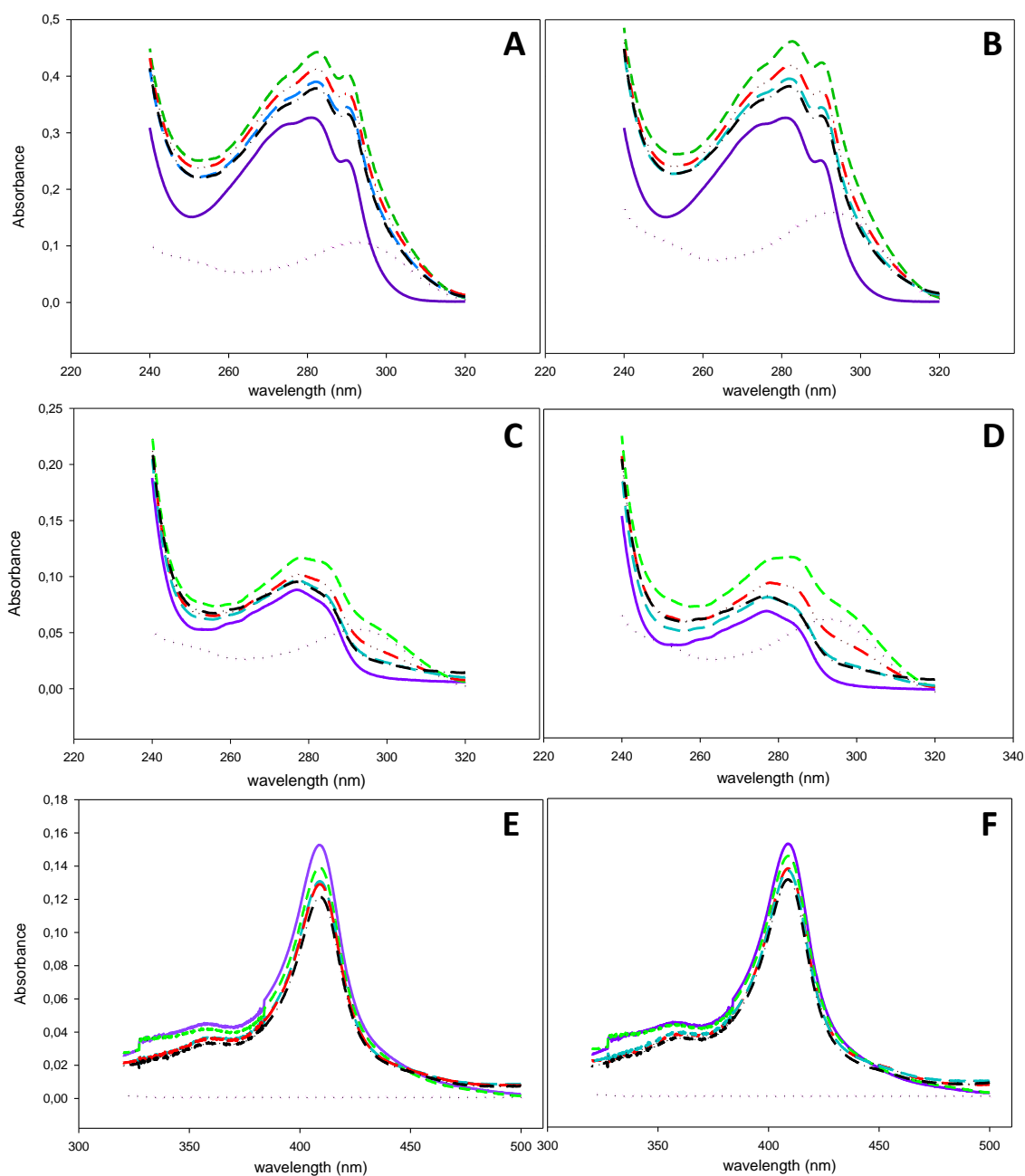
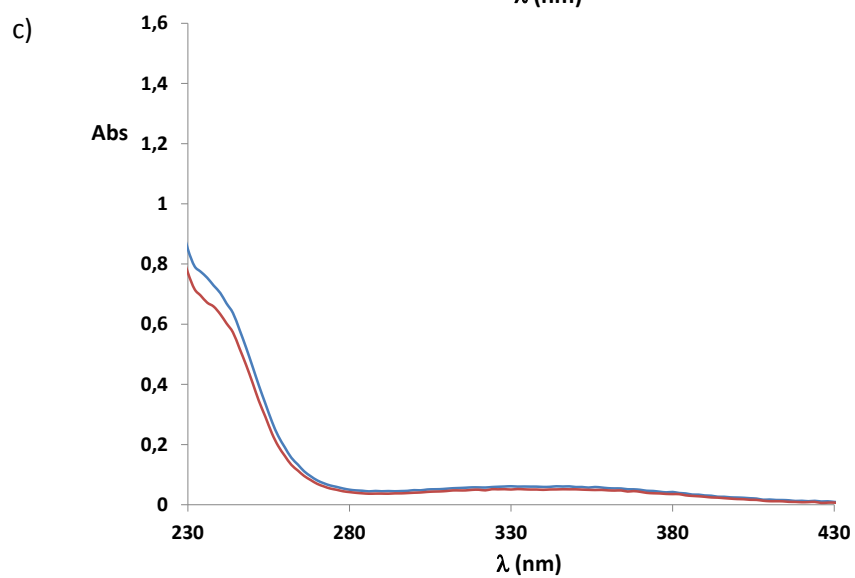
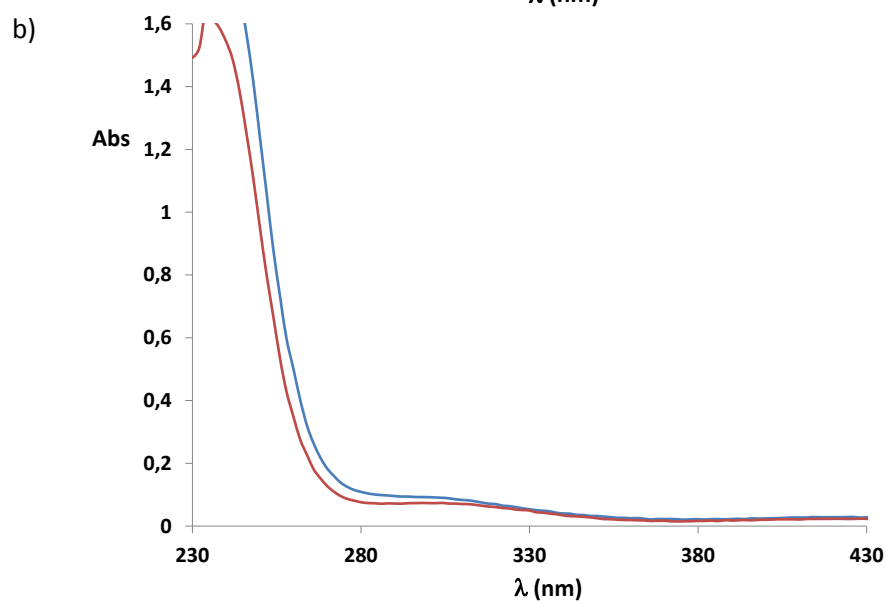
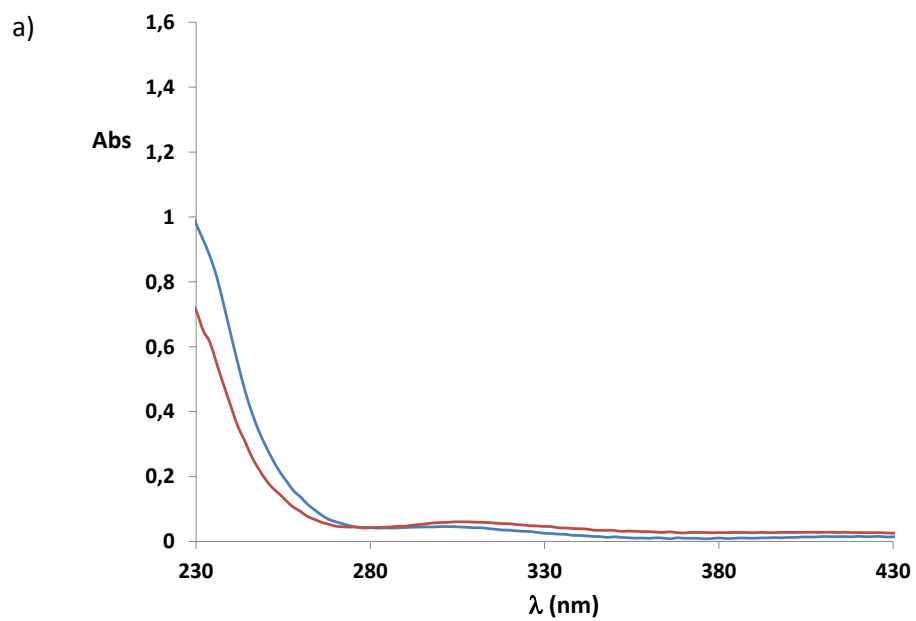
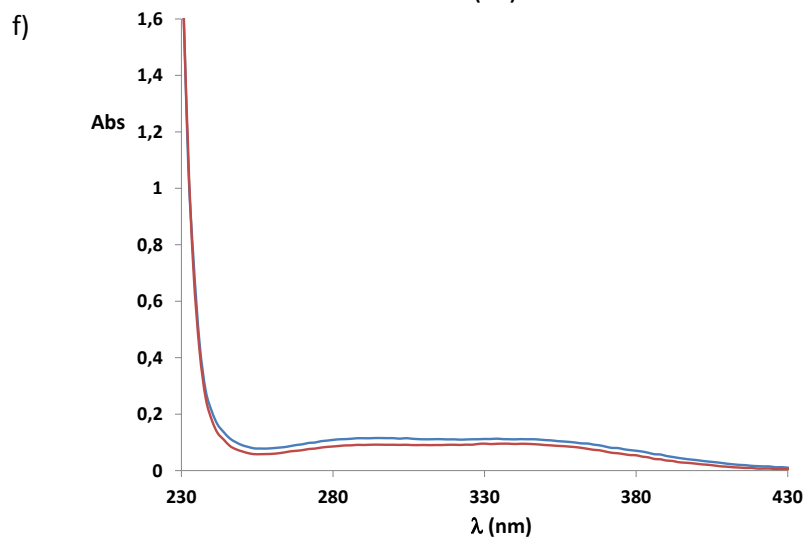
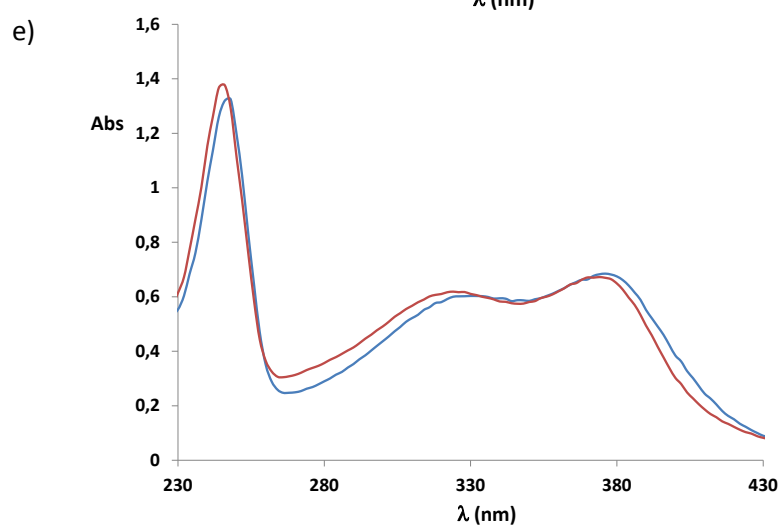
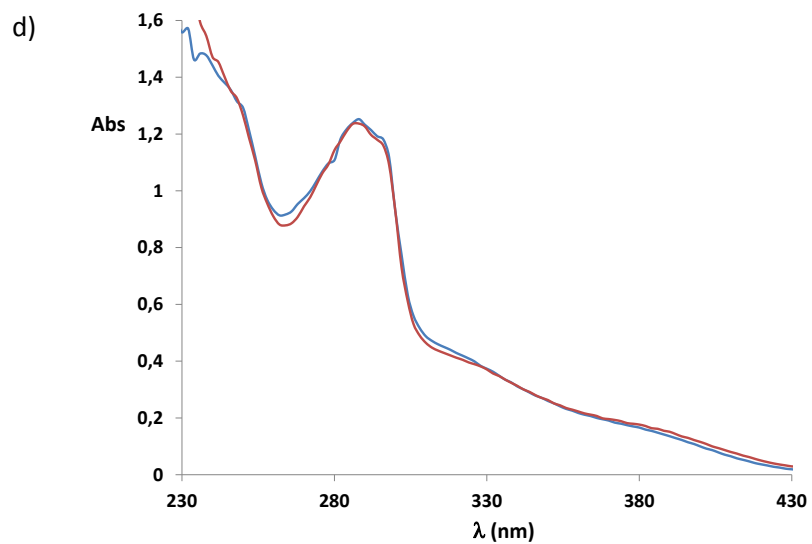


Figure SIV.5.3. Time-course of UV-Vis spectra of compound **Mn10** (B, D and F) and its ligand (-)-L (A, C and E) dissolved in 10 mM phosphate buffer, pH 7.4, in the presence of chicken egg lysozyme (A and B), human pancreatic ribonuclease (C and D) and cytochrome C (E and F) at a stoichiometric ratio of 4:1 (compound or ligand/protein). Pink: spectra of compound or ligand before the addition of the protein; purple: protein spectra before the incubation with the compound or ligand; green: mix of compound 8 or ligand (-)-L with protein at $t=0$ h of incubation; red: at $t=4$ h of incubation; blue: at $t=20$ h of incubation; and black: at $t=48$ h of incubation.





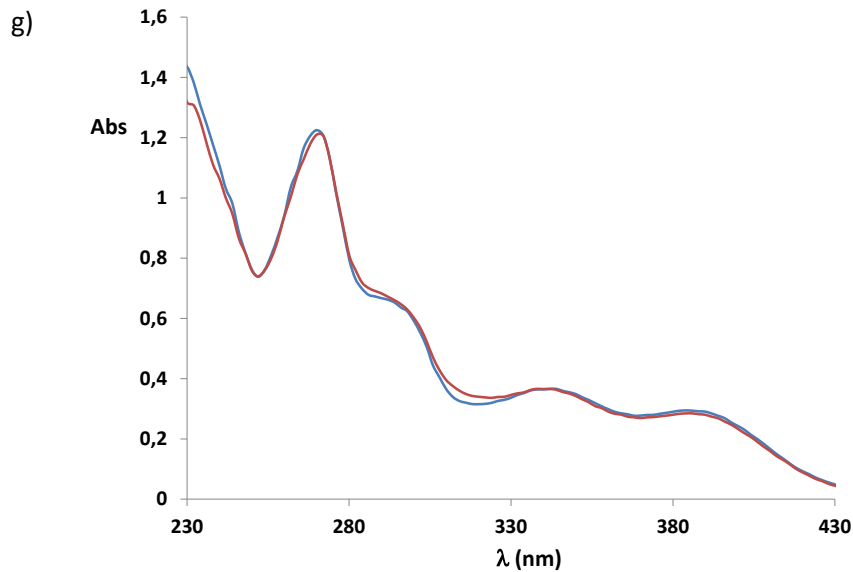


Figure SIV.5.4. UV-Vis spectra registered in H₂O of complexes a) Ru4, b) Ru5, c) Ru6, d) P2, e) Ru12, f) Ru13 (+ 1 % dmsO) and g) Ru14. Blue lines correspond to the initial spectrum registered and red lines after 72 h.

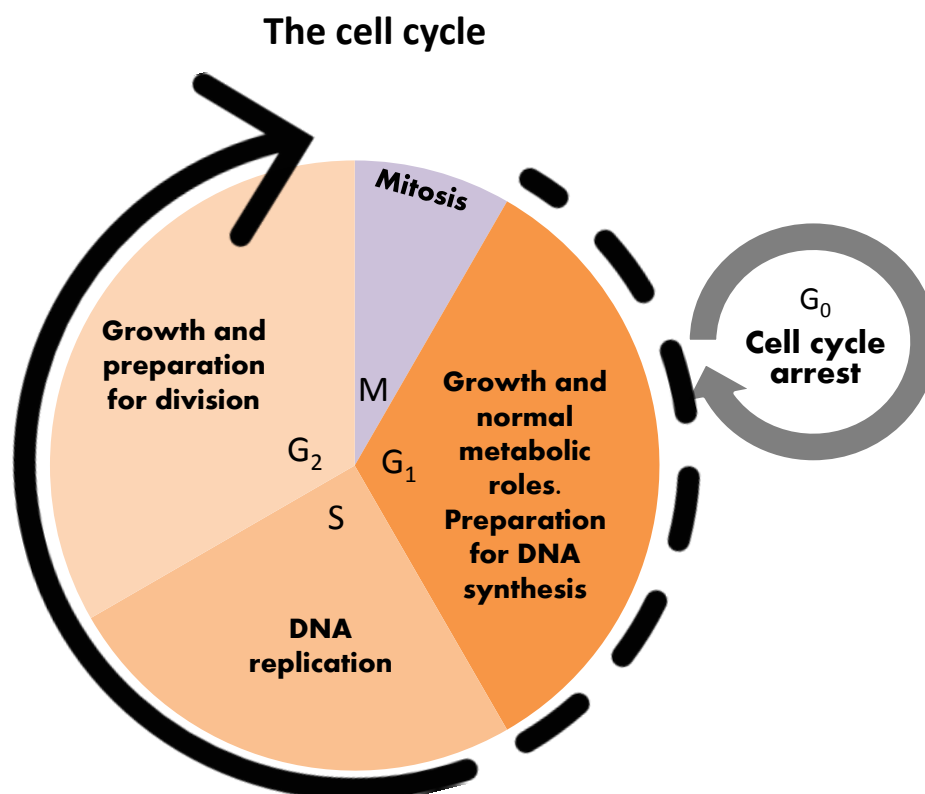


Figure SIV.5.5. The cell cycle phases a) G₀: growth and normal metabolic roles; b) G₁, first growth phase (growth and normal metabolic roles) plus preparation for DNA synthesis: cellular contents excluding the chromosomes, are duplicated; c) S, synthesis phase: duplication of chromosomes; d) G₂, second growth phase and preparation for division: the cell “double checks” the duplicated chromosomes for error, making any needed repairs; and e) M, mitosis: cell division.

